ISBN 978-82-326-5247-7 (printed ver.)
ISBN 978-82-326-5335-5 (electronic ver.)
ISSN 1503-8181 (printed ver.)
ISSN 2703-8084 (electronic ver.)

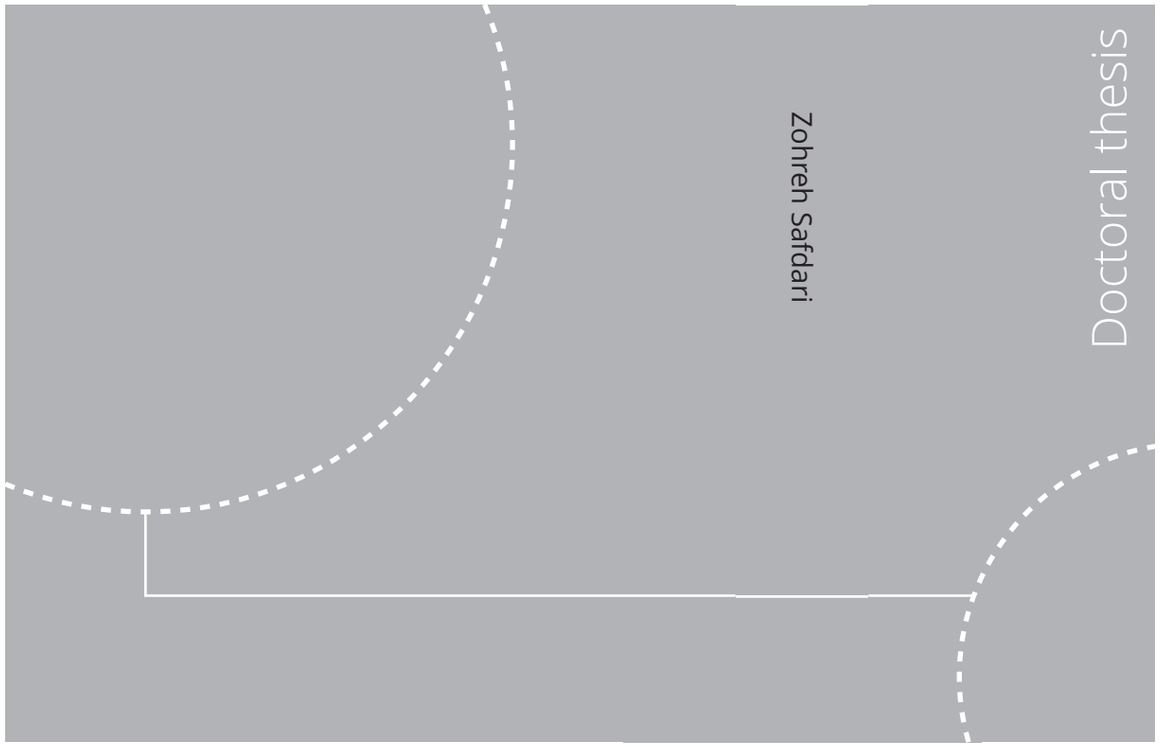

Doctoral theses at NTNU, 2021:377

Zohreh Safdari

Groundwater Level Monitoring across Iran's Main Water Basins Using Temporal Satellite Gravity Solutions and Well Data

NTNU
Norwegian University of Science and Technology
Thesis for the degree of Philosophiae Doctor
Faculty of Engineering
Department of Civil and Environmental Engineering

NTNU
Norwegian University of Science and Technology

Doctoral theses at NTNU, 2021:377

NTNU
Norwegian University of Science and Technology

Zohreh Safdari

Groundwater Level Monitoring across Iran's Main Water Basins Using Temporal Satellite Gravity Solutions and Well Data

Thesis for the degree of Philosophiae Doctor

Trondheim, December 2021

Norwegian University of Science and Technology
Faculty of Engineering
Department of Civil and Environmental Engineering

NTNU
Norwegian University of
Science and Technology

NTNU
Norwegian University of Science and Technology

Thesis for the degree of Philosophiae Doctor

Faculty of Engineering
Department of Civil and Environmental Engineering

ISBN 978-82-326-5247-7 (printed ver.)
ISBN 978-82-326-5335-5 (electronic ver.)
ISSN 1503-8181 (printed ver.)
ISSN 2703-8084 (electronic ver.)

Doctoral theses at NTNU, 2021:377

PRINTED IN NORWAY
NO - 1598

NORDIC SWAN ECOLABEL
Printed matter
2041 0731

Printed by Skipnes Kommunikasjon AS

Abstract

Water is an essential resource for life on the earth; no life can exist without water. During recent decades, because of growth in population and technologies, demands for water resources have been increasing. Due to groundwater's physical properties, it has a special role in human life especially in a dry and semi-dry climate like that in Iran. Therefore, management of sustainability of groundwater is necessary. The first stage in water management is to collect water-table data in order to have a time series of groundwater storage (GWS) changes. Nevertheless, in some areas, there is no continuous, reliable data, or access to these data requires the permission of the respective governments. Sometimes these data are outdated and measured by inconsistent methods between geopolitical boundaries and therefore are not reliable. The acquisition of accurate data is a major challenge. Globally, there are no extensive ground-based networks for monitoring large-scale GWS variations.

Satellite observations from the GRACE (Gravity Recovery and Climate Experiment) mission present a new and valuable tool to fill the gaps in data availability. Standard GRACE modeling of groundwater changes are usually country-wide. These country-scale models, however, cannot be used in finer basin-scales. In this thesis, we developed a technique to move GRACE modelling from the country-scale to the sub-basin scale. We developed the GRACE least square mascon solution method for specific regions of Iran, chosen largely to coincide with main water basin.

We have used 163 months of CSR GRACE Level-2 release 6.0 data (2002 to 2017) and 15 months of GRACE Follow-On (FO) (2018 to 2019). The degree 1 coefficients are computed as described by Swenson et al. (2008). The coefficient of C_{20} is replaced by estimates from Satellite Laser Ranging (SLR) data. The effects of Glacial Isostatic Adjustment (GIA) are removed by subtracting the GIA Stokes coefficients computed by A et al. (2013). Instead of using a decorrelation filter, the Spherical Harmonic coefficients

are smoothed using a Gaussian smoothing function with a 100-km radius. Total water storage changes are synthesized on a 0.5° spatial grid over Iran. The signal from the Caspian Sea and Urmia Lake are removed as described in Swenson and Wahr (2007). Output from a version of the CLM4.5 land surface model has been used to remove contributions from soil moisture, snow, canopy storages, and river storage. We conclude that most of the long-term water loss is due to a decline in GWS. To estimate the time series of groundwater changes using the GRACE data and its necessary corrections, a software package was developed. We have estimated total water storage trends for the whole of Iran inferred from GRACE data -20.49± 1 (GT/yr). Total water storage trends for the largest basin of Iran (central plateau basin) are -7.0 ± 4 (GT/yr).

The other part of this thesis deals with groundwater changes estimation from observation wells data. There are 17,865 active observation wells in the whole of Iran. In order to study well level time series, Iran is divided into six main basins. These six main water basins have 32 sub-basins. Each sub-basin is divided into several study areas too. The Thiessen polygon method has been used to make a time series of the groundwater level across each study area. The total changes in GWS across each sub-basin is computed by adding together the scaled change in GWS of all its study areas. The same procedure is carried out for each main water basin.

By estimating secular trend groundwater storage changes in Iran during 2002–2017, we see that there is an intensive negative trend, even -4,400 Million cubic meter (Mm^3) in some areas. The largest contributions to water consumption in Iran belong to the agriculture section. These estimations show changing in climate and extra extraction from aquifers for agriculture use in some areas in Iran.

The secular trend of groundwater storage changes in the whole of Iran inferred from observation well data is -20.08 GT/yr, and inferred from GRACE data is -20.49 GT/yr. These two trends agree to a good extent. Groundwater changes estimations for each main water basin as a mascon, inferred from GRACE data and observation well data, agree to a good extent.

Acknowledgements

My first appreciation goes to my supervisor Prof. Hossein Nahavandchi for his support, trust and confidence in my abilities to do this PhD research. He has always supported my ideas and provided me with encouragement and guidance in the writing of this thesis. I would also like to appreciate my co-supervisor Dr. Mahdi Motagh who offered me guidance and support in the beginning of this work.

This thesis would not have been possible without the constant support, guidance, and assistance of Dr. Gholamreza Joodaki. His level of patience, knowledge, and ingenuity is something I will always keep aspiring to. Thank you so much Reza!

Many thanks to all of the members of staff in the division of Geomatics at Norwegian University of Science and Technology (NTNU) for their kind support during my PhD study.

Away from work, my deepest thanks must go to my parents for love and inspiration throughout my life.

Last but not the least; my heartfelt gratitude goes to the two loves of my life, my husband and my daughter, Taranom for their love, patience and encouragement all the way through my PhD journey.

This page is intentionally left blank

Table of Contents

	Abstract	i
	Acknowledgments	iii
	Table of Contents	v
	List of Figures	viii
	List of Tables	xiv
1	**Introduction**	1
1.1	Motivation	1
1.2	Background	2
1.3	Case study: Ground water depletion in Iran	8
1.4	Literature Review:	11
1.5	Scientific objectives	12
1.6	Structure of Thesis	13
2	**Groundwater storage changes estimation using well data**	15
2.1	Well data observations	16
2.2	Water basins or drainage basins in Iran	19
2.3	The Caspian Sea catchment	20
2.3.1	The climate and weather system	22
2.3.2	Vegetation	23
2.4	The Persian gulf and the gulf of Oman catchment	23
2.4.1	The climate and weather system	25
2.4.2	Vegetation	26
2.5	Urmia Lake catchment	28
2.6	Central Plateau catchment	30

2.7	Eastern Boundary catchment	33
2.8	Ghareghom catchment	36
3	**Groundwater storage changes estimation using satellite data**	39
3.1	The Earth's Gravity field:	39
3.2	Time-variable gravity	40
3.3	GRACE	42
3.3.1	GRACE data Levels	46
3.3.2	The end of GRACE	48
3.3.3	GRACE Follow-On	48
3.4	Earth's Mass Change Estimation	49
3.5	Estimation of the Earth's mass changing by using GRACE level-2 data	52
3.6	GRACE DATA decorrelation methods	54
3.6.1	Gaussian isotropic smoothing	55
3.6.2	Terms with n=0, 1	56
3.6.3	Terms with n=2 and m=0	57
3.7	Glacial Isostatic Adjustment (GIA)	57
3.8	Spatial averaging	58
3.9.	Least Squares Mascon fitting	60
3.10	Estimating groundwater storage using the GRACE Data	64
3.10.1	Hydrological land surface models (LSMs)	65
3.10.2	Global Land Data Assimilation System	66
4	**Numerical Investigations**	67
4.1.	Groundwater level changes monitoring based on the well data	67
4.1.1	The Central plateau basin (code 4)	70
4.1.2	The Caspian Sea basin (code 1)	76
4.1.3	The Eastern boundary basin (Code 5)	81
4.1.4	The Ghareghom basin (code 6)	84
4.1.5	The Persian Gulf basin and Oman Sea basin (code 2)	86
4.1.6	The Urmia basin (code 3)	92
4.2	Spatial dependence of total water storage	93

4.3	Total water storage inferred from GRACE least squares mascon solution	95
4.3.1	The Persian Gulf and Oman basin	98
4.3.2	The Caspian sea basin	100
4.3.3	The Urmia Lake basin	101
4.3.4	The Central Plateau basin	102
4.3.5	The Eastern Boundary basin	103
4.3.6	The Ghareghom basin	104
4.4	Total water storage inferred from the GRACE Follow-On (FO) least squares mascon solution	105
4.4.1	The Persian Gulf and Oman Sea basin	105
4.4.2	The Caspian Sea basin	106
4.4.3	The Urmia Lake basin	106
4.4.4	The Central Plateau basin	107
4.4.5	The Eastern Boundary basin	107
4.4.6	The Ghareghom basin	108
4.5	Groundwater trends for different water basins in Iran and their uncertainties	108
5	**Conclusion and Remarks**	111
6	**References**	115
7	**Appendix A**	141
8	**Appendix B**	143
9	**Appendix C**	233
10	**Appendix D**	253
11	**Appendix E**	263
12	**Appendix F**	269
13	**Appendix G**	345

List of Figures

2.1	Figure 2.1. Construction of Thiessen polygon.	17
2.2	Iran's main water basins.	20
2.3	The Caspian Sea cachment.	21
2.4	The Persian Gulf and Oman Sea catchment.	24
2.5	The Persian Gulf and Oman Sea.	27
2.6	The Urmia catchment.	28
2.7	The Urmia Lake.	29
2.8	The Central plateau catchment.	33
2.9	The Eastern boundary catchment.	36
2.10	The Ghareghom catchment.	37
3.1	Gravity Recovery and Climate Experiment (GRACE) mission.	44
3.2	The 2002-2011 secular trend map (mm/year) over the world using JPL GRACE level 2 data release 4.0.	53
3.3	Effects of GIA of the lithosphere and mantle.	58
4.1	Secular trend in Million cubic meter ($Mm^3/year$) groundwater storage across Iran, computed from water level inferred from observation wells in 32 sub-basins in Iran, during 2002–2017.	68
4.2	a) Monthly values of groundwater storage, b) long-period of monthly values of groundwater storage, c) short-period of monthly values of groundwater storage across Central plateau basin (code 4).	70
4.3	a) Monthly values of groundwater storage, b) long-period of monthly values of groundwater storage, c) short-period of monthly values of groundwater storage across Daryache Namak (code 41).	71

4.4 a) Monthly values of groundwater storage, b) long-period of monthly values of groundwater storage, c) short-period of monthly values of groundwater storage across Gav Khooni (code 42). 72

4.5 a) Monthly values of groundwater storage, b) long-period of monthly values of groundwater storage, c) short-period of monthly values of groundwater storage across Tashtak-Bakhtegan (code 43). 73

4.6 a) Monthly values of groundwater storage, b) long-period of monthly values of groundwater storage, c) short-period of monthly values of groundwater storage across Abarghoo-Sirjan (code 44). 73

4.7 a) Monthly values of groundwater storage, b) long-period of monthly values of groundwater storage, c) short-period of monthly values of groundwater storage across Hamoon Jazmoorian (code 45). 74

4.8 a) Monthly values of groundwater storage, b) long-period of monthly values of groundwater storage, c) short-period of monthly values of groundwater storage across Kavir Loot (Code: 46). 74

4.9 a) Monthly values of groundwater storage, b) long-period of monthly values of groundwater storage, c) short-period of monthly values of groundwater storage across Kavir Markazi (Code: 47). 75

4.10 a) Monthly values of groundwater storage, b) long-period of monthly values of groundwater storage, c) short-period of monthly values of groundwater storage across Kavir Siah Kooh (Code: 48). 75

4.11 a) Monthly values of groundwater storage, b) long-period of monthly values of groundwater storage, c) short-period of monthly values of groundwater storage across Kavir Daranjir-Saghand (Code: 49). 76

4.12 a) Monthly values of groundwater storage, b) long-period of monthly values of groundwater storage, c) short-period of monthly values of groundwater storage across Caspian Sea basin (code 1). 77

4.13 a) Monthly values of groundwater storage, b) long-period of monthly values of groundwater storage, c) short-period of monthly values of groundwater storage across Aras (code 11). 78

4.14	a) Monthly values of groundwater storage, b) long-period of monthly values of groundwater storage, c) short-period of monthly values of groundwater storage across Talesh (code 12).	78
4.15	a) Monthly values of groundwater storage, b) long-period of monthly values of groundwater storage, c) short-period of monthly values of groundwater storage across Sefidrood Bozorg (code 13).	79
4.16	a) Monthly values of groundwater storage, b) long-period of monthly values of groundwater storage, c) short-period of monthly values of groundwater storage across Sefidrood Bozorg (code 14).	79
4.17	a) Monthly values of groundwater storage, b) long-period of monthly values of groundwater storage, c) short-period of monthly values of groundwater storage across study area of Gharasoo-haraz (code 15).	80
4.18	a) Monthly values of groundwater storage, b) long-period of monthly values of groundwater storage, c) short-period of monthly values of groundwater storage across Gharesoo-Gorganrood (code 16).	81
4.19	a) Monthly values of groundwater storage, b) long-period of monthly values of groundwater storage, c) short-period of monthly values of groundwater storage across Atrak (Code: 17).	81
4.20	a) Monthly values of groundwater storage, b) long-period of monthly values of groundwater storage, c) short-period of monthly values of groundwater storage across Eastern boundary basin (5).	82
4.21	a) Monthly values of groundwater storage, b) long-period of monthly values of groundwater storage, c) short-period of monthly values of groundwater storage across Deghe Petergan-Namakzar Khaf (code 51).	83
4.22	a) Monthly values of groundwater storage, b) long-period of monthly values of groundwater storage, c) short-period of monthly values of groundwater storage across Deghe Petergan-Namakzar Khaf (code 52).	84
4.23	a) Monthly values of groundwater storage, b) long-period of monthly values of groundwater storage, c) short-period of monthly values of groundwater storage across Hamoon Mashkil (code 53).	84

4.24 a) Monthly values of groundwater storage, b) long-period of monthly values of groundwater storage, c) short-period of monthly values of groundwater storage across Ghareghom basin (code 6). 85

4.25 a) Monthly values of groundwater storage, b) long-period of monthly values of groundwater storage, c) short-period of monthly values of groundwater storage across Persian Gulf Basin (Code: 2). 86

4.26 a) Monthly values of groundwater storage, b) long-period of monthly values of groundwater storage, c) short-period of monthly values of groundwater storage across Marzi Gharb (code 21). 87

4.27 a) Monthly values of groundwater storage, b) long-period of monthly values of groundwater storage, c) short-period of monthly values of groundwater storage across Roodkhane Karkhe (code 22). 88

4.28 a) Monthly values of groundwater storage, b) long-period of monthly values of groundwater storage, c) short-period of monthly values of groundwater storage across Karoon Bozorg (code 23). 89

4.29 a) Monthly values of groundwater storage, b) long-period of monthly values of groundwater storage, c) short-period of monthly values of groundwater storage across Jarahi (code 24). 89

4.30 a) Monthly values of groundwater storage, b) long-period of monthly values of groundwater storage, c) short-period of monthly values of groundwater storage across Hele (code 25). 90

4.31 a) Monthly values of groundwater storage, b) long-period of monthly values of groundwater storage, c) short-period of monthly values of groundwater storage across Mand (code 26). 90

4.32 a) Monthly values of groundwater storage, b) long-period of monthly values of groundwater storage, c) short-period of monthly values of groundwater storage across Kalmehran (code 27). 91

4.33 a) Monthly values of groundwater storage, b) long-period of monthly values of groundwater storage, c) short-period of monthly values of groundwater storage across Bandar Abbas (code 28). 91

4.34	a) Monthly values of groundwater storage, b) long-period of monthly values of groundwater storage, c) short-period of monthly values of groundwater storage across Baluchestan Junubi (code 29).	92
4.35	a) Monthly values of groundwater storage, b) long-period of monthly values of groundwater storage, c) short-period of monthly values of groundwater storage across Urmieh basin (code 3).	93
4.36	GRACE-derived secular trend of total water storage across Iran in cm/yr. From 2002 to 2016. CSR monthly solution and a corresponding radius of 300 km.	94
4.37	Sensitivity kernel for the central plateau mascon.	96
4.38	a) Monthly values of groundwater storage, b) long-period of monthly values of groundwater storage, c) short-period of monthly values of groundwater storage, d) long-period of monthly values of groundwater storage, inferred from well data and GRACE data, across Persian Gulf and Oman Sea basin (code2).	99
4.39	a) Monthly values of groundwater storage, b) long-period of monthly values of groundwater storage, c) short-period of monthly values of groundwater storage, d) long-period of monthly values of groundwater storage, inferred from well data and GRACE data, across Caspian Sea basin (code1).	100
4.40	a) Monthly values of groundwater storage, b) long-period of monthly values of groundwater storage, c) short-period of monthly values of groundwater storage, d) long-period of monthly values of groundwater storage, inferred from well data and GRACE data, across Urmieh Lake basin (code 3).	101
4.41	a) Monthly values of groundwater storage, b) long-period of monthly values of groundwater storage, c) short-period of monthly values of groundwater storage, d) long-period of monthly values of groundwater storage, inferred from well data and GRACE data, across Central Plateau basin (code 4).	102

4.42	a) Monthly values of groundwater storage, b) long-period of monthly values of groundwater storage, c) short-period of monthly values of groundwater storage, d) long-period of monthly values of groundwater storage, inferred from well data and GRACE data, across Eastern Boundary basin (code 5).	103
4.43	a) Monthly values of groundwater storage, b) long-period of monthly values of groundwater storage, c) short-period of monthly values of groundwater storage, d) long-period of monthly values of groundwater storage, inferred from well data and GRACE data, across Ghareghom basin (code 6).	104
4.44	Monthly values of groundwater storage, inferred from data and GRACE data and GRACE Follow on data, across Persian Gulf and Oman Sea basin (code 2).	105
4.45	Monthly values of groundwater storage, inferred from data and GRACE data and GRACE Follow on data, across Caspian Sea basin (code 1).	106
4.46	Monthly values of groundwater storage, inferred from data and GRACE data and GRACE Follow on data, across, Urmieh Lake basin (code 3).	106
4.47	Monthly values of groundwater storage, inferred from data and GRACE data and GRACE Follow on data, across Central Plateau basin (code 4).	107
4.48	Monthly values of groundwater storage, inferred from data and GRACE data and GRACE Follow on data, across Eastern Boundary basin (code 5).	107
4.49	Monthly values of groundwater storage, inferred from data and GRACE data and GRACE Follow on data, across Ghareghom basin (code 6).	108

List of Tables

1.1.	Groundwater use by country; FAO, AQUASTAT	6
2.1.	Sub basins of the Caspian Sea catchment.	22
2.2.	Sub basins of the Persian gulf and the gulf of Oman Sea catchment	27
2.3.	Sub basins of the central plateau chatchment.	32
2.4.	Sub basins of the Eastern boundary catchment.	36
2.5.	Sub basins of the Ghareghom catchment	37
4.1.	Secular trends, in Gt/yr, of the total groundwater storage (GRACE-minus- GLDAS/NOAH) for Iran, for 2002-2017. Results are compared with estimates based on well data.	109

Chapter 1

Introduction

The main goal of this Ph.D. is study of the feasibility of using the Gravity Recovery and Climate Experiment (GRACE) satellite to monitor groundwater storage (GWS) changes at the scale of Iran's six main water basins. Using in situ data and the GRACE mission helps us to compare these two sets of data. We developed the GRACE least squares mascon solution (mass concentrated) method for specific regions of Iran, chosen largely to coincide with main water basin. The Iran water resources management company has collected a large number of observation wells data for 40 years that are used in different hydrological studies. To the best of our knowledge, there has been no study to date about groundwater depletion in the whole of Iran. Study of groundwater changes by the two above-mentioned methods demonstrates the application of using GRACE as a fast and reliable form of estimating regionally integrated changes in GWS in Iran.

1.1. Motivation

In recent years, the public concern about future of the Earth, its climate, its environment and shortage of its natural resources has been more pressing than ever before. Among different resources, water is the most vital. Because of the properties of groundwater, it has the most important contribution. Management of the sustainability of groundwater is essential in arid and semi-arid areas like most of the regions in Iran. Feasible methods of GWS changes estimation are the most important requirement of an appropriate management of water resources. Satellite gravity missions such as GRACE and GRACE

Follow-On are powerful tools for groundwater monitoring. This thesis demonstrates the feasibility of GRACE temporal gravity data as a fast and reliable form of estimating regionally integrated changes in GWS in Iran. The Iran Water resources Management Company have used collected well data for different hydrological purposes. As far as we are aware, these data have not been used for large-scale water-level monitoring. Analysis of these data in order to estimate GWS changes and comparison with GRACE results will show the GRACE mission's ability to monitor groundwater depletion as an alternative quantitative tool for monitoring GWS changes when in situ measurements are limited or unavailable.

1.2. Background

Water is an essential resource for life on the Earth. Nearly 70% of the Earth's surface is covered with water. Typically, fresh water is defined as water with a salinity of less than 1% that of the oceans (oceans have average salinity of 3.5%). Around 2.8% of all water on the Earth is fresh water. There is 76.8% of fresh water as ice in the Earth's polar glaciers, 22.5% of it is groundwater, and the rest is surface water such as rivers, streams, and lakes (Sultan et al. 2012).

Groundwater is one of the nation's most important natural resources. It constitutes about two-thirds of the freshwater reserves of the world (Chilton 1992, Buchanan 1983). Groundwater globally supplies about 50% of drinking water needs, 40% of the needs of self-supplied industry, and 20% of the demand for irrigation water (Zektser and Lorne 2004, United Nations (UN) report). There are some important reasons to focus on using groundwater all over the world: There is no easy access to rivers, lakes, and streams everywhere, but groundwater is distributed haphazardly in space and time, and there is easy access to pumped wells almost everywhere. Deep beneath the ground, groundwater is unseen, isolated from temperature changes, and protected from evaporation and pollution, which satisfies World Health Organization (WHO) drinking water quality standards (Olumuyiwa et al. 2012). Groundwater serves as a natural storage that is a substitute for surface reservoirs in the dry season as well (Morris et al. 2003).

Nowadays, increase in demand in developing countries results in groundwater depletion (Giordano 2009, Foster and Chilton 2003, and Foster et al. 1997). Groundwater levels in many countries are falling at extraordinary rates, even, in some cases, more than one meter per year. Therefore, we will face different problems; for example, permanent rivers and streams whose base flow was supplied by groundwater are becoming seasonal or have disappeared, and wetlands are drying up or have become shallower. In some areas, use of groundwater for irrigation has become impossible or expensive (Dennehy et al. 2002).

Groundwater depletion can allow salt-water intrusion and increase the risk of contamination of groundwater. The depletion can change the linkages between ground- and surface-water systems (Bergkamp and Cross 2007). It can also reduce soil moisture levels, harmfully changing the composition of natural vegetation and crops, so in this way it contributes to climate change itself. Cities are becoming dependent on groundwater, and the replenishment of groundwater is no longer possible with the amount that it is being consumed (Liamas and Martınez-Santos 2005). Nearly half the world's population depend on groundwater as their primary source of drinking water (Morris et al. 2003).

On the other hand, we face the impacts of droughts that can last for months or even years. Due to global warming, extreme precipitation and temperature events occur much more frequently in most arid and semi-arid regions (Mulinde et al. 2016, Jackson et al. 2001). GWS experiences more stress during these periods. Surface water supplies have been more polluted and lead to more use of clean groundwater instead (Morris et al. 2003, Castle et al. 2014).

Since the dawn of time, wherever humans lived together, water was the important resource to share. There is a complex relationship between water, man and territory. Water is a potential source of conflicts, where aquifers are internationally shared, for example the struggle over aquifer sharing between Israel and the Palestinian territories (Eckstein 2005; Feitelson 2006). Although globally management of transboundary waters has been studied, little discussion has focused on groundwater (Wolf 2007, Puri et al. 2001, Struckmeier et al. 2006, Matsumoto 2009).

Groundwater depletion has also changed properties of aquifers, and drawdown results in permanent compaction that causes reduced ability to retain water in layers of ground in

the future (Foster et al. 2000). The depletion can change the linkages between ground- and surface-water systems (Bergkamp and Cross 2007) and reduce soil moisture levels, harmfully changing the natural composition of aquifers. Groundwater exploitation can change the water level and cause it to decline severely, even up to 40 m. The geological structure naturally has cavities that can hold groundwater. If low-permeability layers limit the ability of the aquifer to retain water, the reduced water pressure in the sand and gravel causes slow drainage of water from layers. Extraction of a large amount of water in a short time can cause subsidence and fracture in the geological structures. Subsidence causes permanent inundation of land, flooding, changes topographic gradients, ruptures the land surface, and reduces the capacity of aquifers to store water (Devin et al. 2011, Olumuyiwa et al. 2012). Subsidence is common in semi-arid and arid climates. Over 150 major cities worldwide have experienced subsidence (Hu et al. 2004, Taylor and Alley 2001).

It has been accepted by the international community that the very first stage in water management is to collect data and knowledge about water resources. This is not a simple affair, despite the power of modern tools and techniques for observation, measurement, data processing, and modeling. Therefore, there is no universal "ready-made" solutions to these issues (Blomquist and Ingram 2003, Jarvis 2006). The Food and Agriculture Organization (FAO) noted that they had not spent much time on groundwater problems, and only in recent years has a global view with involvement of the UN has been taken. The World Water Resources (Shiklomanov 1998) and the FAO's AQUASTAT database[1] are examples. The data of the Worldwide Hydrogeological Mapping and Assessment Programme (WHYMAP), maps of major recharge areas,[2] is another example. Finally, a complementary set of works has separated global patterns from local evidences, such as analyses of agricultural use (Giordano and Villholth 2007, Shah et al. 2007), urban use (Zektse and Everett 2004), and degradation (Foster and Chilton 2003). These cases lack regionally sufficient monitoring networks because of the high cost of monitoring' and lack of regular collection standards across and within countries. AQUASTAT have assembled data at national scales, which can be used to develop internally consistent

[1] http://www. fao.org/nr/water/aquastat/main/index.stm
[2] http://www.whymap.org

figures on global groundwater use. Despite their best work at collecting data, the quality and timelines of data vary considerably by country (Elissason et al. 2003). Recent rapid changes in groundwater use in some regions, especially in Asia, may result in significant changes in reporting, including under reporting. Having these limitations, we have scarcity and uncertainty in groundwater data (Seckler et al. 1999, Tsur 1990).

Despite major groundwater use, global demand is still only 600–700 km^3 about 6% of the estimated water resources. Nevertheless, moving from global to regional scales, there are different regions where extraction of groundwater is more than an annual recharge (Briscoe 1999). Table (1.1) shows the main groundwater-using countries. Just the top five countries account for nearly 80% of total use. The top 10 account for nearly 90%. The main groundwater-consuming countries are limited to specific areas across North Africa and the Middle East (Singh and Singh 2002, Allan 2007). In general, the magnitude of depletion has hardly been measured and is poorly documented. The most direct way to estimate the volume of water depleted from an aquifer is to integrate maps of head changes over the aquifer area. The resulting aquifer volume is multiplied by an appropriate storage coefficient to compute the corresponding volume of water (McGuire et al. 2003). Hydrologists believe most aquifer systems that are monitored have sparse observation networks, discontinuities in data collection leading to data gaps, and limited official data-sharing policies reducing access to essential observational data (Famiglietti et al. 2011, UNECA 2011, Jacobsen et al. 2012).

In order to manage the limited groundwater resources in a way that will ensure reasonable, sustainable, and economically wise decisions, we must improve our existing capability to monitor and predict groundwater availability. Consequently, a better monitoring system is critical to understanding proper management of these resources in developing and developed countries. Although in situ monitoring networks provide high-resolution estimates, in many parts of the world, data is complicated by sparsely distributed and spatially inconsistent monitoring wells, by temporal data gaps, and limitation in access to data by political boundaries. In particular, analysis of groundwater variability requires continuous time series data (Pavelic et al. 2012, Giordano 2009, Sophocleous 2010, Scanlon et al. 2012, Robins et al. 2006).

Table 1.1. Groundwater use by country: FAO, AQUASTAT

Country	Total groundwater withdrawals (km3)	Total renewable groundwater resources (km3)	Percent of withdrawals to total renewable groundwater resources	Percent of national share of global withdrawals
India	190	419	45.3	28.9
United States	110	1,300	8.5	16.7
Pakistan	60	55	109.1	9.1
China	53	828	6.4	8.1
Iran	53	49	108.2	8.1
Mexico	25	139	18.0	3.8
Saudi Arabia	21	2.2	954.5	3.2
Italy	14	43	32.6	2.1
Japan	14	27	51.9	2.1
Bangladesh	11	21	52.4	1.7
Brazil	8	1,874	0.4	1.2
Turkey	8	68	11.8	1.2
Uzbekistan	7	9	77.8	1.1
Germany	7	46	15.2	1.1
Egypt	7	2	350.0	1.1
France	6	100	6.0	0.9
Spain	5	30	16.7	0.8
Bulgaria	5	6	83.3	0.8
Argentina	5	128	3.9	0.8
Libya	4	0.5	800.0	0.6
Rest of the world	76	6,135	1.2	11.6
Total	658	11,282	5.8	100.0

The geophysical gravity method offers a means to estimate changes in subsurface water storage directly by measuring changes in the Earth's gravitational field (Pool et al. 2000, Hoffmann 2004). This method was applied to the Tucson Basin in southern Arizona, USA, for the period 1989–1998 (Konikow and Kendy 2005). Recently, remote sensing has been shown to greatly improve estimates of groundwater depletion. Sequential gravity

surveys may be conducted from satellites to measure changes in GWS professionally over large regions. This technique has the potential to offer near real-time monitoring and assessment of subsurface hydrologic changes. Therefore, remotely sensed data set-up the only source of information for assessing water resources in sparsely monitored regions (Alsdorf et al. 2007). The GRACE satellite mission has attracted much attention since its launch. Satellite observations of time-variable gravity from the GRACE mission measure variations in the Earth's gravity field that reveal mass redistributions. It presents a new and valuable tool to fill the gaps in data availability to monitor water changes (Tapley et al. 2004, Scanlon 2012a). Covering globe, GRACE provides an excellent tool for mapping the gravity field across the world. GRACE maps the static and temporal gravity variations of the Earth's gravity field to a scale of couple of hundred kilometers and with a time interval of about one month. Changes in the gravity field are caused by the redistribution of mass within and on or above the Earth's surface. The great contribution of the change is related to water mass transport (Joodaki and Nahavandchi 2010+ more references). Over land, temporal variations in the gravity field are mainly due to terrestrial water storage changes; GRACE provides a record of variations in total terrestrial water storage across the globe. The GRACE data have been used by many researchers to study changes in land water storage, ocean mass, and changes in land-locked ice, including glaciers. The main advantages of satellite time-variable gravity measurements are that they are sensitive to large bodies like water basins, and that they provide mass estimates with only minimal use of supporting physical assumptions or additional data. The GRACE mission presents a new opportunity to monitor large-scale GWS changes, after removing atmospheric and oceanic effects (Tapley et al. 2004, Rodell and Famiglietti, 1999, Wahr et al. 2004, Ramillien et al. 2004, Syed et al. 2008). TWS is the vertically integrated measure of groundwater, soil moisture, snow, ice, and surface water. To isolate GWS from total TWS, other components must be estimated from models or observations (Yeh et al. 2006, Rodell et al. 2007, Ramillien et al. 2008, Zaitchik et al. 2008). GRACE is a powerful tool in water storage monitoring.

1.3. Case study: Groundwater depletion in Iran

Drought and water shortage in the Middle Eastern countries can lead to economic and consequently political instability. Particularly groundwater declines affect transboundary regions, and the high frequency of conflict is due to disputes over groundwater (Amery and Wolf 2000, Wolf and Newton 2007, Wolf 1998). The recent drought in the Middle East that began in 2007 has further stressed the limited water resources in the region (Integrated Regional Information Networks, 2010; U.S. Department of Agriculture (USDA) 2008). In this area, wetland ecosystems were destroyed, and thousands of farmers migrated to urban centers and cities in search of employment, which caused secondary problems in those cities (Michel et al. 2012, Sullivan 2010). Because of frequent drought and also population growth, the countries in this region experience different problems. In this regard, Iran is one of the most vulnerable countries. Annual precipitation in Iran is 273 millimeters, less than one-third of the world's mean annual precipitation. Iran has been facing water stress, and it is on the fast track to severe water scarcity (see e.g. Mahdavi 2004). One method used to overcome water scarcity in Iran was through underground water and water delivery called qanat. Qanat is traditional sustainable groundwater withdrawal. By using this method, we had access to water any time and everywhere it was needed. In Iran, groundwater resources were sustainable before the importation of motor pumps and construction of large dams. Nowadays, most Qantas have dried up, losing the hydraulic head battle to deep wells (Madani 2014). In 1999, severe drought in Iran began a period of unusually dry conditions, which is still ongoing and likely to continue for the near future (Karami and Hayati 2005). Iran is experiencing significant water challenges that have turned water security into a national priority now. The temporal and spatial distribution of rainfall is not uniform; about 75% of the nation's precipitation falls in a small area on the southern coast of the Caspian Sea, while the rest of the country receives insufficient precipitation. Only 25% of the precipitation falls during plant growth season (Jamab 1998, Mahdavi 2004). In addition, because of the relatively high temperature, evaporation is intensive, and about half of the annual precipitations evaporate, so there are few permanent streams in Iran. Recent estimates indicate that the rate of precipitation has reached its lowest point in more than 40 years. The average surface run-off in this period is 42% less than the long-term

average. All of these factors make people inclined to use more groundwater in Iran. Therefore, groundwater management has become a high-priority matter (Brown 2007, Moridi 2017).

According to the Falkenmark water stress index, countries with per capita renewable water less than 1,700 cubic meters per year are subject to water stress. Therefore, Iran with per capita renewable water equal to 1560 m^3 is under water stress. Besides, 80% of the renewable water in Iran is used by different sectors (Moridi 2017). The Iranian agricultural sector uses over 92% of all water resources and wastes about 70% of this water due to evaporation and lack of well-organized irrigation systems. Although Iranian agricultural production has greatly risen during the past 30 years, its total contribution to the national Gross Domestic Product (GDP) has declined.

Population growth and inappropriate spatial population distribution has caused the 20 most populous Iranian cities currently to experience a medium to extremely high overall water risk, some of which also experience severe land subsidence, forced migration, agricultural losses, salt and sand storms, and frequent occurrences of floods and severe water stress on Iran's wetlands (Madani 2014). The drying wetlands are one of the sources of dust propagation, which affect people's health. It has also increased the desertification and salinization of land (Sinéad 2014, Mahmoudpour 2016). Based on satellite data, about 529 dust storms were identified in the western part of Iran during the period of 2001 to 2011. NASA's satellite Total Ozone Mapping Spectrometer (TOMS) was used to examine sources of dust propagation in Iran for the period 1979–2004, and simultaneously 150 synoptical weather stations showed that the dominant sources of mineral dust are mainly located in the dry lakes of internal drainage (Esmaili et al. 2006, Moridi 2017).

There are many illegal wells in aquifers in Iran, so there is no control over the withdrawals of water there. In addition, rapidly growing demand for crops has put pressure on authorities to give permission to dig new wells. This has caused a reduction in groundwater tables in aquifers, which in turn has resulted in reductions in discharges of wells. Owners of wells have then tried to increase the wells' depths or relocate wells to

improve their water withdrawal efficiency. The number of wells has dramatically increased in the past decade in Iran.

All these above-mentioned issues witness to the importance of appropriate water management. Access to accurate water-level data and update time series is vital. In addition, better water-level monitoring, and better assessment and forecasting of water resources, would help government agencies allocate water more efficiently among competing needs (Jackson et al. 2001). Groundwater withdrawal statistics are often outdated and measured by inconsistent methods between geopolitical boundaries (Shiklomanov and Penkova 2003, Alley 2006). The acquisition of accurate data represents a major challenge. The spatial and temporal variability of groundwater data ought to be good enough for a proper water management studies. However, availability of time series of parameters of GWS is limited and uncertain everywhere (Shah et al. 2000).

We have good groundwater data records in Iran; a lot of data exists, but they are not well organized, and a huge part of this study was to collect all these data and bring them in a database to finally calculate the GWS changes from well data. Despite its importance, there have been few water basin-wide hydrological studies using GWS observational data in Iran. The GRACE mission can provide a record of variations in GWS across water basins. The main advantages of satellite time-variable gravity measurements are that they are sensitive to large bodies like water basins, and they can provide mass estimates with only minimal use of supporting physical assumptions or additional data. GRACE has presented opportunities to monitor large-scale GWS changes, after removing hydrological effects and other proper corrections.

We acknowledge the large degree of uncertainty associated with GRACE at small scales, but we test the use of GRACE by developing a mascon-based technique in these smaller areas (water basins) as an alternative tool to the in-situ existing well data network. This study investigates the application of the GRACE mission as a fast and reliable form of estimating regionally integrated changes in GWS in Iran. We will show the efficiency of the developed method despite smaller areas in some of the basins when compared to the

GRACE footprint, by comparison the GRACE results with in-situ well data in the six water basins across Iran.

1.4. Literature review

Many researchers have used GWS data in order to estimate groundwater depletion, for instance Rodell and Famiglietti (2002), Ramillien et al. (2005), Lettenmaier and Famiglietti (2006), Yeh and Famiglietti (2007), Yamamoto and Taniguchi (2008), Tiwari et al. (2009), Moore and Fisher (2010), Wang et al. (2011), Famiglietti et al. (2011b), Swenson and Famiglietti (2012), Voss et al. (2013), Ahmed (2014), Ouma et al. (2015), Huang et al. (2016), Gemitzi and Lakshmi (2017), and Gong et al. (2018).

Despite, Iran being one of the areas of water reservoir scarcity, few researchers have estimated groundwater depletion in Iran. However Forootan (2014), for instance, studied signal-noise separation problem and the 'signal-signal' separation problem for GRACE data. Voss et al. (2013) and Darama (2014) estimated groundwater depletion in the Middle East from GRACE data with implications for transboundary water management in the Tigris–Euphrates–Western Iran region. Khaki et al. (2018) estimated water storage depletion within Iran by assimilating GRACE data into the W3RA hydrological model. The above-mentioned studies are, somehow, standard methods of using GRACE observations for GWS change estimation with different proper correction terms in each study.

Least squares mascon fitting is a useful method for estimation of groundwater depletion. Joodaki et al. (2013) used the least squares mascon technique to estimate total water storage centered over western Iran and eastern Iraq. They divided a big study area into seven mascons outlined along national boundaries: Iran, Iraq, Syria, eastern Turkey, northern Saudi Arabia, southern Saudi Arabia, and the area immediately west of the Caspian Sea. They showed that the largest groundwater depletion is occurring in Iran, with a mass loss rate of 25±6 Gt/yr during the study period. The conclusion of significant Iranian groundwater loss is further supported by in-situ well data from across the country. Joodaki et al. (2013) used GRACE observations and the mascon technique in a large region. GRACE data at large scales work effectively. The challenging part of this study

is to use the GRACE data at smaller scales in Iran only dividing it into six different mascons.

1.5. Scientific objectives

One objective of this study is to collect, assess, and evaluate all observation well data, producing a nationwide database, and allocating those data across water basins in Iran, to constitute time series of groundwater data for final estimation of GWS changes using in-situ hydrological data. The second objective of this study is to estimate GWS changes across Iran water basins by using GRACE data, proper corrections, and a mathematical tool named least squares mascon technique developed in this study to fit mass amplitudes for each of six mascons simultaneously to the monthly GRACE data. We obtain monthly times series of mass variability for each of the six water basins in Iran during 2003–2018. Each basin is a unit of hydrological studies. We used 163 months of GRACE data (April 2002 to July 2017) and 15 months of GRACE FO data (Jun 2018 to September 2019) to examine the water storage trend in the six water basins in Iran. The developed mascon solutions for GRACE data have significantly increased the spatial localization and amplitude of recovered terrestrial Total Water Storage Anomalies (TWSA).

We took every water basin as a mascon, which are our study units. These water basins are separated by natural topography as their boundaries. In order to examine this method, well data in every water basin has been collected, assessed, and evaluated. Using observation wells data available in Iran, water-table time series are estimated.

We compare GRACE least squares mascon results with estimates obtained from time series of water level in 17,865 active observation wells. We also use these well data to monitor the level of groundwater across the country. The Iran Water Resources Management Company collects the well observations.

GRACE data have other applications such as estimating rates of groundwater depletion by estimating flood potential (Reager and Famiglietti 2009), drought (Andersen et al. 2005, Yirdaw et al. 2008, Leblanc et al. 2009, Agboma et al. 2009, Chen et al. 2010), and reservoir storage changes (Swenson and Wahr 2009, Wang et al. 2011). These different

applications demonstrate the potential of the GRACE mission for the management of water resources at the regional scales.

1.6. Structure of thesis

In chapter 1, the necessity of groundwater management and issues related to nationwide water-level monitoring have been discussed. The severe water-level decline in Iran has been deliberated. The advantage of using satellite gravity solutions, GRACE, for groundwater depletion monitoring has been presented. The motivation and scientific objectives of the thesis has also been discussed. Chapter 2 is devoted to the climate properties and geography of the main water basins in Iran. The mathematical formulations for GWS changes estimation using well hydrological data are presented. In chapter 3, Earth mass change estimation using satellite gravity missions is described. The GRACE gravity mission is presented, and formulas for mass change estimations and proper correction terms are given. The least squares mascon method, developed in this study, is defined in detail. Estimations of TWS and GWS using GRACE data are described. In chapter 4, numerical investigations and results are presented. The GWS changes inferred from well data for the main basins and sub-basins are illustrated. Total water storage for basins inferred from GRACE and GRACE FO data are demonstrated. In chapter 5, conclusions and remarks are presented. In Appendices A-G, the GWS changes inferred from well data for all study areas are illustrated.

This page is intentionally left blank.

Chapter 2

Groundwater Storage Changes Estimation Using Well Data

In this chapter, the method of estimation of groundwater changes using observation well data in Iran is described. And the geographic properties of the main water basins are explained.

Iran is located between 44° 02′-63° 20′ E and 25°03′ to 39° 46′ N. Its total area is about 1,648 million km^2. Iran is located in a high-altitude plateau surrounded by connected ranges of mountains (Road Atlas of Iran 2004). About 16% of the country has an elevation of more than 2,000 m above sea level. The elevation at the Caspian Sea coast is 25 m below the mean sea level, and Mount Damavand stands at 5,610 m (Jafari 2005, Darehshouri and Kasraian 1998). The largest mountain range is the Zagros, with 1,400-km length and 533,512-km^2 area, which ranges from the northwest to the south then continues southeast. There is another mountain chain in the north of Iran along the southern edge of the Caspian Sea called the Alborz Mountains, with an area of 51,500 km^2. Its length is around 950 km. The average height of these ranges is more than 2,000 m; in some areas, these heights reach to more than 5,000 m. There is a range of central

mountains that run from northwest to southeast; its length is 1,460 km, with 143,000 km^2 area. In addition, there are several scattered mountain chains along the eastern boundary and center of the country (Jafari 2005).

The diverse topography and geographic location create a mixed climate in Iran. Temperatures in the interior rise to 55°C, while the temperature in the northwestern part of Iran can reach −40°C. The average precipitation in some parts of Iran can reach 2,400 mm per year, whereas the desert may experience no rainfall in several years (Darehshouri and Kasraian 1998). We can classify the climate of Iran into 10 parts:

Arid Climate; Severe Semi-arid Climate; Moderate Semi-arid Climate; Hot and Dry Mediterranean Climate; Warm Mediterranean Climate; Moderate Mediterranean Climate; Semi-Mediterranean Climate; Exerophire Climate; Cold Exerophire Climate; Cold Steppe Climate (Ghorbani 2013).

2.1. Well data observations

There are 17,865 active observation wells in the whole of Iran. In order to study well level time series, Iran is divided into six main basins. Each main water basin is divided into several sub-basins. On the other hand, based on distribution of the position of monitoring wells, each sub-basin is divided into several study areas too. Generally, the groundwater monitoring wells are established as nonhomogeneous in alluvial plains of the study areas. Therefore, we cannot use these to make a time series of the groundwater level across the whole study areas directly. The Thiessen polygon method has been used to make a time series of the groundwater level across each study area. Thiessen polygons, also known as Voronoi networks and Delaunay triangulations, were used in several fields, including hydrology and climatology, as an essential method for the analysis of proximity and neighbourhood of phenomena, over a century ago. This method is a graphical technique that calculates station weights based on the relative areas of each measuring station in the Thiessen polygon network. The method proposed by Thiessen (1911) assigns to each station a weighted value based on the percentage of the area it represents in relation to the total area of the region in question. In order to achieve accurate estimation of the spatial distribution of the water table in every study area, it is necessary to use a suitable

interpolation method; the Thiessen method is the most appropriate one. This method assigns weight at each gauge station in proportion to the catchment area that is closest to that gauge.

The method of constructing the polygons (Figure 2.1) implies the following steps:

1. The gauge network is plotted on a map of the catchment area of interest.

2. Adjacent stations are connected with lines.

3. Perpendicular bisectors of each line are constructed (perpendicular line at the midpoint of each line connecting two stations).

4. The bisectors are extended and used to form the polygon around each gauge station.

5. The water table value for each gauge station is multiplied by the area of each polygon.

6. All values from step 5 are summed and divided by the total basin area.

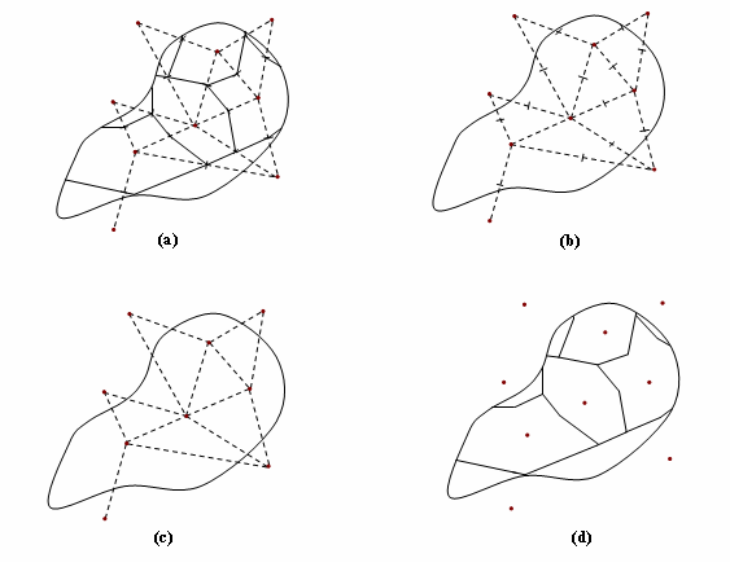

Figure 2.1. Construction of Thiessen polygon.

Each point location in the watershed is assigned a water table equal to that of the closest well. If A_i is area assigned to well *i*, then the water table can be estimated as:

$$\bar{P}_{ave}=\sum_{i=1}^{m}\frac{A_i}{A}P_i \qquad (1.2)$$

where $\bar{P}_{ave}$ is the areal mean level, P_i is water table observed at the i^{th} station inside or outside the basin, A_i is in-region portion of the area of the polygon surrounding the i^{th} station, m is the number of the area, and A is the total basin area. (Olawoyin and Acheampong 2017)

A time series of the changes in Groundwater Storage (GWS) changes across each study area can be computed as its area multiplies its specific yield multiplies the change in groundwater level.

$$\Delta V=\Delta h\times S\times \rho \qquad \Delta h=h-h_{ave} \qquad (2.2)$$

ΔV is groundwater changes, Δh is well-level changes, S is area of Thiessen polygon, ρ is specific yield, h is well level and h_{ave} is average of well level during the period of study. Then we scale up it for each study area by multiplying it by the ratio: $(\frac{\text{area of the study area}}{\text{area of the Thiessen polygon}})$. The total changes in GWS across each sub-basin is computed by adding together the scaled change in GWS of all its study areas. The same procedure is carried out for each main water basin. The results for each of Iran's main water basins and its sub-basins are represented in detail in the following sections. The observations of all well data were collected from Iran Water Resources Management Company. These data are categorized based at monthly intervals, where Iran's water year is defined as the period between October 1st of one year and September 30th of the next. Because of the vast area of Iran, there are 32 sub-basins with 641 study areas. These study areas have long periods of well-level data; some of them have more than 40 years of monthly water-level data. In this thesis, we have monitored all these data. A software package in MATLAB has been developed to estimate the time series of GWS changes across each water basin using well data.

2.2. Water basins or drainage basins in Iran

A drainage basin is an area of land where all precipitation and current water, due to the land slope, collects and drains into a common outlet, such as into a bay, a river, a lake or other body of water. It also known as a water catchment or water basin. The drainage basin includes all the surface water from rain, snowmelt, and nearby streams that run downslope towards the shared outlet, and it includes the groundwater. It means the drainage basin collects all the water within the basin area like a funnel and sends it to a single point. Each drainage basin separates topographically from adjacent basins by a boundary. Drainage basins connect with other drainage basins at lower elevations in a hierarchical pattern, with smaller sub-drainage basins. In closed drainage basins, the water converges to a single point inside the basin, known as a sink, which may be a lake, or a point where surface water is lost underground. Drainage basins have also been named catchments, catchment basins, drainage areas, river basins, water basins and watersheds (Lucien and Brush 1849).

Iran is divided into six main and 31 secondary catchment areas. The six major basins are the Caspian Sea basin in the north (Khazar), the Persian Gulf and Oman Sea basin in the west and south, the Lake Urmia basin in the northwest, the Central Plateau in the center, the Lake Hamun basin in the east (the eastern catchment, or Mashkil Hirmand), and the Ghareghom basin in the northeast (Sarakhs) (Figure 2.2). All these basins, except the Persian Gulf and the Gulf of Oman basin, are interior basins. On the other hand, the Central Plateau basin, covering over 50% of the country, has less than one-third of the total renewable water resources (Iran's Third National Communication to UNFCCC report).

Figure 2.2. Iran's main water basins (Fahmi 2012).

2.3. The Caspian Sea catchment

The Caspian Sea catchment (Figure 2.3) has an area of 175,051-km^2 with seven sub-basins (Table 2.1), and it covers 10.79% of Iran. The Caspian Sea is the largest endorheic water body in the world. It is a lake with no outlets; the Caspian Sea connects to the shores of five countries: Azerbaijan, Iran, Turkmenistan, Kazakhstan, and Russia. The length of its coastline is 5,580 km. The surface of the Caspian Sea lies about 22 to 28 meters below the mean sea level with fluctuation over the years. Because of the inconstancy of the Caspian Sea levels, its area is also inconstant (Aladin and Plotnikov 2004). The water balance of the Caspian Sea is mostly determined by river runoffs, rainfalls, evaporation, and water outflow into Kara-Bogaz-Gol. The groundwater runoff into the Caspian Sea is insignificant. Because of the fluctuation of the Caspian Sea over the years, its level and

its area are sensitive to the weather conditions and drought periods (Aladin and Plotnikov 2004).

The most important part of the incoming water balance is the river runoff of the Volga, which makes up almost 80% of the total riverine inflow. The Caspian is elongated south to north. Its length is 1,225 km. The greatest breadth of the Caspian from the east to the west is 566 km. The surface is equal to 436,000 km^2, and the volume is about 77,000 km^3. The maximum depth of the Caspian is 1,025 m. The Northern part of the Caspian Sea is mostly shallow, and although its area is about 29% of the entire area of the sea, its volume is less than 1%. The average depth is 6 meters, maximal depths do not exceed 10m, and about 20% of the area has depths less than 1 m. (Aladin and Plotnikov 2004). The area of the Middle Caspian makes up about 36%, and its volume is about 35% of the sea. The average depth is about 175 m, and the greatest is 790 m. The Southern Caspian has the largest volume; it is about 64% of the total volume, and its area amounts to 35% of the total area of the sea. It is the deepest part of the sea with the maximum depth reaching 1,025 m. The average depth is 300 m. More than 130 rivers flow into the Caspian Sea, such as the Volga, Ural, Kura, Sefidrood, Atrak and other rivers, from inside Iran, and also precipitation (Aladin and Plotnikov 2004). These Iranian rivers pour water from the North Slope of Alborz to the Caspian Sea, and on their way to the Caspian Sea irrigate the agricultural lands. In the Iranian part of the coastline, the most important river in this catchment is Sefidrood. Its length is 800 km, and its basin area is 50,000 km^2. The Atrak River is the second most important river, being 600 km in length.

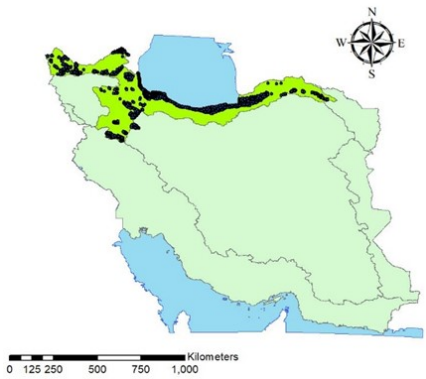

Figure 2.3. The Caspian Sea catchment.

Table 2.1. Sub-basins of the Caspian Sea catchment

Sub-basin	Water basin area (km^2)	Water basin code
Aras River	39534	11
Talesh Rivers and Anzali	6921	12
Sefidrood Bozorg	59429	13
The rivers between Sefidrood and Haraz River	10905	14
The rivers between Gharaso River and Haraz River	18771	15
The rivers between Gharaso River and Gorganrood River	13061	16
Atrak River	26430	17
Total	175051	1

2.3.1. The climate and weather system: Rainfall over the Caspian Sea coast originates from this lake. In winter, the cold front from Central Asia crosses over the Aral and Caspian Seas and absorbs moisture from these large water bodies. When moist winds from the east-northeast reaches the Alborz Mountains, they become condensed and produce large amounts of rainfall. It can even reach 2,000 mm per year. In the Caspian Sea area, the average amount of rainfall in winter and spring is more or less the same. In the autumn, this area has more rainfall compared to the other seasons. In this water basin, we have four types of climate:

Moderate Mediterranean Climate: The Alborz Mountain range acts as a barrier wall, and the moisture coming from the Caspian Sea becomes stuck in this part, and this causes high precipitation. The aridity index is 40–100 days. The region comprises from Anzali to Nowshahr. The average annual rainfall in this region is from 700 to 1,800 mm. This region's climate is considered as mild or moderate.

Semi-Mediterranean Climate: In the southern and eastern parts of the Caspian Sea coast it frequently rains, and the seasonal temperature variation is small. The average annual rainfall is 700–1000 mm. The aridity index is less than 40 days. The coastal lands never

freeze because of high humidity. This climate covers a small area from Babolsar to the Hosseingholi Gulf.

Exerophire Climate: In some parts of the coastal area, the precipitations is so frequent that it does not even experience a dry season. This includes Astara, Fooman, Lakan, Bibalani, and east of the Talesh Mountains. The average annual rainfall in this region varies from 1,000 to 2,000 mm.

Cold Exerophire Climate: This type of climate dominates over heights in Alborz. For almost 5–11 months of the year, there is freezing weather in this region. The average annual rainfall is more than 2,000 mm.

2.3.2 Vegetation: Most trees and shrubs in the Caspian region have managed to survive because of their distance from the glaciers; therefore, although this area is not vast, the Caspian Floral Province includes 80 tree species and about 50 shrub species. This water basin has a European–Siberian origin from a botanical point of view. Forests in the Caspian Province are really a live museum presenting periglacial European plants. There are two kinds of forest in this area: the Caspian Hyrcanian Mixed Forest located from south-eastern Azerbaijan eastwards to Golestan Province spread over 2.1 million hectares, and the Arasbaran Forest located in the northwest with 160,000 hectares. A large part of Caspian forest has been transformed into rice fields, citrus groves, and tea gardens, as well as into housing areas (Ghorbani 2013).

2.4. The Persian Gulf and Oman Sea catchment

This catchment measures 424,029.6 km^2 and it covers 26.22% of Iran (Figure 2.4). It spreads from west to south and southeast of the country with 9 sub-basins (Table 2.2). Almost half of the country's renewable water resources are located in this basin. This area only has even low precipitation, but it has some rivers, so it makes a large contribution to Iran's water resources (Iran's Third National Communication to UNFCCC report, Freshwater and Sanitation Country Profile). The Persian Gulf is located between 24º-30º N latitude and 48º-56.5º E longitude between Iran and the Arabian Peninsula. Around the Persian Gulf, Iran covers most of the northern coast and Saudi Arabia most of the southern

coast (Figure 2.5). The Persian Gulf is an extension of the Indian Ocean and the Gulf of Oman, through the Strait of Hormuz. The Strait of Hormuz connects the Persian Gulf to the Oman Sea and the Arabian Sea and Indian Ocean. The Hormuz Strait is only 56 km wide at its narrowest point. The length of the Persian Gulf on the northern coast, from Shatt al-Arab (Arvandrood) to the Hormuz Strait, is 970 km; the maximum width of the Persian Gulf is 338 km; and the surface area of the Gulf is around 251,000 km^2. The Oman Sea area is 939,009 km^2 (Dariusz and Bugajski, 2016, Kåmpf and Sadrinasab 2006). The Persian Gulf is a low-depth sea with an average depth of 36 m around the Strait, deepening to more than 100 m inside the Strait, and its depth increases quickly to more than 2,000 m within 200 km outside the Strait. The Oman Sea is relatively deep, and its depth even reaches 3,500 m. (Reynolds and Michael 1993). Weak bottom circulation probably causes it to produce pollutants and fine-grained muds (Hughes and Hunter 1979, Reynolds 1992a).

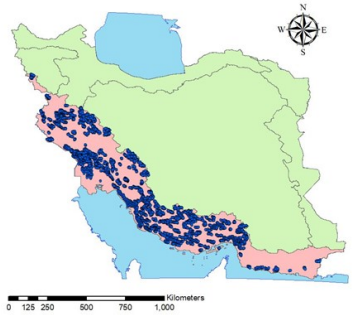

Figure 2.4: The Persian Gulf and Oman Sea catchment.

In this water basin, some of the rivers end in the Persian Gulf and Gulf of Oman, and some of them pour out of Iran to Iraq. Most river inflow into the Persian Gulf is from Iranian rivers. At the western end of Persian Gulf, there is the major river delta of the Shatt al-Arab; this river carries the waters of the Karun, the Euphrates, and the Tigris. These three rivers together drain 808,000 km^2, and they join near the head of the Persian Gulf to form the Shatt al-Arab. Before it reaches the sea across the desert, much of the water evaporates. As the flow reduces, the river's carrying power also reduces and causes the silt to be deposited. So the bed is becoming higher and higher. In Iran, Karun is the longest river with a length of 828 km. While the basin measures only 67,572.79 km², the

Karun drains a mountainous area of moderately heavy precipitation, so it carries a large volume of water (George and Cressey 1958).

The Tigris and Euphrates rivers together bring an annual average of 708 m^3/s and the Karun brings 748 m^3/s. Therefore, the total average outflow of the Shatt al-Arab is 1,456 m^3/s. Other major rivers are the Hendijan with 203 m^3/s outflow, the Hilleh with 444 m^3/s outflow, and the Mand with 1387 m^3/s outflow. The total river runoff reaches 110 km^3/yr; it is equivalent to 46 cm/yr of depth (Reynolds 1993). Iran has some outflow from this area; 10 km^3/year from affluents of the Tigris flows to Iraq. About 24.7 km^3/year flows from the Karun into Iraq, but since this is just before it discharges into the sea, it does not count as inflow into Iraq (FAO. 2008).

2.4.1. The climate and weather system

This region is the boundary between tropical circulations and the weather systems of mid-latitudes. Descending dry air in these latitudes yields arid conditions. The climate in the Gulf of Oman is different from the climate in the Persian Gulf. The Strait of Hormuz is like a boundary between the two systems. The Gulf of Oman is at the northern edge of the tropical weather systems in the Arabian Sea and Indian Ocean. Monsoon circulation produces south winds in the summer and strong northerly winds in the winter. These sets of winds have great force and continue for several days. The summer northerly winds are almost continuous from early June through July. They are associated with the relative strengths of the Indian and Arabian thermal lows. Due to the channeling of the low-level air flow by the Zagros Mountains of western Iran, the strongest of the southerly winds occur on the eastern seaboard. A strong sea breeze occurs along the entire coastline, especially along the Arabian Peninsula because of temperature difference between the land and water surfaces; the sea breeze circulation adds a landward component to all winds. It causes surface pollutants to be deposited on the beach.

Evaporation in the Persian Gulf is much higher than rivers' inflow and precipitation so the area has a Mediterranean, reverse-flow, estuarine circulation. Estimates of evaporation vary from 144 cm/yr to 500 cm/yr. Measurements show that even though the water temperature is considerably higher in the summer, most evaporation occurs in the wintertime because of higher wind speeds. The energy in the sea water motion derives

from different sources: tidal forces, wind forces, and density differences (Reynolds 1993). In this water basin, we have different types of climate:

Severe Semi-arid Climate: This hot and dry climate includes the edge of the deserts. The average annual rainfall is between 100 and 280 mm. The aridity index is 250–300 days.

Hot and Dry Mediterranean Climate: In this weather condition, the aridity index is between 150 and 200 days. The low-pressure cold weather systems coming in from the north or the west of Iran, while passing the Zagros Mountain range, lose temperature and produce some rainfall. The average annual rainfall increases to 200 and 500 mm. It includes the western parts of Iran from Ghasr-e Shirin toward the center to Khoram-abad.

Warm Mediterranean Climate: Western Iran has higher geographic latitude and relatively high elevation; hence, the precipitation mostly is snow in the winter and in the form of showers in the spring. The average annual rainfall is between 300 and 600 mm, and the aridity index is 100–150 days. Cities such as Ravansar, Kermanshah, and southern parts of Arak experience this kind of climate.

Cold Steppe Climate: We have this type of cold and dry climate in some parts of the Zagros Mountains; freezing weather lasts five to eight months. The annual precipitation is around 200 mm.

Cold Exerophire Climate: This type of climate dominates over heights in Zagros. For almost five to 11 months of the year, there is freezing weather in this region. The average annual rainfall is more than 2,000 mm.

2.4.2. Vegetation: This catchment includes Zagros Floral Province and Southern Coastal Plains Floral Province. The vegetation cover in Zagros varies with elevation. In the higher area, the vegetation cover is shorter and grassier. This area includes Zagros Forest, which spreads over six million hectares. In the Southern Coastal Plains Floral Province, because of hot weather in this area, warmth-loving plants prevail, and mostly their origin goes back to tropical Asia or Africa, for instance palm (date) and lotus trees. Their low

resistance to cold weather makes them limited to the southern coastal area, which is quite warm. There is another forest in this area, Gulf Forest covering 1.1 million hectares.

Table 2.2. Sub-basins of the Persian Gulf and Oman Sea catchment

Sub-basin	Water basin area (km^2)	Water basin code
Marzi-e-Gharb rivers	39667	21
Karkeh river	51337	22
Karoon River	67257	23
Jarahi River and Zohreh River	40788	24
Hele River and small rivers around	21274	25
Mand River and closed basin Heram, Karin, and Khanij	47654	26
Mehran River, Kal River, south Masil and islands	62918	27
The rivers between Bandar Abbas and Sadij	44763	28
The rivers between Sadij and Pakistan Boundary (Baloochestan Jonubi)	48551	29
Total	424209	

Figure 2.5. The Persian Gulf and Oman Sea (Reynolds 1993).

2.5. The Urmia Lake catchment

This catchment is 52,000 km^2 and it covers 3.21% of Iran (Figure 2.6). This basin is located in the northwest of Iran, at latitude 37°00' to 38°12' N, and longitude 44°40' to 45°50' E. Urmia Lake is one of the largest permanent lakes in the Middle East and 7% of the total surface water in Iran (Eimanifar and Mohebbi 2007). Urmia is the sixth largest salt lake in the world according to surface area. Urmia Lake is a hypersaline lake, so it has an important role in the ecology and the life of people in this region. The lake is registered as a Biosphere Reserve and a Ramsar Wetland. A causeway divides the lake into southern and northern parts for facilitation of communication between east (Tabriz City) and west (Urmia City) of the lake (West Azarbaijan Regional Water Authority, 2012a) (Figure 2.7). The lake's basin has a continental climate; also, there are mountains near the lake that influence the climate of this basin (Kelts & Shahrabi, 1986).

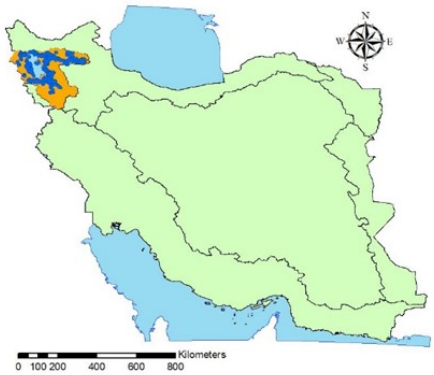

Figure 2.6. The Urmia catchment.

During the last two decades, there has been a rapid decline of the lake's water level. The lake has shrunk from its former size, and the water level has had a negative trend that had never happened before. Agricultural activities use water from the rivers while the rivers are the main source of inflows to the lake. Urmia Lake is a terminal lake, which means that there is no outlet from this lake, it is in-charged by precipitation and inflowing rivers, and there are no outflows from the lake, just evaporation. There are 14 permanent, seven seasonal, and around 39 episodic rivers in this catchment that pour in the lake. On average, the annual incoming water to the lake comprises 4,900 million m^3 water from

rivers, 1,500 million m^3 from precipitation, and 500 million m^3 from floodwaters hence the total inflow to the lake is about 6,900 million m^3 (Ghaheri et al. 1999). Because of irrigation through pumping water, the presence of several dams in the area for agricultural use, and seasonally high evaporation, it is not clear how much water from groundwater resources goes into the lake. In addition to drought periods, the increase of and change in agriculture, the growing population, higher industrial demand, and necessity for implementing more dam and pumping projects are the other reasons for the lake declining. The salinity of Urmia Lake is high and has had fluctuations over the years. It has increased during recent years because it depends on the water level declining. There is a spatial ecosystem and fauna in this catchment that is sensitive to the situation of the lake. The water level declining has an irreversible impact on the ecosystem. The drying up of the lake, turning it into a salt marsh, which will harmfully affect the climate and ecosystem of the region, may lead to the migration of some of the local population since their life is dependent on agriculture (Sangoyomi et al. 1996, Lall et al. 1996, Hassanzadeh et al. 2011 Delju et al. 2012, West Azarbaijan Regional Water Authority 2012a, Ministry of Energy 2007, Khatami and Berndtsson 2013).

The climate of this catchment includes cold mountain, and Mediterranean with spring rains.

Figure 2.7. The Urmia Lake (Google Earth – August 25, 1998–August 13, 2011).

2.6. The Central Plateau catchment

This water basin is in the center of Iran, located between 26º 22′ to 37º 28′ north latitude and 48º 08′ to 61º 23′ east longitude (Figure 2.8). Its area is around 825,000 km^2. It is a vast area and covers half of the total area of Iran with 9 sub-basins (Table 2.3). The border of the Central Plateau catchment in the north is the Alborz Mountains, in the east the eastern mountains, and from the west and south the Zagros Mountains. This basin has no connection to the Caspian Sea or Persian Gulf. There are two deserts in this basin: Dasht-e-Kavir and Kavir-e-Lut. They are very arid and maybe the hottest areas in the world. Kavir-e-Lut is the largest pit inside the Iranian plateau, with maximum annual rainfall of 100 mm. The average altitude of this desert is almost 600 m above sea level. Dasht-e-Kavir is located in the north of Kavir-e-Lut, with minimum altitude of 400 m ASL. The difference in temperature during a year is between 0° and 70° C. The mountains that surround the area act like a barrier, thus the moisture from the Caspian Sea, the Oman Sea and the Persian Gulf do not reach the Central Plateau. Consequently, the average precipitation in this area is low. Because of strong sunshine and excessive vaporization, 70% of precipitation evaporates, and humidity can decrease down to 0%. In these two deserts there is no proper soil and water for plants to grow. This is because these regions are always open to winds and there are not sufficient plants to preserve the soil, wind erodes the earth, and a large amount of sand is always moving and forming sand hills and running sand masses.

The central basin includes 44.5% mountains, 41.9% plain, and 13.6% swamp and desert. It comprises different climates, such as desert, high mountains, plain and salt marsh. Therefore, the meteorological parameters have a vast variety. The existence of two deserts and swamps in the east of this catchment make access to the area difficult. This causes lack of different data such as the grids of synoptic stations and piezometric well data. Thus, the study of drought, total water storage, and other useful parameters in this catchment is difficult and less accurate. The Central Plateau is a closed water basin; no water comes from outside and no water comes inside, and all rivers pour into swamps and lakes inside of this basin, for instance the salt lake and the Gavkhouni Swamp. In this area, surface water is not a considerable portion of water resources; just precipitation and groundwater supply the requirements of big cities in this catchment. Increase in

population makes the study of total water storage for this basin important. A considerable amount of water storage is consumed for agriculture and drinking, and most of the precipitation leaves the area by evapotranspiration. Only a small amount of water is absorbed in the soil and stored as soil moisture or groundwater. So the situation in the area is critical. In this area, some activities stop when it is extremely cold in winter and while summers are long and very dry. This catchment includes different types of climate: hot and dry desert, hot semi-desert, and cold semi-desert.

Hot and Dry Climate: The central part of the Iranian Plateau consists of dry and bare deserts. This area manifests an arid climate; the characteristics of this climate are briefly expressed as very low rainfall, a long hot season and extreme aridness. In addition, there is a big difference between day and night temperatures; days are very hot, and nights are relatively cold. The annual rainfall is 75 mm. Rain falls mostly in the mountainous parts, and it happens over a few days. The aridity index (the number of days with no rainfall) in this area is 300–350 days.

Hot Semi-desert: This climate mostly includes the edge of the deserts and is in surrounding areas with arid climate. This kind of climate is also hot and dry, but cloud systems coming from the north and the west of Iran make it little damp; therefore, in these areas, the average annual rainfall is between 100 and 280 mm. The aridity index in this type of climate is 250–300 days. The average annual temperature in these areas is between 16 and 20°C. The weather becomes moderate in winter with infrequent rainfall that usually leads to floods.

Semi-arid Climate: Parts of Khuzestan Plain, southern parts of Fars Province, and most of Iran's Central Plateau experience this.

Cold Steppe Climate: We have this type of cold and dry climate in some parts of the Alborz and Zagros Mountains; freezing weather lasts five to eight months. The annual precipitation is around 200 mm.

Most regions in Iran have almost dry summers, except the Caspian coasts and the southeast of the country, which have some rain in the summer, due to seasonal Indian Ocean winds that bring rain clouds to the southeast of Iran. These clouds are not so thick

and when mixed with northwest systems lose some of their rain-making abilities. Except for these two areas, other regions in Iran have almost no rain in summer, because the summer weather system that brings summer rain for Europe loses the moisture while crossing the desert (Nabavi, 2018).

Iran's Central Plateau covers about 3/4 of Iran's surface area, and 70% of the flora species of Iran belong to this province. The plants that could survive in this area are adapted to heat, severe aridity, salinity, long summers, and cold winters. The number of trees reduce and are replaced with busheland when moving from the hills toward the plains. Rolling sand dunes in the form of small and large patches are spread throughout some places in this area, which display a special vegetation cover. This vegetation cover is very rich in species variety, and its extent depends on elevation, rainfall, and form of soil. The concentration of brushland in Iran's Central Plateau is notable. There are Irano-Touranian forests dispersed throughout the Central Plateau. This is a special type of forest, and it has distance between trees. This forest comprises 4.5 million hectares of the Central Plateau.

Table 2.3. Sub-basins of the Central Plateau catchment

Sub-basin	Water basin area (km^2)	Water basin code
Daryache Namak	92563	41
Gavkhouni	41550	42
Lakes of Tashtak, Bakhtegan, and Maharloo	31492	43
Abarghoo Sirjan Kaviar	57196	44
Jazmoorian Hamun	69390	45
Loot kaviar	206222	46
Markazi kaviar	226523	47
The deserts of Siahkooh, Rig-e Zarin, and Degh Sorkh	48912	48
The deserts of Daranjir and Saghand	50508	49
Total	824356	4

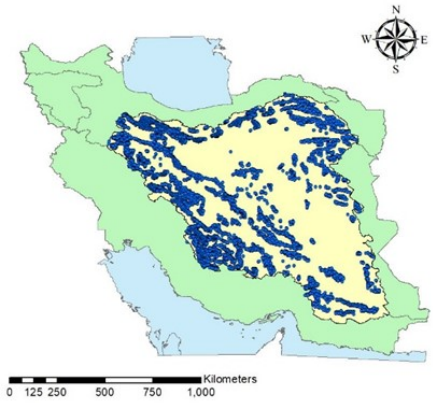

Figure 2.8. The Central Plateau catchment.

2.7. The Eastern Boundary catchment

This catchment is 106,000 km^2 and it covers 6.42% of Iran (Figure 2.9) with 3 sub-basins (Table 2.4). This water basin is located in southeast Iran in the Sistan region, across the neighboring areas of Afghanistan and Pakistan. It also called Hamun or Sarakhs and is limited at the east by the Iranian highlands, at the north by the southern Hindu Kush ranges, at the west by the East Iranian ranges, and at the south by mountain ranges in the Baluchestan province of Pakistan (Whitney 2006). The climate in this area is hot and dry, and there is a large desert that is famous for windstorms, sudden floods, and dryness. The basin receives the water of the Hirmand River (Shirdeli 2014).

In the winter season, the winds blowing from low-pressure zones in Central Asia toward the west remain dry if they do not pass over lakes or other water bodies; therefore, they bring no rainfall to the near east region. Few rain cloud systems coming from low-pressure systems in Asia Minor reach the Iranian Plateau. In the autumn, the seasonal Indian Ocean winds gradually recede toward the southeast allowing the procession of the Atlantic Ocean weather system into Iran, which produces 15% of the average annual rainfall (Ghorbani 2013). The southeast of the country has some rain in the summer, due to seasonal Indian Ocean winds that bring rain clouds. These clouds are not very thick

and when mixed with northwest systems lose some of their rain-making abilities. (Nabavi 1994).

There is a set of winds in the southeast of the country that are known as the 120-day winds, from late May until late August. The speed of these winds reach 25 m/s, and the average speed has been measured to be as much as 10 m/s. The highest speed can reach 90 km/h, and in an extraordinary one-off case, the speed of these winds reached 126 km/h. While these winds are blowing, there will be lots of dust in the area, so all human activities stop. It is damaging and unsafe for human health. These winds are also one of the reasons for high evaporation in this area.

Lake Hamun is located in this catchment. It comprises a gathering of wetlands, marshlands, and shallow lakes in an endorheic basin in the desert. This lake is fed by numerous seasonal secondary branches; the main and permanent stream is the Hirmand River. This river begins in Afghanistan, in the Hindu Kush Mountains, from snowmelt in spring. Hamun Lake is sometimes considered to be three sibling shallow lakes: Hamun-e Hirmand, Hamun-e Sabari, and Hamun-e Puzak. This area includes native wetland ecosystems, and there is wildlife, animals and migratory birds. The situation of Hamun depends on weather conditions, so during the last century, it completely dried up at least three times (Shirdeli 2014). Because Lake Hamun is fed mainly by water catchments on the Afghanistan side, when rivers in Afghanistan were flowing regularly, the amount of water in the lake was relatively high. But if the water level on the Afghanistan side is drawn down, the condition would be critical. It could happen through natural reasons such as droughts in Afghanistan, or by human-induced reasons such as using more water from Hirmand River for irrigation in Afghanistan. Between 1999 and 2001, the lake all dried up and disappeared. Consequently, the end result is that it appears to be a dry lake bed in Iran, and seasonal winds blow fine sands off the bare lake bed. The sand is swirled into huge hills that may cover fishing villages along the former lake shore. Wildlife around the lake is negatively impacted, and fisheries also have stopped operating. Changes in water policies in the region can help to return much of the water to Lake Hamun.

In the past five millennia, people around Hamun Oasis for the most part lived in harmony with the wetlands and their wildlife. The livelihood near the lake mostly was based on

hunting, fishing, and farming. From 4,000 years ago, irrigation was carried out in the area without destroying the wetlands, until the late 20th century, when population rapidly increased and new, more efficient water management technologies were brought to the region. New irrigation methods began to be used in the basin. Farther west, Afghan governments constructed large dams (Arghandab Dam, Kajaki Dam) that diverted water from the upper reaches of the river (Weier 2002).

Arid Climate: This area manifests an arid climate; the characteristics of this climate are briefly expressed as very low rainfall, a long hot season, and extreme aridness. In addition, there is a big difference between day and the night temperatures; days are very hot, and nights are relatively cold. The annual rainfall is 75 mm. Rain falls mostly in the mountainous parts, and it happens over a few days. The aridity index (the number of days with no rainfall) in this area is 300–350 days. Areas such as Jazmurian, Khur and Jandagh, Farrokhi, Biyabanak, Anarak, Nehbandan to Nosrat-abad, Bam, Zahedan, Zabol, and Saravan can be included in this type of climate.

Severe Semi-arid Climate: This climate mostly includes the edge of the deserts, and is in surrounding areas with arid climate. This kind of climate is also hot and dry, but cloud systems coming from the north and the west of Iran make it little damp; therefore, in these areas, the average annual rainfall is between 100 and 280 mm. The aridity index in this type of climate is 250–300 days. The average annual temperature in these areas is between 16 and 20°C. The weather becomes moderate in winter with infrequent rainfall that usually leads to floods.

Cold Semi-desert Climate: These areas have very hot summers and mild or warm winters. Cold semi-arid regions are usually found in temperate zones and are more likely to occur inland, away from large bodies of water. Summers are usually hot and dry, and winters are often cold enough for snow.

The vegetation of this basin includes three types of botanies: desert lowland, steppe, and semi-desert.

Table 2.4. Sub-basins of the Eastern Boundary catchment

Sub-basin	Water basin area (km2)	Water basin code
Petergan Playa and namakzare-khaf	32980	51
Hamoon-Hirmand	33731	52
Mashkil hamun	36458	53
Total	103169	5

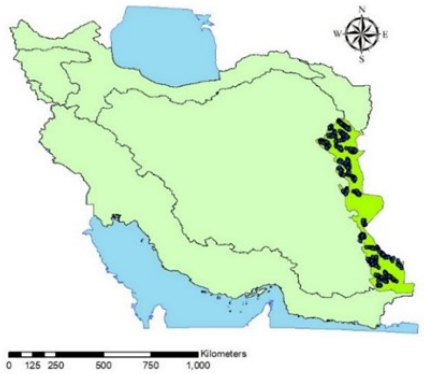

Figure 2.9. The Eastern Boundary catchment.

2.8. The Ghareghom catchment

This catchment is 44,295.5 km^2 and it covers 2.68% of Iran (Figure 2.10) with one sub-basin (Table 2.5). It is located in the northeast of Iran, on the border of Afghanistan and Turkmenistan. This catchment is one of the low precipitation kind, so the rivers are mostly seasonal and episodic. Some of the rivers in this area originate from Afghanistan, such as Harirud. This river flows in direction of the border of three countries; therefore it is a transboundary river. Harirood and Kashafrood together connect to the Tajan River and go to Turkmenistan.

The Ghareghom basin contains 13 sub-basins, four of which are in the border region. In the Sarakhs sub-basin, there is an important transboundary sedimentary aquifer with

approximately $110\times10^6 m^3$ recharge mostly from Harirud River. The Sarakhs Aquifer is an important transboundary aquifer between Iran and Turkmenistan, and it is suggested that it should be included in the second assessment report of United Nations Economic Commission for Europe (UNECE). In other sub-basins, such as Gonbadli, Kalat, Dargze sub-basins, and Atrak basin, transboundary groundwater volume is low and also there is poor information.

To avoid future argument, it is suggested that some integrated studies should be conducted and for there to be programming of transboundary aquifers in Harirud Basin with the cooperation of Afghanistan and Turkmenistan and international organizations.

This catchment includes cold semi-desert, cold mountain, and Mediterranean climate with spring rains.

2.5. Sub-basins of the Ghareghom catchment

Sub-basin	Water basin area (km2)	Water basin code
Ghareghom	44165	60

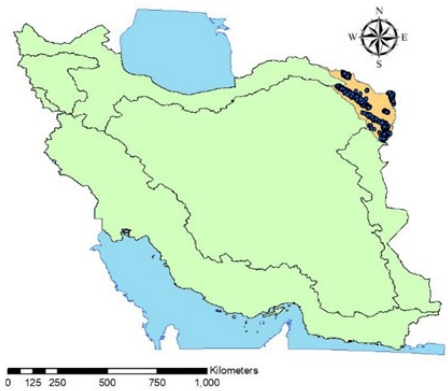

Figure 2.10. The Ghareghom catchment.

This page is intentionally left blank.

Chapter 3

Groundwater Storage Changes Estimation Using Satellite Data

3.1. The Earth's gravity field

According to the Newton's law of universal gravitation, every particle attracts every other particle in the universe with a force that is directly relative to the product of their masses and inversely relative to the square of the distance between their centers. This is a general physical law derived by Isaac Newton (Brackenridg 1996, Moustos 2017). The Earth's gravity field is a product of its mass distribution; this includes mass deep within the Earth and at and above the Earth's surface. Different sources cause constant changes to mass distribution. Tides in the ocean and solid Earth cause large mass variations at 13-hour and 24-hour periods. Atmospheric disturbances related to synoptic storms, seasonal climatic variations, etc., lead to variations in the distribution of mass in the atmosphere and the ocean. In addition to these, mantle convection causes mass variability throughout the mantle that has large amplitudes, but it occurs slowly relative to human timescales; therefore, this source

of variation is not considered. Because of these and other processes, the Earth's gravity field varies with time. Observations of that variability using either satellites or ground-based instrumentation can be made to study a wide variety of geophysical and climatology processes that involve changes in mass such as total water storage (Dickey et al. 1997). Most of the time-variable signal comes from the Earth's fluid envelope: the oceans, the atmosphere, the polar ice sheets and continental glaciers, and the storage of water and snow on land. Fluids (water and gases) are much more mobile than rock. Solid Earth deformation has a significant indirect effect on ground-based gravity measurements. If we assume that a gravimeter is on the Earth's surface, it is sensitive to the vertical motion of that surface. When the Earth surface goes up, the gravimeter moves further from the center of the Earth, and so it senses a smaller gravitational acceleration compared to before this movement. For most solid Earth processes, the signal from the vertical displacement of the meter is far larger than the actual gravity change caused by the displaced mass. Therefore, a surface gravimeter can be considered as a vertical positioning instrument. If we compare a satellite measuring, it is not fixed to the surface; the gravity signals it detects are due entirely to the underlying mass distribution. So, satellite gravity delivers direct dependency on that mass. When we try to find density distribution by using gravity data, there are a variety of possible solutions. It means that when interpreting gravity observations, the limitation is that the inversion of gravity for density is not unique. There are always an unlimited number of possible internal density distributions that can produce the same external gravity field. The gravity field are produced by mass that is uniformly distributed throughout the sphere, or is localized completely at the outer surface, or has any other distribution that is radially-dependent, is the same. So just knowledge about the external field is not sufficient. This non-uniqueness is a major limitation when interpreting the Earth's static gravity field (Lemoine et al. 1998).

3.2. Time-variable gravity

As mentioned above, time-variable gravity changes are caused by a combination of postglacial rebound, fluctuations in atmospheric mass, and the redistribution of water, snow,

or ice stored on or a little below the Earth's surface on land and in the ocean. The spatial resolution of gravity data obtained from satellite measurements has not yet been sufficient to separate the effects of these processes from one another. The time-varying signals can usually come from mass variability at the Earth's surface rather than from deep within the Earth. One of the other sources is the body tide, and the response of the solid Earth to the surface mass load. That loading effect can be linearly related to the load signal through scale-dependent, well-modeled, proportionality factors. Thus, all the seasonal mass anomaly can be assumed to be concentrated within a few kilometers of the surface. Therefore, despite the inversion for mass anomalies still depending on the exact depth of the load, the corresponding uncertainty in the amplitude of the inferred mass anomaly is small. It is still not possible to tell, without additional information, whether a mass anomaly in a continental region, for example, is in the atmosphere, or in the water and snow on the surface, or in the water stored underground. But at least the total amplitude of the mass anomaly can be determined. The struggle with time-variable gravity is that the amplitudes of variations compared to the static field are small. The annually varying geoid is over 1,000 times smaller than the lateral variation in the static field. Most of the Earth's mass, after all, is tied up in the rocky interior and remains relatively immobile on human timescales. Over the last few decades, improvements in ground-based instrumentation have helped us to observe time-variable gravity at local scales. Even though high-precision gravimeters can detect surface displacements caused by solid Earth processes, and also local gravitational changes caused by variations in the covering atmosphere and underlying water storage, we need satellite measurements in order to recover large-scale time-varying signals (Swenson and Wahr 2002).

At the beginning, satellite time-variable gravity solutions were established on Satellite Laser Ranging (SLR) observations such as Laser Geometric Environmental Observation Survey (LAGEOS) (launched by NASA in 1976) and LAGEOS II (launched by NASA and the Italian Space Agency in 1993). Both satellites are orbiting at 6,000 km altitude. They are passives spheres, with outer surfaces covered with corner cube reflectors. A powerful laser on Earth sends a laser pulse up to the satellite, and the light is reflected to the laser. The distance between the laser and the satellite is determined; this is, in fact, the round-trip travel

time between satellite and the point on the Earth. So, by monitoring these distances from lasers around the Earth's surface, the satellite's orbital motion is computed. Since the orbital motion is determined by the Earth's gravity field, this allows for global gravity field solutions at ordered time intervals. Differences between solutions for different time periods provide estimates of time-variable gravity (Wahr 2007). High-altitude satellites such as LAGEOS, however, provide gravity information only at relatively long wavelengths. Accurate detection would require a low-altitude satellite (Wahr and Molenaar 1998). Low-altitude satellites, however, are subject to considerably larger non-gravitational forces, primarily from the atmosphere, and these can greatly degrade the gravity inversions at all wavelengths. SLR measurements have also been used to detect temporal variations in the Earth's gravity field. Laser ranging to LAGEOS and other satellites has provided information about seasonal, decadal, and secular changes in a few (from two to about five, depending on the analysis) of the very largest-scale zonal components of the gravity field (Yoder et al. 1983, Rubincam 1984, Cheng et al. 1989, Gegout and Cazenave 1993, Eanes 1995, Nerem et al. 1993, Dong et al. 1996). The sources of this variability have been proposed as including mass redistribution in the atmosphere (for the seasonal terms), the 18.6-year gravitational tide in the solid Earth and oceans (for the decadal variability), and a combination of postglacial rebound.

3.3. GRACE

The Earth's surface is not uniform as it includes objects with different density, such as mountains, valleys, oceans, lands with stored water, and ice caps. Therefore, the density varies from place to place on the Earth's surface. Consequently, these variations in density make slight variations in the gravitational field. The main driving forces behind temporal variations of the gravity field are atmosphere and ocean circulations and continental water storage changes at periods of several years or shorter. Accurate time-variable gravity field measurements can be used to study mass redistribution within the Earth system. This was the

primary motivation behind the development of the Gravity Recovery and Climate Experiment (GRACE) mission. The chief advantage GRACE had over other space observations was completeness in capturing integrated mass changes at and beneath the land surface. These observations created the potential for applications in drought monitoring and related fire-hazard assessment, flood risk evaluation, regional water budget analysis including quantification of groundwater depletion, ice sheet and glacier mass change monitoring, and non-steric sea level rise assessment. The GRACE mission design made it particularly useful for time-variable gravity studies. GRACE consisted of twin identical satellites in identical orbits, one following the other by about 220 km. Each of these spacecraft was carrying a science payload consisting of a microwave ranging system, GPS receiver, star cameras, accelerometer, and SLR retroreflector providing the primary observations needed for gravity field recovery. The primary objective of the GRACE mission was to accurately measure the temporal changes in the shifting Earth masses and map their effects on the Earth's gravity field, with a high spatial resolution from 400 km to 40,000 km, yield new information on the effects of global climate change. Its secondary objective was to measure globally distributed profiles of the GPS signal excess delay or bending angle of GPS measurements per day caused by the ionosphere and atmosphere (Slobbe 2008).

The GRACE satellite gravity mission was jointly sponsored by NASA and the German Aerospace Center (DLR) (Tapley et al. 2004a). The key partners was the University of Texas Center for Space Research (UTCSR), the GFZ German Research Centre for Geosciences, and the Jet Propulsion Laboratory (JPL). DLR's German Space Operations Center (GSOC) was responsible for mission management and satellite operation. UTCSR and GFZ were responsible for scientific data evaluation. GRACE was launched in March 2002, with an expected five-year lifetime. After all, the mission lasted a good 15 years (more than three times as long as expected). The goal of GRACE was to map Earth's gravity field with unprecedented accuracy. GRACE worked by tracking changes in the distance between the two satellites and combining these measurements with data from onboard accelerometers and GPS receivers. Onboard GPS receivers determined the position of each spacecraft in a geocentric reference frame. These twin satellites flew in one low altitude orbit (450 km) with

inclination of 89°. GRACE satellites were tracking each other in a low Earth orbit (LEO), so it was a Low-Low Satellite to Satellite Tracking (LL-SST) mission (Figure 3.1). When the GRACE satellites was passing over a mass anomaly on or near the surface of the Earth, first the leading satellite was feeling the anomaly as it had caused a small perturbation in the orbit. In a little while, the other satellite was feeling the exact same perturbation caused by the same anomaly, only slightly displaced in time. This perturbation was observed as a change in distance between the two satellites. The Earth's gravity field could be determined using observed changes in the inter-satellite distance, position, and acceleration of each satellite. Changes in the inter-satellite distance was the mission data, while acceleration and position data was made for each satellite.

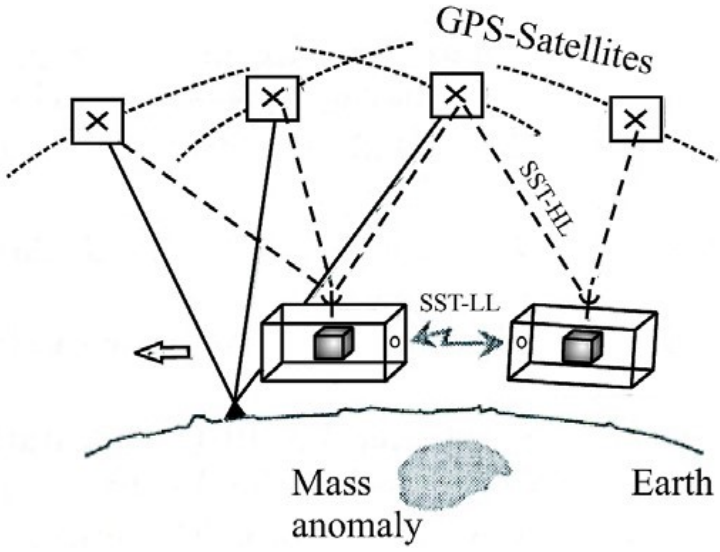

Figure 3.1: Gravity Recovery and Climate Experiment (GRACE) mission (Rummel et al. 2002).

The satellites detected minute variations in the Earth's surface mass below as well as variations in the Earth's gravitational force. When the satellites was traveling 500 km above the Earth in space, the front satellite captured the area with higher gravity; it was slightly

pulled toward the area with higher density and speeds up. As soon as the front satellite passed over the area of higher gravity, it slowed down, but the trailing satellite speeded up. The distance between the two satellites changed again. As the trailing satellite passed the region of higher density, it slowed down as well, which did not affect the front satellite at the same time. These minute expansions and contractions of the distance between satellites were measured using the microwave K-band ranging instrument. That K/Ka-Band Ranging System (KBR) were an extremely precise microwave ranging system (within 10 μm, about 1/100'th the thickness of a human hair). This was actually KBR with sampling frequency of 10Hz and placed at the center of mass of each satellite that measures the inter-satellite distance (Dunn et al. 2003). The measurements of satellite distance were transmitted to the ground where they were used to correct the satellite-to-satellite distance measurements. The position of each satellite was precisely determined by the GPS satellites. The main advantage of the GRACE mission was the high precision of the GPS receiver, which helped to map precisely the Earth's gravity field within 1 micron. Consequently, high-resolution maps enabled observation of the Earth's gravitational field from the large scale to finer scale over both land and sea. The accurate microwaves continually was monitor separation distance changes with time as the satellites flew through spatial gradients in the gravity field. Consequently, by monitoring those changes, the gravity field could be determined and the gravity field solutions at global-scale wavelengths were improved (Tapley et al 2004).

The resolution of the gravity field that could be recovered from the tracking data depends on the orbital height. The lower the orbit, the better the resolution, but also the more drag on the satellites, the shorter the lifetime. Because the satellite altitude was less than 500 km, it made GRACE considerably more sensitive than SLR to short wavelength terms in the gravity field. This not only resulted in better maps of the Earth's static gravity field but also permitted temporal variations in gravity to be determined down to scales of a couple hundred kilometers and shorter every three to four weeks (Wahr and Molenaar 1998). These temporal variations could be used to study a large variety of problems in a number of disciplines, from monitoring changes in water and snow storage on continents, to determining variability in seafloor

pressure, to measuring the redistribution of ice and snow on the polar ice caps, to constraining postglacial rebound deformation within the solid Earth (Dickey et al. 1997).

The disadvantage of having such a low altitude was that GRACE experiences greater atmospheric drag, which could cause large and unpredictable changes in the inter-satellite distance. To reduce this problem, each GRACE satellite had an on-board accelerometer to measure non-gravitational accelerations. Onboard accelerometers were used to detect the non-gravitational acceleration so that its effects could be removed from the satellite-to-satellite distance measurements. This non-gravitational acceleration was due to atmospheric drag, as well as solar and Earth radiation pressure. Afterwards, just the residuals would be used to infer the gravitational acceleration and thus to map the gravity field.

3.3.1. GRACE data levels:

Level-0:

The Level-0 data were the result of the data reception and collection by the Raw Data Center (RDC) of the Mission Operation System (MOS) located in Neustrelitz, Germany. Using tracking antennas in Weilheim (WHM) and Neustrelitz (NST), the MOS received the science instrument and housekeeping data twice per day from each GRACE satellite, which were stored in two appropriate files in the Level-0 rolling archive of the RDC. The Science Data System (SDS) regularly retrieved these files and extracted and reformatted the corresponding instrument and ancillary housekeeping data. Primarily for operational radio occultation data analysis, the raw data were also received during every pass at the GFZ polar Satellite Receiving Station (SRS) in Ny Ålesund (NYA) and forwarded to GFZ in Potsdam.

Level-1:

The Level-1A data products were the result of a non-destructive processing applied to the Level-0 data. The sensor calibration factors were applied in order to convert the binary encoded measurements to engineering units. Where necessary, time tag integer second ambiguity was resolved, and data were time tagged to the respective satellite receiver clock

time. Editing and quality control flags were added, and the data were reformatted for further processing. The Level-1A data were reversible to Level-0, except for the bad data packets. This level also included the ancillary data products needed for processing to the next data level.

The Level-1B data products were the result of a possibly destructive, or irreversible, processing applied to both the Level-1A and Level-0 data. The data were correctly time-tagged, and the data sample rate was reduced from the higher rates of the previous levels. Collectively, the processing from Level-0 to Level-1B was called the Level-1 Processing. This level also included the ancillary data products generated during this processing and the additional data needed for further processing such as the Level-1B Atmosphere and Ocean De-aliasing Product (AOD1B).

Level-2:

Level-2 data referred to the approximately monthly gravity field estimates reported in form of spherical harmonic coefficients. These data included the short term (monthly and weekly) and static gravity field derived from calibrated and validated GRACE Level-1B data products. This level also included ancillary data sets (e.g. mean atmospheric and oceanic mass variations) which are necessary to interpret time variability in gravity field solutions. The Level-2 processing software has been developed independently by all three processing centers. Routine processing was done at UTCSR and GFZ, while JPL was generating Level-2 products for verification purposes. The coefficients were distributed on the Level-2 data archives as GAC, GAD, and GSM files (GAC, GAD, and GSM were file extensions). The GSM files contained spherical harmonic coefficients representing the gravity field of the Earth. The atmospheric and oceanic mass signals effects had been removed from these coefficients. The GAC and GAD files included the modeled atmospheric and oceanic contributions to the GSM coefficients. The GAC files included the global atmospheric and oceanic effects, and the GAD files represented ocean bottom pressure variations. But in these files, signals from large lakes and water reservoirs are not included, so there are nonnegligible

signals in those areas which should be removed. The signal for each lake/water reservoir can be removed by computing the stokes coefficients caused by a uniform 1 m rise of lake/water reservoir, and then scaling those coefficients using monthly altimeter estimates (Birkett et al., 2009) (http://www.pecad.fas.usda.gov/cropexplorer/global_reservoir) of the lake/water reservoir surface height (Swenson and Wahr, 2007).

Level-3:

Level-3 data referred to the gridded version of Level-2 data sets, also were available with higher-sampling (1-degree at writing) spatial scaling factors (Landerer and Swenson 2012).

3.3.2. The end of GRACE

After more than 15 productive years in orbit, three times as long as originally planned, the GRACE satellite mission has ended science operations. Following an age-related battery issue on GRACE-2 in September 2017, it became apparent by mid-October 2017 that GRACE-2's remaining battery capacity would not be sufficient to operate its science instruments and telemetry transmitter. Consequently, the decision was made to decommission the GRACE-2 satellite and end GRACE's science mission.

GRACE was a pioneering mission that advanced our understanding across the Earth system, land, ocean, and ice. Due to the extreme success of GRACE in many Earth science disciplines, there was a long-standing strong request by the international user community to launch a GRACE Follow-On (GRACE-FO) mission to extend the GRACE mass transport time series with the minimum practical data gap between both missions.

3.3.3. GRACE Follow-On

The Gravity Recovery and Climate Experiment Follow-On (GRACE-FO) mission, a joint partnership between NASA and the German Research Centre for Geosciences (GFZ), launched on 22 May 2018. It uses twin satellites to accurately map variations in the Earth's

gravity field and surface mass distribution. It is designed as a successor to the GRACE mission. Conceptually very similar to the original GRACE mission (2002–2017), GRACE-FO consists of two identical satellites flying in formation around Earth at an initial altitude of approximately 490 kilometers and a nominal separation distance of 220±50 kilometers. Instruments on board the satellites precisely measure changes in the distance between them due to orbital perturbations caused by geographical and temporal variations in the Earth's gravity field. GRACE-FO expands GRACE's legacy of scientific achievements. These include tracking mass changes in the Earth's polar ice sheets and mountain glaciers (which impacts global sea level); estimating total water storage on land (from groundwater changes in deep aquifers to changes in soil moisture and surface water); inferring changes in deep ocean currents, a driving force in climate; and even measuring changes within the solid Earth itself, such as postglacial rebound and the impact of major earthquakes.

3.4. Earth's mass change estimation

The Earth's global gravity field is commonly described in terms of the shape of the geoid, a gravity equipotential surface, which best fits, in a least squares sense, global mean sea level. It is usual to expand the geoid shape N as a sum of spherical harmonics (see, e.g., Wahr et al. (1998))

$$N(\vartheta, \lambda, r)=\frac{GM}{r\gamma}\sum_{n=2}^{\infty}\sum_{m=0}^{cn}\left(\frac{r}{a}\right)^{-n}[C_{nm}\cos m\lambda+S_{nm}\sin m\lambda]\bar{P}_{nm}(\cos\vartheta) \tag{1.3}$$

where γ is the normal gravity vector. M is the total mass of the Earth, G is the universal gravitational constant, C_{nm} , S_{nm} are numerical coefficients, ϑ, λ are latitude and eastward longitude of point of computation, a is the Earth radius, and $\bar{P}_{nm}$ are normalized associated Legendre functions

$$\bar{P}_{nm}=\left(\frac{(2-\delta_{m0})(2n+1)(n-m!)}{(n+m)!}\right)^{1/2}P_{nm} \tag{2.3}$$

where δ is the Kronecker delta function. As a spherical approximation and r=a, we have:

$$N(\vartheta,\lambda,r)=a\sum_{n=2}^{\infty}\sum_{m=0}^{n}[C_{nm}\cos m\lambda+S_{nm}\sin m\lambda]\bar{P}_{nm}(\cos\vartheta) \tag{3.3}$$

A geoid model typically consists of numerical values for the C_{nm}, and S_{nm} variables. Redistribution of mass within the Earth and on or above its surface causes changes in the gravity field and geoid. Let $\Delta\rho(r,\vartheta,\lambda)$ be the density redistribution causing the geoid change. ΔN is a time-dependent change in the geoid, either the change in N at one time to another, or as the difference between N at one time and a time average of N, or as some other representation of a changing N. This change can be represented in terms of changes, ΔC_{lm} and ΔS_{lm}, in the spherical harmonic geoid coefficients as

$$\Delta N=a\sum_{n=2}^{\infty}\sum_{m=0}^{n}[\Delta c_{nm}\cos m\lambda+\Delta s_{nm}\sin m\lambda]\bar{P}_{nm}(\cos\vartheta) \tag{4.3}$$

According to Wahr et al. (1998) and Chao and Gross (1987), we have:

$$\begin{pmatrix}\Delta c_{nm}\\ \Delta s_{nm}\end{pmatrix}=\frac{3}{4\pi\rho_{ave}(2n+1)}\int\Delta\rho(r,\vartheta,\lambda)\bar{P}_{nm}(\cos\vartheta)\times\left(\frac{r}{a}\right)^{n+2}\begin{pmatrix}\cos(m\lambda)\\ \sin(m\lambda)\end{pmatrix}\cos\vartheta d\vartheta d\lambda dr \tag{5.3}$$

where ρ_{ave} is the average density of the Earth (=5517kg/m^3). $\Delta\rho$ is concentrated in a thin layer of thickness H at the Earth's surface. This layer must be thick enough to include those parts of the atmosphere, oceans, ice caps, and groundwater storage with significant mass variation. H is customarily determined by the thickness of the atmosphere and is about of 10–15 km. We can then define mass/area as surface density, $\Delta\sigma$, as the radial integral of $\Delta\rho$ through this layer:

$$\Delta\sigma(\vartheta,\lambda)=\int_{\text{thin layer}}\Delta\rho\,(r,\vartheta,\lambda)dr \tag{6.3}$$

The sum over (n, m) in Equation (3.3) can be truncated to degrees $<n_{\max}$, where, n_{max} is different in geoid models, for example in a satellite geoid model, at most, $n_{max}\approx100$. In view of H being thin enough that $(\frac{H}{a})^{n_{\max}+2} \ll 1$ then $(\frac{r}{a})^{n+2} \approx 1$, so Equation (5.3) reduces to

$$\begin{pmatrix}\Delta c_{nm}\\ \Delta s_{nm}\end{pmatrix}_{\text{solid Earth}} = \frac{3}{4\pi\rho_{ave}(2n+1)} \int \Delta\sigma(\vartheta,\lambda)\bar{P}_{nm}(\cos\vartheta)\times \begin{pmatrix}\cos(m\lambda)\\ \sin(m\lambda)\end{pmatrix} \cos\vartheta d\vartheta d\lambda \tag{7.3}$$

Equation (7.3) describes the contribution to the geoid from the direct gravitational attraction of the surface mass. We have also an additional geoid contribution because surface mass also loads and deforms the underlying solid Earth, using k_n as the load Love number of degree n (see Farrell 1972):

$$\begin{pmatrix}\Delta c_{nm}\\ \Delta s_{nm}\end{pmatrix}_{\text{solid Earth}} = \frac{3k_n}{4\pi\rho_{ave}(2n+1)} \int \Delta\sigma(\vartheta,\lambda)\bar{P}_{nm}(\cos\vartheta)\times \begin{pmatrix}\cos(m\lambda)\\ \sin(m\lambda)\end{pmatrix} \cos\vartheta d\vartheta d\lambda \tag{8.3}$$

The total geoid change is the sum of Equation (7.3) and Equation (8.3):

$$\begin{pmatrix}\Delta\hat{C}_{nm}\\ \Delta\hat{S}_{nm}\end{pmatrix} = \begin{pmatrix}\Delta C_{nm}\\ \Delta S_{nm}\end{pmatrix}_{\text{surface mass}} + \begin{pmatrix}\Delta C_{nm}\\ \Delta S_{nm}\end{pmatrix}_{\text{solid Earth}} \tag{9.3}$$

To summarize the results for ΔC_{nm} and S_{nm} , in a more compact form, we expand $\Delta\sigma$ as

$$\Delta\sigma(\vartheta,\lambda)=a\rho_w \sum_{n=0}^{\infty}\sum_{m=0}^{n} [\Delta\hat{C}_{nm}\cos m\lambda + \Delta\hat{S}_{nm}\sin m\lambda]\bar{P}_{nm}(\cos\vartheta) \tag{10.3}$$

where ρ_w is the density of water (assumed to be 1000 kg/m^3) and is included here so that $\Delta\hat{C}_{nm}$ and $\Delta\hat{S}_{nm}$ are dimensionless. We can use a trick to introduce a parameter $\Delta\sigma/\rho_w$ as the change in surface mass expressed in equivalent water thickness. By noting that the $\bar{P}_{nm}$ variables are normalized so that

$$\int_0^{\pi} \bar{P}_{nm}^2(\cos\vartheta)\cos\vartheta d\vartheta = 2(2-\delta_{m,0}) \tag{11.3}$$

we conclude from Equation (10.3) that

$$\begin{pmatrix}\Delta\widehat{C}_{nm}\\ \Delta\hat{S}_{nm}\end{pmatrix}=\frac{1}{4\pi\rho_w}\int_0^{2\pi}d\lambda\int_0^{\pi}\cos\vartheta d\vartheta\times\Delta\sigma(\vartheta,\lambda)\bar{P}_{nm}(\cos\vartheta)\begin{pmatrix}\cos(m\lambda)\\ \sin(m\lambda)\end{pmatrix} \tag{12.3}$$

using (8-3) in (9.3), and using (12.3), results a simple relation between $\Delta\widehat{C}_{nm}$, $\Delta\hat{S}_{nm}$ and ΔC_{nm}, ΔS_{nm}:

$$\begin{pmatrix}\Delta\widehat{C}_{nm}\\ \Delta\hat{S}_{nm}\end{pmatrix}=\frac{\rho_{ave}}{3\rho_w}\frac{2n+1}{1+k_n}\begin{pmatrix}\Delta C_{nm}\\ \Delta S_{nm}\end{pmatrix} \tag{13.3}$$

or, conversely,

$$\begin{pmatrix}\Delta C_{nm}\\ \Delta S_{nm}\end{pmatrix}=\frac{3\rho_w}{\rho_{ave}}\frac{1+k_n}{2n+1}\begin{pmatrix}\Delta\widehat{C}_{nm}\\ \Delta\hat{S}_{nm}\end{pmatrix} \tag{14.3}$$

Now, using Equation (13-3) in Equation (10-3), it is possible to find the change in surface mass density from changes ΔC_{nm} and ΔS_{nm} in the geoid coefficients.

$$\Delta\sigma(\vartheta,\lambda)=\frac{a\rho_{ave}}{3}\sum_{n=0}^{\infty}\sum_{m=0}^{n}\frac{2n+1}{1+k_n}\bar{P}_{nm}(\cos\vartheta)(\Delta C_{nm}\cos(m\lambda)+\Delta S_{nm}\sin(m\lambda)) \tag{15.3}$$

which can be used to find the change in surface mass density from changes ΔC_{nm} and ΔS_{nm} in the geoid coefficients. Similarly, using (14.3) in (4.3) gives

$$\Delta N=\frac{3a\rho_w}{\rho_{ave}}\sum_{n=2}^{\infty}\sum_{m=0}^{n}\frac{1+k_n}{2n+1}[\Delta\widehat{C}_{nm}\cos m\lambda+\Delta\hat{S}_{nm}\sin m\lambda]\bar{P}_{nm}(\cos\vartheta) \tag{16.3}$$

which together with (12.3) gives the change in the geoid from knowledge of the change in surface mass density.

3.5. Estimation of the Earth's mass changes using GRACE Level-2 data

Equation (15.3) is the starting point for using the GRACE Level-2 data to recover changes in surface mass density. The larger the degree in the spherical harmonic coefficients, the larger the errors in the GRACE Level-2 data and the larger the contributions to the sum in

Equation (15.3). There is little hope of GRACE recovering useful time-variable geoid coefficients for $n >\approx 100$. In fact, most of the recoverable time-dependent gravity signal will be concentrated at degrees well below 80 or so. On the other hand, because of the GRACE satellites' orbit geometry, the high-degree-order Stokes coefficients are dominated by noise (Chen et al. 2006). This high-frequency noise generates long and linear features oriented from north to south in the global GRACE fields, called stripes (see Figure 3.2).

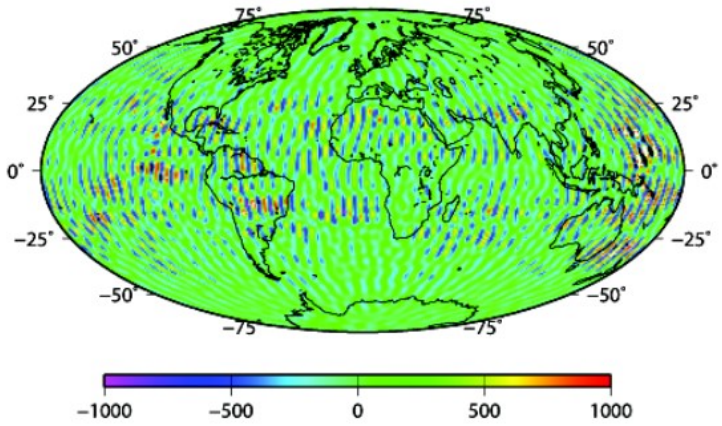

Figure 3.2: The 2002–2011 secular trend map (mm/year) over the world using JPL GRACE Level-2 data release 4.0 (Joodaki 2014).

These stripes do not represent geophysical signals, but they come from the GRACE K-band ranging system. This system provides inter-satellite distance variations, which produce temporal gravity field variations that suffer from a limited spatial resolution. The spatial resolution of GRACE is defined by the degree-order expansion of the GRACE coefficients as it is described in $\frac{20000}{n}$, where the higher coefficients refer to higher frequencies. Therefore, the generated "stripes" suggest a high degree of correlation in the Stokes coefficients at shorter wavelengths, which correspond to higher degree-order coefficients (spectral domain).

One simplified way of reducing and removing the stripes would be to truncate the Stokes coefficients to a relatively low degree and order, but this would cause losing geophysical signal while removing the systematic noise. Instead, different filtering techniques have been widely used to reduce this correlated noise and recover the Earth's surface mass changes that cause the gravity field variations, expressed by the Stokes coefficients' differences. The process of filtering the correlated coefficients as a function of degree and order is called decorrelation.

3.6. GRACE DATA decorrelation methods

By de-correlating the GRACE Stokes coefficients, noise is being suppressed, and the amplitude of the stripes decreases. For the reduction of the noisy GRACE data, a number of methods have been proposed: an isotropic Gaussian filter (Wahr et al. 1998), an anisotropic filter based on the calibrated error spectrum (Han et al. 2005), optimal filters based on a priori estimates of signal and measurement error variances (Swenson and Wahr 2002, Seo and Willson 2005, Chen et al. 2006), empirical decorrelation filters (Swenson and Wahr 2006, Chambers 2006, Wouters and Schrama, 2007, Chen et al. 2007, Duan et al. 2009), and decorrelation filters, which use a-priori data from a synthetic model (Kusche 2007, Klees et al. 2008, Kusche et al. 2009). The striping effects in the spatial domain reduce after de-correlating them, but they still exist after that. These remaining striping effects hint that noise leftovers still exist in higher frequencies, which is due to non-correlated errors (i.e., random or other systematic errors). Smoothing techniques like Gaussian isotropic or anisotropic filtering are usually applied to the de-correlated Stokes coefficients, causing smoothly averaged results. By filtering the GRACE coefficients, a part of the geophysical signals involved might also be removed simultaneously, which cannot be directly estimated. As the level of filtering increases, the geophysical signals reduce. Thus, the selection of the de-correlating and smoothing filtering parameters has a great impact on the geophysical signal loss; therefore, their selection is extremely critical. Additionally, the selection of the Gaussian-smoothing radius is more crucial than of the decorrelation methods. Higher radii

values imply stronger filtering, which decreases the amplitude of noise, thus producing more smoothed surface mass density changing fields. The level of smoothing is capable of reducing the geophysical signals' attendance. Therefore, the final radius and radii selection is based on the different levels of filtering intensity.

3.6.1. Gaussian isotropic smoothing

A Gaussian isotropic smoothing filter is a common isotropic averaging function, which is able to reduce the magnitude and the possible signal distortion at the high-degree-only GRACE coefficients. Jekeli (1981) developed this method to compensate for poorly known, short-wavelength spherical harmonic coefficients to improve estimates of the Earth's gravity field. This smoothing filter is degree-dependent spectrum only and is expressed by Equation (17.3):

$$W_n = \int_0^{\pi} W(\alpha) P_n\big(\cos(\alpha)\big) \sin(\alpha)\, d\alpha \tag{17.3}$$

with

$$W(\alpha) = \frac{b}{2\pi} \frac{\exp\ [-b(1-\cos\alpha)]}{1-e^{-2b}} \qquad \text{and} \qquad b = \frac{\ln\ (2)}{1-\cos\left(\frac{r}{R_E}\right)} \tag{18.3}$$

where α is the spherical distance between two points, r denotes the averaging or smoothing radius at which W has dropped to ½ its value at $\alpha = 0$. It is commonly used to indicate the degree of smoothing. R_E is the Earth's radius. Jekeli (1981) shows that the coefficients W_n can be computed with recursion formulae:

$$W_0 = 1 \tag{19.3}$$

$$W_n = \frac{1+e^{-2b}}{1-e^{-2b}} - \frac{1}{b} \tag{20.3}$$

$$W_{n+1} = -\frac{1+2n}{b} W_n + W_{n-1} \tag{21.3}$$

3.6.2. Terms with n=0, 1

The terms in (15.3) with n=0 and n=1 require discussion. The n=0 term is proportional to the total mass of the Earth where "the Earth" includes not only the solid Earth but also its fluid envelope (the oceans, atmosphere, etc.). This total mass does not change with time, and so ΔC_{00} from GRACE can be assumed to vanish. The n=1 terms are proportional to the position of the Earth's center of mass relative to the center of the coordinate system and so depend on how the coordinate system is chosen. One possibility is to choose a system where the origin always coincides with the Earth's instantaneous center of mass. In that case, all n=1 terms in the geoid are zero by definition, and so the GRACE results for $\Delta C_{nm}=\Delta S_{nm}=0$ for all n=1. Again, the n=1 coefficients for an individual component of the total surface mass need not vanish. Redistribution of mass in the ocean, for example, can change the center of mass of the ocean. However, that will induce a change in the center of mass of the solid Earth, so that the center of mass of the ocean + solid Earth remains fixed. Another possibility is to define the coordinate system so that its origin coincides with the center of figure of the Earth's solid outer surface. That is the usual way of defining the origin, since the coordinate system is determined using geodetic measurements of positions on the solid Earth's surface. In that case, the n=1 GRACE results for $\Delta C_{nm}=\Delta S_{nm}$ need not vanish, and the n=1 terms in (15.3) describe the offset between [the center of mass of the surface mass+ deformed solid Earth] and [the center of figure of the deformed solid Earth surface]. The reference frame origin used in the GRACE gravity field determination is the Earth's center of mass. In this frame, the degree one Stokes coefficients from the combined surface mass plus solid Earth are zero by definition, and so no multiplicative factor could allow the recovery of the (presumably) nonzero contribution of the surface mass alone. Thus, until now, there has been no known algorithm for inferring the degree one mass coefficients from the GRACE fields. But, to improve the accuracy and precision in deriving the Earth's mass changes, the coefficients are generally replaced by those calculated by Swenson et al. (2008).

3.6.3. Terms with n=2 and m=0

The n=2 terms are the longest wavelength terms in the series expansion (1.3). The Earth's oblateness is proportional to the lowest-degree zonal harmonics, C_{20} (or in another format as J_2). There is a secular increase in C_{20} which is consistent with a steady migration of mass from low latitudes towards high latitudes (Yoder et al. 1983, Rubincam 1984) (Appendix A). Due to the GRACE orbit geometry and the separation length between its satellites, C_{20} cannot be well determined from the GRACE data (Tapley et al. 2004b). The C_{20} estimates from GRACE also are well known to be affected by significant long-period tidal aliases. Therefore, some of the previous studies excluded the C_{20} value in the estimation of surface mass density (e.g., Wahr et al. 2004). The replacement of the GRACE C_{20} coefficient by its estimate from SLR improves the estimation of mass variations from GRACE (Chen et al. 2005). The SLR time series are also more precise, with about a third of the noise of the GRACE time series. Therefore, the monthly SLR estimates for C_{20} coefficient are generally used to replace the estimates from GRACE.

3.7. Glacial Isostatic Adjustment (GIA)

The effect of Glacial Isostatic Adjustment (GIA) of the lithosphere and mantle since the Last Glacial Maximum (LGM) is one of the sources of complicity of the extraction of the mass signals from GRACE and interpreting them as changes in the water content of hydrologic basins, or ocean bottom pressure, or ice sheet mass. GRACE detects not only present-day mass loss but also changes in the gravity field caused by ongoing GIA (Wahr et al. 2000, Velicogna and Wahr 2006, Ramilien et al. 2006), and it is not possible to separate these two signals from GRACE observations. Traditionally, separating mass change signals from GIA relies upon modeled estimates. Despite the divergence in spatial distribution and in the magnitudes of the modeled GIA signals, the size of the errors in GIA models constitutes a significant proportion of the signal. The reason for this is that these models involve reconstructions of the past ice load since the LGM and require parameterizations of the

Earth's rheology (elastic and viscous properties) which are generally poorly constrained and uncertain. There are three general sources of error in the GIA estimates: the ice (deglaciation) history, the viscosity profile of the mantle, and physical and numerical approximations in the model. Comparing 14 GIA models from different authors, Guo et. al. (2012) showed that the accuracy and consistency of GIA models need to be substantially improved to fully exploit GRACE data, to enhance the constraints on ice-sheet mass balance and the mass component of global sea level change. Figure 3.3 shows the effects of GIA of the lithosphere and mantle using A et al.'s (2013) model. This model has a compressible Earth and uses the ICE-5G deglaciation history and VM2 viscosity profile, and the same PREM-based elastic structure as Peltier (2004). The model includes polar wander feedback (computed as described in Mitrovica et al. 2005), uses the self-consistent sea level equation to distribute meltwater into the ocean, and includes degree-one terms when computing the uplift rate. The uncertainty of this model is about ± 20%. This uncertainty comes from looking at results for various viscosity values and alternative deglaciation models for Antarctica and Greenland.

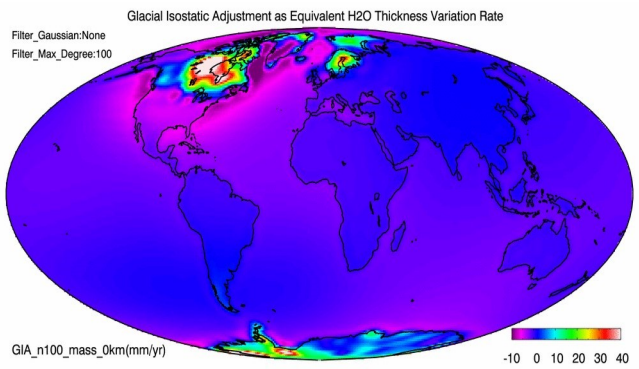

Figure 3.3. Effects of GIA of the lithosphere and mantle (Courtesy to GRACE Tellus et al. 2013).

3.8. Spatial averaging

Because the spatial resolution of GRACE is on the order of a few hundred kilometers, an estimate of a surface mass anomaly will not be a point measurement, but rather a spatial

average. Wahr et al. (1998) introduced an averaging method based on a simple Gaussian filter. However, this method does not isolate a specific region. Many applications require estimates of mass variability for specific regions. Various methods have been used for improving the GRACE mass estimates for specific regions though most of them are similar to one another (Swenson and Wahr 2002, Swenson et al. 2003, Seo and Wilson 2005, Chen et al. 2006, Han et al. 2005). These methods fall into one of two categories: smoothing the surface mass results, or averaging over specific regions. These sorts of problems are better addressed by constructing specific averaging functions optimized for those regions, than by smoothing the surface mass results. For example, an exact regional average would take the form

$$\Delta\sigma_{region}=\frac{1}{\Omega_{region}}\int \Delta\sigma(\vartheta,\lambda)\upsilon(\vartheta,\lambda)\sin\vartheta d\vartheta d\lambda \tag{22.3}$$

where Ω_{region} is the angular area of the region of interest, and $\upsilon(\vartheta,\lambda)$ is a function that describes the shape of the basin (e.g., a river basin, a region of the ocean floor, an ice sheet, a political boundary) according to

$$\nu(\vartheta,\lambda)=\begin{cases}1 & \text{Inside the basin}\\ 0 & \text{Outside the basin}\end{cases} \tag{23.3}$$

Equation (22.3) can be expressed as a sum of Stokes coefficients:

$$\Delta\sigma_{region}=\frac{a\,\rho_{ave}}{3\Omega_{region}}\sum_{n=0}^{\infty}\sum_{m=0}^{n}\frac{(2n+1)}{(1+k_n)}(\nu^c_{nm}\Delta C_{nm}+\nu^s_{nm}\Delta S_{nm}) \tag{24.3}$$

where ν^c_{nm} and ν^s_{nm} are the harmonic coefficients describing $\nu(\vartheta,\lambda)$:

$$\nu(\vartheta,\lambda)=\frac{1}{4\pi}\sum_{n=0}^{\infty}\sum_{m=0}^{n}\bar{P}_{nm}(\cos\vartheta)\,(\nu^c_{nm}\cos m\lambda+\nu^s_{nm}\sin m\lambda) \tag{25.3}$$

$$\begin{Bmatrix}\nu^c_{nm}\\ \nu^s_{nm}\end{Bmatrix}=\int \nu(\vartheta,\lambda)\bar{P}_{nm}(\cos\vartheta)\begin{Bmatrix}\cos m\lambda\\ \sin m\lambda\end{Bmatrix}d\Omega \tag{26.3}$$

One effect of the basin coefficients in equation (24.3) is to reduce the contribution to $\Delta\sigma_{region}$ from the stockes coefficients for large n. Since the averaging function, $\nu(\vartheta,\lambda)$ in this case, changes abruptly from 1 to 0 along the edge of the region, it has power at short spatial scales. Thus ν^{c}_{nm} and ν^{s}_{nm} can be relatively large at high degrees, and so this estimate of $\Delta\sigma_{region}$ can be inaccurate. The expansion of an averaging kernel that varies smoothly across the basin boundary has less power in its short wavelength coefficients than does the exact averaging kernel. The basin average computed using a smoothed averaging kernel will less accurately represent the true basin average. This approximate average will be influenced by mass signals outside the basin, referred to as leakage, as well as over- or under-estimating the contribution of the signal inside the basin. While the approximation error cannot be eliminated, one can create smoothed averaging kernels that produce a reduction in satellite measurement error while keeping the amount of leakage error in the basin-averaged estimates of surface-mass change to an acceptable level for basins having length scales of a few hundred kilometers and larger. Swenson and Wahr (2002) described two types of averaging kernels. The first kind, which is relatively simple to visualize and compute, incorporates a Gaussian filter, and the second kind is more complicated but provides a means of minimizing either the leakage error or the satellite measurement error, or the sum of the two.

3.9. Least squares mascon fitting

The concept “mascon” stands for “mass concentration” and is a user-defined region of the Earth’s surface. It originates from Muller and Sjogren (1968), who have used mascons to model the gravity field of the moon. There are three classes of GRACE mascon solutions that are used to study time-variable gravity. The first class of mascon solution is one in which an analytic expression for the mass concentration function is provided, and explicit partial derivatives relating the inter-satellite range-rate measurements to the analytic mascon formulation are used to directly estimate mass variations. An example of this first type of mascon solution is found in Ivins et al. (2011), where spherical cap mascons are estimated directly from range accelerations to interpret the regional ice mass loss and (GIA) processes.

The second class of mascon solution comes from the group at NASA Goddard Space Flight Center (Luthcke et al. 2006a, Rowlands et al. 2010, Sabaka et al. 2010, Luthcke et al. 2013). This type of mascon solution shares commonality with the first type of mascon solution in the sense that the mascon basis functions are directly related to the inter-satellite range-rate measurements through explicit partial derivatives, which are used in the gravity estimation. The difference is that each mascon basis function is represented by a finite truncated spherical harmonic expansion, rather than an analytical expression, such that the functional representation of each mascon has signal power outside of the mascon boundary. Finally, the third class of so-called "mascon" solutions or "Least Squares Mascon Fitting (LSMF)" are when users fit mass elements to spherical harmonic coefficients (from spherical harmonic GRACE solutions) to reduce satellite measurement error, leakage error, and correlated error (striping error). These are not true mascon solutions in the sense that there is no direct relation between the formulation of the mass elements and the inter-satellite range-rate measurements (i.e., there are no explicit partial derivatives relating the observations to the state). Examples of this type of mascon solution include Tiwari et al. (2009), Jacob et al. (2012), Joodaki et al. (2014), Schrama et al. (2014), and Velicogna et al. (2014).

Having more than one mascon is necessary in the LSMF solution. In this solution, mascon amplitudes are fitted to the GRACE Stokes coefficients to obtain estimates of the monthly mass variability of each mascon. For each mascon, the set of Stokes coefficients are found such that they would be resulted by a unit mass distributed uniformly over that mascon. Let the degree n and order m Stokes coefficients for mascon i be (C_{nm}^{i}, S_{nm}^{i}). Let the actual, but unknown, mass of mascon i be M_i. The M_is for all mascons are estimated by fitting them simultaneously to the GRACE monthly Stokes coefficients.

Let (ΔC_{nm}, ΔS_{nm}) be the GRACE coefficients at time t, after removing the mean of all monthly solutions (and after removing the hydrology and GIA models). The mean must be removed because otherwise contributions from the Earth's interior, which dominate the mean signal, would be misinterpreted as surface mass signals. As a result, GRACE can be used to determine change of total water storage, but not total water storage. Before fitting, the

GRACE Stokes coefficients and the Stokes coefficients for each mascon are multiplied by $W_n\,(2n+1)/(1+k_n)$, where W_n are the coefficients of the Gaussian smoothing function, and the k_n are load Love numbers to transform these geoid coefficients into smoothed spherical harmonic coefficients of mass (Wahr et al. 1998). A Gaussian smoothing function is applied to the Stokes coefficients to reduce the noise in the monthly M_i time series. These modified Stokes coefficients are denoted with asterisks (i.e. $\Delta C^{*}_{nm}(t)$, $C^{*,i}_{nm}$, etc.) and the $\{M_i(t)\}$ are found such that they minimize the standard least squares merit function:

$$E=\sum_{n,m}\left[\left(\Delta C^{*}_{nm}(t)-\sum_{i} C^{*,i}_{nm}M_i(t)\right)^2+\left[\left(\Delta S^{*}_{nm}(t)-\sum_{i} S^{*,i}_{nm}M_i(t)\right)^2\right]\right. \tag{27.3}$$

For each monthly time step, t. The $\{Mi(t)\}$ that minimize (27.3) solve

$$Y_j(t)=\sum_{i} B_{ji}\,M_i(t) \tag{28.3}$$

where

$$Y_j(t)=\sum_{nm}(\Delta C^{*}_{nm}(t)C^{*,j}_{nm}+\Delta S^{*}_{nm}(t)S^{*,j}_{nm}) \tag{29.3}$$

$$B_{ji}=\sum_{nm} C^{*,j}_{nm}\,C^{*,i}_{nm}+S^{*,j}_{nm}S^{*,i}_{nm} \tag{30.3}$$

The solution to (28.3) is

$$M_i(t)=\sum_{j} B^{-1}_{ij}Y_j(t) \tag{31.3}$$

Ideally, the solution for $M_i(t)$ would recover the true spatial average of mascon *i*'s mass: It means a spatial average that samples every point inside the mascon with a sensitivity of 1, and every point outside with a sensitivity of 0. Unfortunately, because of the finite number of harmonic degrees in the GRACE solution (for example, n_{max}=60 for CSR solutions), this is not the case. It is possible to determine the sensitivity kernel of each mascon solution,

which not only provides insight into possible biases in those solutions but also can help when deciding how to choose mascon sizes, shapes, and locations.

Let $\Delta\sigma(\vartheta,\lambda, t)$ be the surface mass at co-latitude ϑ, longitude λ, and time t. Because the inverted mascon masses, M_i, are linearly related to the GRACE coefficients (through (31.3)), and those coefficients are linearly related to $\Delta\sigma(\vartheta,\lambda, t)$ (through Newton's Law of Gravity), there must be a linear relation between each M_i and $\Delta\sigma(\vartheta,\lambda, t)$. The most general linear relation has the form

$$M_i(t)=\int \Delta\sigma(\vartheta,\lambda, t)A_i(\vartheta,\lambda)a^2\sin\vartheta d\vartheta\, d\lambda \qquad (32.3)$$

where $A_i(\vartheta,\lambda)$ is the sensitivity kernel for mascon i, and would ideally equal 1 for points inside the mascon and 0 outside, and *a* is the mean radius of the Earth. In order to explain about $A_i(\vartheta,\lambda)$, note that equations (28.3)–(30.3) imply a linear relation between M_i and the GRACE Stokes coefficients:

$$M_i(t)=\sum_{nm}\left[A^{C,i}_{nm}\Delta C_{nm}(t)+A^{S,i}_{nm}\Delta S_{nm}(t)\right] \qquad (33.3)$$

where the factors $A^{C,i}_{nm}$, $A^{S,i}_{nm}$ can be determined as described below. The relation between the Stokes coefficients and $\Delta\sigma(\vartheta,\lambda, t)$, implied by Newton's Law of Gravity, is (Wahr et al. 1998)

$$\begin{pmatrix}\Delta C_{nm}(t)\\ \Delta S_{nm}(t)\end{pmatrix}=\frac{3(k_n+1)}{4\pi\rho_{ave}a^3(2n+1)}\int \Delta\sigma(\vartheta,\lambda,t)P_{nm}(\cos\vartheta)\begin{pmatrix}\cos(m\lambda)\\ \sin(m\lambda)\end{pmatrix}a^2\sin\vartheta d\vartheta d\lambda \qquad (34.3)$$

where the $P_{nm}(\cos\vartheta)$ are Associated Legendre functions, and ρ_{ave} is the Earth's mean density. Putting (34.3) into (33.3) gives

$$M_i(t)=\int \Delta\sigma(\vartheta,\lambda,t)\, a^2\sin\vartheta d\vartheta d\varphi\sum_{nm}\frac{3(k_n+1)}{4\pi\rho_{ave}a^3(2n+1)}P_{nm}(\cos\vartheta)(A^{c,i}_{nm}(t)\cos(m\lambda)+A^{s,i}_{nm}\sin(m\lambda))$$

(35.3)

Comparing (35.3) with (32.3), the sensitivity kernel is:

$$A_i(\vartheta,\lambda)=\sum_{nm} P_{nm}(\cos\vartheta)\left(A_{nm}^{C,i}\cos(m\lambda)+A_{nm}^{S,i}\sin(m\lambda)\right)\frac{3(k_n+1)}{4\pi\rho_{ave}a^3(2n+1)} \tag{36.3}$$

Consequently, the sensitivity kernel can be determined from knowledge of $A_{nm}^{C,i}$ and $A_{nm}^{S,i}$. We can determine these terms numerically, as follows.

Define a synthetic set of Stokes coefficients, where $\Delta C_{n'm'}(t) = 1$ for a single (n', m'), and all other Stokes coefficients are 0. Apply the fitting procedure described in (29.3)–(31.3) to this simple set of Stokes coefficients. From (33.3) we know the result for $M_i(t)$ equals $A_{n'm'}^{c,i}$. Repeating this for each (n', m'), and then for the $\Delta S_{n'm'}$'s as well, yields every $A_{n'm'}^{c,i}$, and $A_{n'm'}^{s,i}$, one at a time, which can then be put into (36.3) to obtain the sensitivity kernel. These steps can be repeated for every mascon i. It can be shown that the mascon sensitivity kernels have the following useful property. Let *i* and j represent any two mascons used in a simultaneous mascon fit, and let $A_i(\vartheta,\varphi)$ be the sensitivity kernel for mascon *i*. Then

$$\frac{1}{S_j}\int_{S_j} A_i(\vartheta,\varphi)\sin\vartheta d\vartheta d\varphi=\delta_{i,j} \tag{37.3}$$

where S_j is the surface area of mascon j: it means that the area-averaged sensitivity kernel of a mascon is 1 over itself and 0 over any other mascon used in the simultaneous inversion. This implies that if a mass anomaly is distributed uniformly across a mascon, the solution for that mascon will deliver the true mascon average, and that this mass anomaly will not contaminate the solution for any other mascon.

3.10. Estimating groundwater storage using GRACE data

GRACE data have no vertical resolution, in the sense that it is impossible to use the GRACE data alone to determine how much of the mass variability comes from surface water or snow, how much comes from water stored in the soil, and how much comes from water in the sub-

soil layers (i.e., from groundwater). The GRACE-based anomaly of total water storage (ΔTWS) refers to all forms of water stored on and underneath the Earth's surface:

$$\Delta TWS=\Delta W_{Surface\ water}+\Delta W_{Soil\ water}+\Delta W_{Snow}+\Delta W_{Groundwater} \quad (38.3)$$

According to Equation (38.3), to isolate the changes in groundwater storage, the contributions of the other hydrological reservoirs, i.e., surface water ($\Delta W_{Surface\ water}$), soil water ($\Delta W_{Soil\ water}$), and snow ($\Delta W_{Snow}$) should be removed from ΔTWS:

$$\Delta W_{Groundwater}=\Delta TWS-\Delta W_{Surface\ water}-\Delta W_{Soil\ water}-\Delta W_{Snow} \quad (39.3)$$

The contributions from the individual hydrological reservoirs are obtained from external sources, e.g., hydrological model outputs, in-situ data, or other remotely sensed observations. If in-situ observations were publicly unavailable during the time period of interest, this separation will be done using monthly output from global, gridded hydrological land surface models (LSMs).

3.10.1. Hydrological land surface models (LSMs)

Land models are classically used as tools to integrate terrestrial contributions and responses to weather, climate variability, and climate change. In addition, modern land models are increasingly expected to provide insight into weather and climate impacts of societally relevant quantities such as water availability, crop and timber yields, wildfire risk, human heat stress, and other ecosystem services (Bonan and Doney 2018). Two kind of hydrological models are generally used to remove the contributions of the different hydrological reservoirs from the GRACE-based anomaly of total water storage (ΔTWS): different versions of NASA's Global Land Data Assimilation System (GLDAS) model, and a version of the Community Land Model (CLM). These models afford values for soil moisture, snow cover, and canopy storage. The CLM includes a groundwater component, but GLDAS models do not. None of the models include surface storage in lakes or rivers or marshes, and none of them include anthropogenic contributions.

Community Land Model (CLM)

The CLM, which is the land component of the Community Earth System Model (CESM) (Gent et al. 2011) simulates the partitioning of mass and energy from the atmosphere, the redistribution of mass and energy within the land surface, and the export of fresh water and heat to the oceans. To realistically simulate these interactions, the CLM includes terrestrial hydrological processes such as interception of precipitation by the vegetation canopy, through fall, infiltration, surface and subsurface runoff; snow and soil moisture evolution; evaporation from soil and vegetation; and transpiration (Oleson et al. 2013). The current version of CLM is CLM 5.0, and the other versions are CLM 2.0, CLM 2.1, CLM 3.0, CLM 3.5, CLM 3.0, and CLM 3.5.

3.10.2. Global Land Data Assimilation System

GLDAS) is a high-resolution, offline (uncoupled to the atmosphere) terrestrial modeling system that integrates a large quantity of satellite- and ground-based and model (re)analysis data by using them to parameterize, force, and constrain sophisticated numerical (LSMs) towards the goal of producing physically consistent, high-resolution fields of land surface states (e.g., snow, land surface temperature, soil moisture) and fluxes (e.g., evapotranspiration, runoff) (Rodell et al. 2004). GLDAS can run on local, regional, continental, or global domains at spatial resolutions from 1˚ down to 1 km. GLDAS typically executes at 1/4˚ and 1˚ spatial and three-hourly to monthly temporal resolution. A primary objective of GLDAS is to allow users to run multiple LSMs without specific knowledge of the model's architecture or physics. GLDAS currently drives four LSMs, namely Noah, the CLM, VIC, and MOSAIC. GLDAS simulations go back to 1979 and run through to the present.

Chapter 4

Numerical Investigations

The main goal of this Ph.D. is to study monitoring the groundwater storage changes (GWS) across the six main water basins of Iran. We based our research on two methods of monitoring. The first is a traditional method based on well observation data, and the second method is the GRACE least squares mascon fitting solution, which has been described in section 3.9. Groundwater changes for all of the study areas have been computed and presented in separate figures. The groundwater trends for every water basin have been computed for these two methods. To estimate the time series of groundwater storage changes using both the GRACE data and its necessary corrections and well data, a software package has been developed. The practical methods for both well data and GRACE data will be explained in the beginning of the coming sections.

4.1. Groundwater level changes monitoring based on the well data

There are 17,865 active observation wells in the whole of Iran. In order to study well level time series in six main basins, each main water basin is divided into several sub-basins, which have been described in chapter 2. Each sub-basin is divided into several study areas too. The Thiessen polygon method has been used to make a time series of the groundwater level across each study area. Then we scale up it for each study area by multiplying it by

the ratio: ($\frac{\text{area of the study area}}{\text{area of the Thiessen polygon}}$). The total change in groundwater storage across each sub-basin is computed by adding together the scaled change in groundwater storage of all its study areas. The same procedure is carried out for each main water basin. The results for each of Iran's main water basins and its sub-basins are represented in detail in the following sections.

The observations of all well data have been collected from Iran Water Resources Management Company. These data are categorized based at monthly intervals, where Iran's water year is defined as the period between October 1st of one year and September 30th of the next.

Figure 4.1 shows groundwater storage from observation well water level in 32 sub-basins across Iran, during 2002–2017. This map shows contours of water-level declines, in ($Mm^3/year$=Million cubic meter per year).

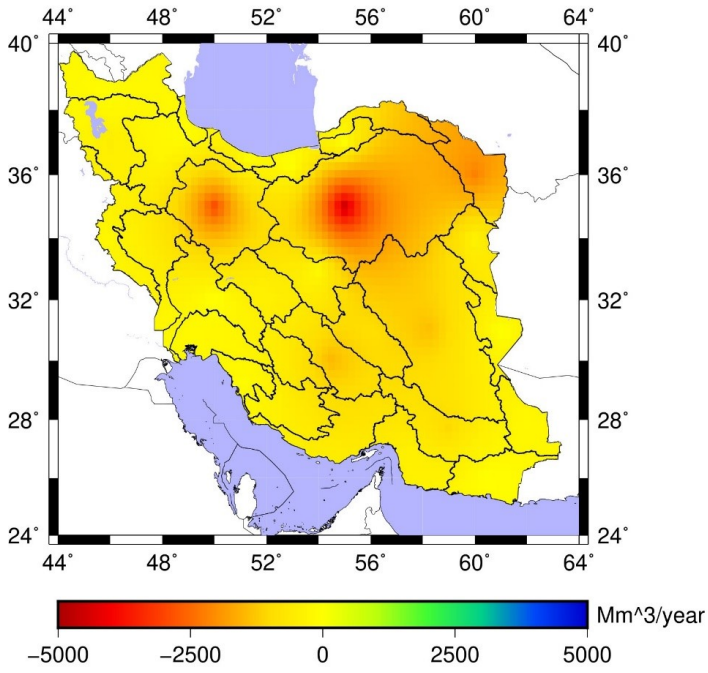

Figure 4.1. Secular trend in Million cubic meter ($Mm^3/year$) groundwater storage across Iran, computed from water level inferred from observation wells in 32 sub-basins in Iran, during 2002–2017.

We see a significant negative trend of water level in most of the sub-basins in Iran, with the exception of some of the sub-basins in the Persian Gulf water basin. Obviously, there are two intensive trends of water decline in the Central Plateau.

We can recognize the variety of secular trend in groundwater storage from 600 to -4,400 Mm^3 across Iran. There are two intensive negative trends in this figure. These two areas are in the Central Plateau basin and mostly located in arid and semi-arid areas. The most populated cities are located there. As mentioned before, the agriculture sector is the largest consumer of water in Iran. These estimations represent climate variability and changes in agriculture pattern. It also needs to be remembered that during a drought period, there is intensive pressure on groundwater storage especially in arid areas. All these reasons cause severe negative trends in the Central Plateau.

There are some positive trends in the southwest located in the Persian Gulf and the Oman Sea catchment and in the southeast. As mentioned in chapter 2, the Persian Gulf water basin has almost half of the country's renewable water resources. This area even has low precipitation, but it has some rivers, so it provides a large contribution to Iran's water resources. Therefore, in this area, rivers provide some of the requirements of the agriculture sector, and there is less pressure on the groundwater. In addition to this, irrigating with surface water might be a new means of groundwater recharge. Another possible reason for these positive features is the construction of new dams in the region. Constructing dams probably results in more recharge aquifers in the area.

The positive features of the southeast may be explained by new irrigation methods that are starting to be used in the basin. Farther west, various Afghan governments constructed large dams (Arghandab Dam, Kajaki Dam) that diverted water from the upper reaches of the river (Weier 2002).

In order to investigate water level time series, we need long periods and short periods of these data. We use a general expression of the following formula to obtain them:

$$f = A + Bt + \sum_i C_i \cos(\omega_i t) + D_i \sin(\omega_i t) + \varepsilon \tag{1.4}$$

where f is water level for each study area, A is a static value, B is the secular trend, C_i and D_i are amplitude of angular frequencies ω_i. The variable ε characterizes noise.

To show the groundwater level changes better in each water basin, These changes has been divided in two components: long-period (inter-annual and secular trend) components and short-period (semi-annual) components.

4.1.1. The Central Plateau basin (code 4)

Based on 13,000 active well data, the main water basin is divided into nine sub-basins, which have been described in section 2.6. (see Table 2.3). These nine sub-basins have 233 study areas, and the well data of 190 of them are available. Using the Thiessen method described in Appendix A and section 4.1., the water level for every study area has been computed. The total change in groundwater storage across each sub-basin is computed by adding together the scaled change in groundwater storage of all the study areas in that sub-basin. The same procedure is carried out for each main water basin. The results for the Central Plateau water basin and its sub-basins are represented in detail in the following sections.

Based on time series of the well data across each study area, using formula (1.4), we have computed the long period (i.e, inter-annual and secular trend) components of groundwater changes and the short period (i.e, semi-annual) components for that area. Since a picture is worth a thousand words, we decided to illustrate the numerical results in a graphical form. Figure 4.2 shows changes in monthly values of groundwater storage inferred from the well data, its long-period and short-period:

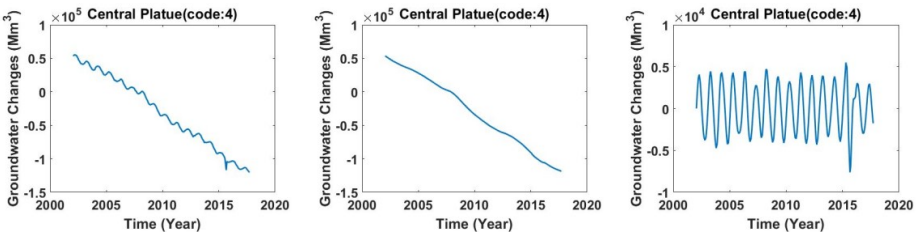

a b c

Figure 4.2. a) Monthly values of groundwater storage, b) long-period of monthly values of groundwater storage, c) short-period of monthly values of groundwater storage across the Central Plateau basin (code 4).

Figure 4.2 b) shows steady groundwater depletion in the Central Plateau, during 2002 to 2017. This basin was depleted by more than 1.5×10^5 Mm^3 during these 15 years. Figure

4.2 c) clearly shows seasonal groundwater changes in the Central Plateau. These seasonal changes are between -0.5×10^5 and 0.5×10^5 Mm^3.

In most of the study areas in the Central Plateau, there is minimum groundwater storage around 2008. We know that a drought occurred in 2007 in Iran. Therefore, it could be explained by a delay in the soil absorbing the water and reaching aquifers. This delay depended on the specific yield for each area.

After calculating groundwater storage changes for the whole Central Plateau, we focus on sub-basins' groundwater changes. Based on time series of the well data across each sub-basin, using formula (1.4), we have computed a trend of groundwater depletion for that area, and its annual and semi-annual signal. We can see changes in monthly values of groundwater storage inferred from the well data, its long-period and short-period, for each study area of the Central Plateau in Appendix B. The water level of the sub-basins of the Central Plateau will be shown in the following sections, and in following figures, the groundwater changes in the nine sub-basins of the Central Plateau will also be shown.

Daryache Namak (code 41)

This sub-basin is located between 33°-37° N and 48°-42° E with 35 study areas, of which the groundwater level data of 29 are available. Changes in monthly values of groundwater storage inferred from the well data, its long-period and short-period, for 29 study areas have been illustrated in Appendix B (figures B.1 to B.29).

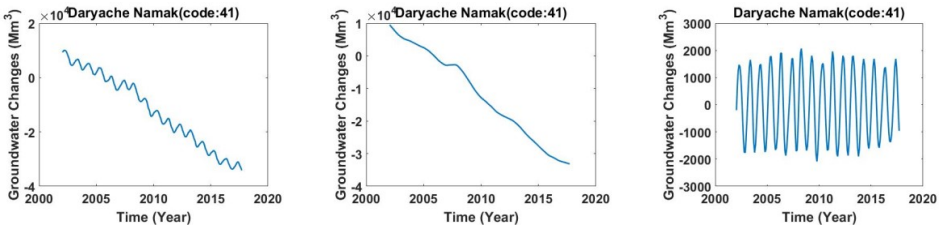

Figure 4.3. a) Monthly values of groundwater storage, b) long-period of monthly values of groundwater storage, c) short-period of monthly values of groundwater storage across Daryache Namak (code 41).

Figure 4.3 shows changes in monthly values of groundwater storage inferred from the well data, its long-period and short-period.

GavKhouni (code 42)

This sub-basin is located between 32° 10′-33° 40′N and 50° 30′-43° 23′E with an area of 41,552.3 km^2. This sub-basin has 21 study areas, of which the groundwater level data of 17 are available. Changes in monthly values of groundwater storage inferred from the well data, its long-period and short-period (inter-annual and semi-annual signal), for 17 study areas have been illustrated in Appendix B (figures B.30 to B.46). Figure 4.4 shows changes in monthly values of groundwater storage inferred from the well data, its long-period and short-period.

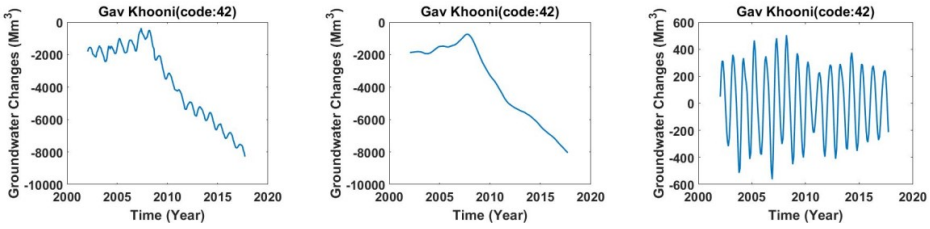

a b c

Figure 4.4. a) Monthly values of groundwater storage, b) long-period of monthly values of groundwater storage, c) short-period of monthly values of groundwater storage across GavKhouni (code 42).

Tashtak-Bakhtegan (code 43)

This sub-basin is located between 29°10′-31°14′ N and 51°42-44°32′E with an area of 31,451.8 km^2. This sub-basin has 26 study areas, of which the groundwater level data of 19 are available. Changes in monthly values of groundwater storage inferred from the well data, its long-period and short-period (inter-annual and semi-annual signal), for 19 study areas have been illustrated in Appendix B (figures B.47 to B.71). Figure 4.5 shows changes in monthly values of groundwater storage inferred from the well data, its long-period and short-period.

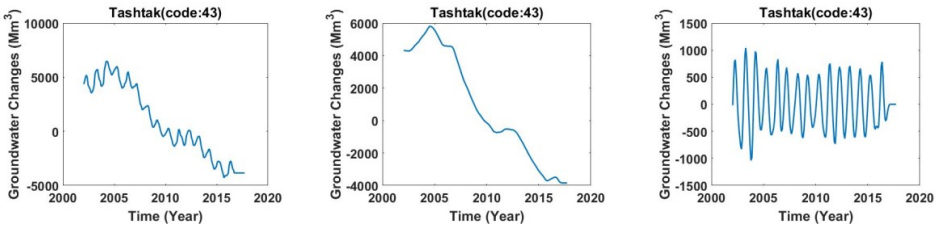

a b c

Figure 4.5. a) Monthly values of groundwater storage, b) long-period of monthly values of groundwater storage, c) short-period of monthly values of groundwater storage across Tashtak-Bakhtegan (code 43).

Abarghoo-Sirjan (code 44)

This sub-basin is located between 29°-32° N and 52°-46° 25′E with an area of 57,124.3 km^2. This sub-basin has 19 study areas, and the groundwater level data of all are available. Changes in monthly values of groundwater storage inferred from the well data, its long-period and short-period (inter-annual and semi-annual signal), for 19 study areas have been illustrated in Appendix B (figures B.72 to B.90). Figure 4.6 shows changes in monthly values of groundwater storage inferred from the well data, its long-period and short-period.

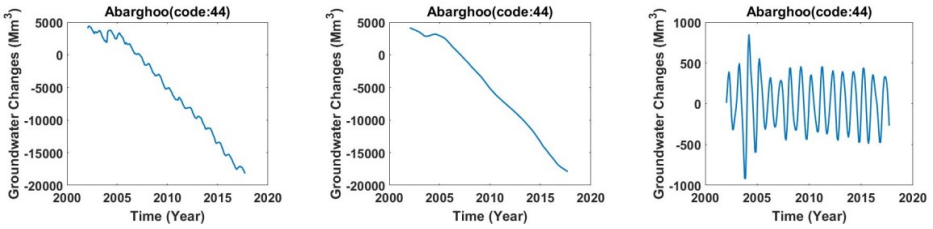

a b c

Figure 4.6. a) Monthly values of groundwater storage, b) long-period of monthly values of groundwater storage, c) short-period of monthly values of groundwater storage across Abarghoo-Sirjan (code 44).

Hamoon Jazmoorian (code 45)

This sub-basin is located between 26°20′-29°30′ N and 56°20′-61° 30′E with an area of 69374.80 km^2. This sub-basin has 20 study areas, of which the groundwater level data of 11 are available. Changes in monthly values of groundwater storage inferred from the well data, its long-period and short-period (inter-annual and semi-annual signal), for 11 study areas have been illustrated in Appendix B (figures B.91 to B.101). Figure 4.7 shows

changes in monthly values of groundwater storage inferred from the well data, its long-period and short-period.

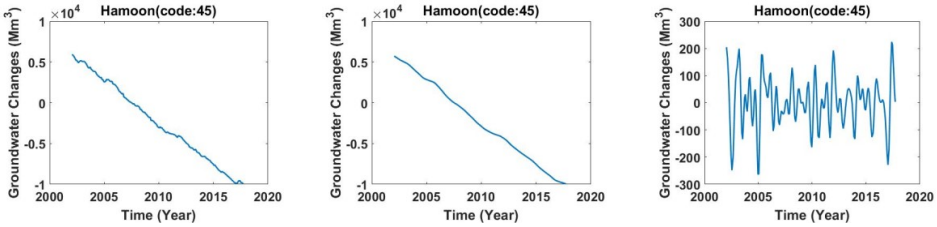

a b c

Figure 4.7. a) Monthly values of groundwater storage, b) long-period of monthly values of groundwater storage, c) short-period of monthly values of groundwater storage across Hamoon Jazmoorian (code 45).

Kavir Loot (code 46)

This sub-basin is located between 27°7′-34° N and 55°17′-61° 11′E with an area of 206,354.03 km^2. This sub-basin has 36 study areas, of which the groundwater level data of 25 are available. Changes in monthly values of groundwater storage inferred from the well data, its long-period and short-period (inter-annual and semi-annual signal), for 25 study areas have been illustrated in Appendix B (figures B.102 to B.126). Figure 4.8 shows changes in monthly values of groundwater storage inferred from the well data, its long-period and short-period.

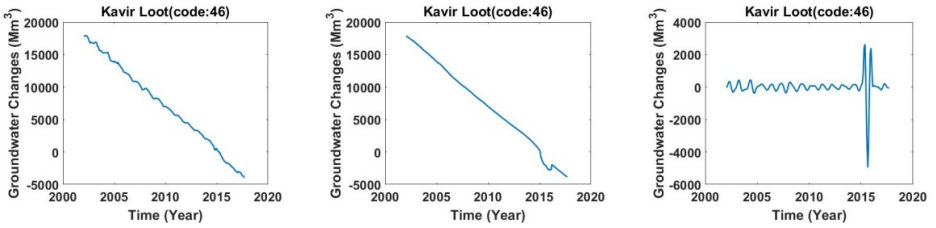

a b c

Figure 4.8. a) Monthly values of groundwater storage, b) long-period of monthly values of groundwater storage, c) short-period of monthly values of groundwater storage across Kavir Loot (code 46).

Kavir Markazi (code 47)

This sub-basin is located between 32°35′-37°26′ N and 51°45′-49° 34′E with an area of 226,533 km^2. This sub-basin has 49 study areas, of which the groundwater level data of

44 are available. Changes in monthly values of groundwater storage inferred from the well data, its long-period and short-period (inter-annual and semi-annual signal), for 44 study areas have been illustrated in Appendix B (figures B.127 to B.171). Figure 4.9 shows changes in monthly values of groundwater storage inferred from the well data, its long-period and short-period.

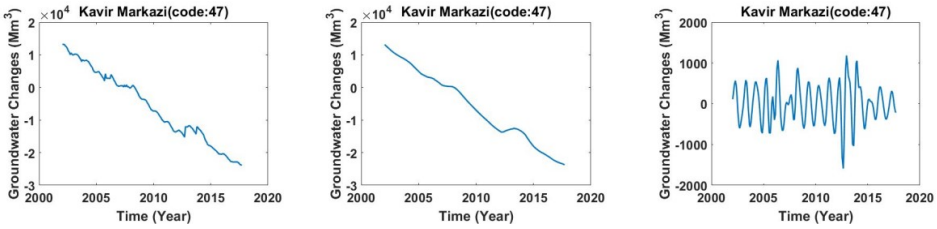

a b c

Figure 4.9. a) Monthly values of groundwater storage, b) long-period of monthly values of groundwater storage, c) short-period of monthly values of groundwater storage across Kavir Markazi (code 47).

Kavir SiahKooh (code 48)

This sub-basin is located between 31°15′-34° N and 51°30′-45° 30′E with an area of 48,599 km^2. This sub-basin has 11 study areas, of which the groundwater level data of 10 are available. Changes in monthly values of groundwater storage inferred from the well data, its long-period and short-period (inter-annual and semi-annual signal), for 10 study areas have been illustrated in Appendix B (figures B.172 to B.181). Figure 4.10 shows changes in monthly values of groundwater storage inferred from the well data, its long-period and short-period.

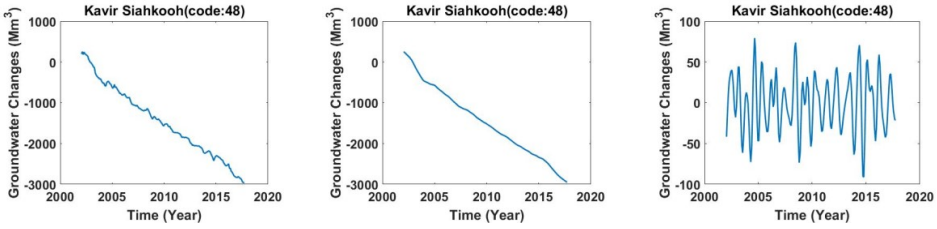

a b c

Figure 4.10. a) Monthly values of groundwater storage, b) long-period of monthly values of groundwater storage, c) short-period of monthly values of groundwater storage across Kavir SiahKooh (code 48).

Kavir Daranjir-Saghand (code 49)

This sub-basin is located between 29°30′-32°30′ N and 54°30′-47° 30′E with an area of 50,736.5 km^2. This sub-basin has 11 study areas, of which the groundwater level data of nine are available. Changes in monthly values of groundwater storage inferred from the well data, its long-period and short-period (inter-annual and semi-annual signal), for nine study areas have been illustrated in Appendix B (figures B.181 to B.190). Figure 4.11 shows changes in monthly values of groundwater storage inferred from the well data, its long-period and short-period.

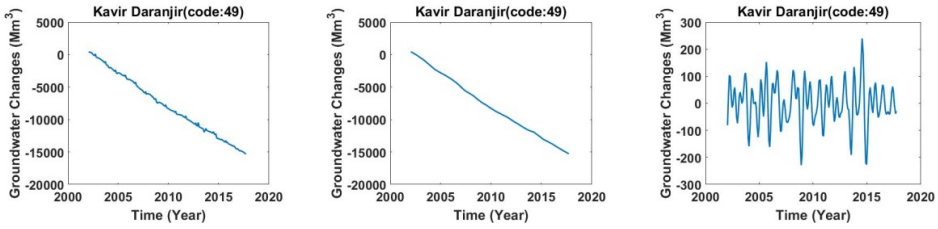

a b c

Figure 4.11. a) Monthly values of groundwater storage, b) long-period of monthly values of groundwater storage, c) short-period of monthly values of groundwater storage across Kavir Daranjir-Saghand (code 49).

4.1.2. The pian Sea basin (code 1)

Based on 3,280 active well data, the main water basin is divided into seven sub-basins, which have been described in section 2.3 (see Table 2.1). These seven sub-basins have 31 study areas, of which the well data of 27 are available. Using the Thiessen method described in Appendix A and section 4.1., the water level for every study area has been computed. The total change in groundwater storage across each sub-basin is computed by adding together the scaled change in groundwater storage of all the study areas in that sub-basin. The same procedure is carried out for each main water basin. The results for the Caspian Sea water basin and its sub-basins are represented in detail in the following sections.

Based on time series of the well data across each study area, using formula (1.4), we have computed the long period (i.e, inter-annual and secular trend) components of groundwater changes and the short period (i.e, semi-annual) components for that area. Since a picture is worth a thousand words, we decided to illustrate the numerical results in a graphical

form. Figure 4.12 shows changes in monthly values of groundwater storage inferred from the well data, its long-period and short-period.

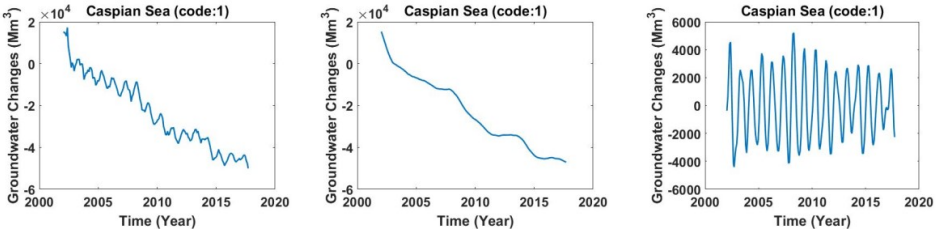

a b c

Figure 4.12. a) Monthly values of groundwater storage, b) long-period of monthly values of groundwater storage, c) short-period of monthly values of groundwater storage across the Caspian Sea basin (code 1).

In the Caspian Sea basin, we can find a sharp negative trend around 2003, and after it, the situation improved. This is probably because of establishing more control over water extraction from illegal wells in this region and changes in agricultural patterns.

This basin depleted by more than 6×10^4 Mm^3 during these 15 years. Figure 4.12 c) clearly' shows seasonal groundwater changes in the Caspian Sea basin. These seasonal changes approximately are between -4,000 and 4,000 Mm^3. Compared to the Central Plateau, the changes are fewer. This is due to the large area of the Central Plateau and intensive evaporation especially in dry and hot seasons.

We can see changes in monthly values of groundwater storage inferred from the well data, its long-period and short-period, for each study area of the Caspian Sea basin in Appendix C. The water level of the sub-basins of the Caspian Sea basin will be shown in the following figures:

Aras (code 11)

This sub-basin is located between 4250000-4280000 N and 610000-698000 E in UTM with an area of 39,778.8 km^2. It has 12 study areas, and the groundwater level data of all are available. Changes in monthly values of groundwater storage inferred from the well data, its long-period and short-period (inter-annual and semi-annual signal), for nine study areas have been illustrated in Appendix C (figures C.1 to C.12). Figure 4.13 shows

changes in monthly values of groundwater storage inferred from the well data, its long-period and short-period.

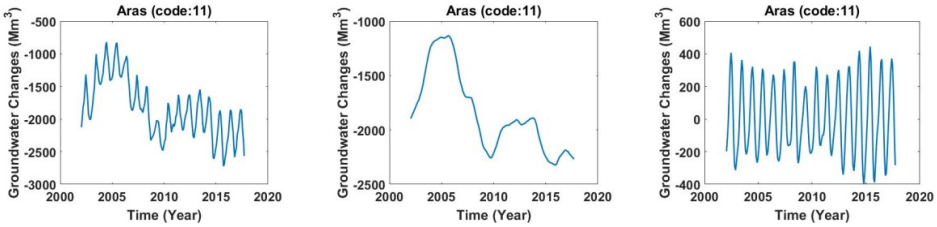

a b c

Figure 4.13. a) Monthly values of groundwater storage, b) long-period of monthly values of groundwater storage, c) short-period of monthly values of groundwater storage across Aras (code 11).

Talesh Rivers and Anzali (code 12)

This sub-basin is located between 36°45′-38°20′ N and 48°45′-49°45′ E with an area of 7,036.2 km^2. It has two study areas, and the groundwater level data of both are available. Changes in monthly values of groundwater storage inferred from the well data, its long-period and short-period (inter-annual and semi-annual signal), for the two study areas have been illustrated in Appendix C (figures C.13 to C.14). Figure 4.14 shows changes in monthly values of groundwater storage inferred from the well data, its long-period and short-period.

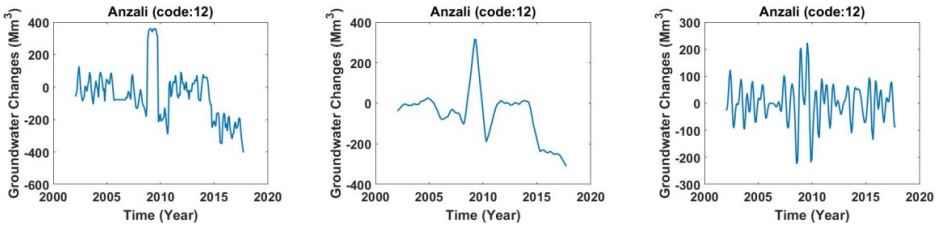

a b c

Figure 4.14. a) Monthly values of groundwater storage, b) long-period of monthly values of groundwater storage, c) short-period of monthly values of groundwater storage across Talesh Rivers and Anzali (code 12).

Sefidrood Bozorg (code 13)

This sub-basin is located between 34°50′-37°55′ N and 47°40′-41° E with an area of 7,036.2 km^2. It has 11 study areas, of which the groundwater level data of nine are available. Changes in monthly values of groundwater storage inferred from the well data,

its long-period and short-period (inter-annual and semi-annual signal), for nine study areas have been illustrated in Appendix C (figures C.15 to C.22). Figure 4.15 shows changes in monthly values of groundwater storage inferred from the well data, its long-period and short-period.

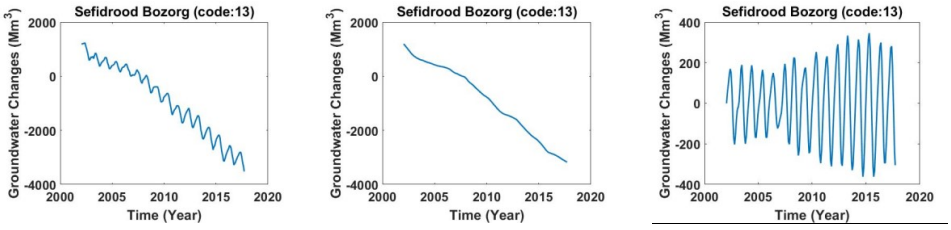

a b c

Figure 4.15. a) Monthly values of groundwater storage, b) long-period of monthly values of groundwater storage, c) short-period of monthly values of groundwater storage across Sefidrood Bozorg (code 13).

Sefidrood-Haraz (code 14)

This sub-basin is located between 3990000 to 4140000 N and 400000 to 620000 E with an area of 10,893.4 km^2. It has three study areas, of which the groundwater level data of one are available. Changes in monthly values of groundwater storage inferred from the well data, its long-period and short-period (inter-annual and semi-annual signal), for this study area have been illustrated in Appendix C (figure C.23). Figure 4.16 shows changes in monthly values of groundwater storage inferred from the well data, its long-period and short-period.

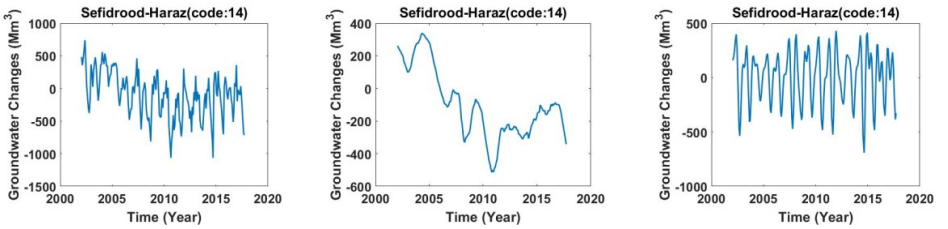

a b c

Figure 4.16. a) Monthly values of groundwater storage, b) long-period of monthly values of groundwater storage, c) short-period of monthly values of groundwater storage across Sefidrood-Haraz (code 14).

Gharasoo-Haraz (code 15)

This sub-basin is located between 3970000 to 4750000 N and 530000 to 830000 E with an area of 6.804.11 km^2. It has four study areas, and the groundwater level data of all are available. Changes in monthly values of groundwater storage inferred from the well data, its long-period and short-period (inter-annual and semi-annual signal), for the four study areas have been illustrated in Appendix C (figures C.24 to C.27). Figure 4.17 shows changes in monthly values of groundwater storage inferred from the well data, its long-period and short-period.

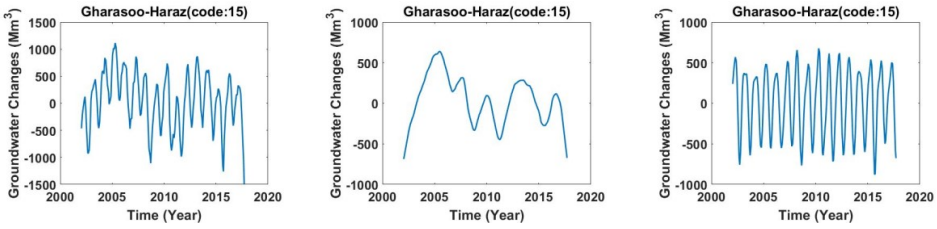

a b c

Figure 4.17. a) Monthly values of groundwater storage, b) long-period of monthly values of groundwater storage, c) short-period of monthly values of groundwater storage across study area of Gharasoo-Haraz (code 15).

Gharasoo-Gorganrood (code 16)

This sub-basin is located between 36°40′-37°55′ N and 54°-46°30′ E with an area of 12,987 km^2. It has two study areas, of which the groundwater level data of one are available. Changes in monthly values of groundwater storage inferred from the well data, its long-period and short-period (inter-annual and semi-annual signal), for this study area have been illustrated in Appendix C (figure C.28). Figure 4.18 shows changes in monthly values of groundwater storage inferred from the well data, its long-period and short-period.

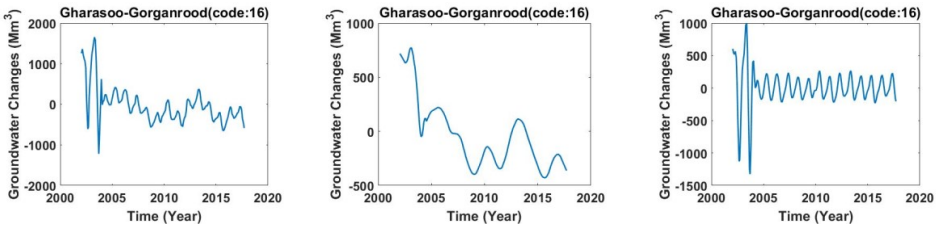

a b c

Figure 4.18. a) Monthly values of groundwater storage, b) long-period of monthly values of groundwater storage, c) short-period of monthly values of groundwater storage across Gharesoo-Gorganrood (code 16).

Atrak (code 17)

This sub-basin is located between 36°55′-38°16′ N and 53°57′-49°5′ E with an area of 26,394.7 km^2. It has eight study areas, of which the groundwater level data of five are available. Changes in monthly values of groundwater storage inferred from the well data, its long-period and short-period (inter-annual and semi-annual signal), for five study areas have been illustrated in Appendix C (figures C.29 to C.33). Figure 4.19 shows changes in monthly values of groundwater storage inferred from the well data, its long-period and short-period.

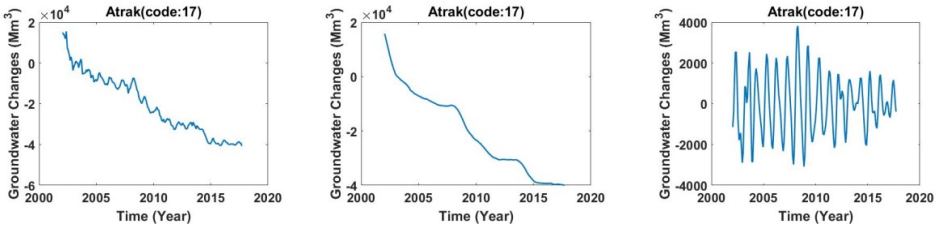

a b c

Figure 4.19. a) Monthly values of groundwater storage, b) long-period of monthly values of groundwater storage, c) short-period of monthly values of groundwater storage across Atrak (code 17).

4.1.3. The Eastern Boundary basin (code 5)

Based on 498 active well data, the main water basin is divided into nine sub-basins, which have been described in section 2.7 (see Table 2.4). These three sub-basins have 23 study areas, of which the well data of 16 are available. Using the Thiessen method described in Appendix A and section 4.1., the water level for every study area has been computed. The total change in groundwater storage across each sub-basin is computed by adding together

the scaled change in groundwater storage of all the study areas in that sub-basin. The same procedure is carried out for each main water basin. The results for the Eastern Boundary water basin and its sub-basins are represented in detail in the following sections.

Based on time series of the well data across each study area, using formula (1.4), we have computed the long period (i.e, inter-annual and secular trend) components of groundwater changes and the short period (i.e, semi-annual) components for that area. Since a picture is worth a thousand words, we decided to illustrate the numerical results in a graphical form. Figure 4. 20 shows changes in monthly values of groundwater storage inferred from the well data, its long-period and short-period.

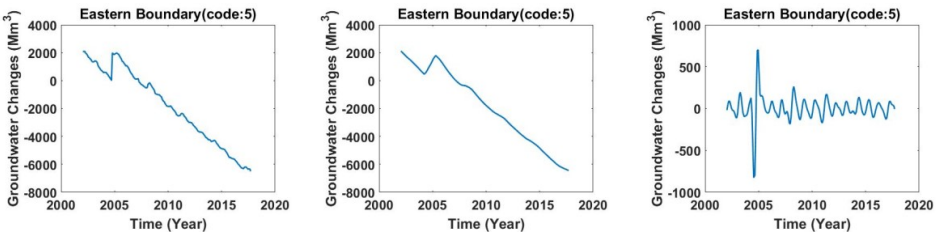

a b c

Figure 4.20. a) Monthly values of groundwater storage, b) long-period of monthly values of groundwater storage, c) short-period of monthly values of groundwater storage across the Eastern Boundary basin (code 5).

In figure 4.20. b) the changes in groundwater around 2005 are due to Afghan governments constructing large dams (Arghandab Dam, Kajaki Dam) that diverted water from the mountains in Afghanistan that charges some of rivers and water storages in this basin (Weier 2002).

This basin was depleted by more than 0.8×10^4 Mm^3 during these 15 years. Figure 4.20 c) clearly shows seasonal groundwater changes in the Eastern Boundary basin. These seasonal changes mostly are between -200 and 200 Mm^3. Compared with other water basins, these changes are very small.

Petergan Playa and namakzare-khaf (code 51)

This sub-basin is located between 32°-35° N and 58°-62°E with an area of 33,086 km^2. It has 12 study areas, of which the groundwater level data of 10 are available. Changes in monthly values of groundwater storage inferred from the well data, its long-period and short-period (inter-annual and semi-annual signal), for 10 study areas have been illustrated in Appendix C (figure D.1 to D.10). Figure 4.21 shows changes in monthly values of groundwater storage inferred from the well data, its long-period and short-period.

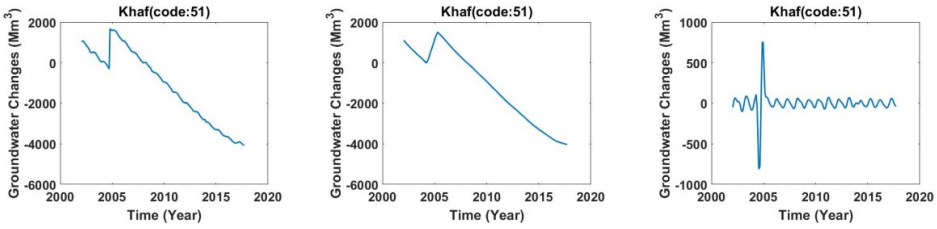

a b c

Figure 4.21. a) Monthly values of groundwater storage, b) long-period of monthly values of groundwater storage, c) short-period of monthly values of groundwater storage across Petergan Playa and namakzare-khaf (code 51).

Hirmand hamun (code 52)

This sub-basin is located between 29°-33° N and 59°-61°E with an area of 33,589.6 km^2. It has 12 study areas, of which the groundwater level data of 10 are available. Changes in monthly values of groundwater storage inferred from the well data, its long-period and short-period (inter-annual and semi-annual signal), for 10 study areas have been illustrated in Appendix C (figures D.11 to D.16). Figure 4.22 shows changes in monthly values of groundwater storage inferred from the well data, its long-period and short-period.

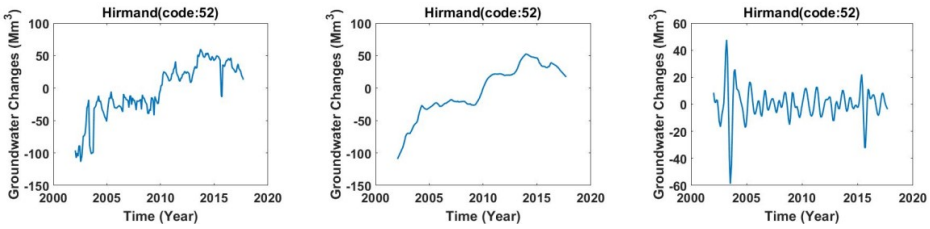

a b c

Figure 4.22. a) Monthly values of groundwater storage, b) long-period of monthly values of groundwater storage, c) short-period of monthly values of groundwater storage across Hirmand hamun (code 52).

Mashkil Hamun (code 53)

This sub-basin is located between 27˚-30˚ N and 60˚ 30′-63˚E with an area of 36,507.6 km^2. It has 12 study areas, of which the groundwater level data of 10 are available. Changes in monthly values of groundwater storage inferred from the well data, its long-period and short-period (inter-annual and semi-annual signal), for 10 study areas have been illustrated in Appendix D (figures D.17 to D.23). Figure 4.23 shows changes in monthly values of groundwater storage inferred from the well data, its long-period and short-period.

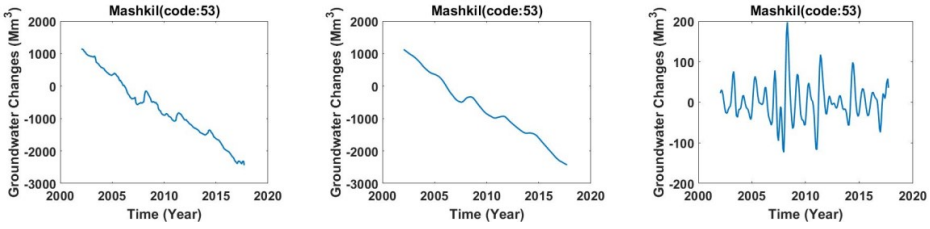

a b c

Figure 4.23. a) Monthly values of groundwater storage, b) long-period of monthly values of groundwater storage, c) short-period of monthly values of groundwater storage across Mashkil Hamun (code 53).

4.1.4. The Ghareghom basin (code 6)

This basin is located between 34˚23′-37˚52′ N and 57˚49′-61˚17′ E with an area of 44,294.5 km^2. This is the smallest basin in Iran. Based on 295 active well data, the main water basin is divided into 13 sub-basins, which have been described in section 2.8 (see Table 2.5). These three sub-basins have 23 study areas, of which the well data of 16 are

available. Using the Thiessen method described in Appendix A and section 4.1., the water level for every study area has been computed. The total change in groundwater storage across each sub-basin is computed by adding together the scaled change in groundwater storage of all the study areas in that sub-basin. The same procedure is carried out for each main water basin. The results for the Ghareghom water basin and its sub-basins are represented in detail in the following sections.

Based on time series of the well data across each study area, using formula (1.4), we have computed the long period (i.e, inter-annual and secular trend) components of groundwater changes and the short period (i.e, semi-annual) components for that area. Since a picture is worth a thousand words, we decided to illustrate the numerical results in a graphical form. Figure 4.24 shows changes in monthly values of groundwater storage inferred from the well data, its long-period and short-period.

Changes in monthly values of groundwater storage inferred from the well data, its long-period and short-period (inter-annual and semi-annual signal), for 10 study areas have been illustrated in Appendix E (figures E.1 to E.9).

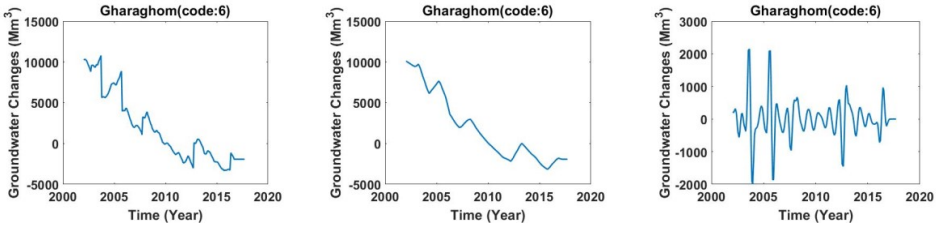

a b c

Figure 4.24. a) Monthly values of groundwater storage, b) long-period of monthly values of groundwater storage, c) short-period of monthly values of groundwater storage across the Ghareghom basin (code 6).

This basin was depleted by more than 0.8×10^4 Mm^3 during these 15 years. Figure 4.24 c) clearly shows seasonal groundwater changes in the Ghareghom basin. These seasonal changes mostly are between -2,000 and 2,000 Mm^3. Compared with other water basins, these changes are very small. The area of the Ghareghom basin is less than half of the area of the Eastern Boundary basin, but the amount of water depletion in this basin is almost two times more. The long-term changes of groundwater has some fluctuations in this basin.

There is an important transboundary sedimentary aquifer in this basin. It is shared between Turkmenistan, Afghanistan, and Iran.

4.1.5. The Persian Gulf and Oman Sea basin (code 2)

Based on 5,404 active well data, the main water basin is divided into nine sub-basins, which have been described in section 2.4 (see Table 2.2). These nine sub-basins have 256 study areas, of which the well data of 195 are available. Using the Thiessen method described in Appendix A and section 4.1., the water level for every study area has been computed. The total change in groundwater storage across each sub-basin is computed by adding together the scaled change in groundwater storage of all the study areas in that sub-basin. The same procedure is carried out for each main water basin. The results for the Persian Gulf and Oman Sea water basin and its sub-basins are represented in detail in the following sections.

Based on time series of the well data across each study area, using formula (1.4), we have computed the long period (i.e, inter-annual and secular trend) components of groundwater changes and the short period (i.e, semi-annual) components for that area. Since a picture is worth a thousand words, we decided to illustrate the numerical results in a graphical form. Figure 4.25 shows changes in monthly values of groundwater storage inferred from the well data, its long-period and short-period:

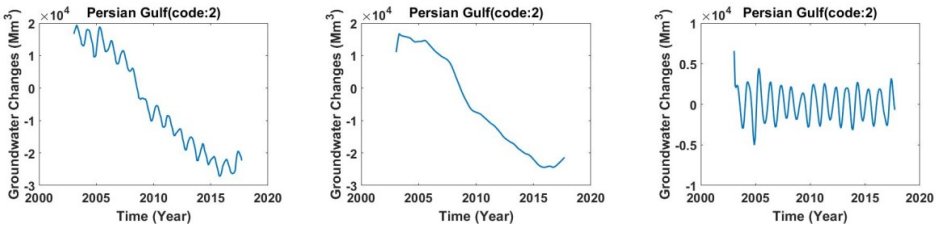

a b c

Figure 4.25. a) Monthly values of groundwater storage, b) long-period of monthly values of groundwater storage, c) short-period of monthly values of groundwater storage across the Persian Gulf and Oman Sea basin (code 2).

In the Persian Gulf and Oman Sea basin, we can find a sharp positive trend around 2003. It is probably because of the construction of numbers of dams in this region. But after that

period, there is a negative trend in the water storage in the basin, which is probably due to intensive groundwater extractions for irrigation. There is also a sharp negative trend around 2008; this is maybe because of the occurrence of a drought in 2007. Around 2017, the trend of water storage is positive, which could be due to more precipitation in this year.

The area of this basin is half of the Central Plateau, but the depletion amount of water in the Central Plateau is more than three times that of this basin, which may be because of the most populated cities being located in the Central Plateau basin and intensive immigration to these cities.

This basin was depleted by more than 4×10^4 Mm^3 during these 15 years. Figure 4.25 c) clearly shows seasonal groundwater changes in the Persian Gulf and Oman Sea basin. These seasonal changes approximately are between -4,000 are 5,000 Mm^3. Compared to the Central Plateau, these changes are 10 times less. This is due to there being fewer rivers and dams in the Central Plateau and more pressure on groundwater in it. In the Persian Gulf and Oman Sea basin, there are large permanent rivers such as the Karoon River.

We can see changes in monthly values of groundwater storage inferred from the well data, its long-period and short-period, for each study area of the Persian Gulf and Oman Sea basin in Appendix F. The water level of sub-basins of the Persian Gulf and Oman Sea basin will be shown in the following figures:

Marzi-e-Gharb Rivers (code 21)

This sub-basin has an area of 39,297.8 km^2. It has 24 study areas, of which the groundwater level data of 14 are available. Changes in monthly values of groundwater storage inferred from the well data, its long-period and short-period (inter-annual and semi-annual signal), for 14 study areas have been illustrated in Appendix F (figures F.1 to F.14). Figure 4.26 shows changes in monthly values of groundwater storage inferred from the well data, its long-period and short-period.

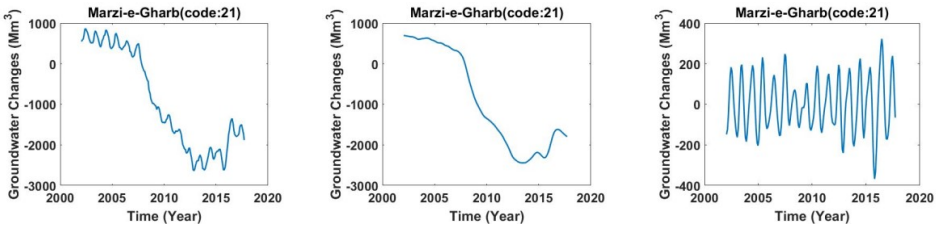

a b c

Figure 4.26. a) Monthly values of groundwater storage, b) long-period of monthly values of groundwater storage, c) short-period of monthly values of groundwater storage across Marzi-e-Gharb (code 21).

Karkhe River(code 22)

This sub-basin is located between 31°-35° N and 46° 5′-49°E with an area of 51,912.3 km^2. It has 35 study areas, of which the groundwater level data of 27 are available. Changes in monthly values of groundwater storage inferred from the well data, its long-period and short-period (inter-annual and semi-annual signal), for 27 study areas have been illustrated in Appendix F (figures F.15 to F.41). Figure 4.27 shows changes in monthly values of groundwater storage inferred from the well data, its long-period and short-period.

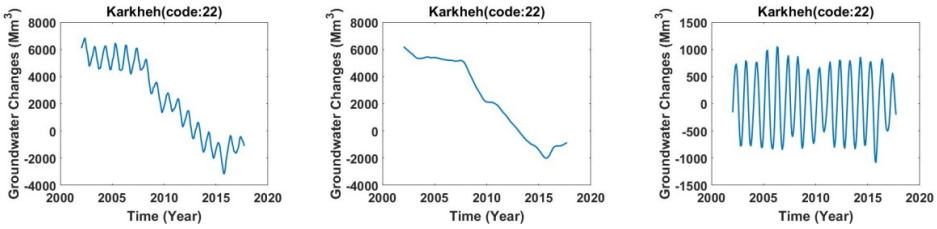

a b c

Figure 4.27. a) Monthly values of groundwater storage, b) long-period of monthly values of groundwater storage, c) short-period of monthly values of groundwater storage across Karkhe River (code 22).

Karoon (Karun) River (code 23)

This sub-basin is located between 3300000°-3780000° N and 200000°-600000°E in UTM, with an area of 66,674.9 km^2. It has 42 study areas, of which the groundwater level data of 32 are available and shown in Appendix F. Changes in monthly values of groundwater storage inferred from the well data, its long-period and short-period (inter-annual and semi-annual signal), for 32 study areas have been illustrated in Appendix F (figures F.42

to F.73). Figure 4.28 shows changes in monthly values of groundwater storage inferred from the well data, its long-period and short-period.

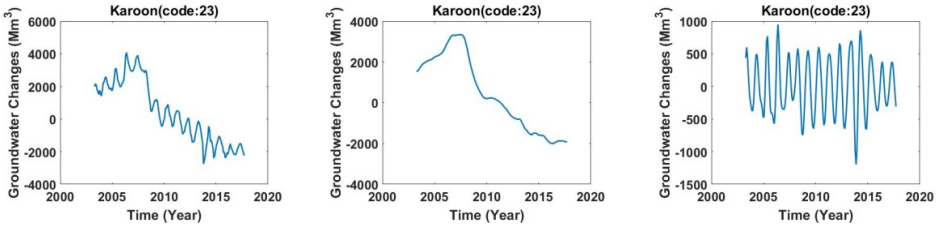

a b c

Figure 4.28. a) Monthly values of groundwater storage, b) long-period of monthly values of groundwater storage, c) short-period of monthly values of groundwater storage across Karoon River (code 23).

Jarahi River(code 24)

This sub-basin is located between 29°45′-31°30′ N and 48°10′-42°15′E, with 40,820.8 km^2 area. It has 42 study areas, of which the groundwater level data of 32 are available. Changes in monthly values of groundwater storage inferred from the well data, its long-period and short-period (inter-annual and semi-annual signal), for 32 study areas have been illustrated in Appendix F (figures F.74 to F.88). Figure 4.29 shows changes in monthly values of groundwater storage inferred from the well data, its long-period and short-period.

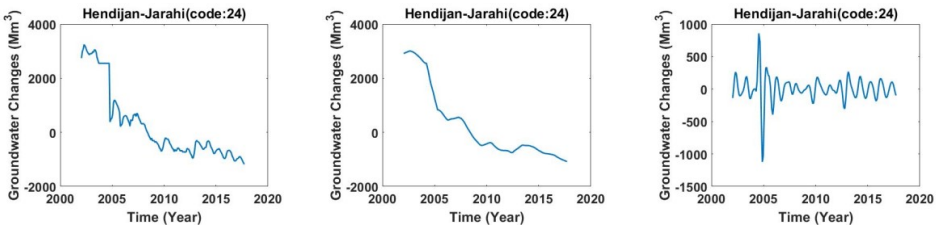

a b c

Figure 4.29. a) Monthly values of groundwater storage, b) long-period of monthly values of groundwater storage, c) short-period of monthly values of groundwater storage across Jarahi River (code 24).

Hele River (code 25)

This sub-basin is located between 3100000°-3360000° N and 390000°- 630000°E in UTM, with an area of 21,309.1 km^2. It has 42 study areas, of which the groundwater level

data of 32 are available. Changes in monthly values of groundwater storage inferred from the well data, its long-period and short-period (inter-annual and semi-annual signal), for 32 study areas have been illustrated in Appendix F (figures F.89 to F.99). Figure 4.30 shows changes in monthly values of groundwater storage inferred from the well data, its long-period and short-period.

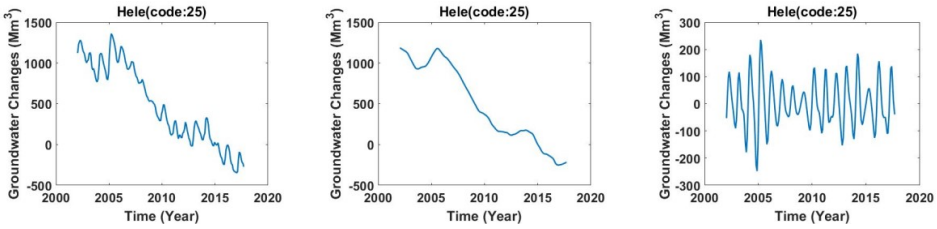

a b c

Figure 4.30. a) Monthly values of groundwater storage, b) long-period of monthly values of groundwater storage, c) short-period of monthly values of groundwater storage across Hele River (code 25).

Mand River (code 26)

This sub-basin is located between 27°35′ -28°55′ N and 51°10′-42 35′E, with an area of 47,802 km^2. It has 47 study areas, of which the groundwater level data of 44 are available. Changes in monthly values of groundwater storage inferred from the well data, its long-period and short-period (inter-annual and semi-annual signal), for 44 study areas have been illustrated in Appendix F (figures F.100 to F.142). Figure 4.31 shows changes in monthly values of groundwater storage inferred from the well data, its long-period and short-period.

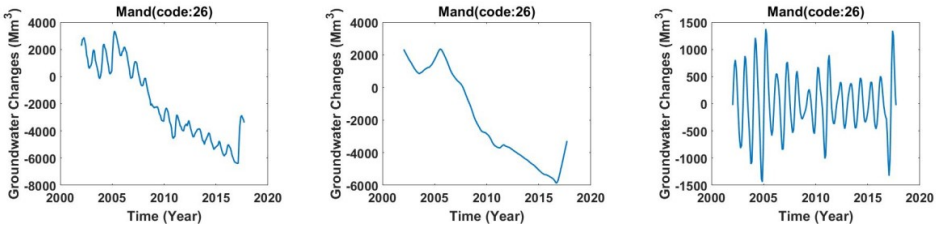

a b c

Figure 4.31. a) Monthly values of groundwater storage, b) long-period of monthly values of groundwater storage, c) short-period of monthly values of groundwater storage across Mand River (code 26).

Mehran River, Kal River (code 27)

This sub-basin is located between -40000°-49000° N and 2930000°-322500010′E in UTM, with an area of 62,894.8 km^2. It has 28 study areas, and the groundwater level data of all are available. Changes in monthly values of groundwater storage inferred from the well data, its long-period and short-period (inter-annual and semi-annual signal), for 28 study areas have been illustrated in Appendix F (figures F.143 to F.175). Figure 4.32 shows changes in monthly values of groundwater storage inferred from the well data, its long-period and short-period.

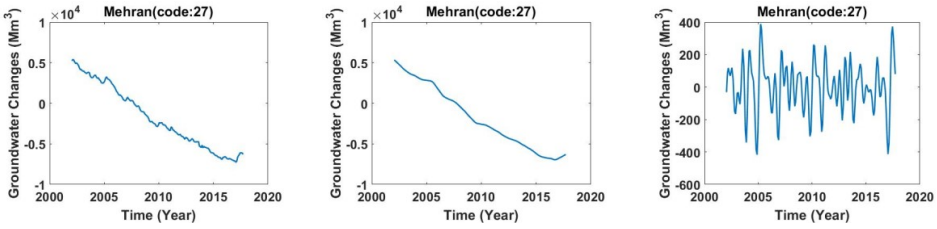

a b c

Figure 4.32. a) Monthly values of groundwater storage, b) long-period of monthly values of groundwater storage, c) short-period of monthly values of groundwater storage across Kalmehran (code 27).

Bandar Abbas (code 28)

This sub-basin is located between 25°30′-28°15′ N and 56°-49°E, with an area of 44,792.2 km^2. It has 20 study areas, of which the groundwater level data of 18 are available. Changes in monthly values of groundwater storage inferred from the well data, its long-period and short-period (inter-annual and semi-annual signal), for 18 study areas have been illustrated in Appendix F (figures F.176 to F.193). Figure 4.33 shows changes in monthly values of groundwater storage inferred from the well data, its long-period and short-period.

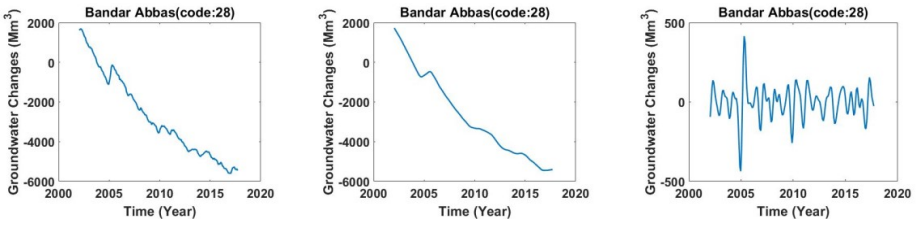

a b c

Figure 4.33. a) Monthly values of groundwater storage, b) long-period of monthly values of groundwater storage, c) short-period of monthly values of groundwater storage across Bandar Abbas (code 28).

Baloochestan Jonubi (code 29)

This sub-basin is located between 25°-27° N and 59°-63°E, with an area of 48,523.7 km^2. It has 13 study areas, of which the groundwater level data of two are available. Changes in monthly values of groundwater storage inferred from the well data, its long-period and short-period (inter-annual and semi-annual signal), for 32 study areas have been illustrated in Appendix F (figures F.193 to F.195). Figure 4.34 shows changes in monthly values of groundwater storage inferred from the well data, its long-period and short-period.

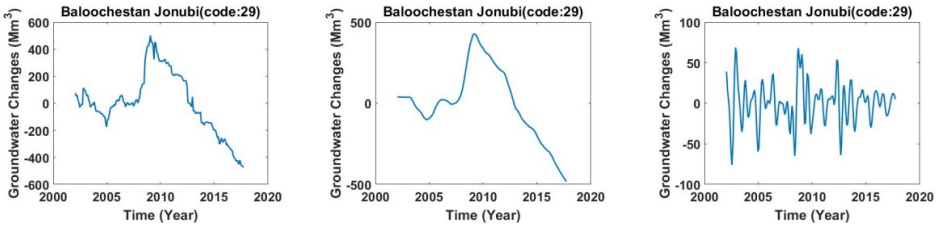

a b c

Figure 4.34. a) Monthly values of groundwater storage, b) long-period of monthly values of groundwater storage, c) short-period of monthly values of groundwater storage across Baloochestan Jonubi (code 29).

4.1.6. The Urmia basin (code 3)

Based on 1,308 active well data, the main water basin is divided into nine sub-basins, which have been described in section 2.5. There are 25 study areas, of which the well data of 23 are available. Using the Thiessen method describe in Appendix A and section 4.1., the water level for every study area has been computed. The total change in groundwater storage across this basin is computed by adding together the scaled change in groundwater storage of all its study areas in the basin. The results for the Urmia water basin are represented in detail in the following sections.

Based on time series of the well data across each study area, using formula (1.4), we have computed the long period (i.e, inter-annual and secular trend) components of groundwater changes and the short period (i.e, semi-annual) components for that area. Since a picture is worth a thousand words, we decided to illustrate the numerical results in a graphical form. Figure 4.35 shows changes in monthly values of groundwater storage inferred from the well data, its long-period and short-period:

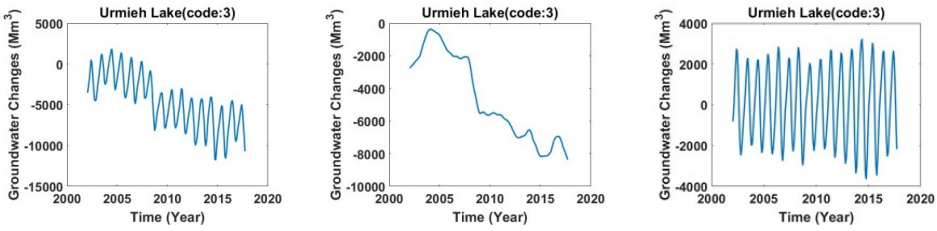

a b c

Figure 4.35. a) Monthly values of groundwater storage, b) long-period of monthly values of groundwater storage, c) short-period of monthly values of groundwater storage across the Urmia basin (code 3).

The trend in the Urmia basin is not a smooth one; it has some fluctuation. There is an intensive negative trend from 2007 to 2008, which might be due to drought in 2007. As mentioned in section 2.5, the water level in the Urmia Lake depends on precipitation. The water table in this basin is directly influenced by the lake level, and the drought period had severe effects on this level. Therefore, the irrigation pattern changes the water level in the area directly.

This basin was depleted by more than 0.8×10^4 Mm^3 during these 15 years. Figure 4.35 c) clearly shows seasonal groundwater changes in the Urmia basin. These seasonal changes are between -4,000 and 4,000 Mm^3.

Well data in the six main basins show steady groundwater depletion in Iran during the last few decades. This is a valuable result of our estimation for water management.

4.2. Spatial dependence of total water storage

We have estimated the secular trend of total water storage across Iran using a standard method and appropriate corrections. In order to examine this method, we have used 15 years (April 2002 to December 2016) of GRACE de-striped Level-2 release 6.0 data. It has been computed at the Center for Space Research (CSR) at the University of Texas at Austin. Release 6.0 coefficients are distributed on the Level-2 data archives as GSM files (GSM is a file extension).

This method requires filtering of the GRACE data to reduce noise (Swenson and Wahr 2006). Then we restore the associated lost signal over Iran by scaling the data in order to

recover the mass change estimate for the region (Velicogna and Wahr 2006). The leakage effects have been removed by the scale-up method. A scale factor of 1.09 was required in this work. The Monthly solution of GRACE has been smoothed by Gaussian filter radii 300 km. The monthly SLR estimates for C_{20} coefficient are used to replace the estimate from GRACE. For estimating total water storage changes in Iran, the surface mass density changes (in terms of equivalent water thickness in cm) is computed using Eq.(15-3), on a $1^{\circ} \times 1^{\circ}$ grid (Figure 4.36).

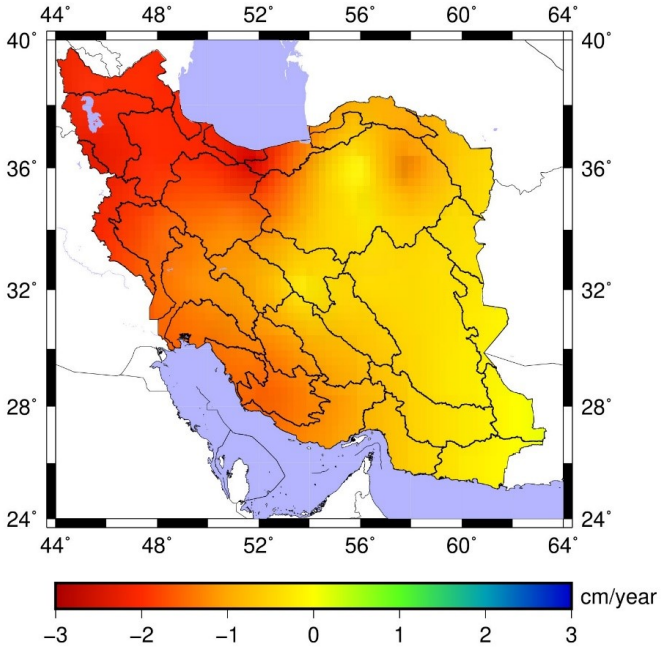

Figure 4.36. GRACE-derived secular trend of total water storage across Iran in cm/yr. From 2002 to 2016. CSR monthly solution and a corresponding radius of 300 km.

Figure 4.36 shows a large negative trend in the GRACE total water storage estimates over north and western Iran. In compare with figure 4.1, it seems that the GRACE standard method for GWS estimation illustrates large wavelengths of GWS changes, and does not present detailed information for hydrological effort. The standard method is not properly designed for obtaining hydrological information in small areas such as water basins.

Developing least square mascon fitting theory for each water basin has made powerful tools for GWS estimations.

4.3. Total water storage inferred from the GRACE least squares mascon solution

In order to compare observation well data results' and the GRACE least squares mascon solution, we divided Iran into six mascons according to the same border in the main water basins. We developed the GRACE least squares mascon solution method by adjusting mascon shapes so that they were the same shapes and sizes of hydrological main basins in Iran. The GRACE least squares mascon solution has been described in section 3.9.

Because GRACE data have finite resolution, it is impossible to obtain a perfect unweighted average of mass variability within a basin, no matter what technique is used for the GRACE analysis or what basin is considered. Results from a mascon fitting method are no exception. A GRACE estimate for the mass change in the central plateau basin, for example, will include contamination from mass variations outside the basin and will not weight every point inside the basin equally. Figure 4.37, for example, shows our sensitivity kernel for the Central Plateau mascon, when fitting all six mascons to the Stokes coefficients. The kernel's value is small outside the Central Plateau and is close to unity inside the Central Plateau, but it does depart somewhat from those ideal values.

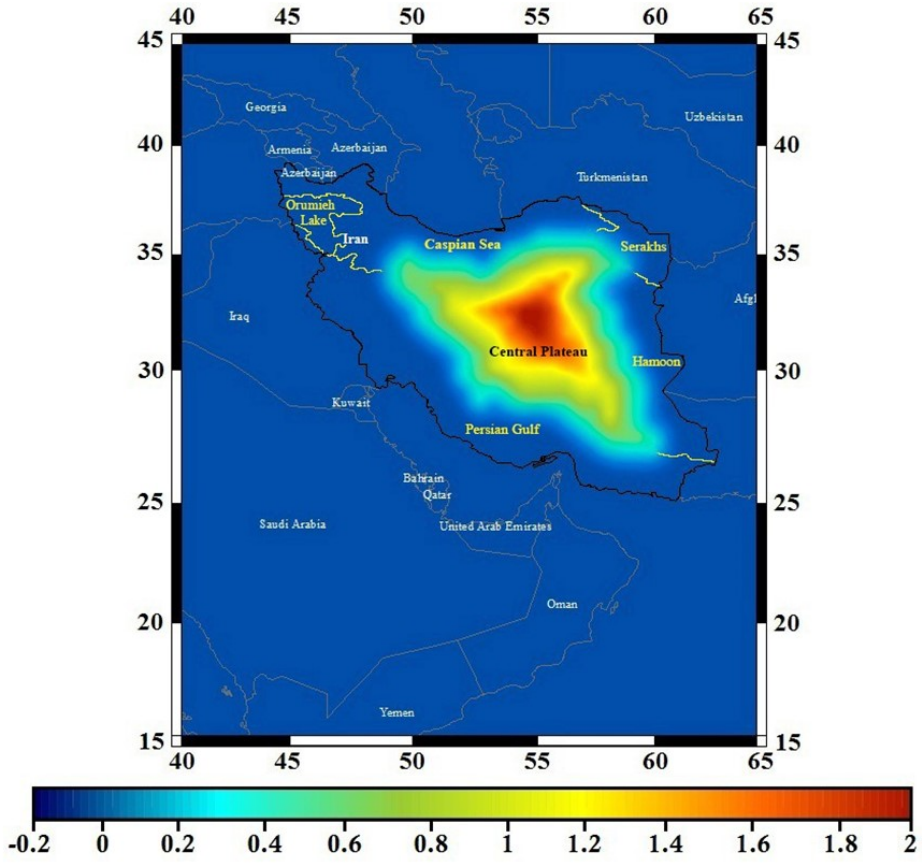

Figure 4.37. Sensitivity kernel for the Central Plateau mascon.

Using the GRACE least squares mascon solution method by adjusting mascon shapes so that they were the same shapes and sizes of hydrological basins in Iran is a new method. In order to calculate the TWS across Iran, 163 months of CSR GRACE Level-2 release 6.0 data (April 2002 to July 2017) and 15 months of GRACE FO (Jun 2018 to September 2019) have been collected, then the computed degree 1 coefficients are included as described by Swenson et al. (2008). The coefficient of degree 2 and order 0 (C20) is replaced by estimates from SLR (Cheng et al. 2013). The time-mean of the coefficients from April 2002 to July 2017 is subtracted from the monthly fields. The effects of Glacial Isostatic Adjustment (GIA) are removed by subtracting the GIA Stokes coefficients computed by A et al. 2013. Spherical Harmonic (SH) coefficients are smoothed using a

Gaussian smoothing function with a 100-km radius. TWS is synthesized on a 0.5° spatial grid over Iran. The Caspian Sea, Persian Gulf, and Oman Sea signal is removed following Swenson and Wahr (2007). Urmia Lake storage contributions are removed using altimeter lake level observations following Swenson and Wahr (2007). The de-aliasing product for non-tidal ocean and atmosphere variability (GAD) is added back.

In summary, the following processing steps were performed in calculating the total water storage across Iran, from 163 months of CSR GRACE Level-2 release 6.0 data.

1. The computed degree 1 coefficients are included as described by Swenson et al. (2008).

2. The coefficient of (C_{20}) is replaced by estimates from SLR (Cheng et al. 2013).

3. The time-mean of the coefficients from April 2002 to July 2017 is subtracted from the monthly fields.

4. The effects of GIA are removed by subtracting the GIA Stokes coefficients computed by A et al. (2013); nevertheless, in this region it is small.

4. Instead of using a decorrelation filter, the SH coefficients are smoothed using a Gaussian smoothing function with a 100-km radius.

7. Total water storage is synthesized on a 0.5° spatial grid over Iran.

8. The Caspian Sea, Persian Gulf, and Oman Sea signal is removed following Swenson and Wahr (2007).

9. Urmia Lake storage contributions are removed using altimeter lake level observations following Swenson and Wahr (2007).

10. Output from a version of the Community Land Model (CLM) 4.5, which is a land surface model, has been used to remove contributions from soil moisture, snow, canopy storage, and river storage; we conclude that most of the long-term water loss is due to a decline in groundwater storage. The CLM4.5 land surface model have not accuracy of local hydrological models. So we will see some fluctuation in the GRACE long-term figures.

GRACE data include measurement error, leakage error, and correlated error or striping error. One of the best methods to decrease all these errors together is least squares mascon fitting. The mascon analysis has less leakage error and can be used for hydrological applications without applying any gain factors or any post processing in comparison with other solutions such as the spherical harmonics solutions.

The following figures show changes in monthly values of total water storage of the main water basins of Iran, inferred from the GRACE least squares mascon solution, its long-period (secular trend and inter-annual) and short-period (seasonal), and compared with well data. The long-period manifest trend of total water changes is inferred from 15 years of study of GRACE data. The short-period shows us the ability of GRACE to indicate seasonal variation in water storage remotely.

4.3.1. The Persian Gulf and Oman basin

Figure 4.38 shows changes in monthly values of total water storage inferred from GRACE data, its long-period, short-period, and compared with well data.

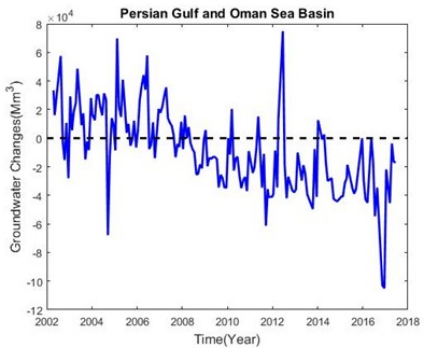

a

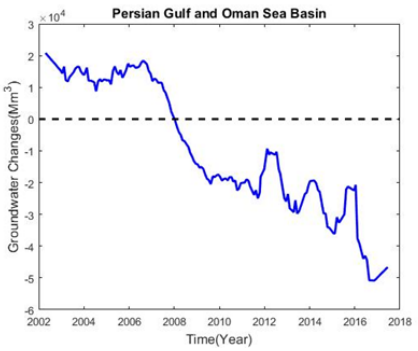

b

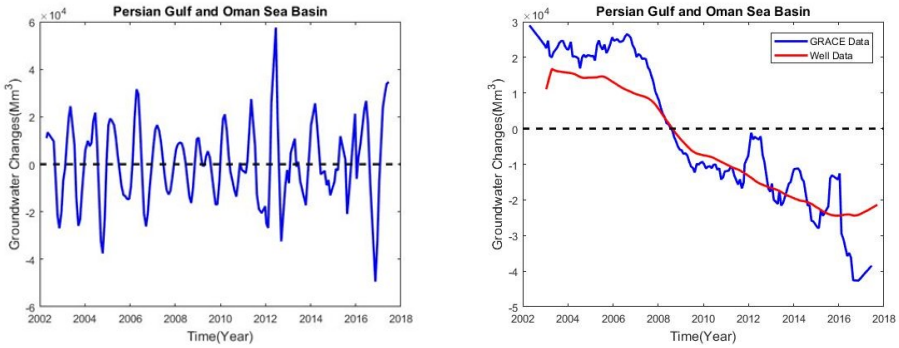

c d

Figure 4.38. a) Monthly values of groundwater storage, b) long-period of monthly values of groundwater storage, c) short-period of monthly values of groundwater storage, d) long-period of monthly values of groundwater storage, inferred from well data and GRACE data, across the Persian Gulf and Oman Sea basin (code 2).

Figure 4.38.c) clearly shows seasonal total water storage changes inferred from GRACE data. Figure 4.38.d) shows the total water storage trend in the Persian Gulf and Oman Sea basin from well data and GRACE data. Regarding the secular trend of the well-based estimates, computed using the GRACE sensitivity kernel, we conclude that most of the GRACE-based long-term water loss is due to a decline in groundwater storage.

There is relatively good agreement between these two sets of data for this basin. The differences between these two sets of data may originate from inadequate global hydrological models and other sources of noise. The other guesstimate is occurrence of more precipitation after 2016, which could reduce the water extraction from wells, since when we have sufficient surface water, we have less requirement for groundwater for irrigation.

4.3.2. The Caspian Sea basin

Figure 4.39 shows changes in monthly values of groundwater storage inferred from GRACE data, its long-period, short-period, and compared with well data.

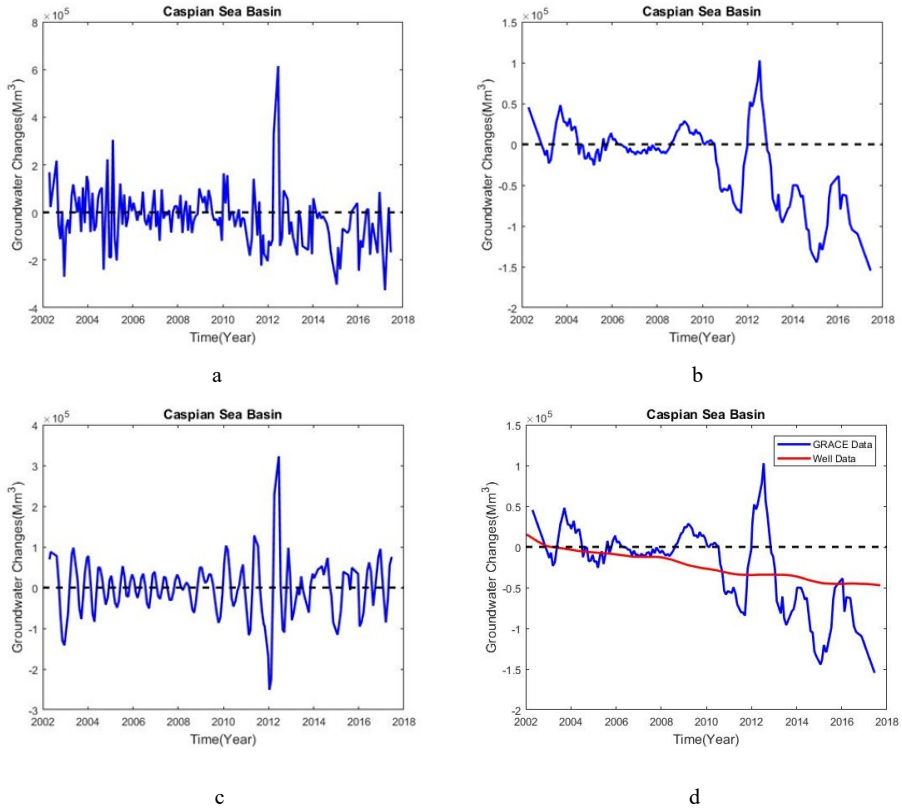

Figure 4.39. a) Monthly values of groundwater storage, b) long-period of monthly values of groundwater storage, c) short-period of monthly values of groundwater storage, d) long-period of monthly values of groundwater storage, inferred from well data and GRACE data, across the Caspian Sea basin (code 1).

In this picture, we can see that GRACE overestimates water storage. The fluctuations in this picture may be due to inadequacy of the hydrological model.

4.3.3. The Urmia Lake basin

Figure 4.40 shows changes in monthly values of groundwater storage inferred from GRACE data, its long-period, short-period, and compared with well data.

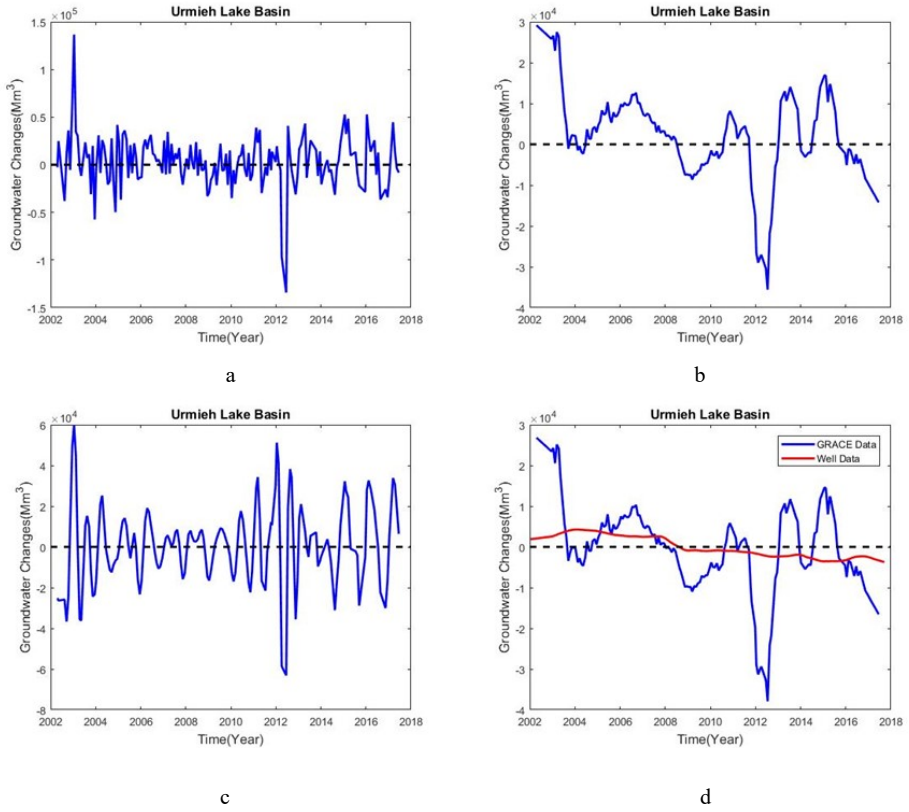

Figure 4.40. a) Monthly values of groundwater storage, b) long-period of monthly values of groundwater storage, c) short-period of monthly values of groundwater storage, d) long-period of monthly values of groundwater storage, inferred from well data and GRACE data, across the Urmia Lake basin (code 3).

Figure 4.40 b) shows long-term changes in the Urmia lake basin. We can see some fluctuations in this figure. As it mentioned in 2.5., the Urmia lake level is dependent on precipitation and evaporation. During the last 20 years, there has been lot of illegal well digging and extra water extraction in the basin due to agricultural pattern changes. GRACE data affected by the lake level changes immediately, but well levels show the fluctuations in delay. Because of the small area of this basin, there is mismatch in d) between GRACE data and well data.

4.3.4. The Central Plateau basin

Figure 4.41 shows changes in monthly values of groundwater storage inferred from GRACE data, its long-period, short-period, and compared with well data.

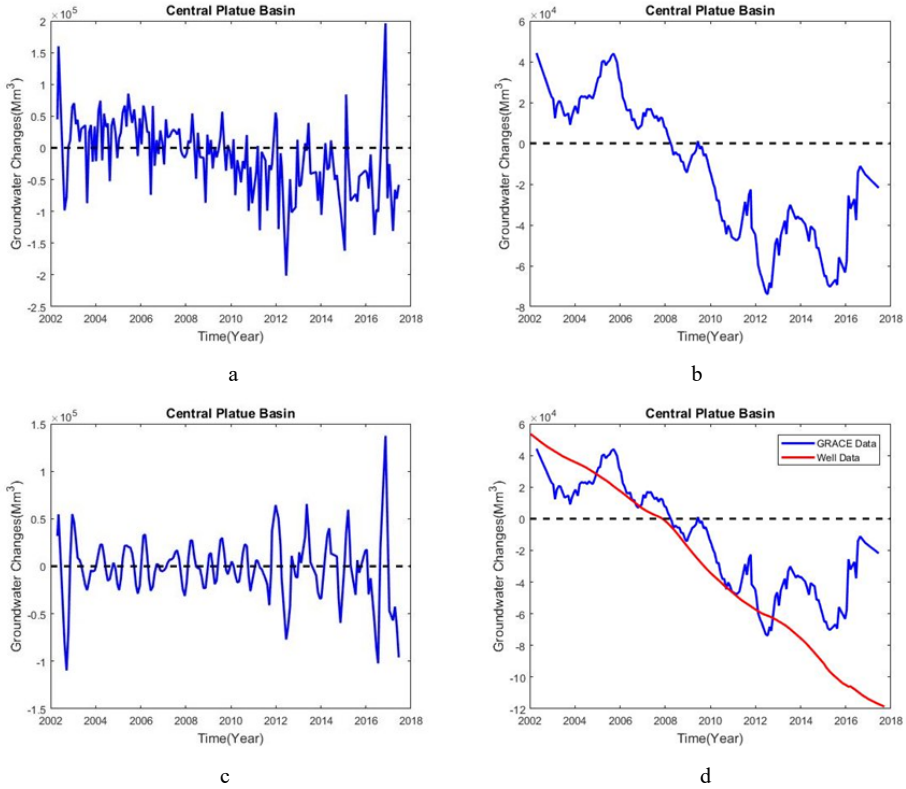

Figure 4.41. a) Monthly values of groundwater storage, b) long-period of monthly values of groundwater storage, c) short-period of monthly values of groundwater storage, d) long-period of monthly values of groundwater storage, inferred from well data and GRACE data, across the Central Plateau basin (code 4).

Figure 4.41 d) shows long-term changes in the Central Plateau. There is an intensive negative trend in this figure. Around 2013, GRACE data did not follow well data. In chapter 1, page 4, it mentioned that extraction of a large amount of water in a short time permanently reduces the capacity of aquifers to store water. Therefore, in spite of increase in precipitation and surface water around 2013, the aquifer could not recharge. These phenomena caused changes in the ecosystem of the region and more frequent flooding in

the area. Unfortunately, it resulted in desertification and dusty storms in the area, affected people's everyday lives as well as the agriculture

4.3.5. The Eastern Boundary basin

Figure 4.42 shows changes in monthly values of groundwater storage inferred from GRACE data, its long-period, short-period, and compared with well data.

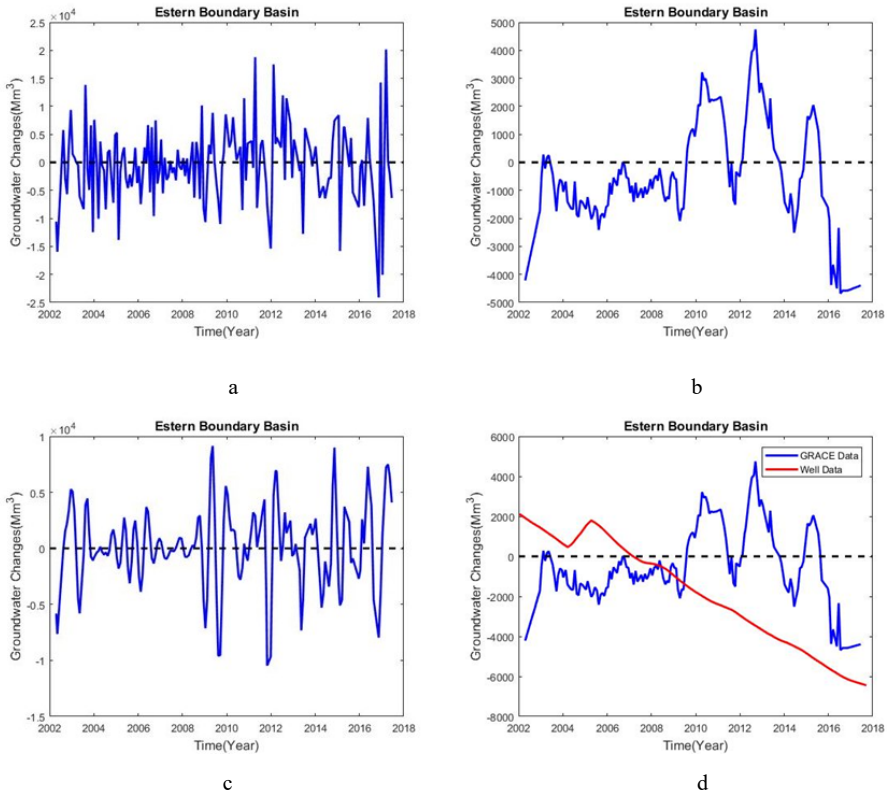

Figure 4.42. a) Monthly values of groundwater storage, b) long-period of monthly values of groundwater storage, c) short-period of monthly values of groundwater storage, d) long-period of monthly values of groundwater storage, inferred from well data and GRACE data, across the Eastern Boundary basin (code 5).

Figure 4.42 b) shows the Easter Boundary total water storage changes; this figure has some fluctuation, which may be because of changes in rules in Afghanistan, where surface water such as Hamoon Lake originates. Figure 4.42 d) shows GRACE mismatched results in a small area. In addition to this, when the mascon shape is far from a circle or square shape, the GRACE result would not be as accurate.

4.3.6. The Ghareghom basin

Figure 4.43 shows changes in monthly values of groundwater storage inferred from GRACE data, its long-period, short-period, and compared with well data.

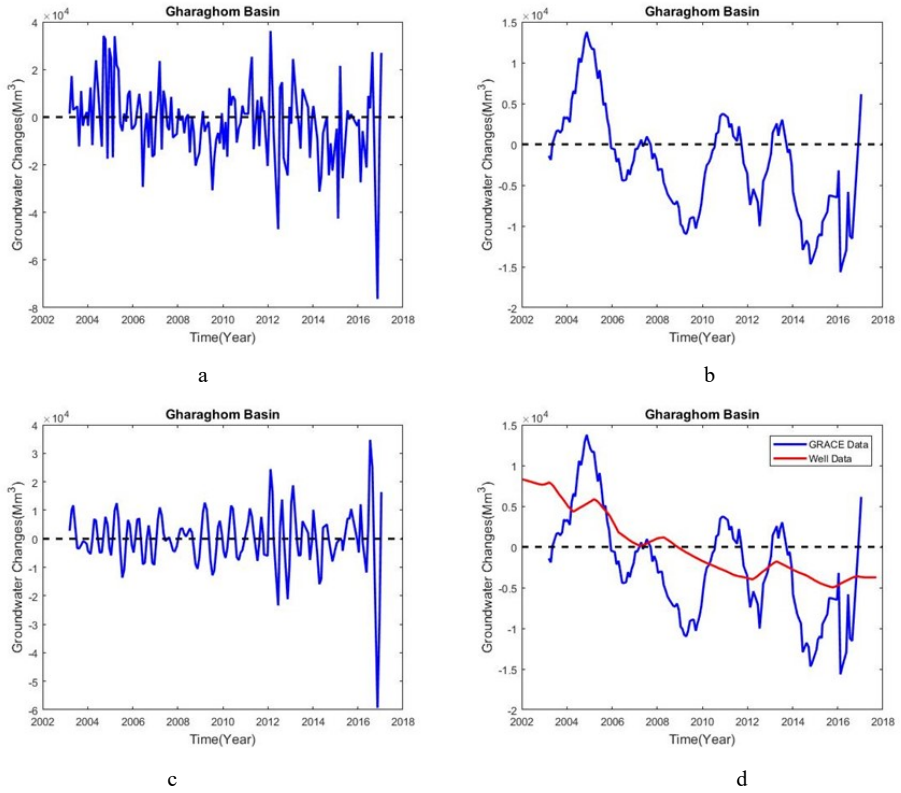

Figure 4.43. a) Monthly values of groundwater storage, b) long-period of monthly values of groundwater storage, c) short-period of monthly values of groundwater storage, d) long-period of monthly values of groundwater storage, inferred from well data and GRACE data, across the Ghareghom basin (code 6).

This figure has some fluctuation, which may be because of shared transboundary aquifers in this basin. We do not have well data information from the Afghanistan part and changes in rules in Afghanistan. It is obvious that the well level shows increase in water storage with some delay. The most significant signal in the long term of GRACE data is due to groundwater storage changes, and some of the mismatch of it with the well data is because of an insufficient hydrological model for the region (Joodaki and Nahavandchi 2010). In addition to this, it is not possible to remove all GRACE noise, such as stripe error, and leakage in and out. In all these six figures, we can see good agreement between GRACE

results and well data results. This outcome is a valuable one and shows the great ability of GRACE to assist in climate studies and water management requirements.

4.4. Total water storage inferred from the GRACE Follow-On (FO) least squares mascon solution

The GRACE mission sent data until June 2017; after that, the GRACE (FO) mission was launched and sent data. Using the same procedure as with the GRACE least squares mascon solution, we divided Iran into six mascons according to the main water basins. The following figures show changes in monthly values of groundwater storage of the main water basins of Iran, inferred from the GRACE (FO) least squares mascon solution.

4.4.1. The Persian Gulf and Oman Sea basin

Figure 4.44 shows changes in monthly values of groundwater storage inferred from GRACE (FO) data.

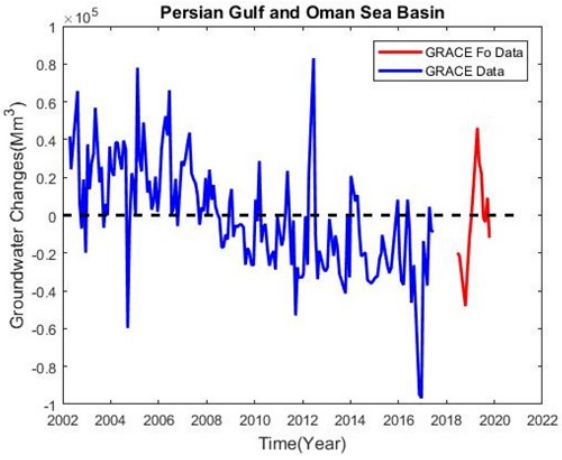

Figure 4.44. Monthly values of groundwater storage, inferred from GRACE data and GRACE (FO) data, across the Persian Gulf and Oman Sea basin (code 2).

4.4.2. The Caspian Sea basin

Figure 4.45 shows changes in monthly values of groundwater storage inferred from GRACE (FO) data.

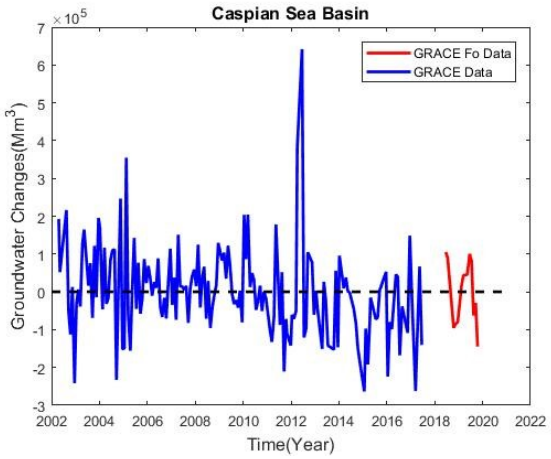

Figure 4.45. Monthly values of groundwater storage, inferred from GRACE data and GRACE (FO) data, across the Caspian Sea basin (code 1).

4.4.3. The Urmia Lake basin

Figure 4.46 shows changes in monthly values of groundwater storage inferred from GRACE (FO) data.

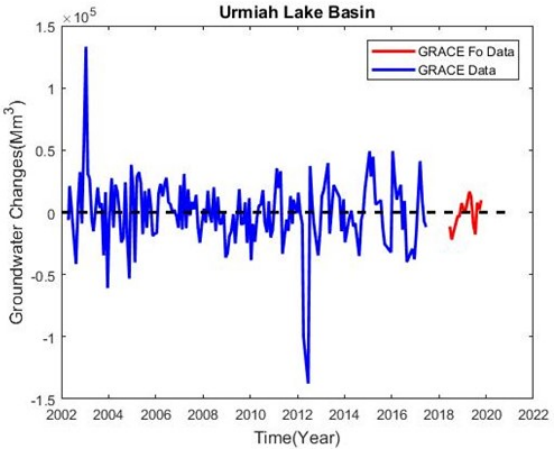

Figure 4.46. Monthly values of groundwater storage, inferred from GRACE data and GRACE (FO) data, across the Urmia Lake basin (code 3).

4.4.4. Central Plateau basin

Figure 4.47 shows changes in monthly values of groundwater storage inferred from GRACE (FO) data.

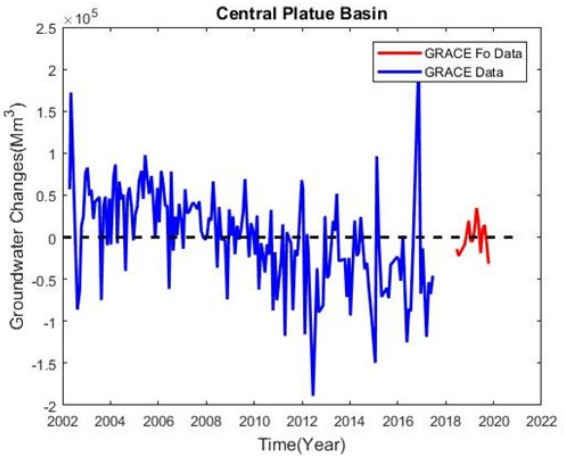

Figure 4.47. Monthly values of groundwater storage, inferred from GRACE data and GRACE (FO) data, across the Central Plateau basin (code 4).

4.4.5. The Eastern Boundary basin

Figure 4.48 shows changes in monthly values of groundwater storage inferred from GRACE (FO) data.

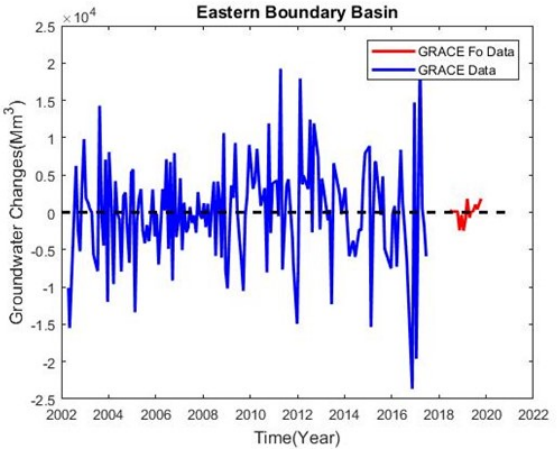

Figure 4.48. Monthly values of groundwater storage, inferred from GRACE data and GRACE (FO) data, across the Eastern Boundary basin (code 5).

4.4.6. The Ghareghom basin

Figure 4.49 shows changes in monthly values of groundwater storage inferred from GRACE (FO) data.

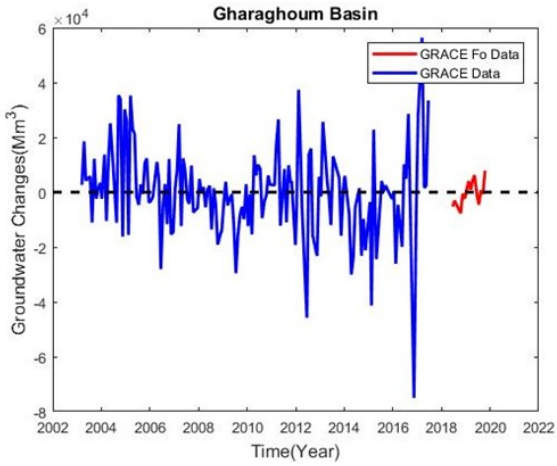

Figure 4.49. Monthly values of groundwater storage, inferred from GRACE data and GRACE (FO) data, across the Ghareghom basin (code 6).

Figures 4.44–4.49 show total water storage inferred from GRACE and GRACE (FO). There is good agreement between these sets of estimations.

The agreement between GRACE measurements and GRACE FO estimates demonstrates the value of GRACE (FO) time series as an alternative quantitative tool for monitoring groundwater storage changes when in-situ measurements are limited or unavailable. In these figures, it seems there is less noise and fluctuation in the GRACE FO results.

4.5. Groundwater trends for different water basins in Iran and their uncertainties

The general agreement between the well data and the GRACE-minus-Global Land Data Assimilation System (GLDAS) estimates for the main water basins in Iran gives us confidence in the overall trends of our GRACE-minus-GLDAS groundwater time series for the region. Table 4.1 lists the trends for the main basins.

Table 4.1. Secular trends, in Gt/yr, of the total groundwater storage changes (GRACE-minus- GLDAS/Noah) for Iran, for 2002–2017. Results are compared with estimates based on well data.

Mascons	GRACE – GLDAS/Noah (GT/yr)	Well data (GT/yr)
Mascon 1 (Caspian Sea)	-7.82 ± 4	-3.60
Mascon 2 (Persian Gulf and Oman Sea)	-4.44 ± 1	-3.0
Mascon 3 (Urmia Lake)	-1.0 ± 1	-0.53
Mascon 4 (Central Plateau)	-7.0 ± 4	-11.55
Mascon 5 (Eastern Boundary)	0.80 ± 2	-0.57
Mascon 6 (Ghareghom)	-0.23 ± 1	-0.83
Total	-20.49± 1	-20.08

Table 4.1 shows groundwater trends for water basins inferred from well data and TWS trends inferred from GRACE data. There is an acceptable agreement between well data and GRACE data in most of the water basins, except the Eastern Boundary. Probably this mismatch is because of the small area of this mascon and the shape of it. The total amounts of trends of water level from GRACE data and well data have very good agreement. The total amount of uncertainty is quite small; it demonstrated the strong ability of GRACE in groundwater storage estimations in large areas. Using local hydrological models in small areas would reduce the uncertainties.

The agreement between results of GRACE and GRACE FO, and results of well data demonstrates that GRACE and GRACE FO are valuable tools for groundwater monitoring.

This page is intentionally left blank.

Chapter 5

Conclusion and Remarks

The GRACE and GRACE FO missions have the unique ability to sense gravity fluctuation at long- to medium-wavelength across the world. Using hydrological models and making other corrections on GRACE data, it is possible to estimate total water storage and carry out groundwater storage monitoring. This thesis is deals with the study of the fluctuation of the water table in Iran's six main water basins, by using GRACE and GRACE FO Level-2 data. Then in order to verify GRACE data ability in water-level monitoring, we use observation well level in the six water basins in Iran.

The Level-2 GRACE data are released as spherical harmonic coefficients in monthly time resolutions. In order to monitor the water table in every water basin, first, we have to estimate total water storage for them. GRACE data include measurement error, leakage error, and correlated error or striping error. One of the best methods to decrease all these errors together is least squares mascon fitting. This method has been used when users fit mass elements to spherical harmonic coefficients to reduce the errors. The mascon analysis has less leakage

error and can be used for hydrological applications without applying any gain factors or any post processing in comparison with other solutions such as the spherical harmonics solutions.

In this thesis, the mascons are the six main water basins of Iran. In order to validate the ability of GRACE for monitoring the water table in small water basins, 17,865 piezometer wells were monitored monthly in 32 sub-basins in Iran. The sub-basins were also divided into more than 500 study areas. The total changes in groundwater storage across each sub-basin is computed by adding together the scaled changes in groundwater storage in Mm^3 of all its study areas. The same procedure is carried out for each main water basin. All these computations have been illustrated in chapter 4 and in the appendixes. There are some valuable results that have come out of these computations, some of which we can see in the following:

The study presented here suggests that groundwater depletion is the largest single contributor to the observed negative trend, the majority of which occurred after the drought in 2007. The groundwater loss that has been accrued during the study period is particularly alarming for Iran, which is already facing severe water scarcity.

In figure 4.1, we have a secular trend of groundwater storage in the whole of Iran, in the period of 2002–2017. Secular trend groundwater storage is estimated to be from -4,400 to 600 Mm^3 across Iran. In the most of regions, we can see sever water depletion. There are two intensive negative trends concentrated around Tehran. Land subsidence has been reported in Tehran and other areas because of water depletion (Voss et al. 2013). Maybe there is a correlation between these two.

- Considering the figures in the appendixes, we found that in some of the study areas we have no significant signal. It shows inadequacy and sometimes uncertainty of well data in those study areas because of the enormous number of wells, difficulty in frequent access to some wells, and having no digital system for data records. But in large-scale sub-basins and basins, having lots of study areas helped us to have acceptable results.

- Water use behaviour in Iran during the study period followed the pattern of increased groundwater extraction in reaction to drought and decreasing surface water accessibility.

- After the drought of 2007, without water from surface water to replenish supplies', there was only one choice: to increase reliance on groundwater. So the Iran's government dug new wells after 2007, to meet their agricultural and domestic needs. This rapid increase in groundwater consumption, with no replenishment from precipitation or streamflow, is an important driver of the groundwater losses that are estimated in this thesis.

- There is not an effective international water management strategy; each country is free to act individually, probably without thinking about the sustainability of groundwater. Iran uses much of the inadequate water resources to support the goals of the agriculture sector (FAO, 2009). Economically, this crisis resulted in the loss of agricultural yields, unemployment, and migration. Politically, the response to the drought represents a missed opportunity for cooperative transboundary water management on the Afghanistan border.

This study highlights the role that the GRACE mission plays in advancing hydrologic remote sensing. This mission can create essential tools for regional and transboundary environmental decision making. This study described a valuable and unique opportunity to estimate hydrologic trends in a data-inaccessible region.

In Iran, there are many illegal wells, and sometimes there is no control over their water withdrawals. Probably changing crop patterns, inefficient irrigation systems, and high water wastage with traditional irrigation causes increased water extraction. So there are some pressures on decision makers to grant permission for new wells in aquifers with negative water balances. When the groundwater table in an aquifer is decreased, discharges of wells are usually decreased. So even by digging deeper wells, the yield of wells has been reduced.

All these issues lead us to the necessity of appropriate water management. Establishing applicable and proper rules for water usage permission and having standards for the amount of water withdrawal from groundwater as a safe yield from wells helps to reduce the water depletion and its effects in Iran. Therefore, access to accurate water level data to have updated time series is required for proper management. Better monitoring, assessment, and forecasting of water resources would help government agencies allocate water more efficiently among competing needs (Robert et al. 2001).

TWS is the vertically integrated measure of groundwater, soil moisture (SM), snow, ice, and surface water. To isolate GWS from total TWS, other components must be estimated from models or observations (Yeh et al. 2006, Rodell et al. 2007, Ramillien et al. 2008, Zaitchik et al. 2008).

The agreement between the results of GRACE, GRACE FO, and of well data shows that GRACE and GRACE FO are valuable tools for groundwater monitoring.

Remarks

According to the results of this study, the following is recommended:

- Using local hydrological models can make satellite monitoring of the hydrological parameters such as groundwater, precipitation, run-off water, and soil moisture more effective.
- GRACE and GRACE FO data can be used for water management in small areas, for example around 44,295.5 km^2 (Ghareghom water basin).
- The results in the Eastern Boundary basin show that GRACE and GRACE FO data can be used for transboundary water study.
- GRACE and GRACE FO data can be used for monitoring of groundwater agricultural consumption.

References:

- Agboma, C., Yirdaw, S. and Snelgrove, K., (2009), Intercomparison of the total storage deficit index (TDSI) over two Canadian Prairie catchments, J. Hydrol, 374(3/4), 351–359, doi:10.1016/j.jhydrol.2009.06.034.

- Ahmed, M., Sultan, M., Wahr, J. and Yan, E., (2014), The use of GRACE data to monitor natural and anthropogenic induced variations in water availability across Africa, Earth-Science Reviews, 136, 289-300, doi: http://dx.doi.org/10.1016/j.earscirev.2014.05.009.

- Aladin, N. and Plotnikov, I., (2004), The Caspian Sea, Lake Basin Management Initiative Thematic Paper. Brookhaven National Laboratory Upton NY 11973 USA.

- Allan JAT. (2007), Rural economic transitions: groundwater use in the Middle East and its environmental consequences. See Ref. 27, pp. 63–78

- Alley, W. M. (2006), Tracking U.S. groundwater reserves for the future, Environment. Science and policy for sustainable development 48(3), 10–25 DOI: 10.3200/ENVT.48.3.10-25.

- Alsdorf, D.E., Rodriguez, E. and Lettenmaier, D.P. (2007), Measuring surface water from space. Reviews of Geophysics 45, RG2002, DOI: 10.1029/2006RG000197.

- Amery, H.A., Wolf, A.T. (2000). Water in the Middle East: A Geography of Peace, University of Texas Press, Austin, Tex.

- Andersen, O., Seneviratne, S., Hinderer, J. and Viterbo, P., (2005), GRACE derived terrestrial water storage depletion associated with the 2003 European heat wave, Geophys. Res. Lett., 32, L18405, doi:10.1029/ 2005GL023574.

- Benjamin, D., Wahr, J., Ray, R.D., Egbert, G.D., and S.D. Desai (2006), Constraints on Mantle Anelasticity From Geodetic Observations, and Implications for the J2 Anomaly. Geophys. J. Int., 165, 3-16.

- Bergkamp, G.,Cross,K., (2007), Groundwater and ecosystem services: options for sustainable use. International Symposium on Groundwater Sustainability (ISGWAS), pp. 177–93

- Blomquist, WA., Ingram, HM., (2003), Boundaries seen and unseen : resolving transboundary groundwater problems. Water Int. 28:162–69

- Bonan, G. and Doney, S., (2018), Climate, ecosystems, and planetary futures: The challenge to predict life in Earth system models. Science. 359. Eaam 8328. 10.1126/science.aam8328.

- Briscoe, J., (1999), Water resources management in Yemen, results of a consultation. Off. memo., World Bank, Washington, DC

- Brown, L., (2007), Water tables falling and rivers running dry: international situation. Int. J. Environ. Consum. 3:1–5

- Castle, S. L., Thomas, B. F., Reager, J. T., Rodell, M., Swenson, S. C. and Famiglietti, J. S., (2014), Groundwater depletion during drought threatens future water security of the Colorado River Basin, Geophys. Res. Lett., 41, 5904–5911, doi:10.1002/2014GL061055.

- Chambers, D. P., (2006), Observing seasonal steric sea level variations with GRACE and satellite altimetry, J. Geophys. Res., 111, C03010, doi:10.1029/2005JC002914.

- Chao, B. F., Richard, S.G., (1987), Changes in the Earth's rotation and low-degree gravitational field induced by earthquakes. Geophys.J.R.astr.Soc.(1987)91, 569-596.

- Chao, B.F. and Au, A.Y., (1991), Temporal variation of the Earth's low-degree zonal gravitational field caused by atmospheric mass distribution, 1980-1988. J. Geophys. Res., 96 (B4), 6569-6575.

- Chen, J. L., Wilson, C. R. and Seo, K.-W., (2006), Optimized smoothing of Gravity Recovery and Climate Experiment (GRACE) time-variable gravity observations, JOURNAL OF GEOPHYSICAL RESEARCH, VOL. 111, B06408, doi: 10.1029/2005JB004064, 2006.

- Chen, J., Wilson, C., Famiglietti, J. S. and Rodell, M., (2005), Spatial sensitivity of the Gravity Recovery and Climate Experiment (GRACE) time-variable gravity observations J. Geophys. Res., 110, B08408, doi:10.1029/2004JB003536, 2005

- Chen, J., Wilson, C., Tapley, B., Longuevergne, L., Lang, Z. and Scanlon, B. (2010), Recent La Plata basin drought conditions observed by satellite gravimetry, J. Geophys. Res., 115, D22108, doi:10.1029/2010JD014689.

- Cheng, M. and Tapley, B.D., (2004), Variations in the Earth's oblateness during the past 28 years, J. Geophys. Res., 109, B09402.

- Cheng, M., Eanes, R., Shum, C., Schutz, B. and Tapley, B., (1989), Temporal variations in low degree zonal harmonics from Starlette orbit analysis, Geophys. Res. Lett., 16, 393-396, 1989.

- Cheng, M., Tapley, B.D., (2004), Variations in the earth's oblateness during the past 28 years. Journal of Geophysical Research: Solid Earth 109(B9)

- Cheng, M.K. and Tapley B.D., (1999), Seasonal variations in low degree zonal harmonics of the Earth's gravity field from satellite laser ranging observations. J. Geophys. Res., 104 (B2), 2667-2681.

- Cheng, M.K., Shum C.K. and Tapley B.D., (1997), Determination of long-term changes in the Earth's gravity field from satellite laser ranging observations. J. Geophys. Res., 102 (B10), 22377-22390.

- Chilton J. (1992), Women and Water. Waterlines J. 2(110): 2-4. EPA (2005). "Protecting Water Quality from Agricultural Runoff" Fact Sheet No. EPA-841-F-05-001.

- Cox, C. M., and Chao, B. F., (2002), Detection of a large-scale mass redistribution in the terrestrial system since 1998, Science, 297, 831-832.

- Darama, Y. (2014), Comment on "Groundwater depletion in the Middle East from GRACE with implications for transboundary water management in the Tigris-Euphrates-Western Iran Region" by Katalyn A. Voss et al, Water Resources Research, 50(1), 754-757, doi: http://dx.doi.org/10.1002/2013WR014084.

- Darehshouri, B. F. and Kasraian, N., (1998), Nature of Iran. Rowzaneh Kar Publication, Tehran.

- Dariusz, R. and Bugajski, (2016), The Persian Gulf in the light of law of the sea, Prawo Morskie 2016, t. XXXII, ISSN 0860-7338

- Davis, J. L., Tamisiea, M. E., Elósegui, P., Mitrovica, J. X. and Hill, E. M., (2008), A statistical filtering approach for Gravity Recovery and Climate Experiment (GRACE) gravity data, J. Geophys. Res., 113, B04410, doi: 10.1029/2007JB005043.

- Delju, A.H., Ceylan, A., Piguet, E. and Rebetez, M., (2012), Observed climate variability and change in Urmia Lake Basin, Iran. Theoretical and Applied Climatology, doi: 10.1007/s00704-012-0651- 9.

- Dennehy, K.F., Litke, DW., McMahon, PB., (2002), The High Plains aquifer, USA: groundwater development and sustainability. In: Hiscock KM, Rivett MO, Davison RM (eds) Sustainable groundwater development. Geol Soc Lond DuMars CT, Minier JD (2004)

- Devin L. Galloway and Thomas J. Burbey, Review: (2011), Regional land subsidence accompanying groundwater extraction, Hydrogeology Journal, Official Journal of the International, Association of Hydrogeologists, ISSN 1431-2174 Volume 19 Number 8 Hydrogeol J (2011) 19:1459-1486 DOI 10.1007/s10040-011-0775-5

- Dickey, J.O., Bentley, C.R., Bilham, R., Carton, J.A., Eanes, R.J., Herring, T.A., Kaula, W.M., Lagerloef, G.S.E., Rojstaczer, S., Smith, W.H.F., van den Dool, H.M., Wahr, J.M., Zuber, M.T., (1997), Satellite Gravity and the Geosphere, National Research Council Report, National Academy Press, 112 pp

- Dickey, J.O., Marcus, S.L., de Viron, O. and Fukumori, I., (2002), Recent Earth oblateness variations: Unraveling climate and postglacial rebound effects Science, 298, 1975-1977.

- Dong, D., Gross, R.S. and Dickey, J.O., (1996), Seasonal variations of the Earth's gravitational field: An analysis of atmospheric and oceanic tidal excitation, Geophys. Res. Lett., 23, 725-728.

- Dunn, C., Bertiger, W., Bar-Sever, Y., desai, Sayali., Haines, B., Kuang, Da., Franklin, G., Harris, I., Kruizinga, G., Meehan, T., Nandi, S., Nguyen, D., Rogstad, T., Thomas, J.B., Tien, J., Romans, L., Watkins, M., Wu, S.-C, Bettadpur, S. and Kim, J. (2003), Instrument of Grace: GPS augments gravity measurements. GPS World. 14. 16-28.

- Eanes, R.J., (1995), A study of temporal variations in Earth's gravitational field using LAGEOS-1 laser ranging observations, Ph.D. thesis, 128 pp., Univ. of Tex., Austin.

- Eckstein, G., (2005), Protecting a hidden treasure: the U.N. International Law Commission and the international law of transboundary ground water resources. Am. Univ. Sustain. Dev. Law Policy 5:5–12

- Eckstein, Y., Eckstein, G., (2003), Groundwater resources and international law in the Middle East peace process. Water Int. 28:154–61

- Eimanifar, A and Mohebbi, F., (2007), Urmia Lake (Northwest Iran): A Brief Review. Saline systems. Aquat. Biosyst. 3, 5. 10.1186/1746-1448-3-5.

- Elissason, A., Faures, JM., Frenken, K. and Hoogeveen, J., (2003), Getting to grips with water information for agriculture. Presented at 6th Water Inf. Summit, Sept. 9–12, Delft, Neth.

- Esmaili, O., Tajrishy, M., and Daneshkar Arasteh, P., (2006), Evaluation of dust sources in Iran through remote sensing and synoptical analysis. Atlantic Europe conference on remote imaging and, spectroscopy.

- Famiglietti, J. S., Lo, M., Ho, S. L., Bethune, J. Anderson, K. J., Syed, T. H., Swanson, S. C., deLineage, C. R. and Rodell, M., (2011b), Satellites measure recent rates of groundwater depletion in California's Central Valley, Geophys. Res. Lett., 38, LO3403, doi:10.1029/2010GL046442

- FAO 2008. Water Report 34 [online]. [Access 16.03.2017]. Available at: http://www.fao.org/nr/water/aquastat/countries_regions/irn/index.stm

- Feitelson, E., (2006), Impediments to the management of shared aquifers: a political economy perspective. Hydrogeol.J. 14:319–29

- Forootan, E., (2014), Statistical Signal Decomposition Techniques for Analysing Time-Variable Satellite Gravimetry Data, Inaugural-Dissertation zur Erlangung des akademischen Grades Doktor-Ingenieur (Dr.-Ing.) der Landwirtschaftlichen Fakultät der Rheinischen Friedrich-Wilhelms-Universität Bonn vorgelegt am.

- Foster, S. S. D. and Chilton, P. J., (1957), Groundwater: the processes and global significance of aquifer degradation Phil. Trans. R. Soc. Lond. B 2003 358, 1957-1972, doi: 10.1098/rstb.2003.1380

- Foster, S. S. D., Chilton, P. J., (2003), Groundwater: the processes and global significance of aquifer degradation. Philos.Trans.R.Soc.Lond.Ser.B 358:1957–72

- Foster, S. S. D., Chilton, P. J., Moench, M., Cardy, F., Schiffler, M., (2000), Groundwater in rural development: facing the challenges of supply and resource sustainability. World Bank Tech. Pap. 463, Washington, DC.

- Foster, S. S. D., Lawrence, AR., Morris, BL., (1997), Groundwater in urban development: assessing management needs and formulating policy strategies.World Bank Tech. Pap. 390, Washington, DC.

- Gegout, P., and Cazenave, A., (1993), Temporal variations of the Earth gravity field for 1985-1989 derived from LAGEOS, Geophys. J. Int., 114, 347-359, 1993.

- Gemitzi, A., and Lakshmi, V., (2017), Evaluating Renewable Groundwater Stress with GRACE Data in Greece. J. Hydrol., 403, 130–140.

- Gent, P. R. and Coauthors, (2011), The Community Climate System Model version 4. J. Climate, 24, 4973–4991

- George, B., Cressey, The Shatt al-Arab (1958), Middle East Journal, Vol. 12, No. 4 , pp. 448-460 Published by: Middle East Institute.

- Ghaheri, M., Baghal-Vayjooee, M.H. and Naziri, J., (1999), Lake Urmia, Iran: A summary Review. International Journal of Salt Lake Research, 8, pp.19-22.

- Ghorbani, M., (2013), The economic geology of Iran, mineral deposits and natural resources, Springer, ISBN 978-94-007-5624-3. DOI 10.1007/978-94-007-5625-0.

- Giordano, M., (2009), Global Groundwater? Issues and Solutions. Annual review of Environment and Resources. 34. 153-178. 10.1146/annurev.environ.030308.100251.

- Giordano, M., Villholth, K., eds, (2007), The Agricultural Groundwater Revolution: Opportunities and Threats to Development. Vol. 3: Comprehensive Assessment. Wallingford, UK: CABI Publ. 419 pp.

- Gong, H. L., Pan, Y., Zheng, L. Q., Li, X. J., Zhu, L., Zhang, C., Huang, Z. Y., Li, Z. P., Wang, H. G. and Zhou, C. F., (2018), Long-term groundwater storage changes and

land subsidence development in the North China Plain (1971-2015), Hydrogeology Journal, 26, 1417-1427. https://doi.org/10.1007/s10040-018-1768-4.

- Guo, J. Y. Duan, X. J., Shum, C. K., (2010), Non-isotropic Gaussian smoothing and leakage reduction for determining mass changes over land and ocean using GRACE data, Geophysical Journal International, Volume 181, Issue 1, 1 April 2010, Pages 290–302, https://doi.org/10.1111/j.1365-246X.2010.04534.x

- Guo, J. Y., Duan, X. J., and Shum, C. K., (2010), Non-isotropic Gaussian smoothing and leakage reduction for determining mass changes over land and ocean using GRACE data, Geophys. J. Int. (2010) 181, 290–302 doi: 10.1111/j.1365-246X.2010.04534.x).

- Guo, J.Y. and Shum, C.K., (2009), Application of the cosine-Fourier series expansion in the transformation of data between latitude–longitude grids, Comput. Geosci., 35, 1439–1444, doi:10.1016/j.cageo.2008.09.010.

- Guo, J.Y., Huang, Z.W., Shum, C.K., and Van Der Wal, W., (2012), comparison among contemporary glacial isostatic adjustment models, J Geodyn, 61(0), 129-137.

- Han, S.C., Shum, C.K., Jekeli, C., Kuo, C.Y., Wilson C. and Seo K.W., (2005b), Non-isotropic filtering of GRACE temporal gravity for geophysical signal enhancement. Geophys. J. Int., 163, 18–25, doi:10.1111/j.1365-246X.2005.02756.

- Hassanzadeh, E., Zarghami, M. and Hassanzadeh, Y., (2011), Determining the Main Factors in Declining the Urmia Lake Level by Using Dynamics Modeling. Water Resources Management, 26(1), pp.129-145, doi: 10.1007/s11269-011-9909-8.

- Hawking, S.W. and Israel, W., (1979), General relativity, An Einstein centenary survey, edited by: Cambridge university press, 1979, ISBN 0521222850.

- Heiskanen, W.A. and Moritz, H., (1967), Physical geodesy. Bulletin Géodésique (1946-1975), 86(1), 491-492.

- Hernandez-M. N., Martinez, Cortina. L., Fornes, J. (2003), Intensive Groundwater Use in Spain. Ref. 142, pp. 387–414

- Hoffmann, J., (2004), The future of satellite remote sensing in hydrogeology. Hydrogeology Journal. 13. 247-250. 10.1007/s10040-004-0409-2.

- Hofmann-Wellenhof, B. and Moritz, H.: (2005), Physical Geodesy. Springer-Verlag Wien.

- Hu R., Yue Z., Wang Lu., Wang S., (2004), Review on current status and challenging issues of land subsidence in China. Eng Geol. 76:65–77.

- Huang, J. L., Pavlic, G. Rivera, A., Palombi, D. and Smerdon, B. (2016), Mapping groundwater storage variations with GRACE: a case study in Alberta, Canada, Hydrogeology Journal, 24(7), 1663-1680. https://dx.doi.org/10.1007/s10040-016-1412-0.

- Hughes, P. and Hunter., J.R., (1979), A Proposal for a Physical Oceanography Program and Numerical Modeling of the KAP Region. UNESCO, Div. Mar. Sci., Paris, MARINF/27, 16 Oct. 1979. 102 pp.

- IPCC. Intergovernmental Panel on Climate Change. Climate Change 2007: impacts, adaptation and vulnerability; summary for policy makers; 2007. Available at: www.ipcc.cg/SPM13apr07.pdf (accessed 3 November 2012)

- Iran's Third National Communication to UNFCCC report, National Climate Change Office at the Department of Environment on behalf of the Government of the Islamic Republic of Iran, Department of Environment, National Climate Change Office, No. 152, Environmental Research Center, Pardisan Eco-park, Hakim Expressway, Tehran, Iran. P.O.Box: 14155-7383. www.climate-change.ir & www.doe.ir

- Jacob, T., Wahr, J., Pfeffer, W. T. and Swenson, S., (2012), Recent contributions of glaciers and ice caps to sea level rise, Nature, 482, 514–518 doi: 10.1038/nature10847.

- Jacobsen, M., M. Webster, and K. Vairavamoorthy (Eds.) (2012), The Future of Water in African Cities: Why Waste Water?, World Bank Publ., Washington, D. C.

- Jamab Consulting Engineers Company. 1998. National Master Plan of Water: Final Report. Iranian Ministry of Energy Press (in Persian).

- Jarvis, WT., (2006), Transboundary groundwater: geopolitical consequences, commons sense, and the law of the hiddensea. Unpubl. PhD diss. Oregon State Univ.

- Jekeli, C., (1981), Modifying Stokes' function to reduce the error of geoid undulation computations, J. Geophys. Res., 86(B8), 6985–6990, doi: 10.1029/JB086iB08p06985.

- Joodaki, Gh. and Nahavandchi, H., (2010), Greenland mass balance estimation from satellite gravity measurements, ESA Living Planet Conference, ESA Special Publication SP-686.

- Joodaki, Gh., Wahr, J., Swenson, S., (2014), Estimating the human contribution to groundwater depletion in the Middle East, from GRACE data, land surface models, and well observations. Water Resour. Res. 50, 2679–2692 (2014).

- Kåmpf, J. and Sadrinasab, M., (2006), The circulation of the Persian Gulf: a numerical study. Ocean Sci., 2, 27–41, 2006 www.ocean-sci.net/2/27/2006/ Ocean Science,

- Karami, E., Hayati, D., (2005), Rural Poverty and Sustainability: The Case of Groundwater Depletion in Iran, Journal: Asian Journal of Water, Environment and Pollution, vol. 2, no. 2, pp. 51-61, 2005.

- Kaula, W.M., (1966), Theory of satelite geodesy, Blaicdell, Waltham, MA, 1966.

- Kelts, K. and Shahrabi, M., (1986), Holocene sedimentalogy of hypersaline Lake Urmia, northwestern Iran. Paleogeography, Paleoclimatology and Paleoecology, 54, pp.105-30.3

- Khaki, M., Forootan, E., Kuhn, M., Awange, J., van Dijk, A., Schumacher, M. and Sharifie, M. A., (2018), Determining water storage depletion within Iran by assimilating GRACE data into the W3RA hydrological model, Adv.Water Resour., 114, 1-18. http://dx.doi.org/10.1016/j.advwatres.2018.02.008.

- Khatami, S. and Berndtsson, R., (2013), Urmia Lake Watershed Restoration in Iran: Short- and Long-Term Perspectives, 6th International Perspective on Water Resources & the Environment conference (IPWE 2013).

- Klees, R., Liu, X., Wittwer, T. et al. Surv Geophys (2008), 29: 335. https://doi.org/10.1007/s10712-008-9049-8.

- Konikow, L.F. and Kendy, E., (2005), Groundwater depletion: A global problem, Hydrogeol J (2005) 13: 317. https://doi.org/10.1007/s10040-004-0411-8

- Kusche, J., (2007), Approximate decorrelation and non-isotropic smoothing of time-variable GRACE-type gravity field models, J Geod, 81: 733. https://doi.org/10.1007/s00190-007-0143-3

- Kusche, J., Schmidt, R., Petrovic, S., and Rietbroek, R., (2009), Decorrelated GRACE time-variable gravity solutions by GFZ, and their validation using a hydrological model. J Geod (2009) 83:903–913, DOI 10.1007/s00190-009-0308-3.

- Lall, U., Sangoyomi, T. and Abarbanel, H.D.I., (1996), Nonlinear Dynamics of the Great Salt Lake: Nonparametric Short-Term Forecasting. Water Resources Research, 32(4), pp.975–985, doi:10.1029/95WR03402.

- Landerer F.W. and Swenson, S. C., (2012), Accuracy of scaled GRACE terrestrial water storage estimates. Water Resources Research, Vol 48, W04531, 11 PP, doi:10.1029/2011WR011453.

- Leblanc, M., Tregoning, P., Ramillien, G., Tweed, S. and Fakes, A., (2009), Basin-scale, integrated observations of the early 21st century multiyear drought in southeast Australia, Water Resour. Res., 45, W04408, doi:10.1029/2008WR007333.

- Lemoine, F.G., Pavlis, N.K., Kenyon, S.C., Rapp, R.H., Pavlis, E.C., Chao, B.F., (1998), New high-resolution model developed for earth' gravitational field. EOS Trans AGU 79(9):117–118. doi:10.1029/98EO00076/pdf

- Leonard, F. Konikow, Eloise Kendy, (2005), Groundwater depletion: A global problem. Published online: Springer-Verlag 2005 Hydrogeol J (2005) 13:317–320 DOI 10.1007/s10040-004-0411-8

- Lettenmaier, D. P. and Famiglietti, J. S., (2006), Hydrology: Water on high, Nature, 444, 562–563, doi:10.1038/444562a.

- Liamas, MR., Martınez-Santos, P. (2005), Intensive groundwater use: silent revolution and potential source of social conflicts. J. Water Resour.Plan.Manag. 131:337–41.

- Lucien, M., Brush, JR., (1849), Flow Characteristics of Selected Streams in Central Pennsylvania, Physiographic and hydraulic studies of revers, geological survey professional paper 282-F, US Department of interior, 1849

- Luthcke, S. B., Zwally, H. J., Abdalati, W., Rowlands, D. D. Ray, R. D., Nerem, R. S., Lemoine, F. G., Mccarthy, J. J. and Chinn, D. S., (2006a), Recent Greenland Ice Mass Loss by Drainage System from Satellite Gravity Observations. Science, 24 NOV 2006: 1286-1289

- Luthcke, SB., Sabaka, TJ., BD Loomis, Arendt, AA., McCarthy, JJ., Camp, J., (2013), Antarctica, Greenland and Gulf of Alaska land-ice evolution from an iterated GRACE global mascon solution, Journal of Glaciology 59 (216), 613-631.

- Madani, K., (2014), Water management in Iran: what is causing the looming crisis? , J Environ Stud Sci (2014) 4:315–328 DOI 10.1007/s13412-014-0182-z.

- Mahdavi, M. (2004), Applied Hydrology Vol. 2 (Fifth Ed.). University of Tehran Press, Iran, 420 (in Persian).

- Mahmoudpour, M., Khamehchiyan, M., Nikudel, M. R., Ghassemi, M. R., (2016), Numerical simulation and prediction of regional land subsidence caused by groundwater exploitation in the southwest plain of Tehran, Iran. Engineering Geology 201 (2016) 6–28.

- Matsumoto, K., (2009), Treaties with groundwater provisions. In Managing and Transforming Water Conflicts, ed. PJ Delli, A Wolf, pp. 266–73. Cambridge: Cambridge Univ. Press.

- McGuire, VL., Johnson, MR., Schieffer, RL., Stanton, JS., Sebree, SK., Verstraeten, IM., (2003), Water in storage and approaches to groundwater management, High Plains aquifer, 2000. US Geol Surv Circ 1243.

- Michel, D., A. Pandya, S. I. Hasnain, R. Sticklor, and S. Panuganti (2012), Water Challenges and Cooperative Response in the Middle East and North Africa, Brookings Insititution, Washington, D.C. Available at http://www.brookings.edu/research/papers/2012/11/water-security-mid dle-east-iwf.

- Mitrovica, J.X., Wahr, J., Matsuyama, I. and Paulson, A., (2005), The rotational stability of an ice age Earth, Geophys. J.Int. Doi: 10.1111/j.1365-246X.2005.02609.x.

- Moore, P., Zhang, Q., and Alothman, A., (2005), Annual and semiannual variations of the Earth's gravitational field from satellite laser ranging and CHAMP. J. Geophys. Res., 110 (B6), B06401.

- Moore, S., and Fisher, J., (2010), Challenges and Opportunities in GRACE-Based Groundwater Storage Assessment and Management: An Example from Yemen, Water Resources Management, 26(6), 1425-1453, doi: http://dx.doi.org/10.1007/s11269-011-9966-z.

- Moridi, A., (2017), State of water resources in Iran, Med Crave, International Journal of Hydrology, Volume 1 Issue 4 – 2017:111–114. DOI: 10.15406/ijh.2017.01.00021.

- Morris, BL., Lawrence ARL., Chilton, PJC, Adams, B, Calow, RC, Liknck, B.A., (2003), Groundwater and its susceptibility to degradation: a global assessment of the problem and options for management. EarlyWarn.Assess.Rep.Ser.RS.03–3. UN Environ. Program., Nairobi, Kenya.

- Moustos, D., (2017), Gravity as a thermodynamic phenomenon, M.Sc. Thesis, Department of Physics, University of Patras, Greece.

- Mulinde, C., Mwanjalolo, M. Twesigomwe, E., Egeru, A., (2016), METEOROLOGICAL DROUGHT OCCURRENCE AND SEVERITY IN UGANDA. 185-215.

- Muller, PM., Sjogren, WL., (1968), Mascons: lunar mass concentrations. Science. 1968 Aug 16;161(3842):680-4. doi: 10.1126/science.161.3842.680. PMID: 17801458.

- Nabavi M (1976), An introduction to geology of Iran. Geological Survey of Iran, Tehran.

- Nabavi M. (1994), Climatological Map of Iran.

- Nabavi, E., (2018), Failed policies, falling aquifers, Unpacking groundwater over abstraction in Iran. Water Alternatives 11(3): 699-724.

- Nerem, R.S., Chao, B.F., Au, A.Y., Chan, J.C., Klosko, S.M., Pavlis, N.K. and Williamson, R.G., (1993), Time variations of the Earth's gravitational field from satellite laser ranging to Lageos, Geophys. Res. Left., 20, 595-598, 1993.

- Nerem, R.S., Eanes, R.J., Thompson, P.F., Chen, J.L., (2000), Observations of annual variations of the Earth's gravitational field using satellite laser ranging and geophysical models. Geophys. Res. Lett., 27 (12), 1783-1786.

- Olawoyin, R., Acheampong, P. K., Objective assessment of the Thiessen polygon method for estimating areal rainfall depths in the River Volta catchment in Ghana. Ghana Journal of Geography Vol. 9(2) (Special Issue), 2017 Pages 151–174.

- Oleson, K., Lawrence, D. M., Bonan, G. B., Drewniak, B., Huang, M., Koven, C. D., Yang, Z. -L., (2013), Technical description of version 4.5 of the Community Land Model (CLM) (No. NCAR/TN-503+STR). doi:10.5065/D6RR1W7M.

- Olumuyiwa I. Ojo., Fred A.O. Otieno and George M. Ochieng, (2012), Groundwater: Characteristics, qualities, pollutions and treatments: An overview, International Journal of Water Resources and Environmental Engineering Vol. 4(6), pp. 162-170, Available

online at http://www.academicjournals.org/IJWREE DOI: 10.5897/IJWREE12.038 ISSN 1991-637X ©2012 Academic Journals.

- Ouma, Y. O., Aballa, D. O. Marinda, D. O., Tateishi, R. and Hahn, M., (2015), Use of GRACE time-variable data and GLDAS-LSM for estimating groundwater storage variability at small basin scales: a case study of the Nzoia River Basin, International Journal of Remote Sensing, 36(22), 5707-5736, doi: http://dx.doi.org/10.1080/01431161.2015.1104743.

- Pavelic, P., Giorgano, M., Keraita, B., Ramesh, V. and Rao, T., (2012), Groundwater availability and use in Sub-Saharan Africa, A review of 15 countries, 276 Colombo, Sri Lanka: International Water Management Institute (IWMI), Sri Lanka, doi:10.5337/2012.213.

- Pool, DR., Winster, D., Cole, K.C., (2000), Land-subsidence and groundwater storage monitoring in the Tucson Active Management Area, Arizona. US Geol Surv Fact Sheet 084-00 Service RF (2004) As the West goes dry. Science 303:1124–1127.

- Puri, S., Appelgren B., Arnold G., Aureli A., Burchi S., et al. (2001), Internationally shared (transboundary) aquifer resources management, their significance and sustainable management: a frame work document. IHP-VI, IHPNonSerialPubl.Hydrol.SC-2001/WS/40.UNEduc.Sci.Cult.Organ. (UNESCO),Paris, Fr.

- Ramillien, G., Cazenave, A. and Brunau, O., (2004), Global time variations of hydrological signals from GRACE satellite gravimetry, Geopyhs. J. Int., 158(3), 813–826, doi:10.1111/j.1365-246X.2004.02328.x.

- Ramillien, G., Famiglietti, J. S. and Wahr, J. (2008), Detection of continental hydrology and glaciology signals from GRACE: A review, Surv. Geophys., 29(4/5), 361–374, doi:10.1007/s10712-008-9048-9.

- Ramillien, G., Frappart, F., Cazenave, A. and Guntner, A., (2005), Time variations of land water storage from an inversion of 2 years of GRACE geoids, Earth and Planetary Science Letters, 235(1-2), 283, doi: http://dx.doi.org/10.1016/j.epsl.2005.04.005.

- Ramilliena, P. G., Lombarda, A., Cazenavea, A., Ivinsb, E. R. Llubesa, M., Remya F. , Biancalec R., (2008), Interannual variations of the mass balance of the Antarctica and Greenland ice sheets from GRACE Author links open overlay. Global and planetary change. Volume 53, Issue 3, Pages 198-208.

- Reager, J. T. and Famiglietti, J. S., (2009), Global terrestrial water storage capacity and flood potential using GRACE, Geophys. Res. Lett., 36, L23402, doi:10.1029/2009GL040826.

- Reigber, C., Luhr, H. and Schwintzer, P., (2002), CHAMP mission status *Adv. Space Res.* 30 129–34.

- Reynolds, R. M., (1992a), Report of Activities – Leg I of the Mt. Mitchell Expedition. National Oceanic and Atmospheric Administration, HMRAD, HMRAD 92-9, Seattle WA USA. 110 pp.

- Reynolds, R.M., (1993), Physical Oceanography of the Persian Gulf, Strait of Hormoz, and the Gulf of Oman-Results from the Mt. Mitchell Expedition. Mitchell Cruise, Vol, 27, 1993, pp. 3-59.

- Roads atlas of Iran, Gitashenasi Cartographic and Geographic Institute (2004).

- Robert, B., Jackson, Stephen R., Carpenter, Clifford N., Dahm, Diane M., McKnight, Robert J., Naiman, Sandra L., Postel, and Steven, W. Running, (2001), Water in a Changing World, Issues in ecology.

- Rodell, M., and Famiglietti, J. S., (1999), Detectability of variations in continental water storage from satellite observations of the time dependent gravity field, Water Resour. Res., 35(9), 2705–2723, doi:10.1029/ 1999WR900141.

- Rodell, M., and Famiglietti, J. S., (2002), The High Plains aquifer, Central US, Journal of Hydrology, 263(1-4), 245, doi: http://dx.doi.org/10.1016/S0022-1694(02)00060-4.

- Rodell, M., Chen, J., Kato, H., Famiglietti, J. S., Nigro, J. and Wilson, C. R. (2007), Estimating groundwater storage changes in the Mississippi River basin (USA) using GRACE, Hydrogeol. J., 15(1), 159–166, doi:10.1007/s10040-006-0103-7.

- Rodell, M., Houser, P. Jambor, U.E.A. Gottschalck, J. Mitchell, Kieran Meng, Jesse Arsenault, Kristi Brian, Cosgrove Radakovich, J. MG, Bosilovich Entin, J. Walker, Jeffrey Lohmann, D. and DL, Toll., (2004), The Global Land Data Assimilation System. bams. 85. 381-394. 10.1175/BAMS-85-3-381.

- Rodell, M., Velicogna, I. and Famiglietti, J. S., (2009), Satellite-based estimates of groundwater depletion in India, Nature, 460(7258), 999–1002, doi: 10.1038/nature08238.

- Rowlands, D. D., Luthcke, S. B., McCarthy, J. J., Klosko, S. M., Chinn, D. S., Lemoine, F. G., Boy, J.-P., and Sabaka, T. J., (2010), Global mass flux solutions from GRACE: A comparison of parameter estimation strategies—Mass concentrations versus Stokes coefficients, J. Geophys. Res., 115, B01403, doi: 10.1029/2009JB006546.

- Rubincam, D.P., (1984), Postglacial rebound observed by Lageos and the effective viscosity of the lower mantle, J. Geophys. Res., 89, 1077-1088, 1984.

- Rubincam, D.P., (1984), Postglacial rebound observed by Lageos and the effective viscosity of the lower mantle, J. Geophys. Res., 89, 1077-1088.

- Sabaka, T. J., Rowlands, D. D., Luthcke, S. B. and Boy, J. P., (2010), Improving global mass flux solutions from Gravity Recovery and Climate Experiment (GRACE) through forward modeling and continuous time correlation. J. Geophys. Res., 115 (B11): B11403 [10.1029/2010JB007533].

- Sadik, B. J., Karam, A. H., (1988), Groundwater monitoring network rationalization using statistical analyses of piezometric fluctuation, Hydrological Sciences, Journal, 33:2, 181-191, DOI: 10.1080/02626668809491237).

- Sangoyomi, T.B., Lall, U. and Abarbanel, H.D.I., (1996), Nonlinear Dynamics of the Great Salt Lake: Dimension Estimation. Water Resources Research, 32(1), pp.149–159, doi:10.1029/95WR02872.

- Sasgen, I., Martinec, Z. and Fleming, K., (2006), Wiener optimal filtering of GRACE data, Stud. Geophys. Geod., 50(4), 499–508.

- Scanlon, B. R., C. C. Faunt, L. Longuevergne, R. C. Reedy, W. M. Alley, V. L. McGuire, and P. B. McMahon (2012b), Groundwater depletion and sustainability of irrigation in the US High Plains and Central Valley, Proc. Natl. Acad. Sci., 109(24), 9320–932.

- Scanlon, B. R., L. Longuevergne, and D. Long (2012a), Ground referencing GRACE satellite estimates of groundwater storage changes in the California Central Valley, USA, Water Resour. Res., 48, W04520, doi:10.1029/2011WR011312.

- Schrama, E. J. O., Wouters, B. and Lavalle´e, D. A., (2007), Signal and noise in Gravity Recovery and Climate Experiment (GRACE) observed surface mass variations, J. Geophys. Res., 112, B08407, doi:10.1029/2006JB004882.

- Schrama, E. J. O., Wouters, B., and Rietbroek, R., (2014), A mascon approach to assess ice sheet and glacier mass balances and their uncertainties from GRACE data, J. Geophys. Res. Solid Earth, 119, 6048–6066, doi:10.1002/2013JB010923.

- Schrama, E., Rietbroek, R. and Wouters, B., (2013), A new mascon approach to assess global ice sheet and glacier mass balances from GRACE. INPROCEEDINGS 2013EGUGA..15.5216S.

- Seckler, D., Barker R., Amarasinghe, UA., (1999), Water scarcity in the twenty-first century. Int. J. Water Resour.Dev. 15:29–42.

- Seo, K. W. and Wilson, C.R., (2005), Simulated estimation of hydrological loads from GRACE. J. Geod., 78, 442 – 456, doi:10.1007/ s00190-004-0410-5.

- Shah, T., (2007), Energy-irrigation nexus in South Asia: improving groundwater conservation and power sector viability. In The Agricultural Groundwater Revolution: Comprehensive Assessment of Water Management in Agriculture, Vol. 3, ed. M Giordano, K Villholth. Wallingford, UK: CABI Publ. 155–164.

- Shah, T., Molden D, Sakthivadivel R, Seckler D., (2000), The global groundwater situation: overview of opportunities and challenges. International Water Management Institute.

- Shah, T., Singh, OP., Mukherji, A., (2006), Groundwater irrigation and south Asian agriculture: empirical analyses fromalarge-scale survey of India, Pakistan, Nepal Terai and Bangladesh. Hydrogeol.J.14:286– 309.

- Shahrabi, M., (1994), Seas and Lakes of Iran, treatise on the Geology of Iran. Ministry of Mines and Metals, Tehran.

- Shiklomanov, I. A., and Penkova, N. V. (2003), Methods for assessing and forecasting global water use and water availability, in World Water Resources at the Beginning of the 21st Century2, edited by I. A. Shiklomanov and J. C. Rodda, 452 pp., Cambridge Univ. Press, Cambridge, U. K.

- Shiklomanov, IA., (1998), World water resources: an appraisal for the 21st century. IHP Rep. UN Educ. Sci. Cult. Organ. (UNESCO), Paris, Fr.

- Shirdeli, A., (2014), Hydropolitics and hydrology issues in Hirmand/Helmand international river basin. – Management Science Letters, 4: 807–812. [DOI].

- Sinéad, L., (2014), The Iranian Water Crisis, Global Food and Water Crises Research Programme, 2014.

- Singh, DK., Singh, AK., (2002), Groundwater situation in India: problems and perspectives. Int. J. Water Resour.Dev. 18:563–80.

- Singh, S., Singh, P., Kumar, R. and Saharan, S., (2012), Groundwater Quality Analysis of Safidon and Julana Blocks of District Jind, Haryana, India, Vol.4

No.1(2012), Article ID:16735,9 pages DOI:10.4236/jwarp.2012.41006 ,Journal of Water Resource and Protection.

- Slobbe, C., (2008), Towards a combined estimation of Greenland's ice sheet mass balance using GRACE and ICESat data. MSc. Geomatics Thesis, TUDelft.

- Sophocleous, MA., (2010), Groundwater legal framework and management practices in the High Plains aquifer, USA. In: Findikakis AN, Sato K (eds) Practices in groundwater management, IAHR Monograph, IAHR, in press.

- Struckmeier, W., Richts, A., Acworth, I., Arduino, G., Bocanegra, E., et al., (2006), WHYMAP and the World Map of Transboundary Aquifer Systems, Special Edition from World-Wide Hydrogeological 1:50000,000. Paris/Hanover, Ger.: BGR/UNESCO.

- Sullivan, P. J., (2010), Syria's liquid worries, in Circle of Blue Water News. Available at http:www.circleofblue.org; accessed 16 February 2010.

- Swenson, S. C., and Wahr, J., (2009), Monitoring the water balance of Lake Victoria, East Africa, from space, J. Hydrol., 370(1–4), 163–176, doi:10.1016/j.jhydrol.2009.03.008.

- Swenson, S., and Famiglietti, J., (2012), Sustainable groundwater management for large aquifer systems; tracking depletion rates from space, in Climate change effects on groundwater resources; a global synthesis of findings and recommendations, edited by H. Treidel, J. L. Martin-Bordes and J. J. Gurdak, pp. 367-375, A.A. Balkema Rotterdam - Brookfield International (III), International (III); Leiden, Netherlands.

- Swenson, S., and Wahr, J., (2002), Methods for inferring regional surface mass anomalies from GRACE measurements of time-variable gravity. J. Geophys. Res., 107(B9), 2193, doi:10.1029/2001JB000576.

- Swenson, S., Chambers, D., and Wahr, J., (2008), Estimating geocenter variations from a combination of GRACE and ocean model output. Journal of Geophysical research, VOL. 113, B08410, doi: 10.1029/2007JB005338, 2008.

- Syed, T. H., Famiglietti, J. S., Rodell, M., Chen, J., and Wilson, C. R., (2008), Analysis of terrestrial water storage changes from GRACE and GLDAS, Water Resour. Res., 44, W02433, doi:10.1029/2006WR005779.

- Tapley, B. D., Bettadpur, S. Watkins, M. and Reigber, C. (2004a), The gravity recovery and climate experiment: Mission overview and early results, Geophys. Res. Lett., 31, L09607, doi:10.1029/2004GL019920.

- Tapley, B. D., Bettadpur, S., Ries, J. C., Thompson, P. F. and Watkins, M. M., (2004b), GRACE measurements of mass variability in the Earth system, Science, 305, 503– 505.

- Tapley, B. D., Bettadpur, S., Ries, J. C., Thompson, P. F. and Watkins, M. M., (2004b), GRACE measurements of mass variability in the Earth system, Science, 305, 503– 505.

- Tapley, B., Bettadpur, S., Watkins, M. and Reigber, Ch., (2004), The Gravity Recovery and Climate Experiment: Mission overview and early results. Geophysical Research Letters. 31. 4 PP. 10.1029/2004GL019920.

- Tapley, B.D., Bettadpur, S., Ries, J.C., Thompson, P.F. and Watkins, M.M., (2004), "Grace Measurements of Mass Variability in the Earth System." *Science* 305, (2004): 503–505.

- Tapley, B.D., et al., The joint gravity field model 3, J. Geophys. Res., 101, 28,029-28,049, 1996.

- Taylor, C. J., Alley W. M., (2001), Ground-Water-Level Monitoring and the Importance of Long-Term Water-Level Data U.S. Geological Survey Circular 1217. Denver, Colorado, U.S. department of the interior gale a norton, Secretary. U.S. geological survey Charles G. Groat, Director.

- Taylor, Charles J., Alley, William M., (2001), Ground-water-level monitoring and the importance of long-term water-level data, p. cm. (U.S. Geological Survey circular; 1217) Includes bibliographical references (p.). 1. Groundwater-United States-

Measurement. 2. Water levels-- Alley, William M. II. Geological Survey (U.S.) III. Title. IV. Series. Library of Congress Cataloging-in-Publications Data, United States T GB1015 .T28 2001 551.49'2'0973-dc21.

- Teclaff, L. A., (1985); water law in historical perspective, natural resources journal,45 (William S. Hein. Co., New York,; L.A., The river basin in history and law (Martinus Nijhoff the hague, 1976).

-.Thiessen, A. H. (1911). Precipitation averages for large areas. *Monthly Weather Review,* 39(7), 1082-1089.

- Tiwari, V. M., Wahr, J. and Swenson, S., (2009), Dwindling groundwater resources in northern India, from satellite gravity observations, Geophysical Research Letters, 36, L18401, doi: http://dx.doi.org/10.1029/2009GL039401.

- Tiwari, V. M., Wahr, J. and Swenson, S., (2009), Dwindling groundwater resources in northern India, from satellite gravity observations, Geophys. Res. Lett., 36, L18401, doi:10.1029/2009GL039401.

- Trupin, A., (1993), Effects of polar ice on the Earth's rotation and gravitational potential. Geophys. J. Int., 113, 273-283.

- Tsur, Y., (1990), The stabilization role of groundwater when surface supplies are uncertain: the implications for groundwater development. Water Resource. Res. 26:811–18.

- UNECA (2011), Climate science, information, and services in Africa: status, gaps and policy implications, working paper, Available at http://www.uneca.org/sites/default/files/publications/wp1-climate_science_data_and_info_formated_draft_final.pdf.

- Velicogna I., Sutterley, T. C., and van den Broeke, M. R,(2014), Regional acceleration in icemass loss from Greenland and Antarctica using GRACE time-variable gravity data, J. Geophys. Res. Space Physics, 41, 8130–8137, doi:10.1002/2014GL061052.

- Velicogna, I., Sutterley, T. C. and van den Broeke, M. R., (2014), Regional acceleration in ice mass loss from Greenland and Antarctica using GRACE time-variable gravity data, Geophysical Research Letters, 41(22), 8130-8137, doi: http://dx.doi.org/10.1002/2014gl061052.

- Velicogna,I., Wahr,J., (2006), Measurements of Time-Variable Gravity Show Mass Loss in Antarctica. Scienc, Vol. 311, Issue 5768, pp. 1754-1756 DOI: 10.1126/science.1123785.

- Voss, K. A., Famiglietti, J. S., Lo, M., De Linage, C., Rodell, M. and Swenson, S. C., (2013), Groundwater depletion in the Middle East from GRACE with implications for transboundary water management in the Tigris-Euphrates-Western Iran region, Water Resources Research, 49(2), 904-914, doi: http://dx.doi.org/10.1002/wrcr.20078.

- Wahr, J. and Molenaar, M., (1998), Time variability of the Earth's gravity field's Hydrological and oceanic effects and their possible detection using GRACE Journal of Geophysical Research, VOL. 103, NO. B12, pages 30,205-30,229.

- Wahr, J., Molenaar, M. and Bryan, F., (1998), Time variability of the Earth's gravity field: Hydrological and oceanic effects and their possible detection using GRACE, J. Geophys. Res., 103(B12), 30205–30229, doi:10.1029/98JB02844.

- Wahr, J., Molenaar, M. and Bryan, F., (1998), Time variability of the Earth's gravity field: Hydrological and oceanic effects and their possible detection using GRACE, J. Geophys. Res., 103(B12), 30205–30229, doi:10.1029/98JB02844.

- Wahr, J., Swenson, S., Zlotnicki, V. and Velicogna, I., (2004), Time-variable gravity from GRACE: First results, Geophys. Res. Lett., 31, L11501, doi:10.1029/2004GL019779.

- Wahr, J., Swenson, S., Zlotnicki, V. and Velicogna, I., (2004), Time-variable gravity from GRACE: First results. Geophysical research letters, VOL. 31, L11501, doi:10.1029/2004GL019779, 2004

- Wahr, J., Wingham,D., Bentley, C., (2000), A method of combining ICESat and GRACE satellite data to constrain Antarctic mass balance J. Geophys. Res., 105 (B7) (2000), pp. 16,279-16,294.

- Wahr, J.M., (2007), Time-Variable Gravity From Satellites, Department of Physics and Cooperative Institute for Research in Environmental Sciences University of Colorado Boulder, Colorado 80309-0390.

- Wang, D., Hejazi, M., (2011), Quantifying the relative contribution of the climate and direct human impacts on mean annual streamflow in the contiguous United States. *Water Resour. Res.* 2011, *47*, W00J12.

- Wang, J., Huang, J., Rozelle, S., Huang, Q., Blanke, A., (2007), Agriculture and groundwater development in northern China: trends, institutional responses and policy options. Water Policy 9(Suppl. 1):61–74.

- Wang, X., De Linage, C., Famiglietti, J. and Zender, C. S., (2011), Gravity Recovery and Climate Experiment (GRACE) detection of water storage changes in the Three Gorges Reservoir of China and comparison with in situ measurements, Water Resources Research, 47(12), W12502, doi: http://dx.doi.org/10.1029/2011WR010534.

- Weier, J., (2002), From Wetland to Wasteland; Destruction of the Hamon Oasis, NASA Earth Observatory, retrieved 2010-09-24.

- West Azarbayejan Regional Water Authority, (2012a), [Online] Available at: http://www.agrw.ir/Farsi/AreaF.asp Id=3 [Accessed 16 September 2012].

- Whitney, J. W., (2006), Geology, water, and wind in the lower Helmand Basin, southern Afghanistan: U.S. Geological Survey Scientific Investigations Report: 2006–5182.

- Wolf, A. T., (1998), Conflict and cooperation along international waterways, Department of Geosciences, Oregon State University, 104 Wilkinson Hall, Corvallis, OR 97331-5506, USA, Water Policy 1 (1998) 251±265.

- Wolf, A.T., Newton, J.T., (2007). Case study transboundary dispute resolution: The Tigris- Euphrates Basin, Transboundary Freshwater Dispute Database (TFDD), Oregon State University, http://www.transboundarywaters.orst.edu/.

- Wolf, AT., (2007). Shared waters: conflict and cooperation. Annu.Rev.Environ.Resour. 32:241–69

- World Resour. Inst. (2000–2001). Table FW2. Groundwater and desalinization. http://earthtrends.wri.org/ pdf library/data tables/fw2n 2000.pdf.

- World Resour. Inst. (2005). Water resources and fisheries. http://earthtrends.wri.org/pdf library/data tables/watcoa1 2005.pdf

- Wouters, B. and Schrama, E. J. O., (2007), Improved accuracy of GRACE gravity solutions through empirical orthogonal function filtering of spherical harmonics, Geophys. Res. Lett., 34, L23711, doi:10.1029/2007GL032098.

- Yamamoto, K., Fukuda, Y. and Taniguchi, M. (2008), Study of Sub-basin Scale Groundwater Variations in Asia Using GRACE, Satellite Altimetry and in-situ Data, edited, p. 1003, American Geophysical Union.

- Yeh, P. J. F., Swenson, S. C., Famiglietti, J. S. and Rodell, M., (2006), Remote sensing of groundwater storage changes in Illinois using the Gravity Recovery and Climate Experiment (GRACE), Water Resour. Res., 42, W12203, doi:10.1029/2006WR005374.

- Yeh, P., and Famiglietti, J. S., (2007), Remote Sensing of Groundwater Storage Changes in Illinois Using GRACE (Gravity Recovery and Climate Experiment), in 2007 Joint Assembly; Acapulco; Mexico; 22-25 May 2007, edited, pp. H54A-01, American Geophysical Union 2000 Florida Ave NW Washington DC 20009-1277 USA URL:http://www.agu.org.

- Yirdaw, S. Z., Snelgrove, K. R. and Agboma, C. O., (2008), GRACE satellite observations of terrestrial moisture changes for drought characterization in the Canadian Prairie, J. Hydrol., 356(1/2), 84–92, doi:10.1016/ j.jhydrol.2008.04.004.

- Yoder, C.F., Williams, J.G., Dickey, J.O., Schutz, B.E., Eanes, R.J. and Tapley, B.D., (1983), Secular variations of Earth's gravitational harmonic J sub2 coefficient from Lageos and the non-tidal acceleration of Earth rotation, Nature, 303, 757-762, 1983.

- Zaitchik, B. F., Rodell, M. and Reichle, R. H., (2008), Assimilation of GRACE terrestrial water storage data into a land surface model: Results for the Mississippi River Basin, J. Hydrometeorol., 9, 535–548, doi:10.1175/2007JHM951.1.

- Zektse, IS., Everett, LG., (2004), Groundwater resources of the world and their use. UN Educ. Sci. Cult. Organ. (UNESCO),IHP-VISer.Groundw., Paris, Fr.

- Zektser, I.S.; Lorne, E., (2004), Groundwater Resources of the World: And Their Use; United Nations Educational, Scientific and Cultural Organization: Paris, France.

- Zonn, I. S., (2000), Three centuries at the Caspian (The Synchronism of Major Historical Events of XVIII–20 cc.). Moscow, 1-72. (in Russian).

Appendix A

Changes in the Earth's oblateness

A change in the earth's oblateness was first interpreted as due to the Earth's continuing response to the removal of the ice loads at the end of the last Ice Age (Post-Glacial Rebound (PGR)). The areas that lay underneath the ice loads placed over Hudson Bay and over the region around the North and Baltic Seas are still depressed from the weight of those ancient ice sheets, and they are still slowly uplifting as material deep within the mantle flows in from lower latitudes. The observed secular change in C_{20} has been used in PGR models to help constrain the Earth's viscosity profile.

More recent SLR solutions give C_{20} trends that are in general agreement with those early estimates (Cox and Chao et al. 2002, Cheng and Tapley 2004), though the actual rate is sensitive to the time span of the data and the analysis method used (Benjamin et al. 2006). There is large seasonal variability, due presumably to a combination of atmospheric pressure variations and variations in the distribution of water in the oceans and on land (Chao and Au 1991, Dong et al. 1996, Cheng and Tapley 1999, Nerem et al. 2000). A trend is also clearly evident in the results and is more obvious after the data have been low-pass filtered. But there are also signs of inter-annual variability. In particular, notice the anomalous wiggle during 1998–2002 (Cox and Chao 2002). This feature has been variously explained as the result of climatically driven oscillations in the ocean (Cox and Chao 2002, Dickey et al. 2002); in the storage of water, snow, and ice on land (Dickey et al. 2002); and as partly the consequence of the effects of anelasticity on the 18.6-year solid Earth tide (Benjamin et al. 2006). Anyway, its existence shows why solutions for the secular trend depend on the time span.

In addition, it has become increasingly evident in recent years that there could be other processes that include enough mass transfer between low- and high-latitudes to have a significant impact on the C_{20} trend; therefore, this can confuse the PGR interpretation.

The most significant of these processes could be changes in ice of the Greenland and Antarctic ice sheets. For example, a rate of Antarctic ice mass loss equivalent to 0.6 mm/yr of global sea level rise averaged over the last 30 years would cause a C_{20} rate of increase that is about equal in magnitude to the SLR value, however with the opposite sign (Trupin 1993). If the ice mass trend was even a sizable fraction of this amount, it would have a significant impact on the C_{20} PGR constraint.

These uncertainties arise because knowledge of the single harmonic, C_{20}, is not sufficient to determine the spatial location of the signal. SLR has provided time-variable solutions for a handful of other harmonics (Cheng et al. 1997, Cheng and Tapley 1999, Nerem et al. 2000, Moore et al. 2005). But there are not nearly enough of these harmonics to give the spatial resolution necessary to certainly address these issues. The basic limitation comes from the high altitude of LAGEOS (6,000 km) and the other SLR satellites. Shorter-scale harmonics in (1.3) are sufficiently weakened at those high altitudes that their time-dependence will not be simply sensed. The solution to this problem is to use a satellite in a lower-altitude orbit. That is the motivation for Challenging Mini-satellite Payload (CHAMP) (Reigber et al. 2002) and, especially, for GRACE (Tapley et al. 2004a, b).

Appendix B

B.1.1. Study area of Daryache Namak (Code: 4101)

This area is located between 34°-35° 10′N and 50° 35′-52° 30′E with an area of 8137.42 km^2. Figure B.1 shows changes in monthly values of groundwater storage inferred from the well data, its long-period and short-period.

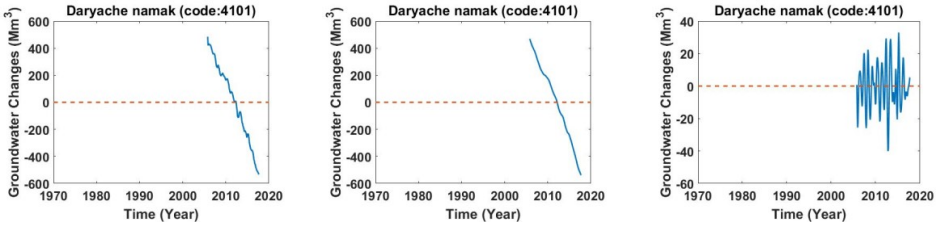

a b c

Figure B.1. a) Monthly values of groundwater storage, b) long-period of monthly values of groundwater storage, c) short-period of monthly values of groundwater storage across study area of Daryache Namak (Code: 4101).

B.1.2. Study area of Zarand Saveh (Code: 4102)

This area is located between 35° 15′-35 to 35° 40′ N and 47°-50°E with an area of 1263.4 km^2. Figure B.2 shows changes in monthly values of groundwater storage inferred from the well data, its long-period and short-period.

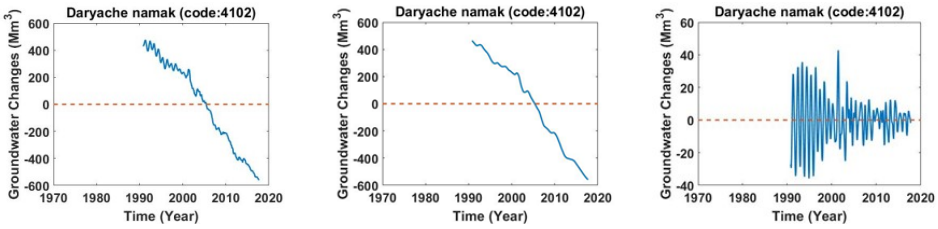

a b c

Figure B.2. a) Monthly values of groundwater storage, b) long-period of monthly values of groundwater storage, c) short-period of monthly values of groundwater storage across study area of Zarand Saveh (Code: 4102).

B.1.3. Study area of Eshtehard (Code: 4104)

This area is located between 35° 30′-35° 50′N and 50° 10′-50° 45′E with an area of 805.5 km^2. Figure B.3 shows changes in monthly values of groundwater storage inferred from the well data, its long-period and short-period.

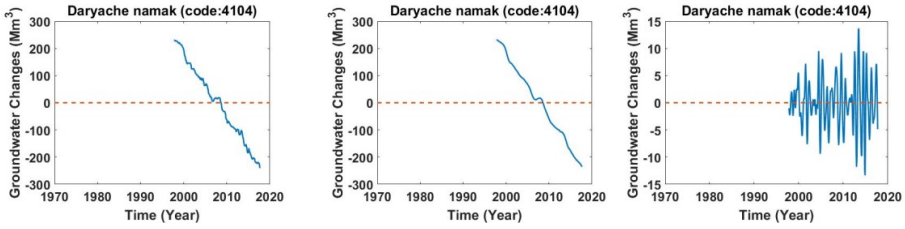

a b c

Figure B.3. a) Monthly values of groundwater storage, b) long-period of monthly values of groundwater storage, c) short-period of monthly values of groundwater storage across study area of Eshtehard (Code: 4104).

B.1.4. Study area of Hashtgerd (Code: 4105)

This area is located between 35° 47′-36° 7′N and 50° 25′-51° 8′E with an area of 1170.6 km^2. Figure B.4 shows changes in monthly values of groundwater storage inferred from the well data, its long-period and short-period.

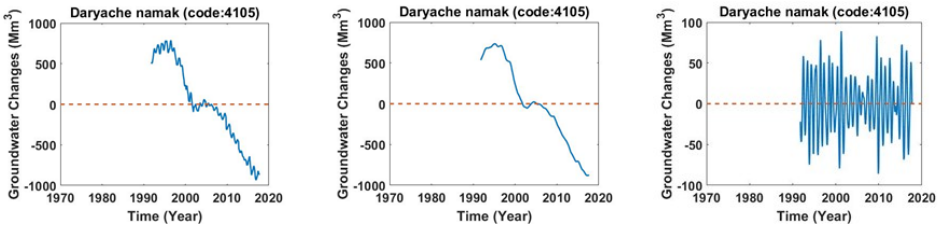

a b c

Figure B.4. a) Monthly values of groundwater storage, b) long-period of monthly values of groundwater storage, c) short-period of monthly values of groundwater storage across study area of Hashtgerd (Code: 4105).

B.1.5. Study area of Ghazvin (Code: 4106)

This area is located between 35° 20′-36° 30′N and 49° 9′-50° 42′E with an area of 9551.67 km^2. Figure B.5 shows changes in monthly values of groundwater storage inferred from the well data, its long-period and short-period.

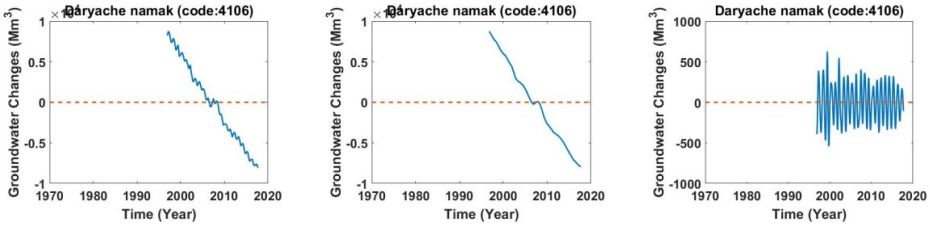

a b c

Figure B.5. a) Monthly values of groundwater storage, b) long-period of monthly values of groundwater storage, c) short-period of monthly values of groundwater storage across study area of Ghazvin (Code: 4106).

B.1.6. Study area of Abhar (Code: 4107)

This area is located between 35° 55′-36° 31′N and 48°50′-49° 25′E with an area of 1926.5 km^2. Figure B.6 shows changes in monthly values of groundwater storage inferred from the well data, its long-period and short-period.

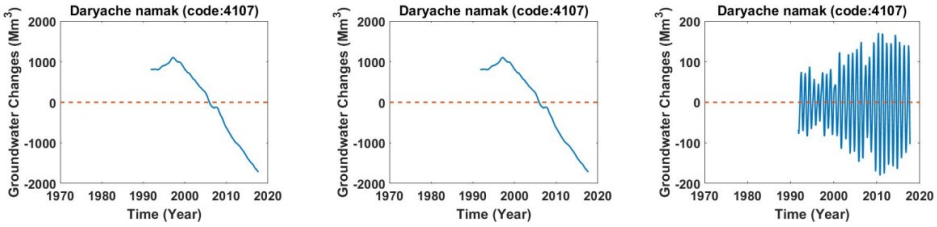

a b c

Figure B.6. a) Monthly values of groundwater storage, b) long-period of monthly values of groundwater storage, c) short-period of monthly values of groundwater storage across study area of Abhar (Code: 4108).

B.1.7. Study area of Gheidar (Code: 4109)

This area is located between 35°35′-36° 16′N and 48° 30′-49° 20′E with an area of 2521.61 km^2. Figure B.7 shows changes in monthly values of groundwater storage inferred from the well data, its long-period and short-period.

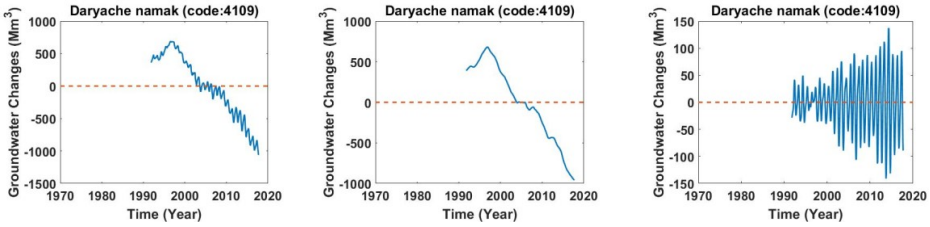

a b c

Figure B.7. a) Monthly values of groundwater storage, b) long-period of monthly values of groundwater storage, c) short-period of monthly values of groundwater storage across study area of Gheidar (Code: 4109).

B.1.8. Study area of Masile (Code: 4110)

This area is located between 34°33′-35N and 51°2 ′-51° 46′E with an area of 1475.49 km^2. Figure B.8 shows changes in monthly values of groundwater storage inferred from the well data, its long-period and short-period.

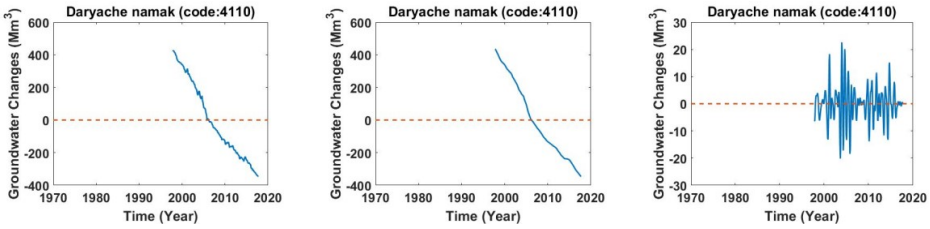

a b c

Figure B.8. a) Monthly values of groundwater storage, b) long-period of monthly values of groundwater storage, c) short-period of monthly values of groundwater storage across study area of Masile (Code: 4110).

B.1.9. Study area of Nobaran (Code: 4111)

This area is located between 34°58′-35° 25′N and 49°22′-50° 15′E with an area of 2175.4 km^2. Figure B.9 shows changes in monthly values of groundwater storage inferred from the well data, its long-period and short-period.

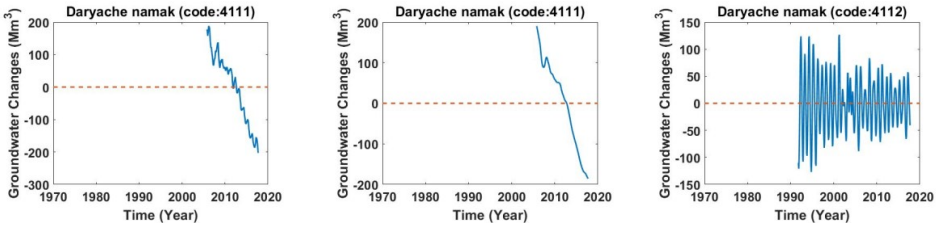

a b c

Figure B.9. a) Monthly values of groundwater storage, b) long-period of monthly values of groundwater storage, c) short-period of monthly values of groundwater storage across study area of Nobaran (Code: 4111).

B.1.10. Study area of Saveh (Code: 4112)

This area is located between 34°27′-35° 12′N and 50°0′-51° 5′E with an area of 4069.4 km^2. Figure B.10 shows changes in monthly values of groundwater storage inferred from the well data, its long-period and short-period.

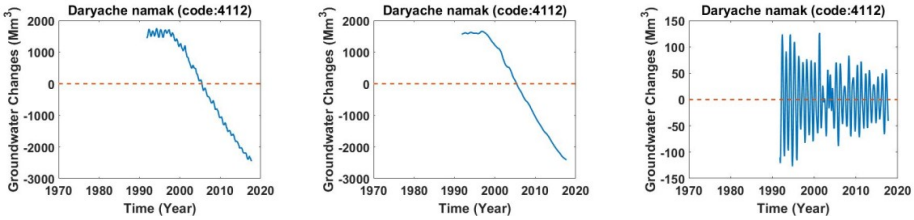

a b c

Figure B.10. a) Monthly values of groundwater storage, b) long-period of monthly values of groundwater storage, c) short-period of monthly values of groundwater storage across study area of Saveh (Code: 4112).

B.1.11. Study area of Tafresh (Code: 4113)

This area is located between 34°36′-34° 53′N and 49°50′-50° 8′E with an area of 420.17 km^2. Figure B.11 shows changes in monthly values of groundwater storage inferred from the well data, its long-period and short-period.

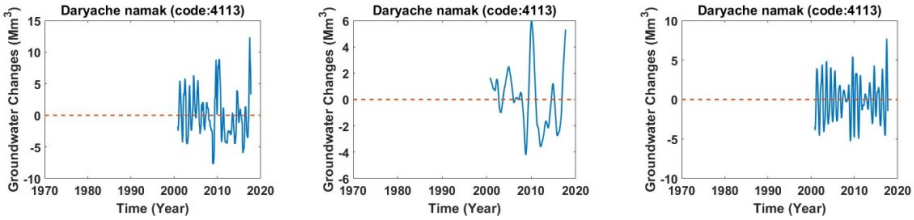

a b c

Figure B.11. a) Monthly values of groundwater storage, b) long-period of monthly values of groundwater storage, c) short-period of monthly values of groundwater storage across study area of Tafresh (Code: 4113).

B.1.12. Study area of Razan-Ghahavand (Code: 4115)

This area is located between 34°45′-35° 37′N and 48°47′-49° 25′E with an area of 3168.28 km^2. Figure B.12 shows changes in monthly values of groundwater storage inferred from the well data, its long-period and short-period.

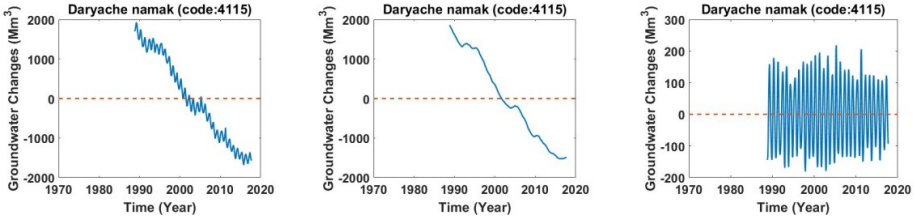

a b c

Figure B.12. a) Monthly values of groundwater storage, b) long-period of monthly values of groundwater storage, c) short-period of monthly values of groundwater storage across study area of Nobaran (Code: 4115).

B.1.13. Study area of Kaboodar-Ahang (Code: 4116)

This area is located between 34°52′-35° 40′N and 48°17′-49° 3′E with an area of 3470 km^2. Figure B.13 shows changes in monthly values of groundwater storage inferred from the well data, its long-period and short-period.

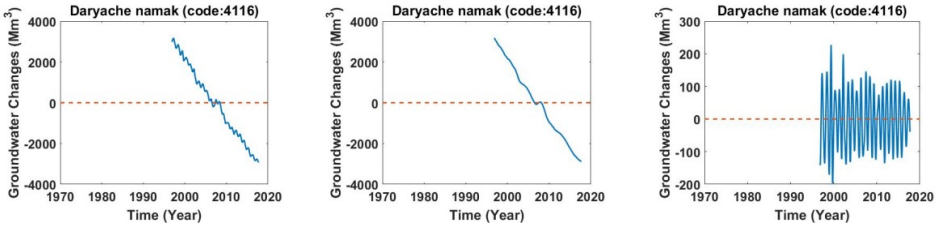

a b c

Figure B.13. a) Monthly values of groundwater storage, b) long-period of monthly values of groundwater storage, c) short-period of monthly values of groundwater storage across study area of Kaboodar-Ahang (Code: 4116).

B.1.14. Study area of Hamedan-Bahar (Code: 4117)

This area is located between 34°35′-35° 11′N and 48°8′-48° 50′E with an area of 2463 km^2. Figure B.14 shows changes in monthly values of groundwater storage inferred from the well data, its long-period and short-period.

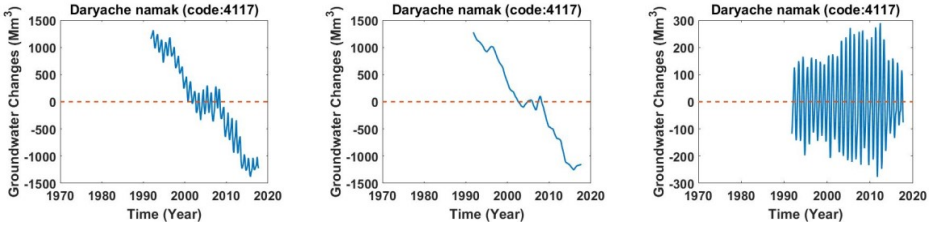

a b c

Figure B.14. a) Monthly values of groundwater storage, b) long-period of monthly values of groundwater storage, c) short-period of monthly values of groundwater storage across study area of Hamedan-Bahar (Code: 4117).

B.1.15. Study area of Komijan (Code: 4118)

This area is located between 34°20′-34° 50′N and 48°40′-49° 27′E with an area of 2547.7 km^2. Figure B.15 shows changes in monthly values of groundwater storage inferred from the well data, its long-period and short-period.

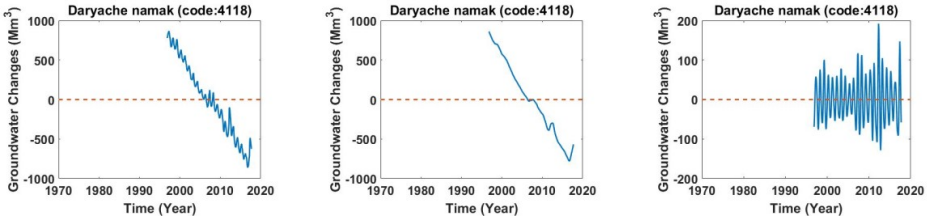

Figure B.15. a) Monthly values of groundwater storage, b) long-period of monthly values of groundwater storage, c) short-period of monthly values of groundwater storage across study area of Nobaran (Code: 4115).

B.1.16. Study area of Blok Shara (Code: 4119)

This area is located between 34°3′-34° 24′N and 49°-49° 32′E with an area of 1020.98 km^2. Figure B.16 shows changes in monthly values of groundwater storage inferred from the well data, its long-period and short-period.

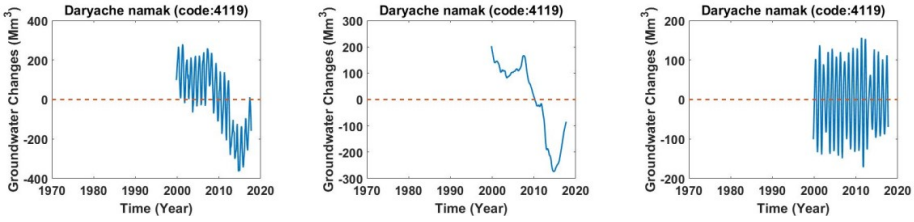

Figure B.16. a) Monthly values of groundwater storage, b) long-period of monthly values of groundwater storage, c) short-period of monthly values of groundwater storage across study area of Blok shara (Code: 4119).

B.1.17. Study area of shazand (Code: 4120)

This area is located between 33°45′-34° 10′N and 49°17′-49° 52′E with an area of 985.62 km^2. Figure B.17 shows changes in monthly values of groundwater storage inferred from the well data, its long-period and short-period.

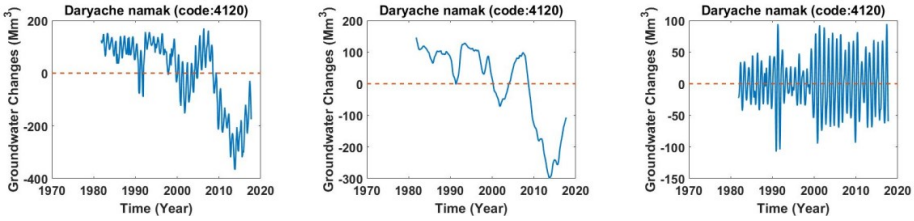

Figure B.17. a) Monthly values of groundwater storage, b) long-period of monthly values of groundwater storage, c) short-period of monthly values of groundwater storage across study area of Shazand (Code: 4120).

B.1.18. Study area of Arak (Code: 4124)

This area is located between 33°49′-34° 45′N and 49° 22′-50° 18′E with an area of 5520.73 km^2. Figure B.18 shows changes in monthly values of groundwater storage inferred from the well data, its long-period and short-period.

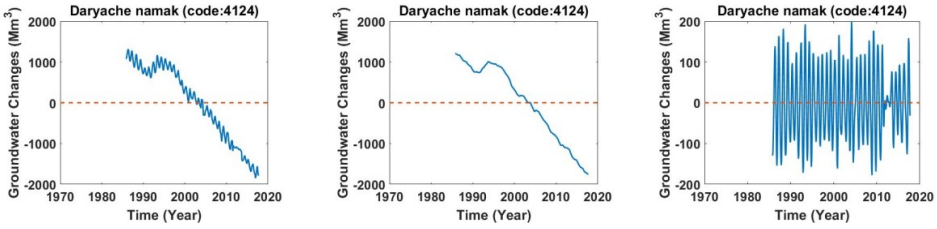

a b c

Figure B.18. a) Monthly values of groundwater storage, b) long-period of monthly values of groundwater storage, c) short-period of monthly values of groundwater storage across study area of Arak(Code: 4124).

B.1.19. Study area of Sharif Abad (Code: 4125)

This area is located between 34°38′-34° 47′N and 50° 52′-51° 18′E with an area of 440.83 km^2. Figure B.19 shows changes in monthly values of groundwater storage inferred from the well data, its long-period and short-period.

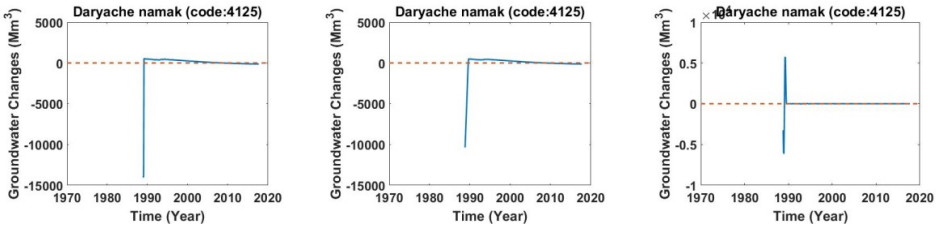

a b c

Figure B.19. a) Monthly values of groundwater storage, b) long-period of monthly values of groundwater storage, c) short-period of monthly values of groundwater storage across study area of Sharif Abad(Code: 4125).

B.1.20. Study area of Ghom-Kahak (Code: 4126)

This area is located between 34°9′-34° 42′N and 50° 41′-51° 32′E with an area of 1835.96 km^2. Figure B.20 shows changes in monthly values of groundwater storage inferred from the well data, its long-period and short-period.

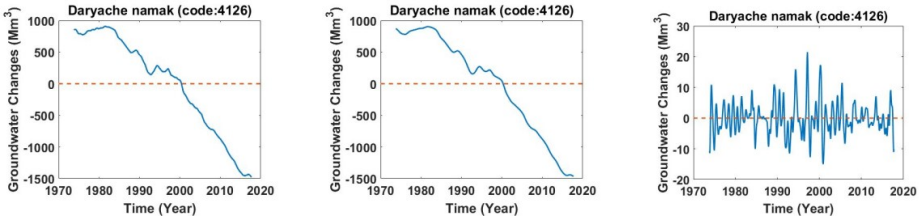

a b c

Figure B.20. a) Monthly values of groundwater storage, b) long-period of monthly values of groundwater storage, c) short-period of monthly values of groundwater storage across study area of Ghom-Kahak(Code: 4126).

B.1.21. Study area of Delijan Mahalat (Code: 4128)

This area is located between 33°38′-34° 12′N and 50° 10′-51° 2′E with an area of 2440.78 km^2. Figure B.21 shows changes in monthly values of groundwater storage inferred from the well data, its long-period and short-period.

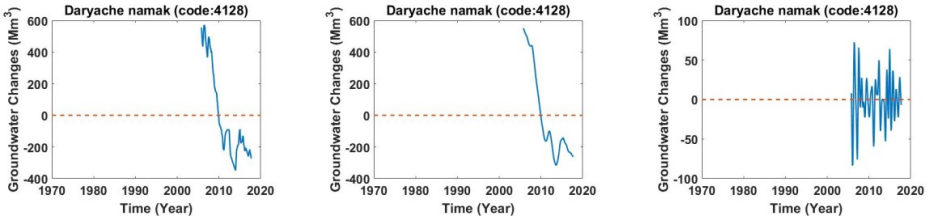

a b c

Figure B.21. a) Monthly values of groundwater storage, b) long-period of monthly values of groundwater storage, c) short-period of monthly values of groundwater storage across study area of Delijan Mahalat (Code: 4128).

B.1.22. Study area of Golpaiegan (Code: 4130)

This area is located between 33°-33° 40′N and 49° 50′-50° 45′E with an area of 3507.87 km^2. Figure B.22 shows changes in monthly values of groundwater storage inferred from the well data, its long-period and short-period.

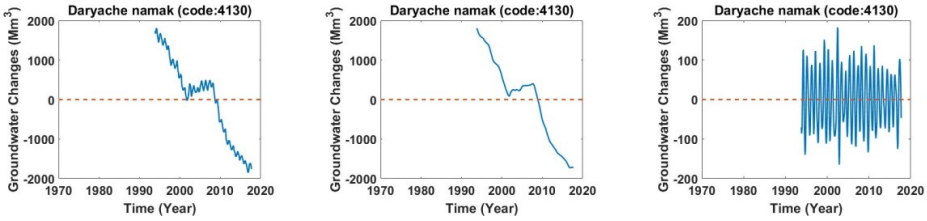

a b c

Figure B.22. a) Monthly values of groundwater storage, b) long-period of monthly values of groundwater storage, c) short-period of monthly values of groundwater storage across study area of Golpaiegan (Code: 4130).

B.1.23. Study area of Khomein (Code: 4131)

This area is located between 31˚22′-33˚ 56′N and 49˚ 41′-50˚ 20′E with an area of 2127.86 km^2. Figure B.23 shows changes in monthly values of groundwater storage inferred from the well data, its long-period and short-period.

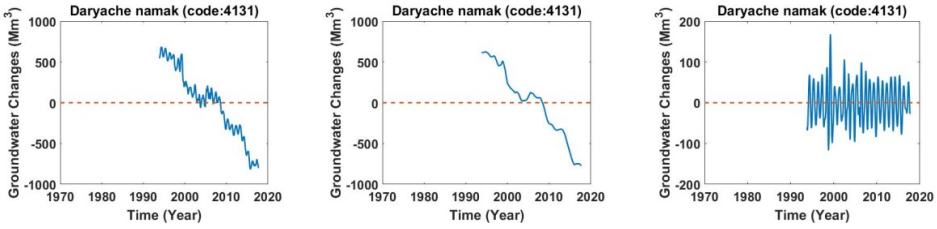

a b c

Figure B.23. a) Monthly values of groundwater storage, b) long-period of monthly values of groundwater storage, c) short-period of monthly values of groundwater storage across study area of Khomein (Code: 4131).

B.1.24. Study area of Kashan (Code: 4132)

This area is located between 33˚37′-34˚ 30′N and 50˚ 55′-52˚ 8′E with an area of 7185.4 km^2. Figure B.24 shows changes in monthly values of groundwater storage inferred from the well data, its long-period and short-period.

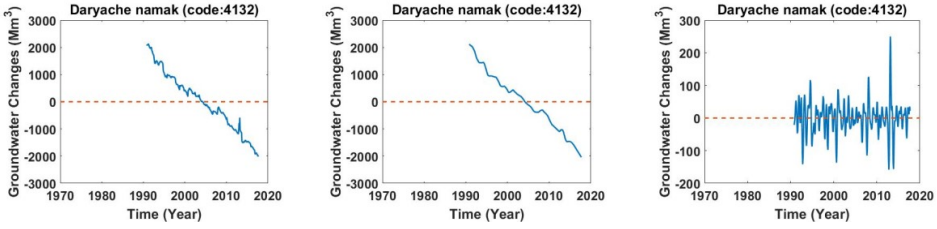

a b c

Figure B.24. a) Monthly values of groundwater storage, b) long-period of monthly values of groundwater storage, c) short-period of monthly values of groundwater storage across study area of Kashan(Code: 4132).

B.1.25. Study area of Tehran-Karaj (Code: 4133)

This area is located between 35˚8′-36˚ 10′N and 50˚ 43′-51˚ 41′E with an area of 5588 km^2. This area is divided to 3 areas. Figure B.25, B.26, B.27 shows changes in monthly values of groundwater storage inferred from the well data, its long-period and short-period.

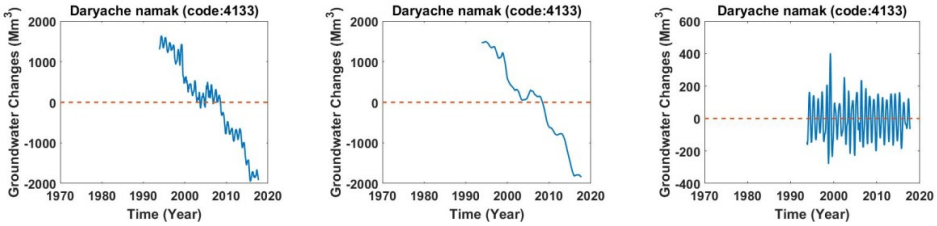

a b c

Figure B.25. a) Monthly values of groundwater storage, b) long-period of monthly values of groundwater storage, c) short-period of monthly values of groundwater storage across first study area of Tehran-Karaj: 1)Dasht Tehran (Code: 4133).

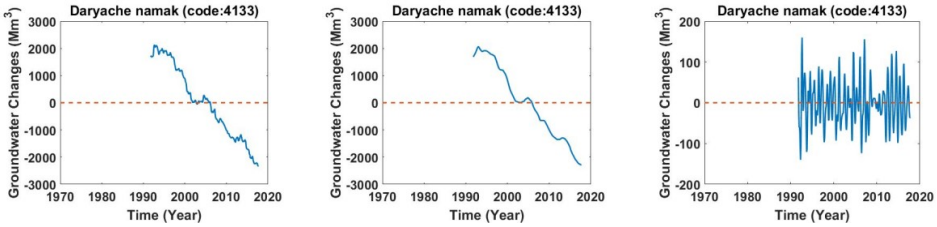

a b c

Figure B.26. a) Monthly values of groundwater storage, b) long-period of monthly values of groundwater storage, c) short-period of monthly values of groundwater storage across second study area of Tehran-Karaj:2) Dasht Karaj (Code: 4133).

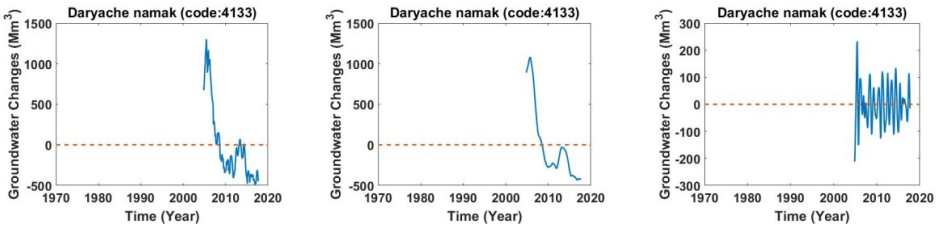

a b c

Figure B.27. a) Monthly values of groundwater storage, b) long-period of monthly values of groundwater storage, c) short-period of monthly values of groundwater storage across third study area of Tehran-Karaj: 3) Dasht Fashafooie (Code: 4133).

B.1.26. Study area of Varamin (Code: 4134)

This area is located between 33°7′-35° 4′N and 51° 20′-51° 55′E with an area of 1642.2 km^2. Figure B.28 shows changes in monthly values of groundwater storage inferred from the well data, its long-period and short-period.

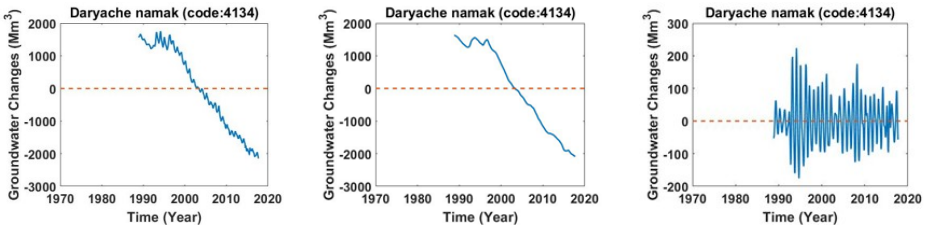

Figure B.28. a) Monthly values of groundwater storage, b) long-period of monthly values of groundwater storage, c) short-period of monthly values of groundwater storage across study area of Varamin(Code: 4134).

B.1.27. Study area of Damavand (Code: 4135)

This area is located between 35°33′-35° 52′N and 51° 45′-52° 13′E with an area of 757.8 km^2. Figure B.29 shows changes in monthly values of groundwater storage inferred from the well data, its long-period and short-period.

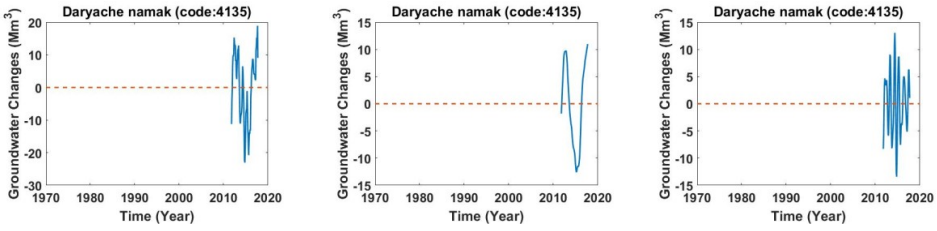

Figure B.29. a) Monthly values of groundwater storage, b) long-period of monthly values of groundwater storage, c) short-period of monthly values of groundwater storage across study area of Damavand (Code: 4135).

B.2.1. Study area of Koohpaie Sagzi (Code: 4201)

This area has 8137.42 km^2. Figure B.30 shows changes in monthly values of groundwater storage inferred from the well data, its long-period and short-period.

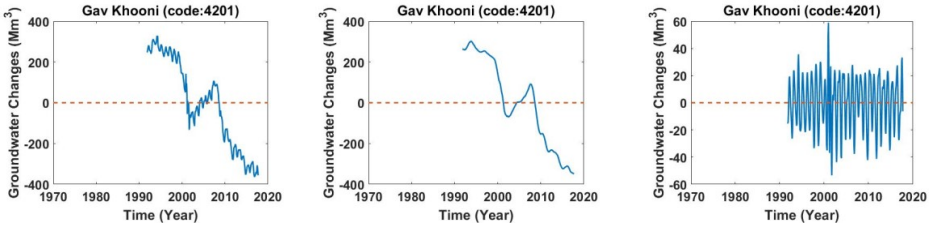

Figure B.30. a) Monthly values of groundwater storage, b) long-period of monthly values of groundwater storage, c) short-period of monthly values of groundwater storage across study area of Koohpaie Sagzi (Code: 4201).

B.2.3. Study area of Esfahan-Barkhordar (Code: 4202)

This area has 357B.6 km^2. Figure B.31 shows changes in monthly values of groundwater storage inferred from the well data, its long-period and short-period.

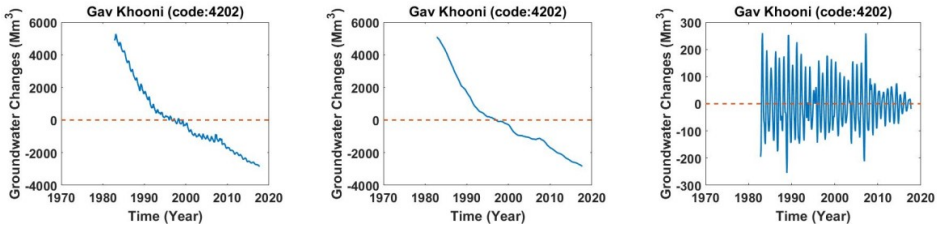

a b c

Figure B.31. a) Monthly values of groundwater storage, b) long-period of monthly values of groundwater storage, c) short-period of monthly values of groundwater storage across study area of Esfahan-Barkhordar (Code: 4202).

B.2.4. Study area of Moorche Khort (Code: 4203)

This area has 220B.9 km^2. Figure B.32 shows changes in monthly values of groundwater storage inferred from the well data, its long-period and short-period.

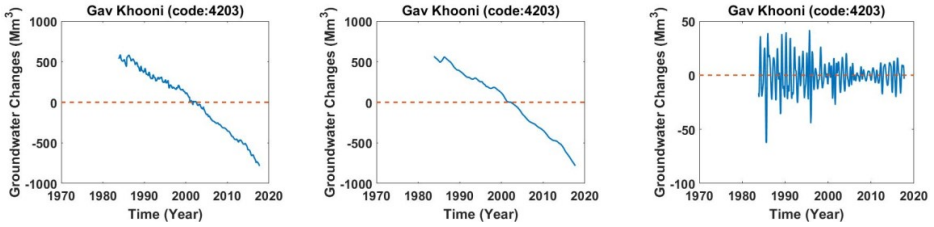

a b c

Figure B.32. a) Monthly values of groundwater storage, b) long-period of monthly values of groundwater storage, c) short-period of monthly values of groundwater storage across study area of Moorche Khort (Code: 4203).

B.2.5. Study area of Alaviche-Dehagh (Code: 4204)

This area has 1443.9 km^2. Figure B.33 shows changes in monthly values of groundwater storage inferred from the well data, its long-period and short-period.

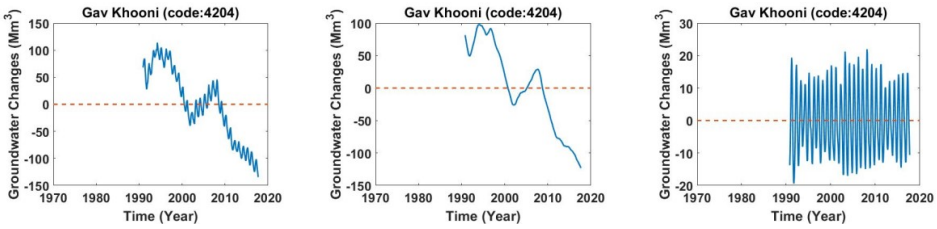

a b c

Figure B.33. a) Monthly values of groundwater storage, b) long-period of monthly values of groundwater storage, c) short-period of monthly values of groundwater storage across study area of Alaviche-Dehagh (Code: 4204).

B.2.6. Study area of Meime (Code: 4205)

This area has 206B.5 km^2. Figure B.34 shows changes in monthly values of groundwater storage inferred from the well data, its long-period and short-period.

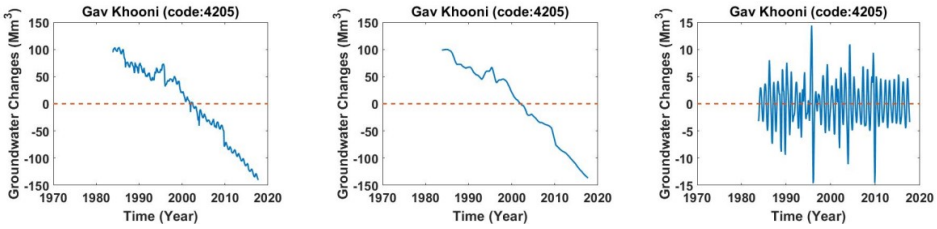

a b c

Figure B.34. a) Monthly values of groundwater storage, b) long-period of monthly values of groundwater storage, c) short-period of monthly values of groundwater storage across study area of Meime (Code: 4205).

B.2.7. Study area of Najaf Abad (Code: 4206)

This area has 175B.9 km^2. Figure B.35 shows changes in monthly values of groundwater storage inferred from the well data, its long-period and short-period.

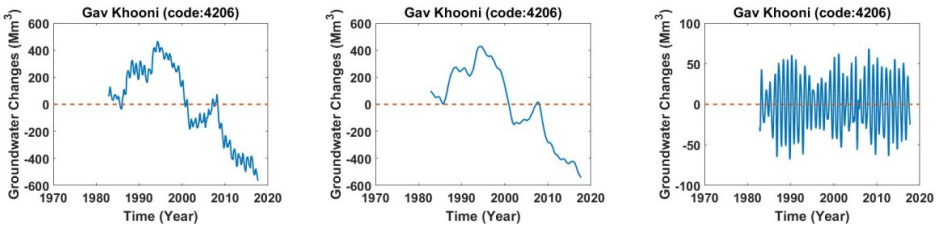

a b c

Figure B.3B. a) Monthly values of groundwater storage, b) long-period of monthly values of groundwater storage, c) short-period of monthly values of groundwater storage across study area of Moorche Khort (Code: 4206).

B.2.8. Study area of Kron (Code: 4207)

This area has 727.9 km^2. Figure B.36 shows changes in monthly values of groundwater storage inferred from the well data, its long-period and short-period.

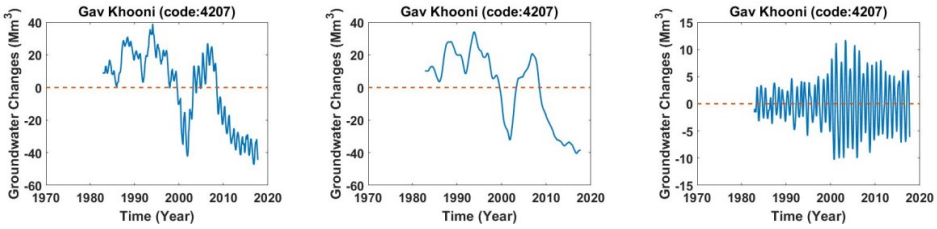

a b c

Figure B.36. a) Monthly values of groundwater storage, b) long-period of monthly values of groundwater storage, c) short-period of monthly values of groundwater storage across study area of Kron (Code: 4207).

B.2.9. Study area of Mahyar Shomali: (4208)

This area has 267.3 km^2. Figure B.37 shows changes in monthly values of groundwater storage inferred from the well data, its long-period and short-period.

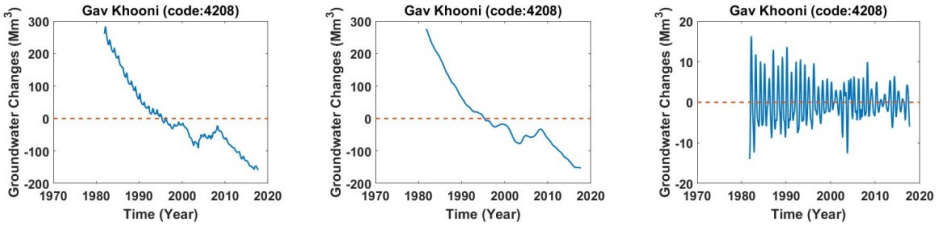

a b c

Figure B.37. a) Monthly values of groundwater storage, b) long-period of monthly values of groundwater storage, c) short-period of monthly values of groundwater storage across study area of Mahyar Shomali (Code: 4208).

B.2.10. Study area of Lenjanat (Code: 4209)

This area has 336B.2 km^2. Figure B.38 shows changes in monthly values of groundwater storage inferred from the well data, its long-period and short-period.

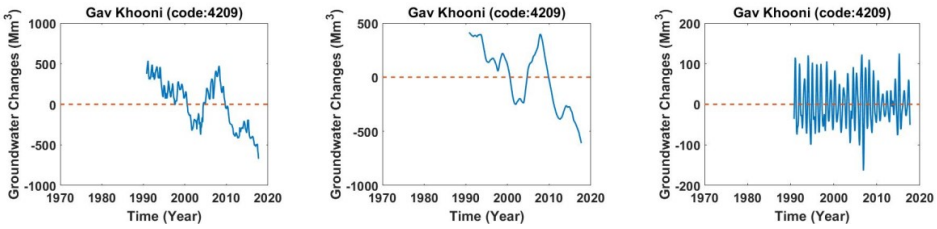

a b c

Figure B.38. a) Monthly values of groundwater storage, b) long-period of monthly values of groundwater storage, c) short-period of monthly values of groundwater storage across study area of Lenjanat (Code: 4209).

B.2.11. Study area of Chadegan (Code: 4211)

This area has 426 km^2. Figure B.39 shows changes in monthly values of groundwater storage inferred from the well data, its long-period and short-period.

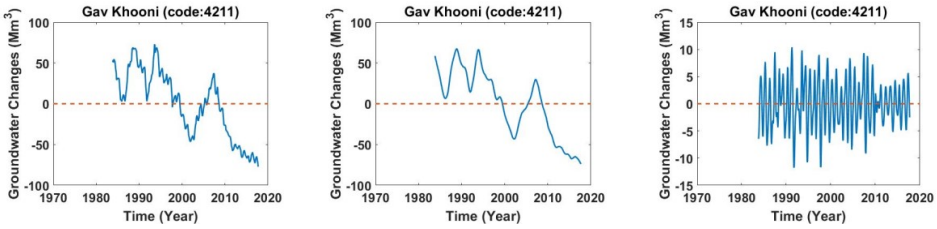

a b c

Figure B.39. a) Monthly values of groundwater storage, b) long-period of monthly values of groundwater storage, c) short-period of monthly values of groundwater storage across study area of Chadegan (Code: 4210).

B.2.12. Study area of Boin-miandasht (Code: 4212)

This area has 982.9 km^2. Figure B.40 shows changes in monthly values of groundwater storage inferred from the well data, its long-period and short-period.

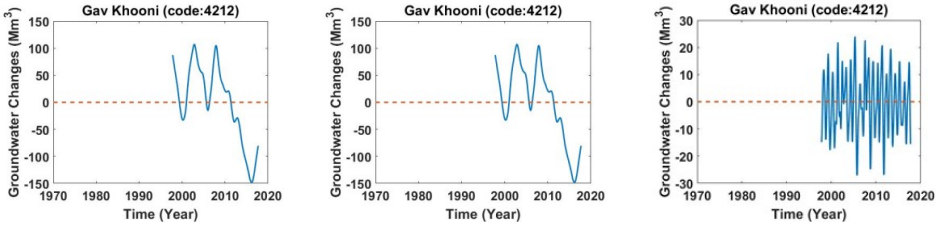

a b c

Figure B.40. a) Monthly values of groundwater storage, b) long-period of monthly values of groundwater storage, c) short-period of monthly values of groundwater storage across study area of Boin-miandasht (Code: 4212).

B.2.13. Study area of Chehel Khane (Code: 4213)

This area has162 km^2. Figure B.41 shows changes in monthly values of groundwater storage inferred from the well data, its long-period and short-period.

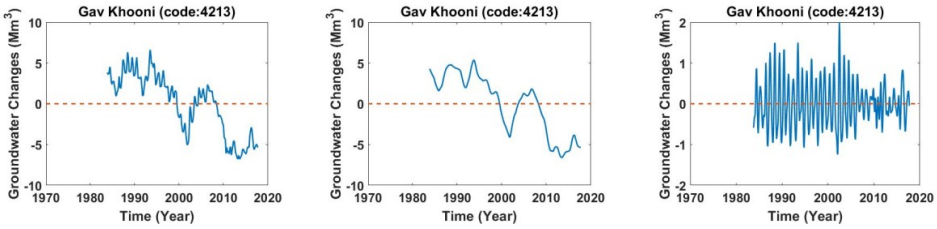

a b c

Figure B.41. a) Monthly values of groundwater storage, b) long-period of monthly values of groundwater storage, c) short-period of monthly values of groundwater storage across study area of Chehel Khanen (Code: 4213).

B.2.14. Study area of Damane Daran (Code: 4214)

This study area of area has 711.2 km^2. Figure B.42 shows changes in monthly values of groundwater storage inferred from the well data, its long-period and short-period.

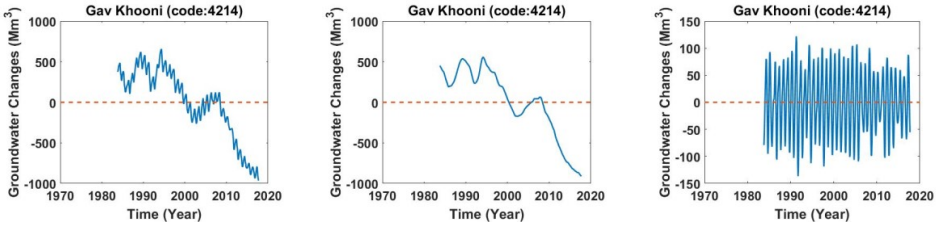

a b c

Figure B.42. a) Monthly values of groundwater storage, b) long-period of monthly values of groundwater storage, c) short-period of monthly values of groundwater storage across study area of Damane Daran (Code: 4214).

B.2.15. Study area of Mahyar Jonobi-Dasht Asman (Code: 4217)

This area has 2559.5 km^2. Figure B.43 shows changes in monthly values of groundwater storage inferred from the well data, its long-period and short-period.

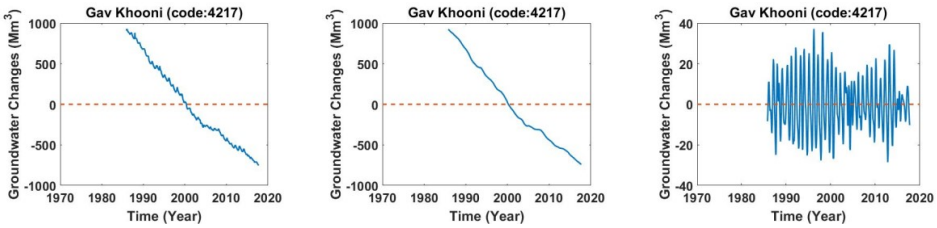

a b c

Figure B.43. a) Monthly values of groundwater storage, b) long-period of monthly values of groundwater storage, c) short-period of monthly values of groundwater storage across study area of Mahyar Jonobi-Dasht Asman (Code: 4217).

B.2.16. Study area of Ghamshe (Code: 4218)

This area has 2557.9 km^2. Figure B.44 shows changes in monthly values of groundwater storage inferred from the well data, its long-period and short-period.

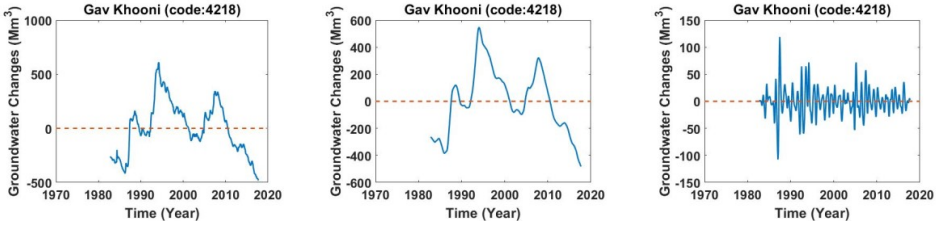

a b c

Figure B.44. a) Monthly values of groundwater storage, b) long-period of monthly values of groundwater storage, c) short-period of monthly values of groundwater storage across study area of Ghamshe (Code: 4218).

B.2.17. Study area of Esfandaran (Code: 4219)

This area has 4786.7 km^2. Figure B.45 shows changes in monthly values of groundwater storage inferred from the well data, its long-period and short-period.

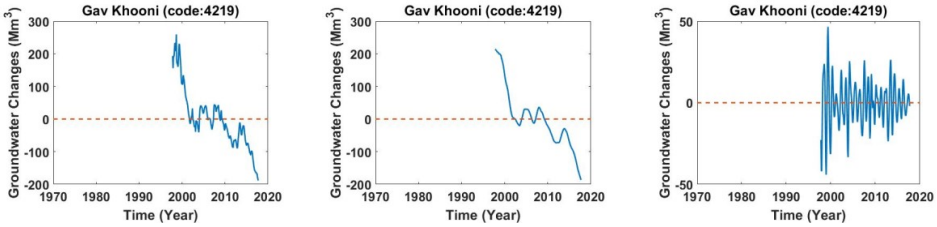

a b c

Figure B.45. a) Monthly values of groundwater storage, b) long-period of monthly values of groundwater storage, c) short-period of monthly values of groundwater storage across study area of Esfandaran (Code: 4219).

B.2.18. Study area of Izadkhast (Code: 4220)

This area has 1117.1 km^2. Figure B.46 shows changes in monthly values of groundwater storage inferred from the well data, its long-period and short-period.

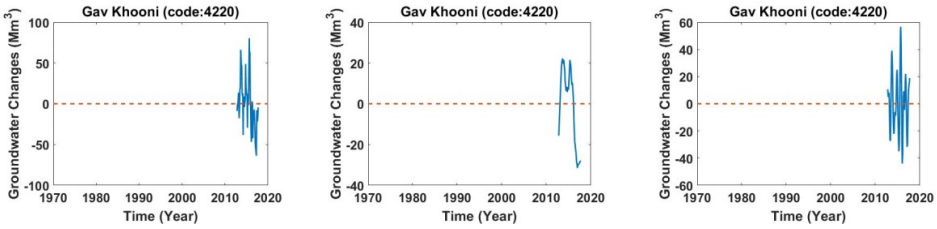

a b c

Figure B.46. a) Monthly values of groundwater storage, b) long-period of monthly values of groundwater storage, c) short-period of monthly values of groundwater storage across study area of Izadkhast (Code: 4220).

B.3.1. Study area of Tavabe Arsanjan (Code: 4301)

This area is located between 3280000 to 3300000 y and 690000 to 730000 x in UTM, with 265.9 km^2. Figure B.47 shows changes in monthly values of groundwater storage inferred from the well data, its long-period and short-period.

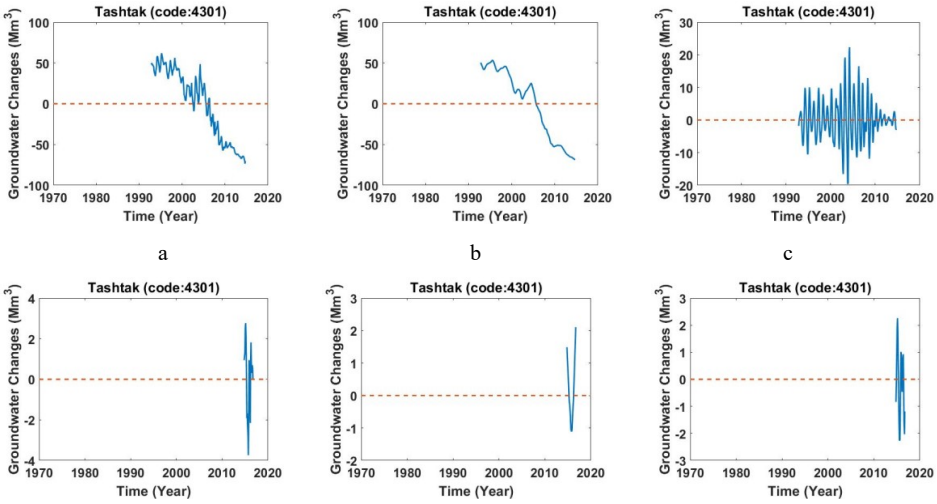

a b c

d e f

Figure B.47. a,d) Monthly values of groundwater storage, b,e) long-period of monthly values of groundwater storage, c,f) short-period of monthly values of groundwater storage across study area of Tavabe Arsanjan (Code: 4301).

B.3.2. Study area of AbadeTashtak-Jahanabad (Code: 4305)

This area is located between 370000 to 3310000 y and 730000 to 800000 x in UTM, with an area of 1941.4 km^2. Figure B.48, B.49, B.50 show changes in monthly values of groundwater storage inferred from the well data, its long-period and short-period.

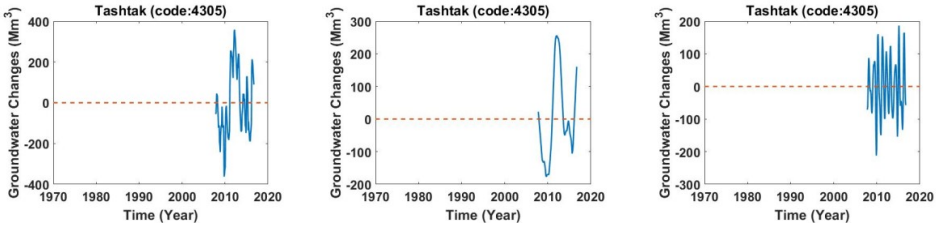

a b c

Figure B.48. a) Monthly values of groundwater storage, b) long-period of monthly values of groundwater storage, c) short-period of monthly values of groundwater storage across study area of Jahanabad (Code: 4305).

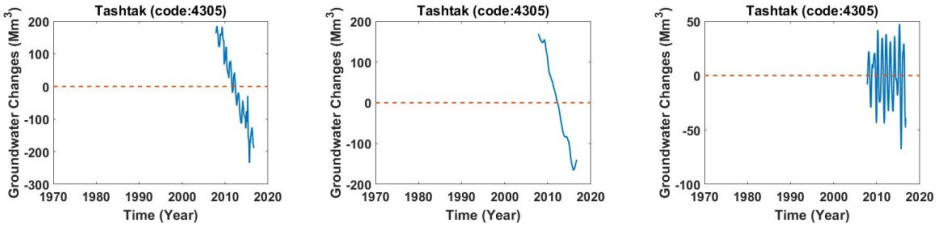

a b c

Figure B.49. a) Monthly values of groundwater storage, b) long-period of monthly values of groundwater storage, c) short-period of monthly values of groundwater storage across study area of AbadeTashtak (Code: 4305).

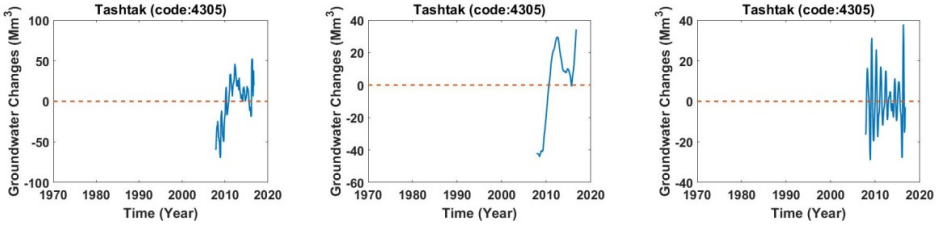

a b c

Figure B.50. a) Monthly values of groundwater storage, b) long-period of monthly values of groundwater storage, c) short-period of monthly values of groundwater storage across study area of Sang kar (Code: 4305).

B.3.3. Study area of Khayer (Code: 4307)

This area is located between 3230000 to 3250000 y and 770000 to 800000 x in UTM, with an area of 233.9 km^2. Figure B.51 shows changes in monthly values of groundwater storage inferred from the well data, its long-period and short-period.

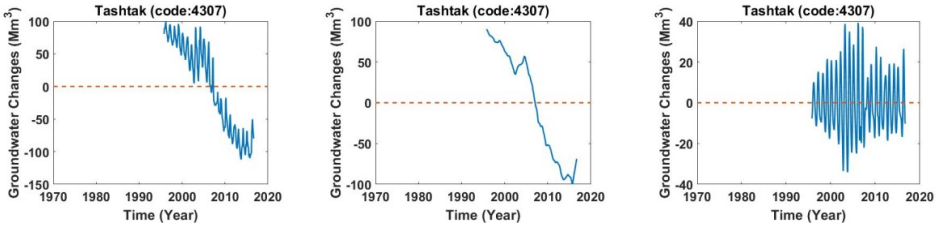

a b c

Figure B.51 a) Monthly values of groundwater storage, b) long-period of monthly values of groundwater storage, c) short-period of monthly values of groundwater storage across study area of Khayer(Code: 4307).

B.3.4. Study area of Estahban (Code: 4308)

This area is located between 3210000 to 3230000 y and 780000 to 800000 x in UTM, with an area of 416.8 km^2. Figure B.52 shows changes in monthly values of groundwater storage inferred from the well data, its long-period and short-period.

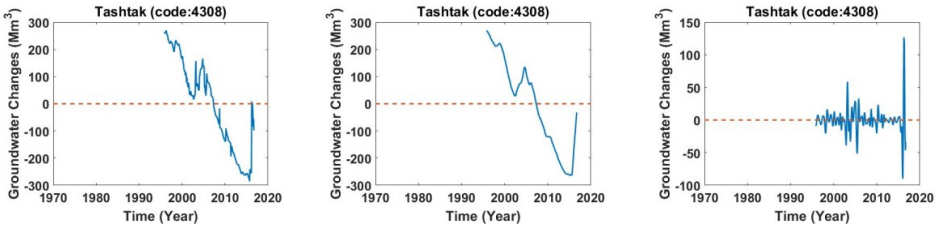

a b c

Figure B.52. a) Monthly values of groundwater storage, b) long-period of monthly values of groundwater storage, c) short-period of monthly values of groundwater storage across study area of Estahban (Code: 4308).

B.3.5. Study area of Neyriz (Code: 4309)

This area is located between 3220000 to 3260000 y and 800000 to 840000 x in UTM, with an area of 99B.1 km^2. Figure B.53 shows changes in monthly values of groundwater storage inferred from the well data, its long-period and short-period.

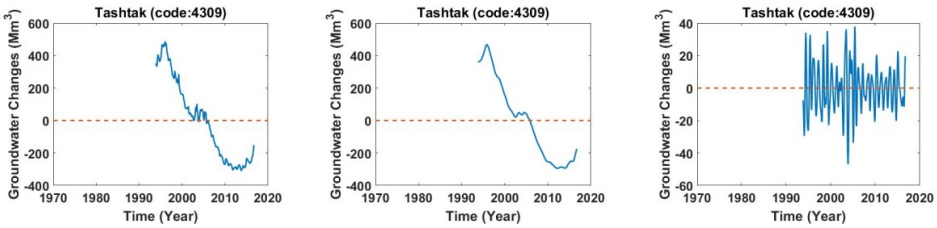

a b c

Figure B.53. a) Monthly values of groundwater storage, b) long-period of monthly values of groundwater storage, c) short-period of monthly values of groundwater storage across study area of Neyriz (Code: 4309).

B.3.6. Study area of Tang Hana-Pichakan (Code: 4310)

This area is located between 3240000 to 3280000 y and 740000 to 820000 x in UTM, with an area of 2106.5 km^2. This study area has two parts. Figures B.54 and B.55 show changes in monthly values of groundwater storage inferred from the well data, its long-period and short-period.

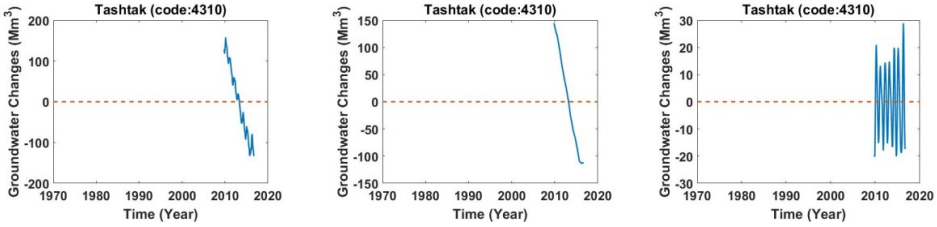

a b c

Figure B.54. a) Monthly values of groundwater storage, b) long-period of monthly values of groundwater storage, c) short-period of monthly values of groundwater storage across study area of Tang Hana (Code: 4310).

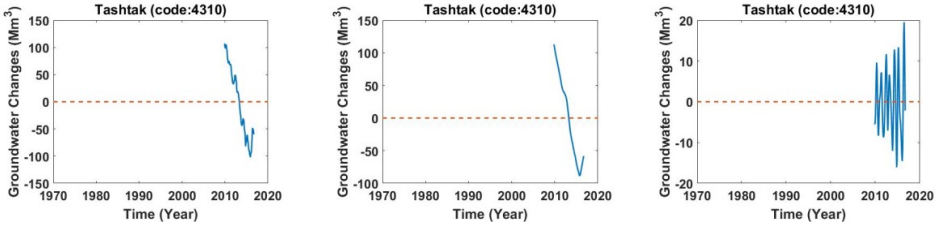

a b c

Figure B.55. a) Monthly values of groundwater storage, b) long-period of monthly values of groundwater storage, c) short-period of monthly values of groundwater storage across study area of Pichakan (Code: 4310).

B.3.7. Study area of Marvdash-Kharame (Code: 4311)

This area is located between 3245000 to 3370000 y and 620000 to 740000 x in UTM, with an area of 3926.1 km^2. Figures B.56, B.57 and B.58 show changes in monthly values of groundwater storage inferred from the well data, its long-period and short-period.

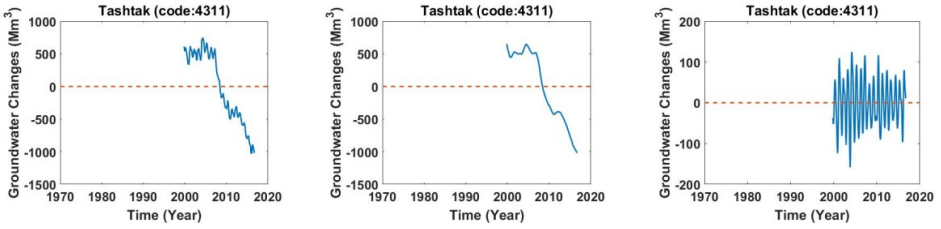

a b c

Figure B.56. a) Monthly values of groundwater storage, b) long-period of monthly values of groundwater storage, c) short-period of monthly values of groundwater storage across study area of Dashtak-Dorodzan (Code: 4311).

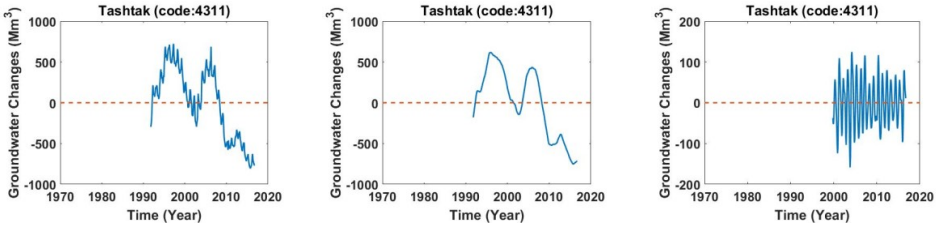

a b c

Figure B.57. a) Monthly values of groundwater storage, b) long-period of monthly values of groundwater storage, c) short-period of monthly values of groundwater storage across study area of Dashtak-Dorodzan (Code: 4311).

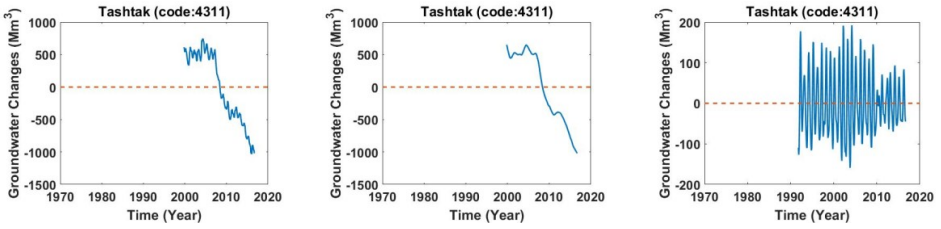

a b c

Figure B.58. a) Monthly values of groundwater storage, b) long-period of monthly values of groundwater storage, c) short-period of monthly values of groundwater storage across study area of Main-Bidkal (Code: 4311).

B.3.8. Study area of Darian (Code: 4312)

This area is located between 3270000 to 3280000 y and 660000 to 700000 x in UTM, with an area of 341.9 km^2. Figure B.59 shows changes in monthly values of groundwater storage inferred from the well data, its long-period and short-period.

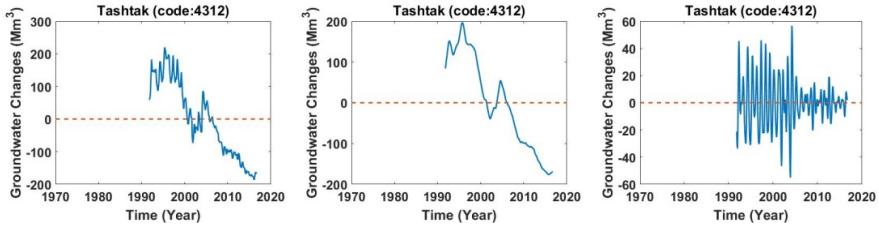

a b c

Figure B.59. a) Monthly values of groundwater storage, b) long-period of monthly values of groundwater storage, c) short-period of monthly values of groundwater storage across study area of Daian (Code: 4312).

B.3.9. Study area of Saadat abad (Code: 4313)

This area is located between 3220000 to 3350000 y and 660000 to 715000 x in UTM, with an area of 726.4 km^2. Figure B.60 shows changes in monthly values of groundwater storage inferred from the well data, its long-period and short-period.

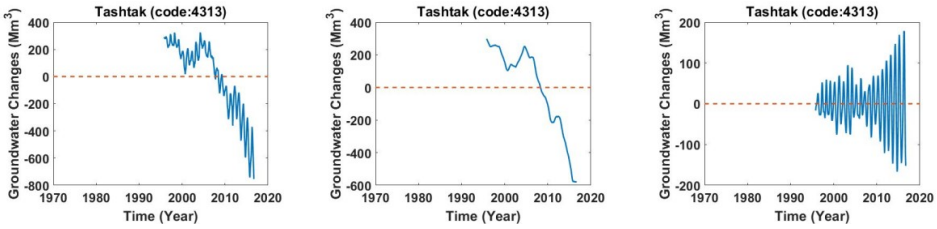

a b c

Figure B.60. a) Monthly values of groundwater storage, b) long-period of monthly values of groundwater storage, c) short-period of monthly values of groundwater storage across study area of Saadat Abad (Code: 4313).

B.3.10. Study area of Sarpaniran (Code: 4314)

This area is located between 3320000 to 3340000 y and 710000 to 750000 x in UTM, with an area of 456.8 km^2. Figure B.61 shows changes in monthly values of groundwater storage inferred from the well data, its long-period and short-period.

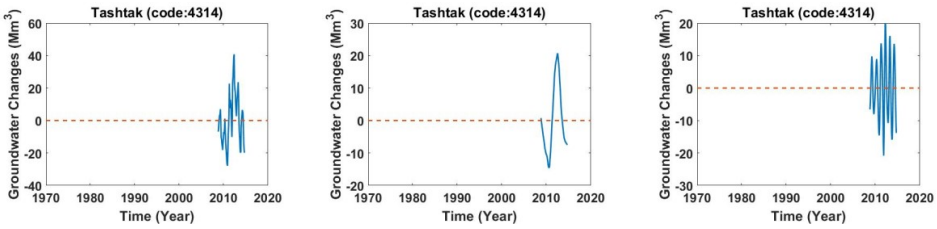

Figure B.61. a) Monthly values of groundwater storage, b) long-period of monthly values of groundwater storage, c) short-period of monthly values of groundwater storage across study area of Sarpaniran (Code: 4314).

B.3.11. Study area of Ghader abad–Madarsoleiman (Code: 4315)

This area is located between 3325000 to 3380000 y and 680000 to 760000 x in UTM, with an area of 2869.2 km^2. Figure B.62 shows changes in monthly values of groundwater storage inferred from the well data, its long-period and short-period.

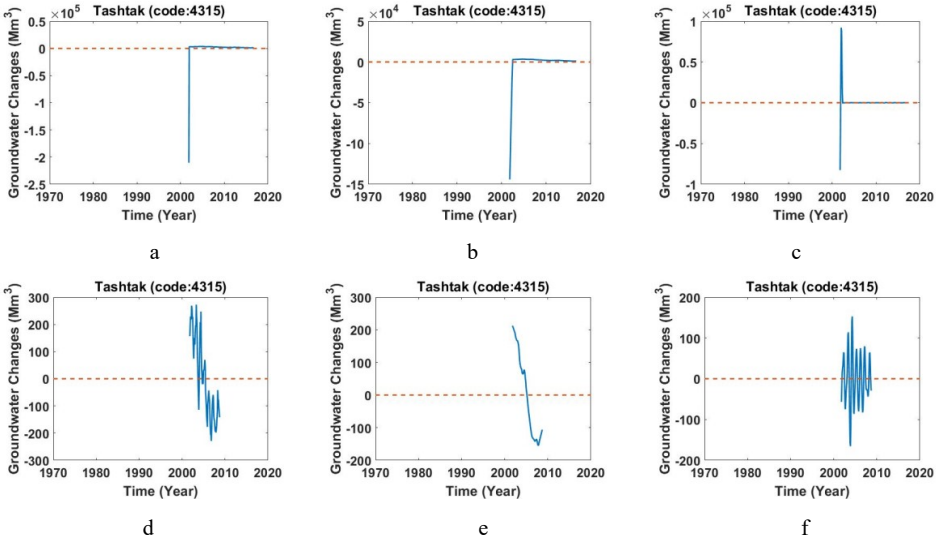

Figure B.62. a,d) Monthly values of groundwater storage, b,e) long-period of monthly values of groundwater storage, c,f) short-period of monthly values of groundwater storage across study area of Ghader abad –Madarsoleiman (Code: 4315).

B.3.12. Study area of Dehbid (Code: 4316)

This area is located between 3360000 to 3410000 y and 660000 to 730000 x in UTM, with an area of 1916.7 km^2. Figure B.63 shows changes in monthly values of groundwater storage inferred from the well data, its long-period and short-period.

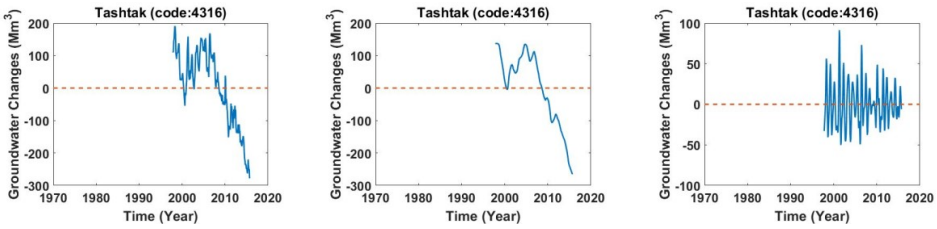

Figure B.63. a) Monthly values of groundwater storage, b) long-period of monthly values of groundwater storage, c) short-period of monthly values of groundwater storage across study area of Dehbid (Code: 4316).

B.3.13. Study area of Namdan (Code: 4317)

This area is located between 3370000 to 3450000 y and 590000 to 690000 x in UTM, with an area of 2813.7 km^2. Figure B.64 shows changes in monthly values of groundwater storage inferred from the well data, its long-period and short-period.

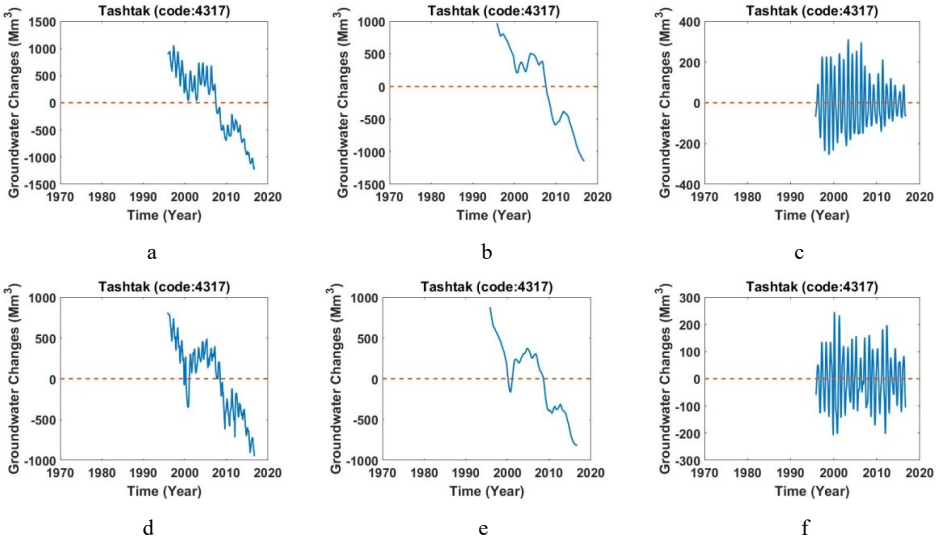

Figure B.64. a,d) Monthly values of groundwater storage, b,e) long-period of monthly values of groundwater storage, c,f) short-period of monthly values of groundwater storage across study area of Namdan (Code: 4317).

B.3.14. Study area of Beiza –Zarghan (Code: 4318)

This area is located between 3380000 to 3345000 y and 610000 to 680000 x in UTM, with an area of 1727.5 km^2. Figure B.65 shows changes in monthly values of groundwater storage inferred from the well data, its long-period and short-period.

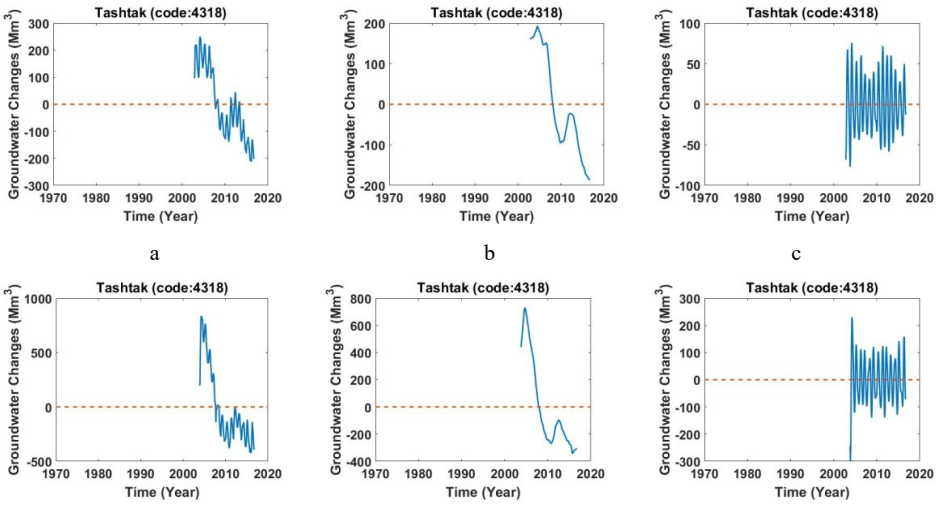

Figure B.65. a,d) Monthly values of groundwater storage, b,e) long-period of monthly values of groundwater storage, c,f) short-period of monthly values of groundwater storage across study area of Beiza –Zarghan (Code: 4318).

B.3.15. Study area of Aspas (Code: 4321)

This area is located between 3350000 to 3450000 y and 600000 to 680000 x in UTM, with an area of 1590.5 km^2. Figure B.66 shows changes in monthly values of groundwater storage inferred from the well data, its long-period and short-period.

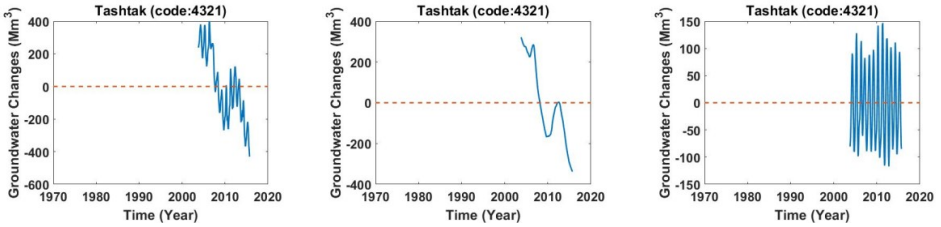

Figure B.66. a) Monthly values of groundwater storage, b) long-period of monthly values of groundwater storage, c) short-period of monthly values of groundwater storage across study area of Aspas (Code: 4321).

B.3.16. Study area of Bakan (Code: 4322)

This area is located between 3360000 to 3380000 y and 600000 to 640000 x in UTM, with an area of 366.6 km^2. Figure B.67 shows changes in monthly values of groundwater storage inferred from the well data, its long-period and short-period.

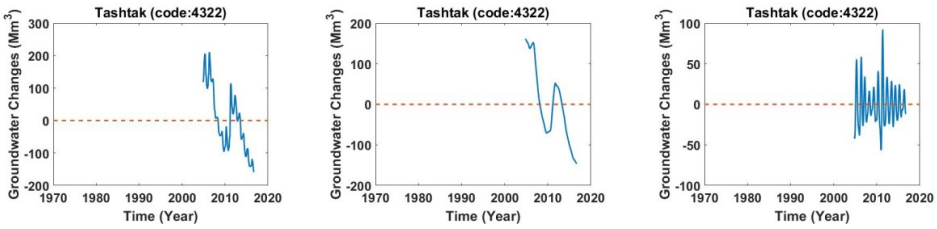

Figure B.67. a) Monthly values of groundwater storage, b) long-period of monthly values of groundwater storage, c) short-period of monthly values of groundwater storage across study area of Dehbid (Code: 4322).

B.3.17. Study area of Shiraz (Code: 4323)

This area is located between 3255000 to 3355000 y and 595000 to 670000 x in UTM, with an area of 1452.2 km^2. Figure B.68 shows changes in monthly values of groundwater storage inferred from the well data, its long-period and short-period.

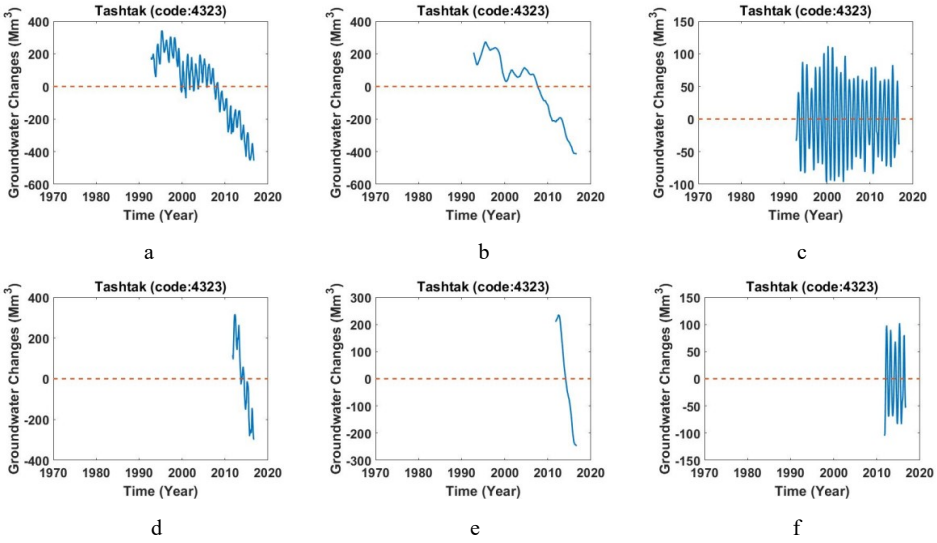

Figure B.68. a,d) Monthly values of groundwater storage, b,e) long-period of monthly values of groundwater storage, c,f) short-period of monthly values of groundwater storage across study area of Shiraz(Code: 4323).

B.3.18. Study area of Gharebagh (Code: 4324)

This area is located between 3245000 to 3275000 y and 595000 to 680000 x in UTM, with an area of 436.6 km^2. Figure B.69 shows changes in monthly values of groundwater storage inferred from the well data, its long-period and short-period.

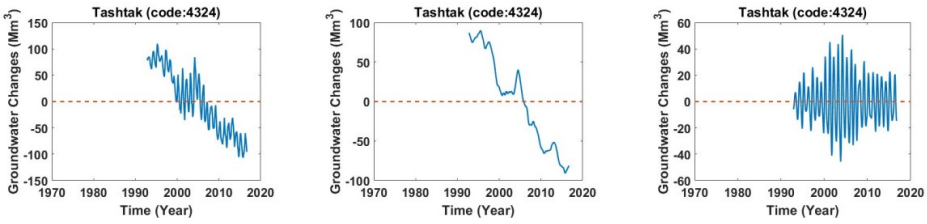

a b c

Figure B.69. a) Monthly values of groundwater storage, b) long-period of monthly values of groundwater storage, c) short-period of monthly values of groundwater storage across study area of Gharebagh (Code: 4324).

B.3.19. Study area of Kovar-Maharloo (Code: 4325)

This area is located between 3225000 to 5y and 660000 to 680000 x in UTM, with an area of 327.6 km^2. Figure B.70 shows changes in monthly values of groundwater storage inferred from the well data, its long-period and short-period.

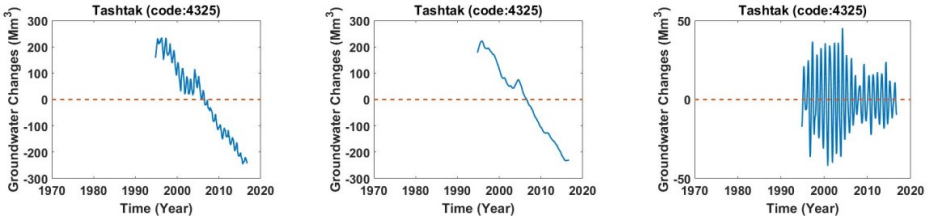

a b c

Figure B.70. a) Monthly values of groundwater storage, b) long-period of monthly values of groundwater storage, c) short-period of monthly values of groundwater storage across study area of Kovar-Maharloo (Code: 4325)

B.3.20. Study area of Sarvestan (Code: 4326)

This area is located between 3200000 to 3260000 y and 660000 to 740000 x in UTM, with an area of 1650.1 km^2. Figure B.71 shows changes in monthly values of groundwater storage inferred from the well data, its long-period and short-period.

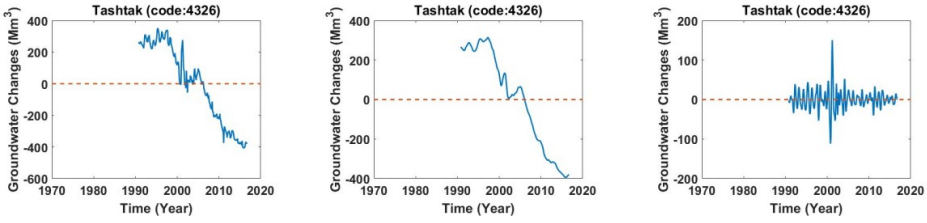

a b c

Figure B.71. a) Monthly values of groundwater storage, b) long-period of monthly values of groundwater storage, c) short-period of monthly values of groundwater storage across study area of Sarvestan (Code: 4326)

B.4.1. Study area of Abarghoo (Code: 4401)

This area is located between 30°40′-31° 30′° N and 52°45′-53° 40′E with an area of 3699.7 km^2. Figure B.72 shows changes in monthly values of groundwater storage inferred from the well data, its long-period and short-period.

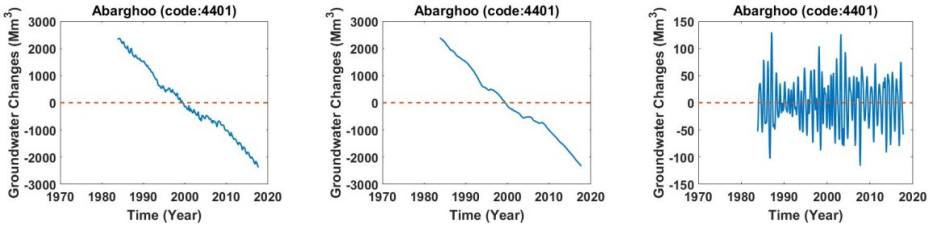

Figure B.72. a) Monthly values of groundwater storage, b) long-period of monthly values of groundwater storage, c) short-period of monthly values of groundwater storage across study area of Abarghoo(Code: 4401).

B.4.2. Study area of Abade Eghlid (Code: 4402)

This area is located between 30°45′-31°30′ N and 52°45′-53°30′E with 2845.2 km^2. Figure B.73 shows changes in monthly values of groundwater storage inferred from the well data, its long-period and short-period.

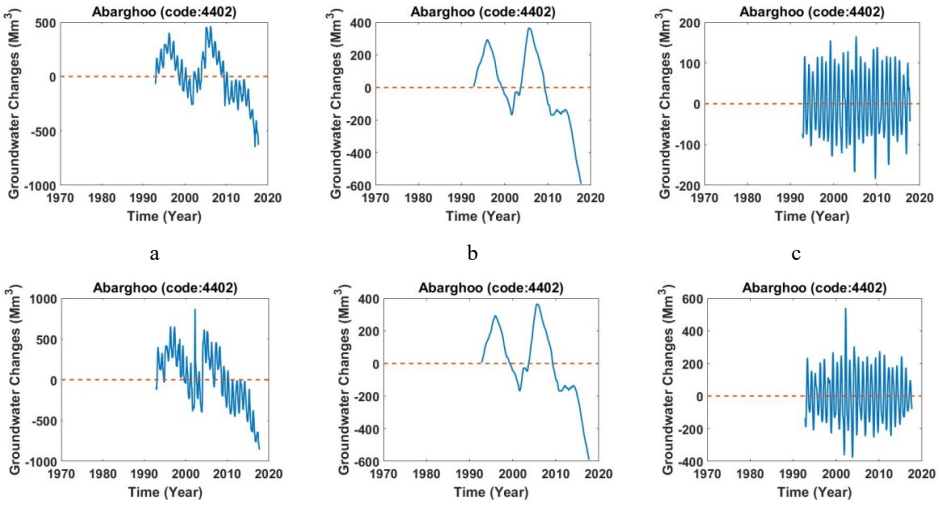

Figure B.73. a,d) Monthly values of groundwater storage, b,e) long-period of monthly values of groundwater storage, c,f) short-period of monthly values of groundwater storage across study area of Abade-Eghlid (Code: 4402).

B.4.3. Study area of Sedgh abad (Code: 4403)

This area is located between 31°-31°20′ N and 52°10′-52°40′E with an area of 732.1 km^2. Figure B.74 shows changes in monthly values of groundwater storage inferred from the well data, its long-period and short-period.

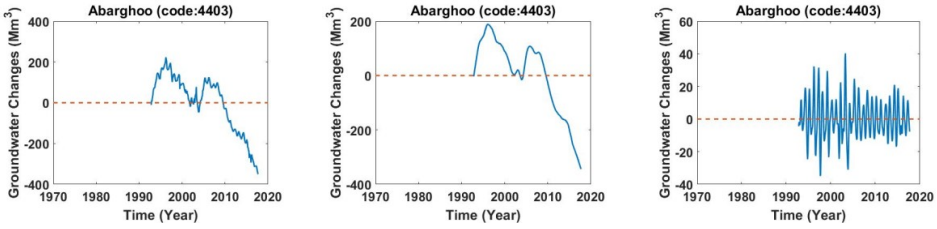

a b c

Figure B.74. a) Monthly values of groundwater storage, b) long-period of monthly values of groundwater storage, c) short-period of monthly values of groundwater storage across study area of Sadeg Abad (Code: 4403).

B.4.4. Study area of Kavir Abarghoo (Code: 4404)

This area is located between 30°40′-31°20′ N and 53°40′-55°E with an area of 7201.3 km^2. This area is divided to 3 parts. Figure B.75 shows changes in monthly values of groundwater storage inferred from the well data, its long-period and short-period.

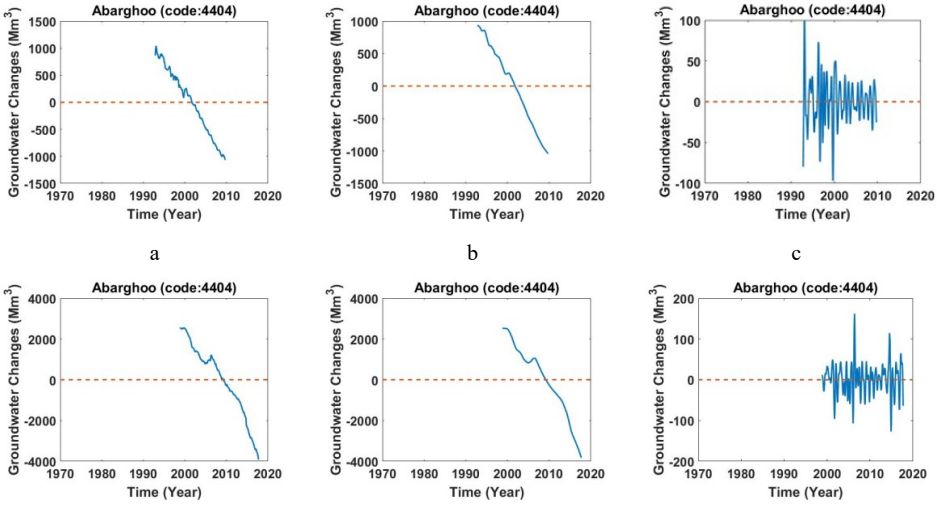

a b c

d e f

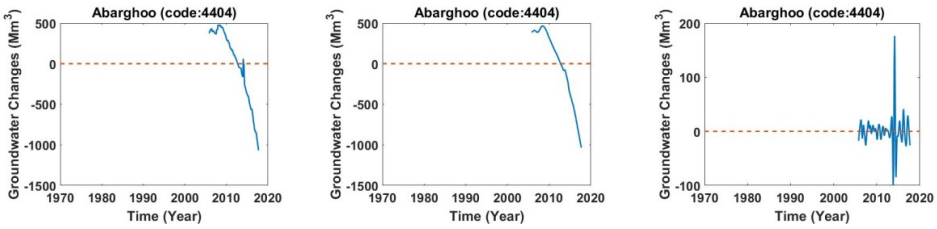

Figure B.75. a,b,g) Monthly values of groundwater storage, b,c,h) long-period of monthly values of groundwater storage, c,f,m) short-period of monthly values of groundwater storage across study area of Kavir Abarghoo (Code: 4404).

B.4.5. Study area of Deh Shir (Code: 4405)

This area is located between 31˚-31˚40′ N and 53˚30′-54˚20′E with an area of 3166 km^2. This area is divided to 2 parts. Figure B.76 shows changes in monthly values of groundwater storage inferred from the well data, its long-period and short-period.

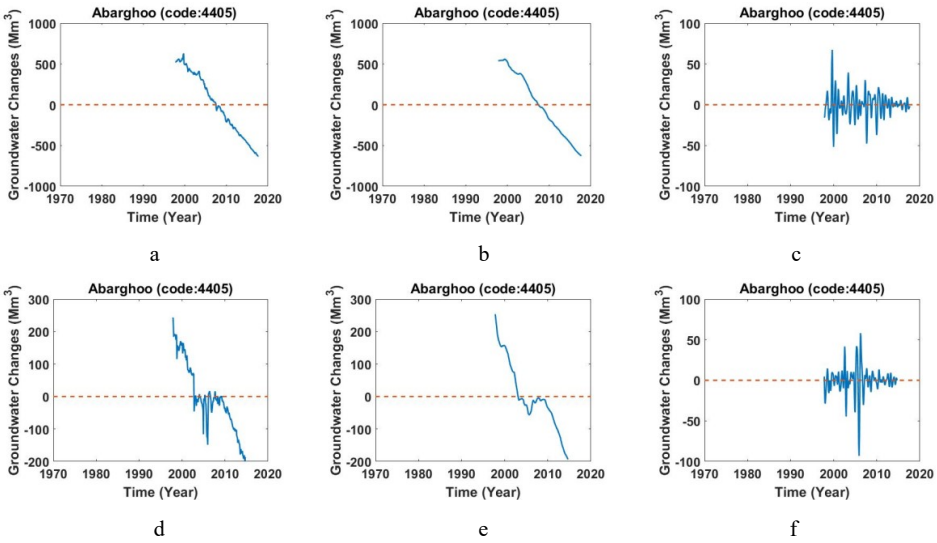

Figure B.76. a,d) Monthly values of groundwater storage, b,e) long-period of monthly values of groundwater storage, c,f) short-period of monthly values of groundwater storage across study area of Deh Shir (Code: 4405).

B.4.6. Study area of Kaf Taghestan (Code: 4406)

This area is located between 31˚20′-32˚ N and 52˚50′-53˚45′E with an area of 3831.5 km^2. Figure B.77 shows changes in monthly values of groundwater storage inferred from the well data, its long-period and short-period.

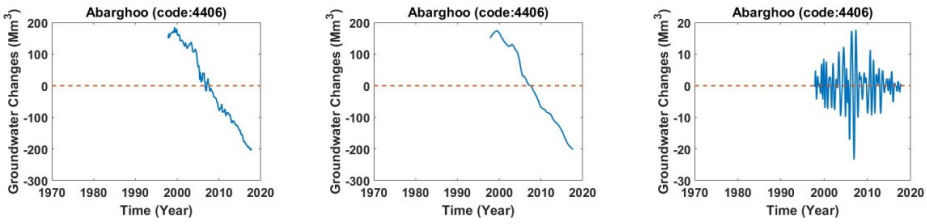

a b c

Figure B.77. a) Monthly values of groundwater storage, b) long-period of monthly values of groundwater storage, c) short-period of monthly values of groundwater storage across study area of Deh Shir (Code: 4405).

B.4.7. Study area of Marvast (Code: 4407)

This area is located between 30°25′-30°50′ N and 54°-54°30′E with 2105.1 km^2. Figure B.78 shows changes in monthly values of groundwater storage inferred from the well data, its long-period and short-period.

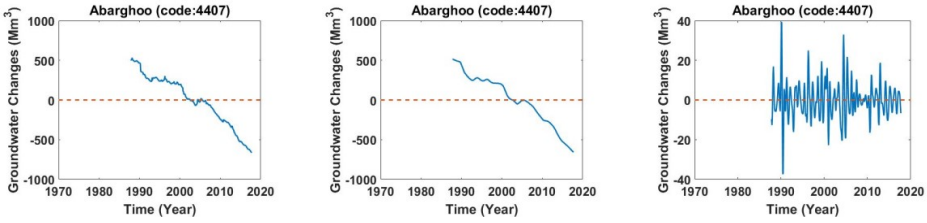

a b c

Figure B.78. a) Monthly values of groundwater storage, b) long-period of monthly values of groundwater storage, c) short-period of monthly values of groundwater storage across study area of Marvast (Code: 4407).

B.4.8. Study area of Bavanat (Code: 4408)

This area is located between 30°20′-30°45′ N and 53 30′′°-54°10′E with an area of 853 km^2. Figure B.79 shows changes in monthly values of groundwater storage inferred from the well data, its long-period and short-period.

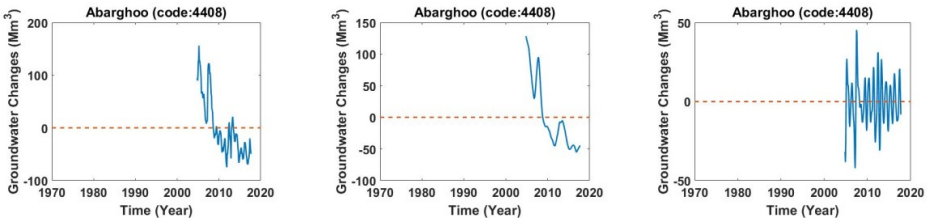

a b c

Figure B.79. a) Monthly values of groundwater storage, b) long-period of monthly values of groundwater storage, c) short-period of monthly values of groundwater storage across study area of Bavanat (Code: 4408).

B.4.9. Study area of Harat (Code: 4409)

This area is located between 30°-30°30′ N and 53° 40′-54°20′E with an area of 1625.6 km^2. This area divided in 2 parts Figure B.80 shows changes in monthly values of groundwater storage inferred from the well data, its long-period and short-period.

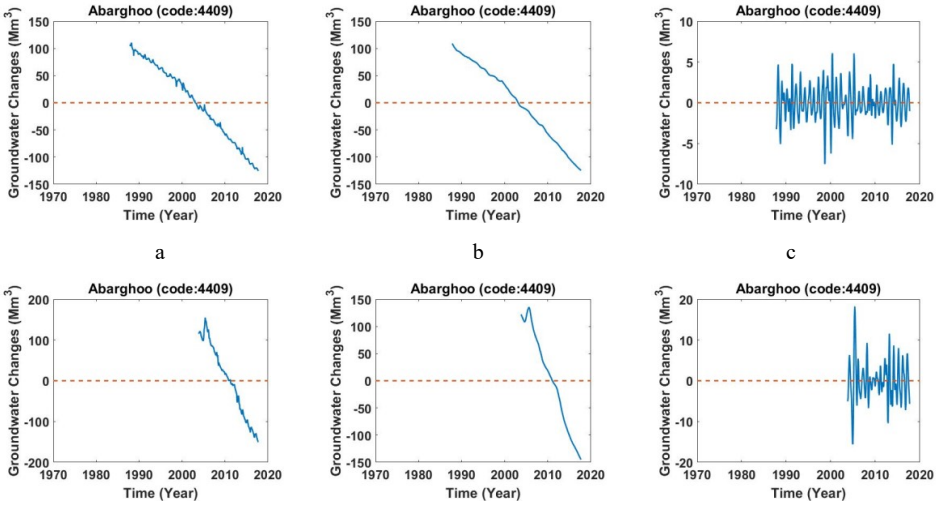

Figure B.80. a,d) Monthly values of groundwater storage, b,e) long-period of monthly values of groundwater storage, c,f) short-period of monthly values of groundwater storage across study area of Harat (Code: 4409).

B.4.10. Study area of Sare Chahan (Code: 4410)

This area is located between 30°-30°20′ N and 53° 30′-54°E with an area of 1107.4 km^2. Figure B.81 shows changes in monthly values of groundwater storage inferred from the well data, its long-period and short-period.

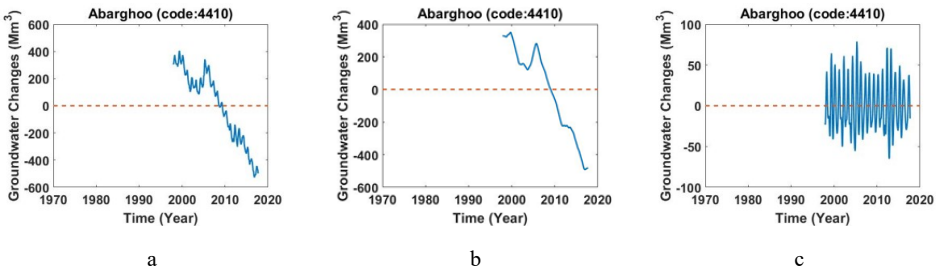

Figure B.81. a) Monthly values of groundwater storage, b) long-period of monthly values of groundwater storage, c) short-period of monthly values of groundwater storage across study area of Sare Chahan (Code: 4410).

B.4.11. Study area of Shahre Babak (Code: 4411)

This area is located between 30°-30°50′ N and 54° 20′-55°10′E with an area of 4002.2 km^2. Figure B.82 shows changes in monthly values of groundwater storage inferred from the well data, its long-period and short-period.

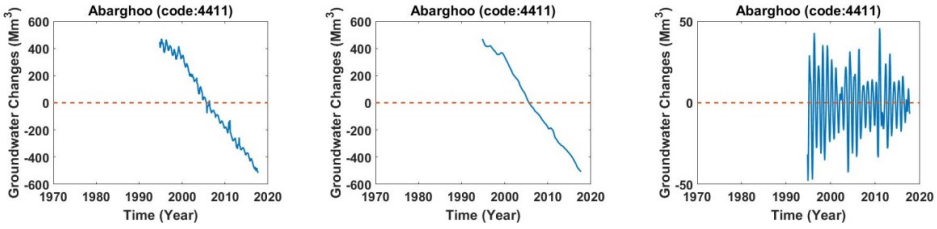

a b c

Figure B.82. a) Monthly values of groundwater storage, b) long-period of monthly values of groundwater storage, c) short-period of monthly values of groundwater storage across study area of Shahre Babak (Code: 4408).

B.4.12. Study area of Chahake Shahriari (Code: 4412)

This area is located between 29°40′-30°10 N and 54°-54°40′E with an area of 2046.1 km^2. Figure B.83 shows changes in monthly values of groundwater storage inferred from the well data, its long-period and short-period.

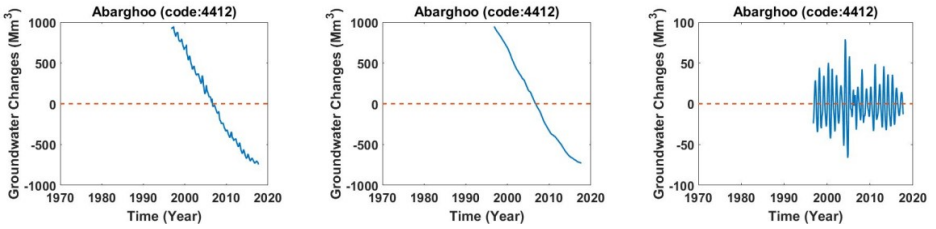

a b c

Figure B.83. a) Monthly values of groundwater storage, b) long-period of monthly values of groundwater storage, c) short-period of monthly values of groundwater storage across study area of Chahake Shahriari (Code: 4412).

B.4.13. Study area of Hasan Abad Ghoori (Code: 4413)

This area is located between 29°25′-29°50 N and 54° 10′-54°30′E with an area of 802.4 km^2. Figure B.84 shows changes in monthly values of groundwater storage inferred from the well data, its long-period and short-period.

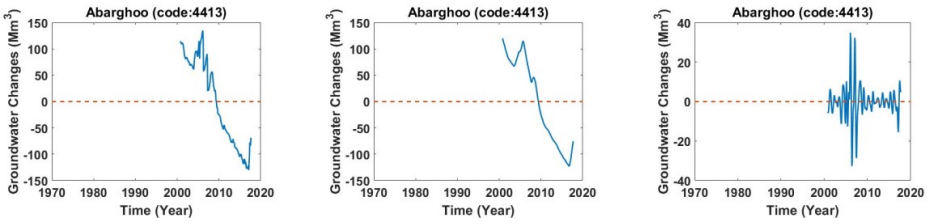

a b c

Figure B.84. a) Monthly values of groundwater storage, b) long-period of monthly values of groundwater storage, c) short-period of monthly values of groundwater storage across study area of Hasan Abade Ghoori (Code: 4413).

B.4.14. Study area of Khatoon Abad (Code: 4414)

This area is located between 30°10′-30°30′ N and 55°-55°30′E with an area of 1343 km^2. Figure B.85 shows changes in monthly values of groundwater storage inferred from the well data, its long-period and short-period.

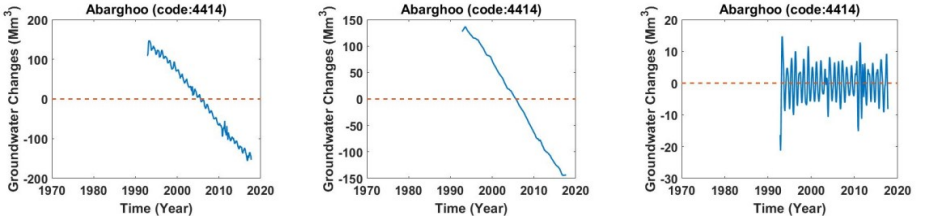

a b c

Figure B.85. a) Monthly values of groundwater storage, b) long-period of monthly values of groundwater storage, c) short-period of monthly values of groundwater storage across study area of Hasan Khatoon Abad (Code: 4414).

B.4.1B. Study area of Kavir Harat va Marvest (Code: 4415)

This area is located between 30°25′-30°45′ N and 54°-54°30′E with an area of 2327.6 km^2. Figure B.86 shows changes in monthly values of groundwater storage inferred from the well data, its long-period and short-period.

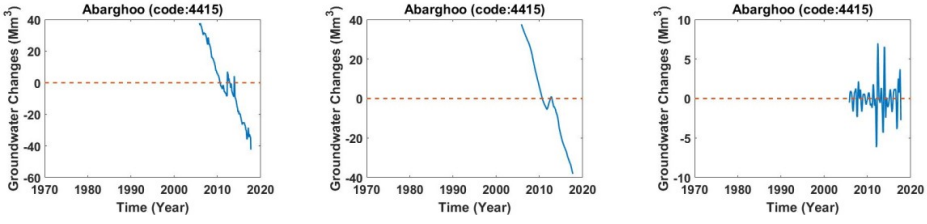

a b c

Figure B.86. a) Monthly values of groundwater storage, b) long-period of monthly values of groundwater storage, c) short-period of monthly values of groundwater storage across study area of Hasan Kavir Harat va Marvest (Code: 4415).

B.4.16. Study area of Ghataroeieh (Code: 4416)

This area is located between 29˚10′-29˚55′ N and 54˚25′-55˚40′E with 4045.8 km^2. Figure B.87 shows changes in monthly values of groundwater storage inferred from the well data, its long-period and short-period.

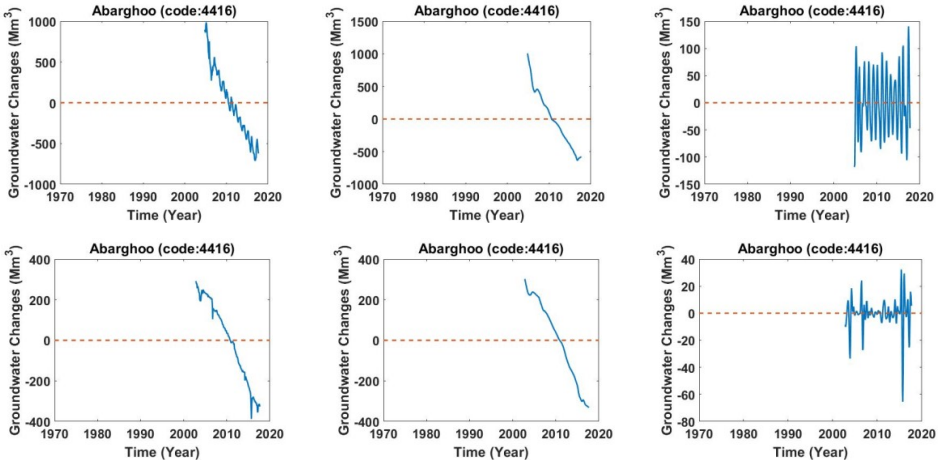

d e f

Figure B.87. a,d) Monthly values of groundwater storage, b,e) long-period of monthly values of groundwater storage, c,f) short-period of monthly values of groundwater storage across study area of Hasan Ghataroeieh (Code: 4416).

B.4.17. Study area of Kavir ghataroeih (Code: 4417)

This area is located between 29˚-29˚20′ N and 54˚30′-5˚30E with an area of 2282.3 km^2. Figure B.88 shows changes in monthly values of groundwater storage inferred from the well data, its long-period and short-period.

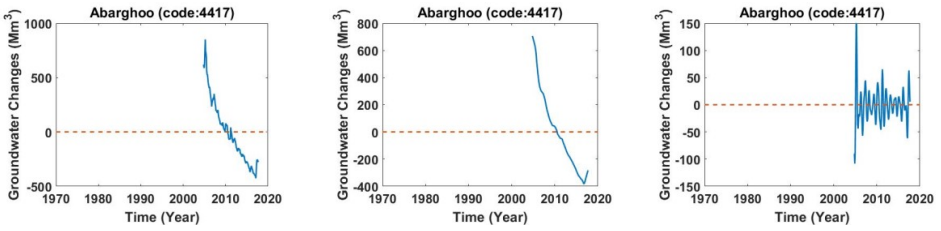

a b c

Figure B.88. a) Monthly values of groundwater storage, b) long-period of monthly values of groundwater storage, c) short-period of monthly values of groundwater storage across study area of Hasan Kavir Ghataroeieh (Code: 4417).

B.4.18. Study area of Kavir Sir Jan (Code: 4418)

This area is located between 29°20′-30°20′ N and 54°30′-56°E with an area of 6121.1 km^2. Figure B.89 shows changes in monthly values of groundwater storage inferred from the well data, its long-period and short-period.

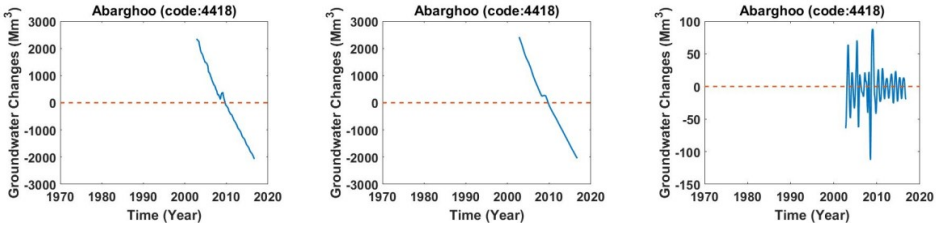

a b c

Figure B.89. a) Monthly values of groundwater storage, b) long-period of monthly values of groundwater storage, c) short-period of monthly values of groundwater storage across study area of Hasan KavirSirJan (Code: 4418).

B.4.19. Study area of Sir Jan (Code: 4419)

This area is located between 29°20′-30°20′ N and 55°5′-56°30′E with an area of 7942.9 km^2. Figure B.90 shows changes in monthly values of groundwater storage inferred from the well data, its long-period and short-period.

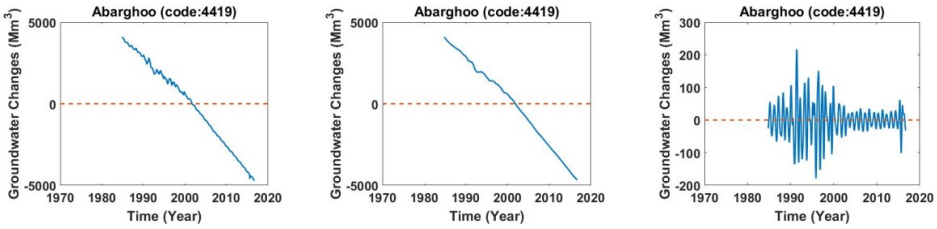

a b c

Figure B.90. a) Monthly values of groundwater storage, b) long-period of monthly values of groundwater storage, c) short-period of monthly values of groundwater storage across study area of Hasan Sirjan (Code: 4419).

B.5.1. Study area of Roodbar Jiroft (Code: 4501)

This area is located between 27°20′-28° 25′ N and 57°30′-59° E with an area of 10788.71 km^2. Figure B.91 shows changes in monthly values of groundwater storage inferred from the well data, its long-period and short-period.

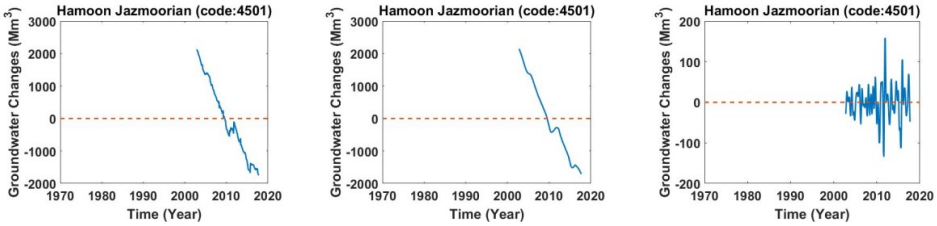

a b c

Figure B.91. a) Monthly values of groundwater storage, b) long-period of monthly values of groundwater storage, c) short-period of monthly values of groundwater storage across study area of Roodbar Jiroft (Code: 4501).

B.5.2. Study area of Fariab sharghi (Code: 4502)

This area is located between 28°-28° 35′ N and 57°30′-57°55′ E with an area of 1742.25 km^2. Figure B.92 shows changes in monthly values of groundwater storage inferred from the well data, its long-period and short-period.

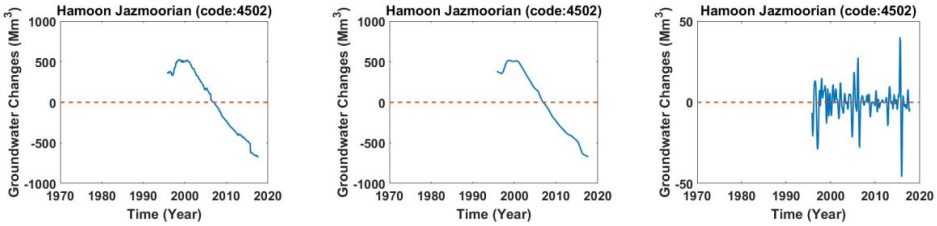

a b c

Figure B.92. a) Monthly values of groundwater storage, b) long-period of monthly values of groundwater storage, c) short-period of monthly values of groundwater storage across study area of Fariab sharghi (Code: 4502).

B.5.3. Study area of Jiroft (Code: 4503)

This area is located between 28°-29° 20′ N and 57°-58°20′ E with an area of 5412.7 km^2. Figure B.93 shows changes in monthly values of groundwater storage inferred from the well data, its long-period and short-period.

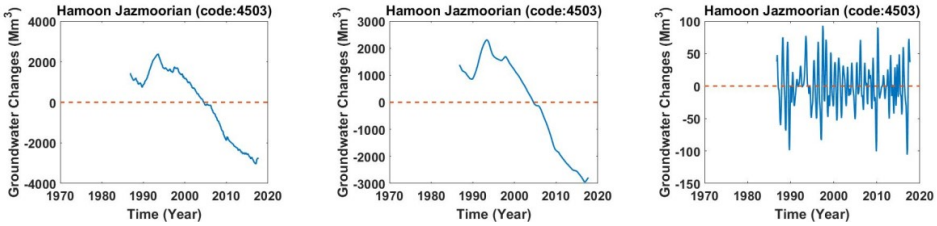

a b c

Figure B.93. a) Monthly values of groundwater storage, b) long-period of monthly values of groundwater storage, c) short-period of monthly values of groundwater storage across study area of Jiroft (Code: 4503).

B.5.4. Study area of Esfandaghe (Code: 4505)

This area is located between 28°20′-28° 45′ N and 56°55′-57°20′ E with an area of 821.83 km^2. Figure B.94 shows changes in monthly values of groundwater storage inferred from the well data, its long-period and short-period.

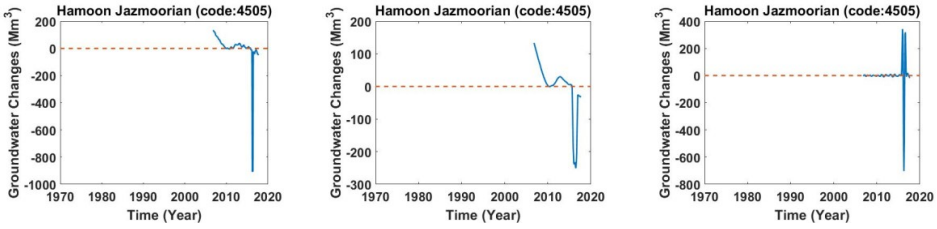

a b c

Figure B.94. a) Monthly values of groundwater storage, b) long-period of monthly values of groundwater storage, c) short-period of monthly values of groundwater storage across study area of Fariab sharghi (Code: 4505).

B.5.5. Study area of Fariab Sharghi (Code: 4509)

This area is located between 28°55′-29° 20′ N and 56°15′-56°40′ E with an area of 938.25 km^2. Figure B.95 shows changes in monthly values of groundwater storage inferred from the well data, its long-period and short-period.

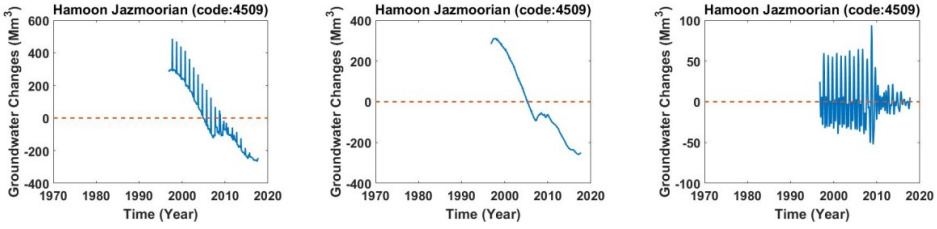

a b c

Figure B.95. a) Monthly values of groundwater storage, b) long-period of monthly values of groundwater storage, c) short-period of monthly values of groundwater storage across study area of Fariab sharghi (Code: 4509).

B.5.6. Study area of Ghale Ganj-Kam Sefid (Code: 4513)

This area is located between 26°45′-27° 40′ N and 57°40′-58°40′ E with an area of 5431.23 km^2. Figure B.96 shows changes in monthly values of groundwater storage inferred from the well data, its long-period and short-period.

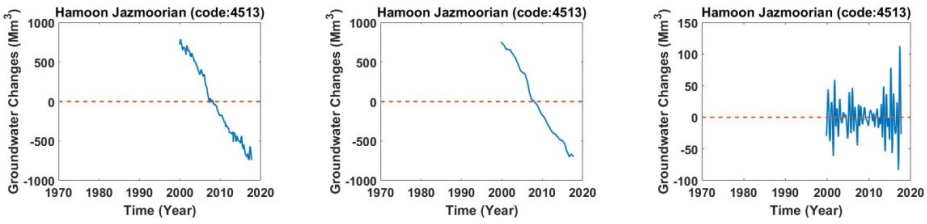

Figure B.96. a) Monthly values of groundwater storage, b) long-period of monthly values of groundwater storage, c) short-period of monthly values of groundwater storage across study area of Fariab sharghi (Code: 4513).

B.5.7. Study area of Chah Hashem (Code: 4514)

This area is located between 26°30′-27° 15′ N and 58°5′-59° E with an area of 5431.23 km^2. Figure B.97 shows changes in monthly values of groundwater storage inferred from the well data, its long-period and short-period.

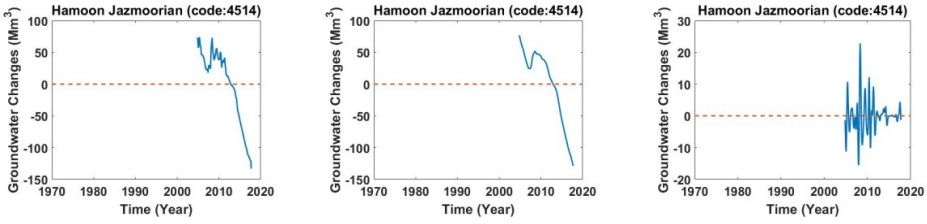

Figure B.97. a) Monthly values of groundwater storage, b) long-period of monthly values of groundwater storage, c) short-period of monthly values of groundwater storage across study area of Chah Hashem (Code: 4514).

B.5.8. Study area of Espake-Maskootan(Code: 4515)

This area is located between 26°30′-27° 10′ N and 58°5′-60°30′ E with an area of 8202.37 km^2. Figure B.98 shows changes in monthly values of groundwater storage inferred from the well data, its long-period and short-period.

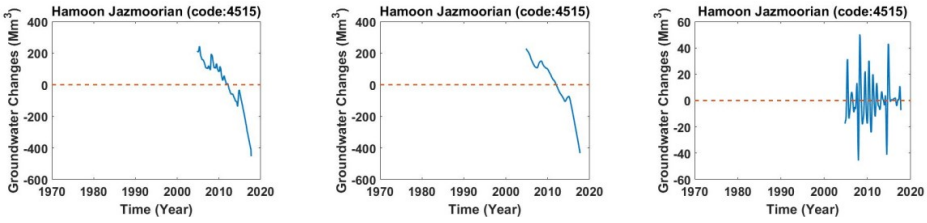

Figure B.98. a) Monthly values of groundwater storage, b) long-period of monthly values of groundwater storage, c) short-period of monthly values of groundwater storage across study area of Espake-Maskootan (Code: 4515).

B.5.9. Study area of Barfan-Sardgal(Code: 4516)

This area is located between 27°-28° N and 59°-60°20′ E with an area of 7261.44km^2. Figure B.99 shows changes in monthly values of groundwater storage inferred from the well data, its long-period and short-period.

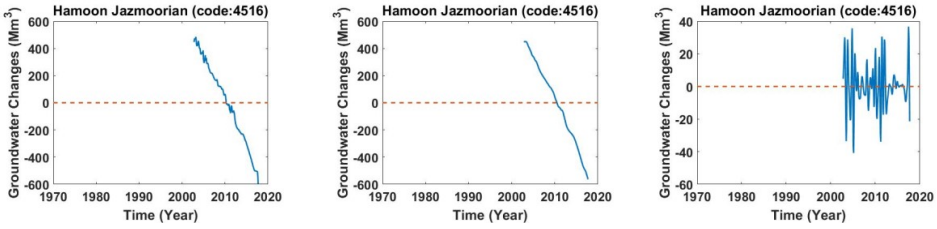

a b c

Figure B.99. a) Monthly values of groundwater storage, b) long-period of monthly values of groundwater storage, c) short-period of monthly values of groundwater storage across study area of Espake-Maskootan (Code: 4516).

B.5.10. Study area of Iran Shahr-Bampoor (Code: 4517)

This area is located between 26°20′-28° N and 60°-61°20′ E with an area of 9436.64 km^2. Figure B.100 shows changes in monthly values of groundwater storage inferred from the well data, its lng-period and short-period.

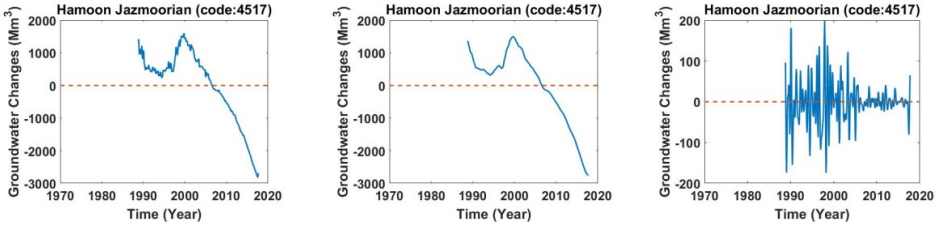

a b c

Figure B.100. a) Monthly values of groundwater storage, b) long-period of monthly values of groundwater storage, c) short-period of monthly values of groundwater storage across study area of Iran Shahr-Bampoor (Code: 4517).

B.5.11. Study area of Volgan-Chah Kichi (Code: 4520)

This area is located between 27°25′-28° N and 59°-59°50′ E with an area of 4762.55 km^2. Figure B.101 shows changes in monthly values of groundwater storage inferred from the well data, its long-period and short-period.

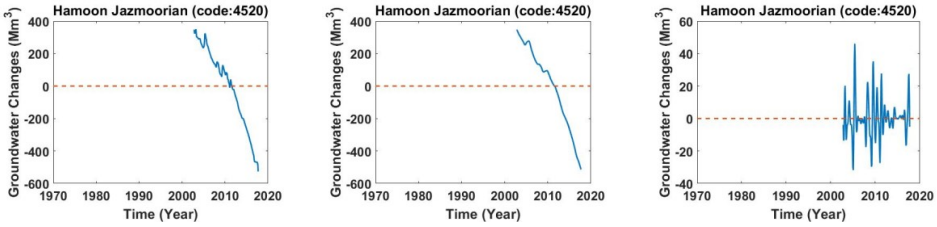

a b c

Figure B.101. a) Monthly values of groundwater storage, b) long-period of monthly values of groundwater storage, c) short-period of monthly values of groundwater storage across study area of Volgan-Chah Kichi (Code: 4520).

B.6.1. Study area of Sarayan (Code: 4601)

This area is located between 33°20′-34°05′ N and 58°-58°48′ E with an area of 2615.6 km^2. Figure B.102 shows changes in monthly values of groundwater storage inferred from the well data, its long-period and short-period.

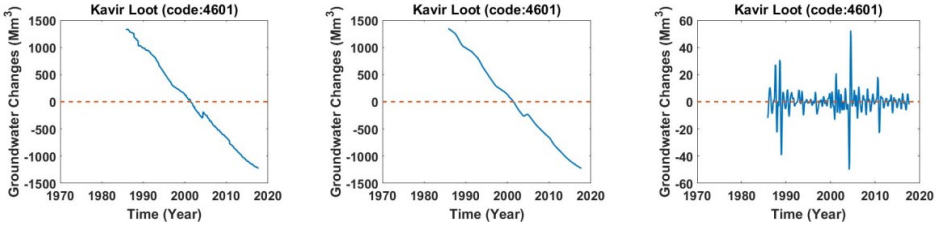

a b c

Figure B.102. a) Monthly values of groundwater storage, b) long-period of monthly values of groundwater storage, c) short-period of monthly values of groundwater storage across study area of Sarayan (Code: 4601).

B.6.2. Study area of Chahak Mosavieh (Code: 4602)

This area is located between 33°-33°47′ N and 58°28′-59°20′ E with an area of 4538.03 km^2. Figure B.103 shows changes in monthly values of groundwater storage inferred from the well data, its long-period and short-period.

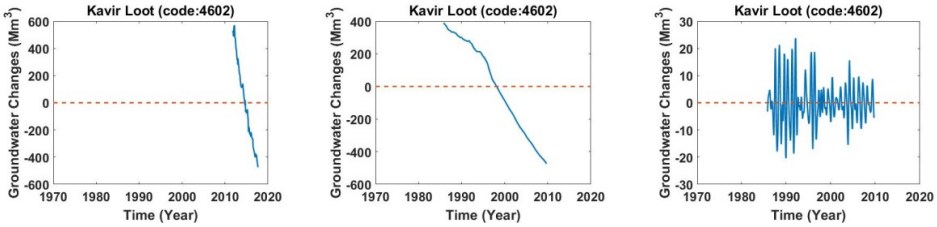

a b c

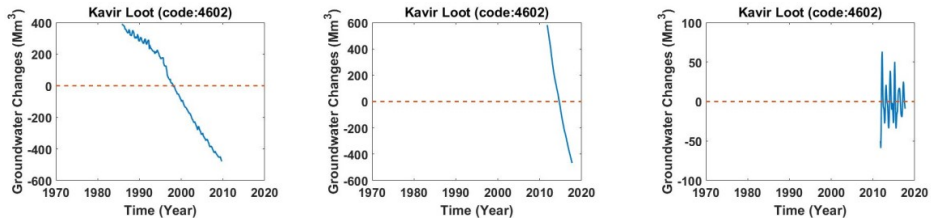

Figure B.103. a,d) Monthly values of groundwater storage, b,b) long-period of monthly values of groundwater storage, c,f) short-period of monthly values of groundwater storage across study area of Chahak Mosavieh (Code: 4602).

B.6.3. Study area of Sadeh (Code: 4603)

This area is located between 33°30′-33°24′ N and 59°11′-59°34′ E with an area of 730.6 km^2. Figure B.104 shows changes in monthly values of groundwater storage inferred from the well data, its long-period and short-period.

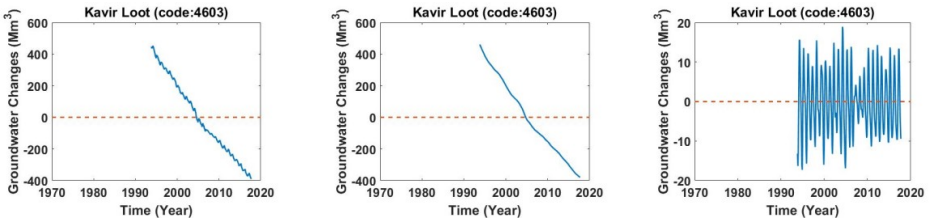

Figure B.104. a) Monthly values of groundwater storage, b) long-period of monthly values of groundwater storage, c) short-period of monthly values of groundwater storage across study area of Sadeh (Code: 4603).

B.6.4. Study area of Tabas (Code: 4604)

This area is located between 32°35′-34°07′ N and 56°13′ -57°31′ E with 12485.85 km^2. Figure B.105 shows changes in monthly values of groundwater storage inferred from the well data, its long-period and short-period.

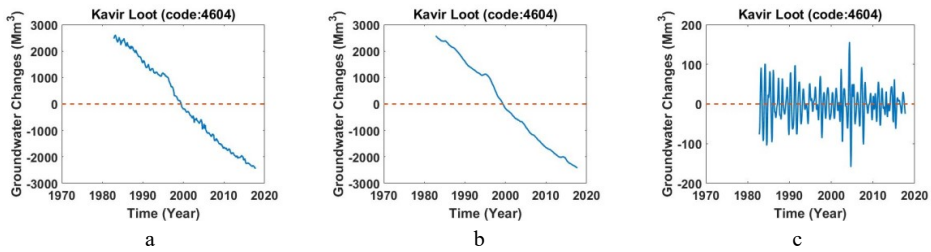

Figure B.105. a) Monthly values of groundwater storage, b) long-period of monthly values of groundwater storage, c) short-period of monthly values of groundwater storage across study area of Tabas (Code: 4604).

B.6.5. Study area of Degh Tel Hamid (Code: 4605)

This area is located between 32°35′-33°25′ N and 55°28′-56°29′ E with 206355.03 km^2. Figure B.106 shows changes in monthly values of groundwater storage inferred from the well data, its long-period and short-period.

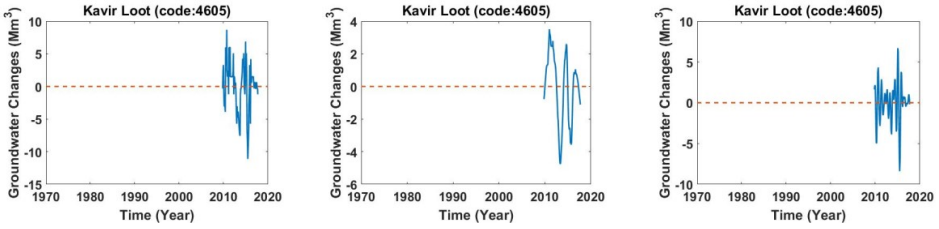

a b c

Figure B.106. a) Monthly values of groundwater storage, b) long-period of monthly values of groundwater storage, c) short-period of monthly values of groundwater storage across study area of Degh Tel Hamid (Code: 4605).

B.6.6. Study area of Sarayan Kavir Ela Abad (Code: 4606)

This area is located between 32°33′-32°56′ N and 55°17′-55°43′ E with an area of 980.17 km^2. Figure B.107 shows changes in monthly values of groundwater storage inferred from the well data, its long-period and short-period.

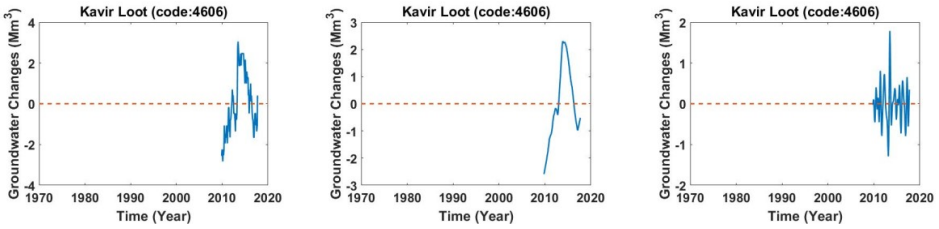

a b c

Figure B.107. a) Monthly values of groundwater storage, b) long-period of monthly values of groundwater storage, c) short-period of monthly values of groundwater storage across study area of Kavir Ela Abad (Code: 4606).

B.6.7. Study area of Bahabad(Code: 4607)

This area is located between 31°33′-32°45′ N and 55°32′-56°19′ E with an area of 5103.32 km^2. Figure B.108 shows changes in monthly values of groundwater storage inferred from the well data, its long-period and short-period.

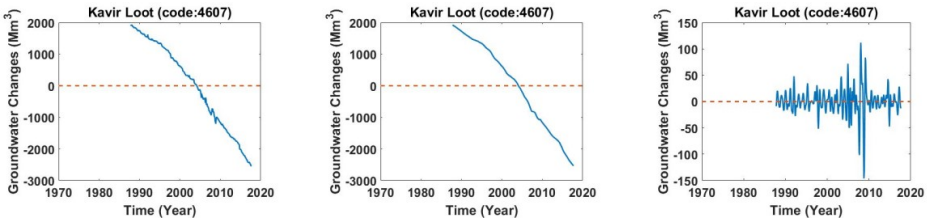

Figure B.108. a) Monthly values of groundwater storage, b) long-period of monthly values of groundwater storage, c) short-period of monthly values of groundwater storage across study area of Bahabad (Code: 4607).

B.6.8. Study area of Ravar (Code: 4610)

This area is located between 30°47′-31°35′ N and 56°26′-57°26′ E with an area of 4127.54 km^2. Figure B.109 shows changes in monthly values of groundwater storage inferred from the well data, its long-period and short-period.

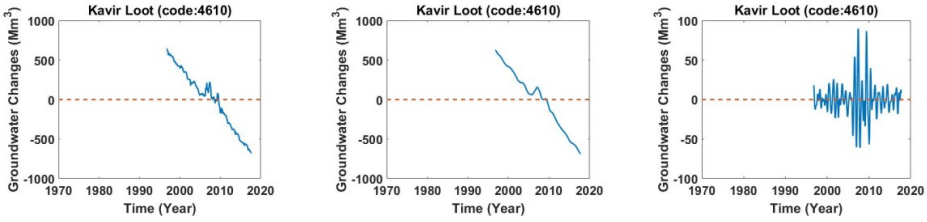

Figure B.109. a) Monthly values of groundwater storage, b) long-period of monthly values of groundwater storage, c) short-period of monthly values of groundwater storage across study area of Ravar (Code: 4610).

B.6.9. Study area of Naiband (Code: 4612)

This area is located between 27°52′-34°7′ N and 55°17′-61°11′ E with an area of 4291.03 km^2. Figure B.110 shows changes in monthly values of groundwater storage inferred from the well data, its long-period and short-period.

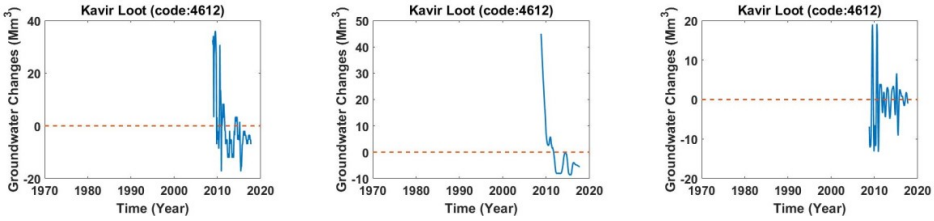

Figure B.110. a) Monthly values of groundwater storage, b) long-period of monthly values of groundwater storage, c) short-period of monthly values of groundwater storage across study area of Naiband (Code: 4612).

B.6.10. Study area of Dihok (Code: 4613)

This area is located between 32°22′-33°39′ N and 57°3′-58°49′ E with 2615.6 km^2. Figure B.111 shows changes in monthly values of groundwater storage inferred from the well data, its long-period and short-period.

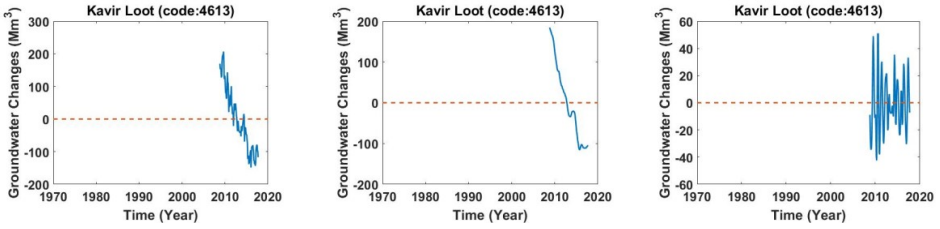

a b c

Figure B.111. a) Monthly values of groundwater storage, b) long-period of monthly values of groundwater storage, c) short-period of monthly values of groundwater storage across study area of Dihok (Code: 4613).

B.6.11. Study area of Ali Abad Hamoon (Code: 4614)

This area is located between 32°6′-33° N and 57°44′-59° E with an area of 4426.77 km^2. Figure B.112 shows changes in monthly values of groundwater storage inferred from the well data, its long-period and short-period.

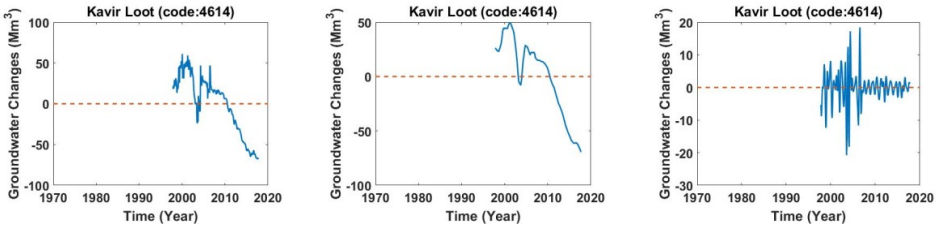

a b c

Figure B.112. a) Monthly values of groundwater storage, b) long-period of monthly values of groundwater storage, c) short-period of monthly values of groundwater storage across study area of Ali Abad Hamoon (Code: 4614).

B.6.12. Study area of Ali Abad Hamoon(Code: 4615)

This area is located between 32°12′-32°47′ N and 58°43′-59°41′ E with an area of 2507.79 km^2. Figure B.113 shows changes in monthly values of groundwater storage inferred from the well data, its long-period and short-period.

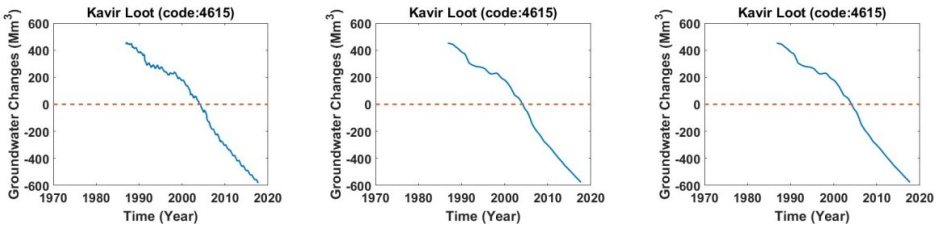

Figure B.113. a) Monthly values of groundwater storage, b) long-period of monthly values of groundwater storage, c) short-period of monthly values of groundwater storage across study area of Ali Abad Hamoon (Code: 4615).

B.6.13. Study area of Birjand (Code: 4616)

This area is located between 32°35′-33°8′ N and 58°41′-59° 46 E with an area of 3406.72 km^2. Figure B.114 shows changes in monthly values of groundwater storage inferred from the well data, its long-period and short-period.

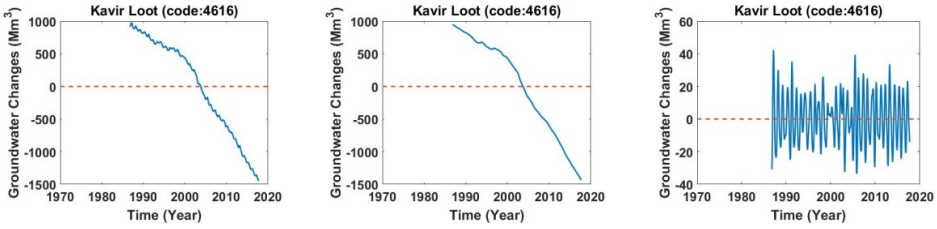

Figure B.114. a) Monthly values of groundwater storage, b) long-period of monthly values of groundwater storage, c) short-period of monthly values of groundwater storage across study area of Birjand (Code: 4616).

B.6.14. Study area of Shahdad (Code: 4617)

This area is located between 29°57′-35°52′ N and 57°7′-58° 8′ E with an area of 5518.2 km^2. Figure B.115 shows changes in monthly values of groundwater storage inferred from the well data, its long-period and short-period.

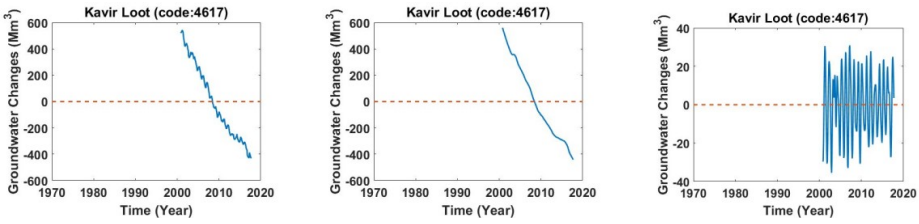

a b c

Figure B.115. a) Monthly values of groundwater storage, b) long-period of monthly values of groundwater storage, c) short-period of monthly values of groundwater storage across study area of Shahdad (Code: 4617).

B.6.15. Study area of Bam Narmashir (Code: 4620)

This area is located between 28°25′-29°26′ N and 57°37′-59° 29′ E with an area of 9658.18 km^2. Figure B.116 shows changes in monthly values of groundwater storage inferred from the well data, its long-period and short-period.

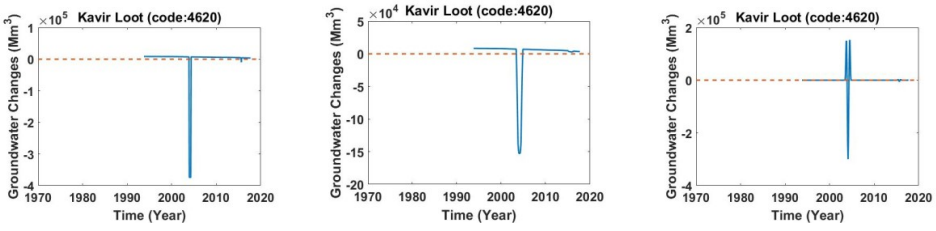

a b c

Figure B.116. a) Monthly values of groundwater storage, b) long-period of monthly values of groundwater storage, c) short-period of monthly values of groundwater storage across study area of Bam Narmashir (Code: 4620).

B.6.16. Study area of Rain (Code: 4621)

This area is located between 29°24′-29°53′ N and 57°14′-57° 55′ E with an area of 1932.95 km^2. Figure B.117 shows changes in monthly values of groundwater storage inferred from the well data, its long-period and short-period.

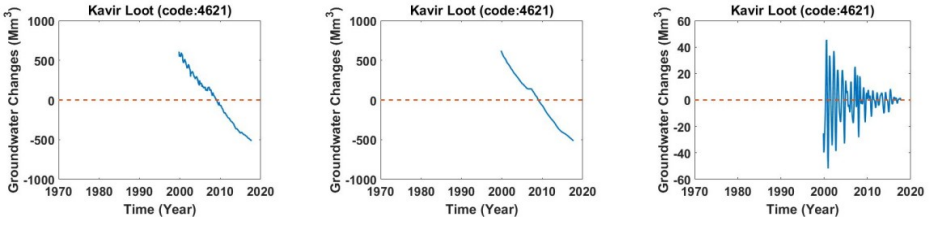

a b c

Figure B.117. a) Monthly values of groundwater storage, b) long-period of monthly values of groundwater storage, c) short-period of monthly values of groundwater storage across study area of Rain(Code: 4621).

B.6.17. Study area of Rahmatabad (Code: 4623)

This area is located between 27°57′-29°11′ N and 58°30′-60° 1′ E with an area of 9369.87 km^2. Figure B.118 shows changes in monthly values of groundwater storage inferred from the well data, its long-period and short-period.

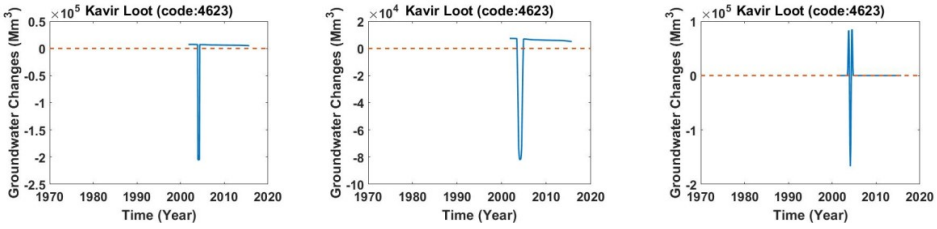

a b c

Figure B.118. a) Monthly values of groundwater storage, b) long-period of monthly values of groundwater storage, c) short-period of monthly values of groundwater storage across study area of Rahmatabad (Code: 4623).

B.6.18. Study area of Gohar kooh (Code: 4625)

This area is located between 28°8′-28°45′ N and 60°11′-61° 1′ E with an area of 9658.18 km^2. Figure B.119 shows changes in monthly values of groundwater storage inferred from the well data, its long-period and short-period.

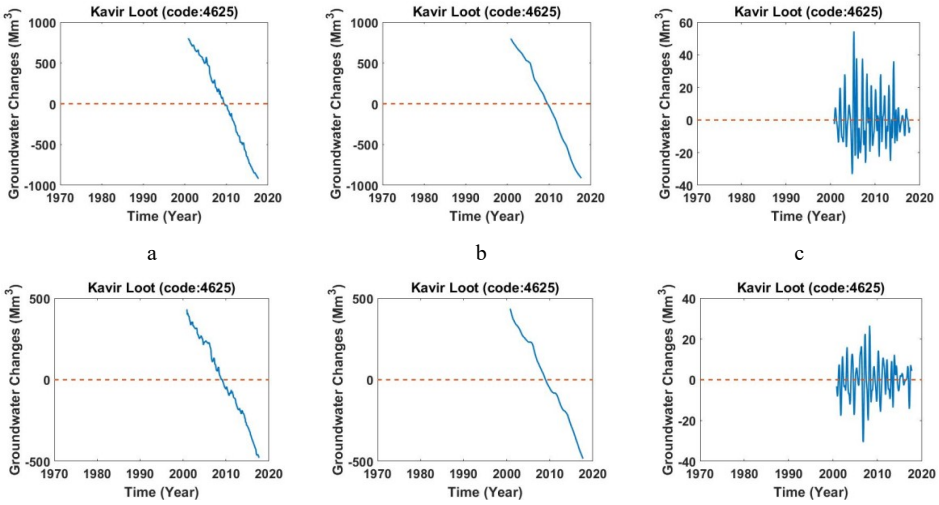

a b c

d e f

Figure B.119. a,d) Monthly values of groundwater storage, b,b) long-period of monthly values of groundwater storage, c,f) short-period of monthly values of groundwater storage across study area of gohar koh (Code: 4625).

B.6.19. Study area of Hesarooie (Code: 4626)

This area is located between 29°7′-29°40′ N and 59°58′-60° 22′ E with 1135.34 km^2. Figure B.120 shows changes in monthly values of groundwater storage inferred from the well data, its long-period and short-period.

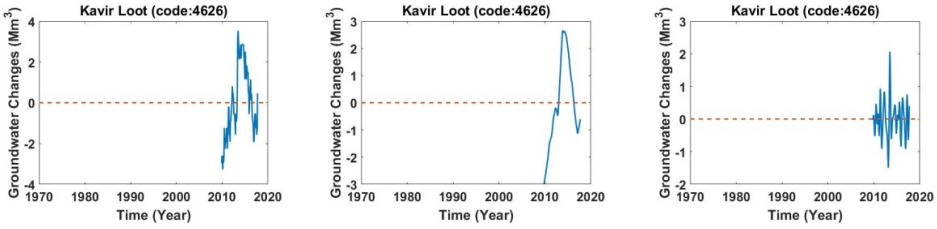

a b c

Figure B.120. a) Monthly values of groundwater storage, b) long-period of monthly values of groundwater storage, c) short-period of monthly values of groundwater storage across study area of Hesarooie (Code: 4626).

B.6.20. Study area of Domak (Code: 4627)

This area is located between 29°8′-29°33′ N and 60°10′-60° 38′ E with an area of 1059.84 km^2. Figure B.121 shows changes in monthly values of groundwater storage inferred from the well data, its long-period and short-period.

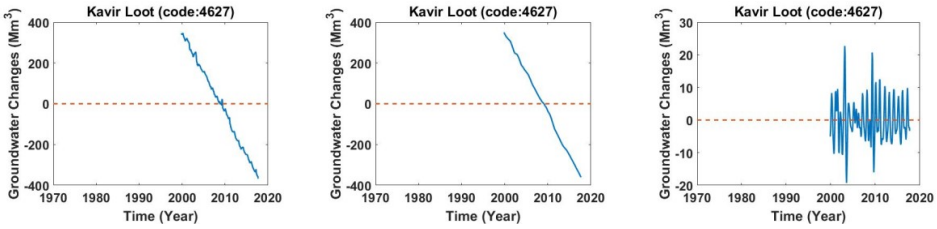

a b c

Figure B.121. a) Monthly values of groundwater storage, b) long-period of monthly values of groundwater storage, c) short-period of monthly values of groundwater storage across study area of Domak (Code: 4627).

B.6.21. Study area of Koorin-Shoro (Code: 4628)

This area is located between 28°42′-29°12′ N and 60°4′-60° 56′ E with an area of 3350.76 km^2. Figure B.122 shows changes in monthly values of groundwater storage inferred from the well data, its long-period and short-period.

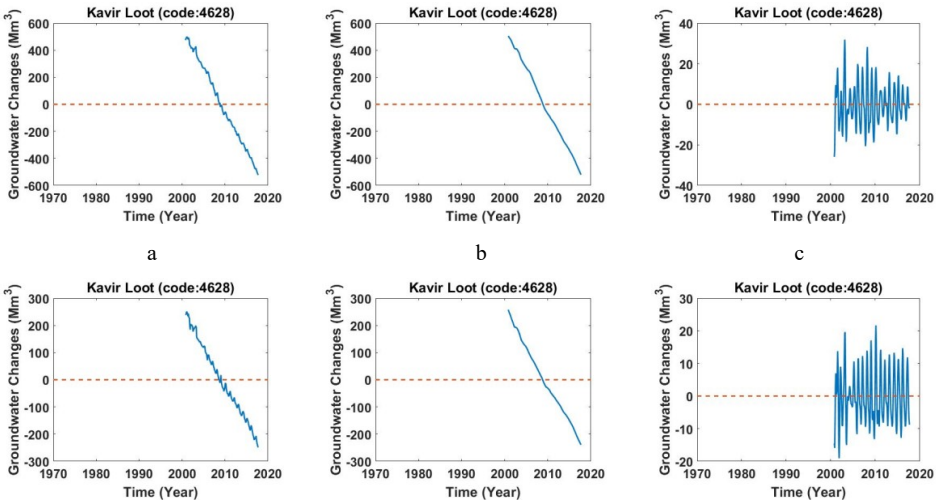

Figure B.122. a,d) Monthly values of groundwater storage, b,e) long-period of monthly values of groundwater storage, c,f) short-period of monthly values of groundwater storage across study area of Koorin-Shoro (Code: 4628).

B.6.22. Study area of Nosratabad (Code: 4630)

This area is located between 29°32′-30°15′ N and 59°30′-60° 18′ E with an area of 3007.56 km^2. Figure B.123 shows changes in monthly values of groundwater storage inferred from the well data, its long-period and short-period.

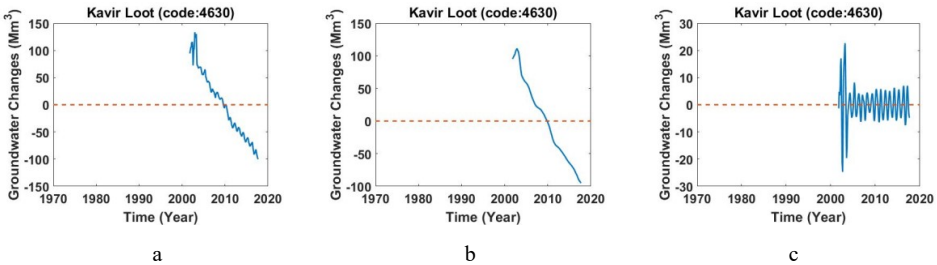

Figure B.123. a) Monthly values of groundwater storage, b) long-period of monthly values of groundwater storage, c) short-period of monthly values of groundwater storage across study area of Nosratabad (Code: 4630).

B.6.23. Study area of Gorgi-Ziarat (Code: 4631)

This area is located between 29°20′-30°46′ N and 60°4′-60° 46′ E with an area of 5199.73 km^2. Figure B.124 shows changes in monthly values of groundwater storage inferred from the well data, its long-period and short-period.

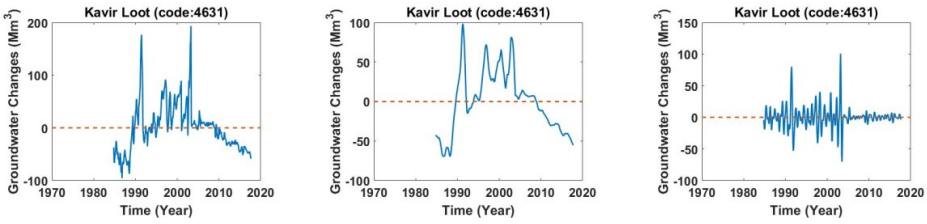

a b c

Figure B.124. a) Monthly values of groundwater storage, b) long-period of monthly values of groundwater storage, c) short-period of monthly values of groundwater storage across study area of Gorgi-Ziarat (Code: 4631).

B.6.24. Study area of Mighan-Dehno (Code: 4632)

This area is located between 30˚4′-32˚5′ N and 59˚8′-60˚ 14′ E with an area of 8148 km^2. Figure B.125 shows changes in monthly values of groundwater storage inferred from the well data, its long-period and short-period.

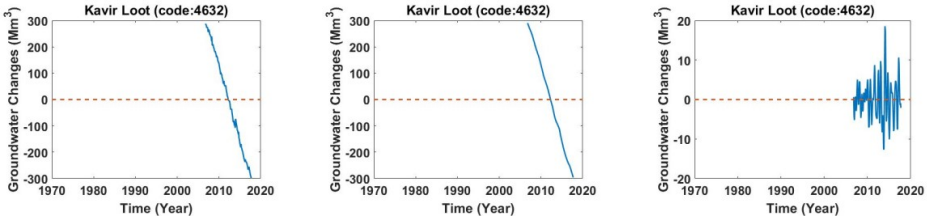

a b c

Figure B.125. a) Monthly values of groundwater storage, b) long-period of monthly values of groundwater storage, c) short-period of monthly values of groundwater storage across study area of Mighan-Dehno (Code: 4632).

B.6.25. Study area of Sahlabad (Code: 4636)

This area is located between 31˚45′-32˚30′ N and 59˚34′-60˚ 14′ E with an area of 2612.4 km^2. Figure B.126 shows changes in monthly values of groundwater storage inferred from the well data, its long-period and short-period.

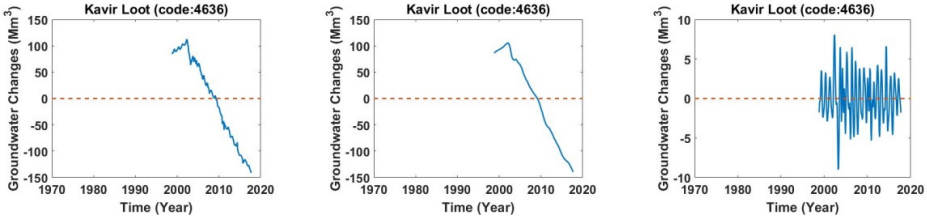

a b c

Figure B.126. a) Monthly values of groundwater storage, b) long-period of monthly values of groundwater storage, c) short-period of monthly values of groundwater storage across study area of Sahlabad (Code: 4636).

B.7.1. Study area of Sorkhe (Code: 4703)

This area is located between 35°30′-35°05′ N and 53°-53°40′ E with 1615.6 km^2. Figure B.127 shows changes in monthly values of groundwater storage inferred from the well data, its long-period and short-period.

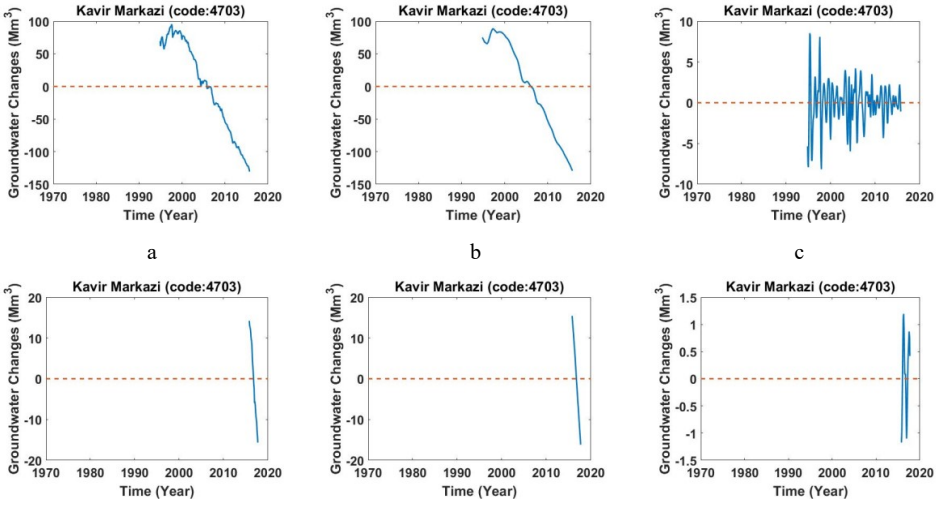

Figure B.127. a,d) Monthly values of groundwater storage, b,e) long-period of monthly values of groundwater storage, c,f) short-period of monthly values of groundwater storage across study area of Sorkhe (Code: 4703).

B.7.2. Study area of Semnan (Code: 4704)

This area is located between 35°-35°40′ N and 53°20′-54 E with an area of 2150.9 km^2. Figure B.128 shows changes in monthly values of groundwater storage inferred from the well data, its long-period and short-period.

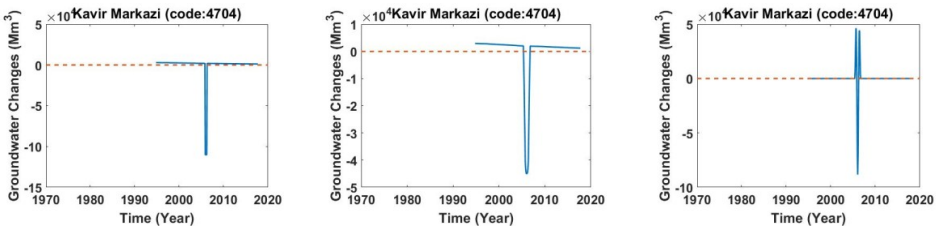

Figure B.128. a) Monthly values of groundwater storage, b) long-period of monthly values of groundwater storage, c) short-period of monthly values of groundwater storage across study area of Semnan (Code: 4704).

B.7.3. Study area of Garmsar (Code: 4705)

This area is located between 34°45′-35°40′ N and 52°34′-53° 14′ E with an area of 5532.1 km^2. Figure B.129 shows changes in monthly values of groundwater storage inferred from the well data, its long-period and short-period.

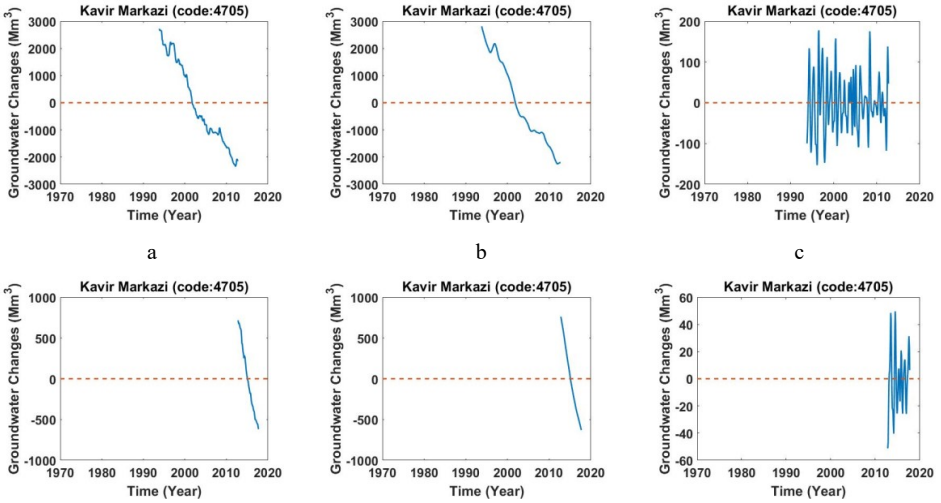

Figure B.129. a,d) Monthly values of groundwater storage, b,e) long-period of monthly values of groundwater storage, c,f) short-period of monthly values of groundwater storage across study area of Garmsar (Code: 4705).

B.7.4. Study area of Firoozkoh (Code: 4706)

This area is located between 35°30′-35°40′ N and 52°30′-53°15′ E with an area of 1651.4 km^2. Figure B.130 shows changes in monthly values of groundwater storage inferred from the well data, its long-period and short-period.

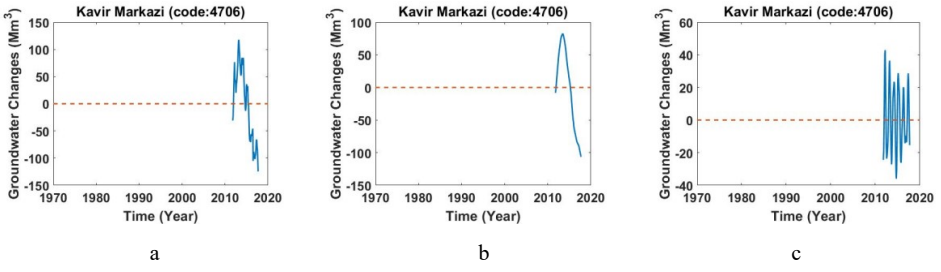

Figure B.130. a) Monthly values of groundwater storage, b) long-period of monthly values of groundwater storage, c) short-period of monthly values of groundwater storage across study area of Firoozkoh (Code: 4706).

B.7.5. Study area of Mobarakie (Code: 4707)

This area is located between 34°20′-35°10′ N and 51°50′-52°45′ E with an area of 3029.7 km^2. Figure B.131 shows changes in monthly values of groundwater storage inferred from the well data, its long-period and short-period.

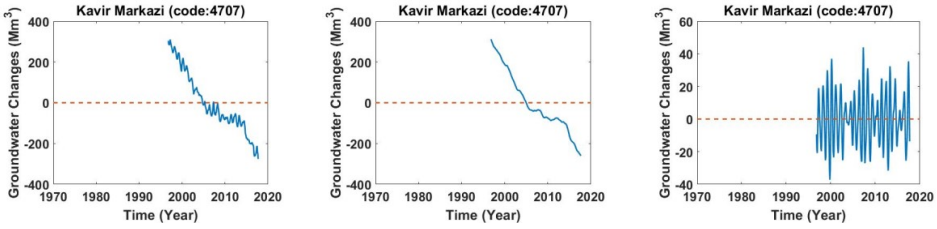

a b c

Figure B.131. a) Monthly values of groundwater storage, b) long-period of monthly values of groundwater storage, c) short-period of monthly values of groundwater storage across study area of Mobarakie (Code: 4707).

B.7.6. Study area of Ivanaki (Code: 4708)

This area is located between 35°10′-35° N and 52°-52°40′ E with 935.2 km^2. Figure B.132 shows changes in monthly values of groundwater storage inferred from the well data, its long-period and short-period.

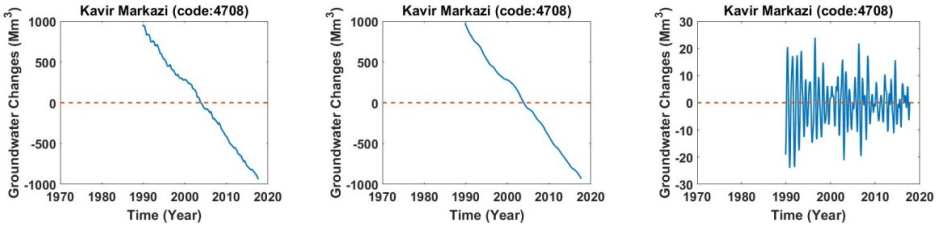

a b c

Figure B.132. a) Monthly values of groundwater storage, b) long-period of monthly values of groundwater storage, c) short-period of monthly values of groundwater storage across study area of Ivanaki (Code: 4708).

B.7.7. Study area of Hoomand Absard (Code: 4709)

This area is located between 35°20′-35°40′ N and 52°15′-53°30′ E with an area of 566.7 km^2. Figure B.133 shows changes in monthly values of groundwater storage inferred from the well data, its long-period and short-period.

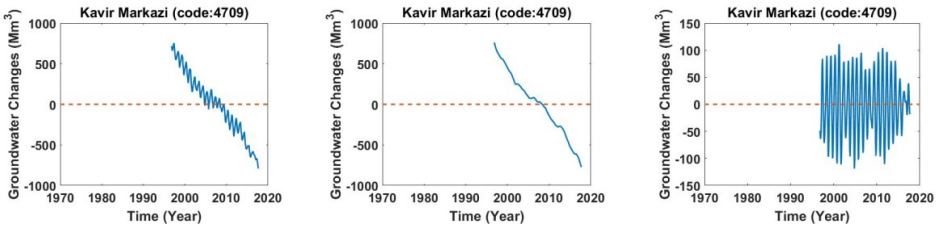

a b c

Figure B.133. a) Monthly values of groundwater storage, b) long-period of monthly values of groundwater storage, c) short-period of monthly values of groundwater storage across study area of Hoomand Absard (Code: 4709).

B.7.8. Study area of Choopanan (Code: 4710)

This area is located between 33˚10′-34˚30′ N and 52˚10′-54˚55′ E with an area of 18128.5 km^2. Figure B.134 shows changes in monthly values of groundwater storage inferred from the well data, its long-period and short-period.

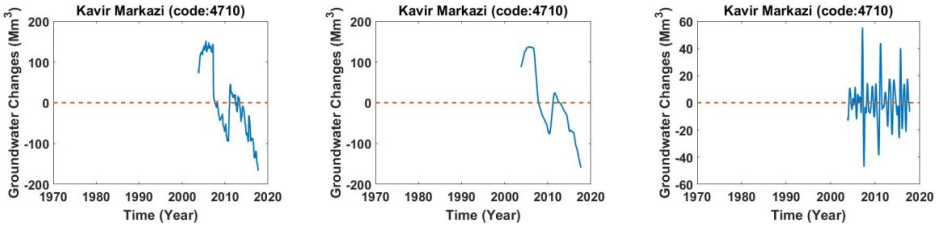

a b c

Figure B.134. a) Monthly values of groundwater storage, b) long-period of monthly values of groundwater storage, c) short-period of monthly values of groundwater storage across study area of Choopanan (Code: 4710).

B.7.9. Study area of Jandagh (Code: 4711)

This area is located between 33˚50′-34˚25′ N and 54˚20′-55˚20′ E with an area of 3830.3 km^2. This area divided to East Jandagh and west Jandagh. Figure B.135 shows changes in monthly values of groundwater storage inferred from the well data, its long-period and short-period.

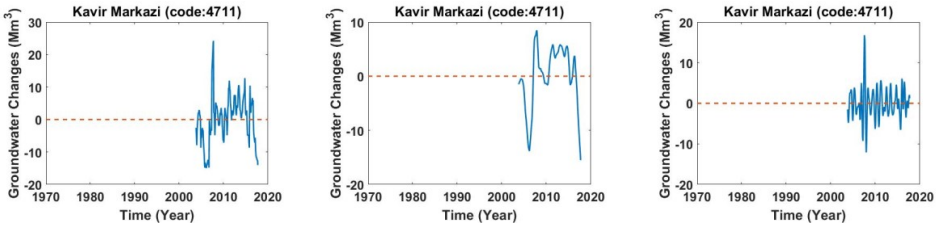

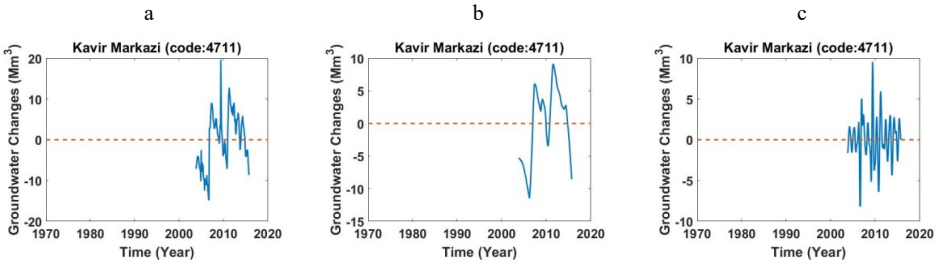

Figure B.135. a,d) Monthly values of groundwater storage, b,e) long-period of monthly values of groundwater storage, c,f) short-period of monthly values of groundwater storage across study area of Jandagh (Code: 4711).

B.7.10. Study area of Khor-Farkhi (Code: 4712)

This area is located between 33°30′-34° N and 54°15′-55°30′ E with an area of 1976.2 km^2. Figure B.136 shows changes in monthly values of groundwater storage inferred from the well data, its long-period and short-period.

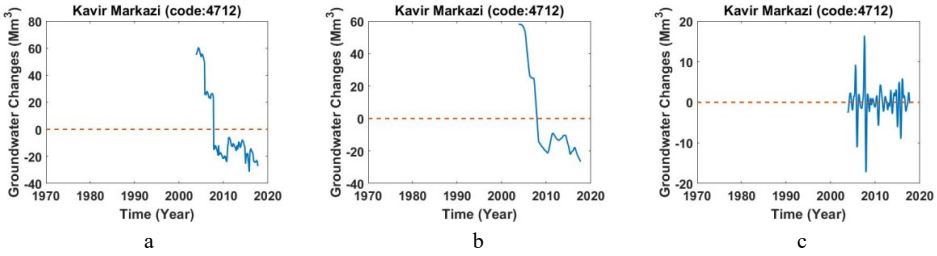

Figure B.136. a) Monthly values of groundwater storage, b) long-period of monthly values of groundwater storage, c) short-period of monthly values of groundwater storage across study area of Khor-Farkhi (Code: 4712).

B.7.11. Study area of Bayaze (Code: 4713)

This area is located between 32°47′-33°32′ N and 54°47′-55°50′ E with an area of 5204 km^2. Figure B.137 shows changes in monthly values of groundwater storage inferred from the well data, its long-period and short-period.

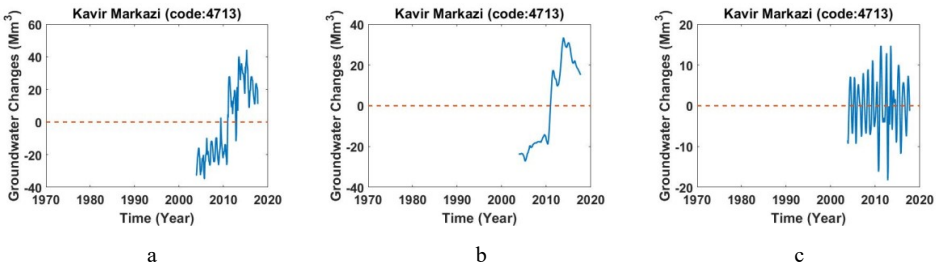

Figure B.137. a) Monthly values of groundwater storage, b) long-period of monthly values of groundwater storage, c) short-period of monthly values of groundwater storage across study area of Bayaze (Code: 4713).

B.7.12. Study area of Halvan-Robatkhan (Code: 47114)

This area is located between 33°-34°20′ N and 55°35′-56°35′ E with an area of 6786.7 km^2. Figure B.138 shows changes in monthly values of groundwater storage inferred from the well data, its long-period and short-period.

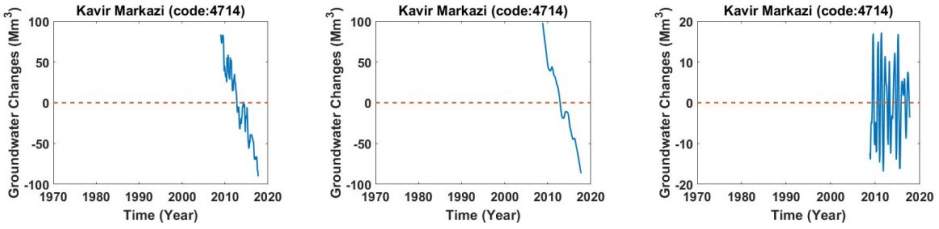

a b c

Figure B.138. a) Monthly values of groundwater storage, b) long-period of monthly values of groundwater storage, c) short-period of monthly values of groundwater storage across study area of Halvan-Robatkhan (Code: 4714).

B.7.13. Study area of Dastgardan (Code: 4715)

This area is located between 33°45′-34°40′ N and 56°15′-57°15′ E with an area of 5842.7 km^2. Figure B.139 shows changes in monthly values of groundwater storage inferred from the well data, its long-period and short-period.

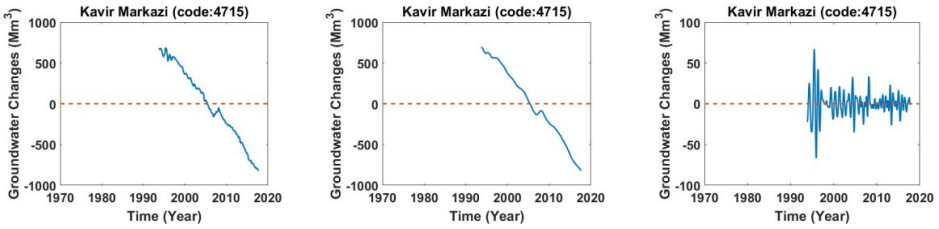

a b c

Figure B.139. a) Monthly values of groundwater storage, b) long-period of monthly values of groundwater storage, c) short-period of monthly values of groundwater storage across study area of Dastgardan (Code: 4715).

B.7.14. Study area of Daroone (Code: 4716)

This area is located between 34°40′-35°32′ N and 56°45′-57°50′ E with an area of 5811.7 km^2. Figure B.140 shows changes in monthly values of groundwater storage inferred from the well data, its long-period and short-period.

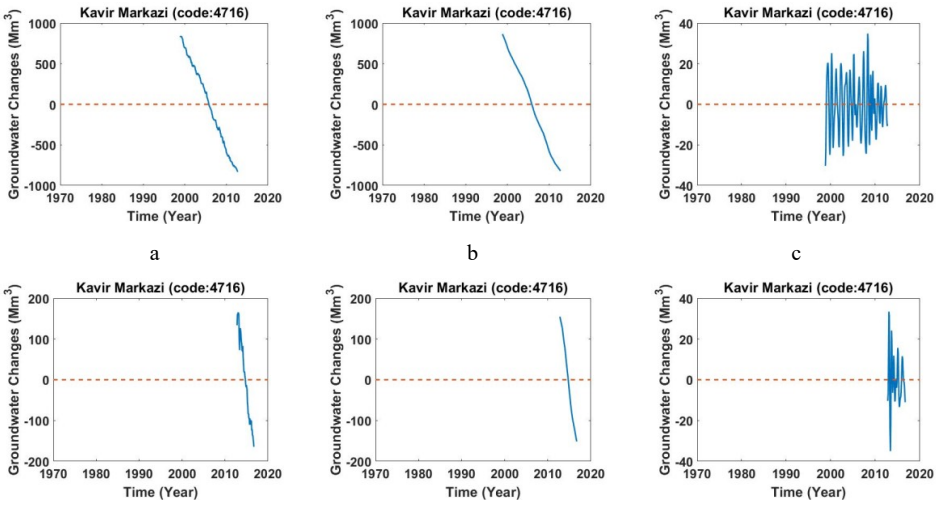

Figure B.140. a) Monthly values of groundwater storage, b) long-period of monthly values of groundwater storage, c) short-period of monthly values of groundwater storage across study area of Danroone (Code: 4716).

B.7.15. Study area of Bardsekan (Code: 4717)

This area is located between 34°50′-35°20′ N and 57°30′-58°10′ E with an area of 2592.5 km^2. Figure B.141 shows changes in monthly values of groundwater storage inferred from the well data, its long-period and short-period.

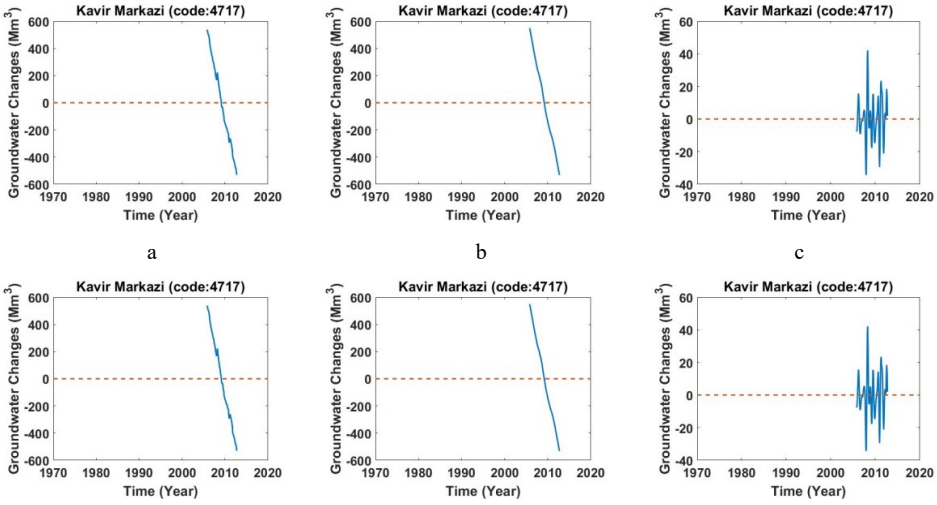

Figure B.141. a,d) Monthly values of groundwater storage, b,e) long-period of monthly values of groundwater storage, c,f) short-period of monthly values of groundwater storage across study area of Bardsekan (Code: 4717).

B.7.16. Study area of Ferdos (Code: 4719)

This area is located between 33°50′-34°15′ N and 57°25′-58°25′ E with an area of 2848.2 km^2. This area is divided to east Ferdos and west Ferdos. Figure B.142 shows changes in monthly values of groundwater storage inferred from the well data, its long-period and short-period.

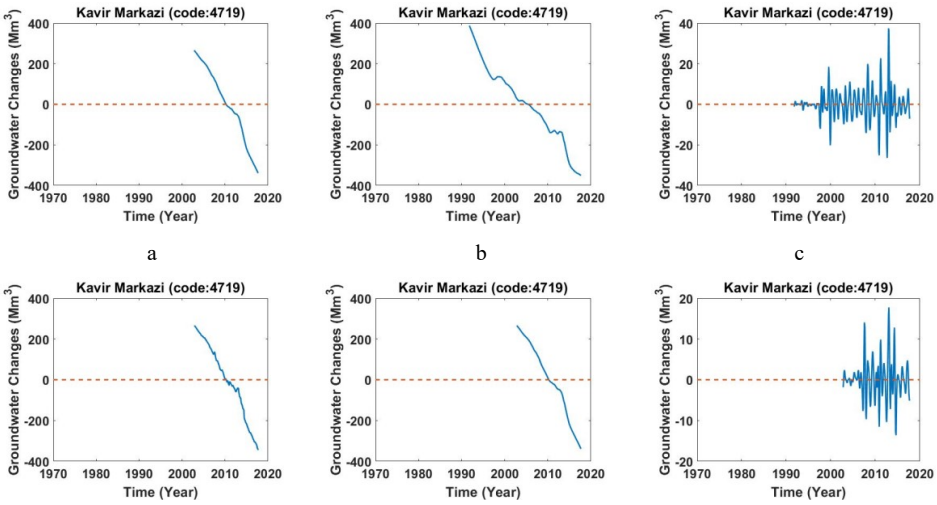

Figure B.142. a,d) Monthly values of groundwater storage, b,e) long-period of monthly values of groundwater storage, c,f) short-period of monthly values of groundwater storage across study area of Ferdos (Code: 4719).

B.7.17. Study area of Bashrooie (Code: 4720)

This area is located between 33°20′-34°20′ N and 57°-58°10′ E with an area of 6427.1 km^2. Figure B.143 shows changes in monthly values of groundwater storage inferred from the well data, its long-period and short-period.

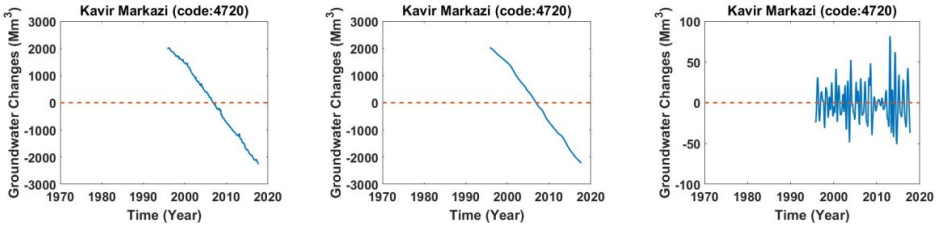

Figure B.143 a) Monthly values of groundwater storage, b) long-period of monthly values of groundwater storage, c) short-period of monthly values of groundwater storage across study area of Bashrooie (Code: 4720).

B.7.18. Study area of Bajestan-Jonesi (Code: 4721)

This area is located between 34°10′-34°45′ N and 57°30′-58°20′ E with an area of 4121.1 km^2. Figure B.144 shows changes in monthly values of groundwater storage inferred from the well data, its long-period and short-period.

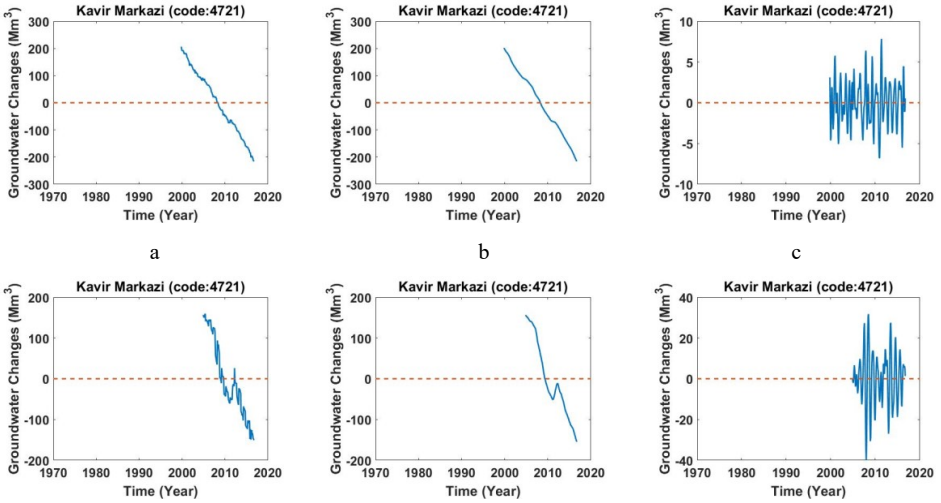

Figure B.144. a,d) Monthly values of groundwater storage, b,e) long-period of monthly values of groundwater storage, c,f) short-period of monthly values of groundwater storage across study area of Bajestan-Jonesi (Code: 4721).

B.7.19. Study area of Mohavalat (Code: 4722)

This area is located between 34°30′-34°50′ N and 58°5′-58°50′ E with an area of 1956.8 km^2. Figure B.145 shows changes in monthly values of groundwater storage inferred from the well data, its long-period and short-period.

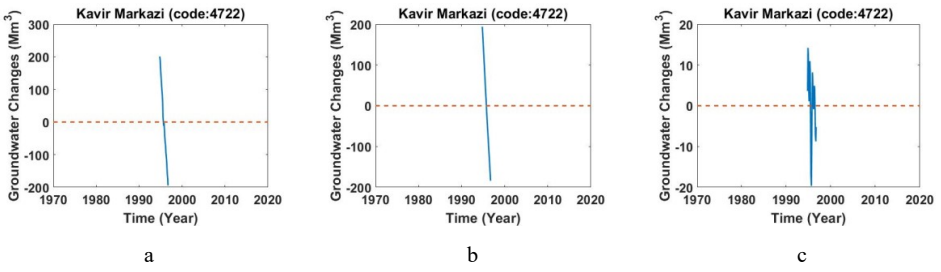

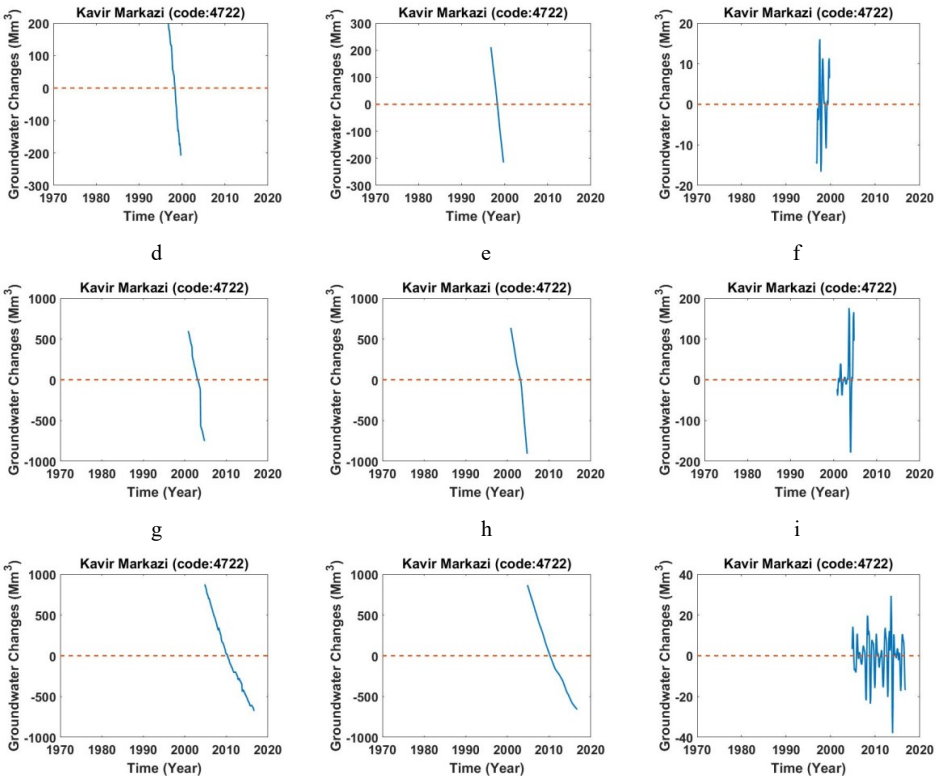

Figure B.145. a,d,g,j) Monthly values of groundwater storage, b,e,h,k) long-period of monthly values of groundwater storage, c,f,i,l) short-period of monthly values of groundwater storage across study area of Mohavalat (Code: 4722).

B.7.20. Study area of Arghand (Code: 4723)

This area is located between 34˚50′-35˚20′ N and 58˚25′-59˚ E with an area of 1953.6 km^2. Figure B.146 shows changes in monthly values of groundwater storage inferred from the well data, its long-period and short-period.

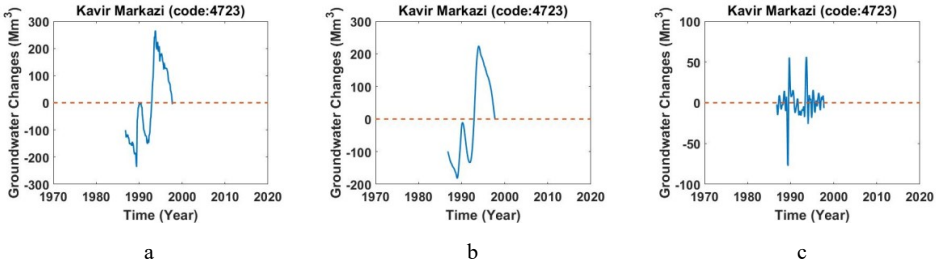

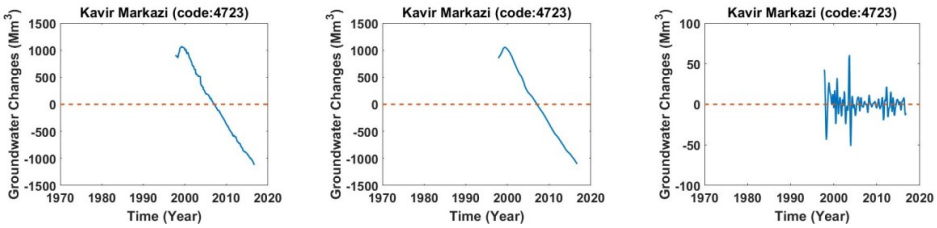

Figure B.146. a,d) Monthly values of groundwater storage, b,e) long-period of monthly values of groundwater storage, c,f) short-period of monthly values of groundwater storage across study area of Arghand (Code: 4723).

B.7.21. Study area of Bimorgh-Omrani (Code: 4724)

This area is located between 34°10′-34°55′ N and 58°15′-59°10′ E with an area of 3249.4 km^2. This area is divided to west and east. Figure B.147 shows changes in monthly values of groundwater storage inferred from the well data, its long-period and short-period.

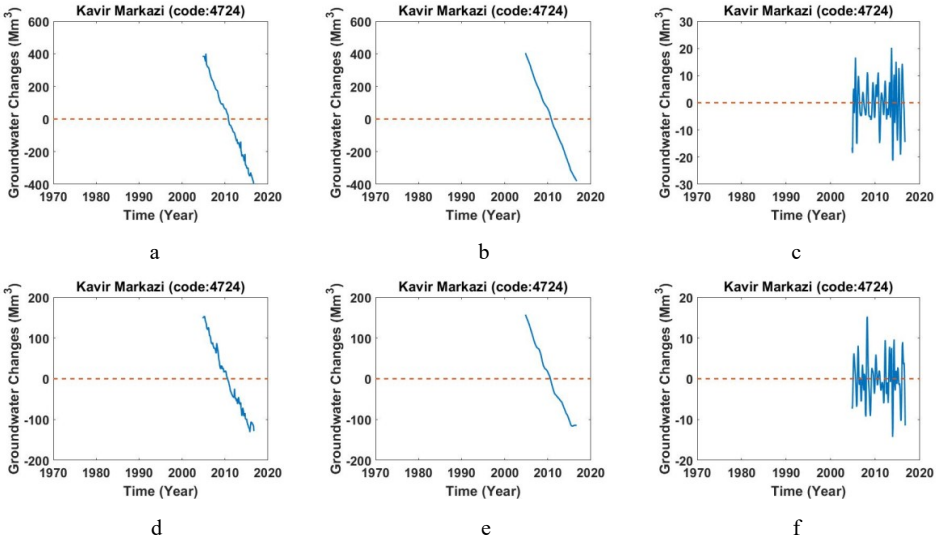

Figure B.147. a,d) Monthly values of groundwater storage, b,e) long-period of monthly values of groundwater storage, c,f) short-period of monthly values of groundwater storage across study area of Bimorgh-Omrani (Code: 4724).

B.7.22. Study area of Gonabad (Code: 4725)

This area is located between 33°50′-34°20′ N and 58°22′-59° E with an area of 1805.9 km^2. Figure B.148 shows changes in monthly values of groundwater storage inferred from the well data, its long-period and short-period.

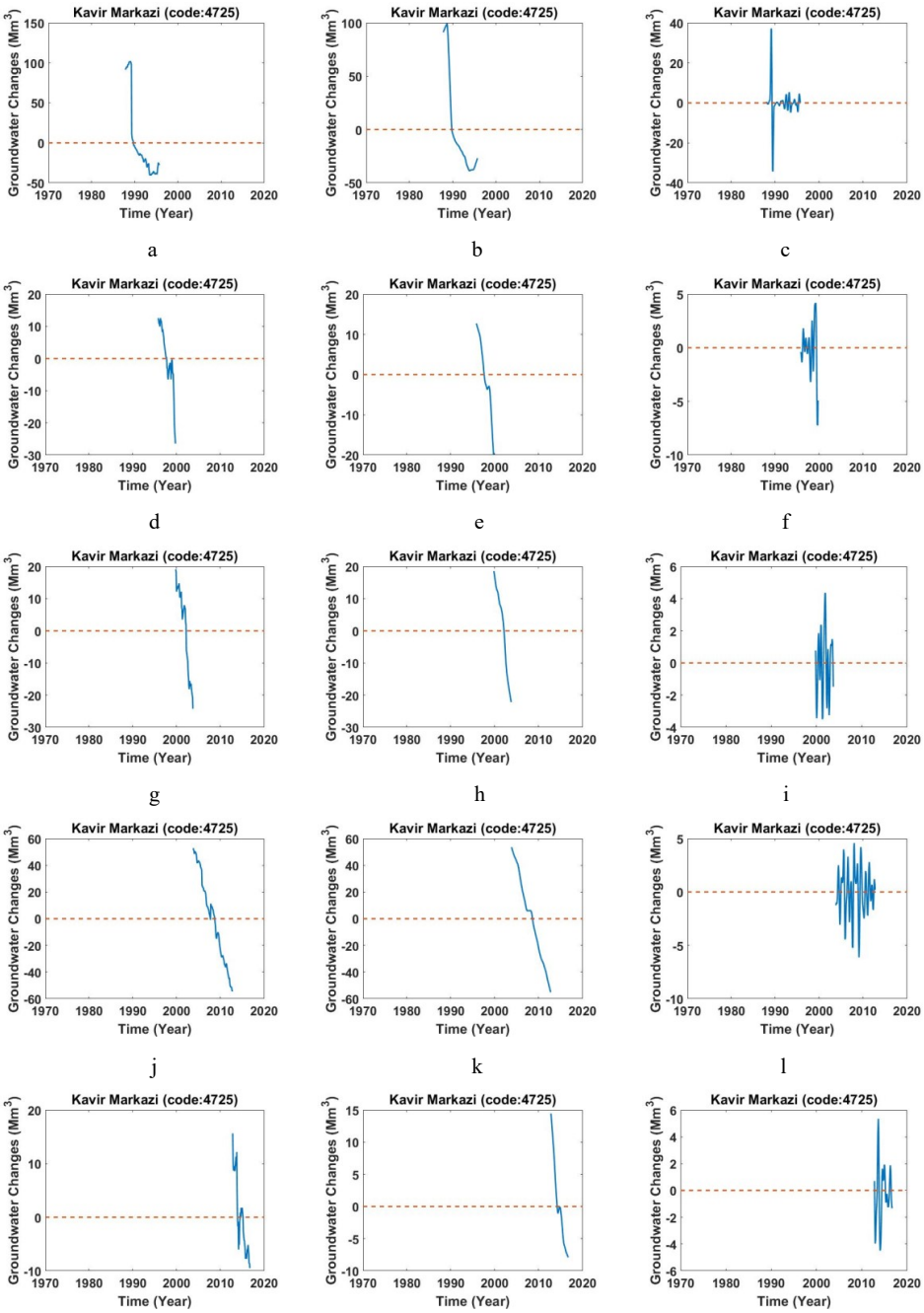

Figure B.148. a,d,g,j,m) Monthly values of groundwater storage, b,e,h,k,n) long-period of monthly values of groundwater storage, c,f,i,l,o) short-period of monthly values of groundwater storage across study area of Gonabad (Code: 4725).

B.7.23. Study area of Jangal (Code: 4726)

This area is located between 34°20′-34°50′ N and 58°48′-59°20′ E with 1295.5 km^2. Figure B.149 shows changes in monthly values of groundwater storage inferred from the well data, its long-period and short-period.

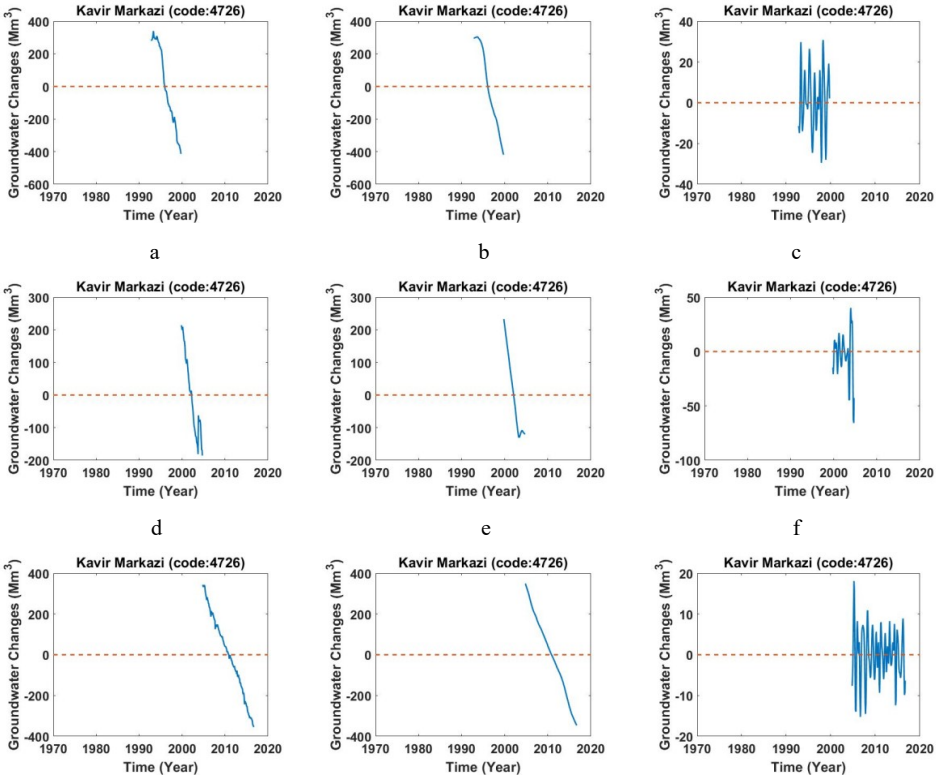

Figure B.149. a,d,g) Monthly values of groundwater storage, b,e,h) long-period of monthly values of groundwater storage, c,f,i) short-period of monthly values of groundwater storage across study area of Jangal (Code: 4726).

B.7.24. Study area of Rashtkhar (Code: 4727)

This area is located between 34°35′-35°10′ N and 59°-59°50′ E with an area of 2343.9 km^2. Figure B.150 shows changes in monthly values of groundwater storage inferred from the well data, its long-period and short-period.

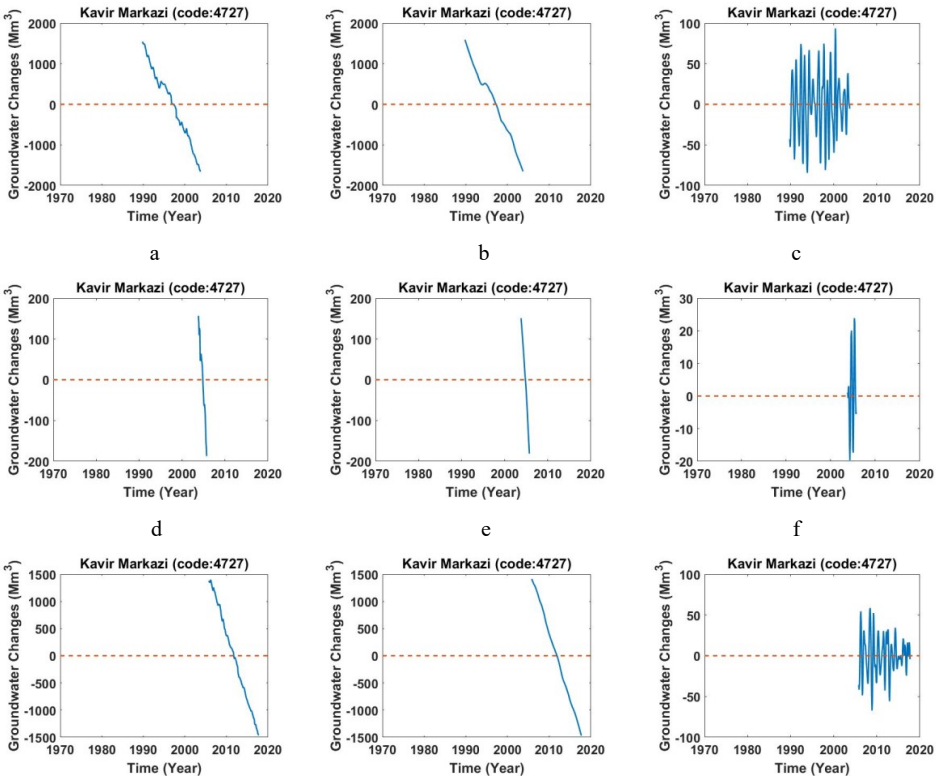

Figure B.150. a,d,g) Monthly values of groundwater storage, b,e,h) long-period of monthly values of groundwater storage, c,f,i) short-period of monthly values of groundwater storage across study area of Rashtkhar (Code: 4727).

B.7.25. Study area of Torbat-Heidarie (Code: 4728)

This area is located between 34°55′-35°20′ N and 59°-59°50′ E with an area of 2502.6 km^2. Figure B.151 shows changes in monthly values of groundwater storage inferred from the well data, its long-period and short-period.

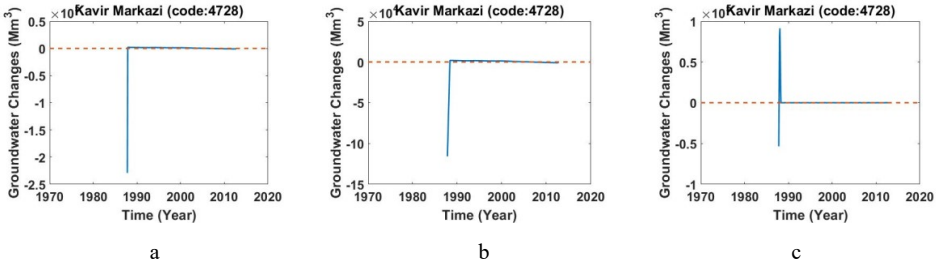

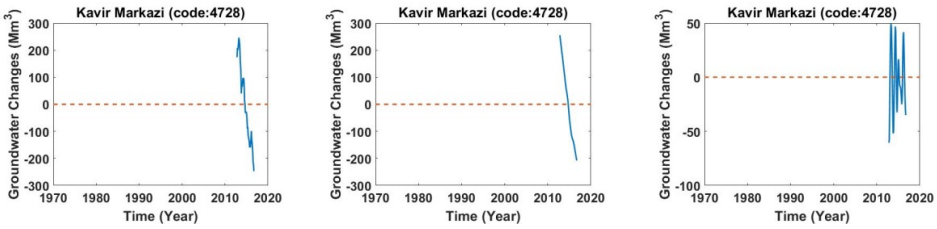

Figure B.151. a,d) Monthly values of groundwater storage, b,e) long-period of monthly values of groundwater storage, c,f) short-period of monthly values of groundwater storage across study area of Torbat-Heidarie (Code: 4728).

B.7.26. Study area of Kashmar (Code: 4729)

This area is located between 34°40′-35°15′ N and 57° 50′-58°35′ E with an area of 1936.2 km^2. Figure B.152, B.153 shows changes in monthly values of groundwater storage inferred from the well data, its long-period and short-period.

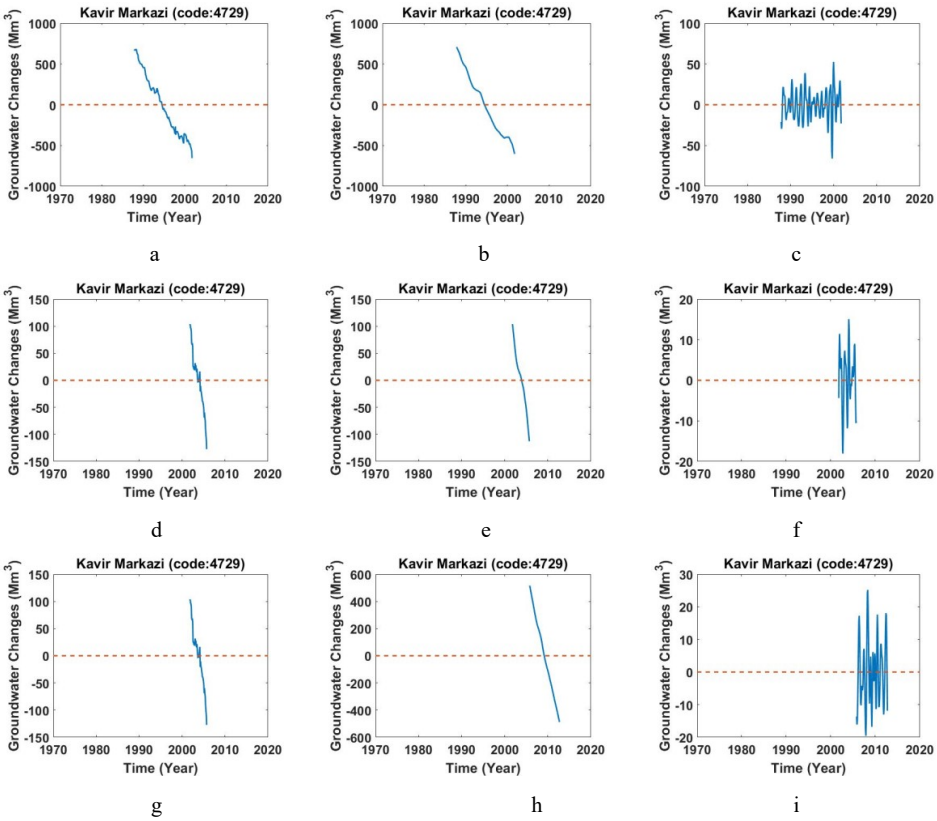

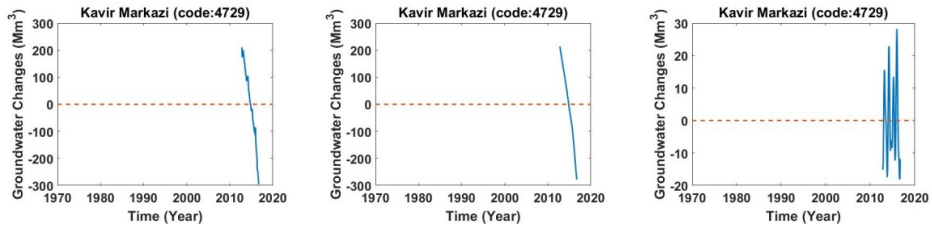

j k l

Figure B.152 a,d,g,j) Monthly values of groundwater storage, b,e,h,k) long-period of monthly values of groundwater storage, c,f,i,l) short-period of monthly values of groundwater storage across study area of Kashmar (Code: 4729).

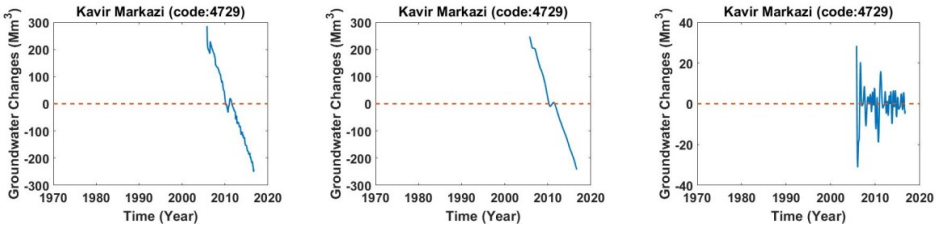

a b c

Figure B.153 a) Monthly values of groundwater storage, b) long-period of monthly values of groundwater storage, c) short-period of monthly values of groundwater storage across study area of Sadodin in Kashmar (Code: 4729).

B.7.27. Study area of riosh (Code: 4730)

This area is located between 35˚15′-35˚28′ N and 58° 8′-58˚35′ E with an area of 622 km^2. Figure B.154 shows changes in monthly values of groundwater storage inferred from the well data, its long-period and short-period.

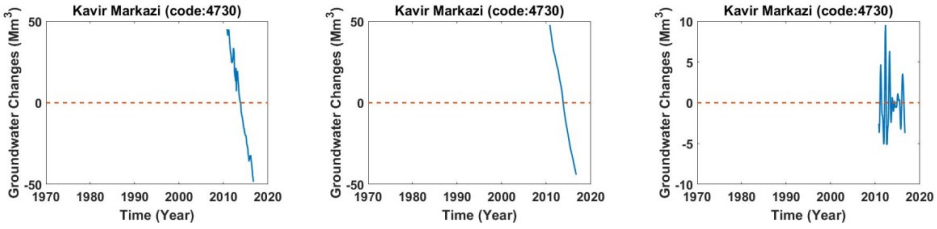

a b c

Figure B.154. a) Monthly values of groundwater storage, b) long-period of monthly values of groundwater storage, c) short-period of monthly values of groundwater storage across study area of Roish (Code: 4730).

B.7.28. Study area of Biararjmand (Code: 4732)

This area is located between 35°45′-36°12′ N and 55°31-56°28′ E with an area of 2763 km^2. Figure B.155 shows changes in monthly values of groundwater storage inferred from the well data, its long-period and short-period.

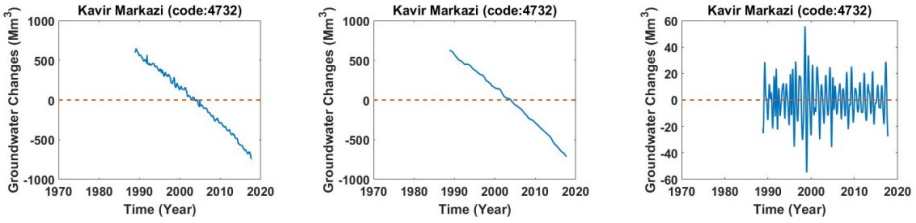

a b c

Figure B.155. a) Monthly values of groundwater storage, b) long-period of monthly values of groundwater storage, c) short-period of monthly values of groundwater storage across study area of Biararjmand (Code: 4732).

B.7.29. Study area of Khartooran (Code: 4733)

This area is located between 35°17′-36° N and 56°31-57°20′ E with an area of 3436.6 km^2. Figure B.156 shows changes in monthly values of groundwater storage inferred from the well data, its long-period and short-period.

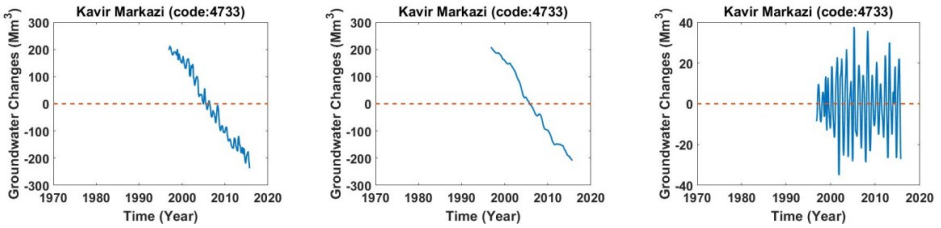

a b c

Figure B.156. a) Monthly values of groundwater storage, b) long-period of monthly values of groundwater storage, c) short-period of monthly values of groundwater storage across study area of Khartooran (Code: 4733).

B.7.30. Study area of Davarzan-Fromad (Code: 4734)

This area is located between 35°40′-36° 30′N and 56°10-57°15′ E with 5175.1 km^2. Figure B.157 shows changes in monthly values of groundwater storage inferred from the well data, its long-period and short-period.

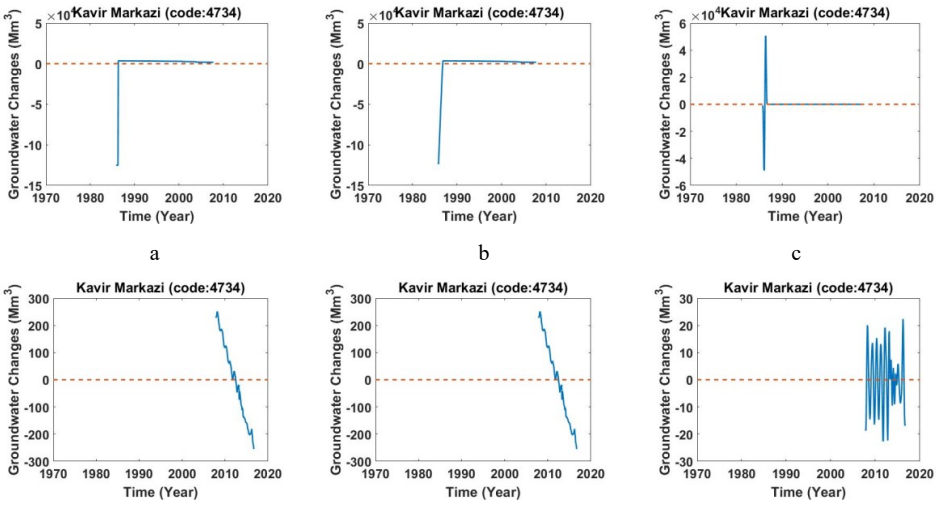

Figure B.157. a,d) Monthly values of groundwater storage, b,e) long-period of monthly values of groundwater storage, c,f) short-period of monthly values of groundwater storage across study area of Davarzan-Fromad (Code: 4734).

B.7.31. Study area of Sabzevar (Code: 4735)

This area is located between 35˚30′-36˚20′ N and 57-58˚ E with an area of 5572.8 km^2. Figure B.158 shows changes in monthly values of groundwater storage inferred from the well data, its long-period and short-period.

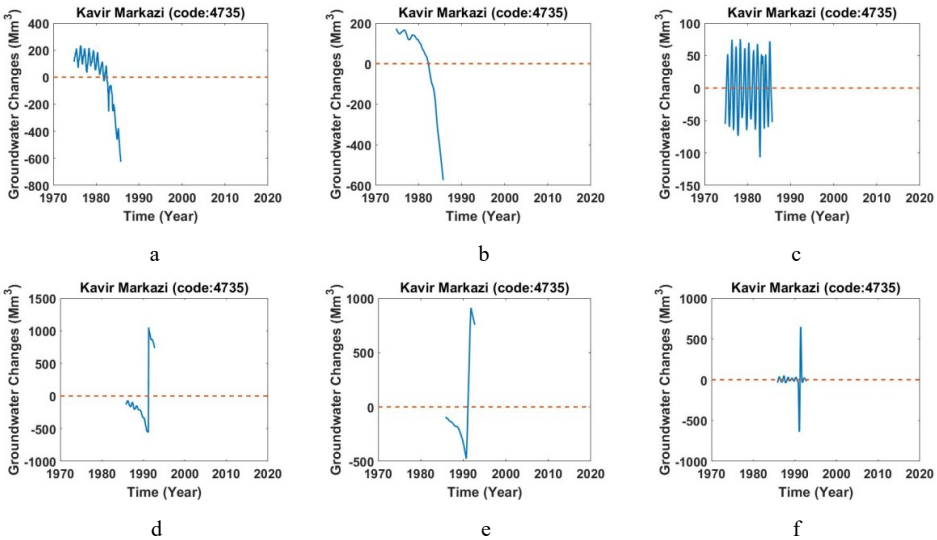

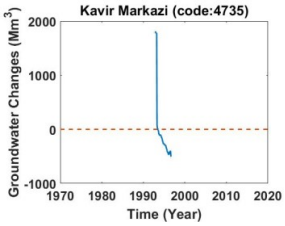

g

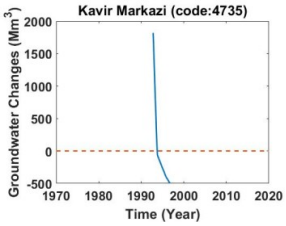

h

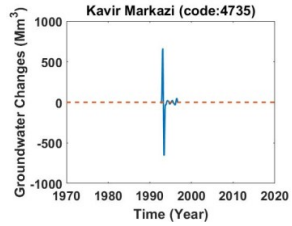

i

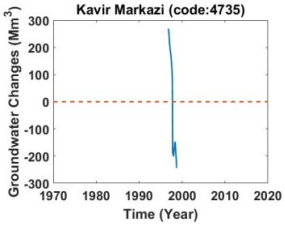

j

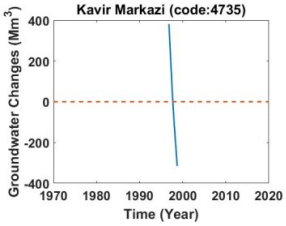

k

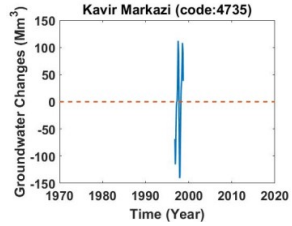

l

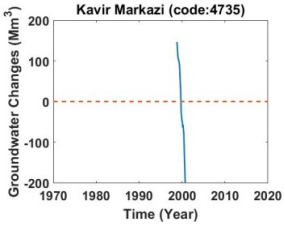

m

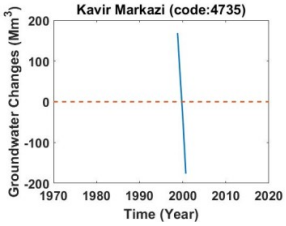

n

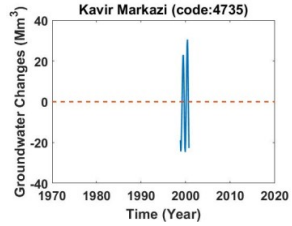

o

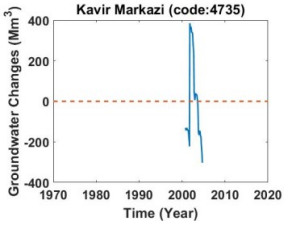

p

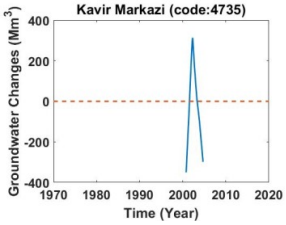

q

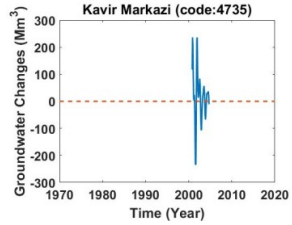

r

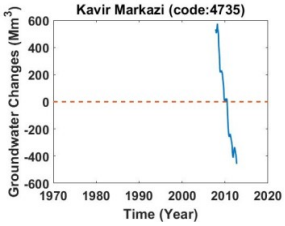

s

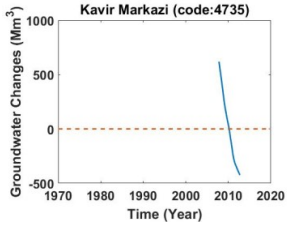

t

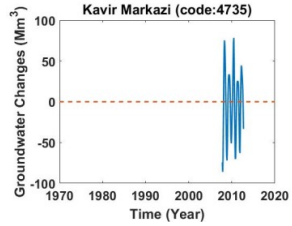

u

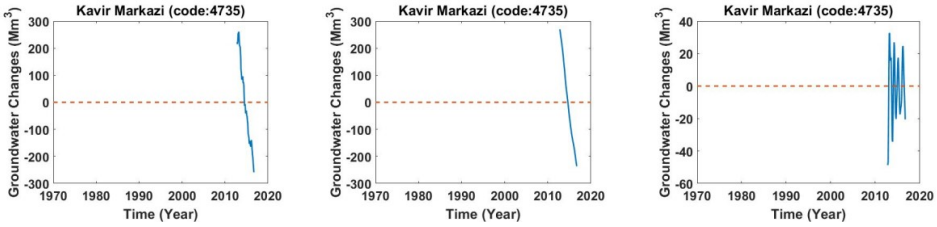

Figure B.158. a,d,g,j,m,p,s,v) Monthly values of groundwater storage, b,e,h,k,n,q,t,w) long-period of monthly values of groundwater storage, c,f,i,l,o,r,u,x) short-period of monthly values of groundwater storage across study area of Sabzevar (Code: 4735).

B.7.32. Study area of Ataieh (Code: 4736)

This area is located between 35°20′-36° 12′N and 57°42-58°40′ E with an area of 3052.9 km^2. Figure B.159 shows changes in monthly values of groundwater storage inferred from the well data, its long-period and short-period.

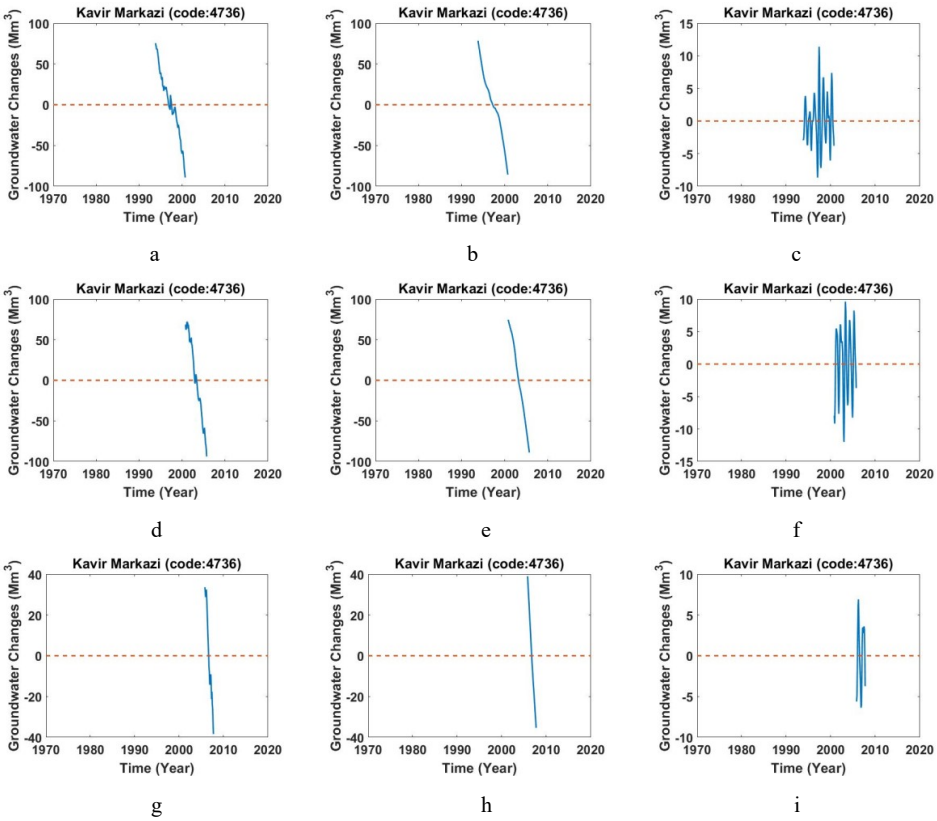

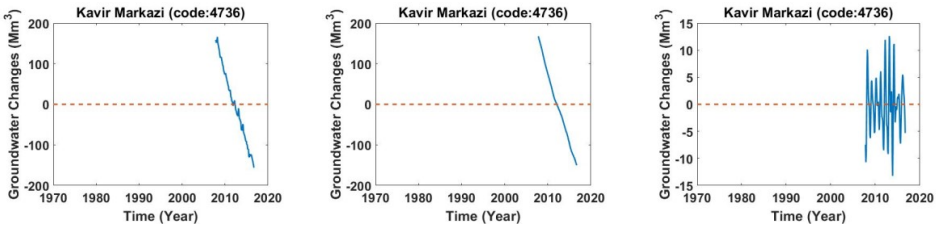

Figure B.159. a,d,g,j) Monthly values of groundwater storage, b,e,h,k) long-period of monthly values of groundwater storage, c,f,i,l) short-period of monthly values of groundwater storage across study area of Ataieh (Code: 4736).

B.7.33. Study area of Neishaboor (Code: 4738)

This area is located between 35°30′-36° 28′N and 58°12′-59°30′ E with an area of 7387.6 km^2. Figure B.160 shows changes in monthly values of groundwater storage inferred from the well data, its long-period and short-period.

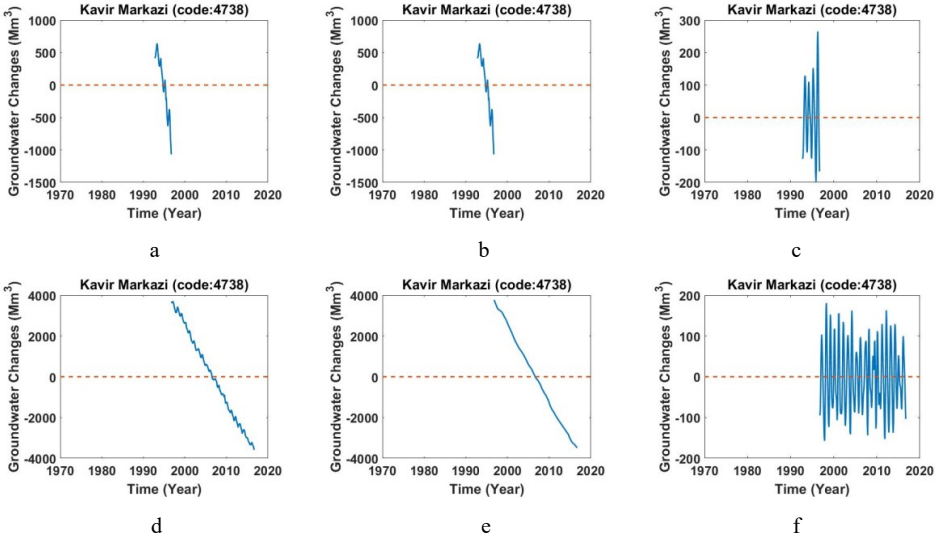

Figure B.160. a,d) Monthly values of groundwater storage, b,e) long-period of monthly values of groundwater storage, c,f) short-period of monthly values of groundwater storage across study area of Neishaboor (Code: 4738).

B.7.34. Study area of Dasht-Rokh (Code: 4739)

This area is located between 34°12′-35° 18′N and 57°55′-58°28′ E with an area of 2061.8 km^2. Figure B.161 shows changes in monthly values of groundwater storage inferred from the well data, its long-period and short-period.

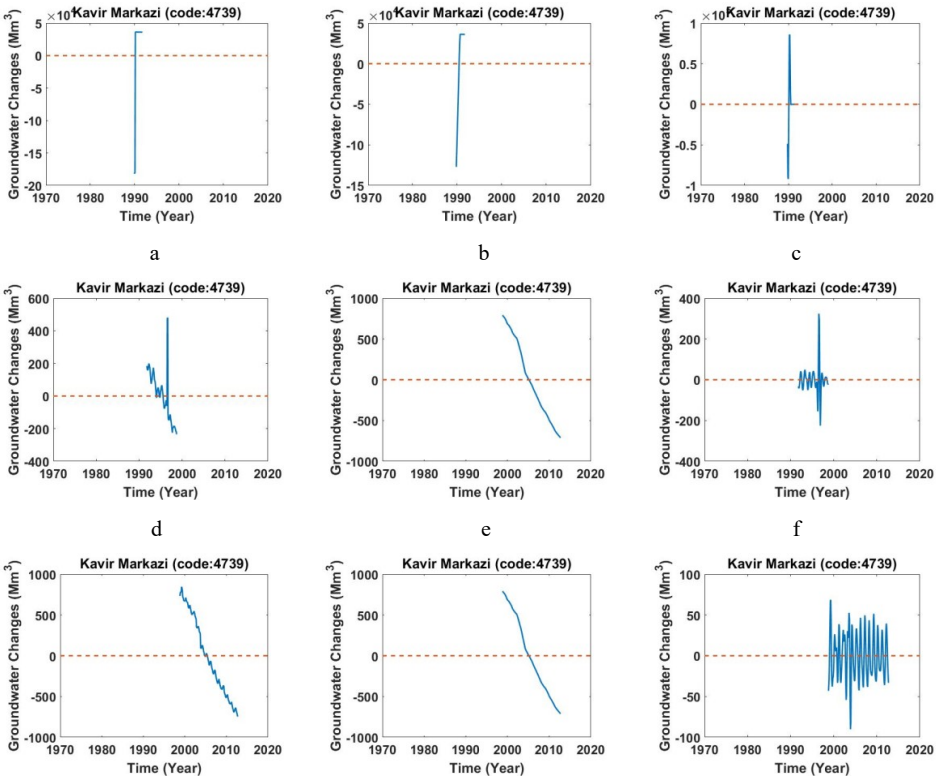

Figure B.161. a,d,g) Monthly values of groundwater storage, b,e,h) long-period of monthly values of groundwater storage, c,f,i) short-period of monthly values of groundwater storage across study area of Dasht-Rokh (Code: 4739).

B.7.35. Study area of Jovin (Code: 4740)

This area is located between 36˚12′-36˚ 40′N and 56˚25′-58˚22′ E with an area of 5687 km^2. Figure B.162 shows changes in monthly values of groundwater storage inferred from the well data, its long-period and short-period.

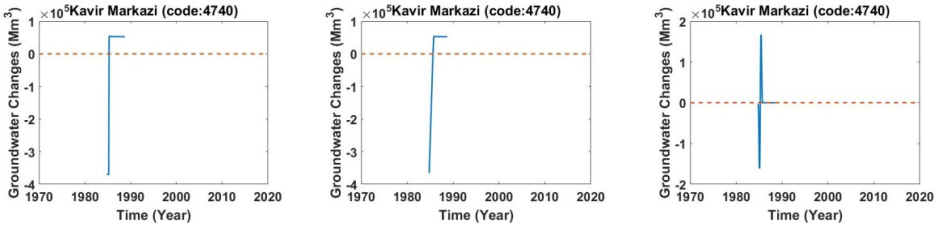

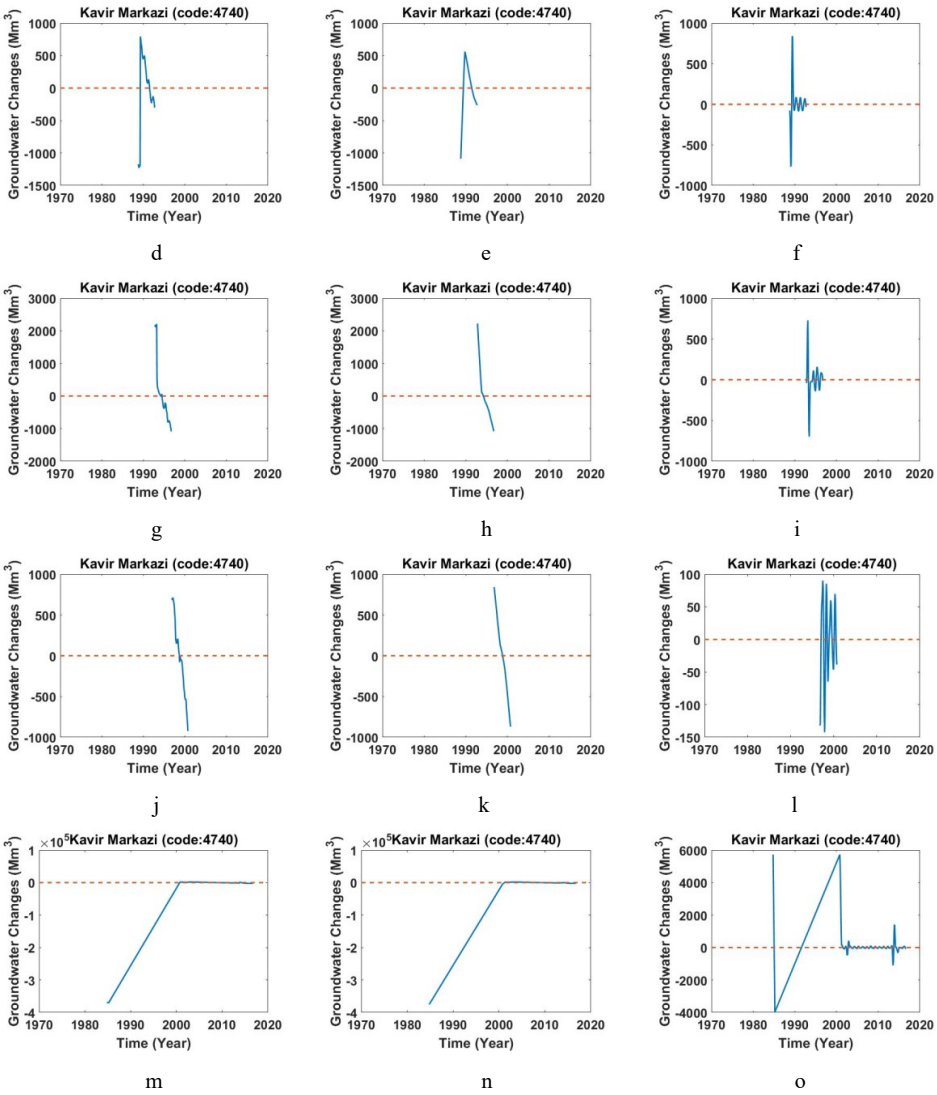

Figure B.162. a,d,g,j,m) Monthly values of groundwater storage, b,e,h,k,n) long-period of monthly values of groundwater storage, c,f,i,l,o) short-period of monthly values of groundwater storage across study area of Jovin (Code: 4740).

B.7.36. Study area of Yengaje (Code: 4741)

This area is located between 36˚20′-36˚ 45′N and 58˚-58˚35′ E with an area of 1507.3 km^2. Figure B.163 shows changes in monthly values of groundwater storage inferred from the well data, its long-period and short-period.

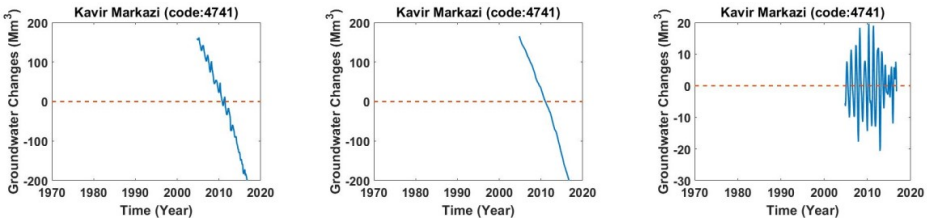

Figure B.163. a) Monthly values of groundwater storage, b) long-period of monthly values of groundwater storage, c) short-period of monthly values of groundwater storage across study area of Yengaje (Code: 4741).

B.7.37. Study area of Jajarm (Code: 4742)

This area is located between 36°32′-37° 5′N and 55°45′-56°35′ E with an area of 2489.6 km^2. Figure B.164 shows changes in monthly values of groundwater storage inferred from the well data, its long-period and short-period.

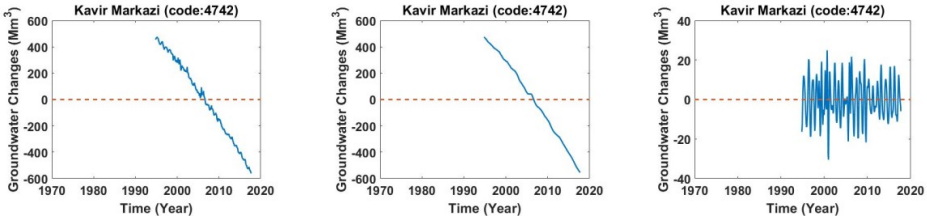

Figure B.164. a) Monthly values of groundwater storage, b) long-period of monthly values of groundwater storage, c) short-period of monthly values of groundwater storage across study area of Jajarm (Code: 4742).

B.7.38. Study area of Esfaraien (Code: 4743)

This area is located between 36°35′-37° 5′N and 56°30′-57°55′ E with an area of 4579.3 km^2. Figure B.165 shows changes in monthly values of groundwater storage inferred from the well data, its long-period and short-period.

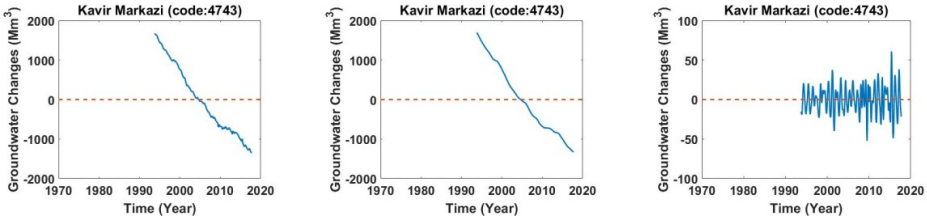

Figure B.165. a) Monthly values of groundwater storage, b) long-period of monthly values of groundwater storage, c) short-period of monthly values of groundwater storage across study area of Esfaraien (Code: 4743).

B.7.39. Study area of Shoghan (Code: 4744)

This area is located between 37-37° 15′N and 56°29′-57°5′ E with an area of 1090.7 km^2. Figure B.166 shows changes in monthly values of groundwater storage inferred from the well data, its long-period and short-period.

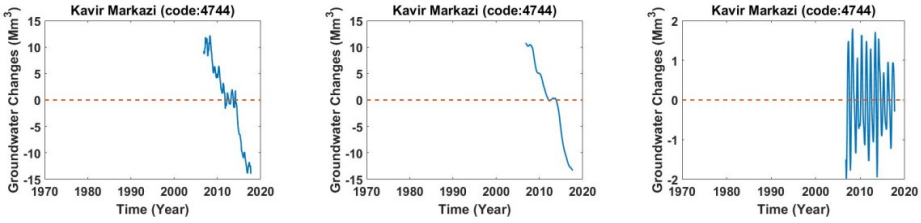

Figure B.166. a) Monthly values of groundwater storage, b) long-period of monthly values of groundwater storage, c) short-period of monthly values of groundwater storage across study area of Shoghan (Code: 4744).

B.7.40. Study area of Safi-Abad (Code: 4745)

This area is located between 36°28′ -36°48′N and 57°10′-58°3′ E with an area of 2548.3 km^2. Figure B.167 shows changes in monthly values of groundwater storage inferred from the well data, its long-period and short-period.

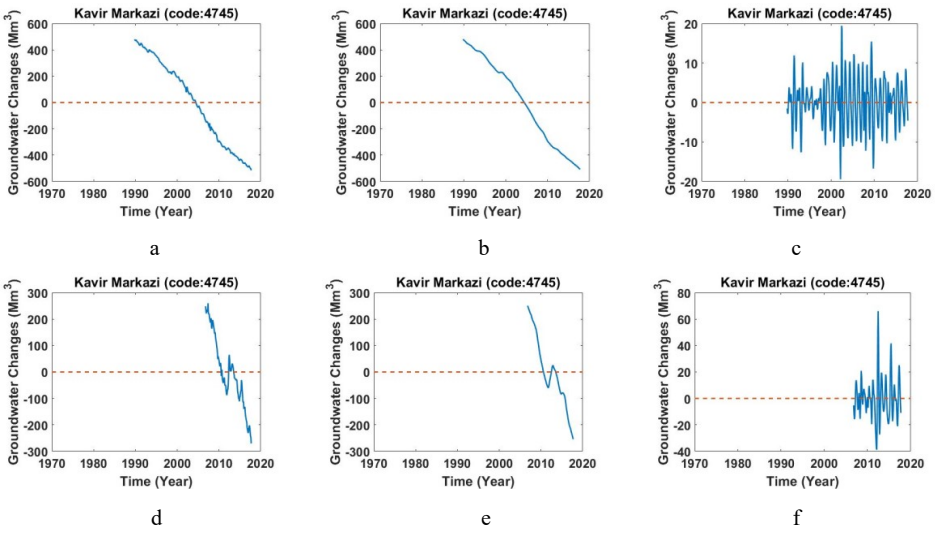

Figure B.167. a,d) Monthly values of groundwater storage, b,e) long-period of monthly values of groundwater storage, c,f) short-period of monthly values of groundwater storage across study area of Safi-Abad (Code: 4745).

B.7.41. Study area of Maiamei (Code: 4746)

This area is located between 36°2′ -36°45′N and 55°14′-55°13′ E with an area of 5083.2 km^2. Figure B.168 shows changes in monthly values of groundwater storage inferred from the well data, its long-period and short-period.

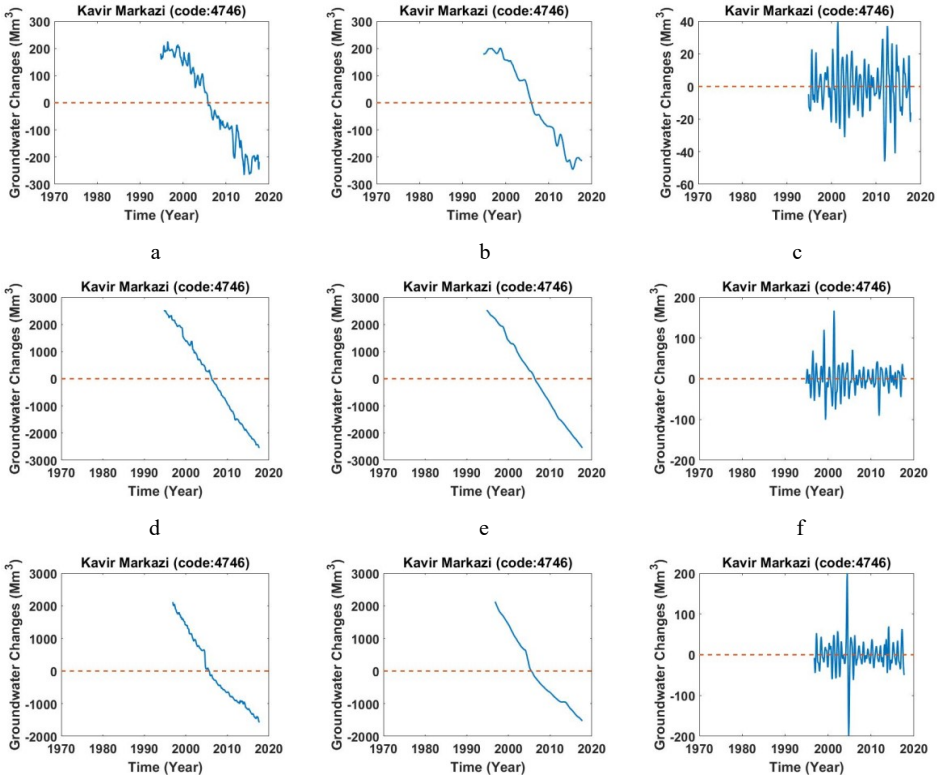

Figure B.168. a,d,g) Monthly values of groundwater storage, b,e,h) long-period of monthly values of groundwater storage, c,f,i) short-period of monthly values of groundwater storage across study area of Maiamei (Code: 4746).

B.7.42. Study area of Damghan (Code: 4747)

This area is located between 35°35′-36° 20′N and 53°30′-54°45′ E with an area of 5946.2 km^2. Figure B.169 shows changes in monthly values of groundwater storage inferred from the well data, its long-period and short-period.

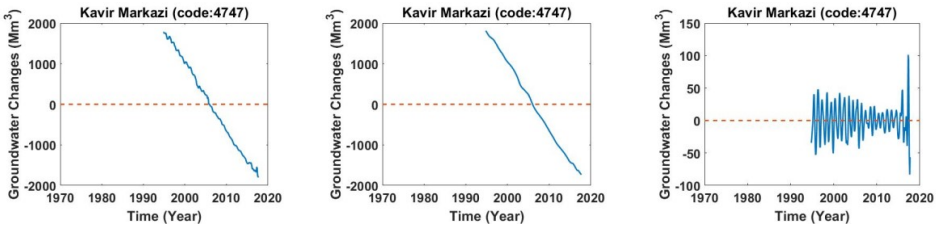

a b c

Figure B.169. a) Monthly values of groundwater storage, b) long-period of monthly values of groundwater storage, c) short-period of monthly values of groundwater storage across study area of Shoghan (Code: 4744).

B.7.43. Study area of Kavire Damghan (Code: 4748)

This area is located between 35°10′-36°10′N and 54°-55°55′ E with an area of 9496.6 km^2. Figure B.170 shows changes in monthly values of groundwater storage inferred from the well data, its long-period and short-period.

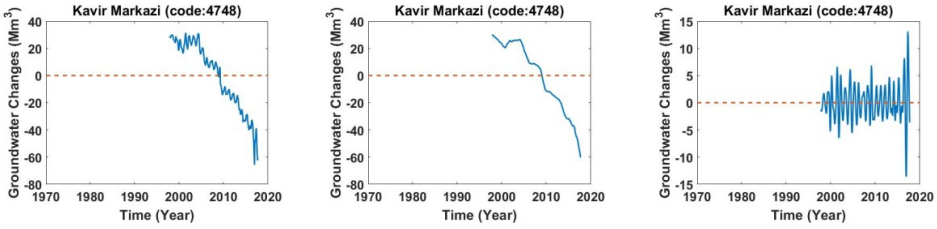

a b c

Figure B.170. a) Monthly values of groundwater storage, b) long-period of monthly values of groundwater storage, c) short-period of monthly values of groundwater storage across study area of Kavire Damghan (Code: 4748).

B.7.44. Study area of Shahrood (Code: 4749)

This area is located between 36°2′ -36°20′N and 54°40′-55°20′ E with an area of 1306.1 km^2. Figure B.171 shows changes in monthly values of groundwater storage inferred from the well data, its long-period and short-period.

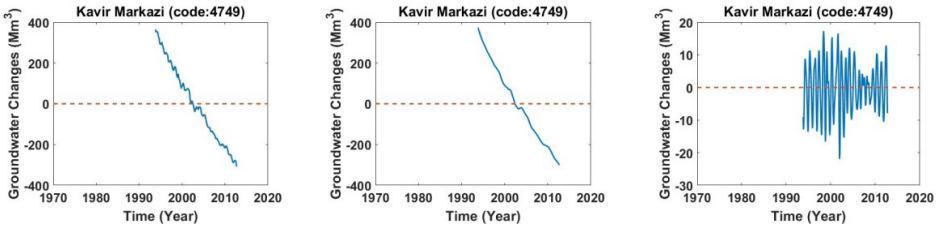

a b c

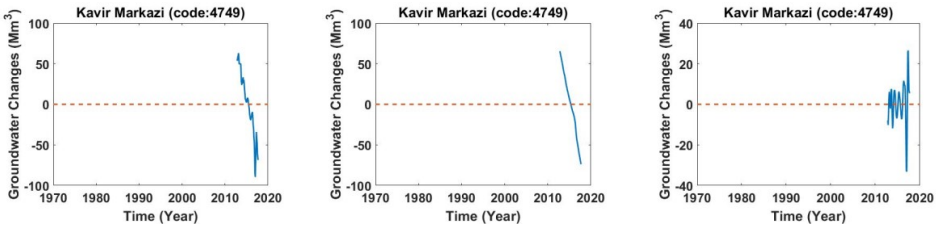

d e f

Figure B.171. a,d) Monthly values of groundwater storage, b,e) long-period of monthly values of groundwater storage, c,f) short-period of monthly values of groundwater storage across study area of Shahrood (Code: 4749).

B.8.1. Study area of Ardestan (Code: 4801)

This area is located between 31˚52′ -33˚57′N and 51˚55′-52˚43′ E with an area of 4377.1 km^2. Figure B.172 shows changes in monthly values of groundwater storage inferred from the well data, its long-period and short-period.

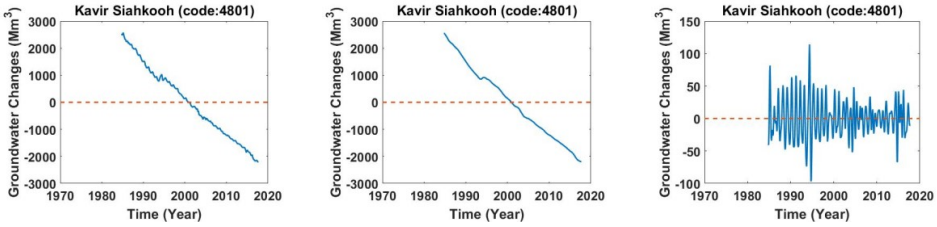

a b c

Figure B.172. a) Monthly values of groundwater storage, b) long-period of monthly values of groundwater storage, c) short-period of monthly values of groundwater storage across study area of Ardestan (Code: 4801).

B.8.2. Study area of Taragh-Abizan (Code: 4802)

This area is located between 33˚-33˚30′N and 51˚32′-52˚17′ E with an area of 1295.7 km^2. Figure B.173 shows changes in monthly values of groundwater storage inferred from the well data, its long-period and short-period.

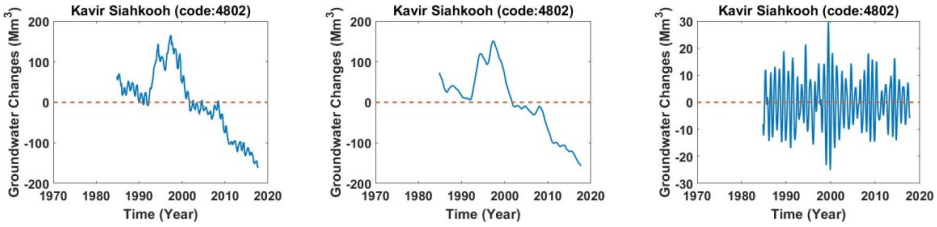

a b c

Figure B.173. a) Monthly values of groundwater storage, b) long-period of monthly values of groundwater storage, c) short-period of monthly values of groundwater storage across study area of Taragh-Abizan (Code: 4802).

B.8.3. Study area of Khaled abad (Code: 4803)

This area is located between 33°25′-34°N and 51°26′-52°23′ E with an area of 1851.4 km^2. Figure B.174 shows changes in monthly values of groundwater storage inferred from the well data, its long-period and short-period.

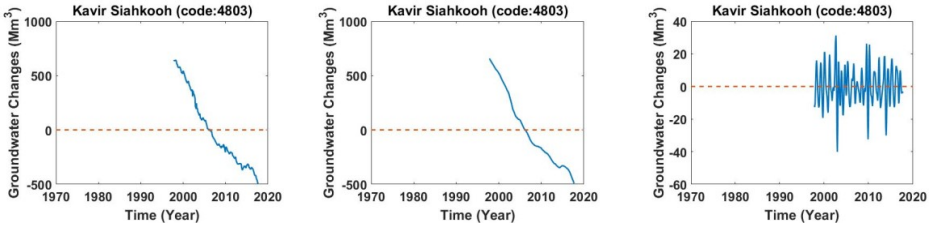

a b c

Figure B.174. a) Monthly values of groundwater storage, b) long-period of monthly values of groundwater storage, c) short-period of monthly values of groundwater storage across study area of Khaled abad (Code: 4803).

B.8.4. Study area of Deghe Sorkh (Code: 4804)

This area is located between 32°-34°N and 52°23′ -53°34′ E with an area of 6249 km^2. Figure B.175 shows changes in monthly values of groundwater storage inferred from the well data, its long-period and short-period.

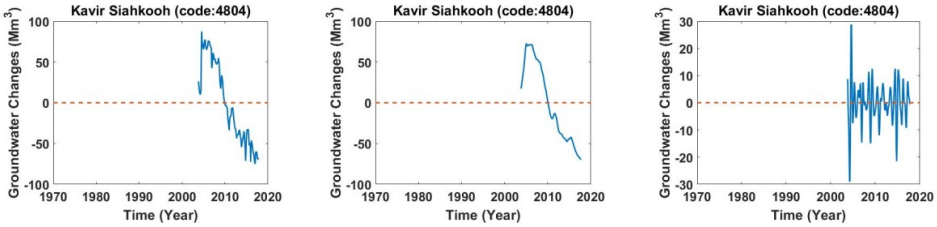

a b c

Figure B.175. a) Monthly values of groundwater storage, b) long-period of monthly values of groundwater storage, c) short-period of monthly values of groundwater storage across study area of Deghe Sorkh (Code: 4804).

B.8.5. Study area of Naein (Code: 4805)

This area is located between 32°-34°N and 52°23′ -53°34′ E with an area of 5018.7 km^2. Figure B.176 shows changes in monthly values of groundwater storage inferred from the well data, its long-period and short-period.

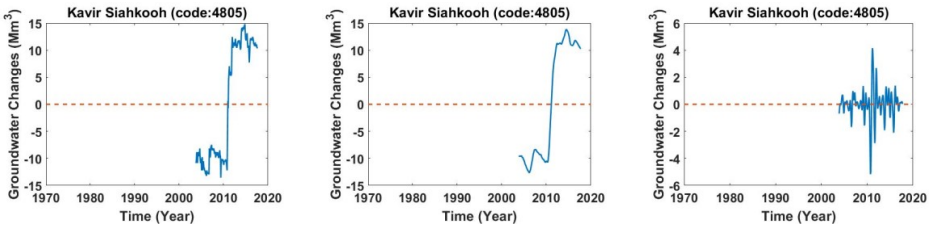

a b c

Figure B.176. a) Monthly values of groundwater storage, b) long-period of monthly values of groundwater storage, c) short-period of monthly values of groundwater storage across study area of Naein (Code: 4805).

B.8.6. Study area of Naein (Code: 4806)

This area is located between 33°-34°N and 51-54° E with an area of 5018.7 km^2. Figure B.177 shows changes in monthly values of groundwater storage inferred from the well data, its long-period and short-period.

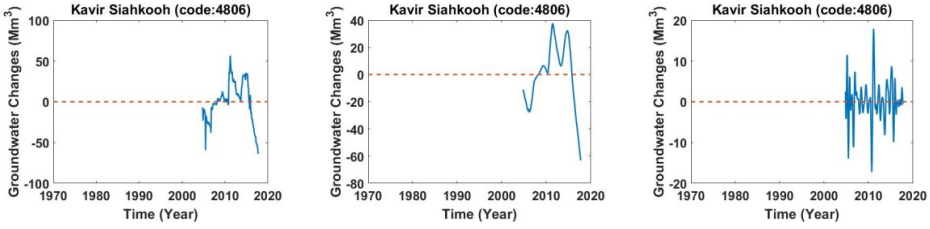

a b c

Figure B.177. a) Monthly values of groundwater storage, b) long-period of monthly values of groundwater storage, c) short-period of monthly values of groundwater storage across study area of Naein (Code: 4806).

B.8.7. Study area of Aghda (Code: 4807)

This area is located between 33°-34°N and 51-54° E with an area of 5018.7 km^2. Figure B.178 shows changes in monthly values of groundwater storage inferred from the well data, its long-period and short-period.

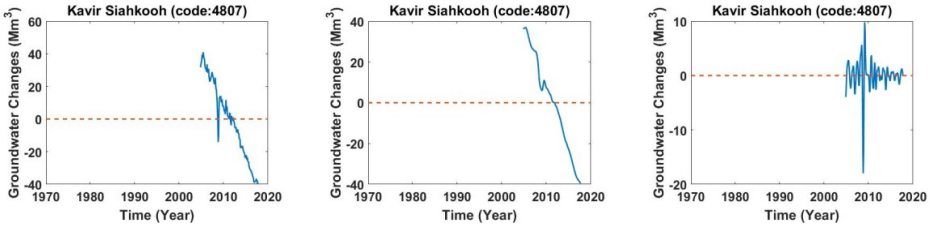

a b c

Figure B.178. a) Monthly values of groundwater storage, b) long-period of monthly values of groundwater storage, c) short-period of monthly values of groundwater storage across study area of Aghda (Code: 4807).

B.8.8. Study area of Yazd-Ardakan (Code: 4808)

This area is located between 31°15′-32°40′ N and 53° 25′-55° E with an area of 11573.0 km^2. Figure B.179 shows changes in monthly values of groundwater storage inferred from the well data, its long-period and short-period.

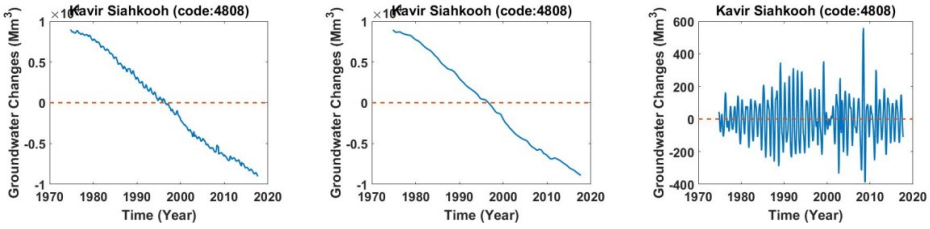

a b c

Figure B.179. a) Monthly values of groundwater storage, b) long-period of monthly values of groundwater storage, c) short-period of monthly values of groundwater storage across study area of Yazd-Ardakan (Code: 4808).

B.8.9. Study area of Kavir Siahkoh (Code: 4810)

This area is located between 32°25′-33°15′ N and 53° 35′-54°35′ E with an area of 3199.6 km^2. Figure B.180 shows changes in monthly values of groundwater storage inferred from the well data, its long-period and short-period.

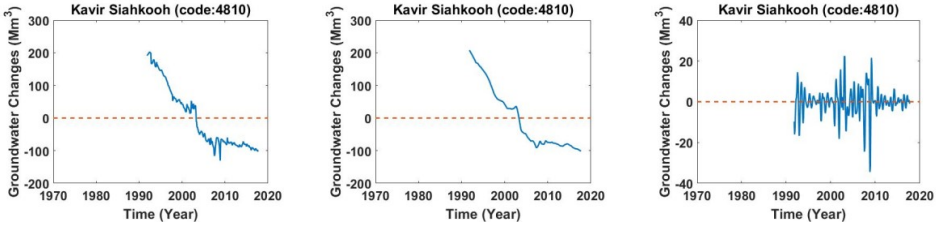

a b c

Figure B.180. a) Monthly values of groundwater storage, b) long-period of monthly values of groundwater storage, c) short-period of monthly values of groundwater storage across study area of Kavir Siahkoh (Code: 4810).

B.8.10. Study area of Kavir Siahkoh (Code: 4811)

This area is located between 32°23′-33°25′ N and 54°-57°27′ E with an area of 10082.2 km^2. Figure B.181 shows changes in monthly values of groundwater storage inferred from the well data, its long-period and short-period.

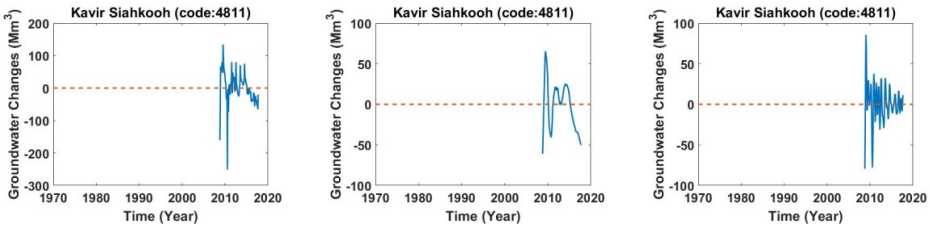

a b c

Figure B.181. a) Monthly values of groundwater storage, b) long-period of monthly values of groundwater storage, c) short-period of monthly values of groundwater storage across study area of Kavir Siahkoh (Code: 4811).

B.9.1. Study area of Kavir Daranjir (Code: 4901)

This area is located between 31°15′-32°27′ N and 54°33′-55°34′ E with an area of 6233.08 km^2. Figure B.182 shows changes in monthly values of groundwater storage inferred from the well data, its long-period and short-period.

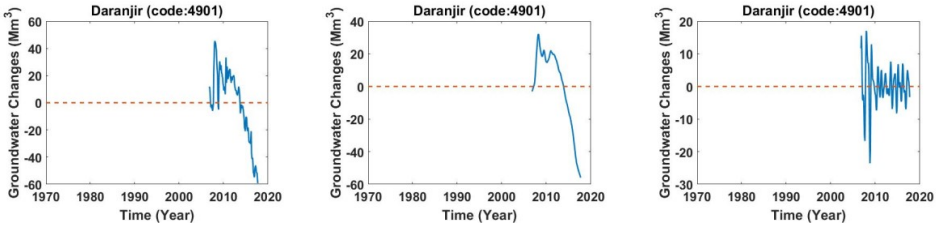

a b c

Figure B.182. a) Monthly values of groundwater storage, b) long-period of monthly values of groundwater storage, c) short-period of monthly values of groundwater storage across study area of Kavir Daranjir (Code: 4901).

B.9.2. Study area of Rafsanjan (Code: 4902)

This area is located between 29°52′-31°30′ N and 54°52′-56°33′ E with an area of 12513.70 km^2. Figure B.183 shows changes in monthly values of groundwater storage inferred from the well data, its long-period and short-period.

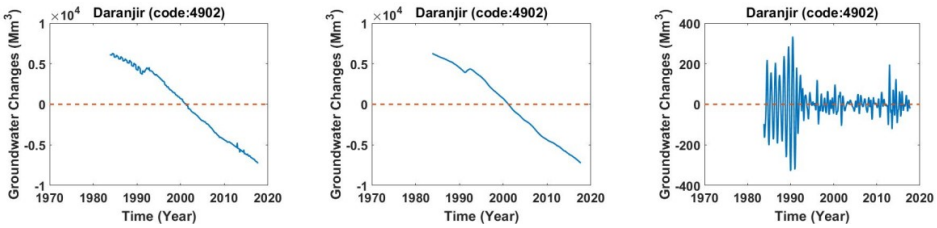

a b c

Figure B.183. a) Monthly values of groundwater storage, b) long-period of monthly values of groundwater storage, c) short-period of monthly values of groundwater storage across study area of Rafsanjan (Code: 4902).

B.9.3. Study area of Bahadoran (Code: 4903)

This area is located between 31°-31°34′ N and 54°44′-55°24′ E with 2285.76 km^2. Figure B.184 shows changes in monthly values of groundwater storage inferred from the well data, its long-period and short-period.

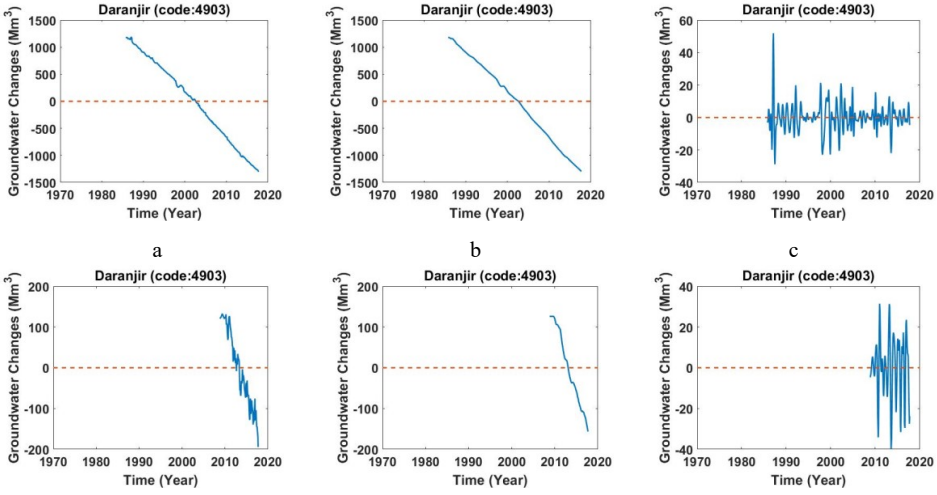

a b c

d e f

Figure B.184. a,d) Monthly values of groundwater storage, b,e) long-period of monthly values of groundwater storage, c,f) short-period of monthly values of groundwater storage across study area of Bahadoran (Code: 4903).

B.9.4. Study area of Arnan-Dehaj (Code: 4904)

This area is located between 30°35′-31°31′ N and 54°8′-55°24′ E with an area of 3985.93 km^2. Figure B.185 shows changes in monthly values of groundwater storage inferred from the well data, its long-period and short-period.

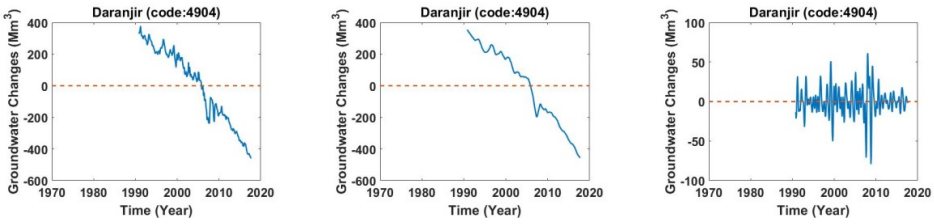

a b c

Figure B.185. a) Monthly values of groundwater storage, b) long-period of monthly values of groundwater storage, c) short-period of monthly values of groundwater storage across study area of Arnan-Dehaj (Code: 4904).

B.9.5. Study area of Kerman-Baghin (Code: 4906)

This area is located between 29°46′-30°32′ N and 56°18′-57°35′ E with an area of 2845.43 km^2. Figure B.186 shows changes in monthly values of groundwater storage inferred from the well data, its long-period and short-period.

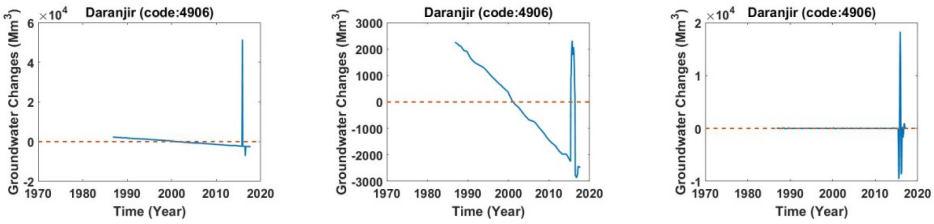

a b c

Figure B.186. a) Monthly values of groundwater storage, b) long-period of monthly values of groundwater storage, c) short-period of monthly values of groundwater storage across study area of Kerman-Baghin (Code: 4906).

B.9.6. Study area of Gharie-Alarab (Code: 4907)

This area is located between 29°23′-29°58′ N and 56°51′-57°19′ E with an area of 1763.96 km^2. Figure B.187 shows changes in monthly values of groundwater storage inferred from the well data, its long-period and short-period.

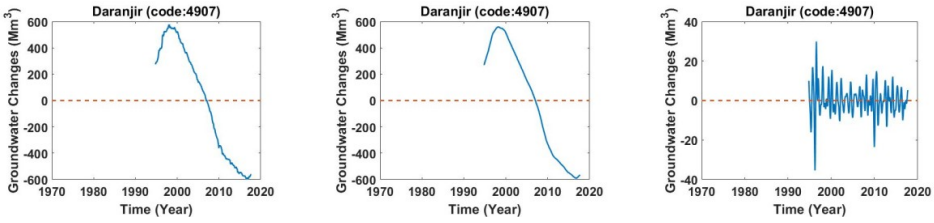

a b c

Figure B.187. a) Monthly values of groundwater storage, b) long-period of monthly values of groundwater storage, c) short-period of monthly values of groundwater storage across study area of Gharie-Alarab (Code: 4907).

B.9.7. Study area of Bafgh (Code: 4908)

This area is located between 31°2′-32°13′ N and 55°14′-55°59′ E with an area of 4793.66 km^2. Figure B.188 shows changes in monthly values of groundwater storage inferred from the well data, its long-period and short-period.

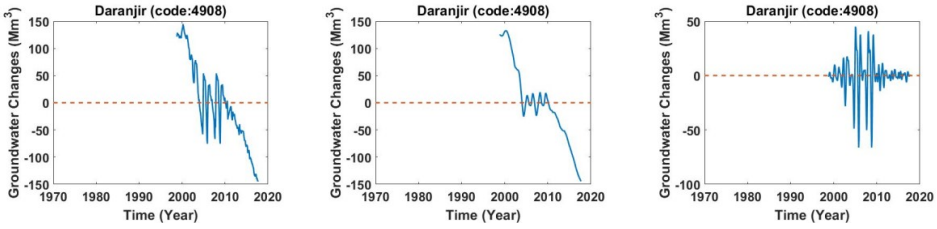

a b c

Figure B.188. a) Monthly values of groundwater storage, b) long-period of monthly values of groundwater storage, c) short-period of monthly values of groundwater storage across study area of Bafgh (Code: 4908).

B.9.8. Study area of Siriz-Toghroljerd (Code: 4910)

This area is located between 30°48′-31°17′ N and 55°46′-56°31′ E with an area of 1715.78 km^2. Figure B.189 shows changes in monthly values of groundwater storage inferred from the well data, its long-period and short-period.

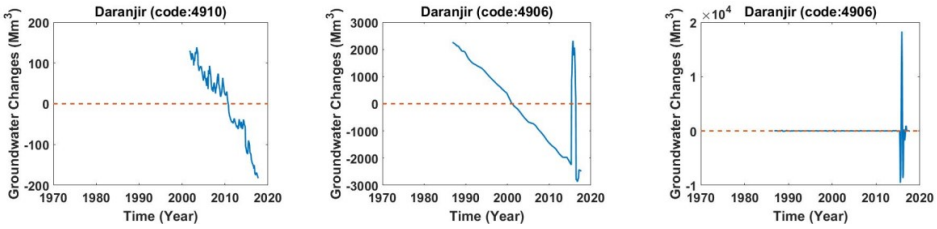

a b c

Figure B.189. a) Monthly values of groundwater storage, b) long-period of monthly values of groundwater storage, c) short-period of monthly values of groundwater storage across study area of Siriz-Toghroljerd (Code: 4910).

B.9.9. Study area of Zarand (Code: 4911)

This area is located between 30°22′-31°14′ N and 56°3′-57°8′ E with an area of 4398.19 km^2. Figure B.190 shows changes in monthly values of groundwater storage inferred from the well data, its long-period and short-period.

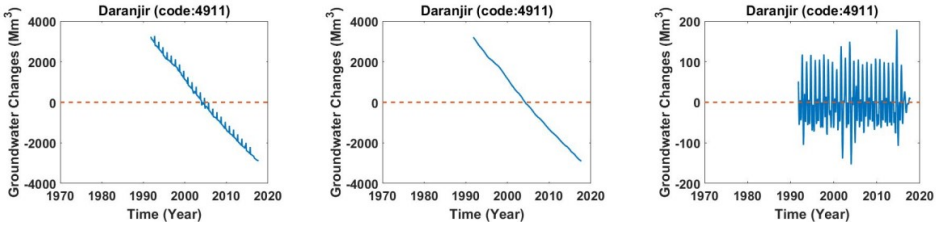

a b c

Figure B.190. a) Monthly values of groundwater storage, b) long-period of monthly values of groundwater storage, c) short-period of monthly values of groundwater storage across study area of Zarand (Code: 4911).

This page is intentionally left blank.

Appendix C

C.1.1. Study area of Moghan-parsabad (Code: 1101)

This area is located between 4250000-4280000 N and 670000-688000 E with an area of 6500 km^2. Figure C.1 shows changes in monthly values of groundwater storage inferred from the well data, its long-period and short-period.

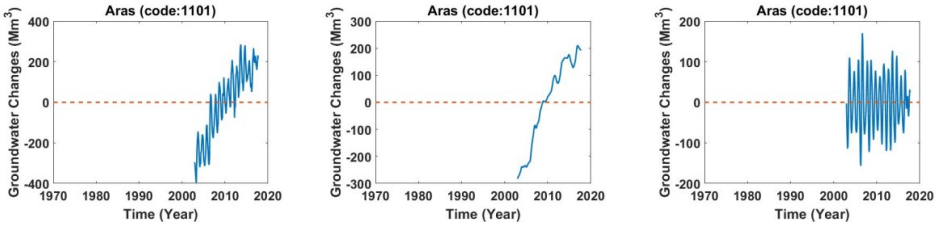

a b c

Figure C.1. a) Monthly values of groundwater storage, b) long-period of monthly values of groundwater storage, c) short-period of monthly values of groundwater storage across study area of Moghan-parsabad (Code: 1101).

C.1.2. Study area of Meshkin Shahr (Code: 1102)

This area is located between 4245000-4260000 N and 670000-688000 E with an area of 2500 km^2 area. Figure C.2 shows changes in monthly values of groundwater storage inferred from the well data, its long-period and short-period.

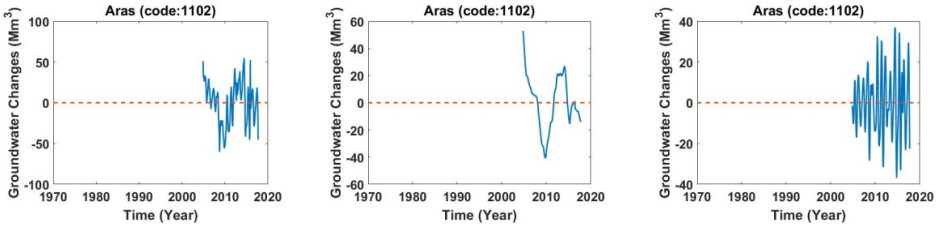

a b c

Figure C.2. a) Monthly values of groundwater storage, b) long-period of monthly values of groundwater storage, c) short-period of monthly values of groundwater storage across study area of Meshkin Shahr (Code: 1102).

C.1.3. Study area of Ardabil (Code: 1103)

This area is located between 4235000-4255000 N and 675000-700000 E with an area of 4300 km^2. Figure C.3 shows changes in monthly values of groundwater storage inferred from the well data, its long-period and short-period.

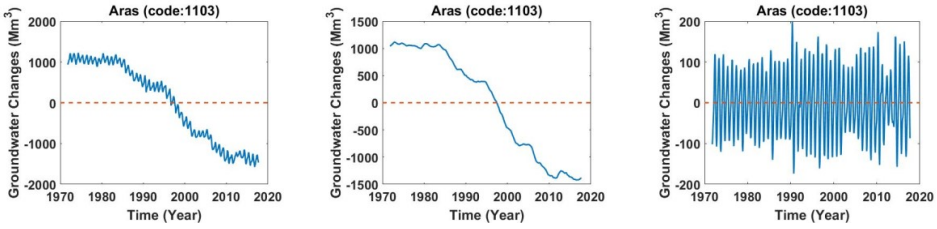

Figure C.3. a) Monthly values of groundwater storage, b) long-period of monthly values of groundwater storage, c) short-period of monthly values of groundwater storage across study area of Ardabil (Code: 1104).

C.1.4. Study area of Ahar-varzaghan (Code: 1104)

This area is located between 4235000-4255000 N and 653000-672000 E with an area of 2152.3 km^2. Figure C.4 shows changes in monthly values of groundwater storage inferred from the well data, its long-period and short-period.

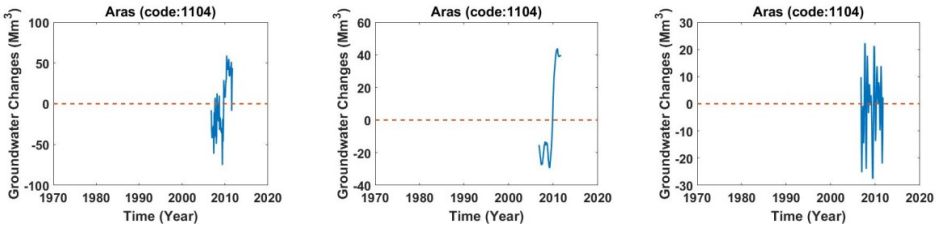

Figure C.4. a) Monthly values of groundwater storage, b) long-period of monthly values of groundwater storage, c) short-period of monthly values of groundwater storage across study area of Ahar-varzaghan (Code: 1104).

C.1.5. Study area of Jolfa-dozal (Code: 1105)

This area is located between 4235000-4255000 N and 635000-675000 E with an area of 4500 km^2. Figure C.5 shows changes in monthly values of groundwater storage inferred from the well data, its long-period and short-period.

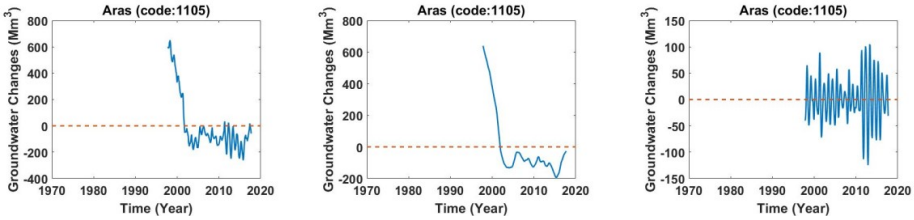

Figure C.5. a) Monthly values of groundwater storage, b) long-period of monthly values of groundwater storage, c) short-period of monthly values of groundwater storage across study area of Jolfa-dozal (Code: 1105).

C.1.6 Study area of Oaghli (Code: 1106)

This area is located between 4250000-4260000 N and 630000-638000 E with an area of 1500 km^2. Figure C.6 shows changes in monthly values of groundwater storage inferred from the well data, its long-period and short-period.

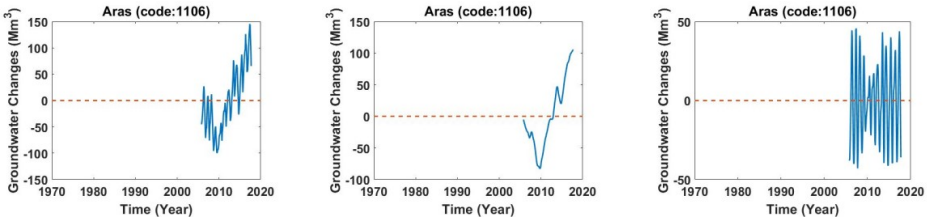

Figure C.6. a) Monthly values of groundwater storage, b) long-period of monthly values of groundwater storage, c) short-period of monthly values of groundwater storage across study area of Oaghli (Code: 1106).

C.1.7. Study area of Marand (Code: 1107)

This area is located between 4256000-4265000 N and 630000-650000 E with an area of 1870 km^2. Figure C.7 shows changes in monthly values of groundwater storage inferred from the well data, its long-period and short-period.

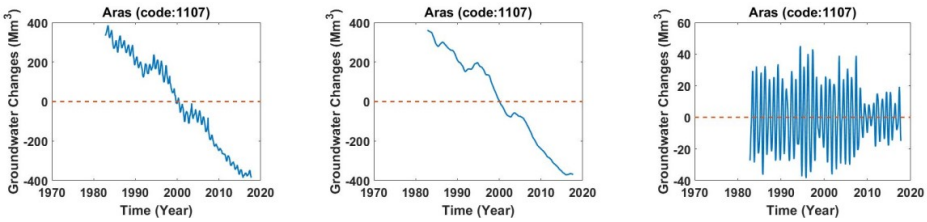

Figure C.7. a) Monthly values of groundwater storage, b) long-period of monthly values of groundwater storage, c) short-period of monthly values of groundwater storage across study area of Marand (Code: 1107).

C.1.8. Study area of Ghare Ziaodin (Code: 1108)

This area is located between 4248000-4255000 N and 610000-630000 E with an area of 2100 km^2. Figure C.8 shows changes in monthly values of groundwater storage inferred from the well data, its long-period and short-period.

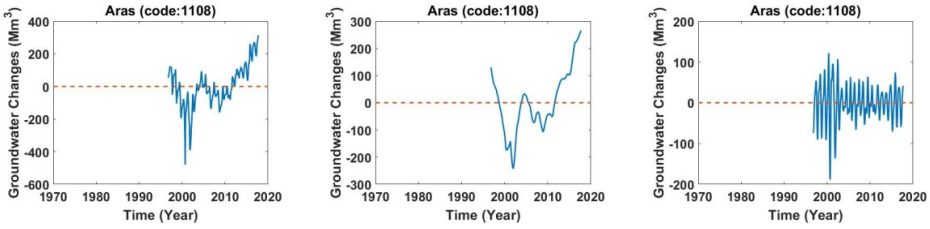

a b c

Figure C.8. a) Monthly values of groundwater storage, b) long-period of monthly values of groundwater storage, c) short-period of monthly values of groundwater storage across study area of Ghare Ziaodin (Code: 1108).

C.1.9. Study area of Khoi (Code: 1109)

This area is located between 4248000-4256000 N and 613000-630000 E with an area of 3600 km^2. Figure C.9 shows changes in monthly values of groundwater storage inferred from the well data, its long-period and short-period.

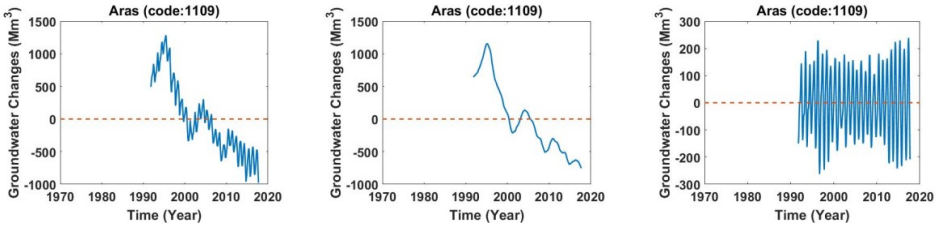

a b c

Figure C.9. a) Monthly values of groundwater storage, b) long-period of monthly values of groundwater storage, c) short-period of monthly values of groundwater storage across study area of Khoi (Code: 1109).

C.1.10. Study area of Poldasht (Code: 1110)

This area is located between 4260000-4274000 N and 620000-635000 E with an area of 3500 km^2. Figure C.10 shows changes in monthly values of groundwater storage inferred from the well data, its long-period and short-period.

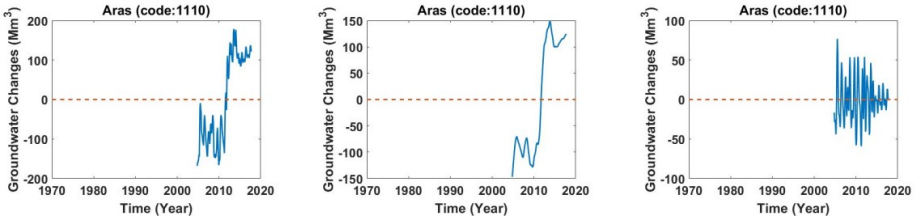

Figure C.10. a) Monthly values of groundwater storage, b) long-period of monthly values of groundwater storage, c) short-period of monthly values of groundwater storage across study area of Poldasht (Code: 1110).

C.1.11. Study area of Bazargan (Code: 1111)

This area is located between 4270000-4280000 N and 610000-622000 E with an area of 900 km^2. Figure C.11 shows changes in monthly values of groundwater storage inferred from the well data, its long-period and short-period.

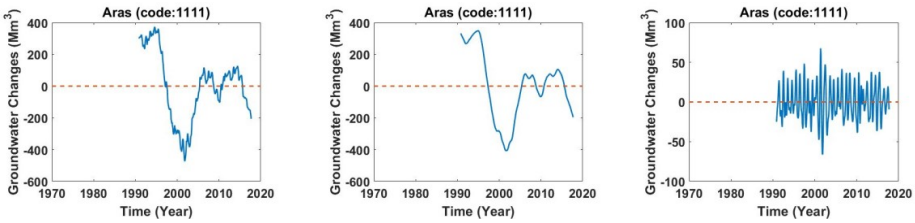

Figure C.11. a) Monthly values of groundwater storage, b) long-period of monthly values of groundwater storage, c) short-period of monthly values of groundwater storage across study area of Bazargan (Code: 1111).

C.1.12. Study area of Chaldoran (Code: 1112)

This area is located between 4260000-4270000 N and 610000-620000 E with an area of 980 km^2. Figure C.12 shows changes in monthly values of groundwater storage inferred from the well data, its long-period and short-period.

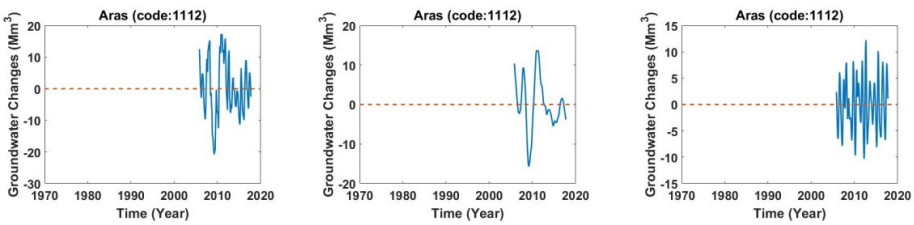

Figure C.12. a) Monthly values of groundwater storage, b) long-period of monthly values of groundwater storage, c) short-period of monthly values of groundwater storage across study area of Chaldoran (Code: 1112).

C.2.1. Study area of Talesh (Code: 1201)

This area is located between 37°15′-38°20′ N and 48°45′-49°15′ E with an area of 3206.7 km^2. Figure C.13 shows changes in monthly values of groundwater storage inferred from the well data, its long-period and short-period.

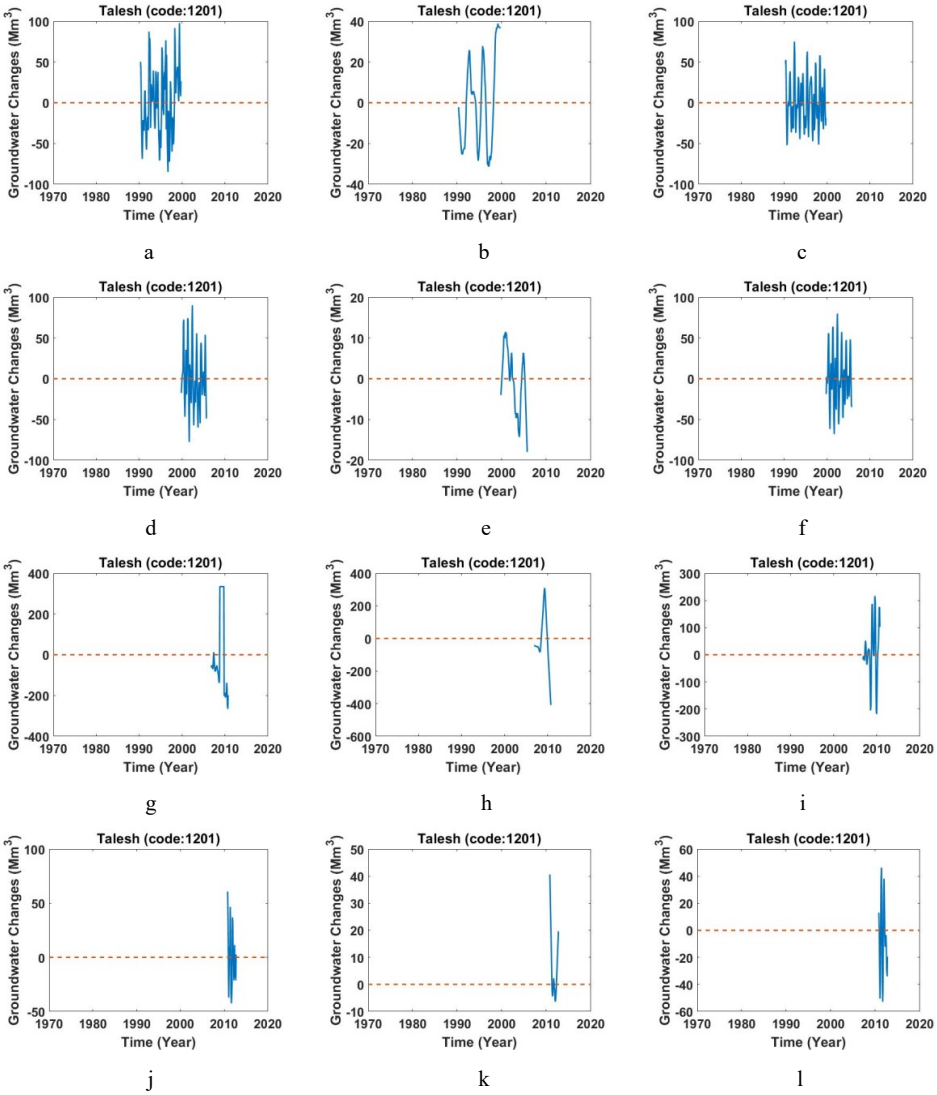

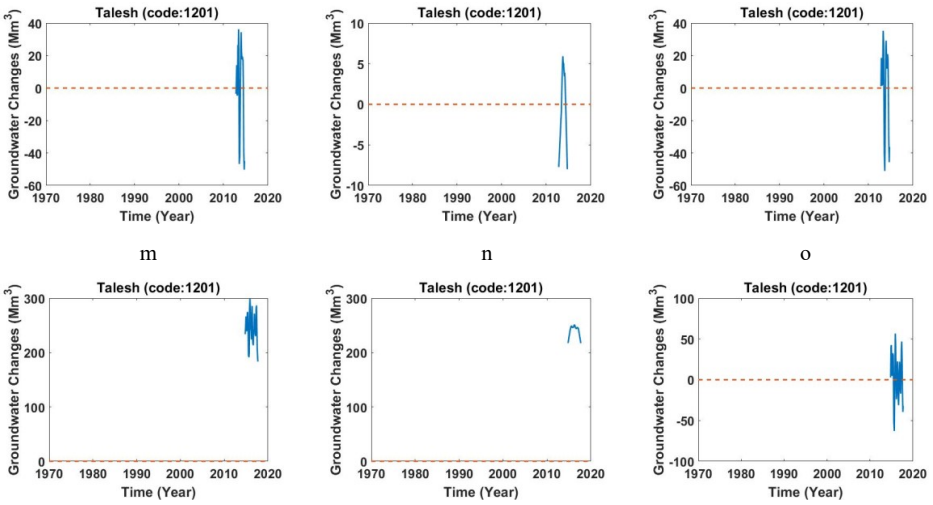

Figure C.13. a,d,g,j,m,p) Monthly values of groundwater storage, b,e,h,k,n,q) long-period of monthly values of groundwater storage, c,f,i,l,o,r) short-period of monthly values of groundwater storage across study area of Talesh (Code: 1201).

C.2.2. Study area of Foomanat (Code: 1202)

This area is located between 36°45′-37°20′ N and 48°45′-49°45′ E with an area of 3829.7 km^2. Figure C.14 shows changes in monthly values of groundwater storage inferred from the well data, its long-period and short-period.

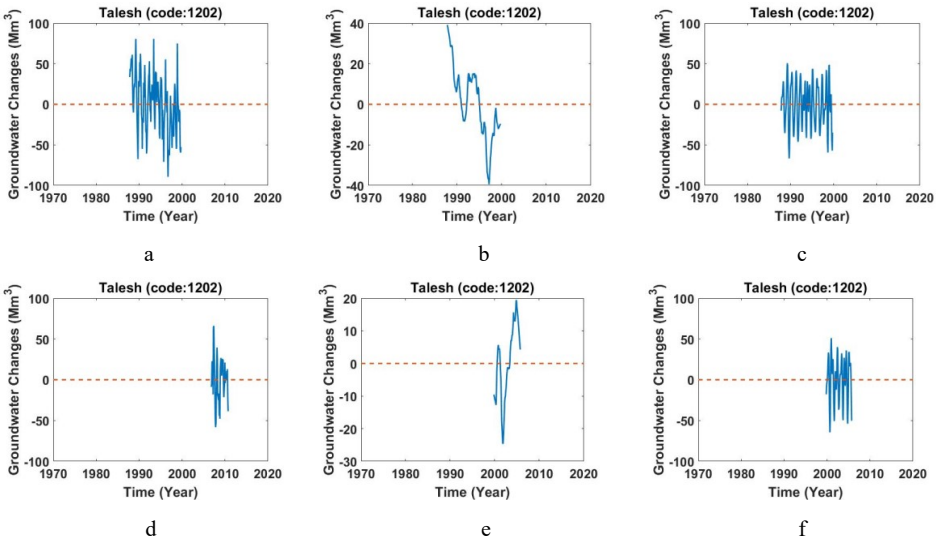

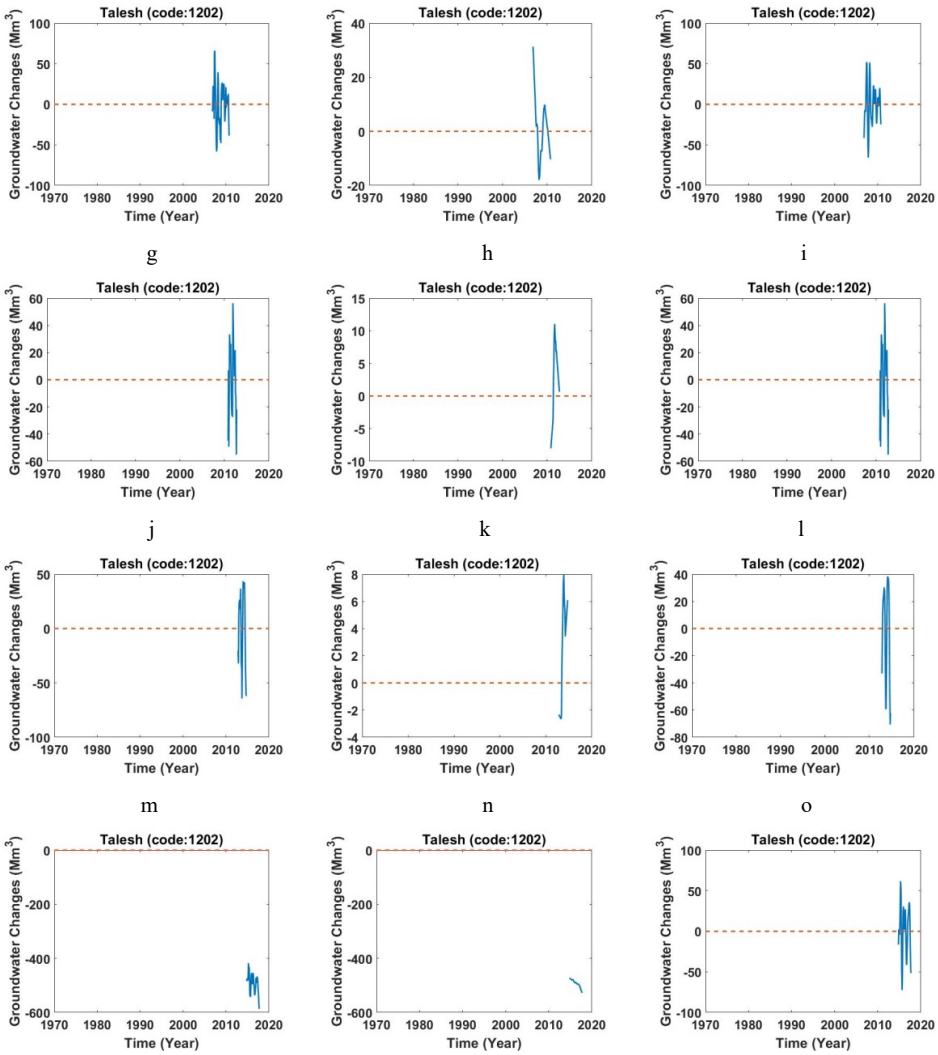

Figure C.14. a,d,g,j,m,p) Monthly values of groundwater storage, b,e,h,k,n,q) long-period of monthly values of groundwater storage, c,f,i,l,o,r) short-period of monthly values of groundwater storage across study area of Foomanat (Code: 1202).

C.3.1. Study area of Kooch-Esfahan (Code: 1301)

This area is located between 36˚43′-37˚28′ N and 49˚15′-50˚11′ E with an area of 2582.7 km^2. Figure C.15 shows changes in monthly values of groundwater storage inferred from the well data, its long-period and short-period.

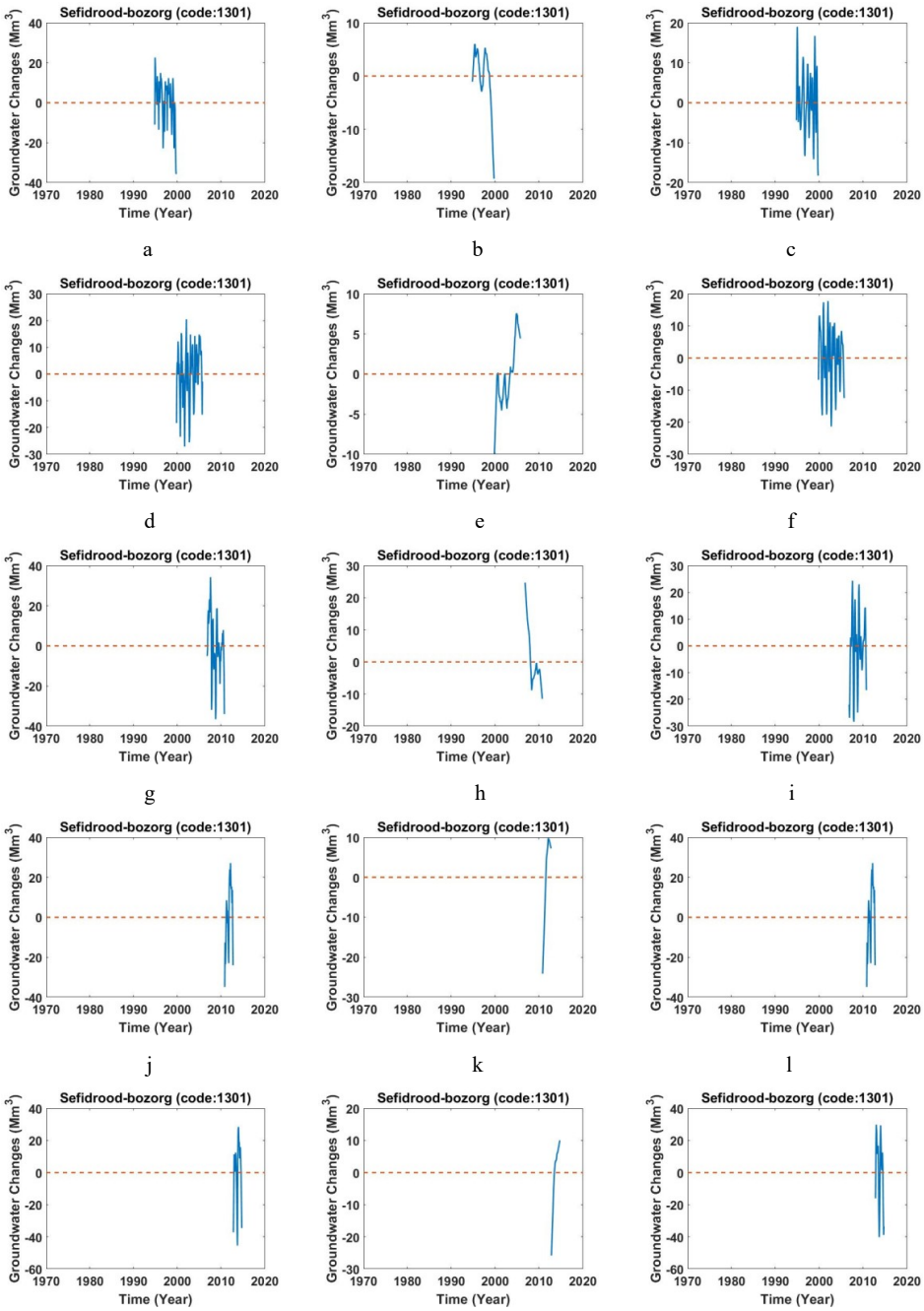

Figure 5.15. a,d,g,j,m) Monthly values of groundwater storage, b,e,h,k,n) long-period of monthly values of groundwater storage, c,f,i,l,o) short-period of monthly values of groundwater storage across study area of Kooch-Esfahan (Code: 1301).

C.3.2. Study area of Tarom-Khalahal (Code: 1302)

This area is located between 36°30′-37°43′ N and 48°-49°10′ E with an area of 8836.8 km^2. Figure C.16 shows changes in monthly values of groundwater storage inferred from the well data, its long-period and short-period.

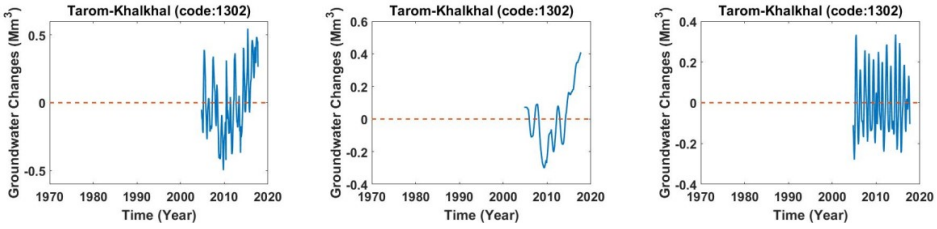

a b c

Figure C.16. a) Monthly values of groundwater storage, b) long-period of monthly values of groundwater storage, c) short-period of monthly values of groundwater storage across study area of Tarom-Khalahal (Code: 1302).

C.3.3. Study area of Miane (Code: 1303)

This area is located between 36°46′-37°43′ N and 46°50′-48°10′ E with an area of 9232.7 km^2. Figure C.17 shows changes in monthly values of groundwater storage inferred from the well data, its long-period and short-period.

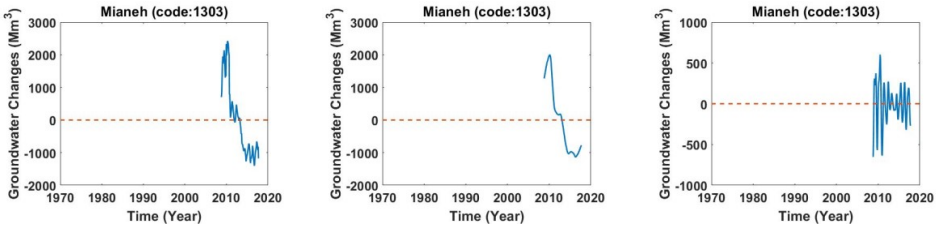

a b c

Figure C.17. a) Monthly values of groundwater storage, b) long-period of monthly values of groundwater storage, c) short-period of monthly values of groundwater storage across study area of Miane (Code: 1303).

C.3.4. Study area of Zanjan (Code: 1304)

This area is located between 36°20′-37°10′ N and 47°55′-49° E with an area of 4667.6 km^2. Figure C.18 shows changes in monthly values of groundwater storage inferred from the well data, its long-period and short-period.

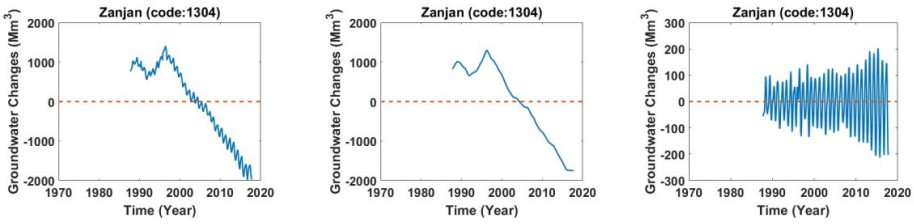

a b c

Figure C.18. a) Monthly values of groundwater storage, b) long-period of monthly values of groundwater storage, c) short-period of monthly values of groundwater storage across study area of Zanjan (Code: 1304).

C.3.5. Study area of Sojas (Code: 1306)

This area is located between 36°-36°30′ N and 48°10′-48°50′ E with an area of 2461.6 km^2. Figure C.19. shows changes in monthly values of groundwater storage inferred from the well data, its long-period and short-period.

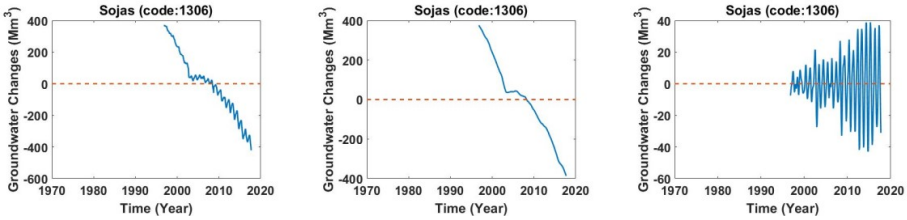

a b c

Figure C.19. a) Monthly values of groundwater storage, b) long-period of monthly values of groundwater storage, c) short-period of monthly values of groundwater storage across study area of Sojas (Code: 1306).

C.3.6. Study area of Goltape-Zarinabad (Code: 1307)

This area is located between 35°5′-36°10′ N and 47°55′-49° E with an area of 5165.6 km^2. Figure C.20 shows changes in monthly values of groundwater storage inferred from the well data, its long-period and short-period.

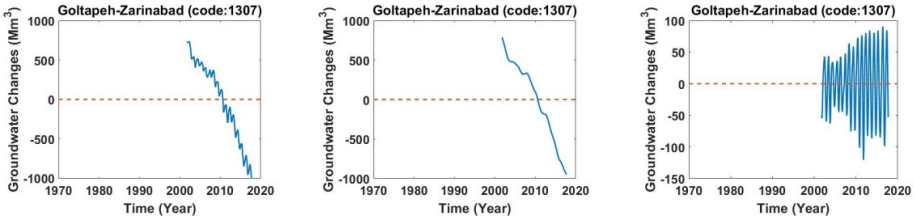

a b c

Figure C.20. a) Monthly values of groundwater storage, b) long-period of monthly values of groundwater storage, c) short-period of monthly values of groundwater storage across study area of Goltape-Zarinabad (Code: 1307).

C.3.7. Study area of Ghorve-Dehgolan (Code: 1308)

This area is located between 34°55′-36° N and 47°10′-48°10′ E with an area of 7236.6 km^2. This area divided to 3 parts. Figure C.21 shows changes in monthly values of groundwater storage inferred from the well data, its long-period and short-period.

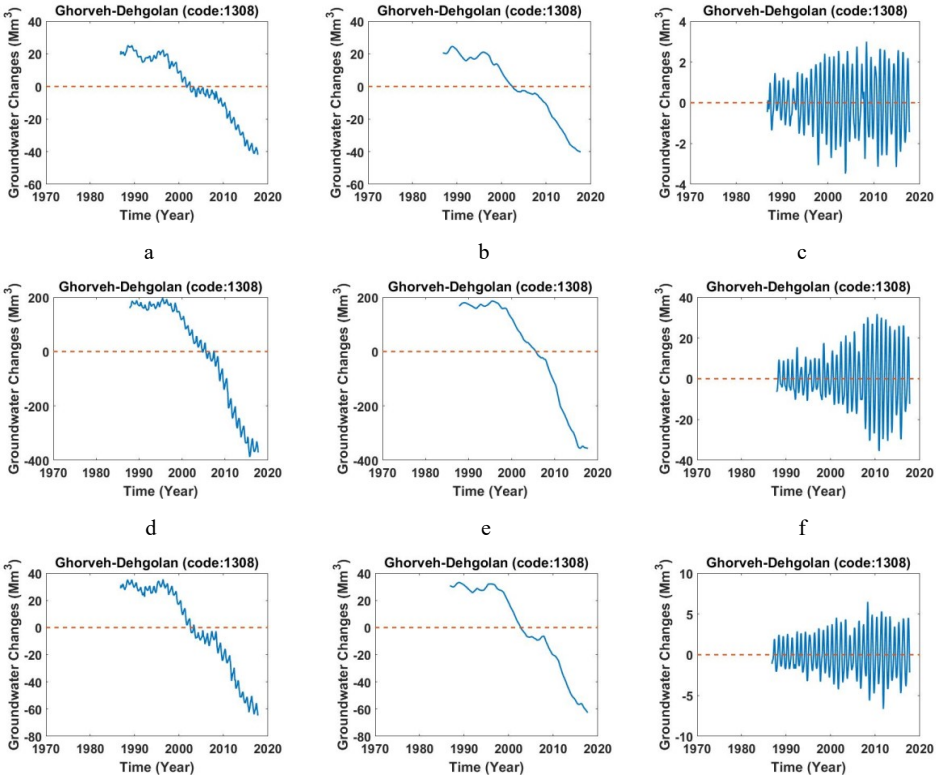

Figure C.21. a,d,g) Monthly values of groundwater storage, b,e,h) long-period of monthly values of groundwater storage, c,f,i) short-period of monthly values of groundwater storage across study area of Goltape-Zarinabad (Code: 1308).

C.3.8. Study area of Divandare-Bijar (Code: 1309)

This area is located between 35°30′-36°20′ N and 46°45′-48° E with an area of 5362.8 km^2. Figure C.22 shows changes in monthly values of groundwater storage inferred from the well data, its long-period and short-period.

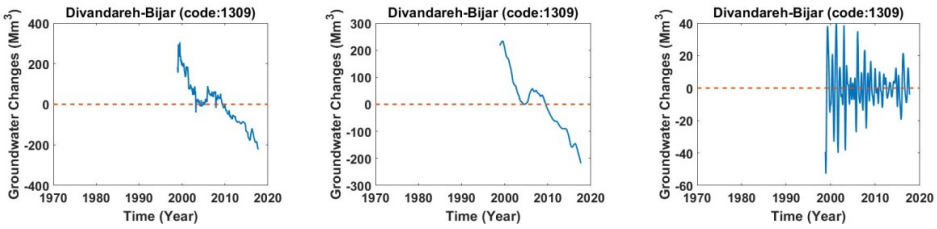

Figure C.22 a) Monthly values of groundwater storage, b) long-period of monthly values of groundwater storage, c) short-period of monthly values of groundwater storage across study area of Divandare-Bijar (Code: 1309).

C.4.1. Study area of Lahijan-chaboksar (Code: 1401)

This area is located between 36°33′-37°23′ N and 49°46′-50°47′ E with an area of 3547.53 km^2. Figure C.23 shows changes in monthly values of groundwater storage inferred from the well data, its long-period and short-period.

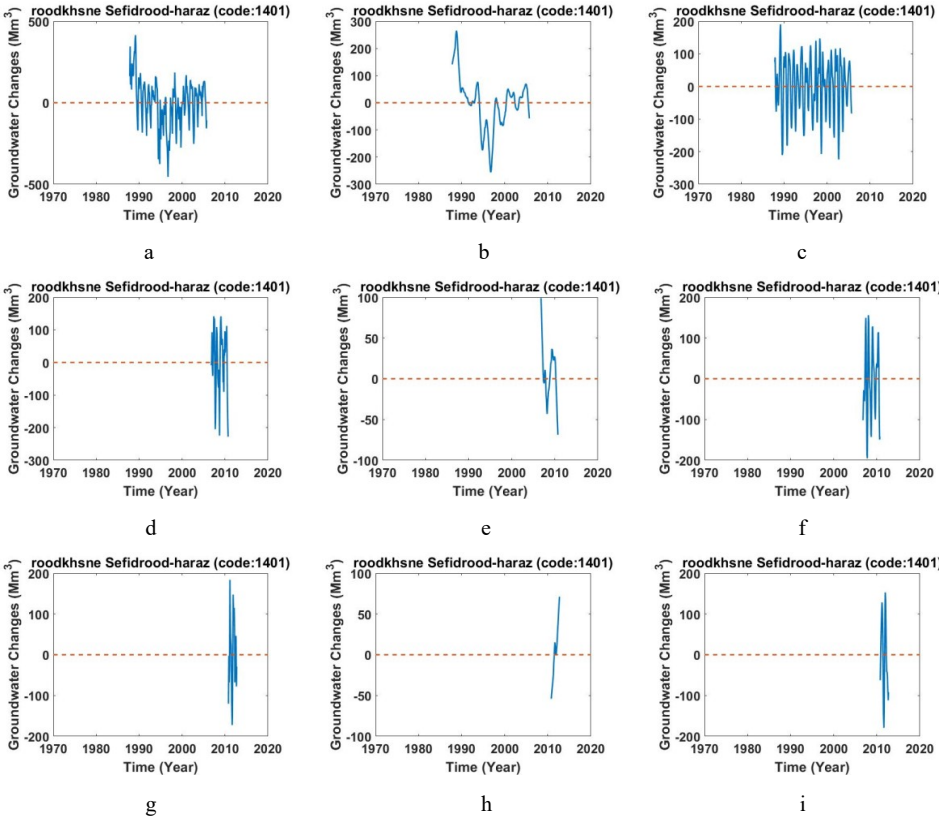

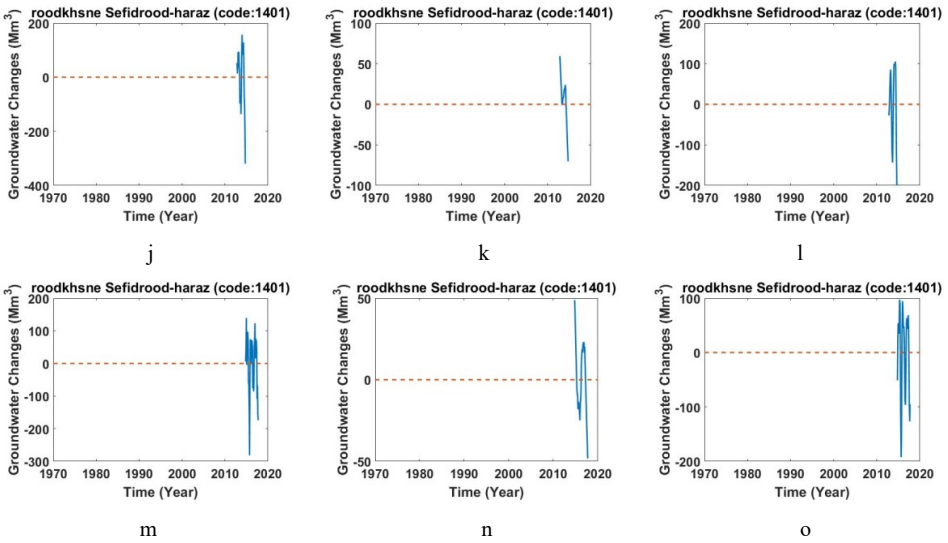

Figure C.23. a,d,g,j,m) Monthly values of groundwater storage, b,e,h,k,n) long-period of monthly values of groundwater storage, c,f,i,l,o) short-period of monthly values of groundwater storage across study area of Talesh (Code: 1401).

C.5.1. Study area of Babol-Amol (Code: 1501)

This area is located between 35°46′-36°43′ N and 51°26′-52°55′ E with an area of 680C.11 km^2. Figure C.24 shows changes in monthly values of groundwater storage inferred from the well data, its long-period and short-period.

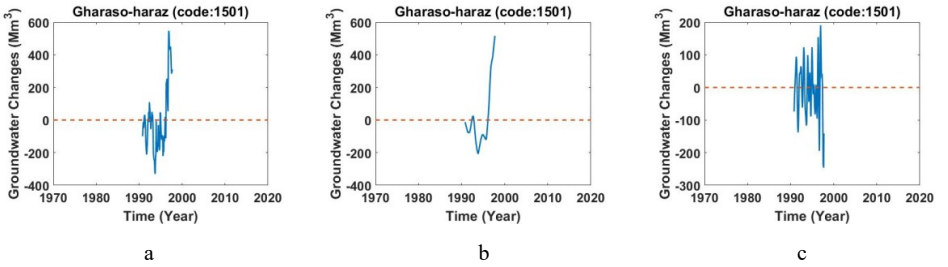

Figure C.24. a) Monthly values of groundwater storage, b) long-period of monthly values of groundwater storage, c) short-period of monthly values of groundwater storage across study area of Babol-Amol (Code: 1501).

C.5.2. Study area of Ghaemshahr-Joibar (Code: 1502)

This area is located between 35°44′-36°47′ N and 52°35′-53°23′ E with an area of 3301.7 km^2. Figure C.25 shows changes in monthly values of groundwater storage inferred from the well data, its long-period and short-period.

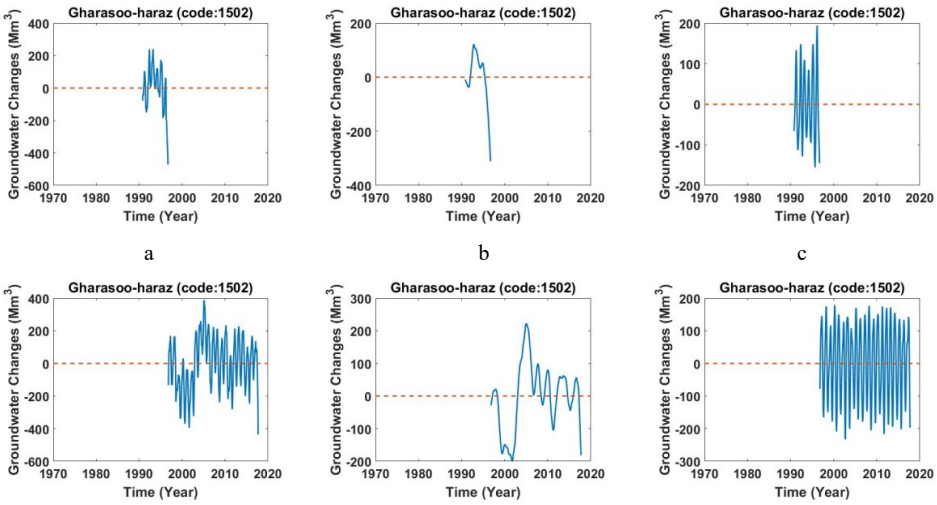

Figure C.25. a,d) Monthly values of groundwater storage, b,e) long-period of monthly values of groundwater storage, c,f) short-period of monthly values of groundwater storage across study area of Ghaemshahr-Joibar (Code: 1502).

C.5.3. Study area of Sari-Neka (Code: 1503)

This area is located between 35°56′-36°52′ N and 52°34′-54°44′ E with an area of 6938.5 km^2. Figure C.26 shows changes in monthly values of groundwater storage inferred from the well data, its long-period and short-period.

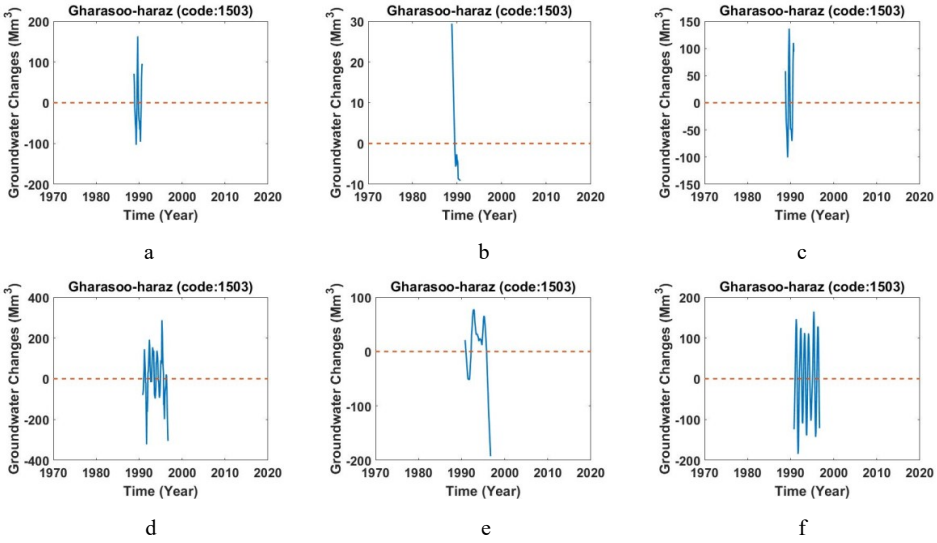

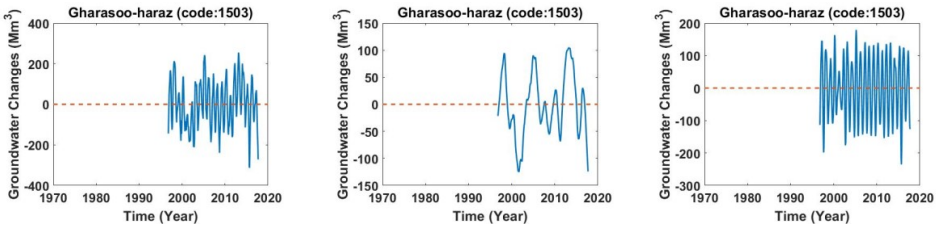

g h i

Figure C.26. a,d,g) Monthly values of groundwater storage, b,e,h) long-period of monthly values of groundwater storage, c,f,i) short-period of monthly values of groundwater storage across study area of Sari-Neka (Code: 1503).

C.5.4. Study area of Behshar-bandargaz (Code: 1504)

This area is located between 36°37′-36°56′ N and 53°19′-54°05′ E with an area of 1730.5 km^2. Figure C.27 shows changes in monthly values of groundwater storage inferred from the well data, its long-period and short-period.

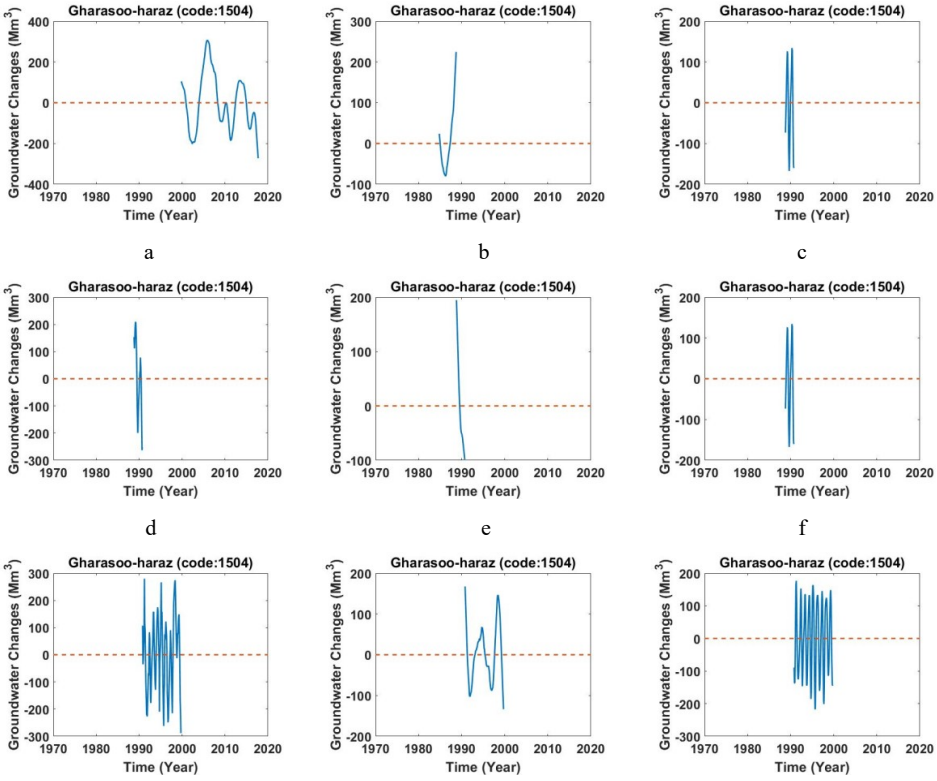

a b c

d e f

g h i

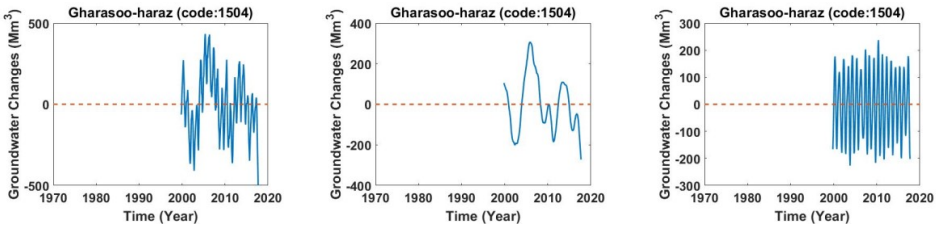

Figure C.27. a,d,g,j) Monthly values of groundwater storage, b,e,h,k) long-period of monthly values of groundwater storage, c,f,i,l) short-period of monthly values of groundwater storage across study area of Behshar-bandargaz (Code: 1504).

C.6.1. Study area of Gorgan (Code: 1601)

This area is located between 36°35′-37°55′ N and 54°-56° E with an area of 11505.5 km^2. Figure 5.28 shows changes in monthly values of groundwater storage inferred from the well data, its long-period and short-period.

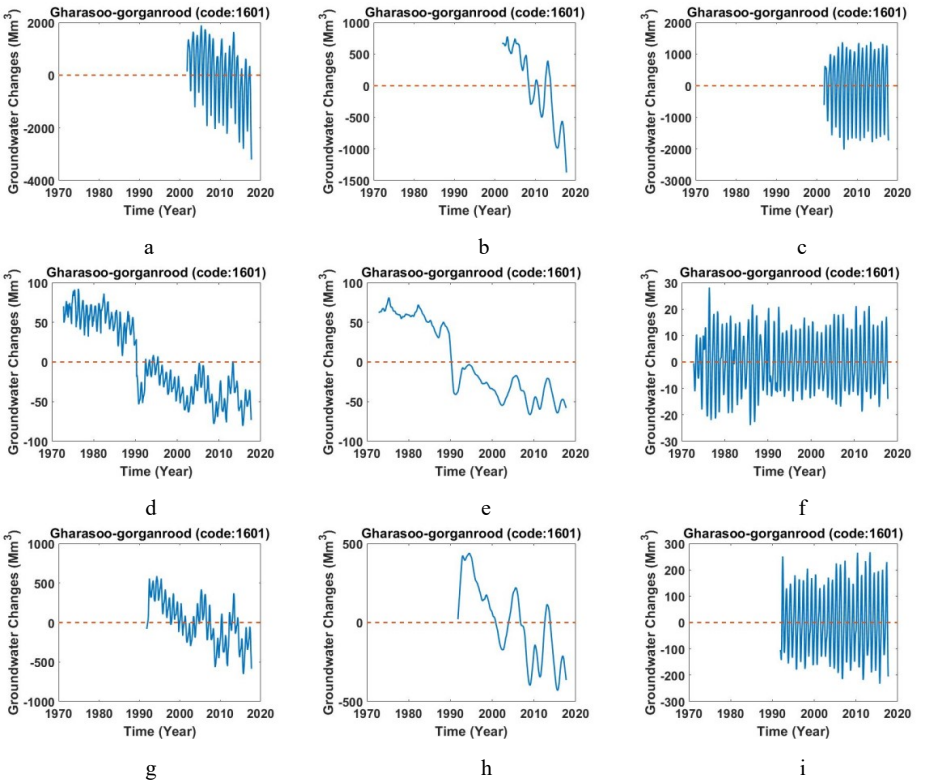

Figure 5.28. a) Monthly values of groundwater storage, b) long-period of monthly values of groundwater storage, c) short-period of monthly values of groundwater storage across study area of Gorgan (Code: 1601).

C.7.1. Study area of Dashli-incheboron (Code: 1701)

This area is located between 37°5′-38°5′ N and 53°55′-55°30′ E. Figure 5.29 shows changes in monthly values of groundwater storage inferred from the well data, its long-period and short-period.

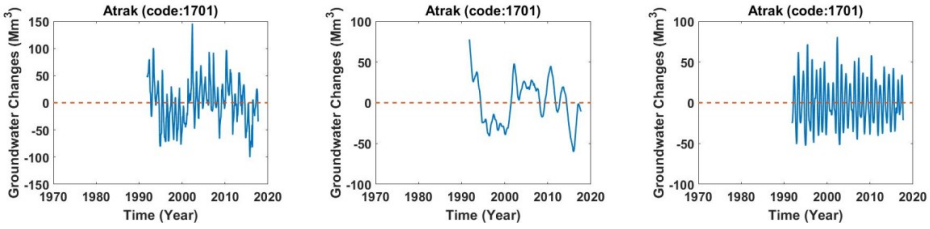

a b c

Figure C.29 a) Monthly values of groundwater storage, b) long-period of monthly values of groundwater storage, c) short-period of monthly values of groundwater storage across study area of Dashli-incheboron (Code: 1701).

C.7.2. Study area of Marave Tape (Code: 1703)

This area is located between 37°45′-38°15′ N and 55°34′-56°30′ E. Figure C.30 shows changes in monthly values of groundwater storage inferred from the well data, its long-period and short-period.

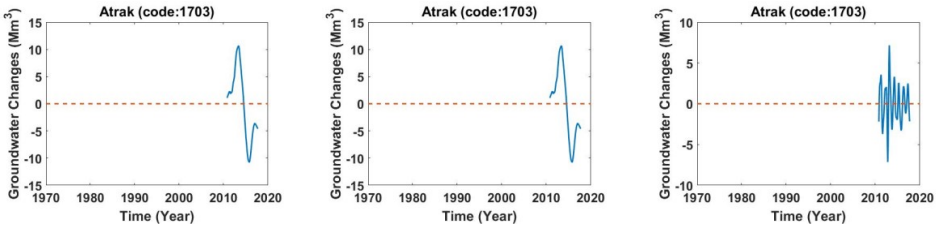

a b c

Figure C.30. a) Monthly values of groundwater storage, b) long-period of monthly values of groundwater storage, c) short-period of monthly values of groundwater storage across study area of Marave Tape (Code: 1703).

C.7.3. Study area of Somlaghan (Code: 1706)

This area is located between 37°20′-37°40′ N and 56°30′-57°05′ E with an area of 1148.52 km^2. Figure C.31 shows changes in monthly values of groundwater storage inferred from the well data, its long-period and short-period.

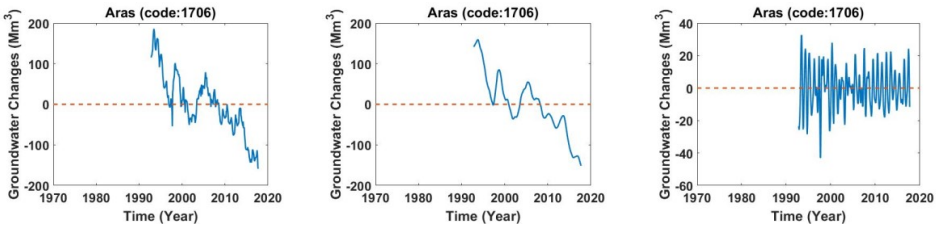

a b c

Figure C.31. a) Monthly values of groundwater storage, b) long-period of monthly values of groundwater storage, c) short-period of monthly values of groundwater storage across study area of Somlaghan (Code: 1706).

C.7.4. Study area of Bojnoord (Code: 1707)

This area is located between 37˚20′-37˚40′ N and 56˚30′-57˚05′ E with an area of 1266.75 km^2. Figure C.32 shows changes in monthly values of groundwater storage inferred from the well data, its long-period and short-period.

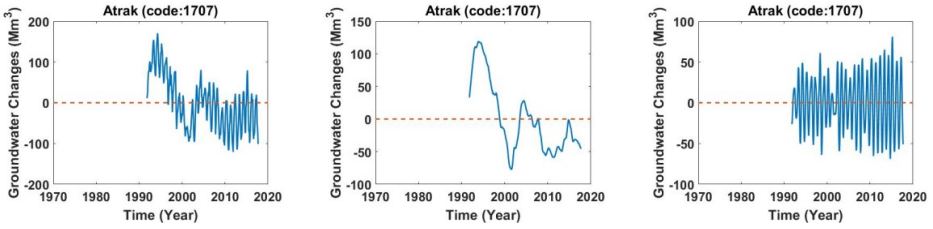

a b c

Figure C.32. a) Monthly values of groundwater storage, b) long-period of monthly values of groundwater storage, c) short-period of monthly values of groundwater storage across study area of Bojnoord (Code: 1707).

C.7.5. Study area of Ghochan-shirvan (Code: 1708)

This area is located between 36˚55′-37˚40′ N and 57˚30′-59˚05′ E with an area of 5538.78 km^2. Figure C.33 shows changes in monthly values of groundwater storage inferred from the well data, its long-period and short-period.

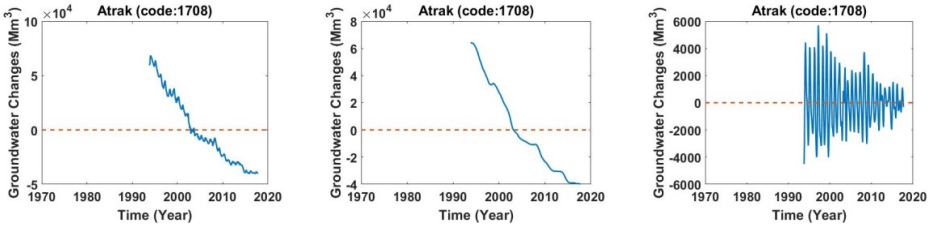

a b c

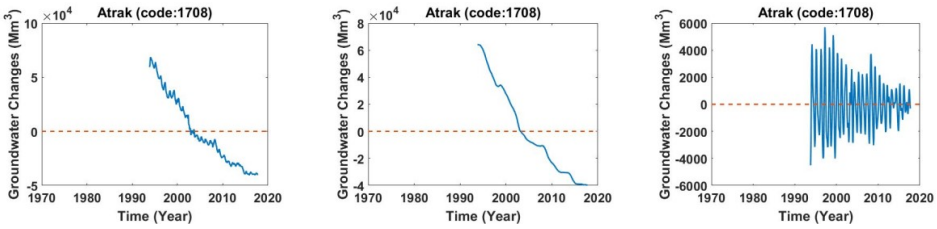

d e f

Figure C.33. a,d) Monthly values of groundwater storage, b,e) long-period of monthly values of groundwater storage, c,f) short-period of monthly values of groundwater storage across study area of Ghochan-shirvan (Code: 1708).

Appendix D

D.1.1. Study area of Khaf (Code: 5101)

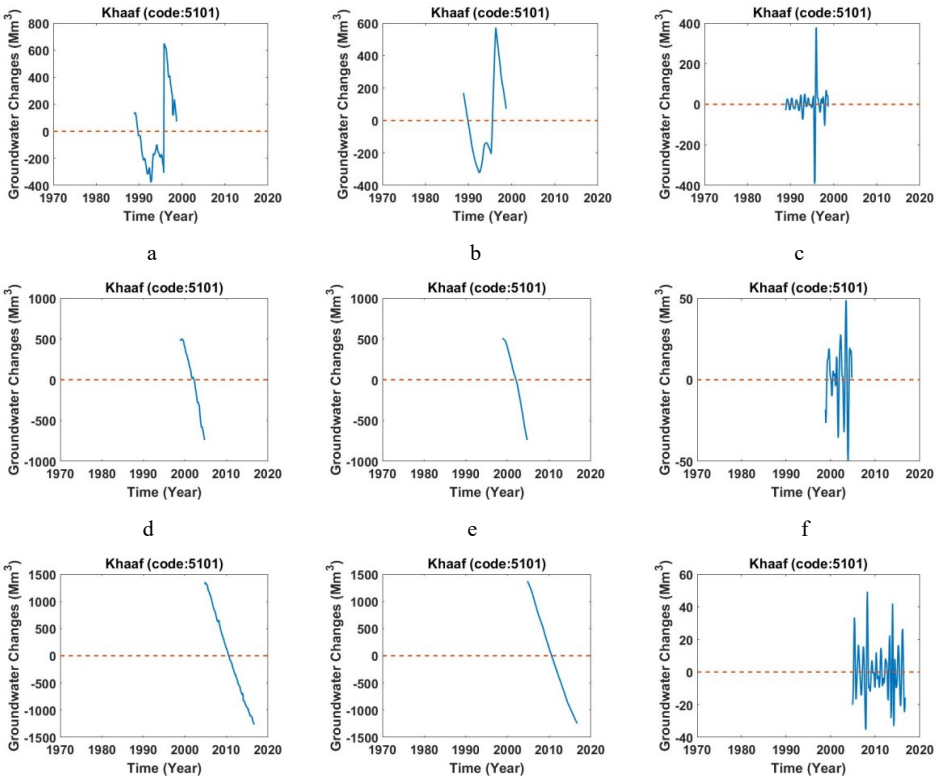

Figure D.1. a,d,g) Monthly values of groundwater storage, b,e,h) long-period of monthly values of groundwater storage, c,f,i) short-period of monthly values of groundwater storage across study area of (Code: 5101).

D.1.2. Study area of Zozan (Code: 5102)

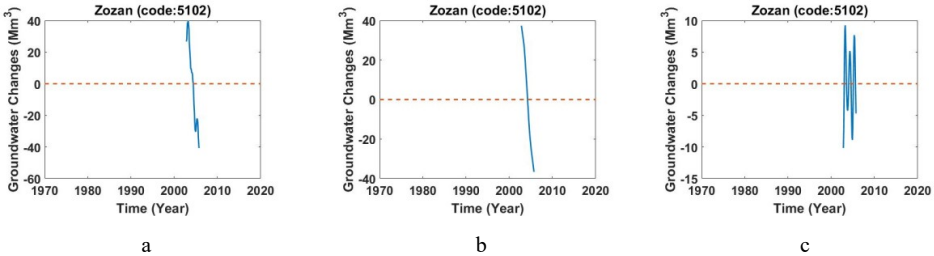

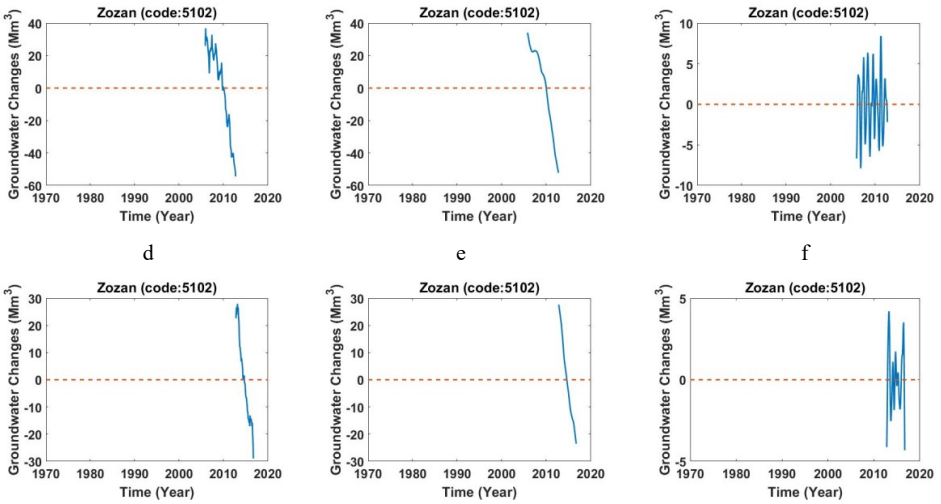

Figure D.2. a,d,g) Monthly values of groundwater storage, b,e,h) long-period of monthly values of groundwater storage, c,f,i) short-period of monthly values of groundwater storage across study area of (Code: 5102).

D.1.3. Study area of Gisoor (Code: 5103)

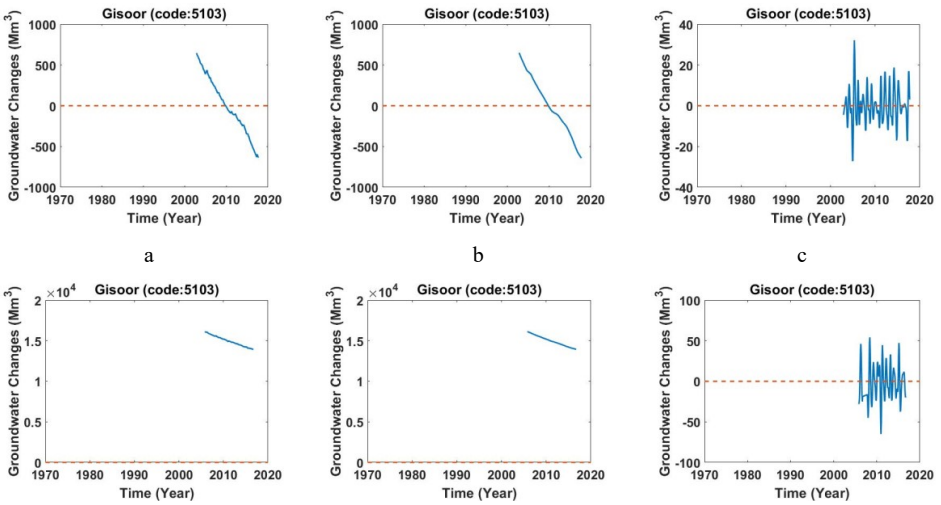

Figure D.3. a,d) Monthly values of groundwater storage, b,e) long-period of monthly values of groundwater storage, c,f) short-period of monthly values of groundwater storage across study area of Gisoor (Code: 5103).

D.1.4. Study area of Asafdan (Code: 5104)

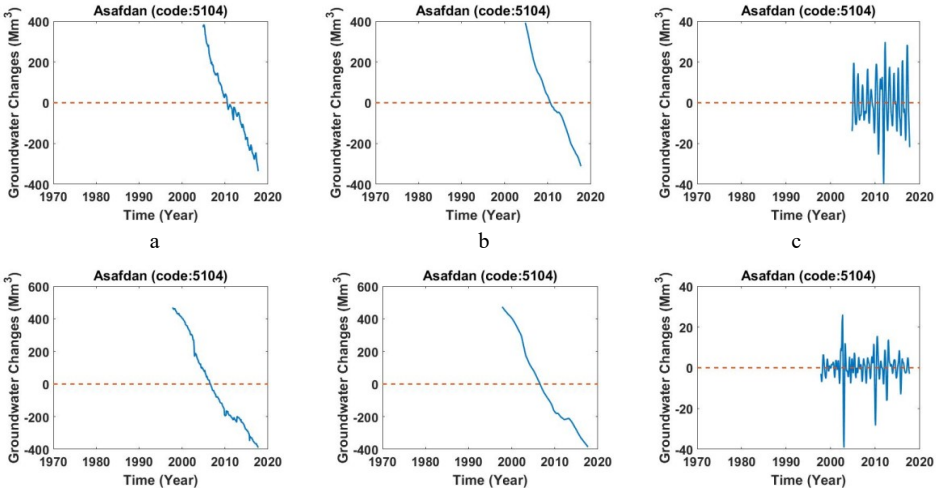

Figure D.4. a,d) Monthly values of groundwater storage, b,e) long-period of monthly values of groundwater storage, c,f) short-period of monthly values of groundwater storage across study area of Asefdan(Code: 5104).

D.1.5. Study area of Ghaen (Code: 5105)

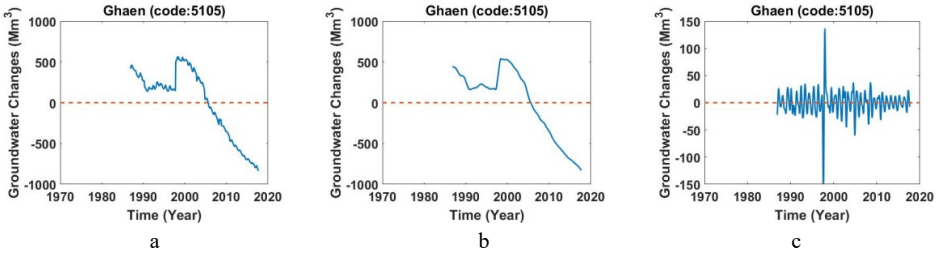

Figure D.5. a) Monthly values of groundwater storage, b) long-period of monthly values of groundwater storage, c) short-period of monthly values of groundwater storage across study area of Ghaen (Code: 5105).

D.1.6. Study area of Ghaenat (Code: 5106)

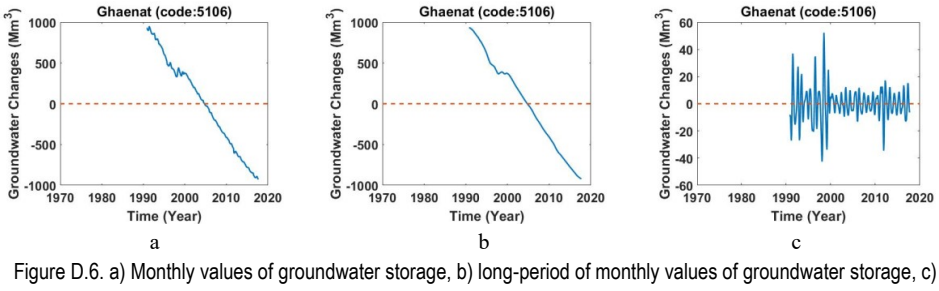

Figure D.6. a) Monthly values of groundwater storage, b) long-period of monthly values of groundwater storage, c) short-period of monthly values of groundwater storage across study area of Ghaenat (Code: 5106).

D.1.7. Study area of Shahrakht-Degh Petergan (Code: 5108)

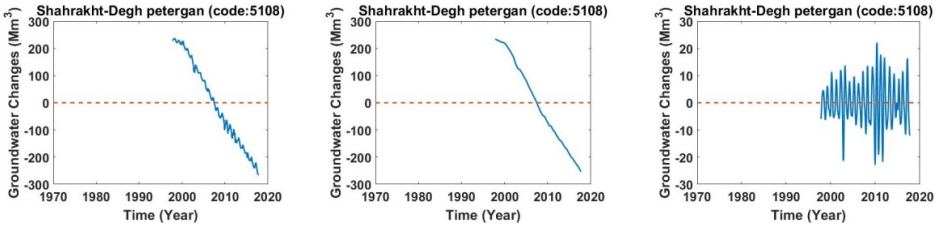

a b c

Figure D.7. a) Monthly values of groundwater storage, b) long-period of monthly values of groundwater storage, c) short-period of monthly values of groundwater storage across study area of Shahrakht-Degh Petergan (Code: 5108).

D.1.8. Study area of Gazik-Avaz (Code: 5110)

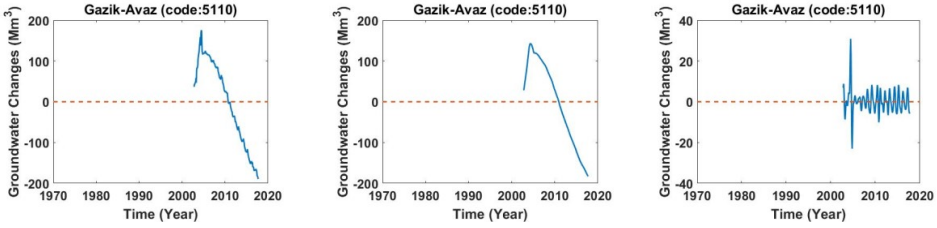

a b c

Figure D.8. a) Monthly values of groundwater storage, b) long-period of monthly values of groundwater storage, c) short-period of monthly values of groundwater storage across study area of Gazik-Avaz (Code: 5110).

D.1.9. Study area of Darmian-Asadabad (Code: 5111)

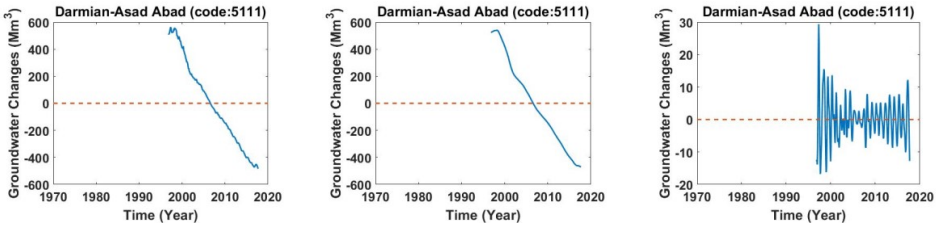

a b c

Figure D.9. a) Monthly values of groundwater storage, b) long-period of monthly values of groundwater storage, c) short-period of monthly values of groundwater storage across study area of Darmian-Asadabad (Code: 5111).

D.1.10. Study area of (Code: 5112)

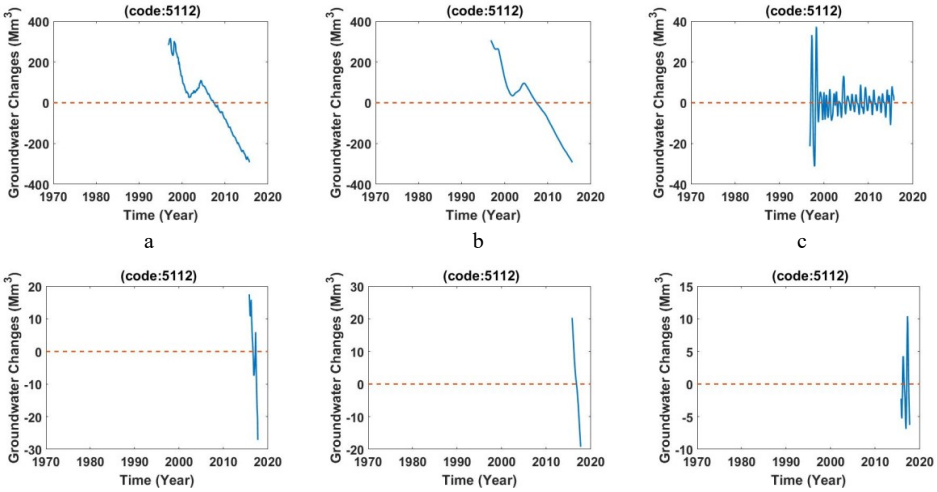

Figure D.10. a,d) Monthly values of groundwater storage, b,e) long-period of monthly values of groundwater storage, c,f) short-period of monthly values of groundwater storage across study area of (Code: 5112).

D.2.1. Study area of Dorah (Code: 5201)

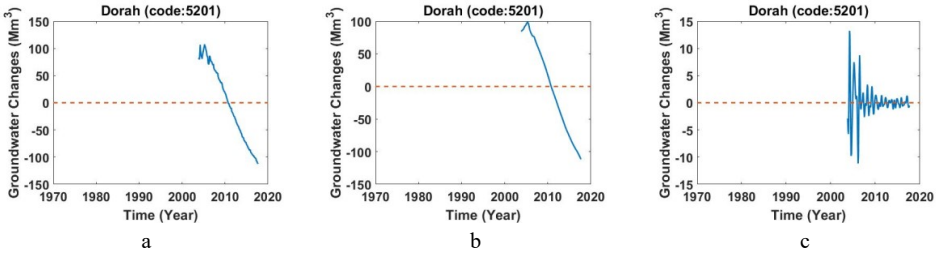

Figure D.11. a) Monthly values of groundwater storage, b) long-period of monthly values of groundwater storage, c) short-period of monthly values of groundwater storage across study area of Dorah (Code: 5201).

D.2.2. Study area of Hossein Abad (Code: 5202)

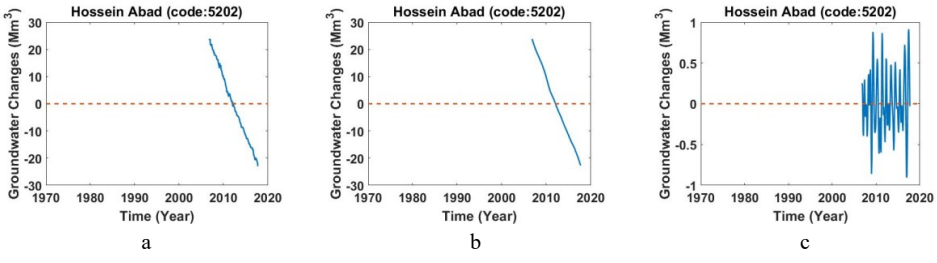

Figure D.12. a) Monthly values of groundwater storage, b) long-period of monthly values of groundwater storage, c) short-period of monthly values of groundwater storage across study area of Hosein Abad (Code: 5202).

D.2.3. Study area of Sarbishe (Code: 5203)

This area divided to two parts.

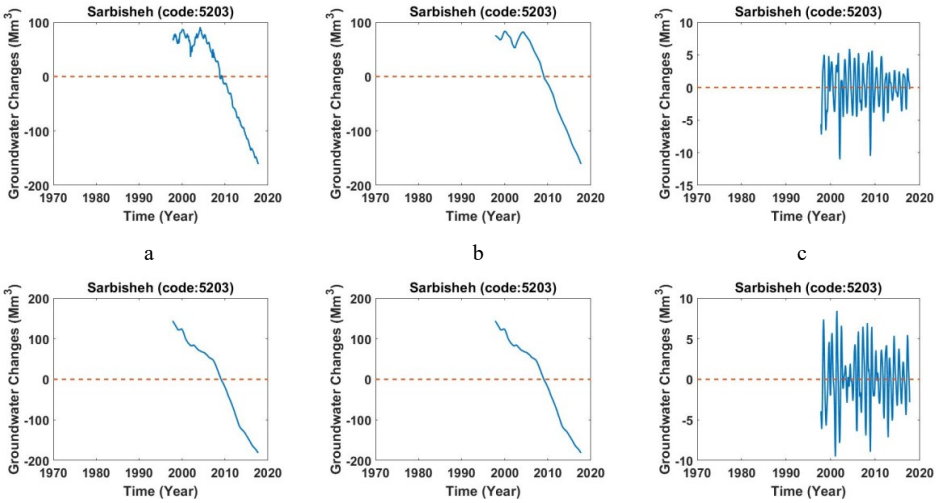

Figure D.13. a,b) Monthly values of groundwater storage, b,e) long-period of monthly values of groundwater storage, c,f) short-period of monthly values of groundwater storage across study area of Sarbishe (Code: 5203).

D.2.4. Study area of Hamoon-Hirmand (Code: 5204)

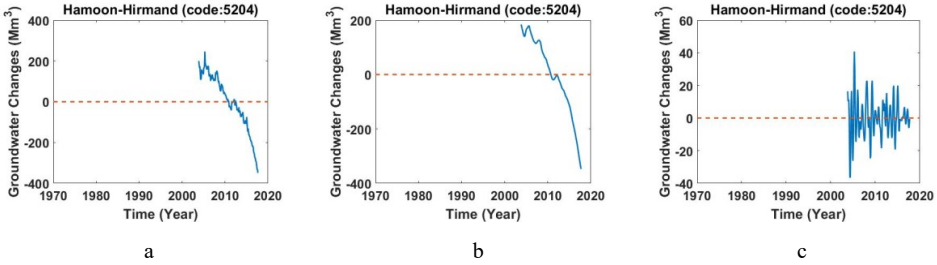

Figure D.14. a) Monthly values of groundwater storage, b) long-period of monthly values of groundwater storage, c) short-period of monthly values of groundwater storage across study area of Hamoon-Hirmand (Code: 5204).

D.2.5. Study area of Hermak (Code: 5208)

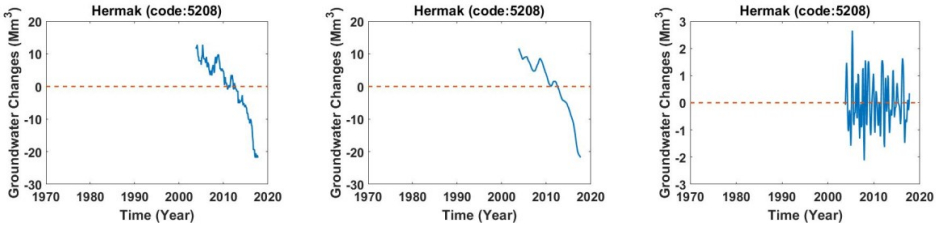

a b c

Figure D.15. a) Monthly values of groundwater storage, b) long-period of monthly values of groundwater storage, c) short-period of monthly values of groundwater storage across study area of Hermak (Code: 5208).

D.2.6. Study area of Zahedan (Code: 5209)

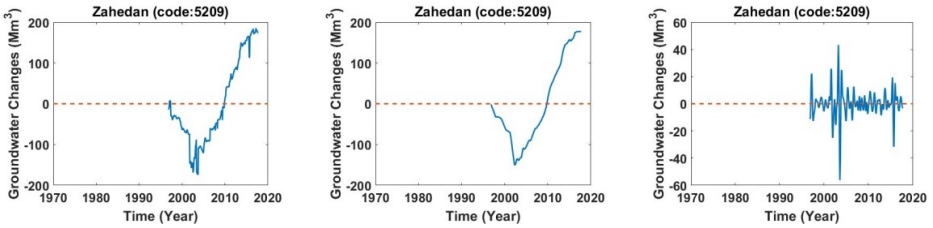

a b c

Figure D.16. a) Monthly values of groundwater storage, b) long-period of monthly values of groundwater storage, c) short-period of monthly values of groundwater storage across study area of zahedan (Code: 5209).

D.3.1. Study area of Tahlab (Code: 5302)

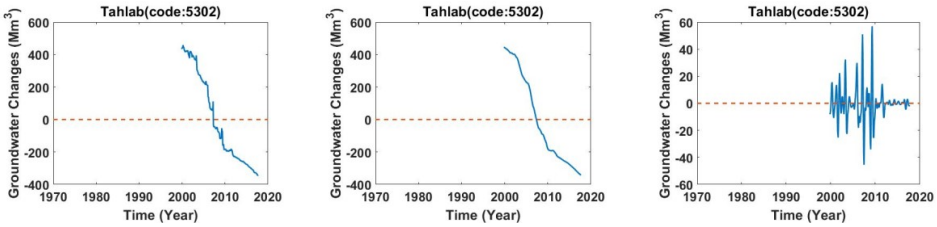

a b c

Figure D.17. a) Monthly values of groundwater storage, b) long-period of monthly values of groundwater storage, c) short-period of monthly values of groundwater storage across study area of Tahlab (Code: 5302).

D.3.2. Study area of Khash (Code: 5303)

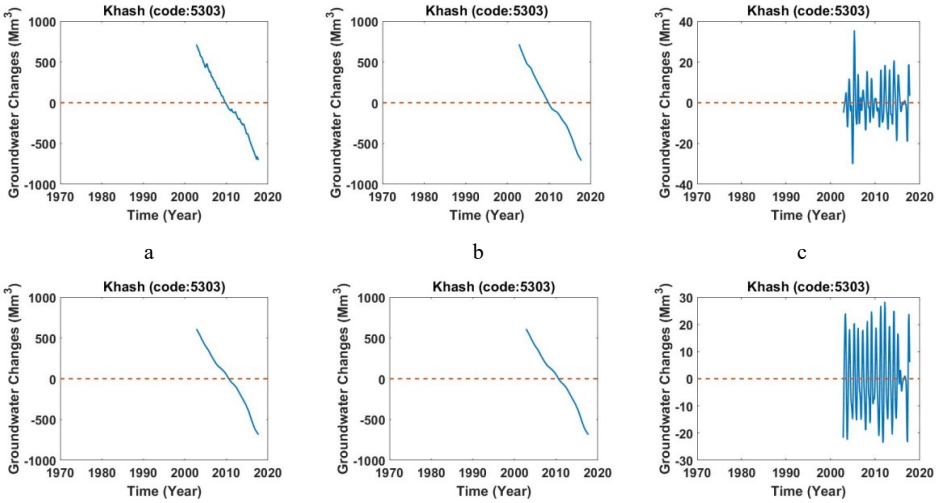

Figure D.18. a,d) Monthly values of groundwater storage, b,e) long-period of monthly values of groundwater storage, c,f) short-period of monthly values of groundwater storage across study area of Khash (Code: 5303).

D.3.3. Study area of Mir Jave (Code: 5304)

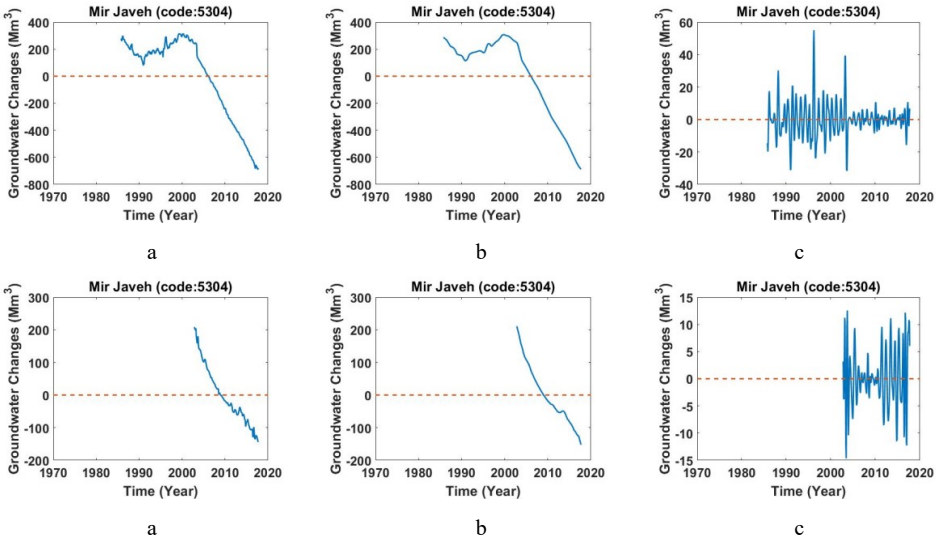

Figure D.19. a,d) Monthly values of groundwater storage, b,e) long-period of monthly values of groundwater storage, c,f) short-period of monthly values of groundwater storage across study area of Mir Jave (Code: 5304).

D.3.4. Study area of Ladiz (Code: 5305)

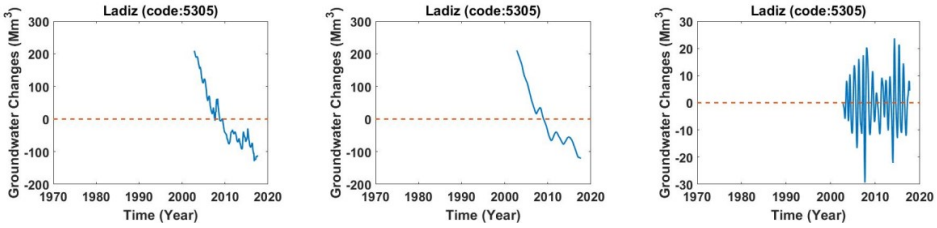

a b c

Figure D.20. a) Monthly values of groundwater storage, b) long-period of monthly values of groundwater storage, c) short-period of monthly values of groundwater storage across study area of Ladiz (Code: 5305).

D.3.5. Study area of Ladiz (Code: 5307)

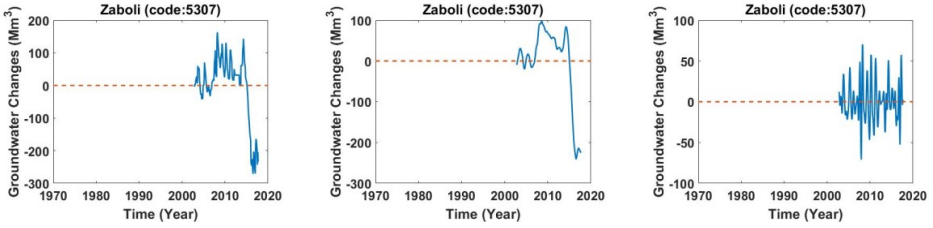

a b c

Figure D.21. a) Monthly values of groundwater storage, b) long-period of monthly values of groundwater storage, c) short-period of monthly values of groundwater storage across study area of Ladiz (Code: 5307).

D.3.6. Study area of Saravan (Code: 5308)

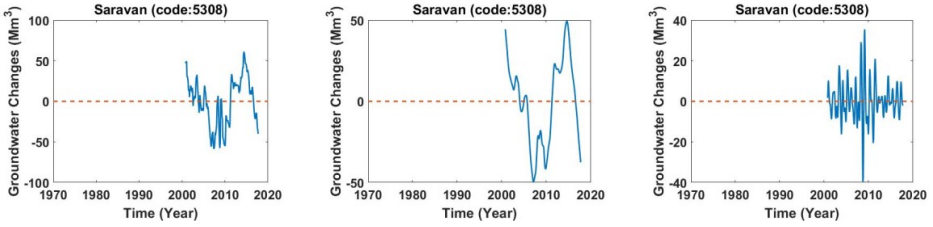

a b c

Figure D.22. a) Monthly values of groundwater storage, b) long-period of monthly values of groundwater storage, c) short-period of monthly values of groundwater storage across study area of Saravan (Code: 5308).

D.3.7. Study area of Sibosoran (Code: 5309)

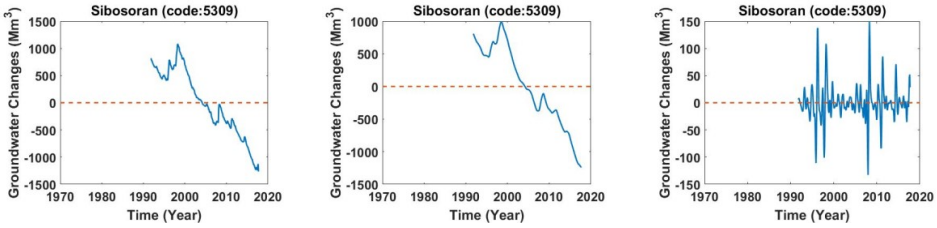

a b c

Figure D.23. a) Monthly values of groundwater storage, b) long-period of monthly values of groundwater storage, c) short-period of monthly values of groundwater storage across study area of Sibosoran (Code: 5309).

Appendix E

E.1. Study area of Daregaz (code 6001)

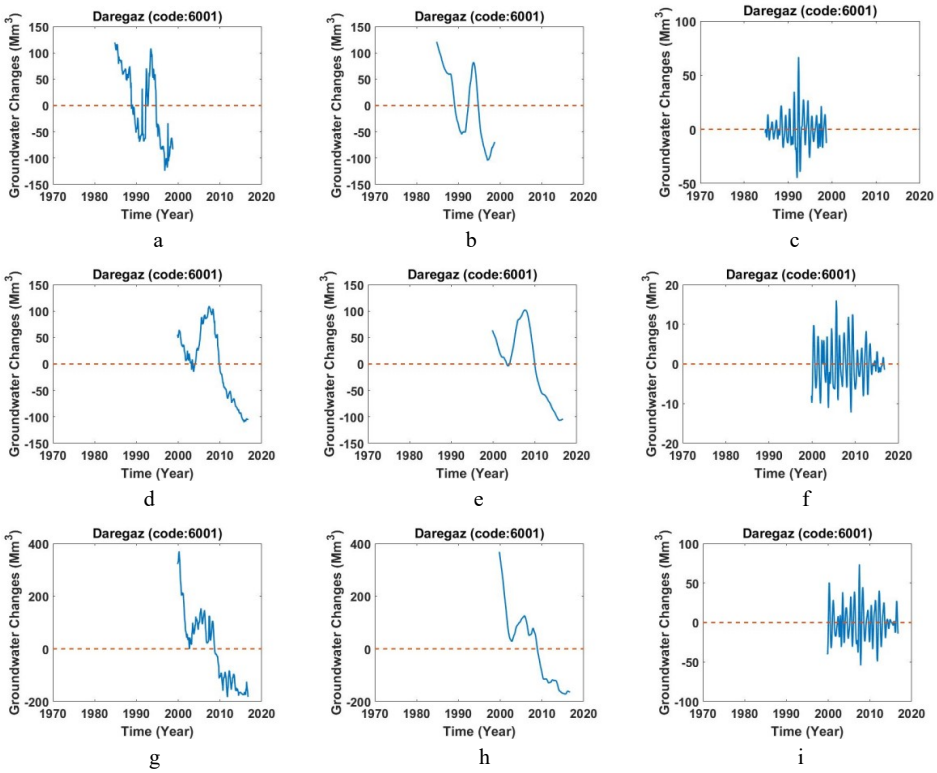

Figure E.1. a,d,g) Monthly values of groundwater storage, b,e,h) long-period of monthly values of groundwater storage, c,f,i) short-period of monthly values of groundwater storage across study area of Dareagaz (Code: 6001).

E.2. Study area of Sarakhs (Code: 6004)

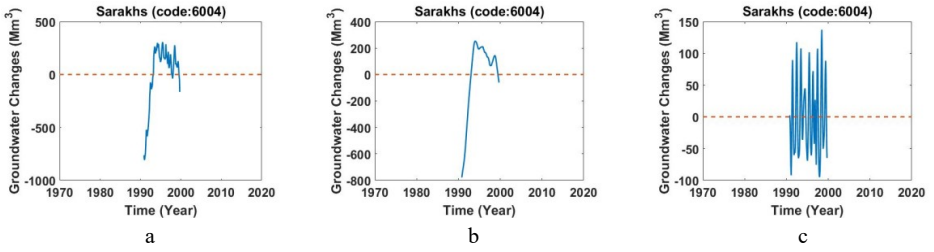

Figure E.2. a) Monthly values of groundwater storage, b) long-period of monthly values of groundwater storage, c) short-period of monthly values of groundwater storage across study area of Sarakhs (Code: 6004).

E.3. Study area of Narimani (Code: 6006)

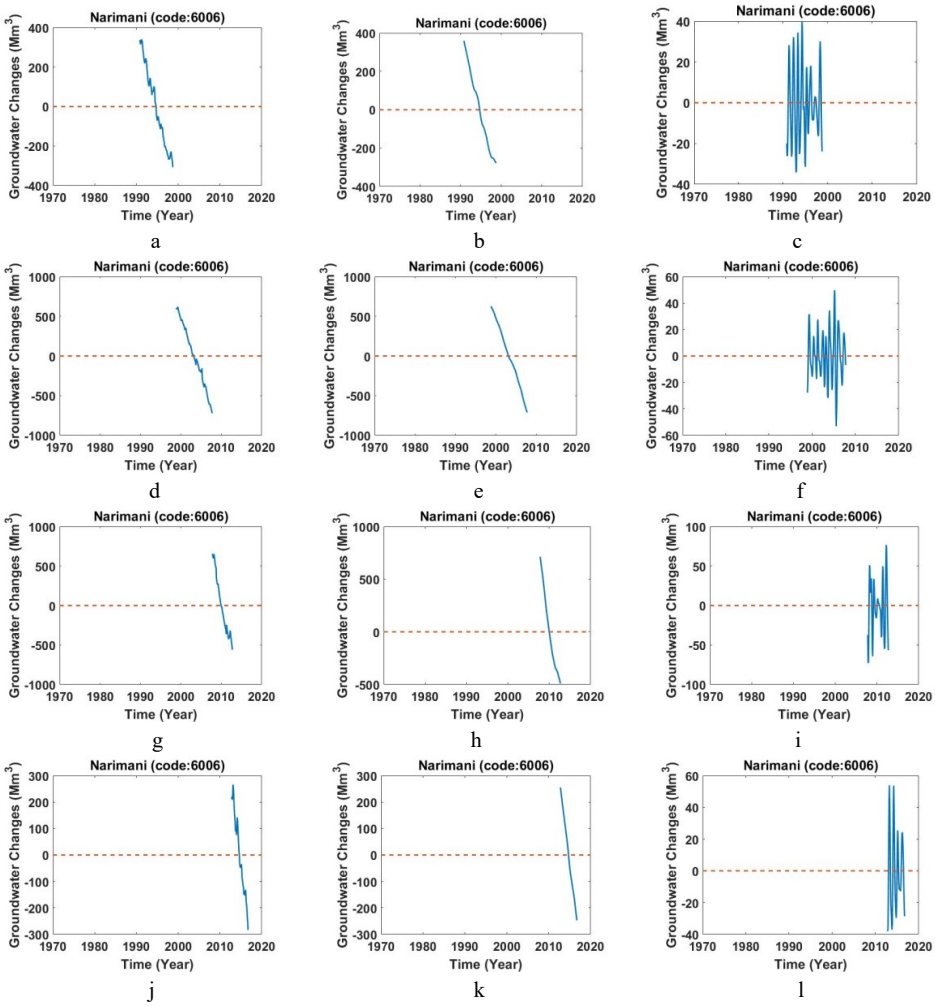

Figure E.3. a,d,g,j) Monthly values of groundwater storage, b,e,h,k) long-period of monthly values of groundwater storage, c,f,i,l) short-period of monthly values of groundwater storage across study area of Narimani (Code: 6006).

E.4. Study area of Mashhad (Code: 6007)

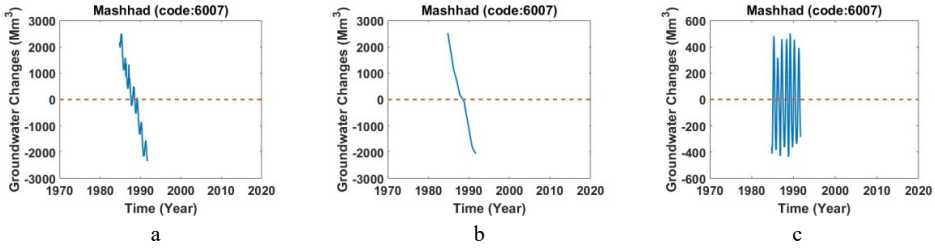

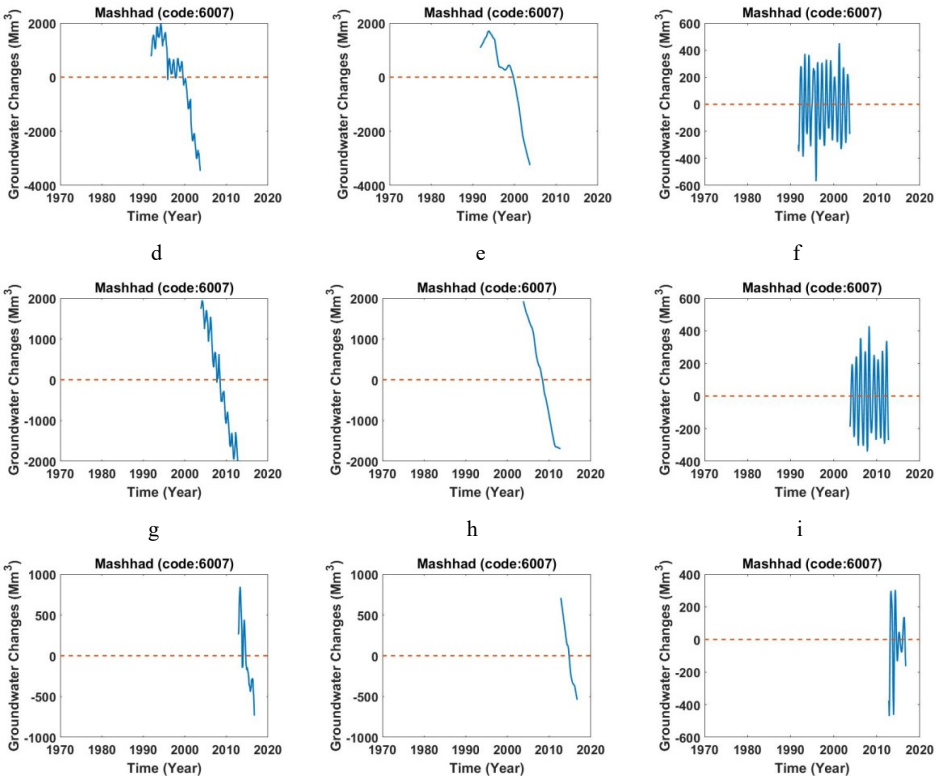

Figure E.4. a,d,g,j) Monthly values of groundwater storage, b,e,h,k) long-period of monthly values of groundwater storage, c,f,i,l) short-period of monthly values of groundwater storage across study area of Mashhad (Code: 6007).

E.5. Study area of Saleh Abad-Janat-Abad (Code: 6009)

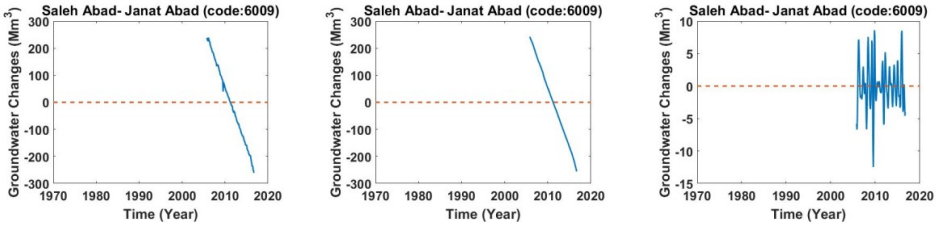

Figure E.5. a) Monthly values of groundwater storage, b) long-period of monthly values of groundwater storage, c) short-period of monthly values of groundwater storage across study area of Saleh Abad-Janat-Abad (Code: 6009).

E.6. Study area of Fariman-Torbatejam (Code: 6010)

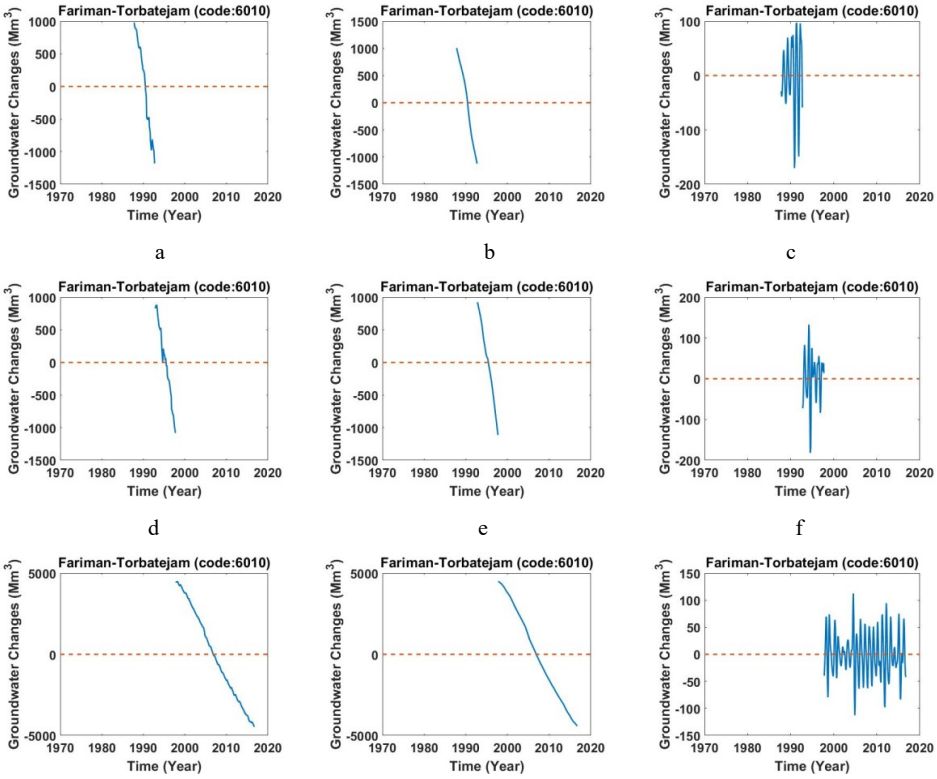

Figure E.6. a,d,g) Monthly values of groundwater storage, b,e,h) long-period of monthly values of groundwater storage, c,f,i) short-period of monthly values of groundwater storage across study area of Fariman-Torbatejam (Code: 6010).

E.7. Study area of Taybad (Code: 6011)

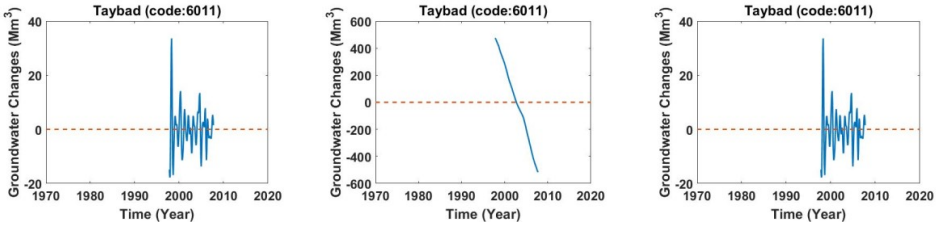

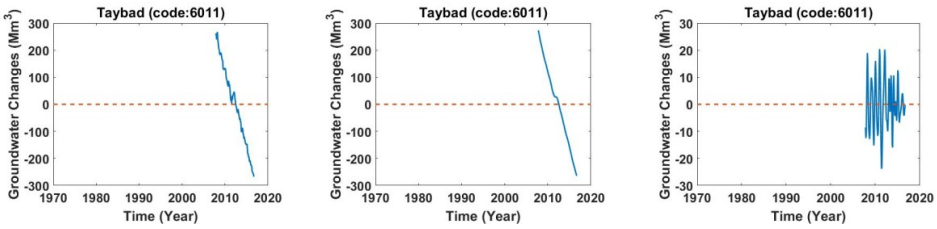

d e f

Figure E.7. a,d) Monthly values of groundwater storage, b,e) long-period of monthly values of groundwater storage, c,f) short-period of monthly values of groundwater storage across study area of Taybad (Code: 6011).

E.8. Study area of Shahreno-Bakhazar (Code: 6012)

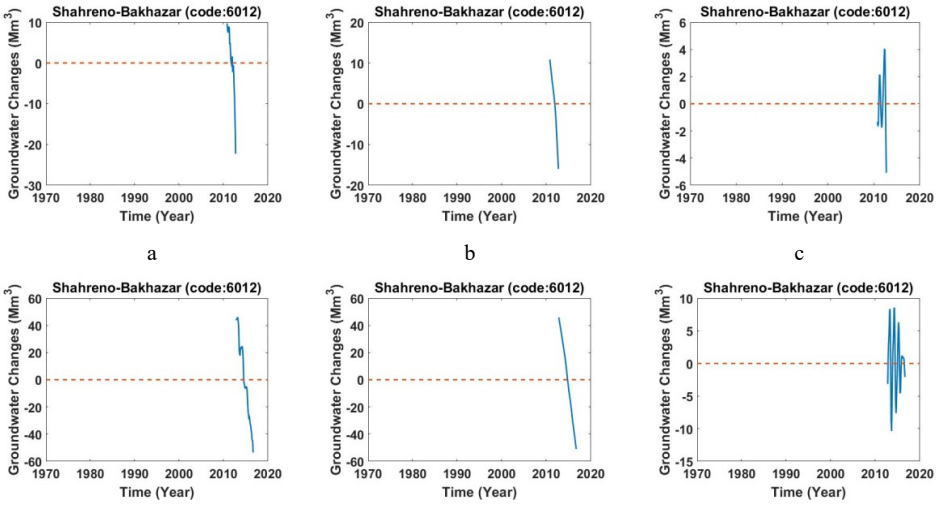

a b c

d e f

Figure E.8. a,d) Monthly values of groundwater storage, b,e) long-period of monthly values of groundwater storage, c,f) short-period of monthly values of groundwater storage across study area of Shahreno-Bakhazar (Code: 6012).

E.9. Study area of Karat (Code: 6013)

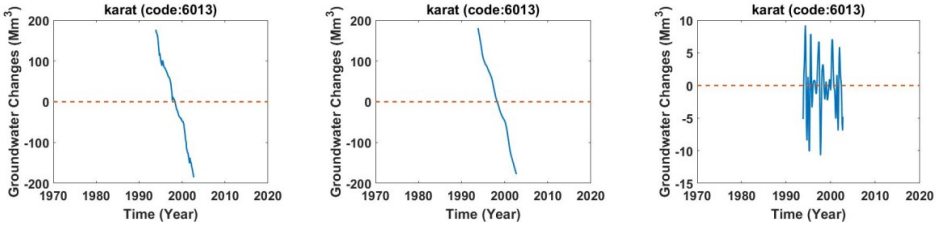

a b c

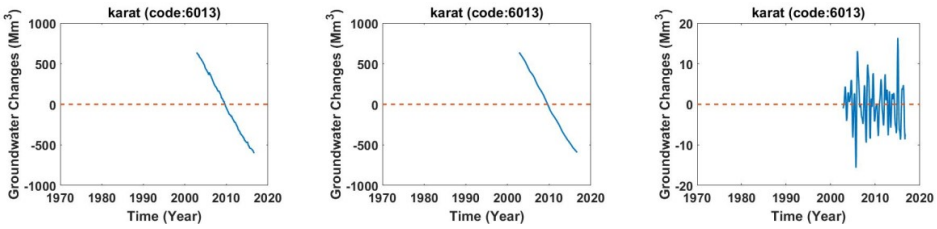

d e f

Figure E.9. a,d) Monthly values of groundwater storage, b,e) long-period of monthly values of groundwater storage, c,f) short-period of monthly values of groundwater storage across study area of Karat (Code: 6013).

Appendix F

F.1.1. Study area of Ghezelche (Code: 2101)

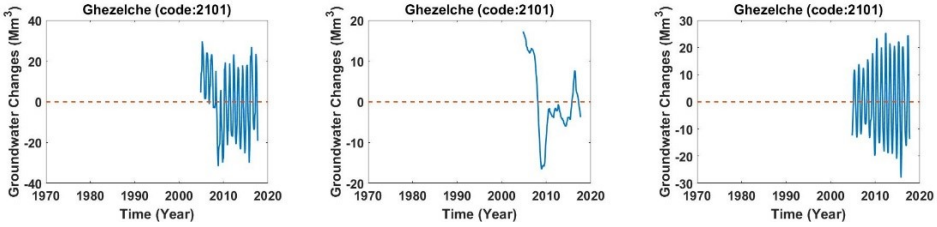

a b c

Figure F.1. a) Monthly values of groundwater storage, b) long-period of monthly values of groundwater storage, c) short-period of monthly values of groundwater storage across study area of Saleh Ghezelche (Code: 2101).

F.1.2. Study area of Piran Shahr (Code: 2104)

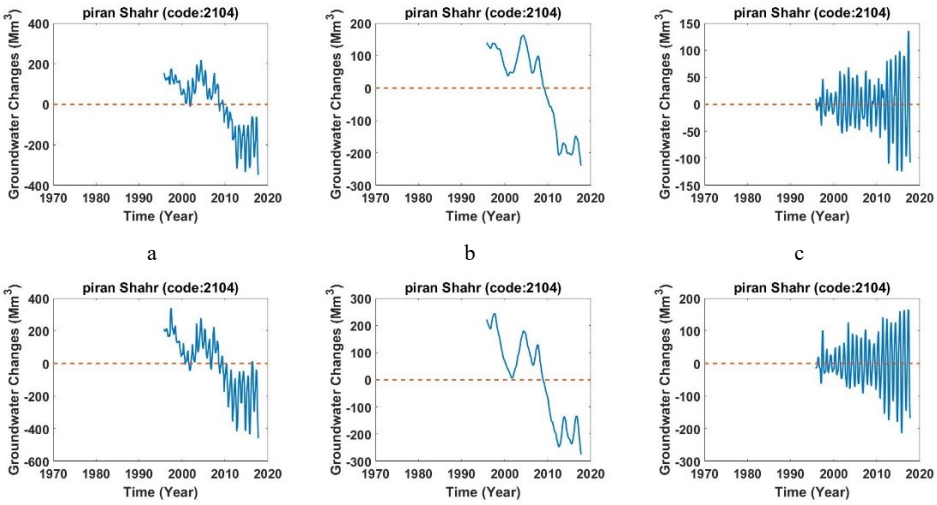

a b c

a b c

Figure F.2. a,d) Monthly values of groundwater storage, b,e) long-period of monthly values of groundwater storage, c,f) short-period of monthly values of groundwater storage across study area of Piran Shahr(Code: 2104).

F.1.3. Study area of Marivan (Code: 2109)

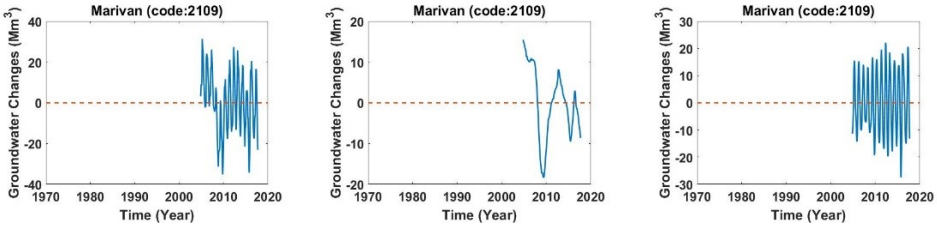

a b c

Figure F.3. a) Monthly values of groundwater storage, b) long-period of monthly values of groundwater storage, c) short-period of monthly values of groundwater storage across study area of Saleh Marivan (Code: 2109).

F.1.4. Study area of Tape Esmail-Amirabad (Code: 2111)

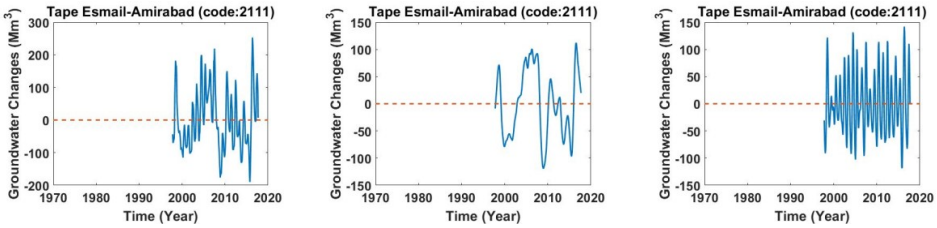

a b c

Figure F.4. a) Monthly values of groundwater storage, b) long-period of monthly values of groundwater storage, c) short-period of monthly values of groundwater storage across study area of Saleh Tape Esmail-Amirabad (Code: 2111).

F.1.F. Study area of Zahab (Code: 2113)

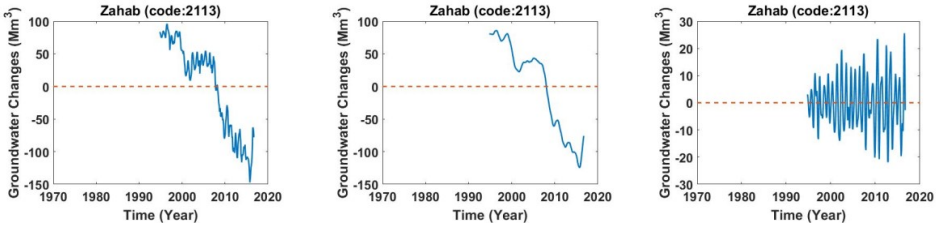

a b c

Figure F.5. a) Monthly values of groundwater storage, b) long-period of monthly values of groundwater storage, c) short-period of monthly values of groundwater storage across study area of Saleh Zahab (Code: 2113).

F.1.6. Study area of GilanGharb (Code: 2114)

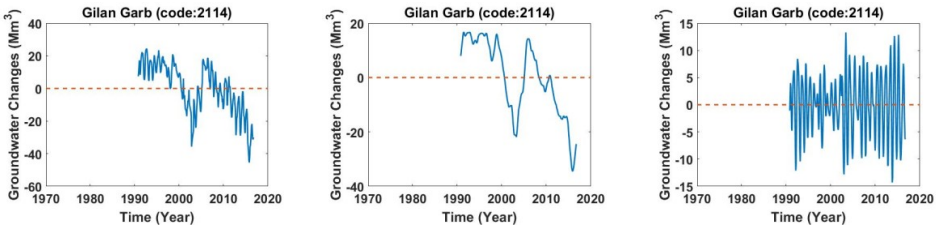

a b c

Figure F.6. a) Monthly values of groundwater storage, b) long-period of monthly values of groundwater storage, c) short-period of monthly values of groundwater storage across study area of Saleh Gilan Gharb (Code: 2114).

F.1.7. Study area of Ghasre shirin (Code: 2116)

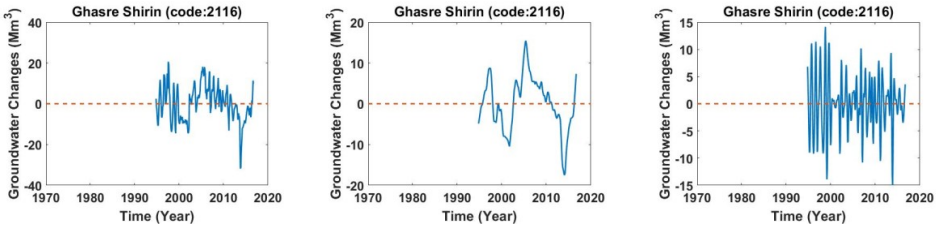

a b c

Figure F.7. a) Monthly values of groundwater storage, b) long-period of monthly values of groundwater storage, c) short-period of monthly values of groundwater storage across study area of Ghasre Shirin (Code: 2116).

F.1.8. Study area of Pole Zahab (Code: 2117)

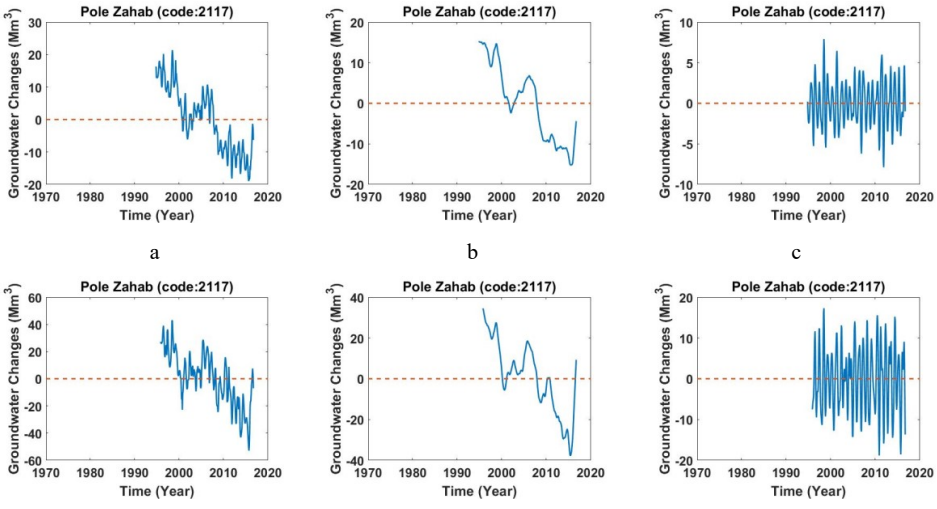

a b c

d e f

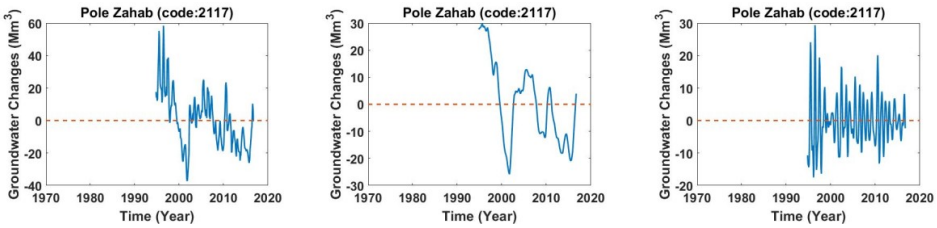

g h i

Figure F.8. a,d,g) Monthly values of groundwater storage, b,e,h) long-period of monthly values of groundwater storage, c,f,i) short-period of monthly values of groundwater storage across study area of Pole Zahab (Code: 2117).

F.1.9. Study area of Ivan –Somar (Code: 2118)

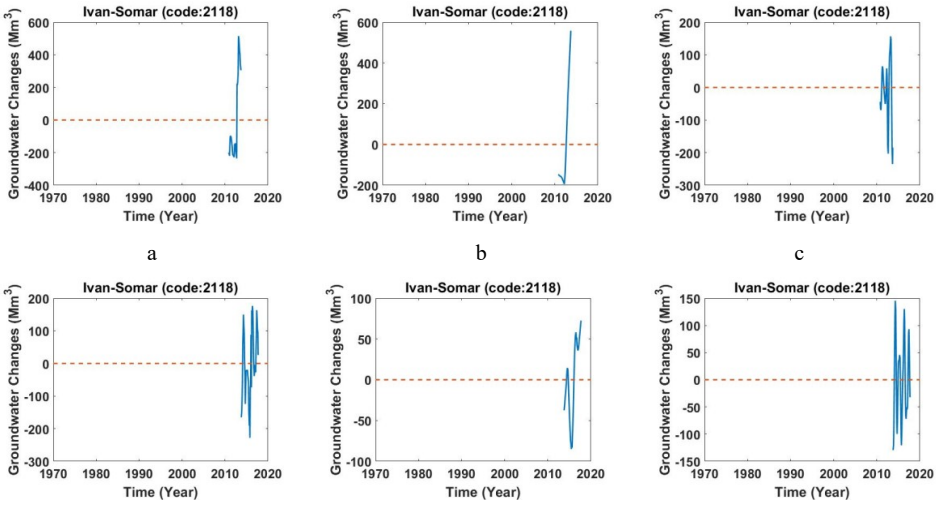

a b c

d e f

Figure F.9. a,d) Monthly values of groundwater storage, b,e) long-period of monthly values of groundwater storage, c,f) short-period of monthly values of groundwater storage across study area of Ivan-Somar (Code: 2118).

F.1.10. Study area of Salehabad (Code: 2120)

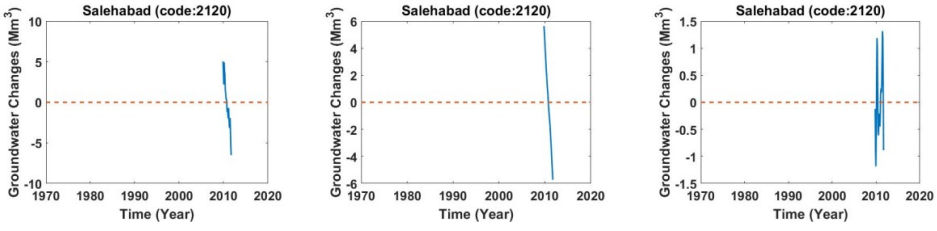

a b c

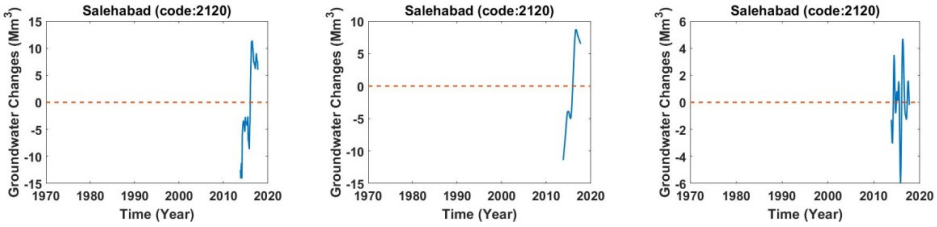

d e f

Figure F.10. a,d) Monthly values of groundwater storage, b,e) long-period of monthly values of groundwater storage, c,f) short-period of monthly values of groundwater storage across study area of Salehabad (Code: 2120).

F.1.11. Study area of Mehran (Code: 2121)

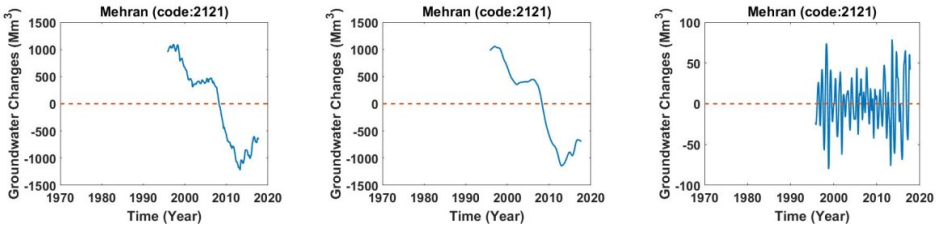

a b c

Figure F.11. a) Monthly values of groundwater storage, b) long-period of monthly values of groundwater storage, c) short-period of monthly values of groundwater storage across study area of Mehran (Code: 2121).

F.1.12. Study area of Dehloran (Code: 2122)

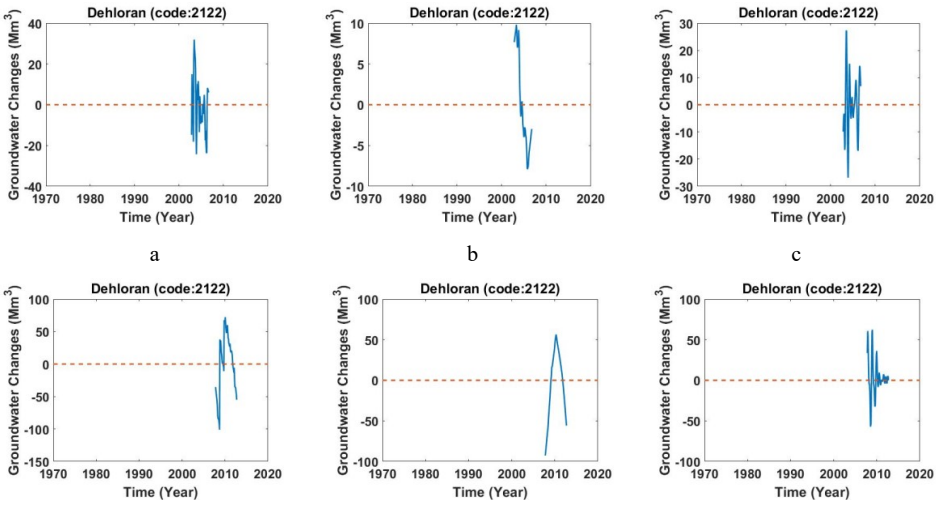

a b c

d e f

Figure F.12. a,d) Monthly values of groundwater storage, b,e) long-period of monthly values of groundwater storage, c,f) short-period of monthly values of groundwater storage across study area of Dehloran (Code: 2122).

F.1.13. Study area of Musian-Abdanan (Code: 2123)

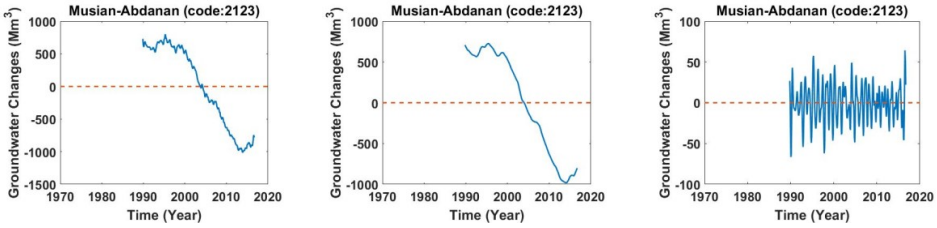

a b c

Figure F.13. a) Monthly values of groundwater storage, b) long-period of monthly values of groundwater storage, c) short-period of monthly values of groundwater storage across study area of Musian-Abdanan (Code: 2123).

F.1.14. Study area of Dasht Abbas (Code: 2124)

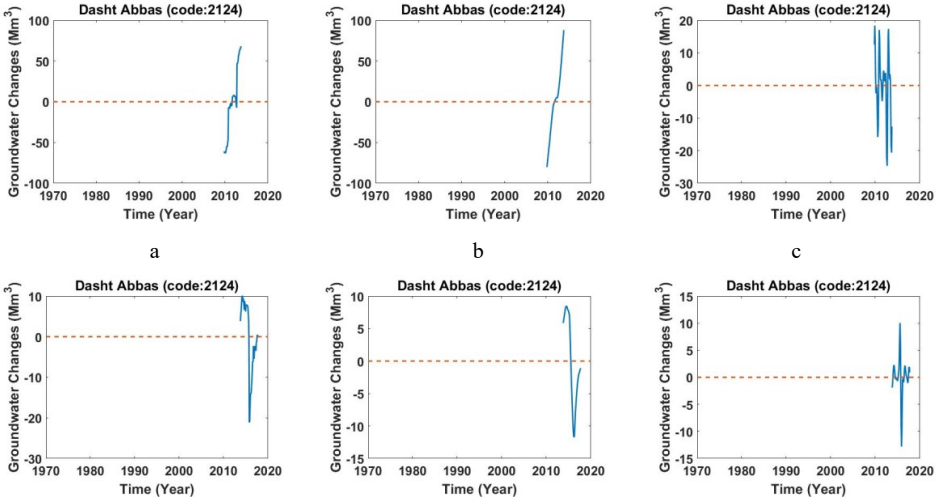

a b c

a b c

Figure F.14. a,d) Monthly values of groundwater storage, b,e) long-period of monthly values of groundwater storage, c,f) short-period of monthly values of groundwater storage across study area of Dasht Abbas (Code: 2124).

F.2.1. Study area of Dasht Azadegan (Code: 2201)

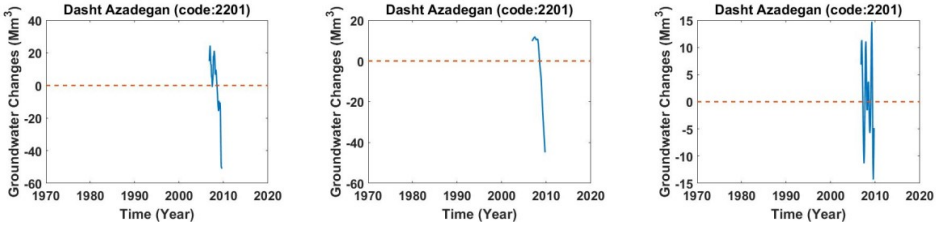

a b c

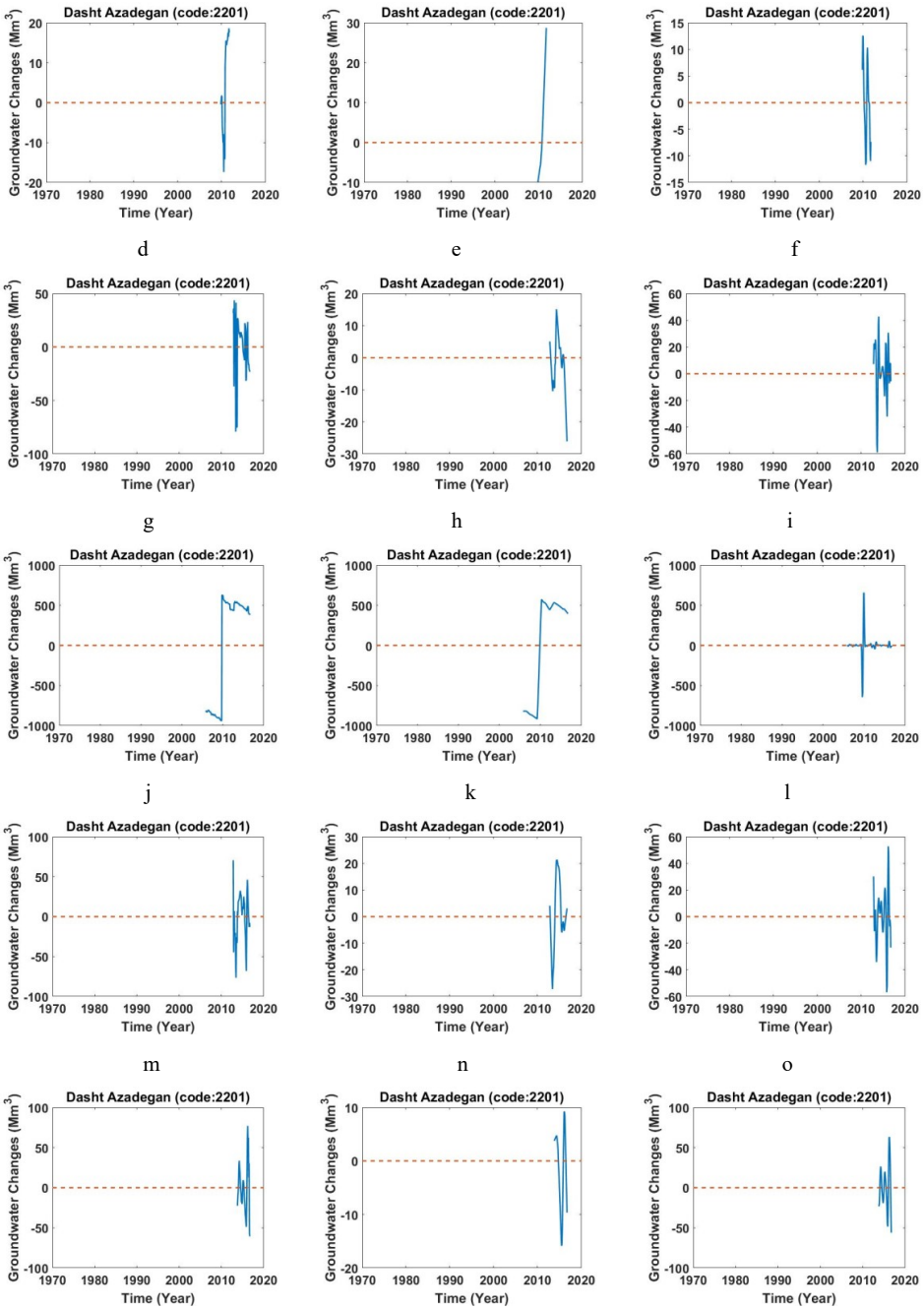

Figure F.15. a,d,g,j,m,p) Monthly values of groundwater storage, b,e,h,k,n,q) long-period of monthly values of groundwater storage, c,f,i,l,o,r) short-period of monthly values of groundwater storage across study area of Dasht Azadegan (Code: 2201).

F.2.2 Study area of Chananeh (Code: 2202)

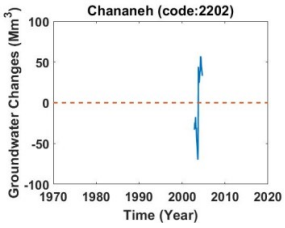

a

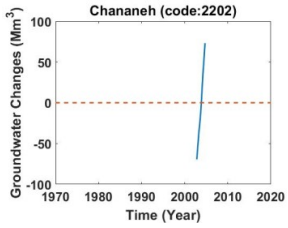

b

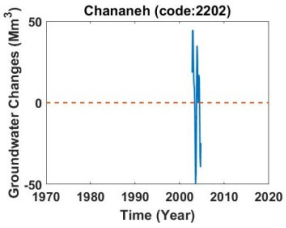

c

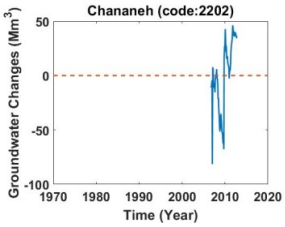

d

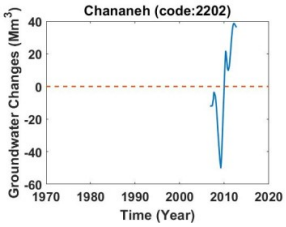

e

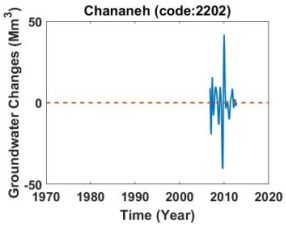

f

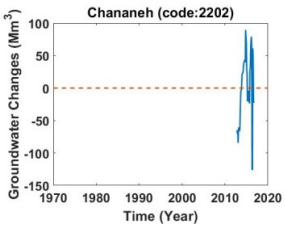

g

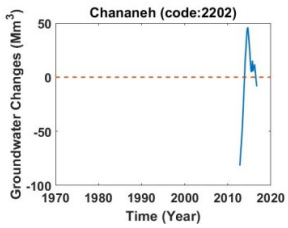

h

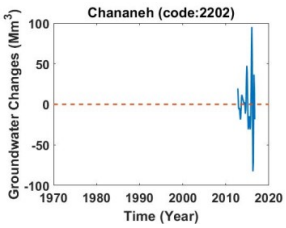

i

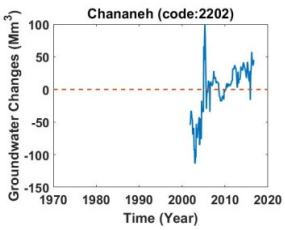

j

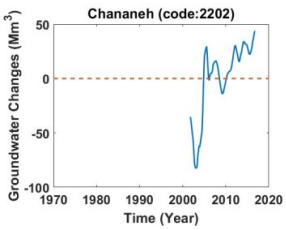

k

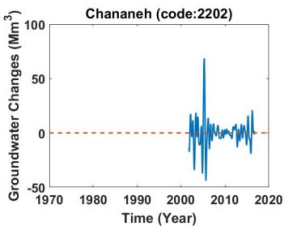

l

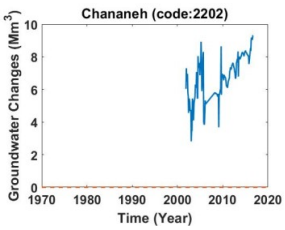

m

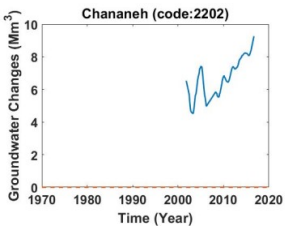

n

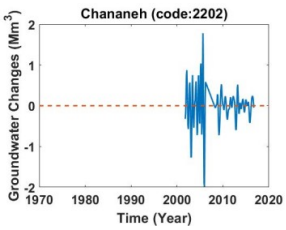

o

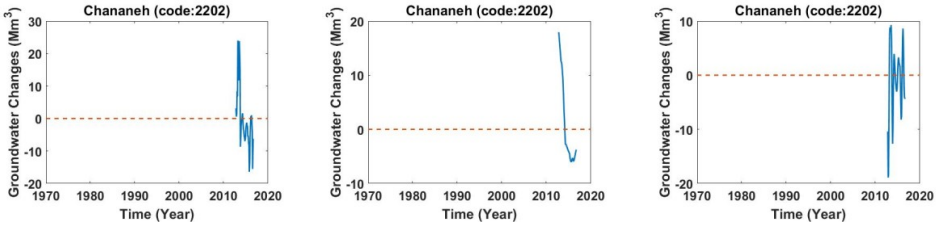

p q r

Figure F.16. a,d,g,j,m,p) Monthly values of groundwater storage, b,e,h,k,n,q) long-period of monthly values of groundwater storage, c,f,i,l,o,r) short-period of monthly values of groundwater storage across study area of Chananeh (Code: 2202).

F.2.3. Study area of Dasht Abbas Sharghi (Code: 2203)

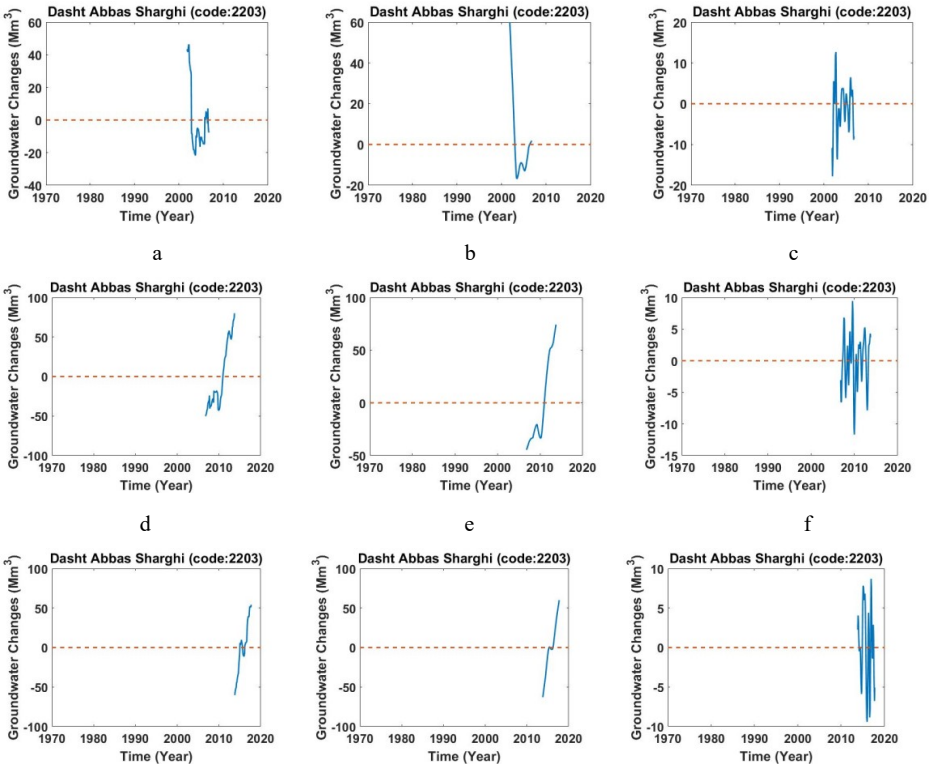

a b c

d e f

g h i

Figure F.17. a,d,g) Monthly values of groundwater storage, b,e,h) long-period of monthly values of groundwater storage, c,f,i) short-period of monthly values of groundwater storage across study area of Dasht Abbas Sharghi (Code: 2203).

F.2.4. Study area of Avan (Code: 2204)

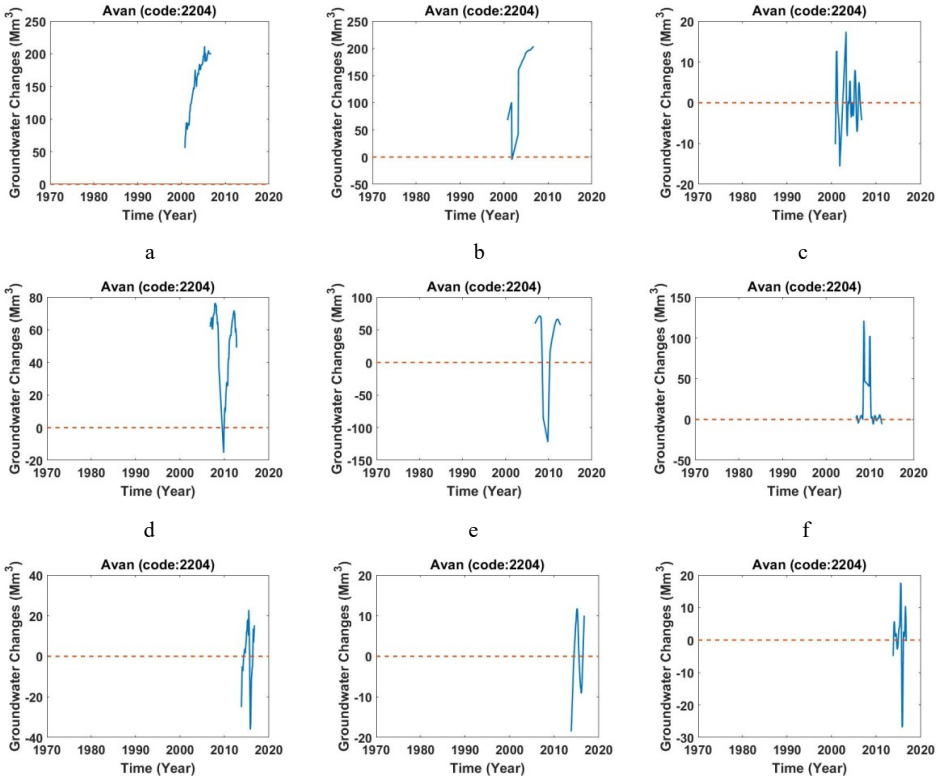

Figure F.18. a,d,g) Monthly values of groundwater storage, b,e,h) long-period of monthly values of groundwater storage, c,f,i) short-period of monthly values of groundwater storage across study area of Avan (Code: 2204).

F.2.5. Study area of Pole Dokhtar (Code: 2206)

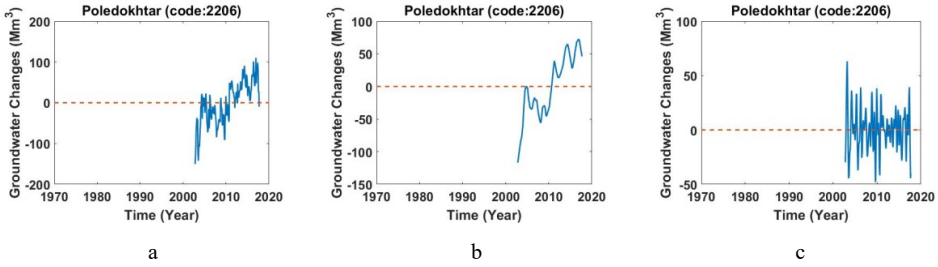

Figure F.19. a) Monthly values of groundwater storage, b) long-period of monthly values of groundwater storage, c) short-period of monthly values of groundwater storage across study area of Pole Dokhtar (Code: 2206).

F.2.6. Study area of Pole Kohdasht (Code: 2207)

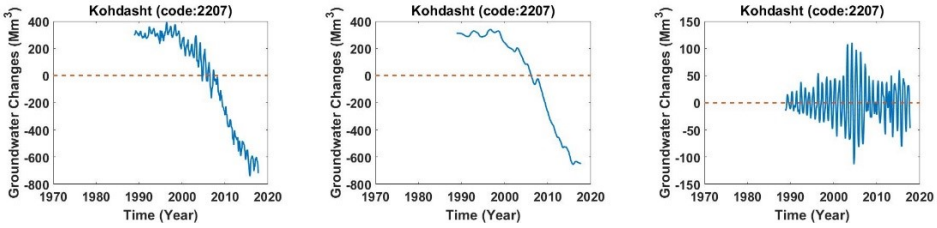

Figure F.20 a) Monthly values of groundwater storage, b) long-period of monthly values of groundwater storage, c) short-period of monthly values of groundwater storage across study area of Pole Kohdasht (Code: 2207).

F.2.7 Study area of Pole Khoramabad (Code: 2208)

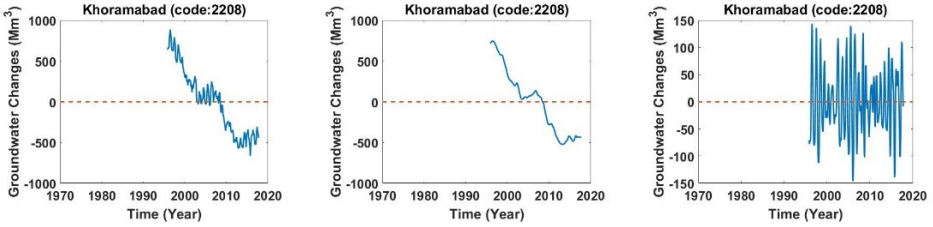

Figure F.21. a) Monthly values of groundwater storage, b) long-period of monthly values of groundwater storage, c) short-period of monthly values of groundwater storage across study area of Pole Khoramabad (Code: 2208).

F.2.8. Study area of Pole Aleshtar (Code: 2210)

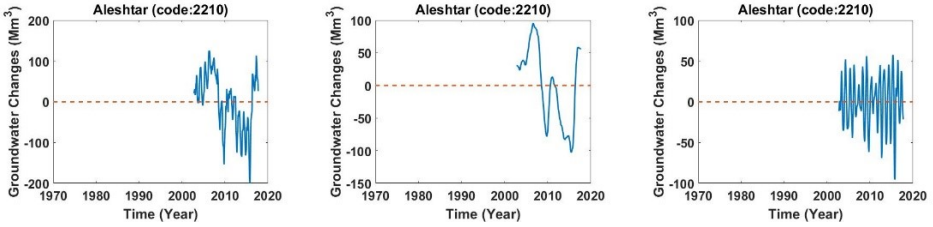

Figure F.22. a) Monthly values of groundwater storage, b) long-period of monthly values of groundwater storage, c) short-period of monthly values of groundwater storage across study area of Aleshtar (Code: 2210).

F.2.9. Study area of Pole chaghalvandi (Code: 2211)

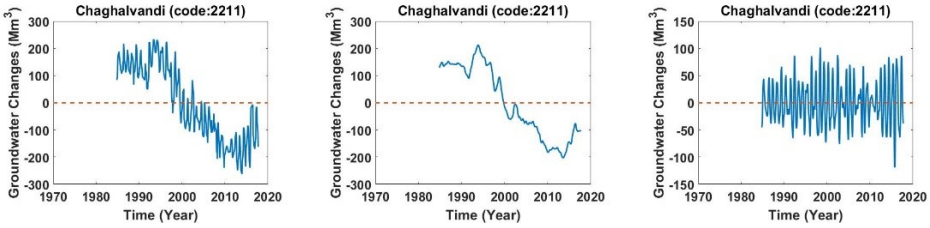

a b c

Figure F.23. a) Monthly values of groundwater storage, b) long-period of monthly values of groundwater storage, c) short-period of monthly values of groundwater storage across study area of Pole Chaghalvandi (Code: 2211).

F.2.10. Study area of Roumishgan (Code: 2213)

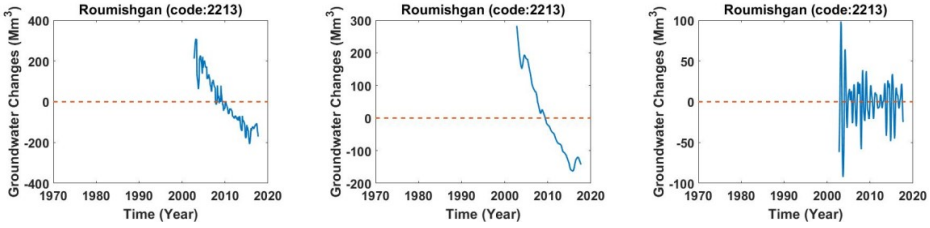

a b c

Figure F.24. a) Monthly values of groundwater storage, b) long-period of monthly values of groundwater storage, c) short-period of monthly values of groundwater storage across study area of Romishgan (Code: 2213).

F.2.11. Study area of Pole Chardavol (Code: 2215)

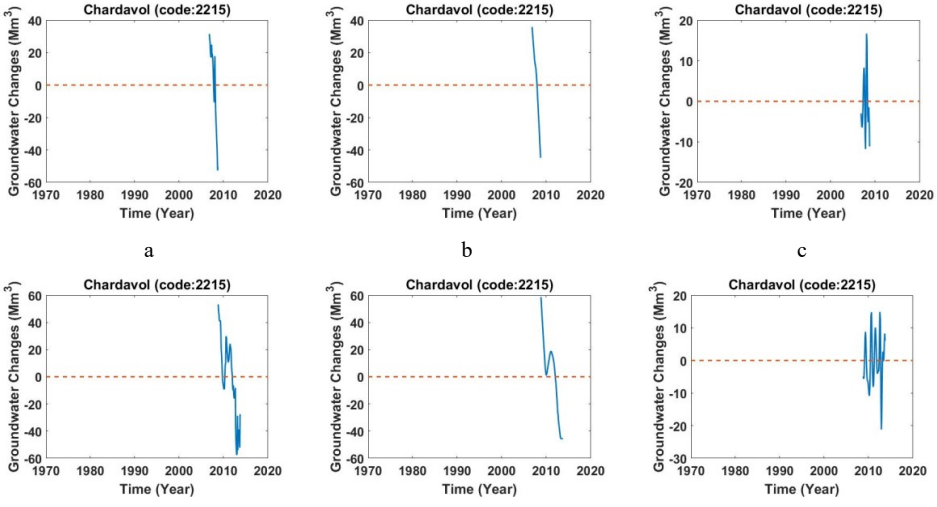

a b c

d e f

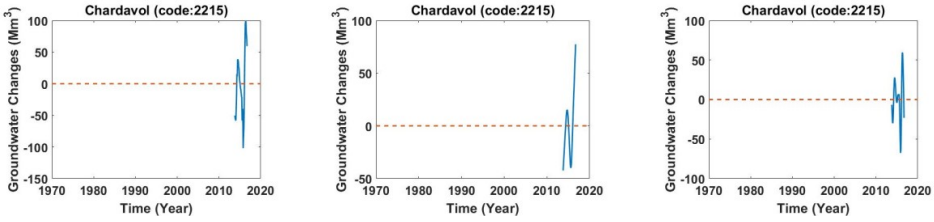

g h i

Figure F.25. a,d,g) Monthly values of groundwater storage, b,e,h) long-period of monthly values of groundwater storage, c,f,i) short-period of monthly values of groundwater storage across study area of Chardavol (Code: 2215).

F.2.12. Study area of Harsem (Code: 2216)

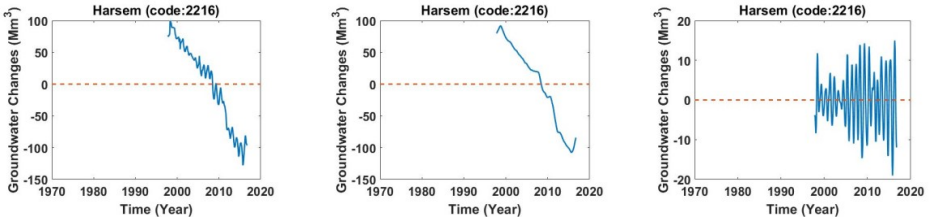

a b c

Figure F.26. a) Monthly values of groundwater storage, b) long-period of monthly values of groundwater storage, c) short-period of monthly values of groundwater storage across study area of Harsem (Code: 2216).

F.2.13. Study area of Hasanabad-Ghaleshian (Code: 2217)

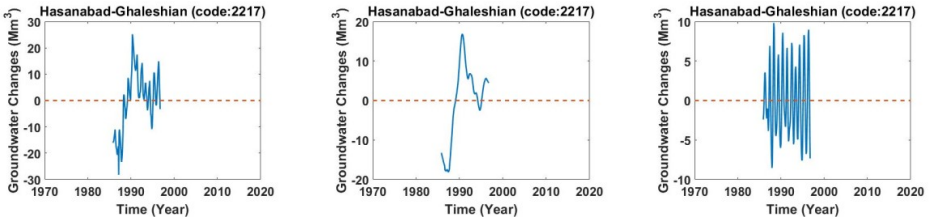

a b c

Figure F.27. a) Monthly values of groundwater storage, b) long-period of monthly values of groundwater storage, c) short-period of monthly values of groundwater storage across study area of Hasanabad-Ghaleshian (Code: 2217).

F.2.14. Study area of Pole Eslamabad (Code: 2218)

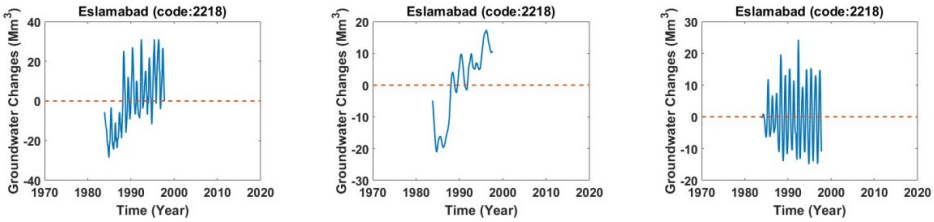

a b c

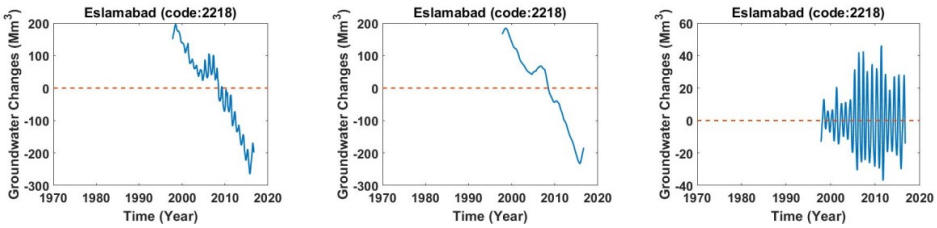

d e f

Figure F.28. a,d) Monthly values of groundwater storage, b,e) long-period of monthly values of groundwater storage, c,f) short-period of monthly values of groundwater storage across study area of Eslamabad (Code: 2218).

F.2.15. Study area of Kerend (Code: 2219)

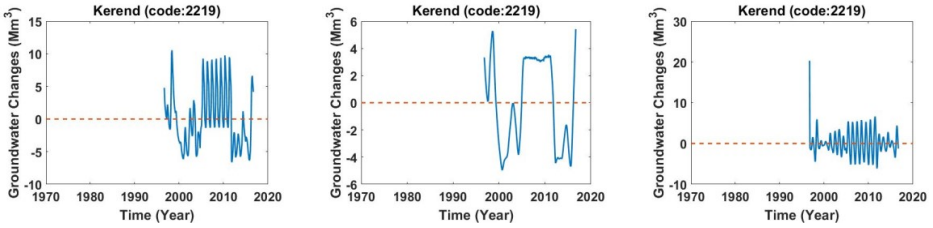

a b c

Figure F.29. a) Monthly values of groundwater storage, b) long-period of monthly values of groundwater storage, c) short-period of monthly values of groundwater storage across study area of Kerend (Code: 2219).

F.2.16. Study area of Helilan (Code: 2220)

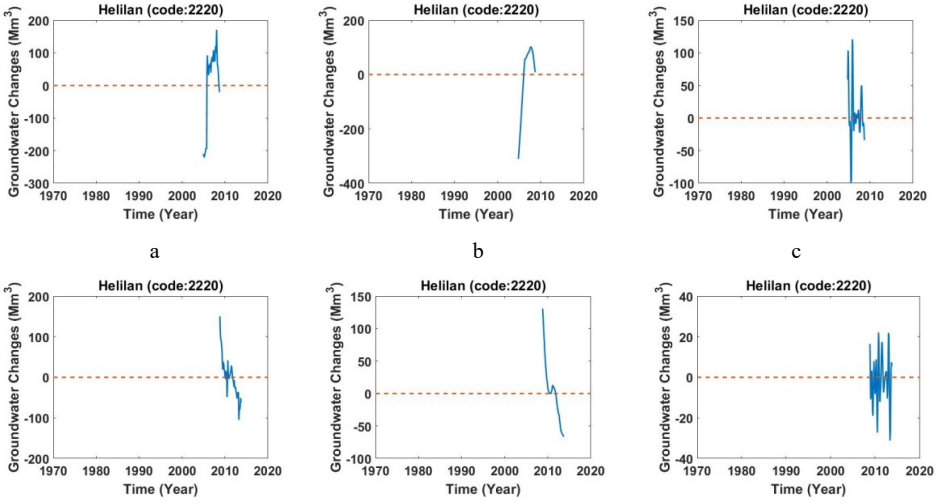

a b c

d e f

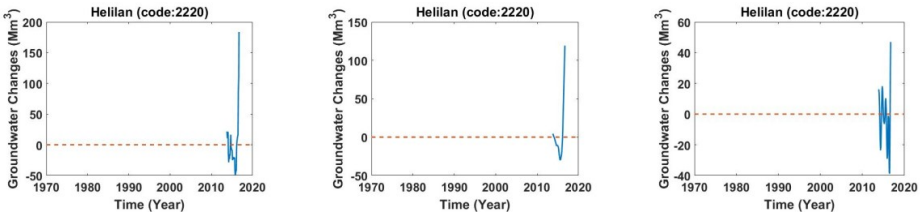

g h i

Figure F.30. a,d,g) Monthly values of groundwater storage, b,e,h) long-period of monthly values of groundwater storage, c,f,i) short-period of monthly values of groundwater storage across study area of Helilan (Code: 2220).

F.2.17. Study area of Noorabad (Code: 2221)

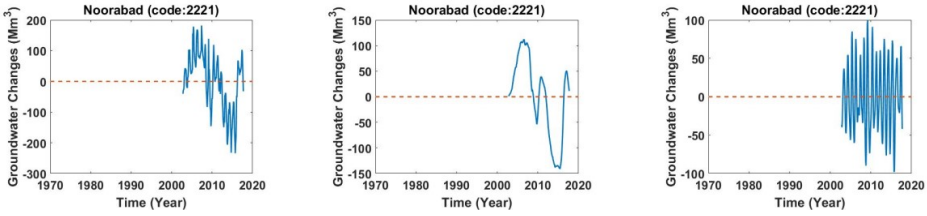

a b c

Figure F.31. a) Monthly values of groundwater storage, b) long-period of monthly values of groundwater storage, c) short-period of monthly values of groundwater storage across study area of Noorabad (Code: 2221).

F.2.18. Study area of Kermanshah (Code: 2222)

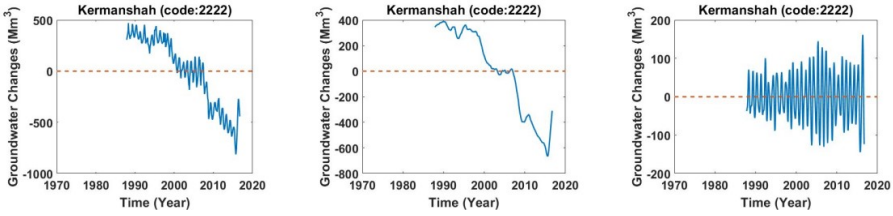

a b c

Figure F.32. a) Monthly values of groundwater storage, b) long-period of monthly values of groundwater storage, c) short-period of monthly values of groundwater storage across study area of Kermanshah (Code: 2222).

F.2.19. Study area of Ravansar (Code: 2224)

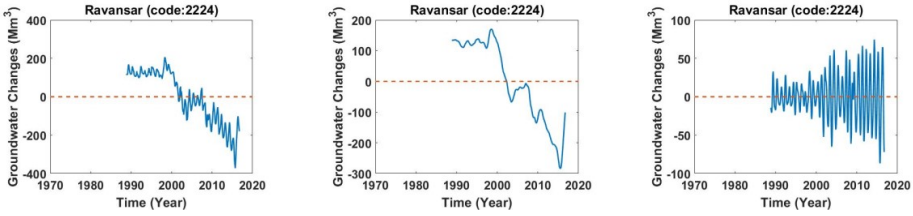

a b c

Figure F.33. a) Monthly values of groundwater storage, b) long-period of monthly values of groundwater storage, c) short-period of monthly values of groundwater storage across study area of Ravansar (Code: 2224).

F.2.20. Study area of Mahi Dasht (Code: 2225)

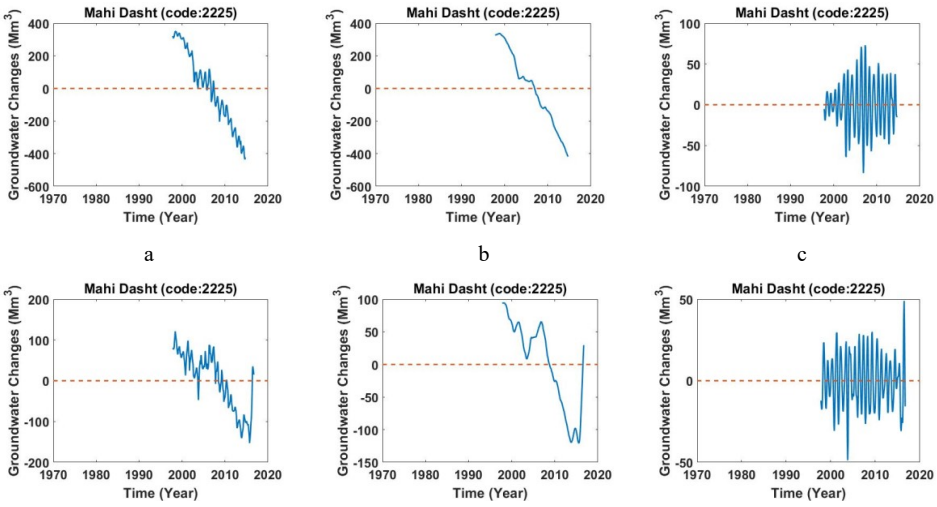

Figure F.34. a,d) Monthly values of groundwater storage, b,e) long-period of monthly values of groundwater storage, c,f) short-period of monthly values of groundwater storage across study area of Mahi Dasht (Code: 2225).

F.2.21. Study area of Main Rahan (Code: 2228)

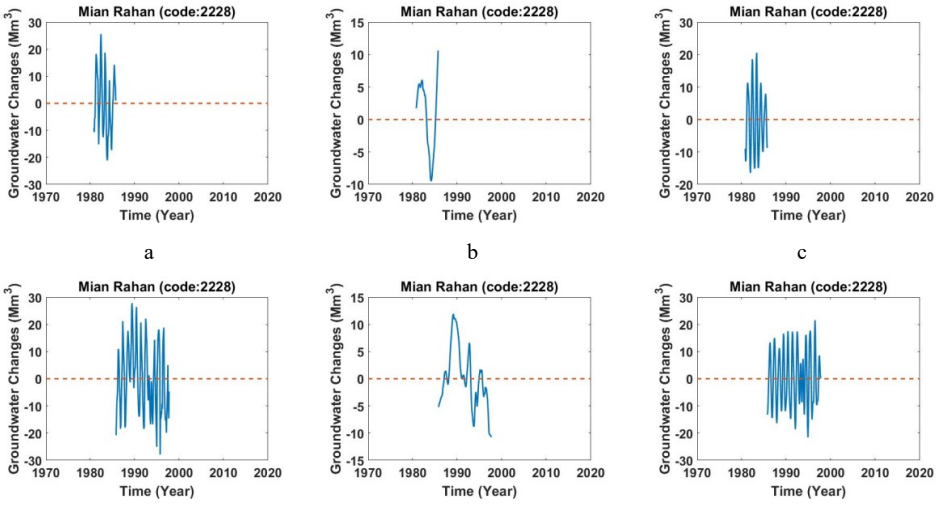

Figure F.35. a,d) Monthly values of groundwater storage, b,e) long-period of monthly values of groundwater storage, c,f) short-period of monthly values of groundwater storage across study area of Mahi Rahan (Code: 2228).

F.2.22. Study area of Songhor (Code: 2229)

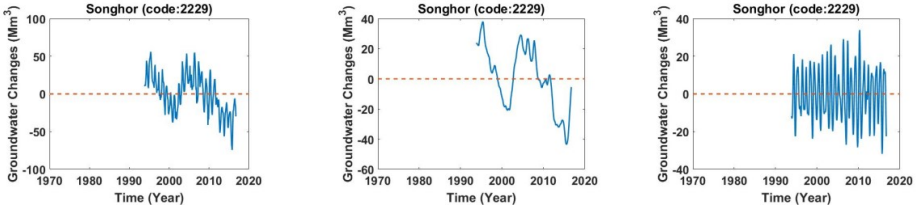

a b c

Figure F.36. a) Monthly values of groundwater storage, b) long-period of monthly values of groundwater storage, c) short-period of monthly values of groundwater storage across study area of Songhor (Code: 2229).

F.2.23. Study area of Sahneh (Code: 2230)

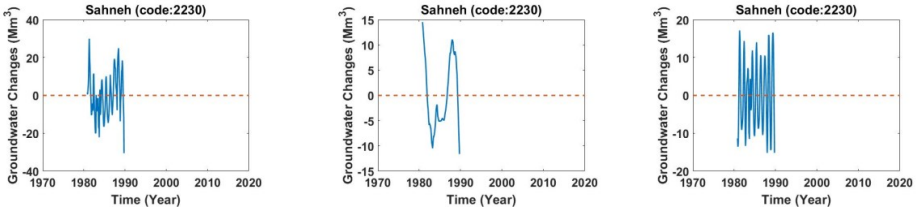

a b c

Figure F.37. a) Monthly values of groundwater storage, b) long-period of monthly values of groundwater storage, c) short-period of monthly values of groundwater storage across study area of Sahneh (Code: 2230).

F.2.24. Study area of Kangavar (Code: 2231)

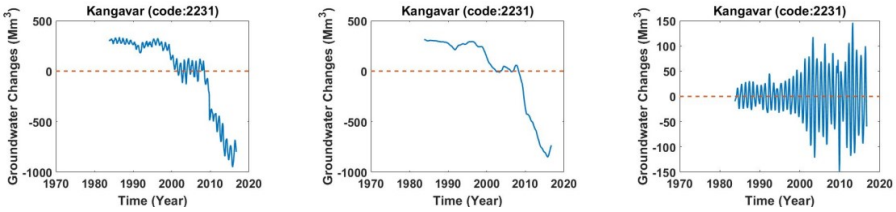

a b c

Figure F.38. a) Monthly values of groundwater storage, b) long-period of monthly values of groundwater storage, c) short-period of monthly values of groundwater storage across study area of Kangavar (Code: 2231).

F.2.25. Study area of Asad Abad (Code: 2232)

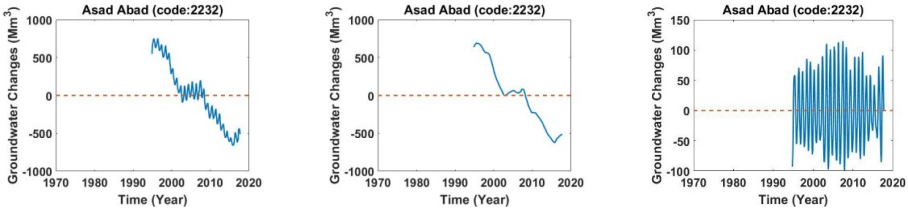

a b c

Figure F.39. a) Monthly values of groundwater storage, b) long-period of monthly values of groundwater storage, c) short-period of monthly values of groundwater storage across study area of Asad Abad (Code: 2232).

F.2.26. Study area of Songhor (Code: 2234)

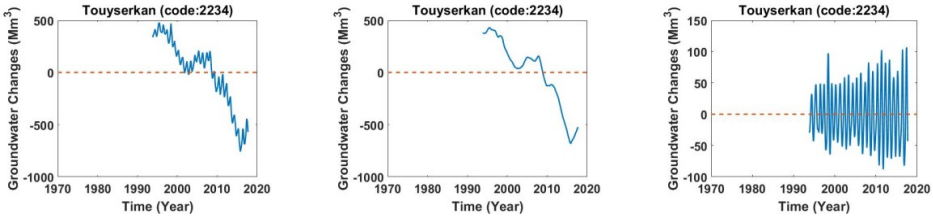

a b c

Figure F.40. a) Monthly values of groundwater storage, b) long-period of monthly values of groundwater storage, c) short-period of monthly values of groundwater storage across study area of Touyserkan (Code: 2234).

F.2.27. Study area of Malayer (Code: 2235)

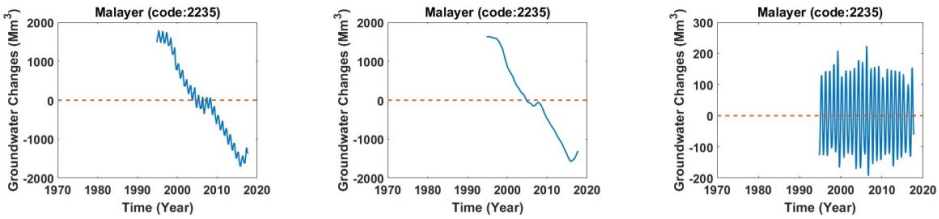

a b c

Figure F.41. a) Monthly values of groundwater storage, b) long-period of monthly values of groundwater storage, c) short-period of monthly values of groundwater storage across study area of Malayer (Code: 2235).

F.3.1. Study area of South Ahvaz (Code: 2302)

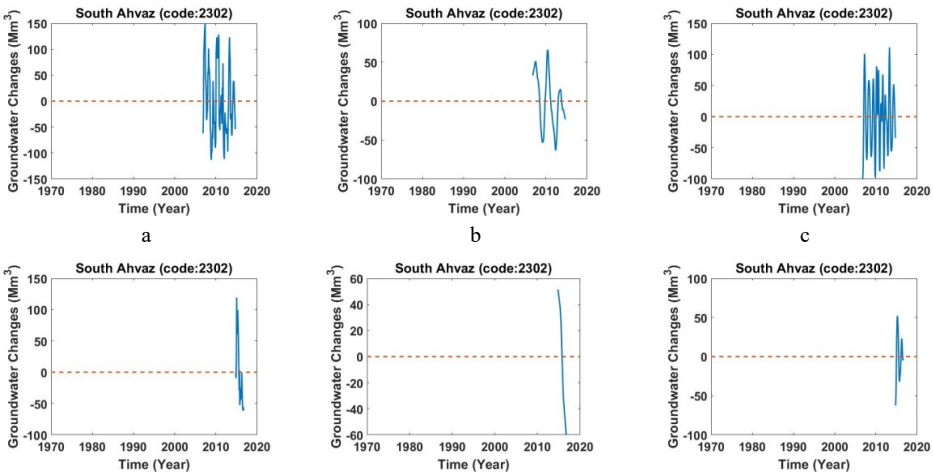

a b c

d e f

Figure F.42. a,d) Monthly values of groundwater storage, b,e) long-period of monthly values of groundwater storage, c,f) short-period of monthly values of groundwater storage across study area of south Ahvaz (Code: 2302).

F.3.2. Study area of North Ahvaz (Code: 2303)

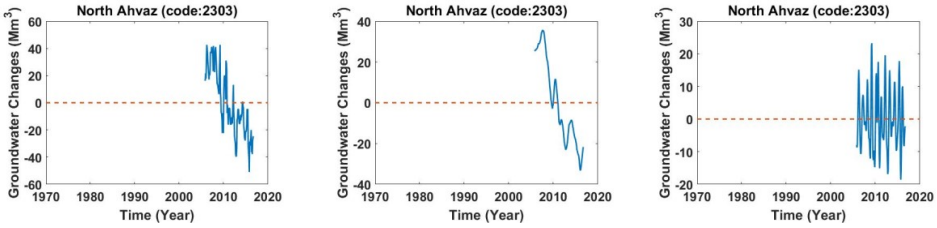

a b c

Figure F.43. a) Monthly values of groundwater storage, b) long-period of monthly values of groundwater storage, c) short-period of monthly values of groundwater storage across study area of North Ahvaz (Code: 2303).

F.3.3. Study area of Shoushtar (Code: 2304)

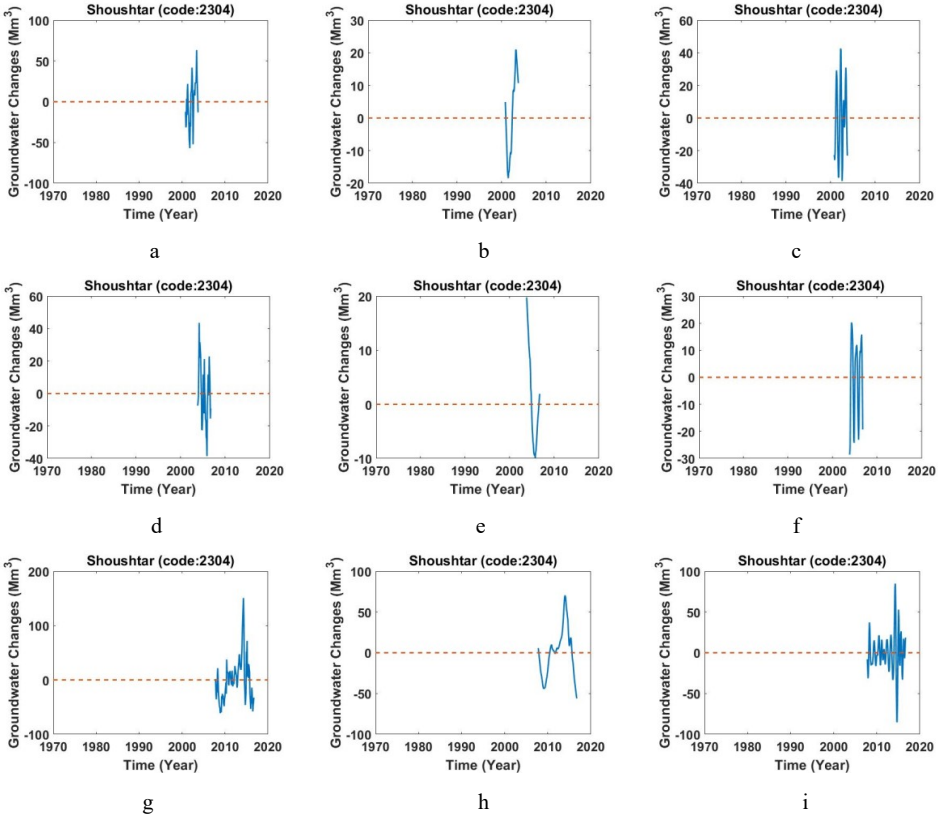

a b c

d e f

g h i

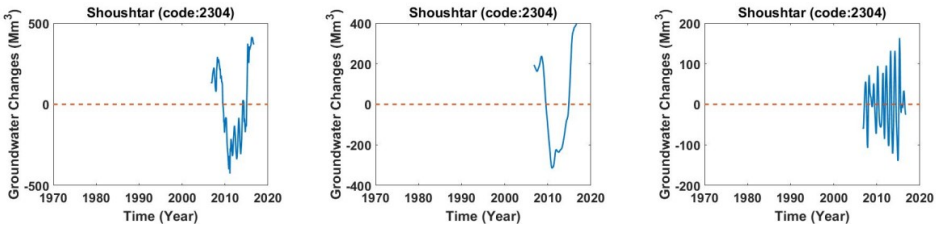

j k l

Figure F.44. a,d,g,j) Monthly values of groundwater storage, b,e,h,k,) long-period of monthly values of groundwater storage, c,f,i,l) short-period of monthly values of groundwater storage across study area of Shoushtar (Code: 2304).

F.3. 4 Study area of Masjed Soleiman (Code: 2305)

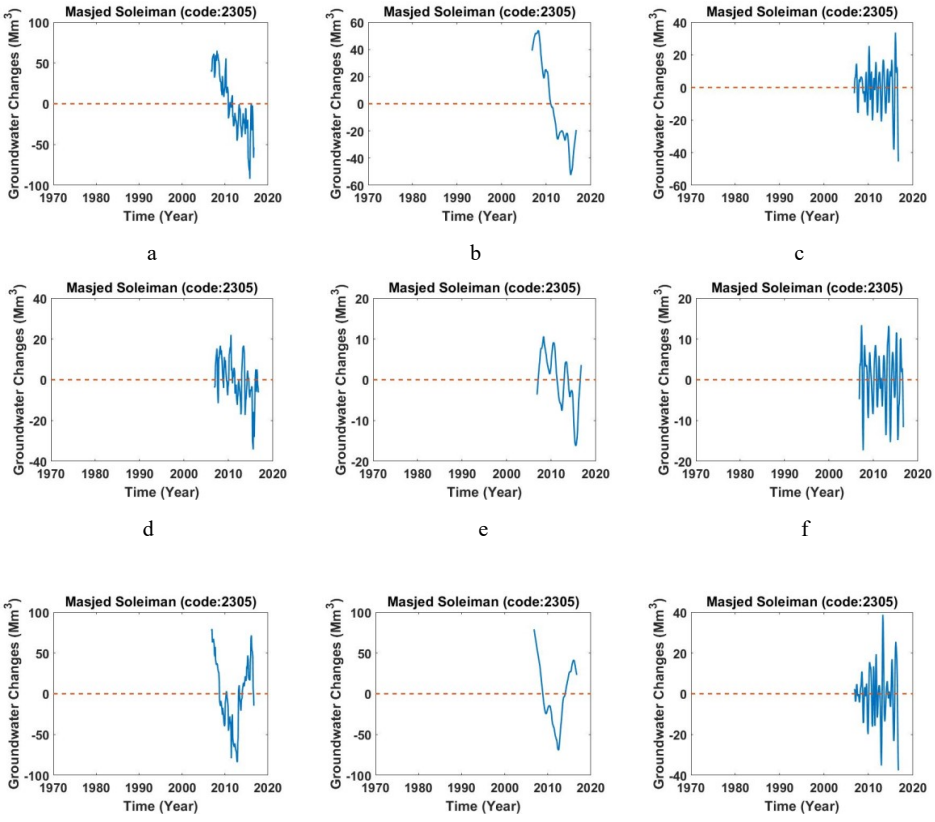

a b c

d e f

g h i

Figure F.45. a,d,g) Monthly values of groundwater storage, b,e,h) long-period of monthly values of groundwater storage, c,f,i) short-period of monthly values of groundwater storage across study area of Masjed Soleiman (Code: 2305).

F.3.5. Study area of Getond-Aghili (Code: 2306)

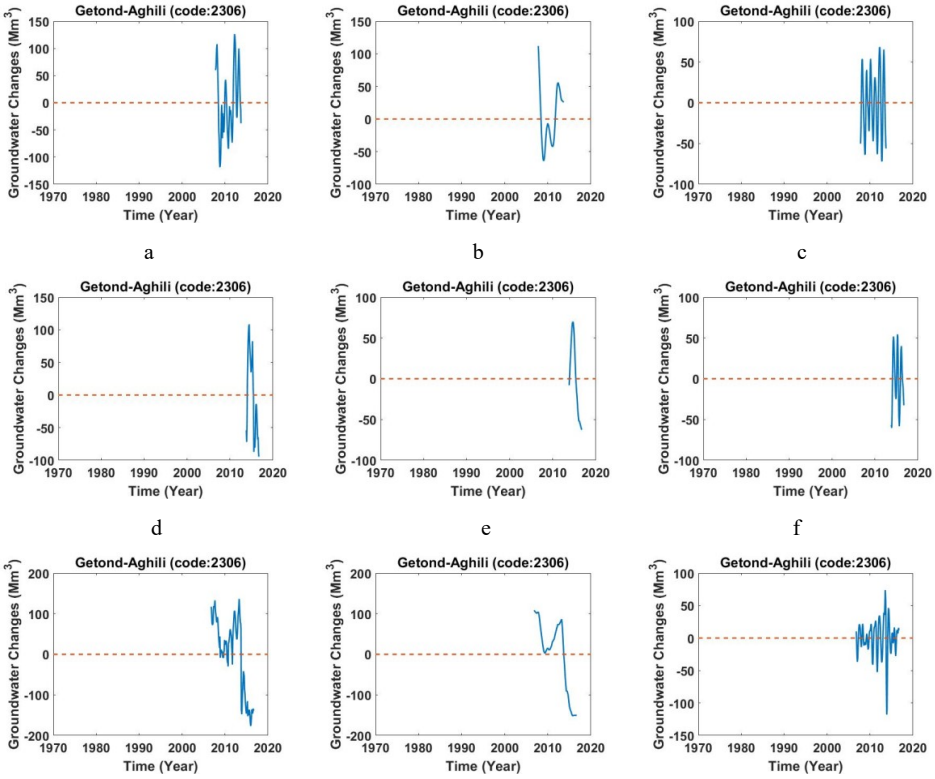

Figure F.46. a,d,g) Monthly values of groundwater storage, b,e,h) long-period of monthly values of groundwater storage, c,f,i) short-period of monthly values of groundwater storage across study area of Getond-Aghili (Code: 2306).

F.3.6. Study area of Lali (Code: 2307)

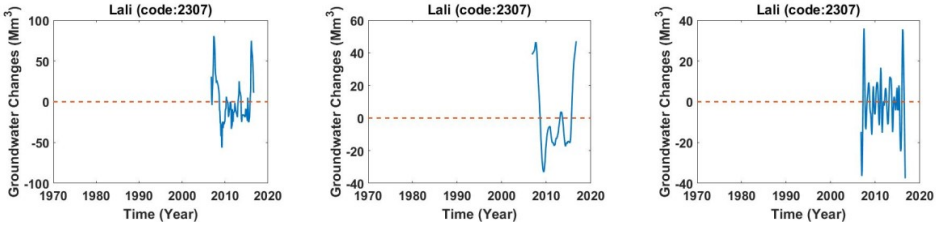

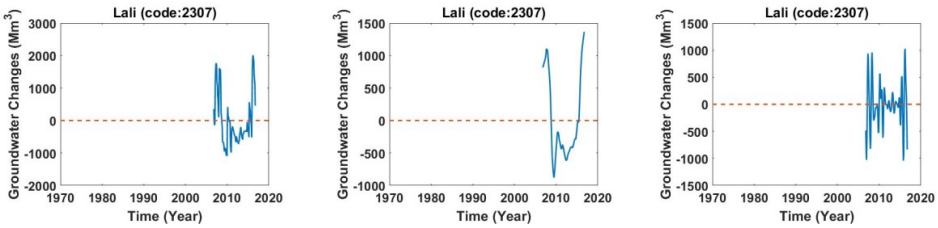

d e f

Figure F.47. a,d) Monthly values of groundwater storage, b,e) long-period of monthly values of groundwater storage, c,f) short-period of monthly values of groundwater storage across study area of Lali (Code: 2307).

F.3.7. Study area of Andika (Code: 2308)

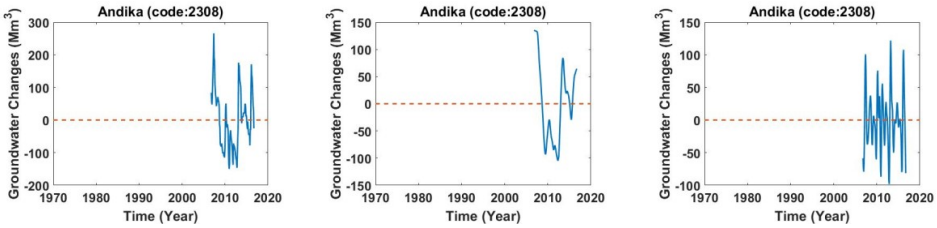

a b c

Figure F.48. a) Monthly values of groundwater storage, b) long-period of monthly values of groundwater storage, c) short-period of monthly values of groundwater storage across study area of Andika (Code: 2308).

F.3.8. Study area of Morghab (Code: 2309)

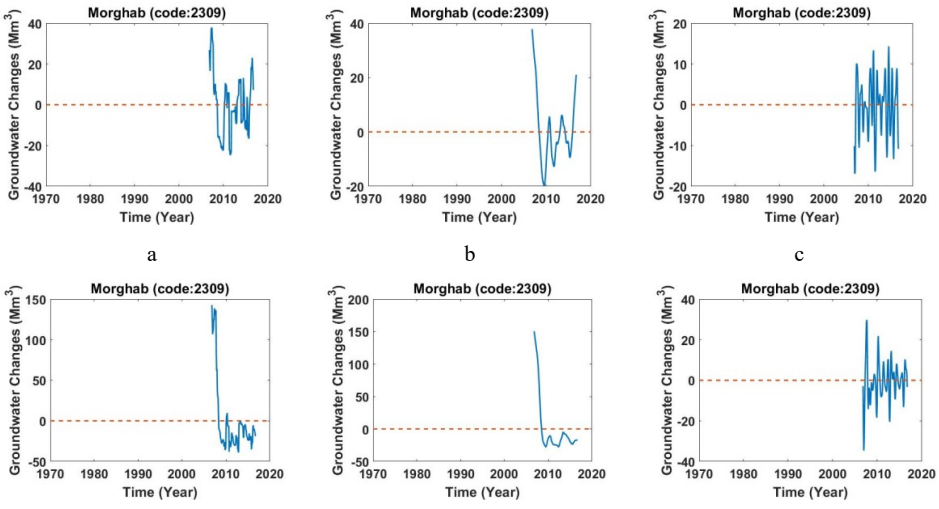

a b c

d e f

Figure F.49. a,d) Monthly values of groundwater storage, b,e) long-period of monthly values of groundwater storage, c,f,) short-period of monthly values of groundwater storage across study area of Morghab (Code: 2309).

F.3.9. Study area of Ize-Pion (Code: 2310)

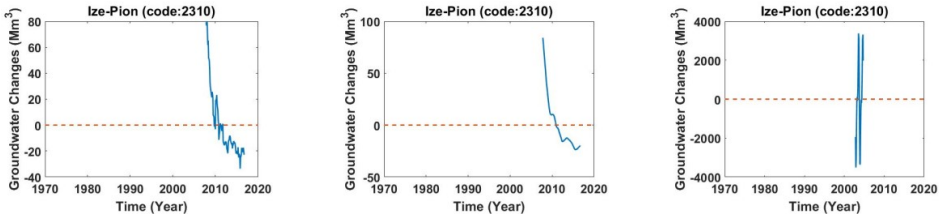

a b c

Figure F.50. a) Monthly values of groundwater storage, b) long-period of monthly values of groundwater storage, c) short-period of monthly values of groundwater storage across study area of Ize-Pion (Code: 2310).

F.3.10. Study area of Dah Sheikh (Code: 2311)

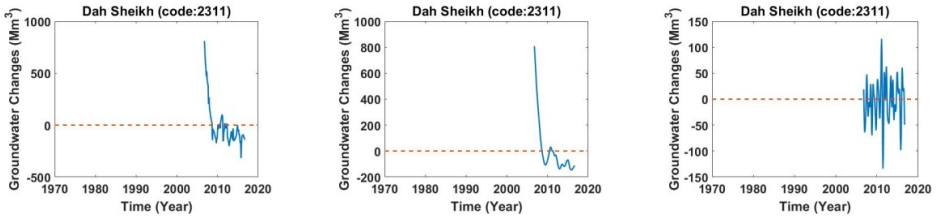

a b c

Figure F.51. a) Monthly values of groundwater storage, b) long-period of monthly values of groundwater storage, c) short-period of monthly values of groundwater storage across study area of Dah Sheikh (Code: 2311).

F.3.11. Study area of Malekhalife (Code: 2313)

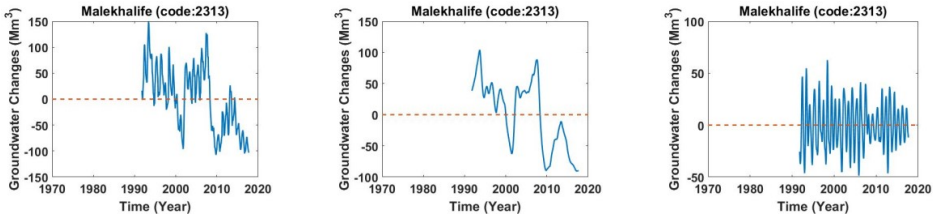

a b c

Figure F.52. a) Monthly values of groundwater storage, b) long-period of monthly values of groundwater storage, c) short-period of monthly values of groundwater storage across study area of Malekhalife (Code: 2313).

F.3.12. Study area of Komeh (Code: 2314)

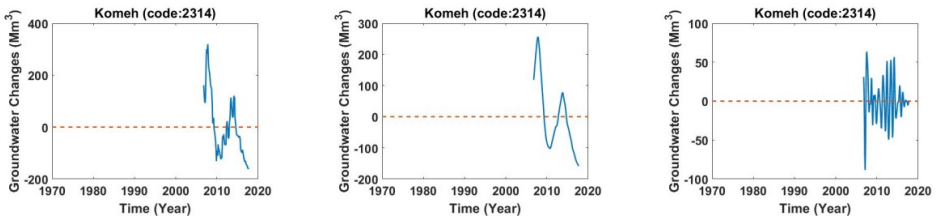

a b c

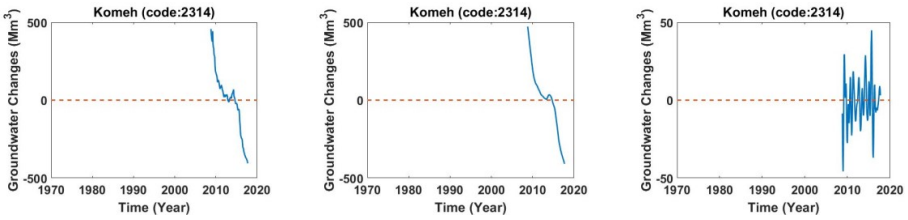

d e f

Figure F.53.4 a,d) Monthly values of groundwater storage, b,e) long-period of monthly values of groundwater storage, c,f,) short-period of monthly values of groundwater storage across study area of Kome (Code: 2314).

F.3.13. Study area of Semirom (Code: 2315)

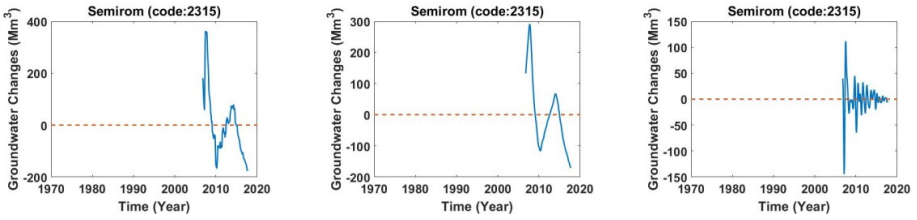

a b c

Figure F.54. a) Monthly values of groundwater storage, b) long-period of monthly values of groundwater storage, c) short-period of monthly values of groundwater storage across study area of Semirom (Code: 2315).

F.3.14 Study area of Ghabre Keykha (Code: 2316)

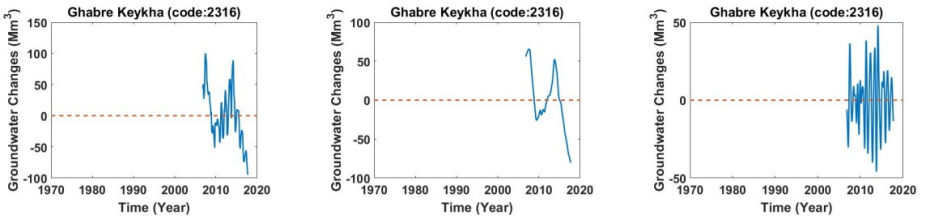

a b c

Figure F.55. a) Monthly values of groundwater storage, b) long-period of monthly values of groundwater storage, c) short-period of monthly values of groundwater storage across study area of Ghabre Keykha (Code: 2316).

F.3.15. Study area of Yasuj (Code: 2317)

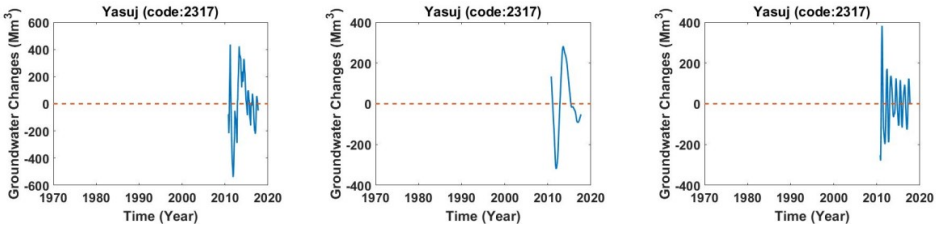

a b c

Figure F.56. a) Monthly values of groundwater storage, b) long-period of monthly values of groundwater storage, c) short-period of monthly values of groundwater storage across study area of Yasuj (Code: 2317).

F.3.16. Study area of Dasht Room (Code: 2318)

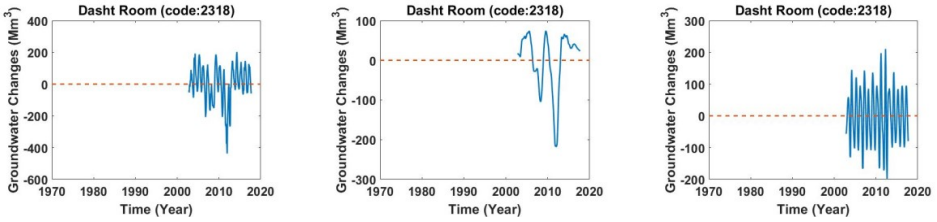

a b c

Figure F.57. a) Monthly values of groundwater storage, b) long-period of monthly values of groundwater storage, c) short-period of monthly values of groundwater storage across study area of Dasht Room (Code: 2318).

F.3.17. Study area of Lordegan (Code: 2319)

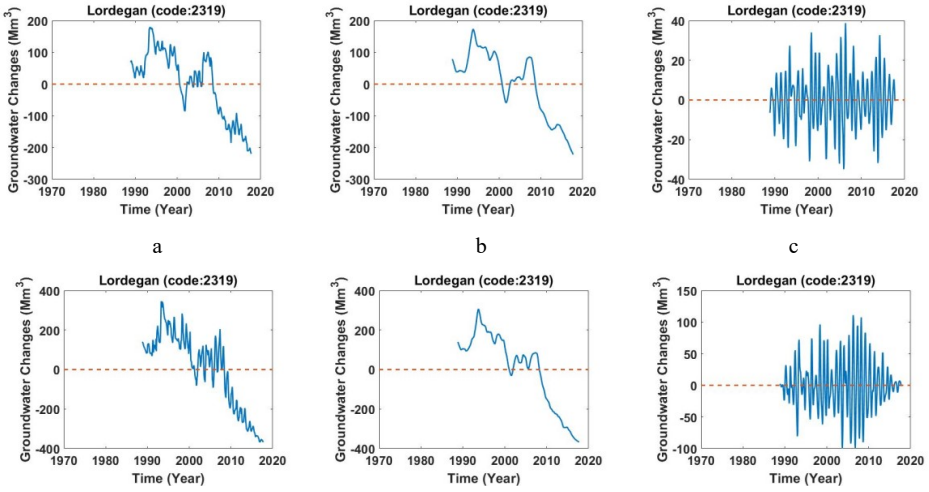

a b c

d e f

Figure F.58. a,d) Monthly values of groundwater storage, b,e) long-period of monthly values of groundwater storage, c,f,) short-period of monthly values of groundwater storage across study area of Lordegan (Code: 2319).

F.3.18. Study area of Javanmardi (Code: 2320)

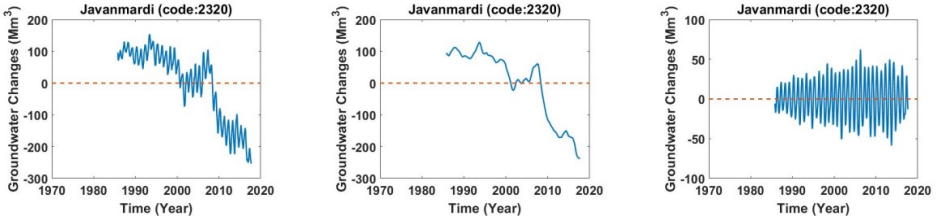

a b c

Figure F.59. a) Monthly values of groundwater storage, b) long-period of monthly values of groundwater storage, c) short-period of monthly values of groundwater storage across study area of Javanmardi (Code: 2320).

F.3.19. Study area of Boldaji (Code: 2323)

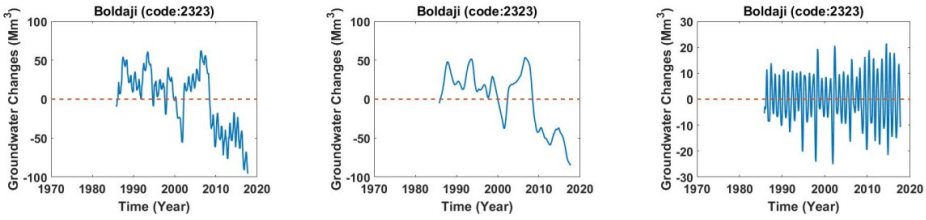

a b c

Figure F.60. a) Monthly values of groundwater storage, b) long-period of monthly values of groundwater storage, c) short-period of monthly values of groundwater storage across study area of Boldaji (Code: 2323).

F.3.20. Study area of Mehrgard (Code: 2324)

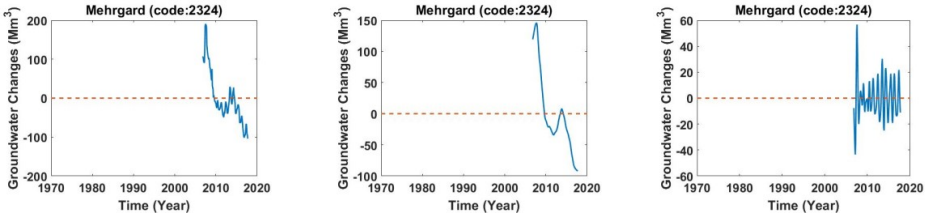

a b c

Figure F.61. a) Monthly values of groundwater storage, b) long-period of monthly values of groundwater storage, c) short-period of monthly values of groundwater storage across study area of Mehrgard (Code: 2324).

F.3.21. Study area of Cheshmeh Soleyman (Code: 2325)

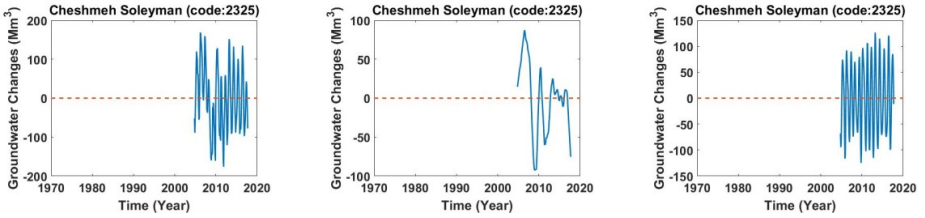

a b c

Figure F.62. a) Monthly values of groundwater storage, b) long-period of monthly values of groundwater storage, c) short-period of monthly values of groundwater storage across study area of Cheshmeh Soleyman (Code: 2325).

F.3.22. Study area of Farsan(Code: 2328)

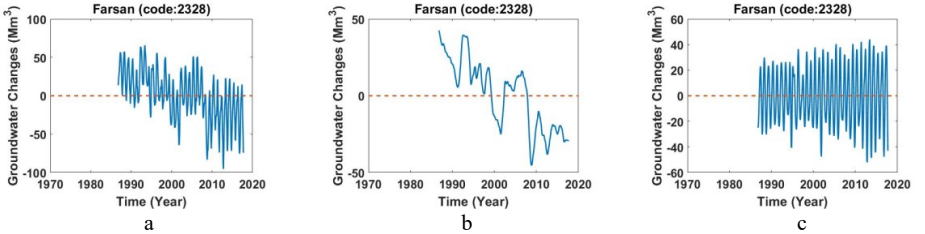

a b c

Figure F.63. a) Monthly values of groundwater storage, b) long-period of monthly values of groundwater storage, c) short-period of monthly values of groundwater storage across study area of Farsan(Code: 2328).

F.3.23. Study area of Shalamzad(Code: 2329)

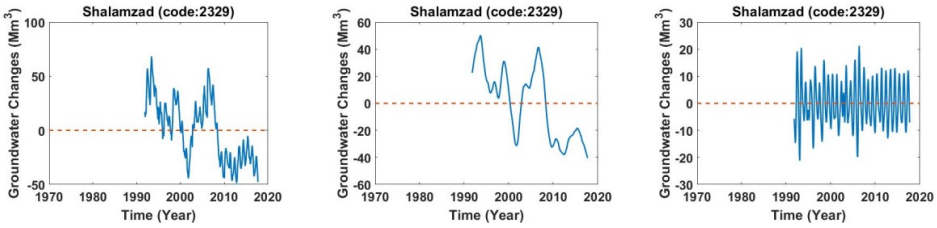

a b c

Figure F.64. a) Monthly values of groundwater storage, b) long-period of monthly values of groundwater storage, c) short-period of monthly values of groundwater storage across study area of Shalamzad (Code: 2329).

F.3.24. Study area of Shahrekord (Code: 2330)

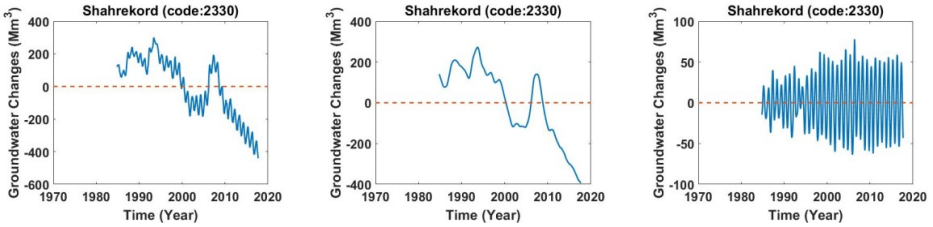

a b c

Figure F.65. a) Monthly values of groundwater storage, b) long-period of monthly values of groundwater storage, c) short-period of monthly values of groundwater storage across study area of Shahrekord (Code: 2330).

F.3.25. Study area of Kiar (Code: 2331)

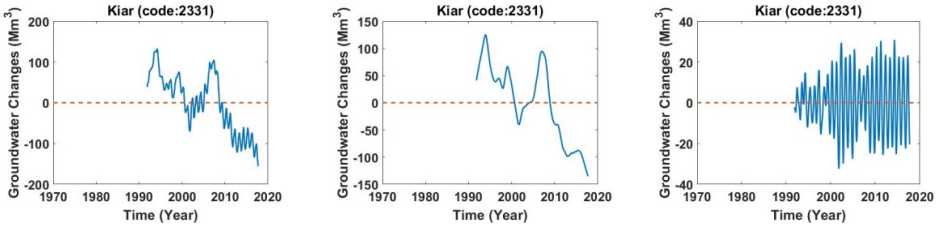

a b c

Figure F.66. a) Monthly values of groundwater storage, b) long-period of monthly values of groundwater storage, c) short-period of monthly values of groundwater storage across study area of Kiar (Code: 2331).

F.3.26. Study area of Sefid Dasht (Code: 2332)

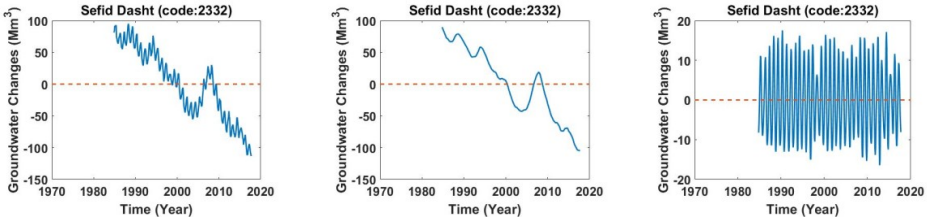

a b c

Figure F.67. a) Monthly values of groundwater storage, b) long-period of monthly values of groundwater storage, c) short-period of monthly values of groundwater storage across study area of Sefid Dasht (Code: 2332).

F.3.27. Study area of Boroujen (Code: 2333)

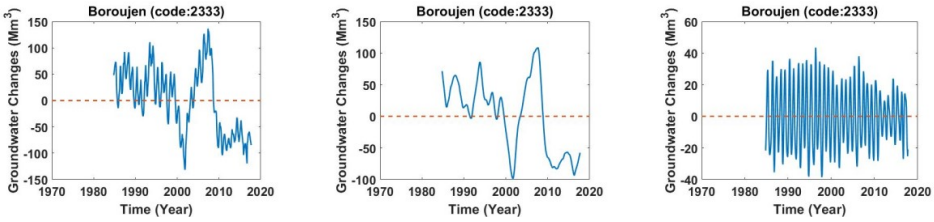

a b c

Figure F.68. a) Monthly values of groundwater storage, b) long-period of monthly values of groundwater storage, c) short-period of monthly values of groundwater storage across study area of Boroujen (Code: 2333).

F.3.28. Study area of Ahoodasht (Code: 2334)

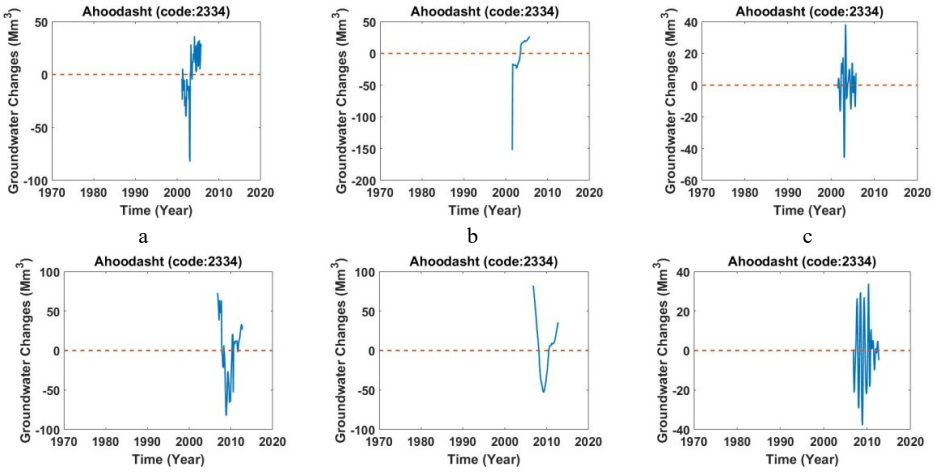

a b c

d e f

Figure F.69. a,d) Monthly values of groundwater storage, b,e) long-period of monthly values of groundwater storage, c,f,) short-period of monthly values of groundwater storage across study area of Ahoodasht (Code: 2334).

F.3.29. Study area of Dezful (Code: 2335)

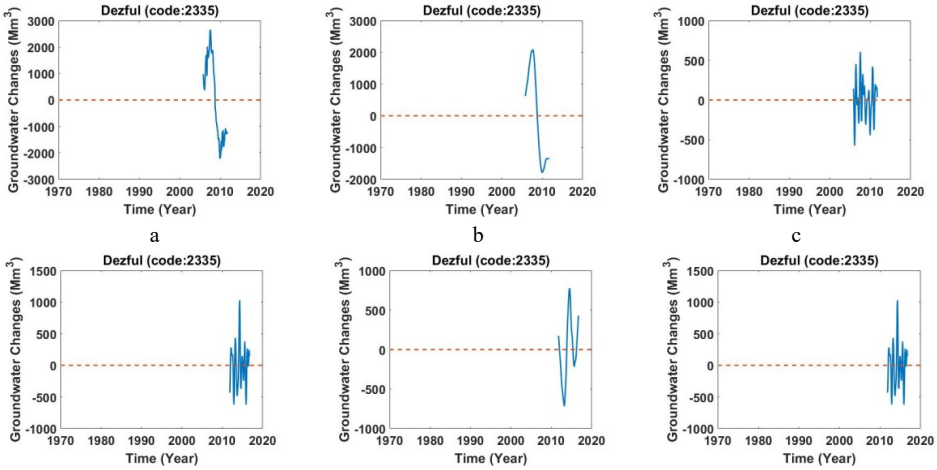

Figure F.70. a,d) Monthly values of groundwater storage, b,e) long-period of monthly values of groundwater storage, c,f,) short-period of monthly values of groundwater storage across study area of Dezful (Code: 2335)

F.3.30. Study area of Boroujerd (Code: 2339)

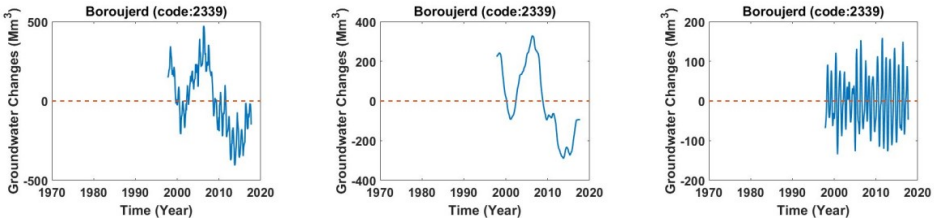

Figure F.71. a) Monthly values of groundwater storage, b) long-period of monthly values of groundwater storage, c) short-period of monthly values of groundwater storage across study area of Boroujerd (Code: 2339).

F.3.31. Study area of Oshtorinan (Code: 2340)

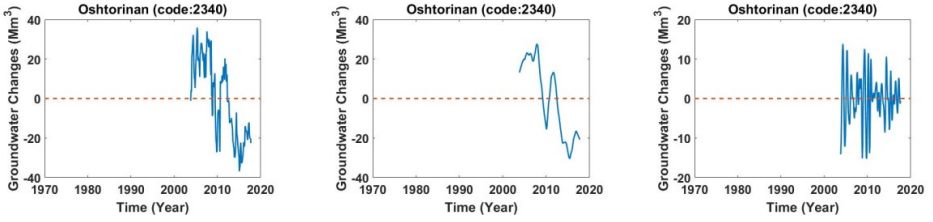

Figure F.72. a) Monthly values of groundwater storage, b) long-period of monthly values of groundwater storage, c) short-period of monthly values of groundwater storage across study area of Oshtorinan (Code: 2340).

F.3.32. Study area of Azna-Aligoudarz (Code: 2342)

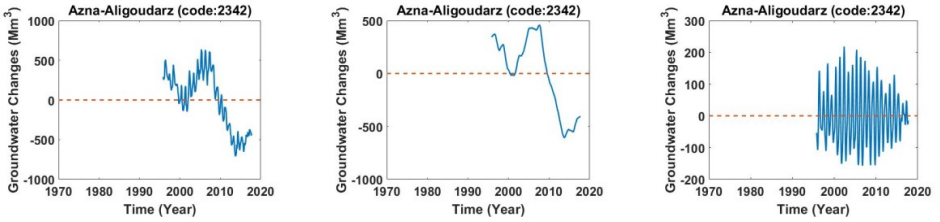

a b c

Figure F.73 a) Monthly values of groundwater storage, b) long-period of monthly values of groundwater storage, c) short-period of monthly values of groundwater storage across study area of Azna-Aligoudarz (Code: 2342).

F.4.1. Study area of Ramhormoz (Code: 2402)

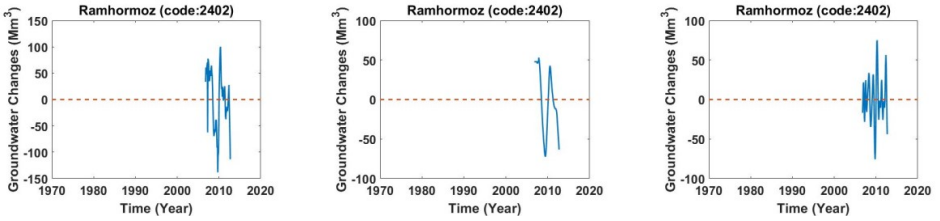

a b c

Figure 5. 74. a) Monthly values of groundwater storage, b) long-period of monthly values of groundwater storage, c) short-period of monthly values of groundwater storage across study area of Ramhormoz (Code: 2402).

F.4.2. Study area of Bagh Malek (Code: 2404)

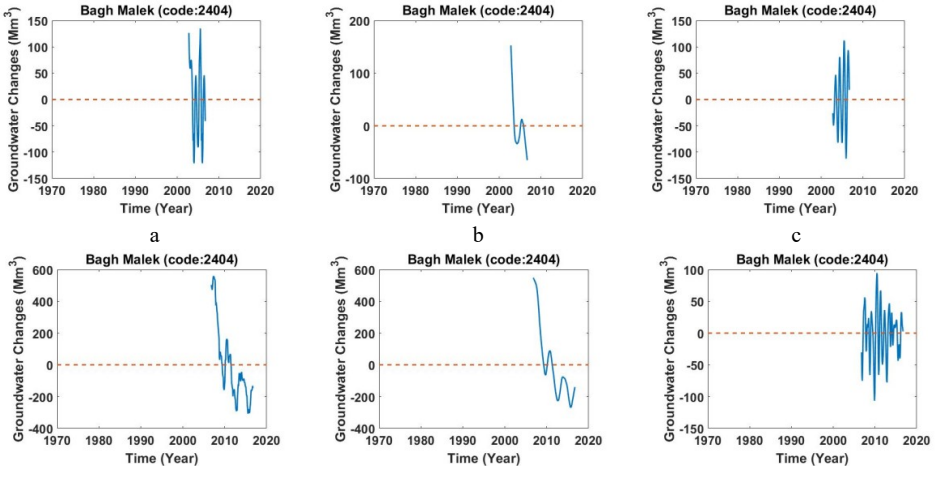

a b c

d e f

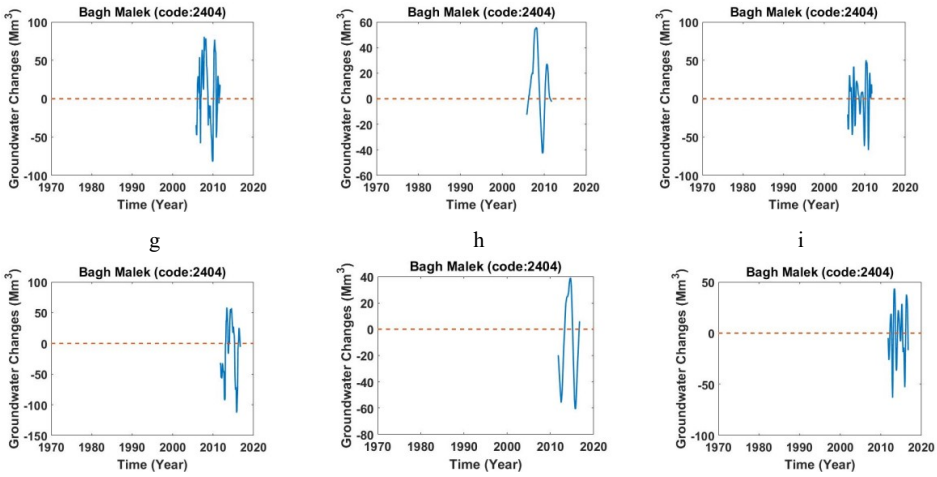

Figure 5.75. a,d,g,j) Monthly values of groundwater storage, b,e,h,k) long-period of monthly values of groundwater storage, c,f,i,l) short-period of monthly values of groundwater storage across study area of Bagh Malek (Code: 2404).

F.4.3. Study area of Jayzan (Code: 2406)

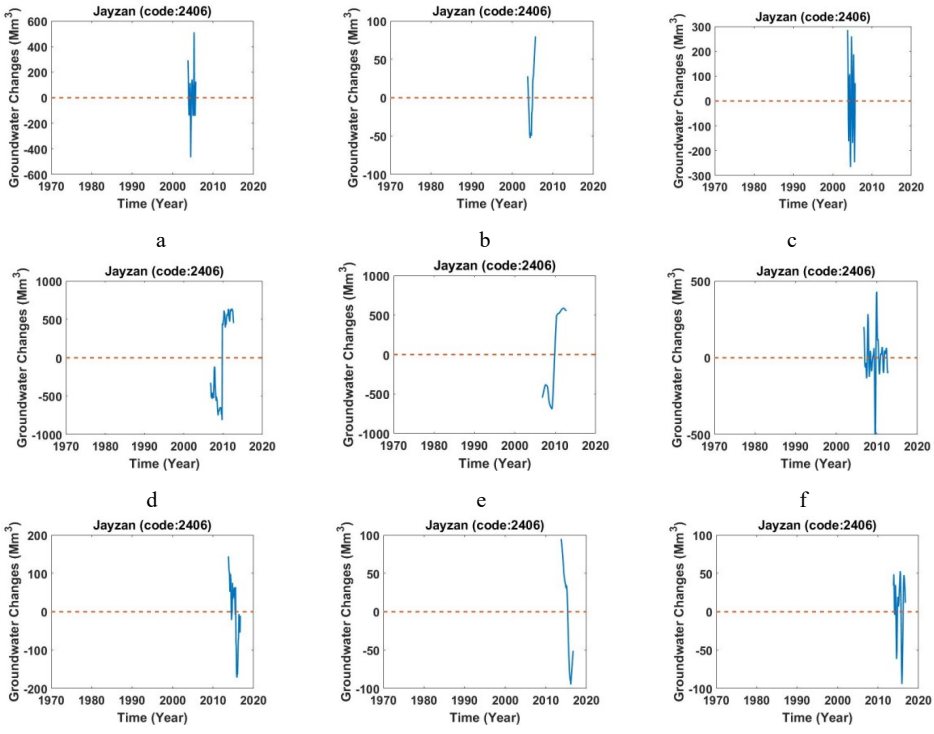

Figure 5.76. a,d,g) Monthly values of groundwater storage, b,e,h) long-period of monthly values of groundwater storage, c,f,i) short-period of monthly values of groundwater storage across study area of Jayze (Code: 2406).

F.4.4. Study area of Behbahan (Code: 2407)

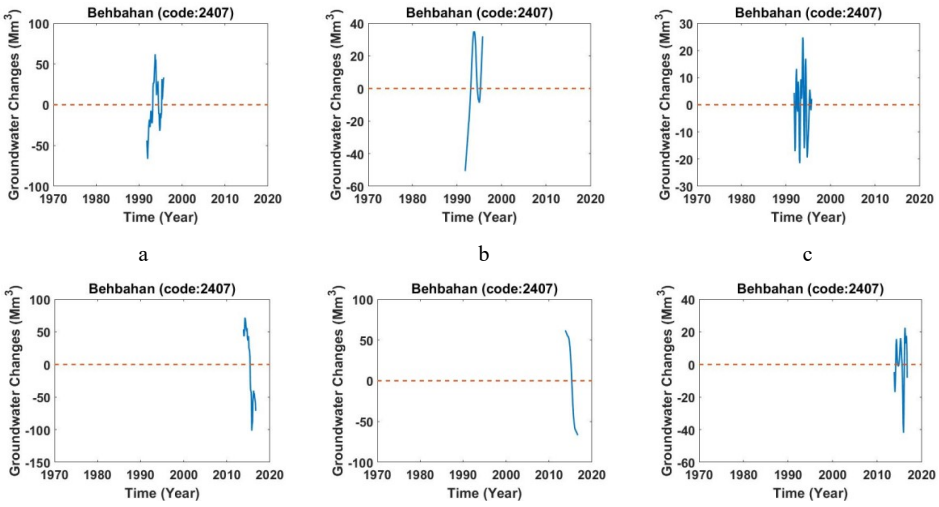

Figure 5.77. a,d) Monthly values of groundwater storage, b,e) long-period of monthly values of groundwater storage, c,f) short-period of monthly values of groundwater storage across study area of Behbahan (Code: 2407).

F.4.5. Study area of Takht Deraz (Code: 2408)

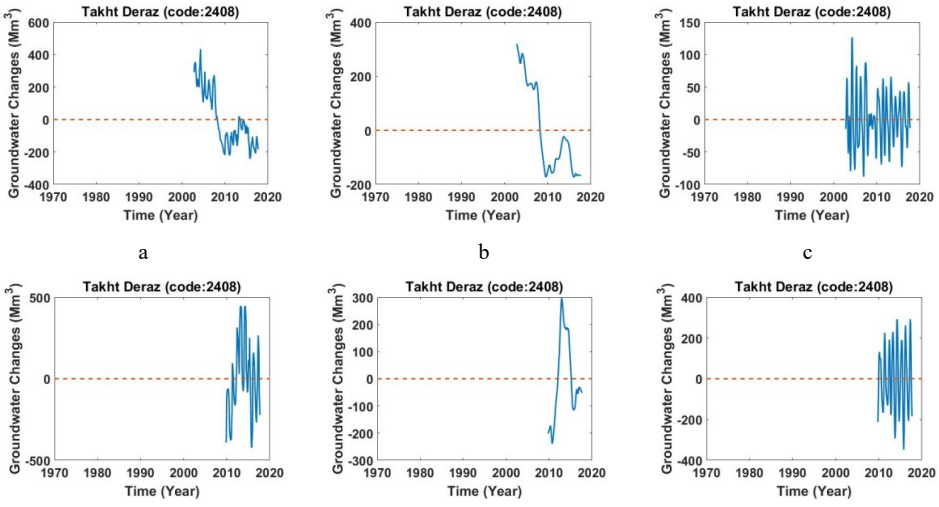

Figure 5.78. a,d) Monthly values of groundwater storage, b,e) long-period of monthly values of groundwater storage, c,f) short-period of monthly values of groundwater storage across study area of Takht Deraz (Code: 2408).

F.4.6. Study area of Zeydoon (Code: 2410)

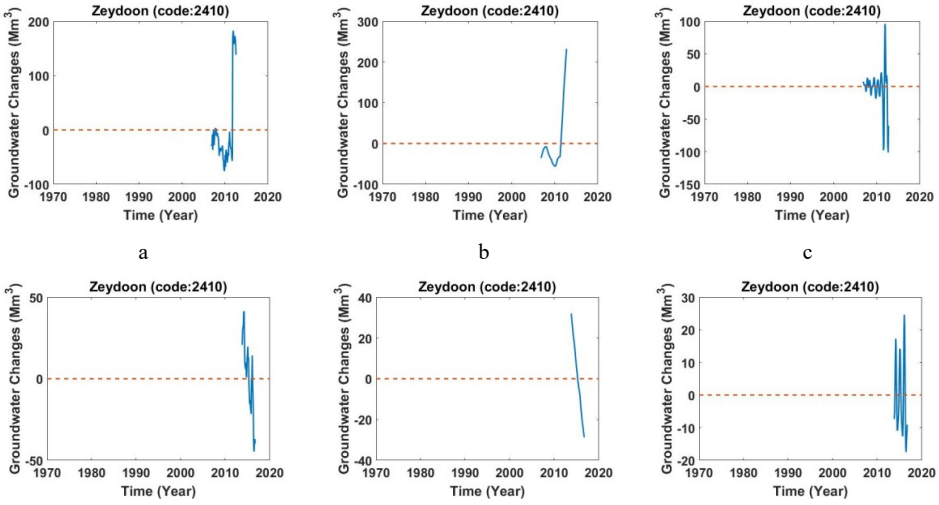

Figure 5.79. a,d) Monthly values of groundwater storage, b,e) long-period of monthly values of groundwater storage, c,f) short-period of monthly values of groundwater storage across study area of Zeydoon (Code: 2410).

F.4.7. Study area of Lishter (Code: 2411)

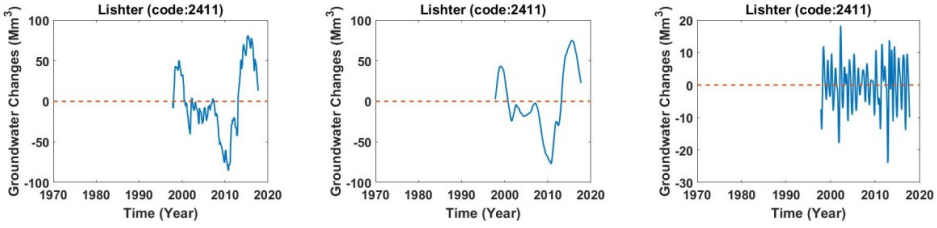

Figure 5.80. a) Monthly values of groundwater storage, b) long-period of monthly values of groundwater storage, c) short-period of monthly values of groundwater storage across study area of Lishter (Code: 2411).

F.4.8. Study area of Dehdasht (Code: 2415)

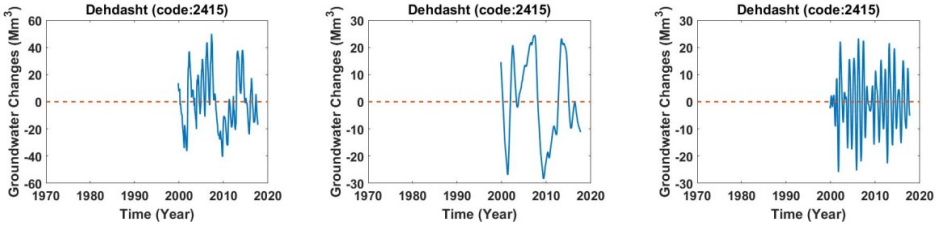

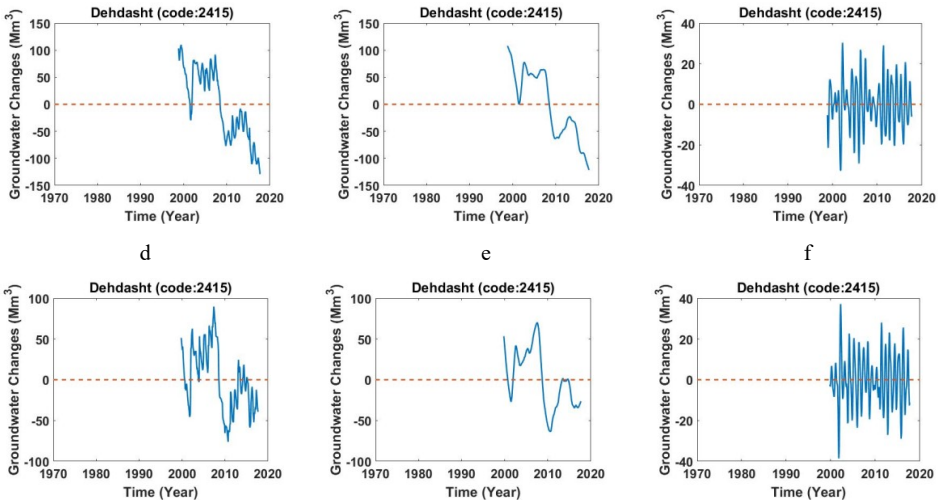

Figure 5.81. a,d,g) Monthly values of groundwater storage, b,e,h) long-period of monthly values of groundwater storage, c,f,i) short-period of monthly values of groundwater storage across study area of Dehdasht (Code: 2415).

F.4.9. Study area of Imamzade (Code: 2417)

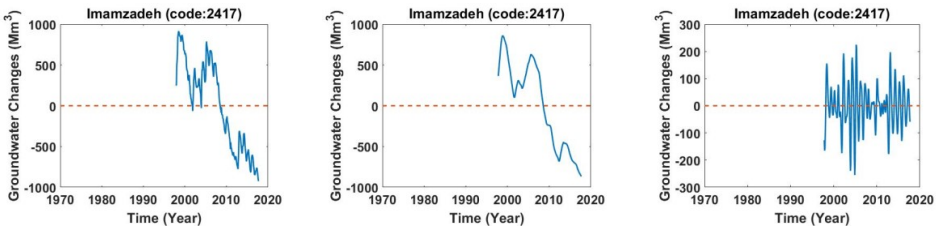

Figure 5.82. a) Monthly values of groundwater storage, b) long-period of monthly values of groundwater storage, c) short-period of monthly values of groundwater storage across study area of Imamzade (Code: 2417).

F.4.10. Study area of Dasht Rostam (Code: 2418)

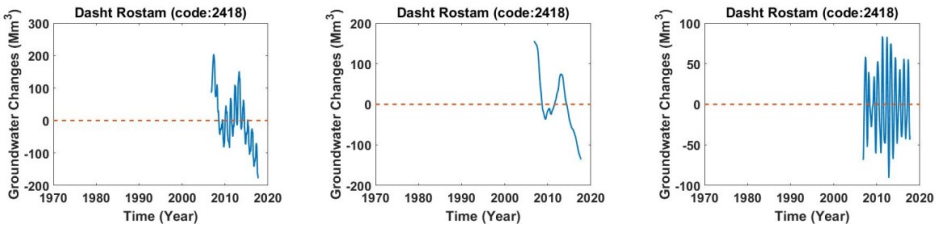

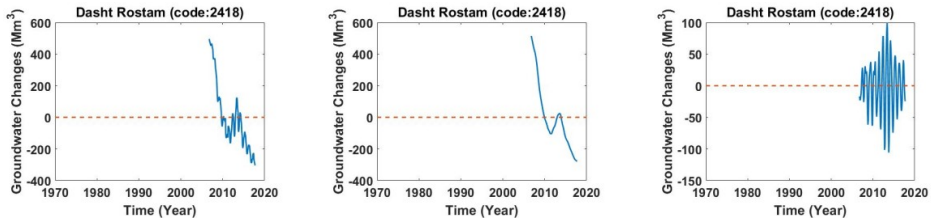

d e f

Figure 5.83. a,d,g) Monthly values of groundwater storage, b,e,h) long-period of monthly values of groundwater storage, c,f,i) short-period of monthly values of groundwater storage across study area of Dasht Rostam (Code: 2418).

F.4.11. Study area of Basht (Code: 2419)

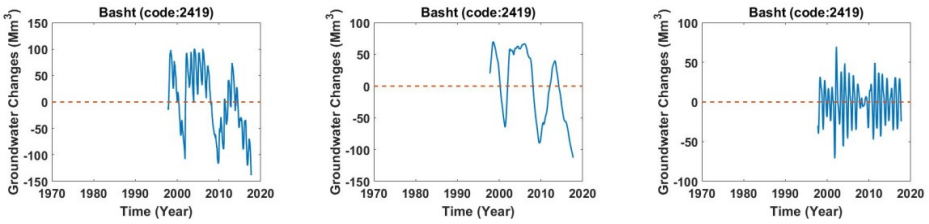

a b c

Figure 5.84. a) Monthly values of groundwater storage, b) long-period of monthly values of groundwater storage, c) short-period of monthly values of groundwater storage across study area of Basht (Code: 2419).

F.4.12. Study area of Noorabad Mamesani (Code: 2420)

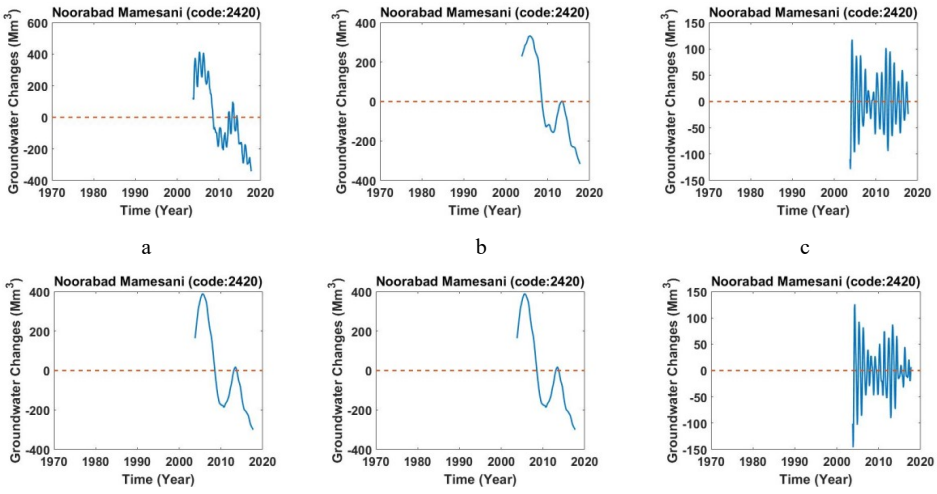

a b c

d e f

Figure 5.85. a,d) Monthly values of groundwater storage, b) long-period of monthly values of groundwater storage, c) short-period of monthly values of groundwater storage across study area of Noorabad Mamesani (Code: 2420).

F.4.13 Study area of Fahlian (Code: 2421)

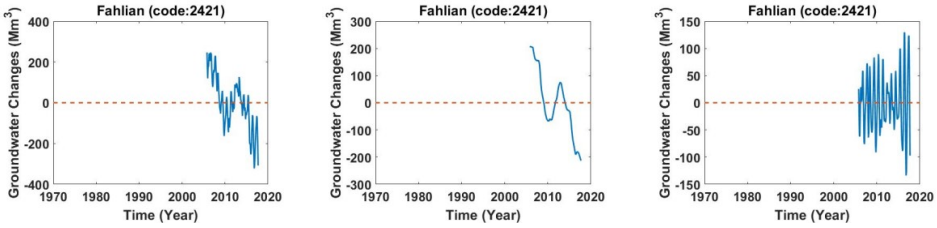

a b c

Figure 5.86. a) Monthly values of groundwater storage, b) long-period of monthly values of groundwater storage, c) short-period of monthly values of groundwater storage across study area of Fahlian (Code: 2421).

F.4.14. Study area of Koodian(Code: 2423)

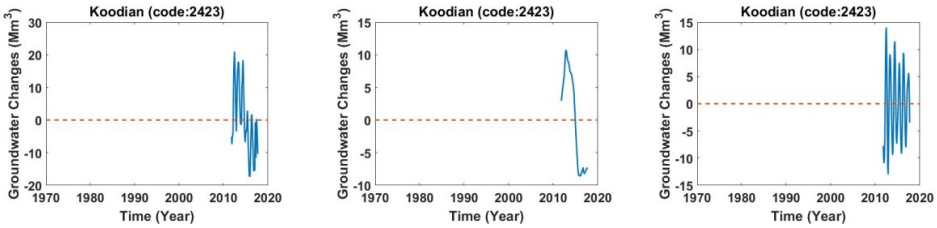

a b c

Figure 5.87. a) Monthly values of groundwater storage, b) long-period of monthly values of groundwater storage, c) short-period of monthly values of groundwater storage across study area of Koodian (Code: 2423).

F.4.15. Study area of Ardakan (Code: 2424)

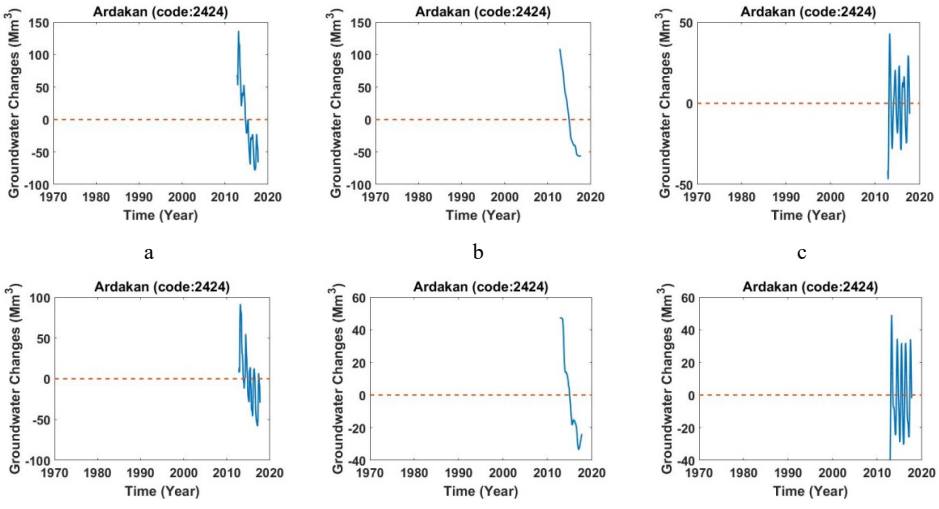

a b c

d e f

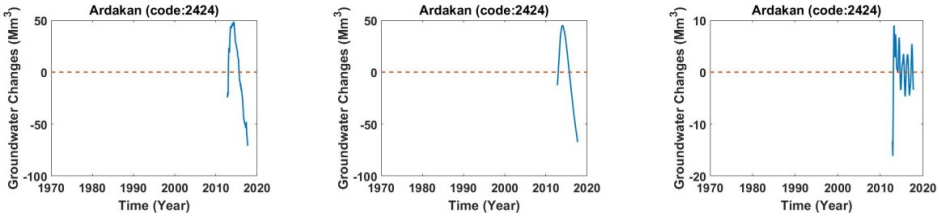

g h i

Figure 5.88. a,d) Monthly values of groundwater storage, b) long-period of monthly values of groundwater storage, c) short-period of monthly values of groundwater storage across study area of Ardakan (Code: 2424).

F.5.1. Study area of Bandar Deylam (Code: 2501)

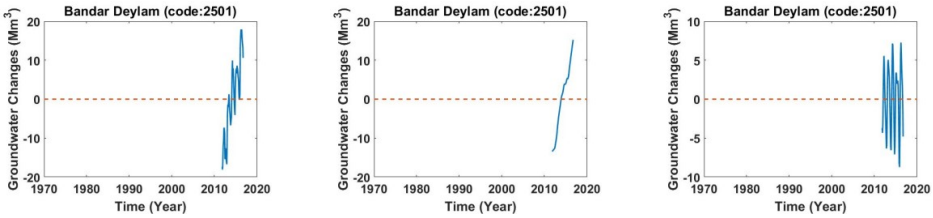

a b c

Figure F.89. a) Monthly values of groundwater storage, b) long-period of monthly values of groundwater storage, c) short-period of monthly values of groundwater storage across study area of Bandar Deylam (Code: 2501).

F.5.2. Study area of Bandar Genaveh (Code: 2502)

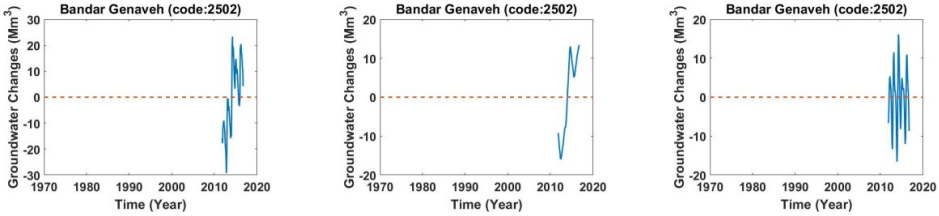

a b c

Figure F.90. a) Monthly values of groundwater storage, b) long-period of monthly values of groundwater storage, c) short-period of monthly values of groundwater storage across study area of Bandar Genaveh (Code: 2502).

F.5.3. Study area of borazjan (Code: 2503)

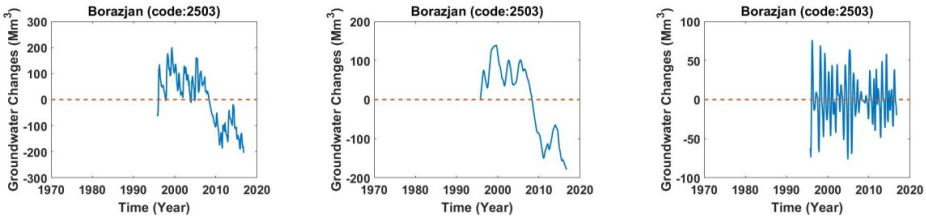

a b c

Figure F.91. a) Monthly values of groundwater storage, b) long-period of monthly values of groundwater storage, c) short-period of monthly values of groundwater storage across study area of Borazjan (Code: 2503).

F.5.4. Study area of Khesht (Code: 2504)

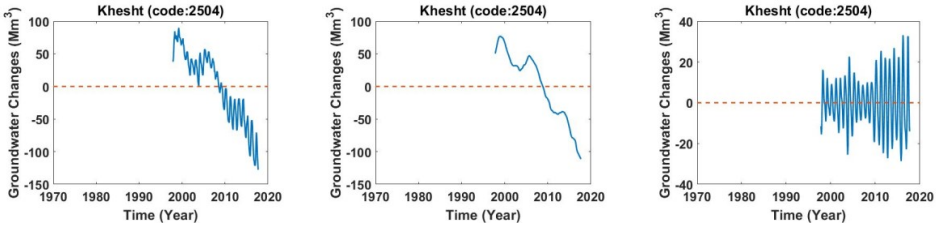

a b c

Figure F.92. a) Monthly values of groundwater storage, b) long-period of monthly values of groundwater storage, c) short-period of monthly values of groundwater storage across study area of Khesht (Code: 2504).

F.5.5. Study area of Kazeroon (Code: 2505)

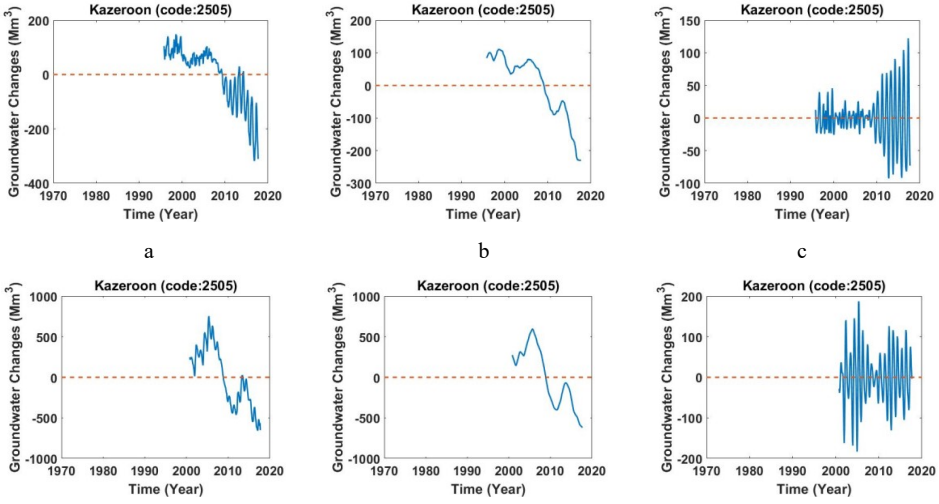

a b c

d e f

Figure F.93. a,d) Monthly values of groundwater storage, b,e) long-period of monthly values of groundwater storage, c,f) short-period of monthly values of groundwater storage across study area of Kazeroon (Code: 2505).

F.5.6. Study area of Beram (Code: 2506)

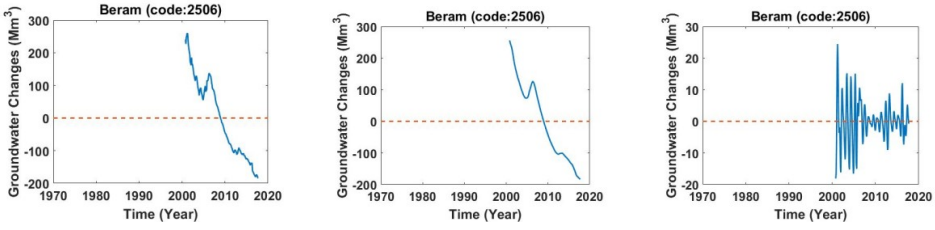

a b c

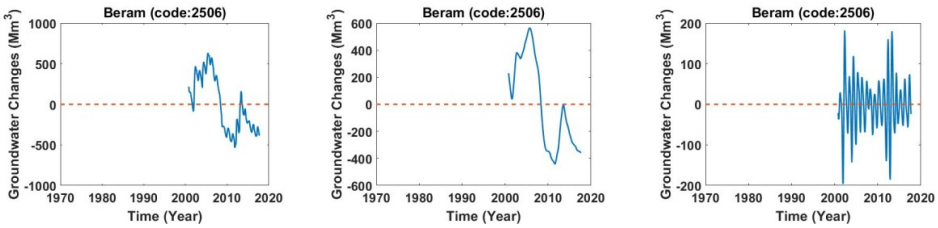

d e f

Figure F.94. a,d) Monthly values of groundwater storage, b,e) long-period of monthly values of groundwater storage, c,f) short-period of monthly values of groundwater storage across study area of Beram (Code: 2506).

F.5.7. Study area of Baladeh (Code: 2507)

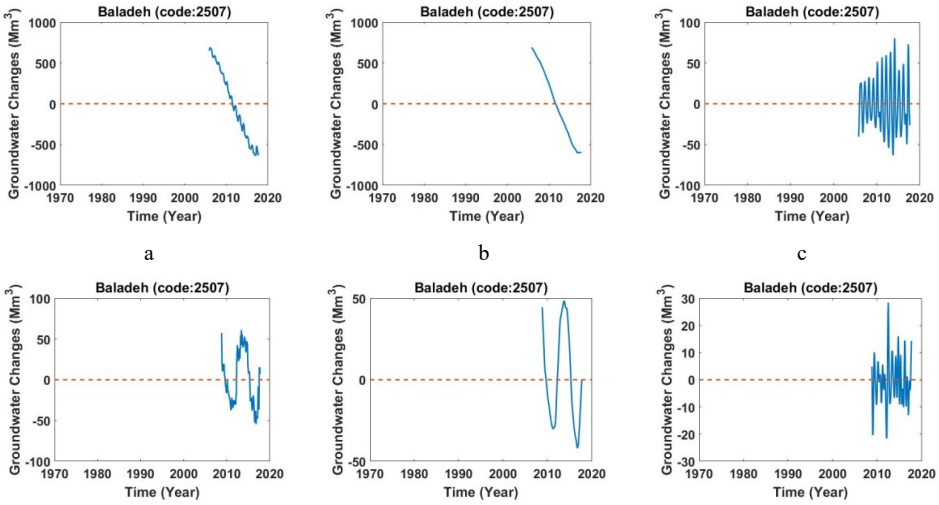

a b c

d e f

Figure F.95. a,d) Monthly values of groundwater storage, b,e) long-period of monthly values of groundwater storage, c,f) short-period of monthly values of groundwater storage across study area of Baladeh (Code: 2507).

F.5.8. Study area of Farashband (Code: 2508)

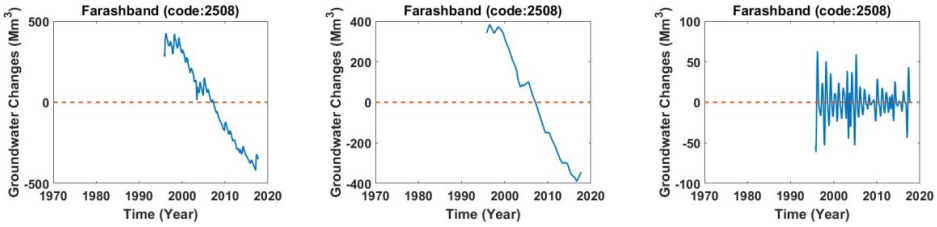

a b c

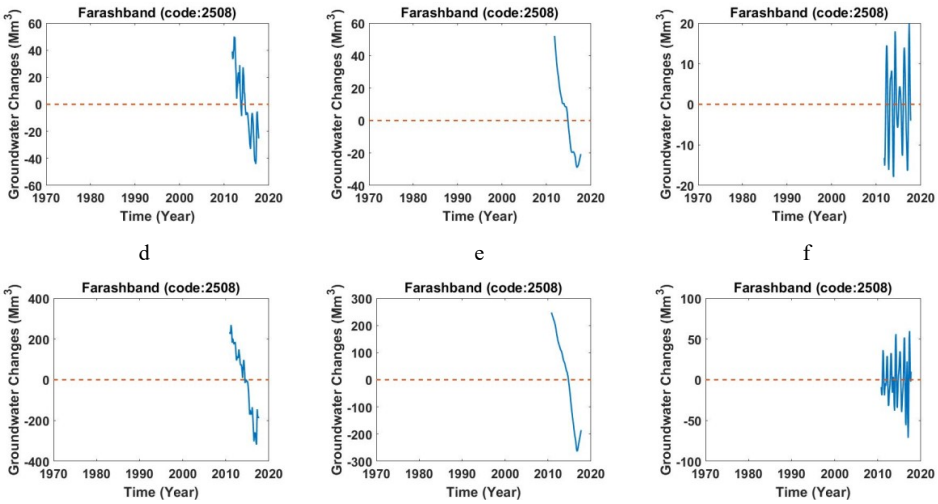

Figure F.96. a,d,g) Monthly values of groundwater storage, b,e,h) long-period of monthly values of groundwater storage, c,f,i) short-period of monthly values of groundwater storage across study area of Farashband (Code: 2508).

F.5.9. Study area of Dasht Arzhan (Code: 2510)

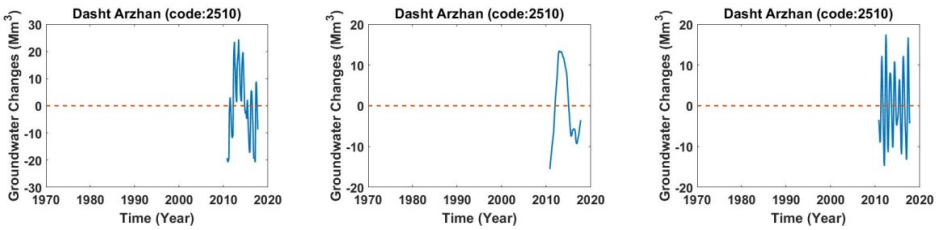

Figure F.97. a) Monthly values of groundwater storage, b) long-period of monthly values of groundwater storage, c) short-period of monthly values of groundwater storage across study area of Dasht Arzhan (Code: 2510).

F.5.10. Study area of Daryache Parishan (Code: 2511)

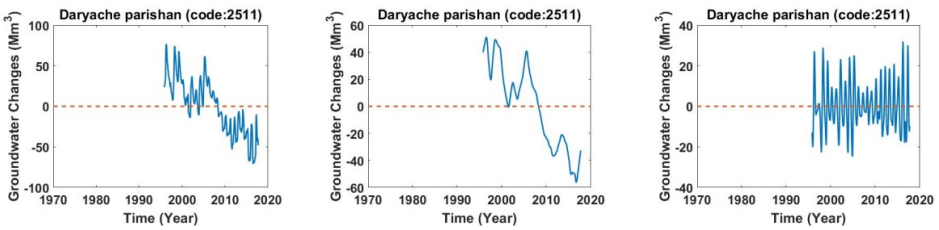

Figure F.98. a) Monthly values of groundwater storage, b) long-period of monthly values of groundwater storage, c) short-period of monthly values of groundwater storage across study area of Daryache Parishan (Code: 2511).

F.5.11. Study area of Ahrom (Code: 2512)

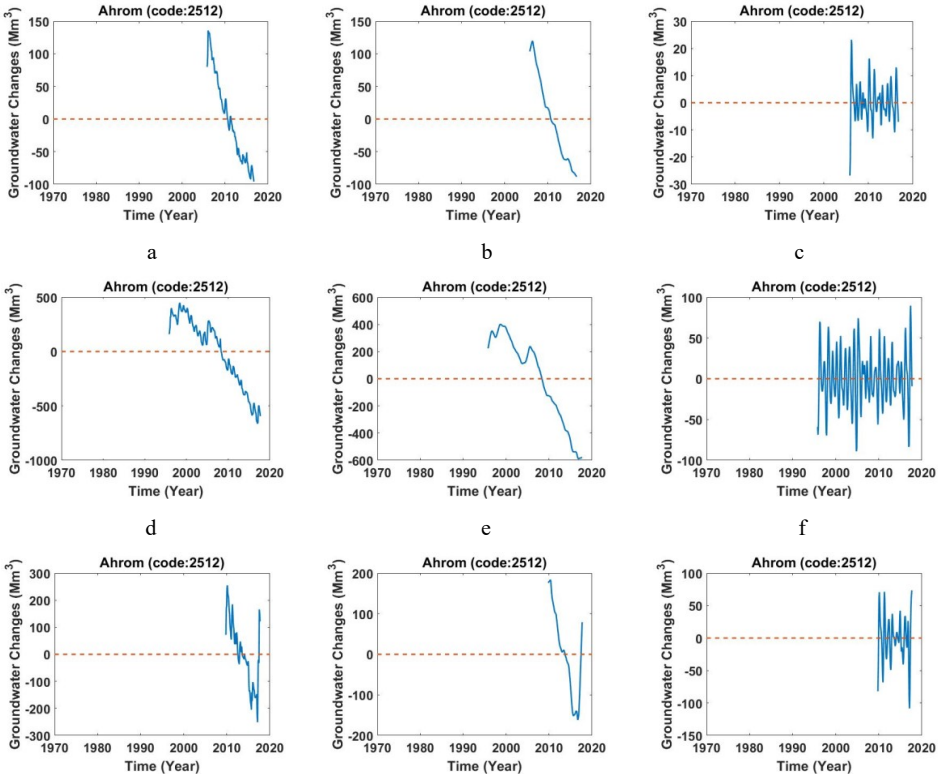

Figure F.99. a,d,g) Monthly values of groundwater storage, b,e,h) long-period of monthly values of groundwater storage, c,f,i) short-period of monthly values of groundwater storage across study area of Ahrom (Code: 2512).

F.6.1. Study area of Mand (Code: 2601)

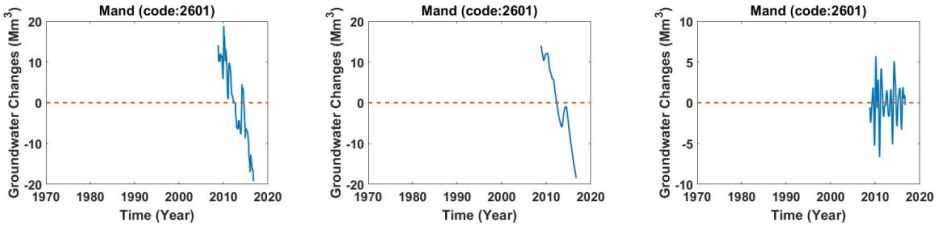

Figure F.100. a) Monthly values of groundwater storage, b) long-period of monthly values of groundwater storage, c) short-period of monthly values of groundwater storage across study area of Mand (Code: 2601).

F.6.2. Study area of Khoormoje (Code: 2602)

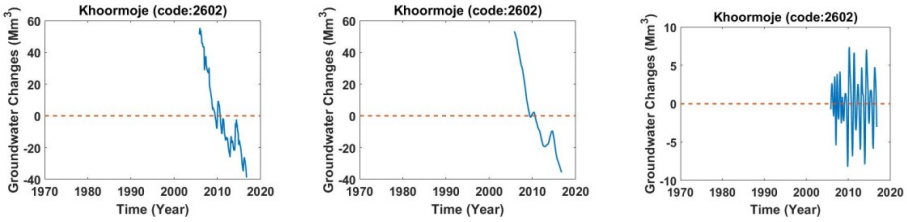

Figure F.101. a) Monthly values of groundwater storage, b) long-period of monthly values of groundwater storage, c) short-period of monthly values of groundwater storage across study area of Khoormoje (Code: 2602).

F.6.3. Study area of Chahgah (Code: 2603)

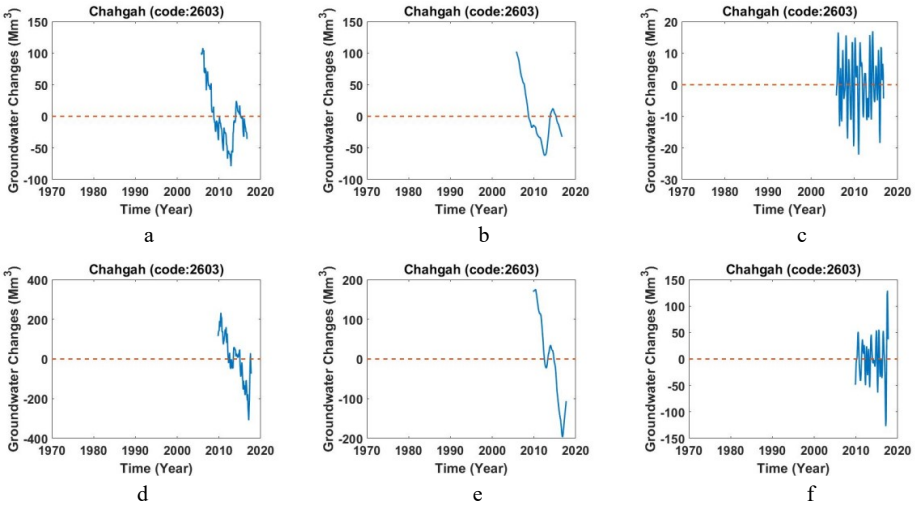

Figure F.102. a,d) Monthly values of groundwater storage, b,e) long-period of monthly values of groundwater storage, c,f) short-period of monthly values of groundwater storage across study area of Chahgah (Code: 2603).

F.6.4. Study area of Baghan (Code: 2604)

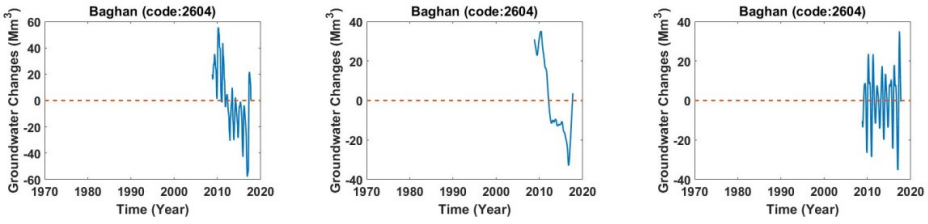

Figure F.103. a) Monthly values of groundwater storage, b) long-period of monthly values of groundwater storage, c) short-period of monthly values of groundwater storage across study area of Baghan (Code: 2604).

F.6.5. Study area of Riz (Code: 2605)

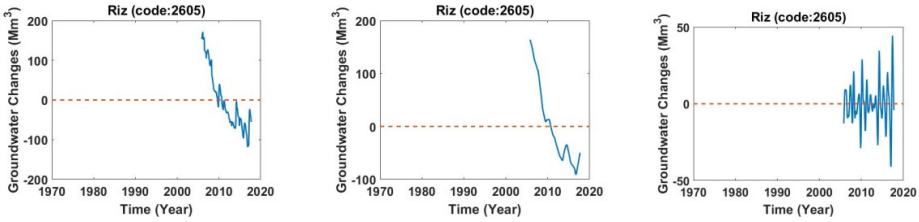

a b c

Figure F.104. a) Monthly values of groundwater storage, b) long-period of monthly values of groundwater storage, c) short-period of monthly values of groundwater storage across study area of Riz (Code: 2605).

F.6.6. Study area of Jam (Code: 2606)

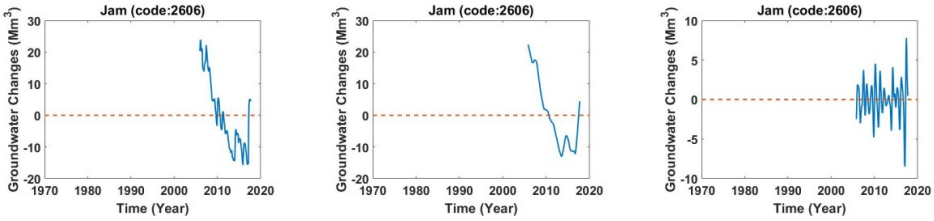

a b c

Figure F.105. a) Monthly values of groundwater storage, b) long-period of monthly values of groundwater storage, c) short-period of monthly values of groundwater storage across study area of Jam (Code: 2606).

F.6.7. Study area of Dejkan (Code: 2607)

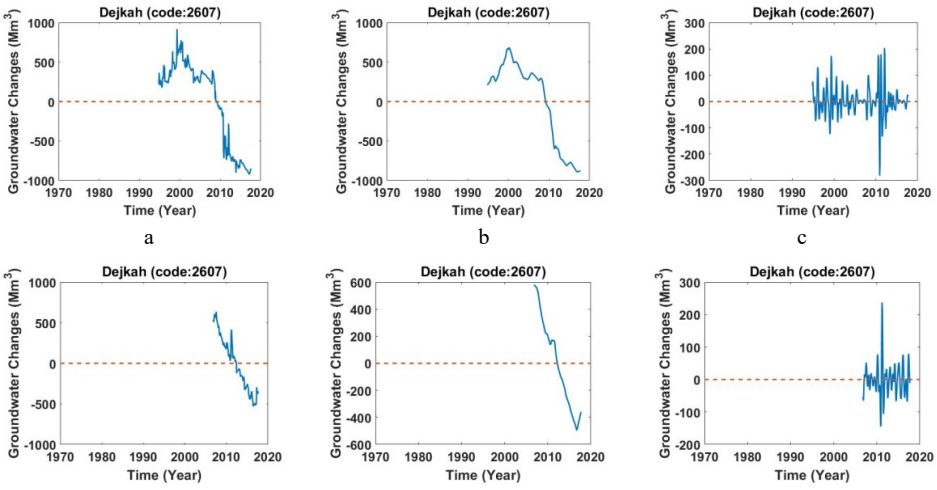

a b c

d e f

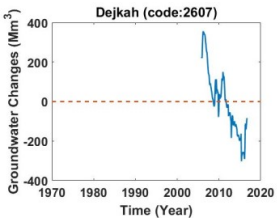

g

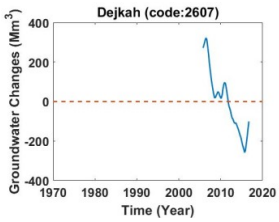

h

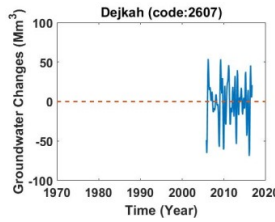

i

Figure F.106. a,d,g) Monthly values of groundwater storage, b,e,h) long-period of monthly values of groundwater storage, c,f,i) short-period of monthly values of groundwater storage across study area of Dejkah (Code: 2607).

F.6.8. Study area of Dsht Palang (Code: 2608)

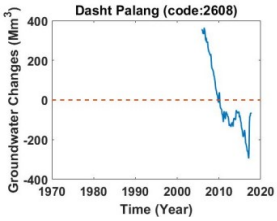

a

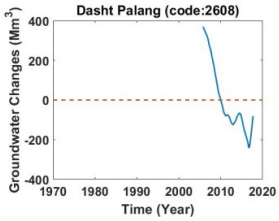

b

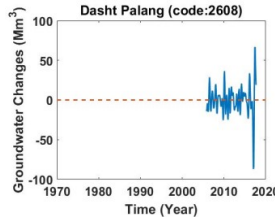

c

Figure F.107. a) Monthly values of groundwater storage, b) long-period of monthly values of groundwater storage, c) short-period of monthly values of groundwater storage across study area of Dasht Palang (Code: 2608).

F.6.9. Study area of Boshgan (Code: 2609)

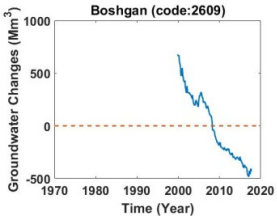

a

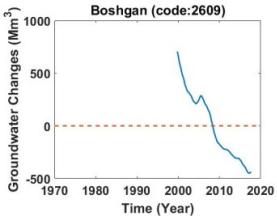

b

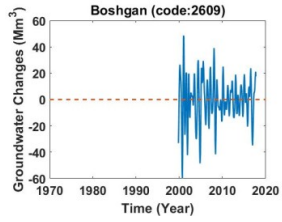

c

Figure F.108. a) Monthly values of groundwater storage, b) long-period of monthly values of groundwater storage, c) short-period of monthly values of groundwater storage across study area of Boshgan (Code: 2609).

F.6.10. Study area of Dehrood-tangeram (Code: 2610)

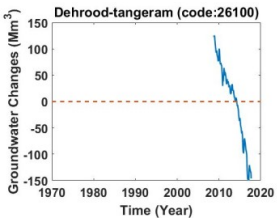

a

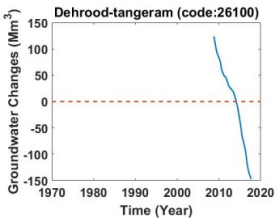

b

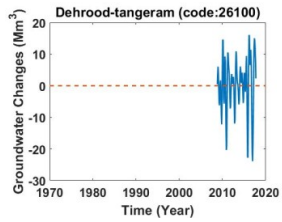

c

Figure F.109. a) Monthly values of groundwater storage, b) long-period of monthly values of groundwater storage, c) short-period of monthly values of groundwater storage across study area of Dehrood-Tangeram (Code: 2610).

F.6.11. Study area of Dehram (Code: 2611)

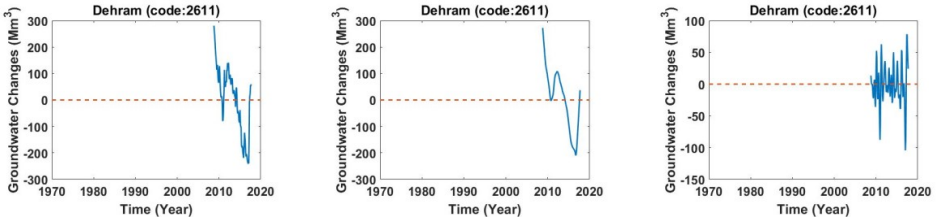

Figure F.110. a) Monthly values of groundwater storage, b) long-period of monthly values of groundwater storage, c) short-period of monthly values of groundwater storage across study area of Dehram (Code: 2611).

F.6.12. Study area of Dehrood-tangeram (Code: 2612)

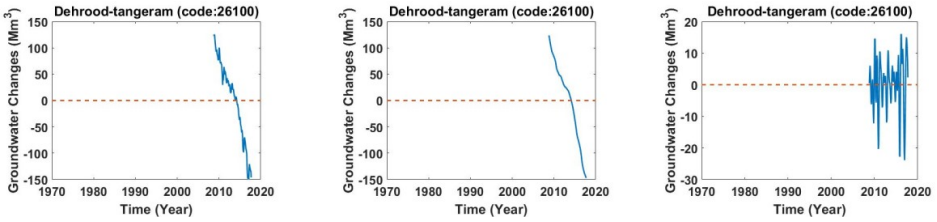

Figure F.111. a) Monthly values of groundwater storage, b) long-period of monthly values of groundwater storage, c) short-period of monthly values of groundwater storage across study area of Dehrood-Tangeram (Code: 2612).

F.6.13. Study area of Mok-Mahkoye (Code: 2613)

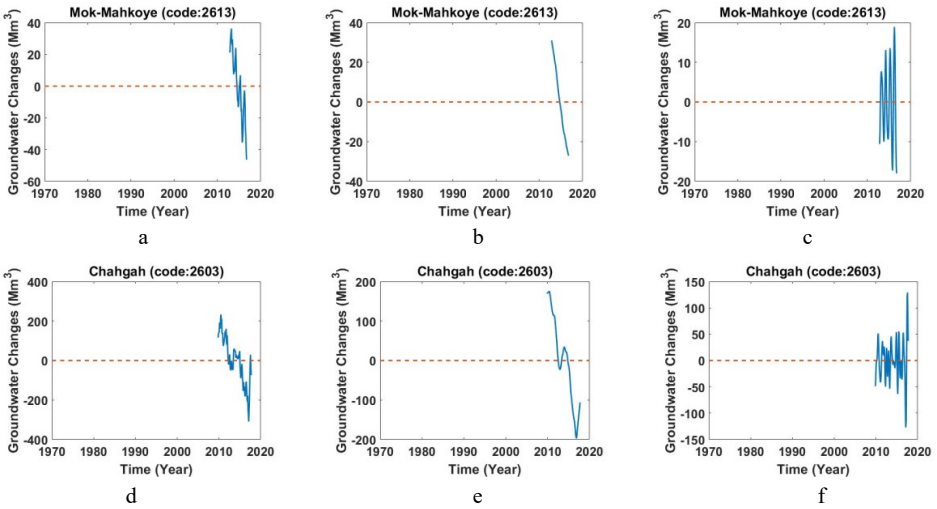

Figure F.112. a,d) Monthly values of groundwater storage, b,e) long-period of monthly values of groundwater storage, c,f) short-period of monthly values of groundwater storage across study area of Mok-Mahkoye (Code: 2613).

F.6.14. Study area of Darangan (Code: 2614)

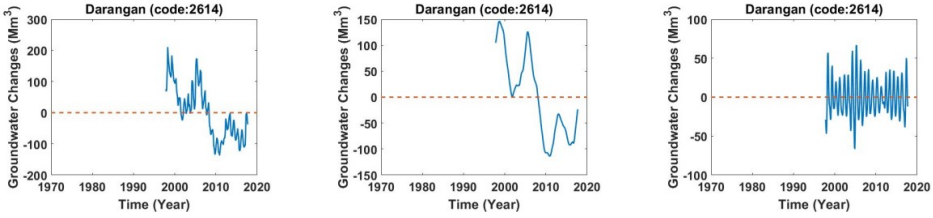

a b c

Figure F.113. a) Monthly values of groundwater storage, b) long-period of monthly values of groundwater storage, c) short-period of monthly values of groundwater storage across study area of Darangan (Code: 2614).

F.6.15. Study area of Daralmizan (Code: 2615)

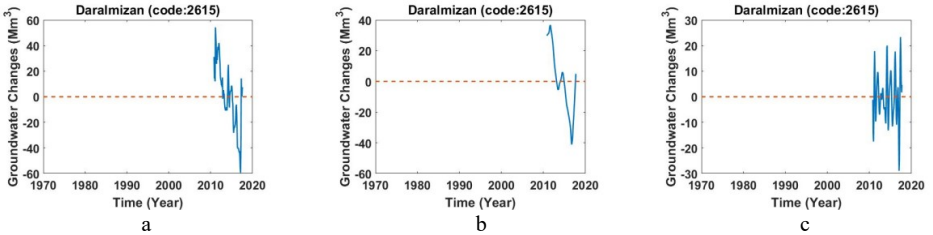

a b c

Figure F.114. a) Monthly values of groundwater storage, b) long-period of monthly values of groundwater storage, c) short-period of monthly values of groundwater storage across study area of Daralmizan (Code: 2615).

F.6.16. Study area of Alamarvdasht-Birom (Code: 2616)

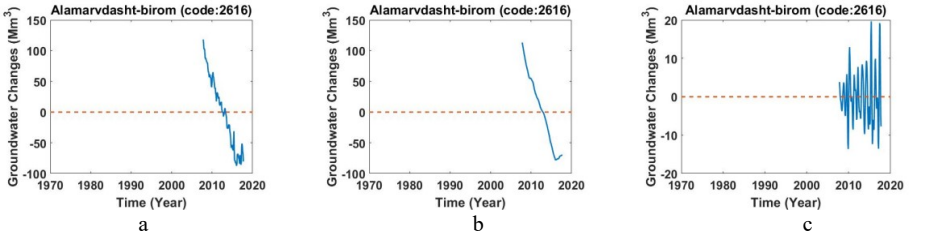

a b c

Figure F.115. a) Monthly values of groundwater storage, b) long-period of monthly values of groundwater storage, c) short-period of monthly values of groundwater storage across study area of Alamarvdasht-Birom (Code: 2616).

F.6.17. Study area of Baghe Lar (Code: 2617)

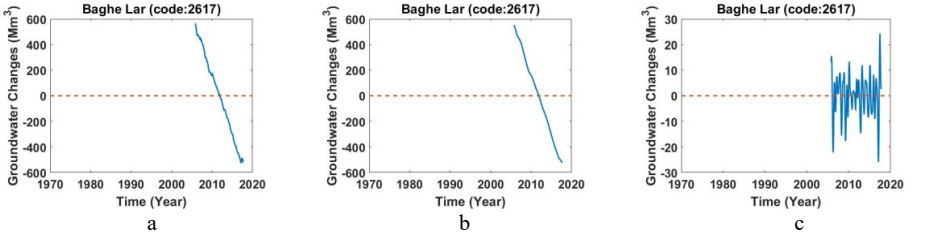

a b c

Figure F.116. a) Monthly values of groundwater storage, b) long-period of monthly values of groundwater storage, c) short-period of monthly values of groundwater storage across study area of Baghe Lar (Code: 2617).

F.6.18. Study area of Hengam (Code: 2620)

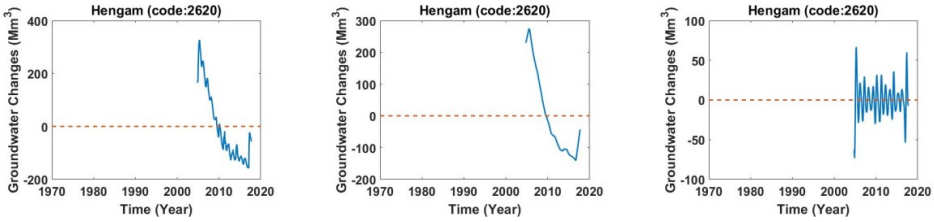

a b c

Figure F.117. a) Monthly values of groundwater storage, b) long-period of monthly values of groundwater storage, c) short-period of monthly values of groundwater storage across study area of Hengam (Code: 2620).

F.6.19. Study area of Seifabad-Laghar (Code: 2621)

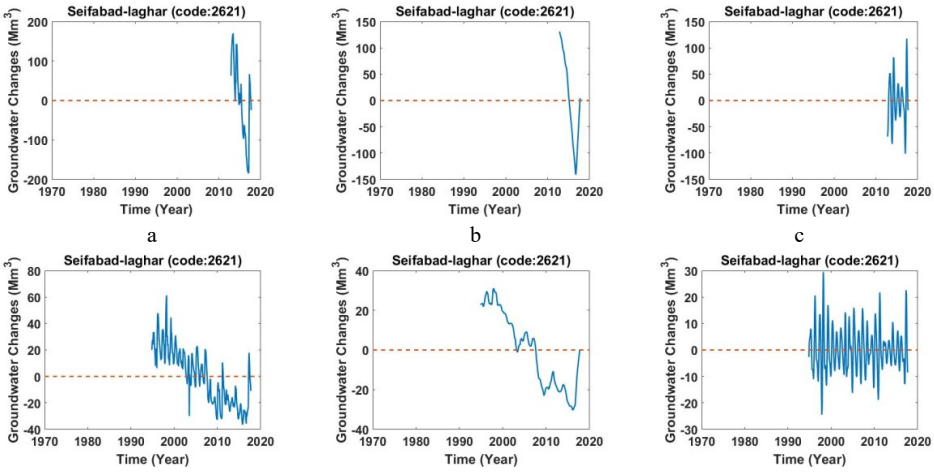

a b c

d e f

Figure F.118. a,d) Monthly values of groundwater storage, b,e) long-period of monthly values of groundwater storage, c,f) short-period of monthly values of groundwater storage across study area of Seifabad-Laghar (Code: 2621).

F.6.20. Study area of Dasht afzar (Code: 2622)

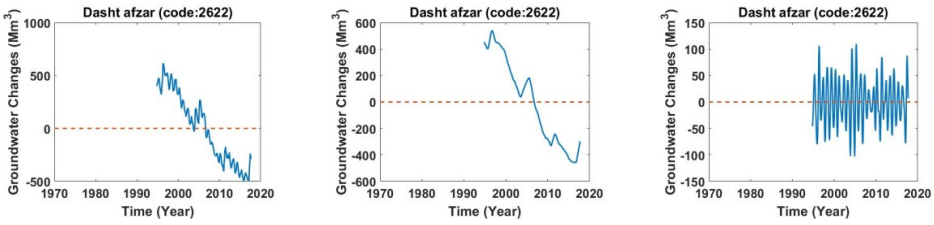

a b c

Figure F.119. a) Monthly values of groundwater storage, b) long-period of monthly values of groundwater storage, c) short-period of monthly values of groundwater storage across study area of Dasht afzar (Code: 2622).

F.6.21. Study area of Ghir-Karzin (Code: 2623)

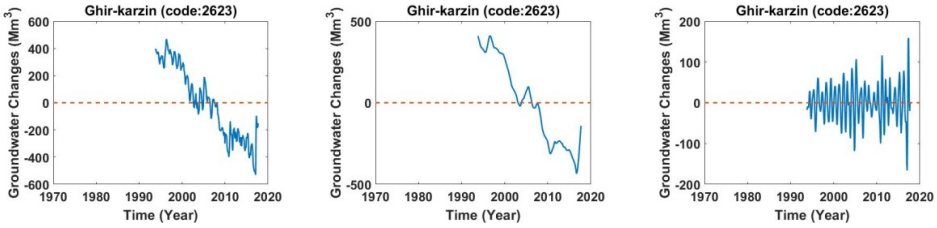

a b c

Figure F.120. a) Monthly values of groundwater storage, b) long-period of monthly values of groundwater storage, c) short-period of monthly values of groundwater storage across study area of Ghir-Karzin (Code: 2623).

F.6.22. Study area of Mobarakabad-baroos (Code: 2624)

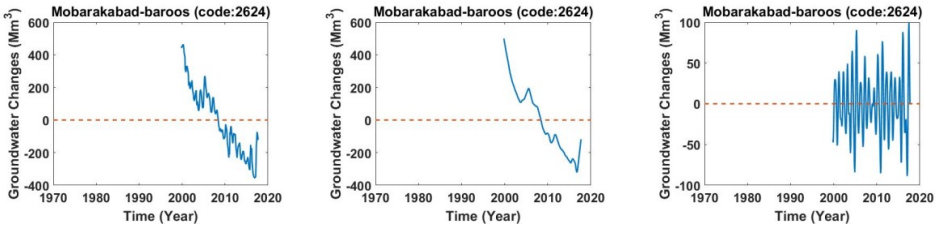

a b c

Figure F.121. a) Monthly values of groundwater storage, b) long-period of monthly values of groundwater storage, c) short-period of monthly values of groundwater storage across study area of Mobarakabad-baroos (Code: 2624).

F.6.23. Study area of Hakan (Code: 2625)

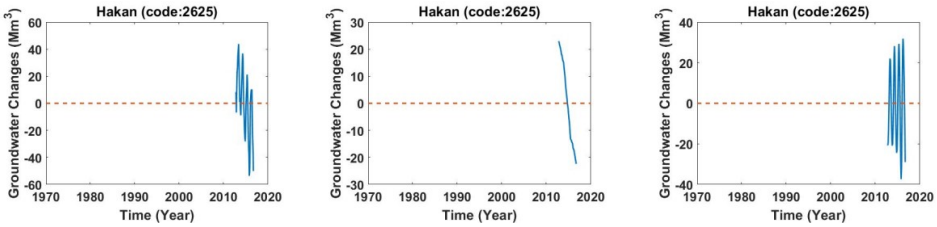

a b c

Figure F.122. a) Monthly values of groundwater storage, b) long-period of monthly values of groundwater storage, c) short-period of monthly values of groundwater storage across study area of Hakan (Code: 2625).

F.6.24. Study area of Dasht afzar (Code: 2626)

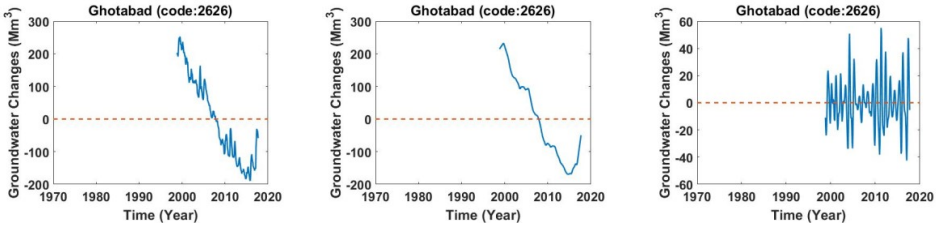

Figure F.123. a) Monthly values of groundwater storage, b) long-period of monthly values of groundwater storage, c) short-period of monthly values of groundwater storage across study area of Dasht afzar (Code: 2626).

F.6.25. Study area of Jahrom (Code: 2627)

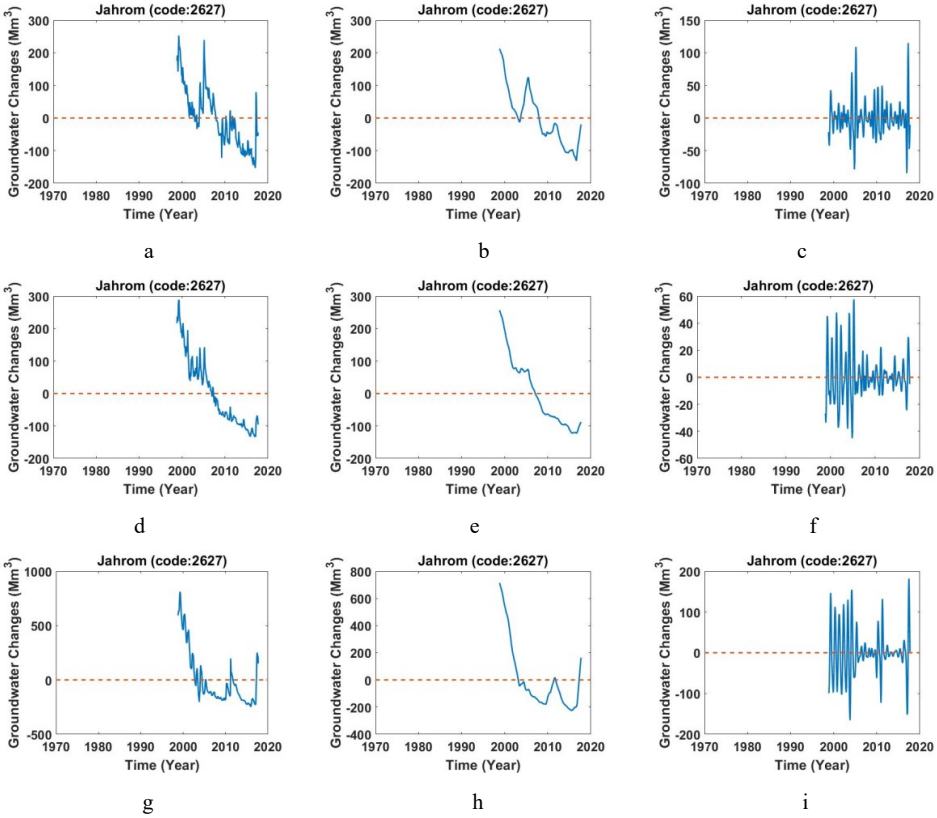

Figure F.124. a,d) Monthly values of groundwater storage, b,e) long-period of monthly values of groundwater storage, c,f) short-period of monthly values of groundwater storage across study area of Jahrom (Code: 2627).

F.6.26. Study area of zahedoon (Code: 2628)

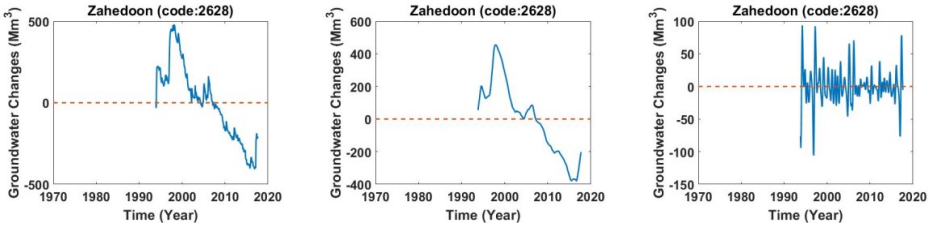

a b c

Figure F.125. a) Monthly values of groundwater storage, b) long-period of monthly values of groundwater storage, c) short-period of monthly values of groundwater storage across study area of zahedoon (Code: 2628).

F.6.27. Study area of Fasa (Code: 2629)

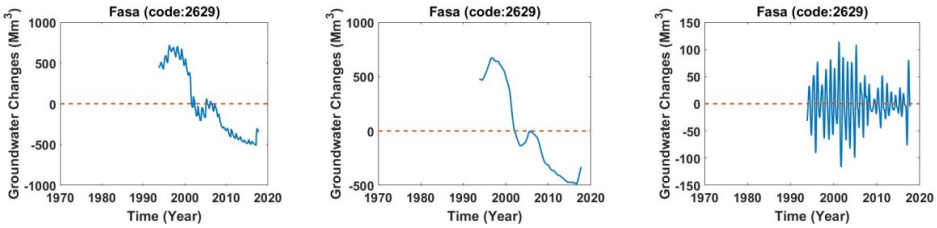

a b c

Figure F.126. a) Monthly values of groundwater storage, b) long-period of monthly values of groundwater storage, c) short-period of monthly values of groundwater storage across study area of Fasas (Code: 2629).

F.6.28. Study area of Mian Jangal (Code: 2630)

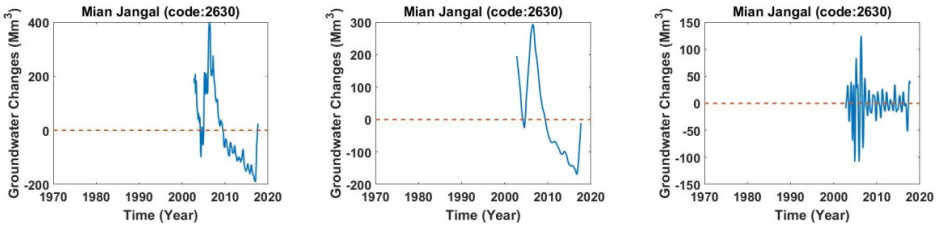

a b c

Figure F.127. a) Monthly values of groundwater storage, b) long-period of monthly values of groundwater storage, c) short-period of monthly values of groundwater storage across study area of Mian Jangal (Code: 2630).

F.6.29. Study area of Roniz (Code: 2631)

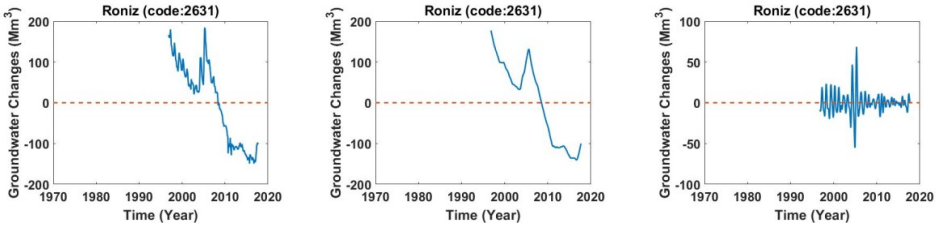

a b c

Figure F.128. a) Monthly values of groundwater storage, b) long-period of monthly values of groundwater storage, c) short-period of monthly values of groundwater storage across study area of Roniz (Code: 2631).

F.6.30. Study area of Nobandegan (Code: 2632)

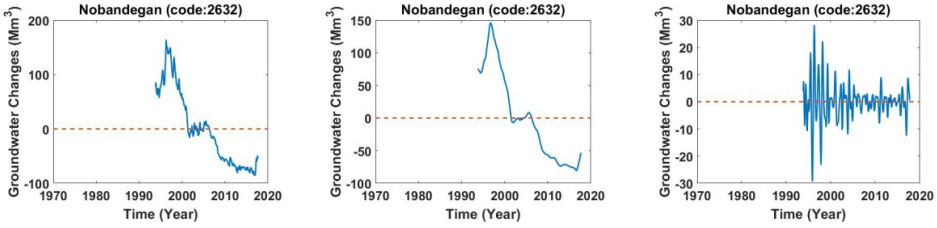

a b c

Figure F.129. a) Monthly values of groundwater storage, b) long-period of monthly values of groundwater storage, c) short-period of monthly values of groundwater storage across study area of Nobandegan (Code: 2632).

F.6.31. Study area of Gharebolagh (Code: 2633)

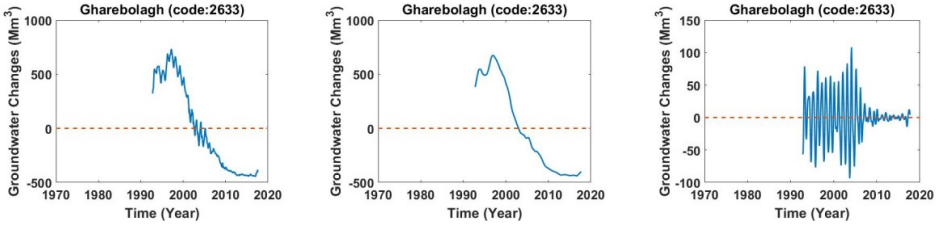

a b c

Figure F.130. a) Monthly values of groundwater storage, b) long-period of monthly values of groundwater storage, c) short-period of monthly values of groundwater storage across study area of Gharebolagh (Code: 2633).

F.6.32. Study area of Eaj (Code: 2634)

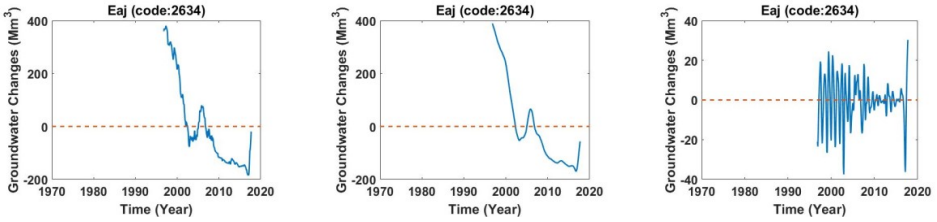

a b c

Figure F.131. a) Monthly values of groundwater storage, b) long-period of monthly values of groundwater storage, c) short-period of monthly values of groundwater storage across study area of Eaj (Code: 2634).

F.6.33. Study area of Meimand Shabankare (Code: 2636)

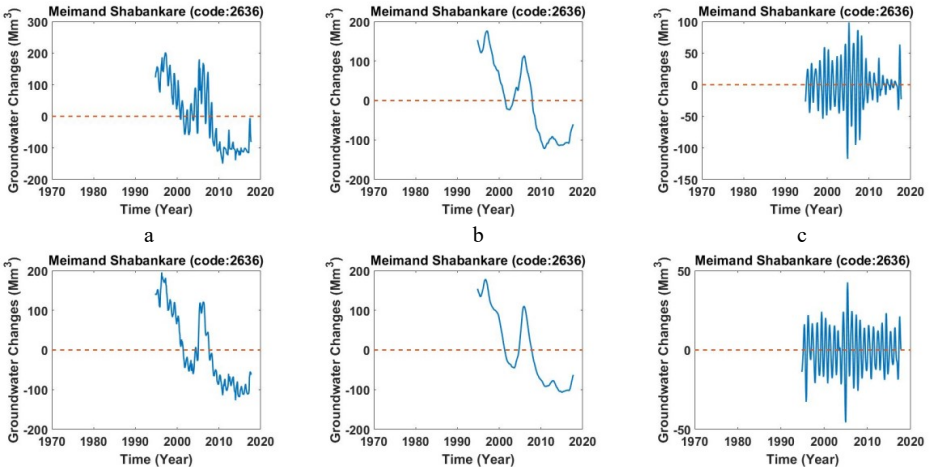

a b c

d e f

Figure F.132. a,d) Monthly values of groundwater storage, b,e) long-period of monthly values of groundwater storage, c,f) short-period of monthly values of groundwater storage across study area of Meimand Shabankare (Code: 2636).

F.6.34. Study area of Khafar (Code: 2637)

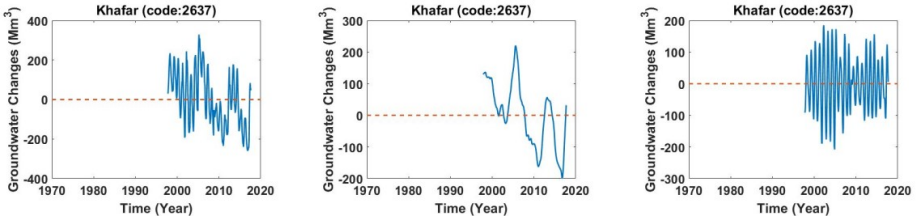

a b c

Figure F.133. a) Monthly values of groundwater storage, b) long-period of monthly values of groundwater storage, c) short-period of monthly values of groundwater storage across study area of Khafar (Code: 2637).

F.6.35. Study area of Kovar (Code: 2638)

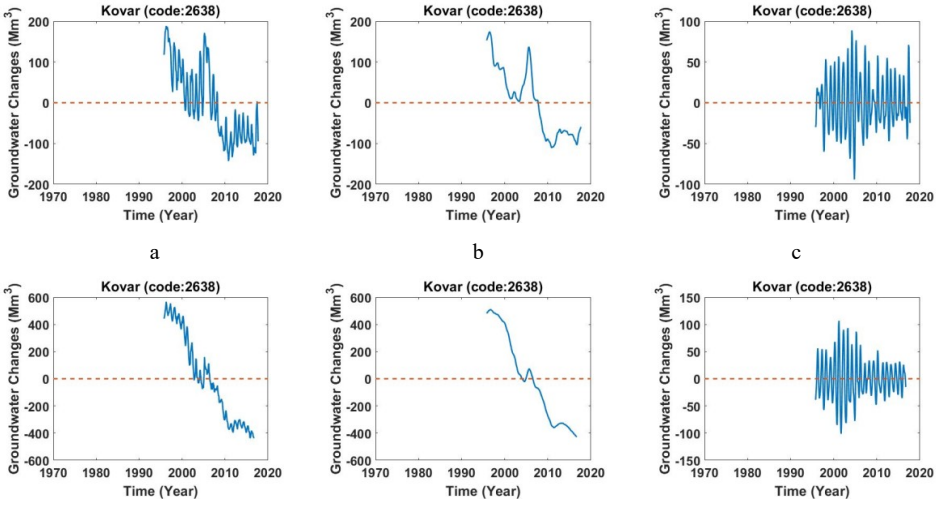

Figure F.134. a,d) Monthly values of groundwater storage, b,e) long-period of monthly values of groundwater storage, c,f) short-period of monthly values of groundwater storage across study area of Kovar (Code: 2638).

F.6.36. Study area of Sikh-Darnegoon (Code: 2639)

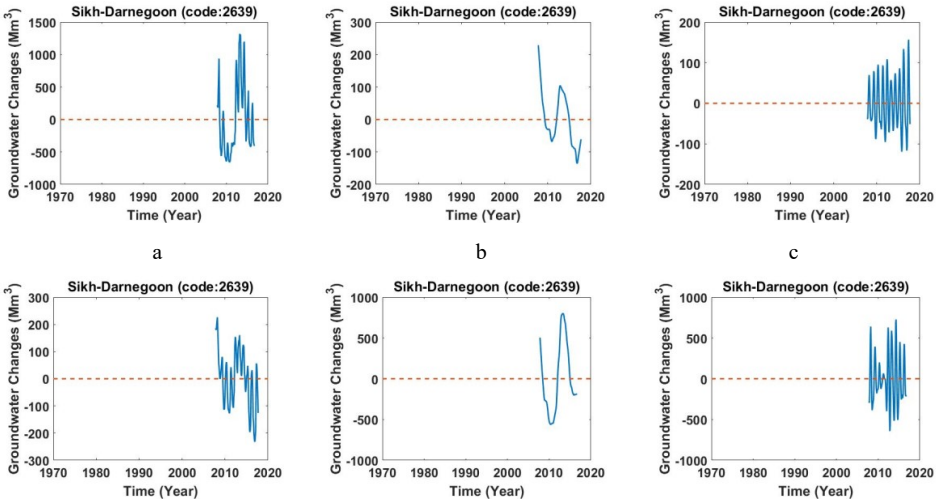

Figure F.135. a,d) Monthly values of groundwater storage, b,e) long-period of monthly values of groundwater storage, c,f) short-period of monthly values of groundwater storage across study area of Sikh-darnegoon (Code: 2639).

F.6.37. Study area of Khane Zanian (Code: 2640)

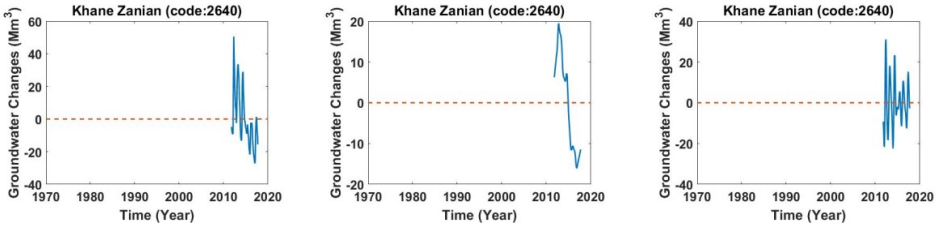

a b c

Figure F.136. a) Monthly values of groundwater storage, b) long-period of monthly values of groundwater storage, c) short-period of monthly values of groundwater storage across study area of Khane Zanian (Code: 2640).

F.6.38. Study area of Benrood Zangane (Code: 2641)

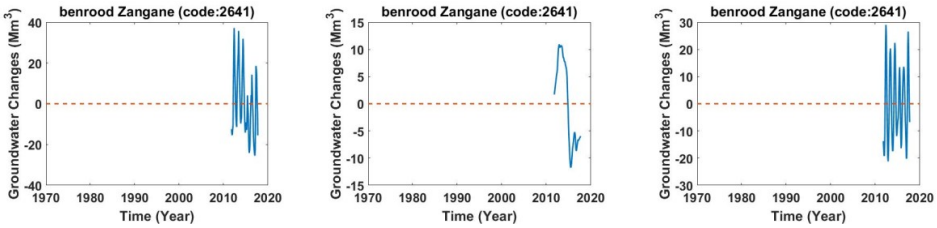

a b c

Figure F.137. a) Monthly values of groundwater storage, b) long-period of monthly values of groundwater storage, c) short-period of monthly values of groundwater storage across study area of Benrood Zangane (Code: 2641).

F.6.39. Study area of Khanj (Code: 2642)

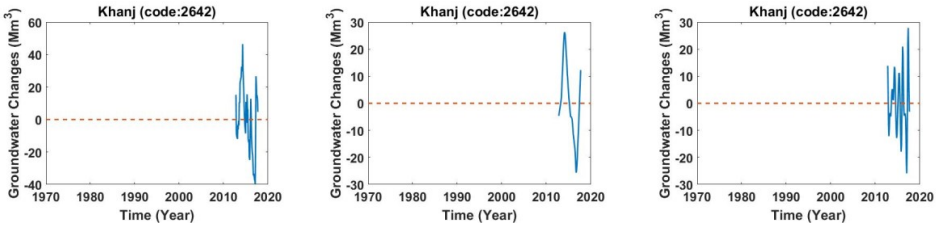

a b c

Figure F.138. a) Monthly values of groundwater storage, b) long-period of monthly values of groundwater storage, c) short-period of monthly values of groundwater storage across study area of Khanj (Code: 2642).

F.6.40. Study area of Bidshar (Code: 2643)

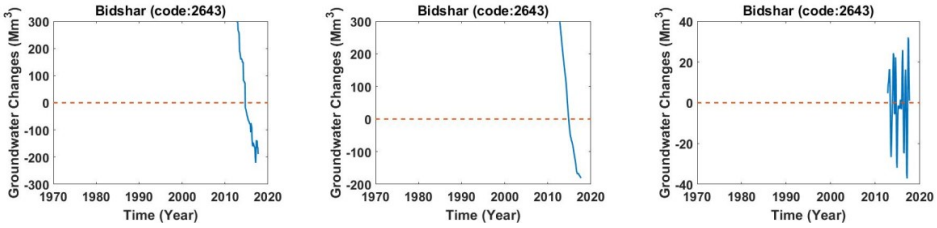

a b c

Figure F.139. a) Monthly values of groundwater storage, b) long-period of monthly values of groundwater storage, c) short-period of monthly values of groundwater storage across study area of Khafar (Code: 2643).

F.6.41. Study area of Jovim-Banarooye (Code: 2644)

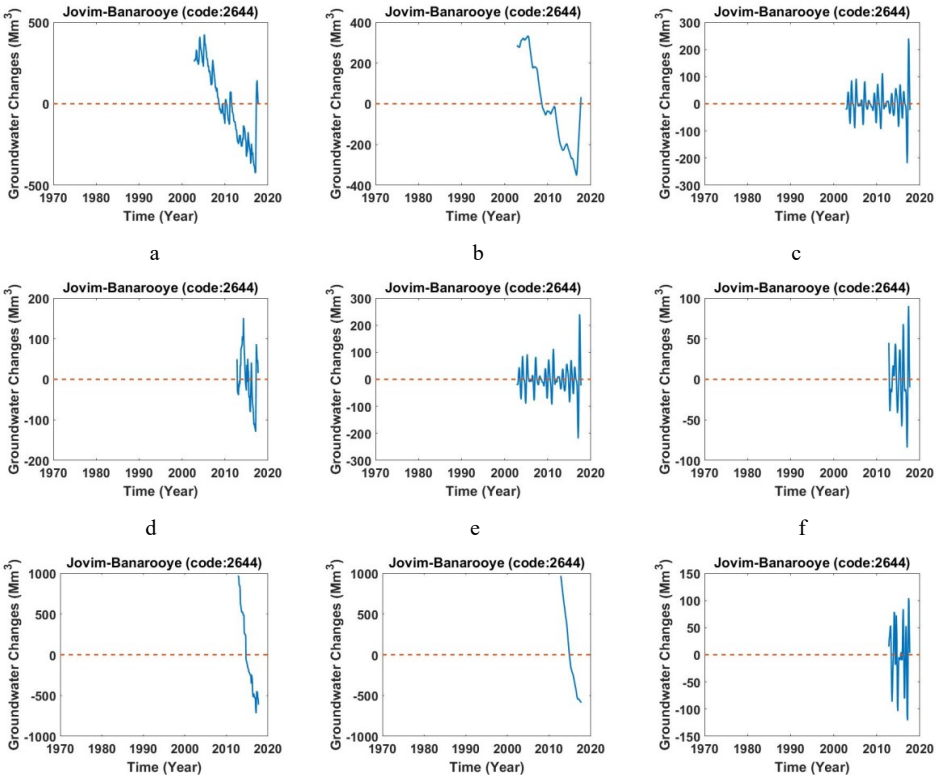

a b c

d e f

g h i

Figure F.140. a,d,g) Monthly values of groundwater storage, b,e,h) long-period of monthly values of groundwater storage, c,f,i) short-period of monthly values of groundwater storage across study area of Jovim-Banarooye (Code: 2644).

F.6.42. Study area of Dehkuyeh (Code: 2646)

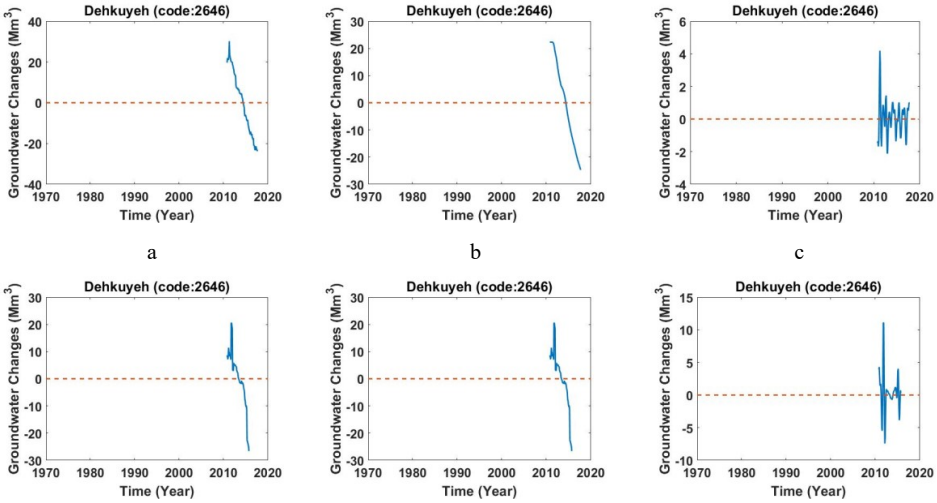

Figure F.141. a,d) Monthly values of groundwater storage, b,e) long-period of monthly values of groundwater storage, c,f) short-period of monthly values of groundwater storage across study area of Dehkuyeh (Code: 2646).

F.6.43. Study area of Izadkhast (Code: 2647)

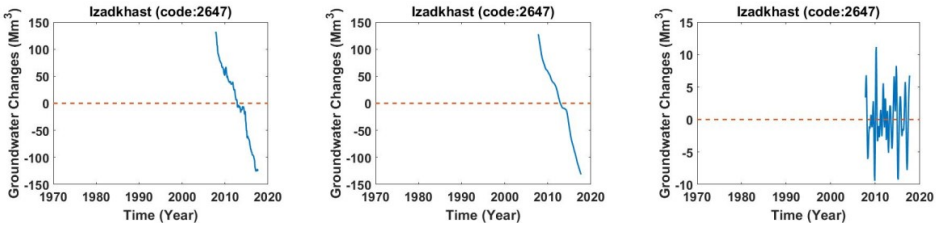

Figure F.142. a) Monthly values of groundwater storage, b) long-period of monthly values of groundwater storage, c) short-period of monthly values of groundwater storage across study area of Izadkhast (Code: 2647).

F.7.1. Study area of Kahoorestan (Code: 2701)

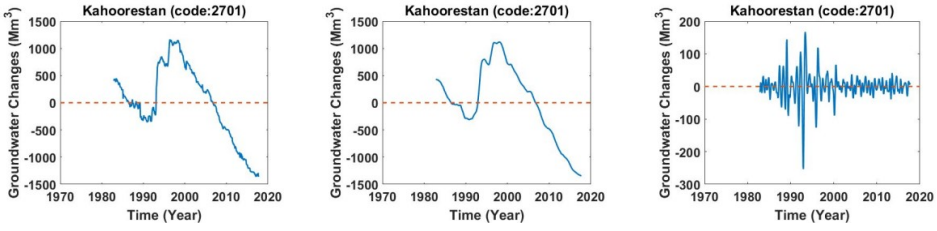

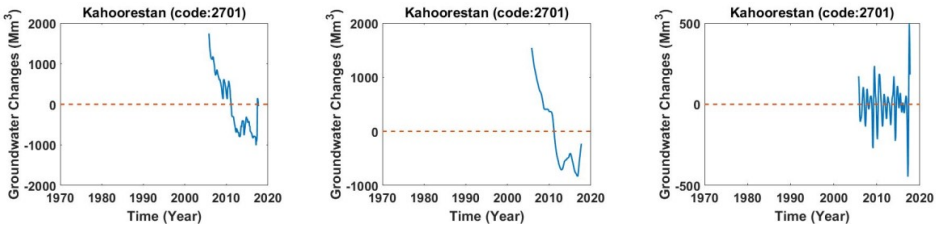

d e f

Figure F.143. a,d) Monthly values of groundwater storage, b,e) long-period of monthly values of groundwater storage, c,f) short-period of monthly values of groundwater storage across study area of Kahoorestan (Code: 2701).

F.7.2. Study area of Aisyn (Code: 2702)

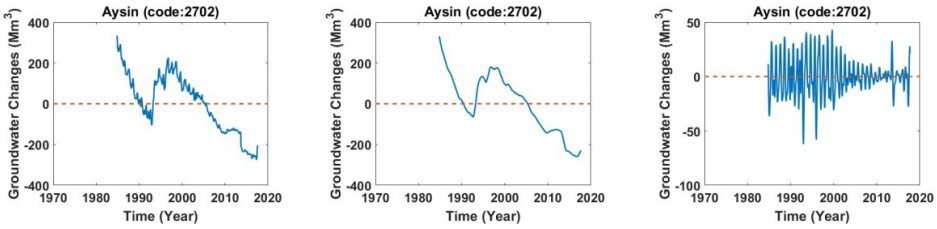

a b c

Figure F.144. a) Monthly values of groundwater storage, b) long-period of monthly values of groundwater storage, c) short-period of monthly values of groundwater storage across study area of Aysin (Code: 2702).

F.7.3. Study area of Rezvan (Code: 2703)

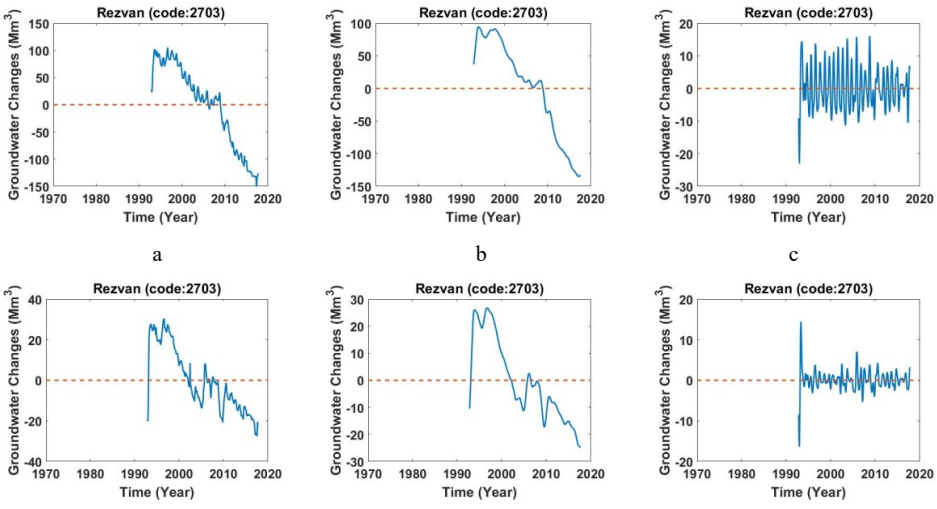

a b c

d e f

Figure F.145. a,d) Monthly values of groundwater storage, b,e) long-period of monthly values of groundwater storage, c,f) short-period of monthly values of groundwater storage across study area of Rezvan (Code: 2703).

F.7.4. Study area of Deh hang (Code: 2704)

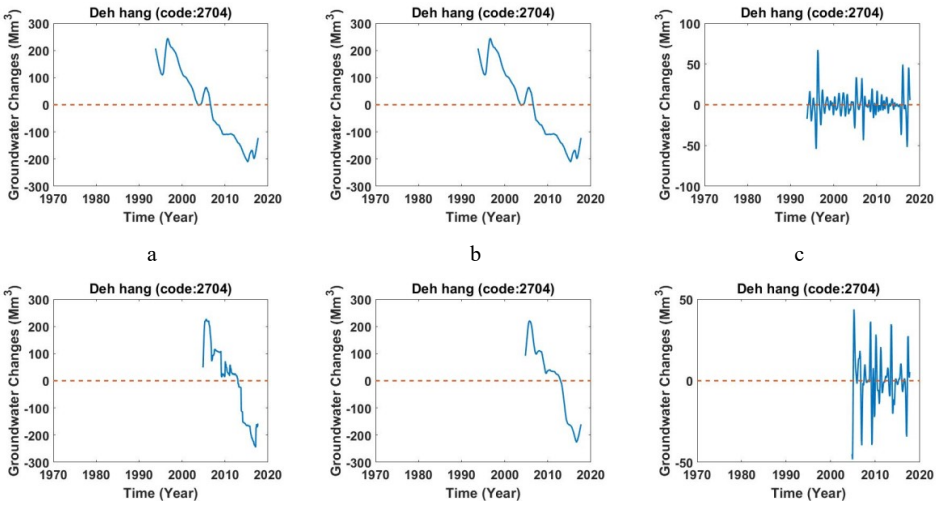

Figure F.146.a,d) Monthly values of groundwater storage, b,e) long-period of monthly values of groundwater storage, c,f) short-period of monthly values of groundwater storage across study area of deh hang (Code: 2704).

F.7.5. Study area of Bashdoo (Code: 2705)

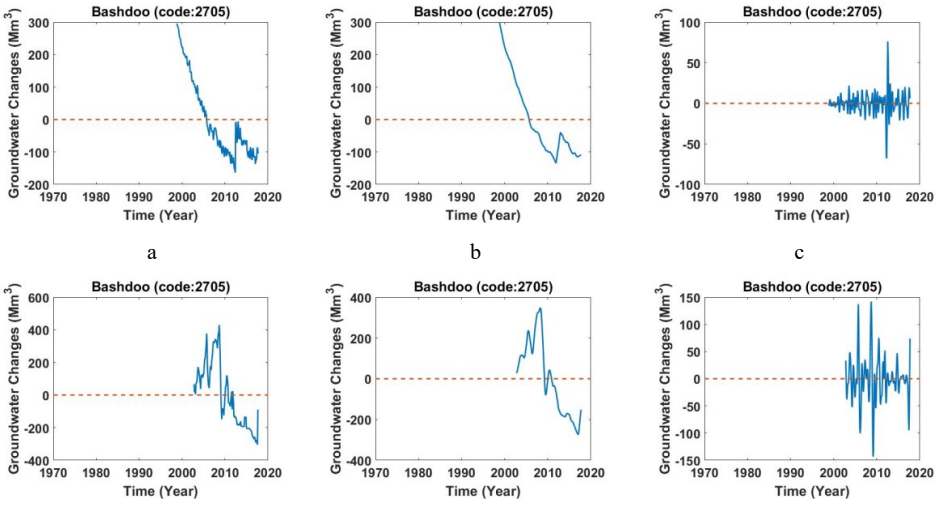

Figure F.147.a,d) Monthly values of groundwater storage, b,e) long-period of monthly values of groundwater storage, c,f) short-period of monthly values of groundwater storage across study area of deh hang (Code: 2705).

F.7.6. Study area of Darz Sayeban (Code: 2706)

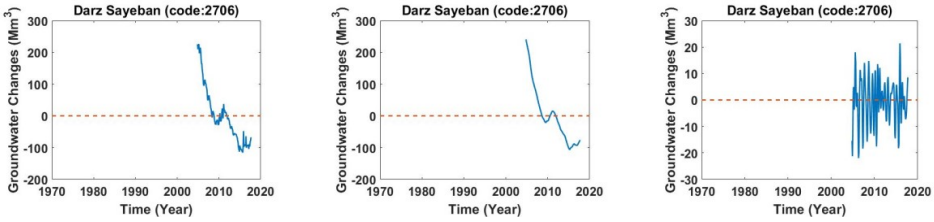

a b c

Figure F.148. a) Monthly values of groundwater storage, b) long-period of monthly values of groundwater storage, c) short-period of monthly values of groundwater storage across study area of Darze Sayeban (Code: 2706).

F.7.7. Study area of Shah Gheyb (Code: 2707)

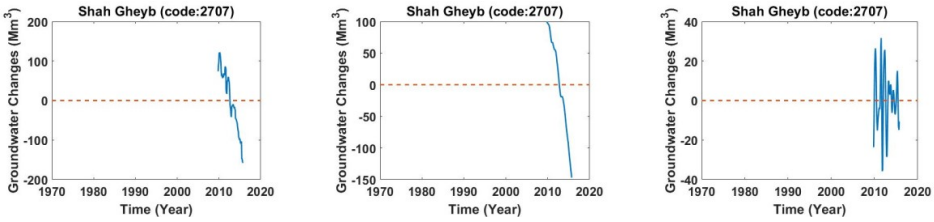

a b c

Figure F.149. a) Monthly values of groundwater storage, b) long-period of monthly values of groundwater storage, c) short-period of monthly values of groundwater storage across study area of Shah Gheyb (Code: 2707).

F.7.8. Study area of Lar (Code: 2708)

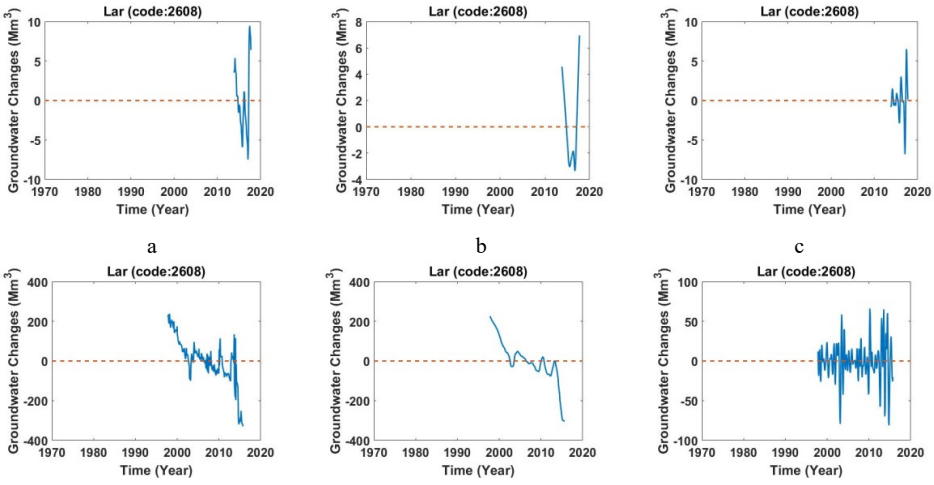

a b c

d e f

Figure F.150. a,d) Monthly values of groundwater storage, b,e) long-period of monthly values of groundwater storage, c,f) short-period of monthly values of groundwater storage across study area of Lar (Code: 2708).

F.7.9. Study area of Garash (Code: 2709)

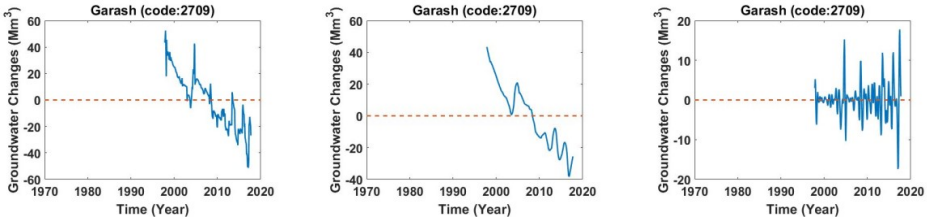

Figure F.151. a) Monthly values of groundwater storage, b) long-period of monthly values of groundwater storage, c) short-period of monthly values of groundwater storage across study area of Garash(Code: 2709).

F.7.10. Study area of Fin-Maram (Code: 2710)

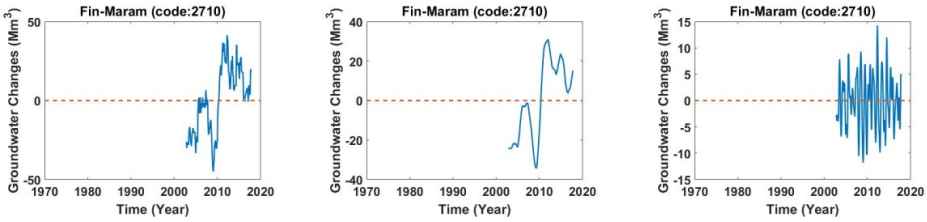

Figure F.152. a) Monthly values of groundwater storage, b) long-period of monthly values of groundwater storage, c) short-period of monthly values of groundwater storage across study area of Fin-Maram (Code: 2710).

F.7.11. Study area of Fin-Kahkam-Saadatabad (Code: 2711)

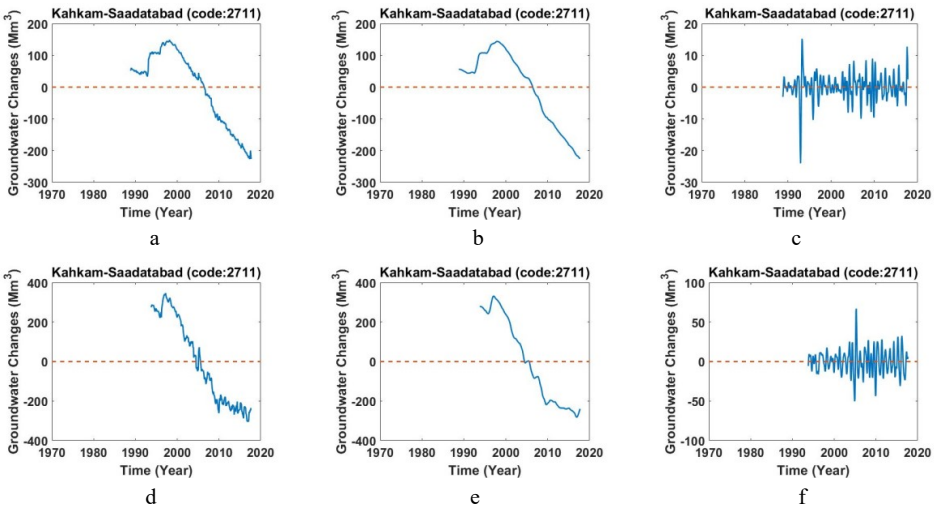

Figure F.153. a,d) Monthly values of groundwater storage, b,e) long-period of monthly values of groundwater storage, c,f) short-period of monthly values of groundwater storage across study area of Kahkam-Saadatabad (Code: 2711).

F.7.12. Study area of Hajiabad (Code: 2712)

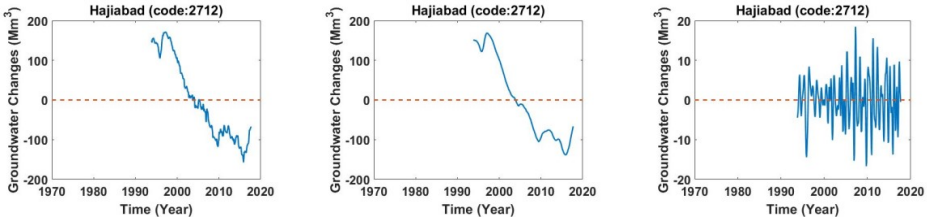

a b c

Figure F.154. a) Monthly values of groundwater storage, b) long-period of monthly values of groundwater storage, c) short-period of monthly values of groundwater storage across study area of Hajiabad (Code: 2712).

F.7.13. Study area of Shamil-Meimand (Code: 2713)

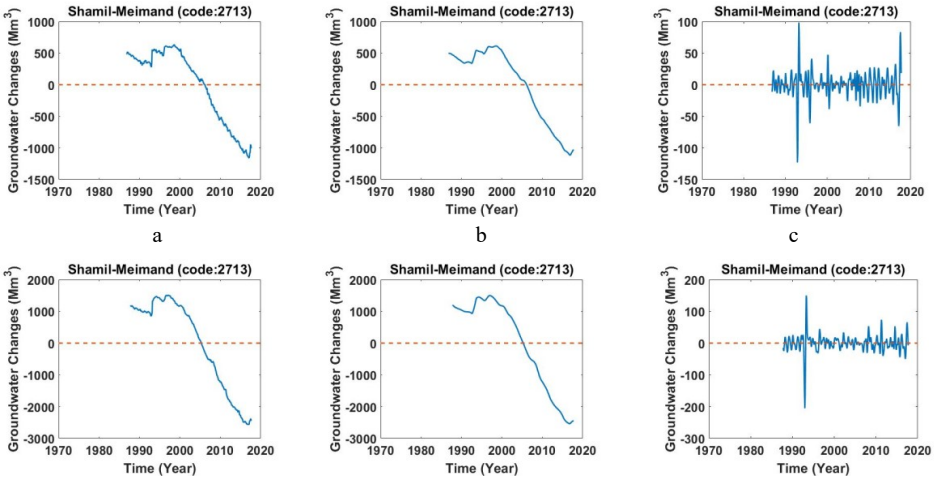

a b c

d e f

Figure F.155. a,d) Monthly values of groundwater storage, b,e) long-period of monthly values of groundwater storage, c,f) short-period of monthly values of groundwater storage across study area of Shamil-Meimand (Code: 2713).

F.7.14. Study area of Dolat Abad (Code: 2714)

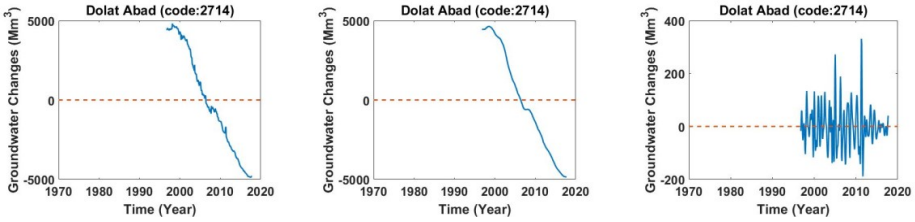

a b c

Figure F.156. a) Monthly values of groundwater storage, b) long-period of monthly values of groundwater storage, c) short-period of monthly values of groundwater storage across study area of Dolat Abad (Code: 2714).

F.7.15. Study area of Soghan (Code: 2715)

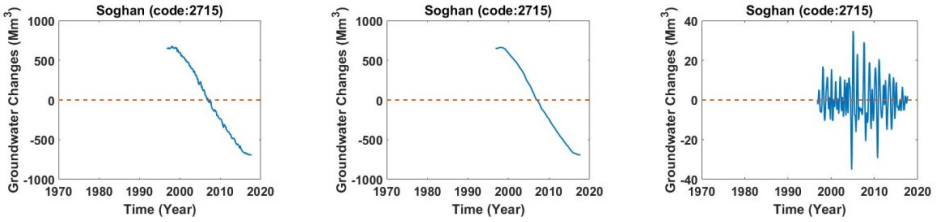

a b c

Figure F.157. a) Monthly values of groundwater storage, b) long-period of monthly values of groundwater storage, c) short-period of monthly values of groundwater storage across study area of Soghan (Code: 2715).

F.7.16. Study area of Baynooj (Code: 2716)

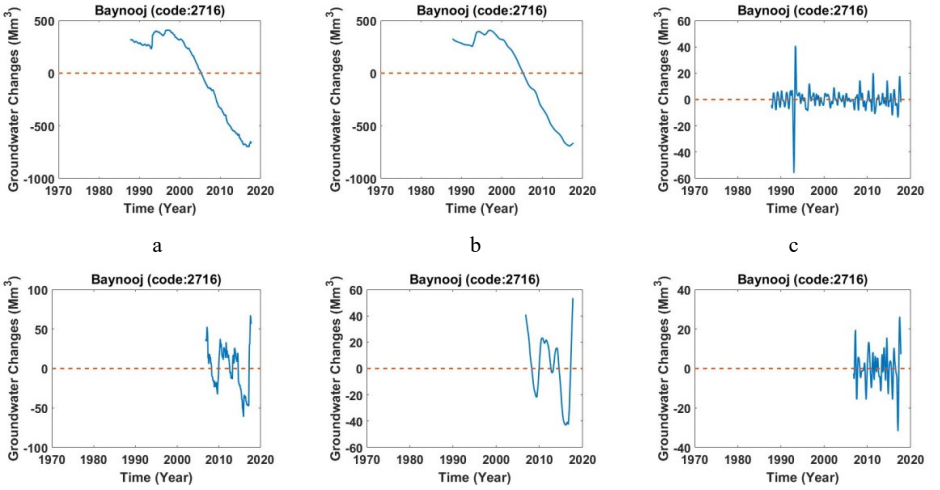

a b c

d e f

Figure F.158. a,d) Monthly values of groundwater storage, b,e) long-period of monthly values of groundwater storage, c,f) short-period of monthly values of groundwater storage across study area of Baynooj (Code: 2716).

F.7.17. Study area of Fakhr Abad (Code: 2717)

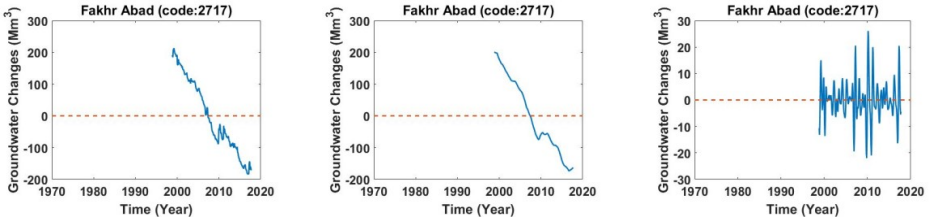

a b c

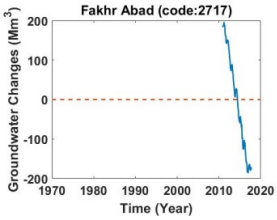

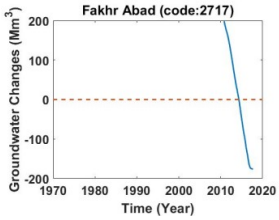

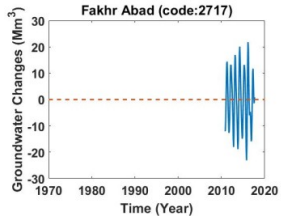

d e f

Figure F.159. a,d) Monthly values of groundwater storage, b,e) long-period of monthly values of groundwater storage, c,f) short-period of monthly values of groundwater storage across study area of Fakhr Abad (Code: 2717).

F.7.18. Study area of Tashkuieh (Code: 2718)

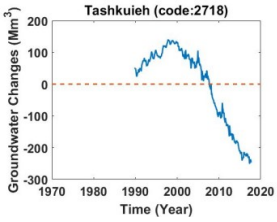

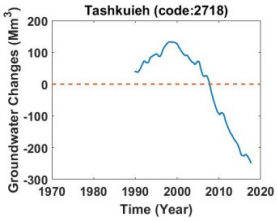

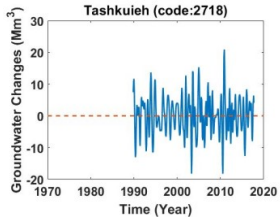

a b c

Figure F.160. a) Monthly values of groundwater storage, b) long-period of monthly values of groundwater storage, c) short-period of monthly values of groundwater storage across study area of Tashkuieh (Code: 2718).

F.7.19. Study area of Fadami (Code: 2719)

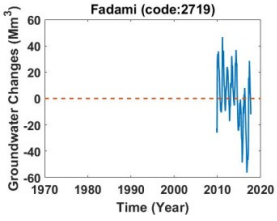

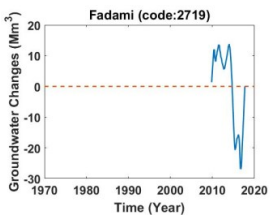

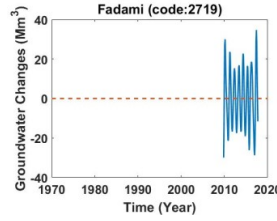

a b c

Figure F.161. a) Monthly values of groundwater storage, b) long-period of monthly values of groundwater storage, c) short-period of monthly values of groundwater storage across study area of Fadami (Code: 2719).

F.7.20. Study area of Rashtagh (Code: 2720)

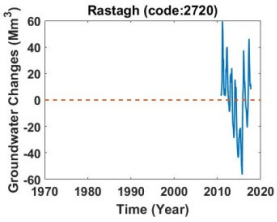

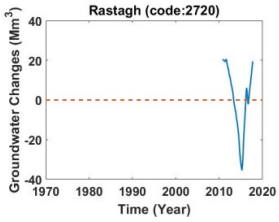

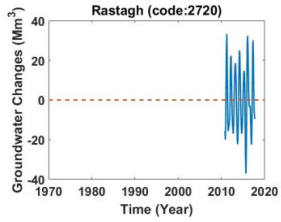

a b c

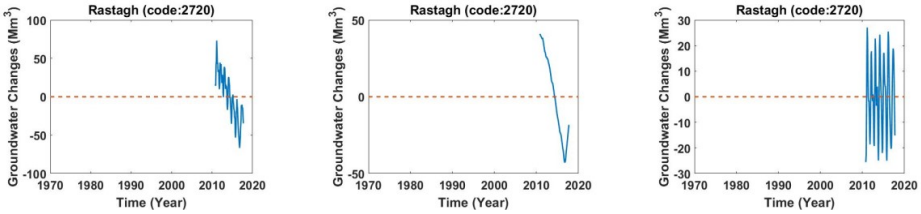

Figure F.162. a,d) Monthly values of groundwater storage, b,e) long-period of monthly values of groundwater storage, c,f) short-period of monthly values of groundwater storage across study area of Rastagh (Code: 2720).

5.2.7.21. Study area of Khasooye-Sachoon (Code: 2721)

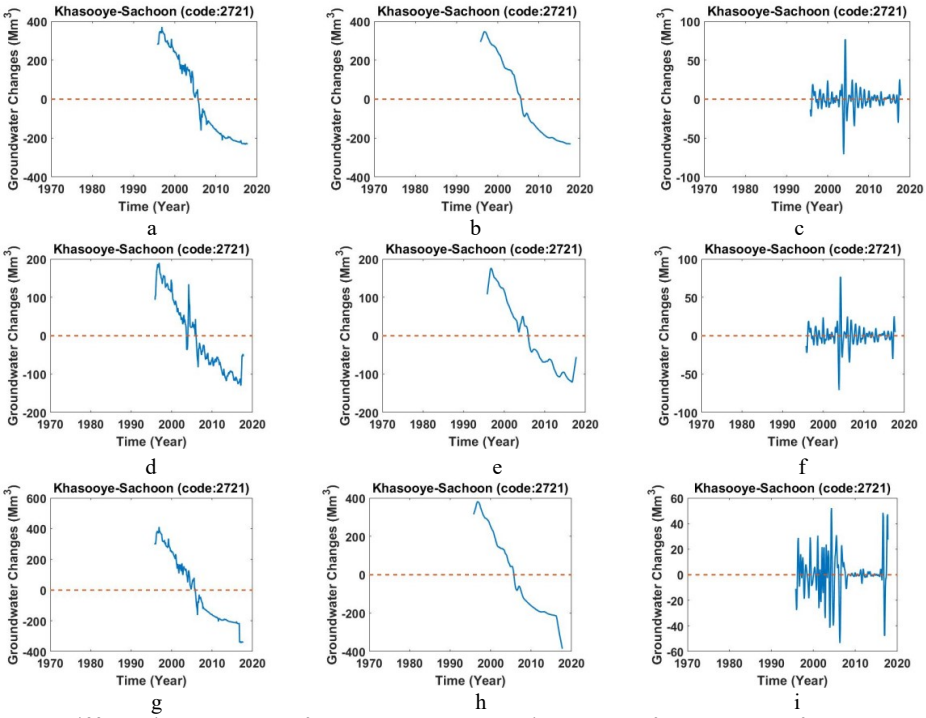

Figure F.163. a,d,g) Monthly values of groundwater storage, b,e,h) long-period of monthly values of groundwater storage, c,f,i) short-period of monthly values of groundwater storage across study area of Khasooye-Sachoon (Code: 2721).

F.7.22. Study area of Darab (Code: 2722)

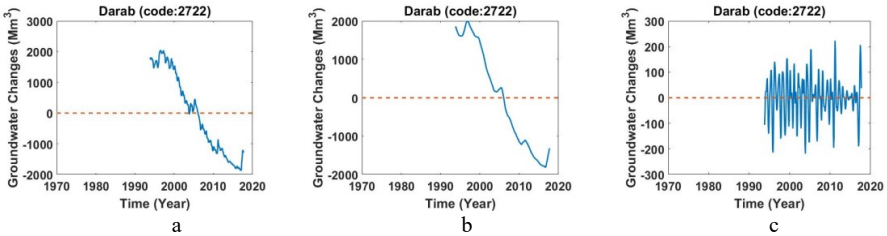

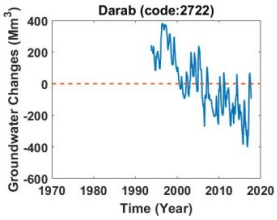

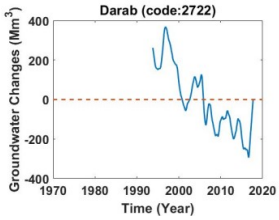

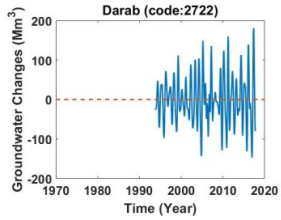

d e f

Figure F.164. a,d) Monthly values of groundwater storage, b,e) long-period of monthly values of groundwater storage, c,f) short-period of monthly values of groundwater storage across study area of Darab (Code: 2722).

F.7.23. Study area of Darakoye (Code: 2723)

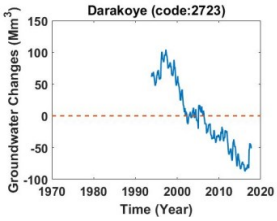

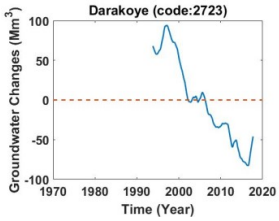

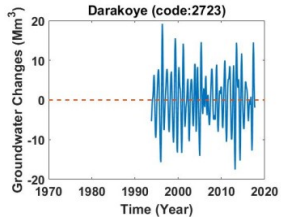

a b c

Figure F.165. a) Monthly values of groundwater storage, b) long-period of monthly values of groundwater storage, c) short-period of monthly values of groundwater storage across study area of Darakoye (Code: 2723).

F.7.24. Study area of Anjirak-Dehvieh (Code: 2724)

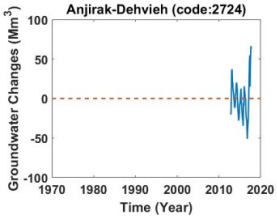

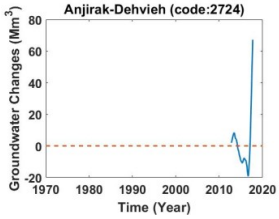

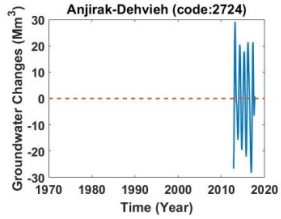

a b c

Figure F.166. a) Monthly values of groundwater storage, b) long-period of monthly values of groundwater storage, c) short-period of monthly values of groundwater storage across study area of Anjirak-Dehvieh (Code: 2724).

F.7.25. Study area of Dejkan (Code: 2725)

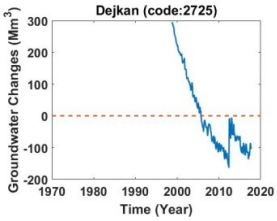

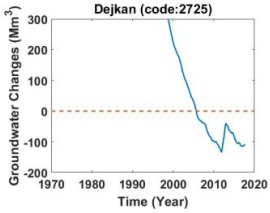

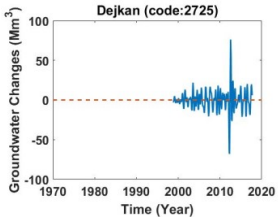

a b c

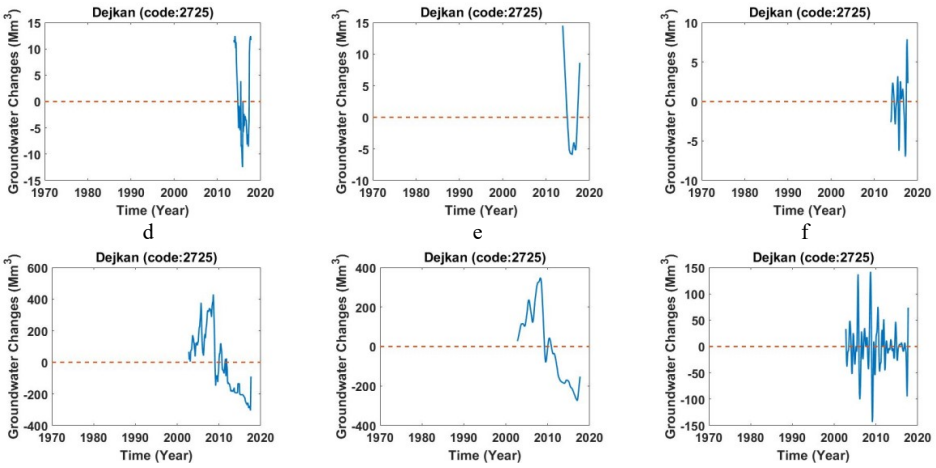

Figure F.167. a,d,g) Monthly values of groundwater storage, b,e,h) long-period of monthly values of groundwater storage, c,f,i) short-period of monthly values of groundwater storage across study area of Dejkan (Code: 2725).

F.7.26. Study area of Jenah-Bastak (Code: 2726)

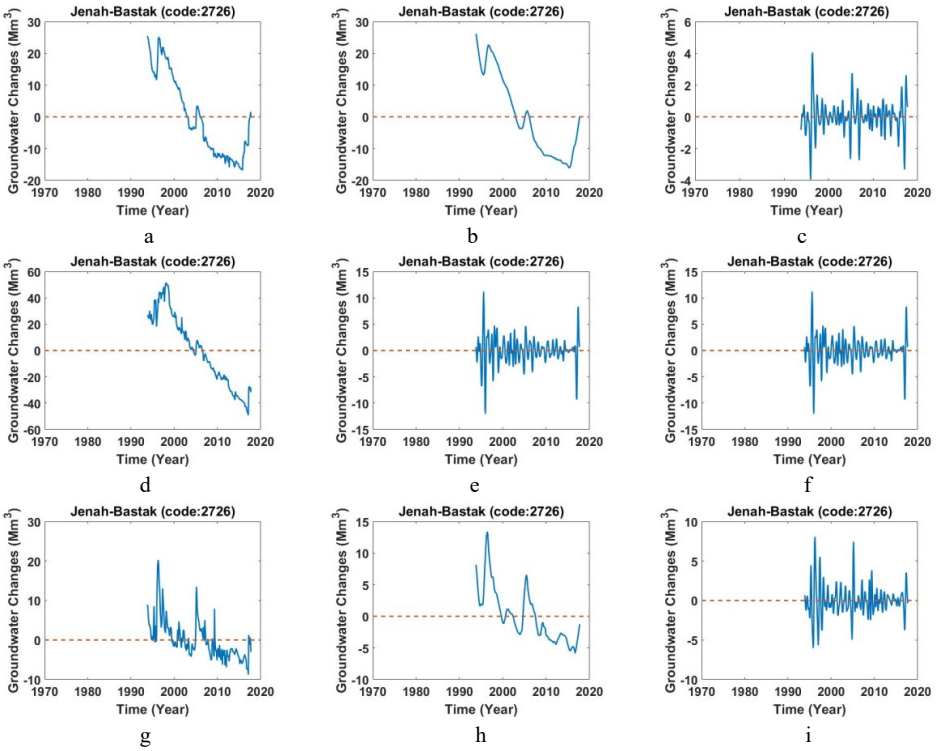

Figure F.168. a,d,g) Monthly values of groundwater storage, b,e,h) long-period of monthly values of groundwater storage, c,f,i) short-period of monthly values of groundwater storage across study area of Jenah-Bastak (Code: 2726).

F.7.27. Study area of Lamard (Code: 2727)

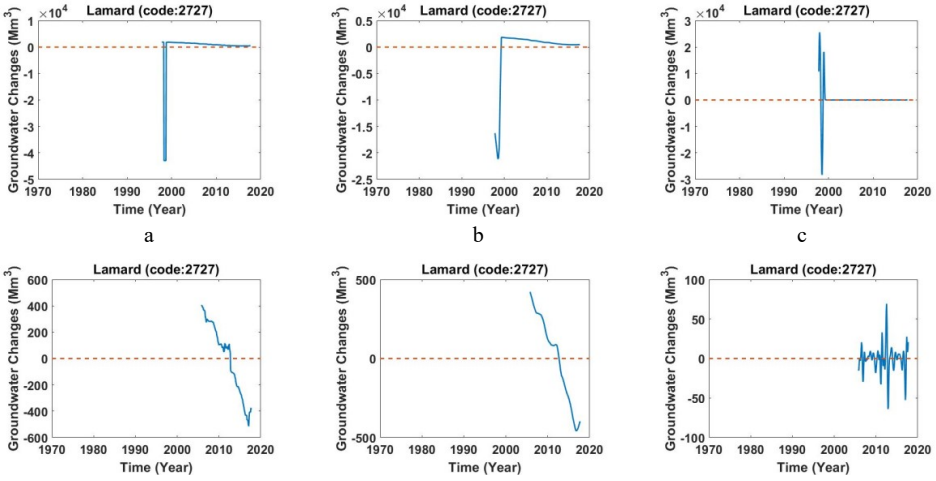

Figure F.169. a,d) Monthly values of groundwater storage, b,e) long-period of monthly values of groundwater storage, c,f) short-period of monthly values of groundwater storage across study area of Lamard (Code: 2727).

F.7.28. Study area of Galedar (Code: 2728)

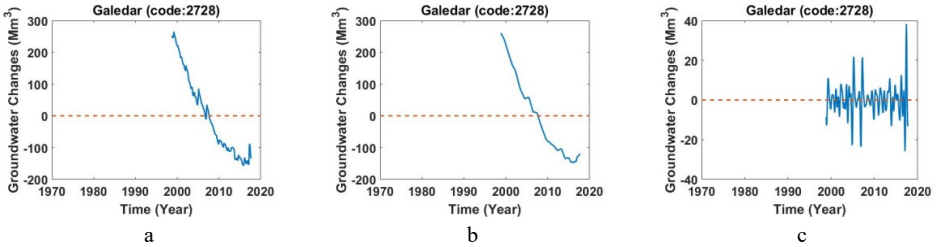

Figure F.170. a) Monthly values of groundwater storage, b) long-period of monthly values of groundwater storage, c) short-period of monthly values of groundwater storage across study area of Galedar (Code: 2728).

F.7.29. Study area of Deyr-Kangan (Code: 2729)

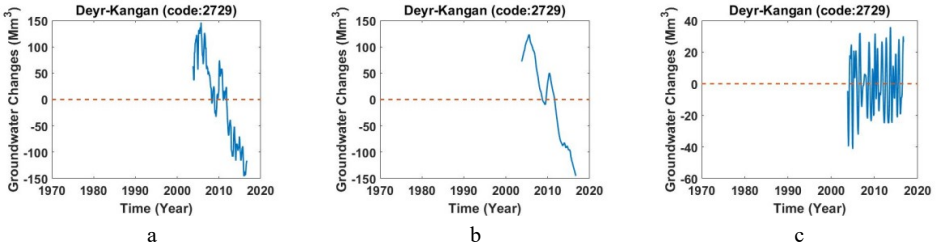

Figure F.171. a) Monthly values of groundwater storage, b) long-period of monthly values of groundwater storage, c) short-period of monthly values of groundwater storage across study area of Deyr-Kangan (Code: 2729).

F.7.30. Study area of Gavbandi (Code: 2730)

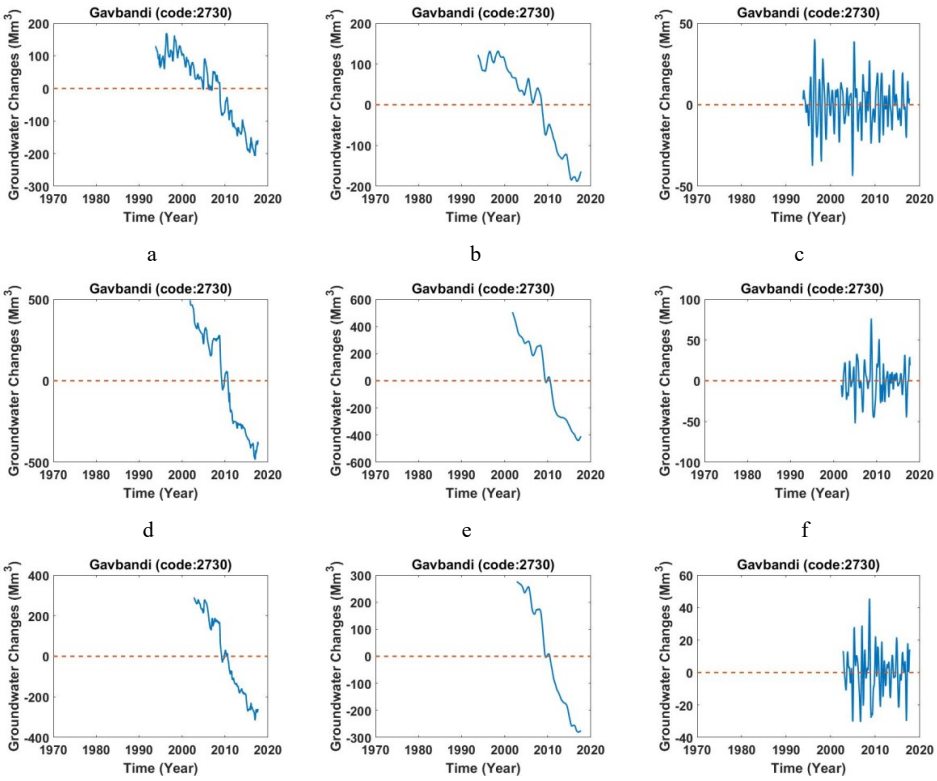

Figure F.172. a,d,g) Monthly values of groundwater storage, b,e,h) long-period of monthly values of groundwater storage, c,f,i) short-period of monthly values of groundwater storage across study area of Gavbandi (Code: 2730).

F.7.31. Study area of Rastagh-Magham (Code: 2731)

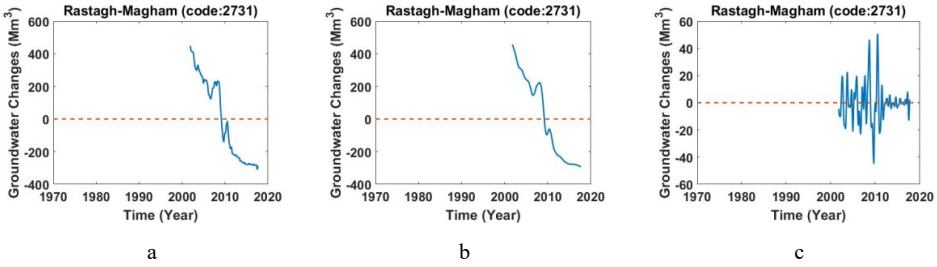

Figure F.173. a) Monthly values of groundwater storage, b) long-period of monthly values of groundwater storage, c) short-period of monthly values of groundwater storage across study area of Rastagh-Magham (Code: 2731).

F.7.32. Study area of Bandar Lenge (Code: 2733)

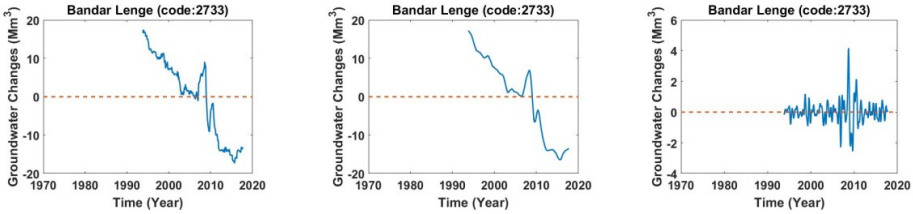

a b c

Figure F.174. a) Monthly values of groundwater storage, b) long-period of monthly values of groundwater storage, c) short-period of monthly values of groundwater storage across study area of Bandar Lenge (Code: 2733).

F.7.33. Study area of Rastagh-Magham (Code: 2739)

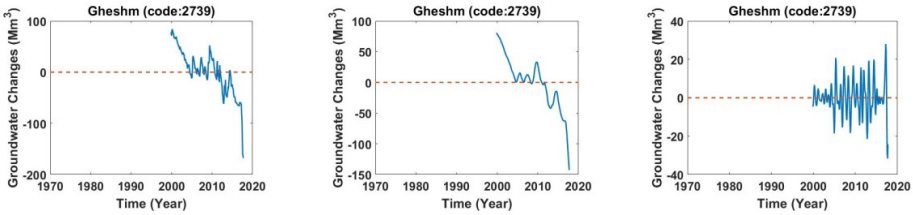

a b c

Figure F.175. a) Monthly values of groundwater storage, b) long-period of monthly values of groundwater storage, c) short-period of monthly values of groundwater storage across study area of Rastagh-Magham (Code: 2739).

F.8.1. Study area of Isin Sharghi (Code: 2802)

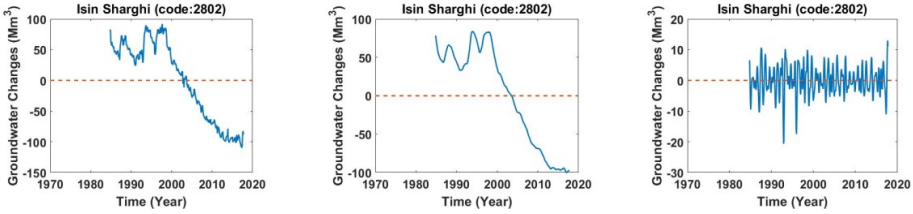

a b c

Figure F.176. a) Monthly values of groundwater storage, b) long-period of monthly values of groundwater storage, c) short-period of monthly values of groundwater storage across study area of Isin Sharghi (Code: 2802).

F.8.2. Study area of Sorkhoon (Code: 2803)

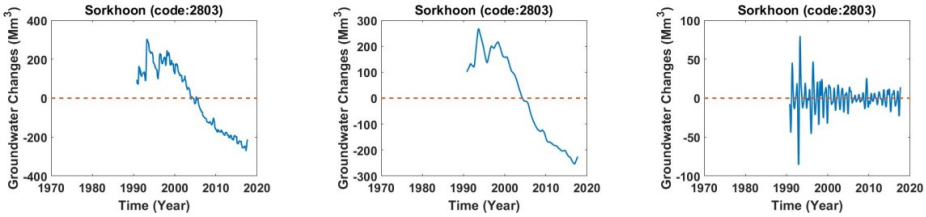

a b c

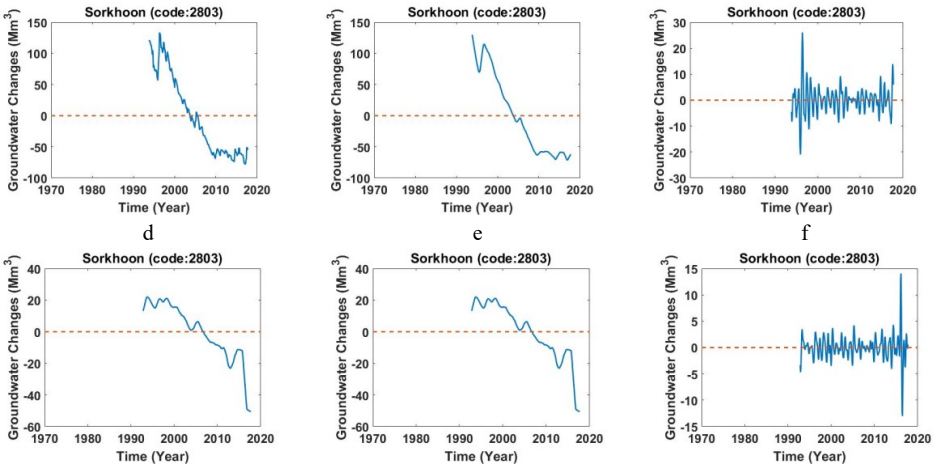

Figure F.177. a,d,g) Monthly values of groundwater storage, b,e,h) long-period of monthly values of groundwater storage, c,f,i) short-period of monthly values of groundwater storage across study area of Sorkhoon (Code: 2803).

F.8.3. Study area of Shamil-Takht (Code: 2804)

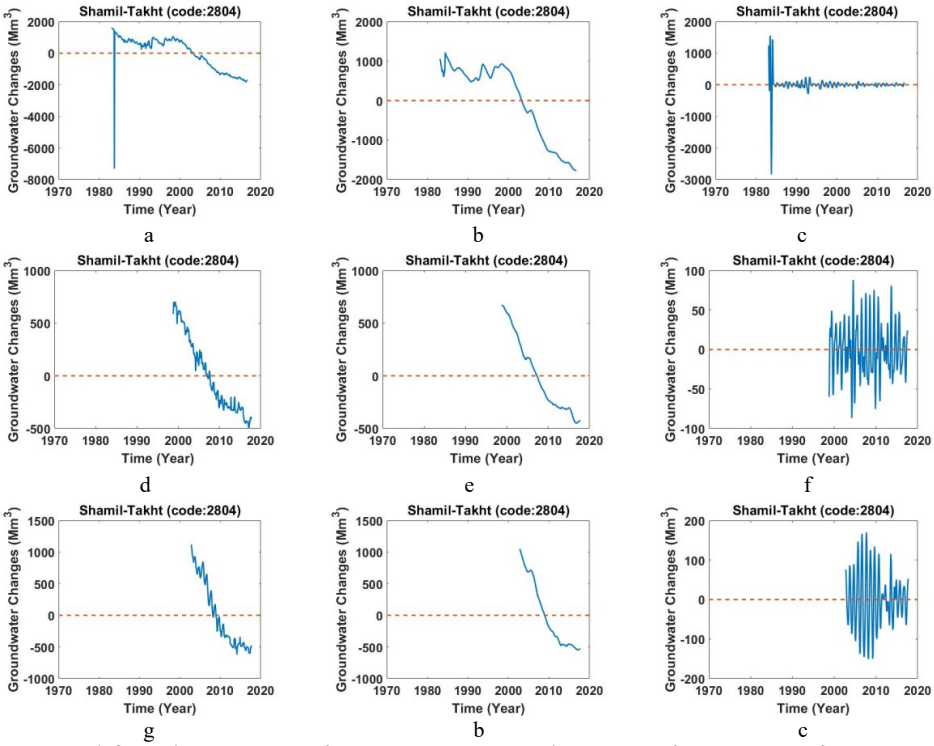

Figure F.178. a,d,g) Monthly values of groundwater storage, b,e,h) long-period of monthly values of groundwater storage, c,f,i) short-period of monthly values of groundwater storage across study area of Shamil-Takht (Code: 2804).

F.8.4. Study area of Sarze-Siahoo (Code: 2805)

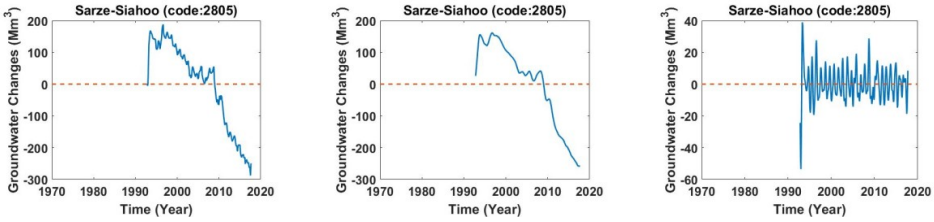

a b c

Figure F.466. a) Monthly values of groundwater storage, b) long-period of monthly values of groundwater storage, c) short-period of monthly values of groundwater storage across study area of Sarze-Siahoo (Code: 2805).

F.8.5. Study area of Ahmadi (Code: 2806)

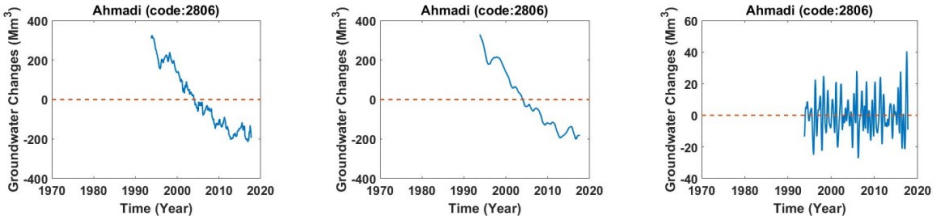

a b c

Figure F.179. a) Monthly values of groundwater storage, b) long-period of monthly values of groundwater storage, c) short-period of monthly values of groundwater storage across study area of Ahmadi (Code: 2806).

F.8.6. Study area of Minab (Code: 2807)

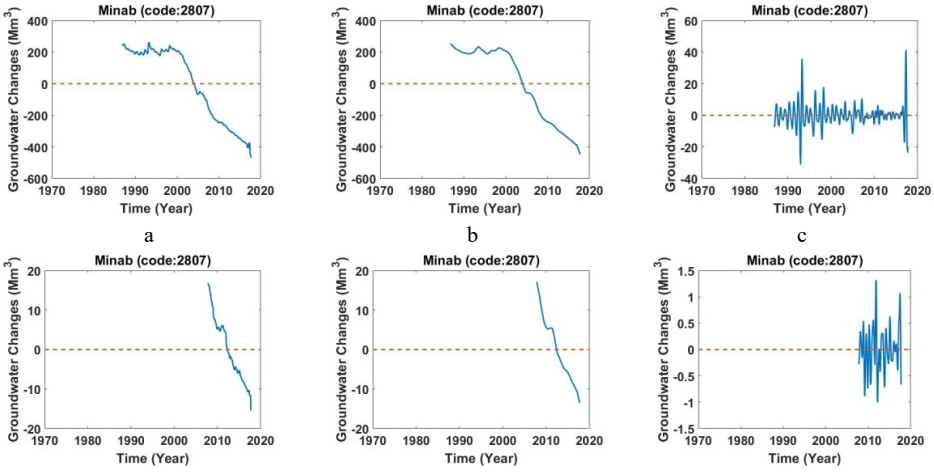

a b c

d e f

Figure F.180. a,d) Monthly values of groundwater storage, b,e) long-period of monthly values of groundwater storage, c,f) short-period of monthly values of groundwater storage across study area of Minab (Code: 2807).

F.8.7. Study area of Joghin-Tokhor (Code: 2808)

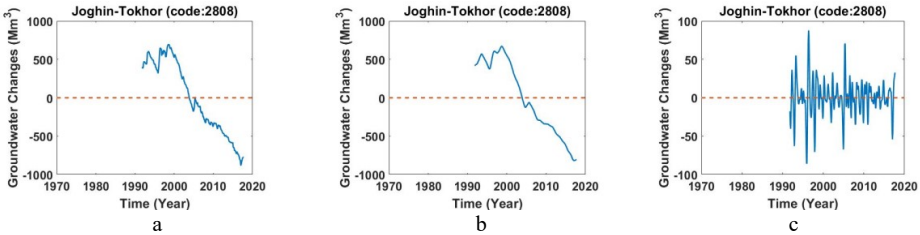

a b c

Figure F.181. a) Monthly values of groundwater storage, b) long-period of monthly values of groundwater storage, c) short-period of monthly values of groundwater storage across study area of Joghin-Tokhor (Code: 2808).

F.8.8. Study area of Manoojan (Code: 2809)

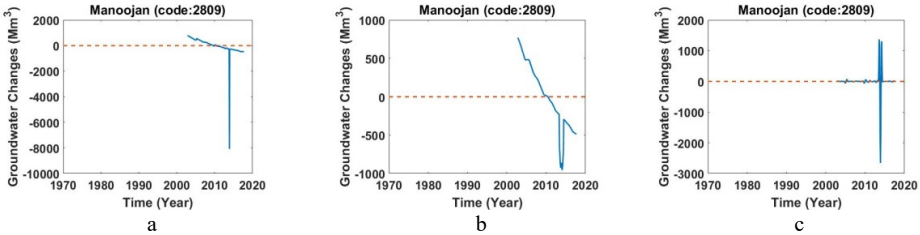

a b c

Figure F.182. a) Monthly values of groundwater storage, b) long-period of monthly values of groundwater storage, c) short-period of monthly values of groundwater storage across study area of Manoojan (Code: 2809).

F.8.9. Study area of Roodan (Code: 2810)

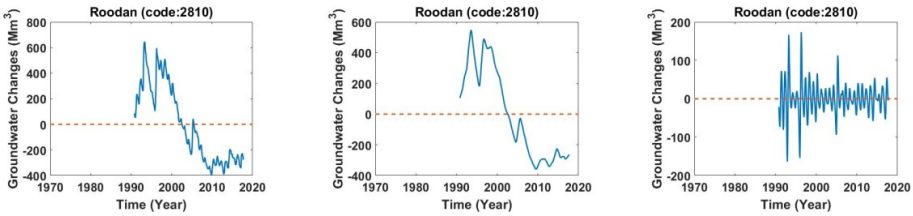

a b c

Figure F.183. a) Monthly values of groundwater storage, b) long-period of monthly values of groundwater storage, c) short-period of monthly values of groundwater storage across study area of Roodan (Code: 2810).

F.8.10. Study area of Nodej (Code: 2811)

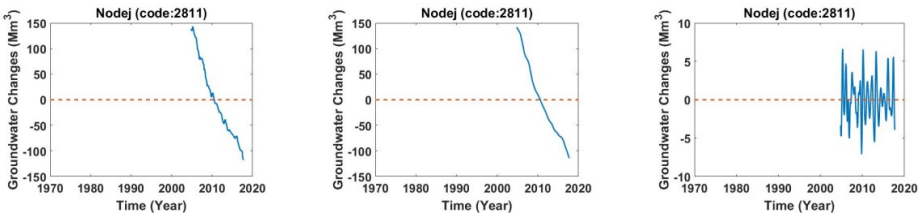

a b c

Figure F.184. a) Monthly values of groundwater storage, b) long-period of monthly values of groundwater storage, c) short-period of monthly values of groundwater storage across study area of Nodej Code: 2811).

F.8.11. Study area of Deh Kahan (Code: 2812)

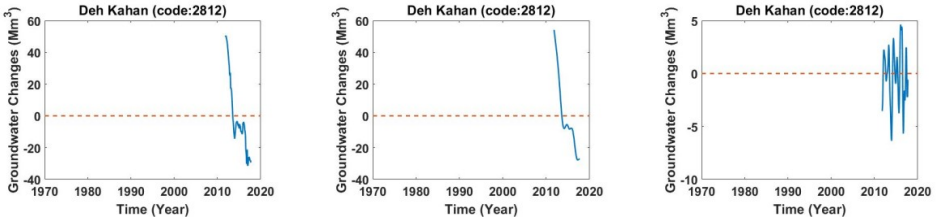

Figure F.185. a) Monthly values of groundwater storage, b) long-period of monthly values of groundwater storage, c) short-period of monthly values of groundwater storage across study area of Deh Kahan (Code: 2812).

F.8.12. Study area of Mosafer Abad (Code: 2813)

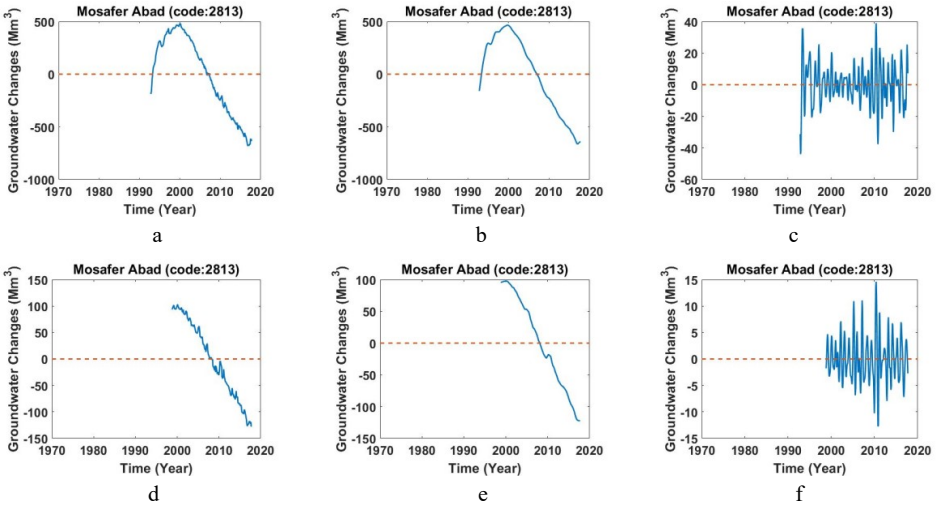

Figure F.186. a,d) Monthly values of groundwater storage, b,e) long-period of monthly values of groundwater storage, c,f) short-period of monthly values of groundwater storage across study area of Mosafer Abad (Code: 2813).

F.8.13. Study area of Faryab-Kalash Gerd (Code: 2814)

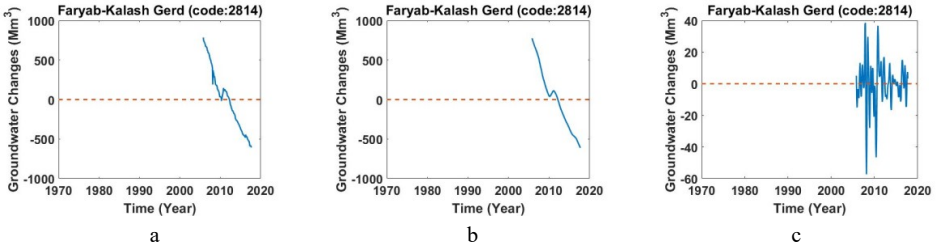

Figure F.187. a) Monthly values of groundwater storage, b) long-period of monthly values of groundwater storage, c) short-period of monthly values of groundwater storage across study area of Faryab-Kalash Gerd (Code: 2814).

F.8.14. Study area of Kordi-Shirazi (Code: 2815)

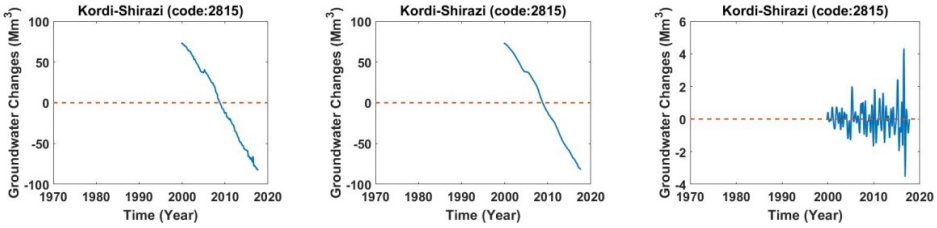

a b c

Figure F.189. a) Monthly values of groundwater storage, b) long-period of monthly values of groundwater storage, c) short-period of monthly values of groundwater storage across study area of Kordi-Shirazi (Code: 2815).

F.8.15. Study area of Karian (Code: 2817)

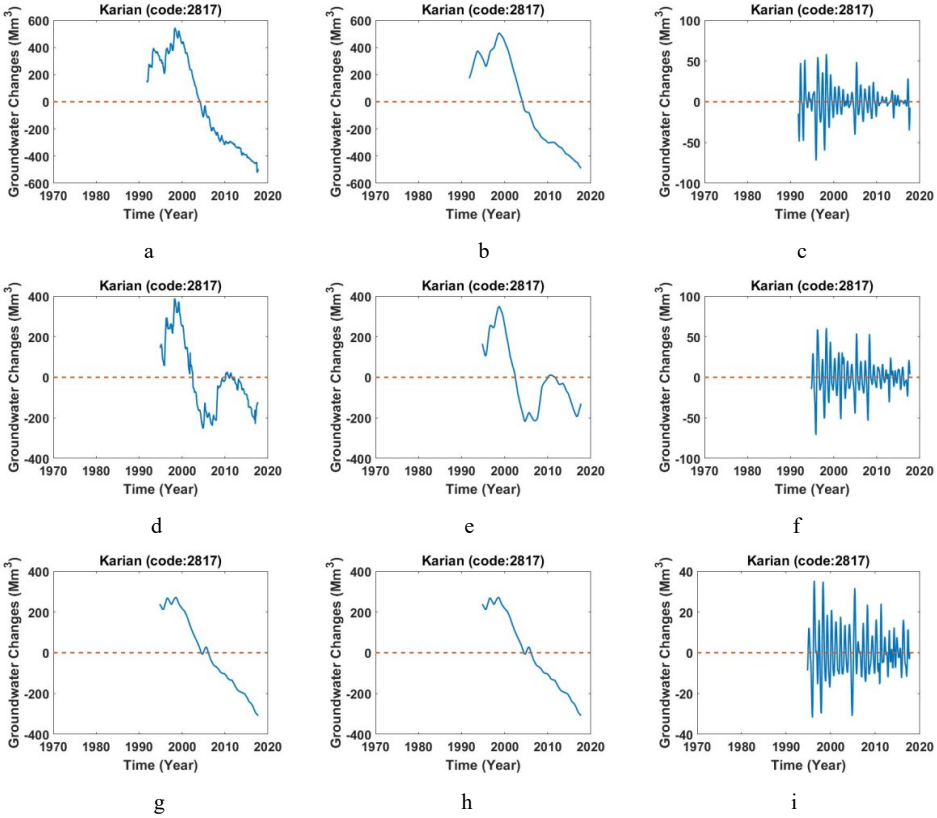

a b c

d e f

g h i

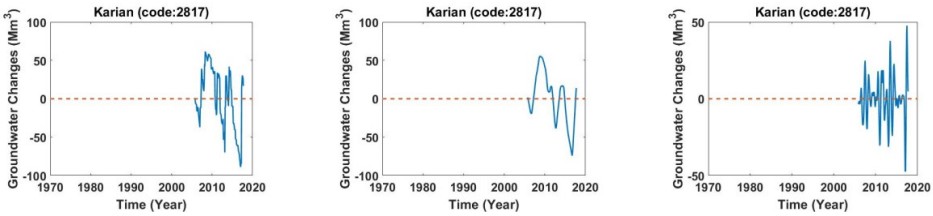

j k l

Figure F.190. a,d,g,j) Monthly values of groundwater storage, b,e,h,k) long-period of monthly values of groundwater storage, c,f,i,l) short-period of monthly values of groundwater storage across study area of Karian (Code: 2817).

F.8.16. Study area of Sirik (Code: 2818)

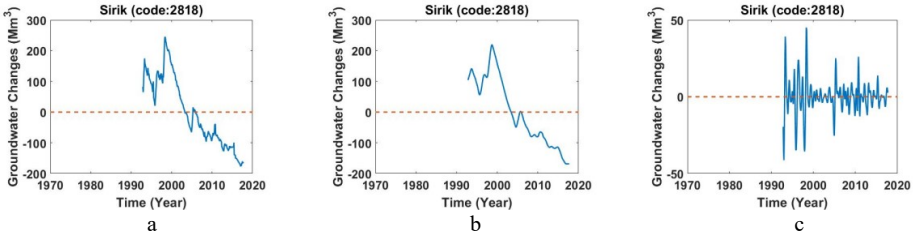

a b c

Figure F.191. a) Monthly values of groundwater storage, b) long-period of monthly values of groundwater storage, c) short-period of monthly values of groundwater storage across study area of Sirik (Code: 2818).

F.8.17. Study area of Jask (Code: 2819)

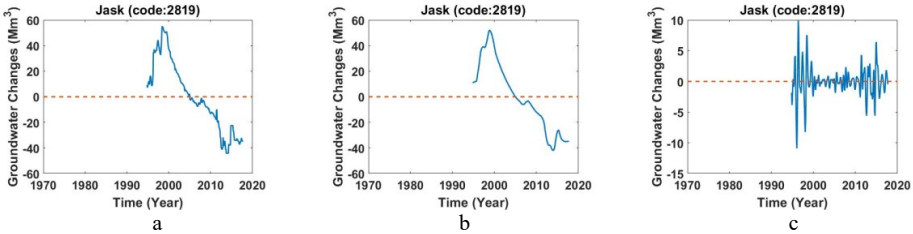

a b c

Figure F.192. a) Monthly values of groundwater storage, b) long-period of monthly values of groundwater storage, c) short-period of monthly values of groundwater storage across study area of Jask (Code: 2819).

F.8.18. Study area of Jagin (Code: 2820)

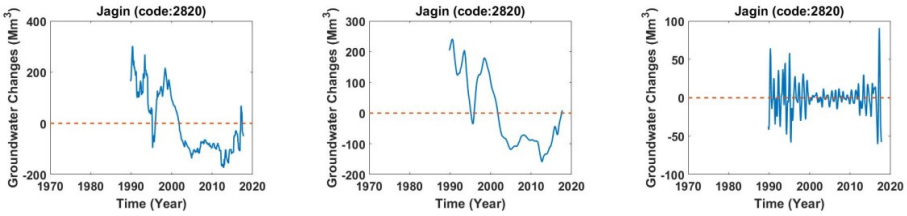

a b c

Figure F.193. a) Monthly values of groundwater storage, b) long-period of monthly values of groundwater storage, c) short-period of monthly values of groundwater storage across study area of Jagin (Code: 2820).

F.9.1. Study area of Pirsohrab-Oraki (Code: 2911)

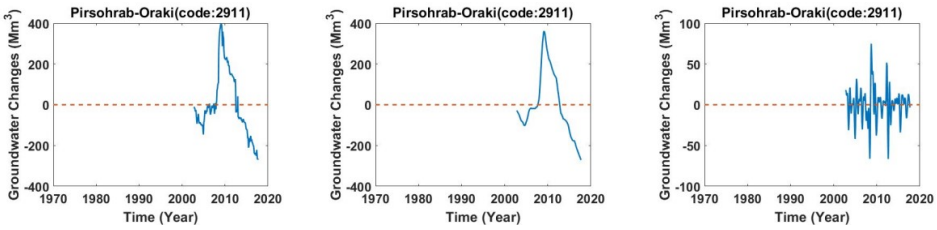

a b c

Figure F.194. a) Monthly values of groundwater storage, b) long-period of monthly values of groundwater storage, c) short-period of monthly values of groundwater storage across study area of Pirsohrab-Oraki (Code: 2911).

F.9.2. Study area of Pishin (Code: 2913)

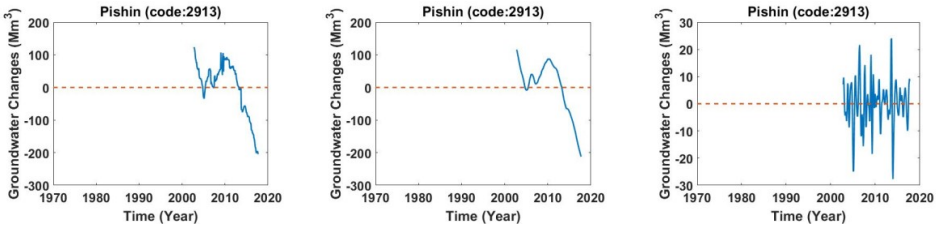

a b c

Figure F.195. a) Monthly values of groundwater storage, b) long-period of monthly values of groundwater storage, c) short-period of monthly values of groundwater storage across study area of Pishin (Code: 2913).

Appendix G

G.1. Study area of Salmas (Code: 3001)

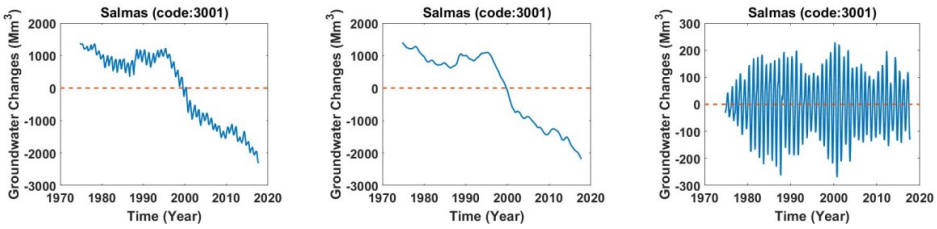

a b c

Figure G.1. a) Monthly values of groundwater storage, b) long-period of monthly values of groundwater storage, c) short-period of monthly values of groundwater storage across study area of Saleh Salmas (Code: 3001).

G.2. Study area of Kahriz (Code: 3002)

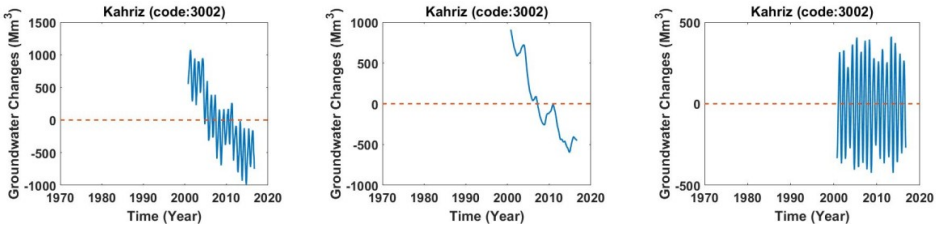

a v b c

Figure G.2. a) Monthly values of groundwater storage, b) long-period of monthly values of groundwater storage, c) short-period of monthly values of groundwater storage across study area of Saleh Kahriz (Code: 3002).

G.3. Study area of Urmieh (Code: 3003)

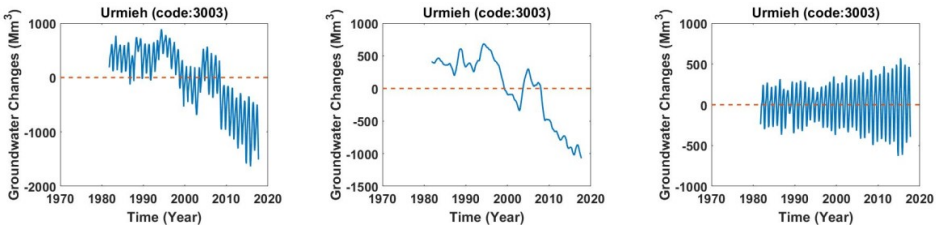

a b c

Figure G.3. a) Monthly values of groundwater storage, b) long-period of monthly values of groundwater storage, c) short-period of monthly values of groundwater storage across study area of Saleh Urmieh (Code: 3003).

G.4. Study area of Serow (Code: 3004)

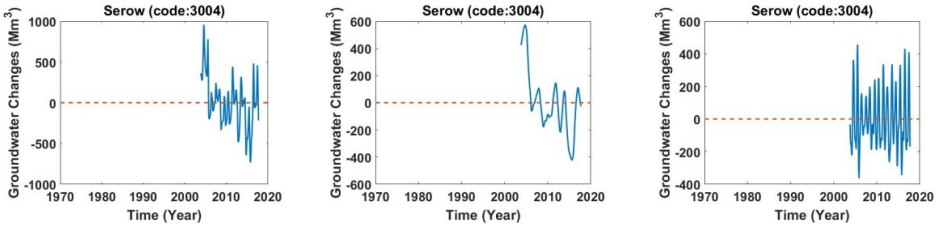

a b c

Figure G.4. a) Monthly values of groundwater storage, b) long-period of monthly values of groundwater storage, c) short-period of monthly values of groundwater storage across study area of Saleh Urmieh (Code: 3004).

G.5. Study area of Cilvana (Code: 3005)

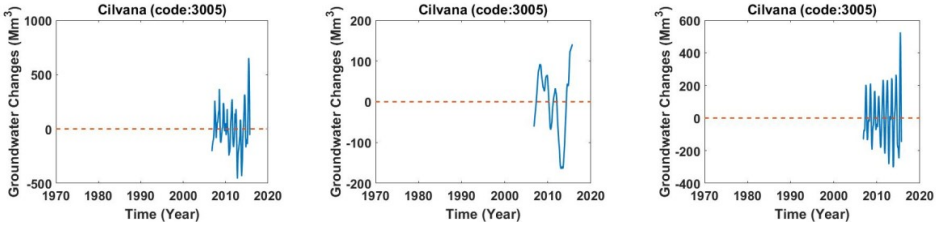

a b c

Figure G.5. a) Monthly values of groundwater storage, b) long-period of monthly values of groundwater storage, c) short-period of monthly values of groundwater storage across study area of Saleh cilvana (Code: 3005).

G.6. Study area of Reshkan (Code: 3006)

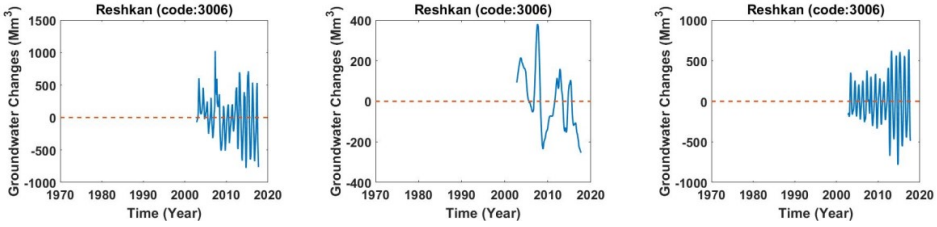

a b c

Figure G.6. a) Monthly values of groundwater storage, b) long-period of monthly values of groundwater storage, c) short-period of monthly values of groundwater storage across study area of Saleh Reshkan (Code: 3006).

G.7. Study area of Naghadeh (Code: 3007)

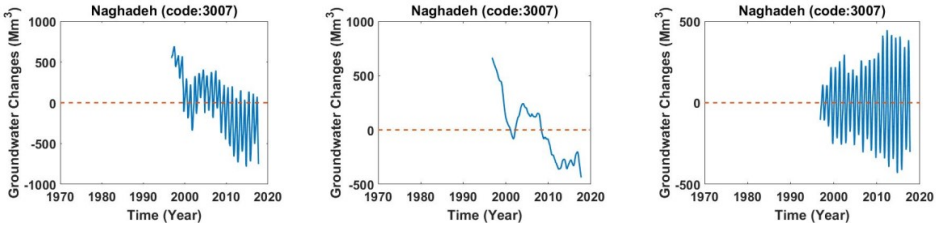

a b c

Figure G.7. a) Monthly values of groundwater storage, b) long-period of monthly values of groundwater storage, c) short-period of monthly values of groundwater storage across study area of Saleh Naghadeh (Code: 3007).

G.8. Study area of Oshnavieh (Code: 3008)

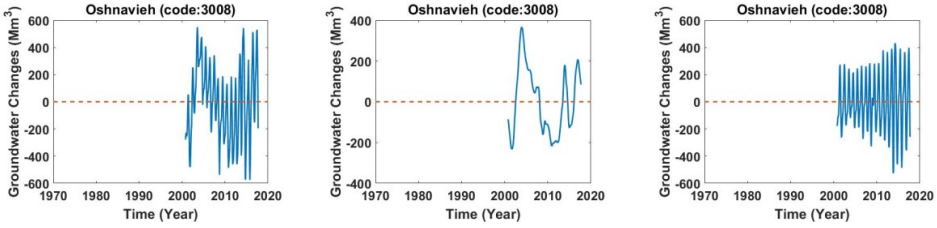

a b c

Figure G.8. a) Monthly values of groundwater storage, b) long-period of monthly values of groundwater storage, c) short-period of monthly values of groundwater storage across study area of Saleh Oshnavieh (Code: 3008).

G.9. Study area of Mahabad (Code: 3009)

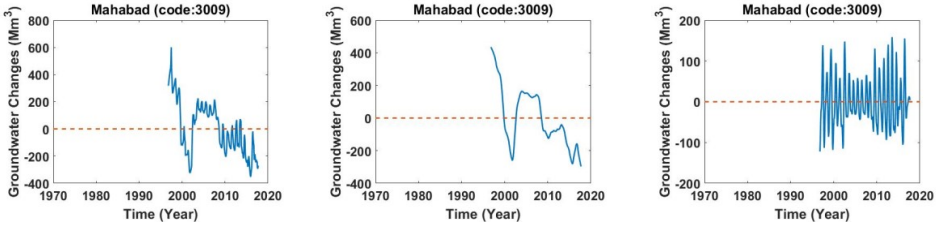

a b c

Figure G.9. a) Monthly values of groundwater storage, b) long-period of monthly values of groundwater storage, c) short-period of monthly values of groundwater storage across study area of Saleh Mahabad (Code: 3009).

G.10. Study area of Miandoab (Code: 3010)

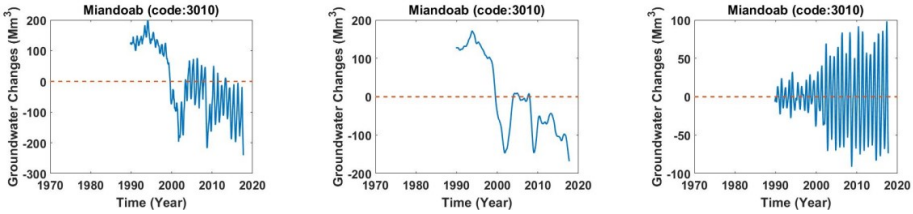

a b c

Figure G.10. a) Monthly values of groundwater storage, b) long-period of monthly values of groundwater storage, c) short-period of monthly values of groundwater storage across study area of Saleh Miandoab (Code: 3010).

G.11. Study area of Bukan (Code: 3011)

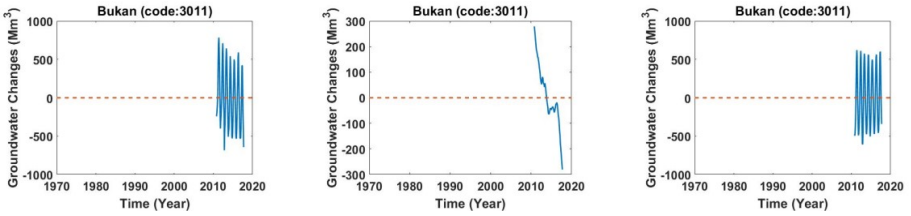

a b c

Figure G.11. a) Monthly values of groundwater storage, b) long-period of monthly values of groundwater storage, c) short-period of monthly values of groundwater storage across study area of Saleh Bukan (Code: 3011).

G.12. Study area of Saeen Ghaleh (Code: 3012)

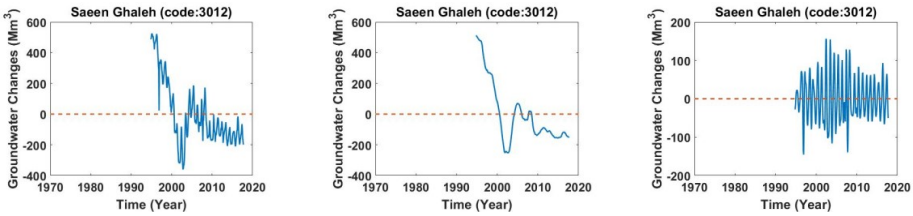

a b c

Figure G.12. a) Monthly values of groundwater storage, b) long-period of monthly values of groundwater storage, c) short-period of monthly values of groundwater storage across study area of Saleh Saeen Ghaleh (Code: 3012).

G.13. Study area of Maraghe (Code: 3015)

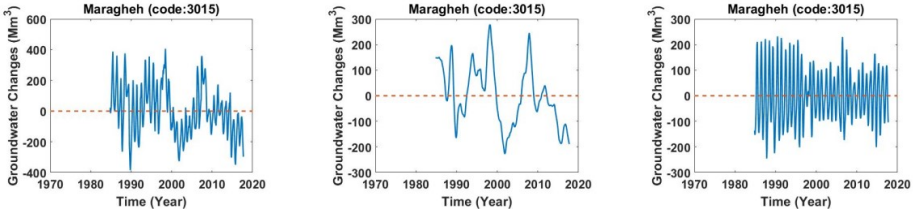

a b c

Figure G.13. a) Monthly values of groundwater storage, b) long-period of monthly values of groundwater storage, c) short-period of monthly values of groundwater storage across study area of Saleh Maraghe (Code: 3015).

G.14. Study area of Ajabshir (Code: 3016)

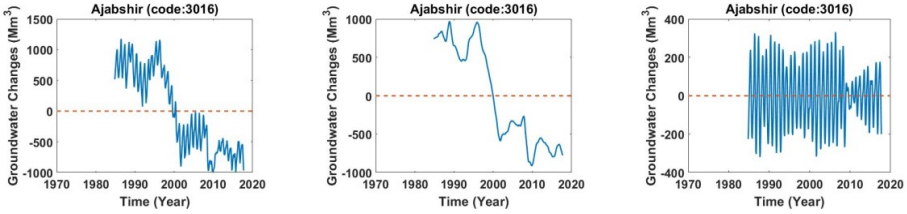

a b c

Figure G.14. a) Monthly values of groundwater storage, b) long-period of monthly values of groundwater storage, c) short-period of monthly values of groundwater storage across study area of Saleh Ajabshir (Code: 3016).

G.15. Study area of Shiramin (Code: 3017)

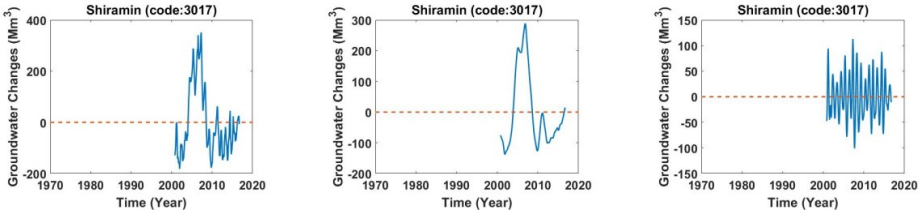

a b c

Figure G.15. a) Monthly values of groundwater storage, b) long-period of monthly values of groundwater storage, c) short-period of monthly values of groundwater storage across study area of Saleh Shiramin (Code: 3017).

G.16. Study area of Azar Shahr (Code: 3018)

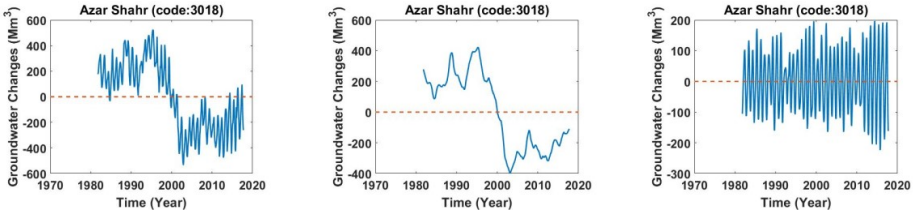

a b c

Figure G.16. a) Monthly values of groundwater storage, b) long-period of monthly values of groundwater storage, c) short-period of monthly values of groundwater storage across study area of Saleh Azar Shahr (Code: 3018).

G.17. Study area of Tabriz (Code: 3019)

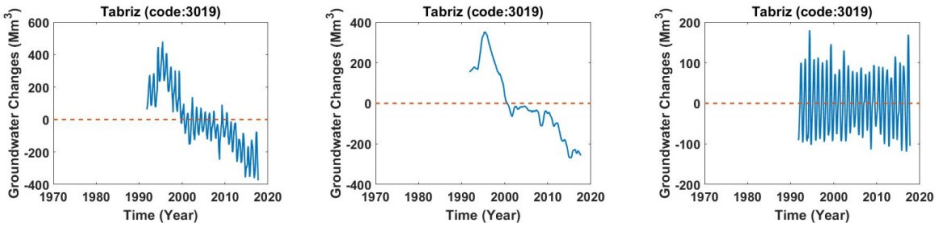

a b c

Figure G.17. a) Monthly values of groundwater storage, b) long-period of monthly values of groundwater storage, c) short-period of monthly values of groundwater storage across study area of Saleh Tabriz (Code: 3019).

G.18. Study area of Bilevardi (Code: 3020)

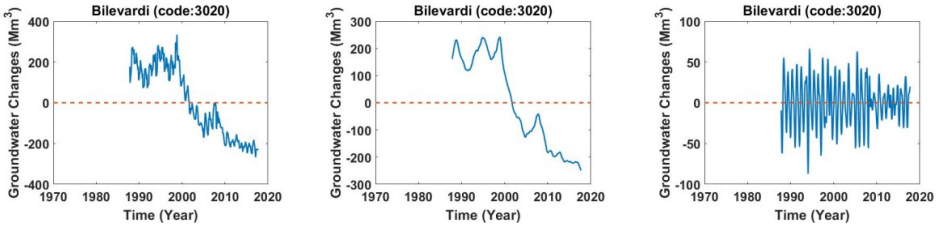

a b c

Figure G.18. a) Monthly values of groundwater storage, b) long-period of monthly values of groundwater storage, c) short-period of monthly values of groundwater storage across study area of Saleh Bilevardi (Code: 3020).

G.19. Study area of Bostan Abad (Code: 3021)

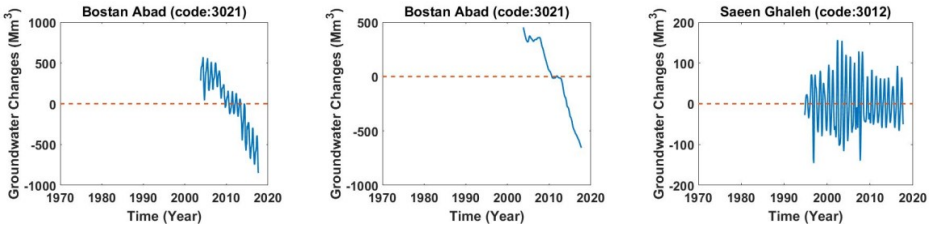

a b c

Figure G.19. a) Monthly values of groundwater storage, b) long-period of monthly values of groundwater storage, c) short-period of monthly values of groundwater storage across study area of Saleh Bostan Abad (Code: 3021).

G.20. Study area of Sarab (Code: 3022)

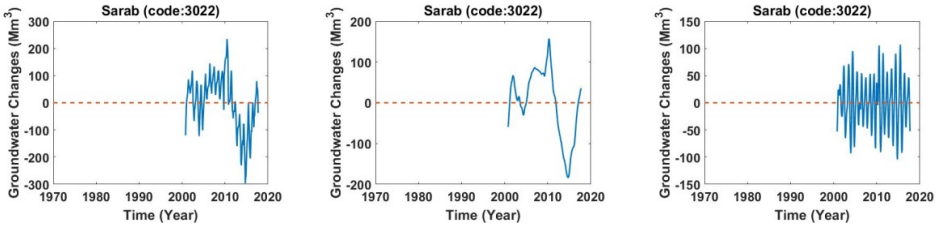

a b c

Figure G.20. a) Monthly values of groundwater storage, b) long-period of monthly values of groundwater storage, c) short-period of monthly values of groundwater storage across study area of Saleh Sarab (Code: 3022).

G.21. Study area of Sufian-Shabestar (Code: 3023)

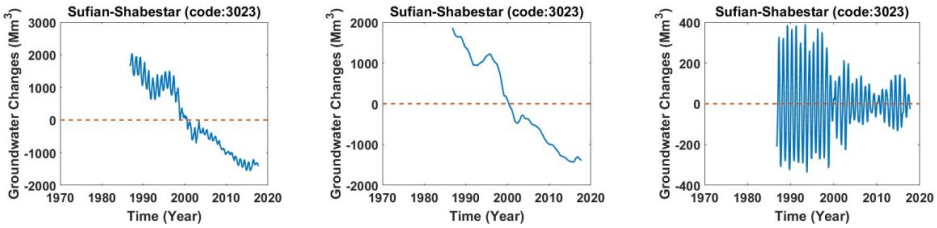

a b c

Figure G.21. a) Monthly values of groundwater storage, b) long-period of monthly values of groundwater storage, c) short-period of monthly values of groundwater storage across study area of Saleh Sufian-Shabestar (Code: 3023).

G.22. Study area of Tasouj (Code: 3024)

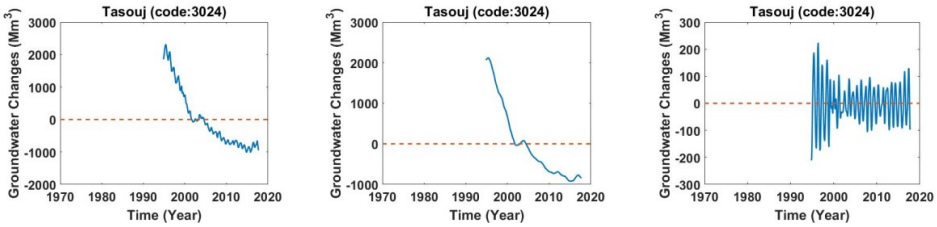

a b c

Figure G.22. a) Monthly values of groundwater storage, b) long-period of monthly values of groundwater storage, c) short-period of monthly values of groundwater storage across study area of Saleh Tasouj(Code: 3024).

G.23. Study area of Jazayer Daryacheh Urmieh (Code: 3025)

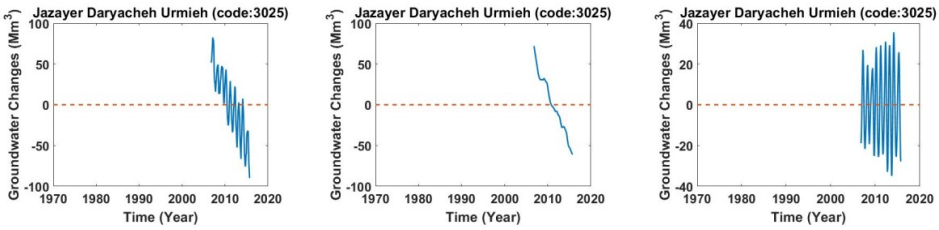

a b c

Figure G.23. a) Monthly values of groundwater storage, b) long-period of monthly values of groundwater storage, c) short-period of monthly values of groundwater storage across study area of Saleh Jazayer Daryacheh Urmieh (Code: 3025)